

**Water and Early City Development in Southeast China: Geoarchaeology
Case Study of the Ancient Liangzhu City**

Huiru Lian
Girton College

March 2021

This thesis is submitted for the degree of Doctor of Philosophy

Declaration

This thesis is the result of my own work and includes nothing which is the outcome of work done in collaboration except as declared in the Preface and specified in the text. I further state that no substantial part of my thesis has already been submitted, or, is being concurrently submitted for any such degree, diploma or other qualification at the University of Cambridge or any other University or similar institution except as declared in the Preface and specified in the text. It does not exceed the prescribed word limit for the relevant Degree Committee.

Huiru Lian

March 2021

Water and Early City Development in Southeast China: Geoarchaeology Case Study of the Ancient Liangzhu City

Huiru Lian

Abstract

Water has been cited as a key factor in influencing the emergence of complex society and the development of early cities throughout the world prehistory. Liangzhu, one of the earliest 'state' societies in East Asia dated from 3300 to 2300 BC, is characterised by its elaborate jade artefacts and hierarchical social structure. The centre of this culture is the 300 ha Liangzhu City located in the Hangzhou Bay area where complex hydraulic systems and waterways have been discovered near colossal man-made earthen mounds. Very little is known about how changes in the local hydrology affected the construction and development of Liangzhu City or how water influenced the complexity of the Liangzhu Culture.

By focusing on Liangzhu City and its nearby landscape, this study applied a series of geoarchaeological methods – namely soil micromorphology, bulk sedimentology, and GIS-modelling – to investigate and model the long-term human-landscape relationships between Liangzhu city, its surrounding landscape and its hydraulic regime. GIS data were processed to reconstruct regional hydrological conditions. Soil profiles were sampled from the Zhongjiagang Watercourse inside Liangzhu City to understand the nature of the infillings and water sequences of this inner-city waterway throughout different stages of city development and its relationship with the near bank mound construction. Settlement sites within the city were studied to examine patterns and details of occupational sequences and their long-term relationship to the changes in local hydrological regimes. Additionally, a series of settlements and profiles outside the city were also sampled in order to understand the sedimentation processes, changes in

hydrological conditions, and the interactions of human occupation and local landscape at a regional scale.

In this research, the major climate and hydrological shifts and the associated cultural responses have been determined from high-resolution sedimentation records, with the changing water regime considered as one of the most important factors influencing the appearance, development and the demise of Liangzhu City. This detailed geoarchaeological research study of Liangzhu City will enhance our understanding of how the management and exploitation of water has contributed to the formation of early state societies, and how changing hydrological conditions contributed to the development and destruction of one of the earliest known cities in East Asia.

Table of contents

CHAPTER 1: INTRODUCTION.....	1
1.1 GENERAL INTRODUCTION	1
1.2 RESEARCH QUESTIONS	2
1.2.1 <i>Water and the development of early cities</i>	2
1.2.2 <i>Liangzhu City in its regional context</i>	5
1.2.3 <i>Research questions</i>	6
1.3 RESEARCH APPROACHES	7
1.4 THESIS OUTLINE	8
CHAPTER 2: ENVIRONMENTAL AND ARCHAEOLOGICAL CONTEXT OF THE LIANGZHU CULTURE AND THE LIANGZHU CITY SITE	10
2.1 INTRODUCTION.....	10
2.2 LIANGZHU CULTURE.....	11
2.2.1 <i>Geographical context and climate of the southern Yangtze River Delta Plain</i>	11
2.2.2 <i>The Neolithic cultures in the southern Yangtze River Delta Plain from 9000 to 3000 BC: An adaption history of the changing water regime</i>	12
2.2.2.1 The beginning of rice exploitation: The Shangshan Culture	12
2.2.2.2 Settlements in swampland: The Kuahuqiao and Hemudu Cultures.....	13
2.2.2.3 Settlements on dry land: The Majiabang and Songze Cultures	14
2.2.3 <i>The distribution and characteristics of the Liangzhu Culture</i>	15
2.3 LIANGZHU CITY SITE: THE EMERGENCE OF EARLY STATE SOCIETY IN CHINA IN 3000 BC.....	19
2.3.1 <i>Introduction: Geographic Settings and Chronology</i>	19
2.3.2 <i>The layout and major archaeological findings of the Liangzhu City site</i>	20
2.3.2.1 Archaeological findings inside Liangzhu City.....	23
2.3.2.2 Archaeological findings from the outer Liangzhu City	25
2.3.2.3 The control and exploitation of water of the Liangzhu City	27
2.3.3 <i>Subsistence of Liangzhu City</i>	30
2.3.3.1 Rice cultivation.....	30
2.3.3.2 The diet of the Liangzhu	31
2.3.4 <i>The social complexity of Liangzhu City</i>	32
2.3.5 <i>The decline of the Liangzhu</i>	34
2.4 THE ENVIRONMENTAL AND SEDIMENTATION HISTORY OF THE LIANGZHU CITY SITE.....	35
2.4.1 <i>Sedimentation history of the Liangzhu Basin and southern Yangtze Delta</i>	35
2.4.1.1 Basal geomorphology of the southern Yangtze Delta	35
2.4.1.2 Sedimentation history of the Liangzhu Basin during the early Holocene	37
2.4.1.3 Sedimentation during Liangzhu time.....	39
2.4.1.4 The demise of Liangzhu	39
2.4.2 <i>History of climate change since the LGM in the Liangzhu Basin</i>	40
2.4.3 <i>Complexity of regional hydrological and sedimentation processes in the Liangzhu Basin</i>	42
2.5 CHARACTERISTICS OF MARINE AND FRESHWATER SEDIMENT.....	43
2.6 UNSOLVED RESEARCH QUESTIONS.....	44

2.7 SUMMARY	45
CHAPTER 3: FIELDWORK AND METHODOLOGY	46
3.1 INTRODUCTION.....	46
3.2 FIELDWORK AND SAMPLING STRATEGY IN THE LIANGZHU CITY SITE.....	46
<i>3.2.1 General working procedure</i>	<i>46</i>
<i>3.2.2 Site selection.....</i>	<i>48</i>
<i>3.2.3 Sampling procedures</i>	<i>50</i>
3.3 METHODOLOGY.....	50
<i>3.3.1 Bulk Sedimentological Analyses</i>	<i>50</i>
3.3.1.1 pH Values.....	51
3.3.1.2 Magnetic Susceptibility.....	51
3.3.1.3 Phosphate Analysis	51
3.3.1.4 Loss-on-Ignition	52
3.3.1.5 Particle Size Analysis.....	52
<i>3.3.2 Soil Micromorphological Analyses.....</i>	<i>53</i>
<i>3.3.3 GIS modelling.....</i>	<i>53</i>
3.4 SUMMARY	54
CHAPTER 4: GIS MODELLING OF THE LIANGZHU REGION	55
4.1 INTRODUCTION.....	55
4.2 PREVIOUS GIS MODELLING OF THE LIANGZHU REGION.....	55
4.3 BASIC GIS MODELLING OF THE HYDROLOGICAL CONDITION OF THE LIANGZHU REGION	59
<i>4.3.1 Modelled water system around Liangzhu region.....</i>	<i>59</i>
<i>4.3.2 Reconstruction of regional inundation condition.....</i>	<i>62</i>
4.3.2.1 Model of inundation condition of the Liangzhu Basin	63
4.4 SUMMARY	65
CHAPTER 5: THE RESULTS OF SOIL MICROMORPHOLOGICAL AND ASSOCIATED CHEMICAL AND PHYSICAL ANALYSES IN THE ZHONGJIAGANG REGION, INNER LIANGZHU CITY	67
5.1 INTRODUCTION.....	67
5.2 MIDDLE ZHONGJIAGANG REGION (T2621).....	68
<i>5.2.1 Field observation and stratigraphy of profile T2621</i>	<i>70</i>
5.2.1.1 The general stratigraphy and findings in the Middle Zhongjiagang region	70
5.2.1.2 Field description of profile T2621	70
<i>5.2.2 Results of soil micromorphological analysis in T2621</i>	<i>72</i>
5.2.2.1 Layer 13.....	72
5.2.2.2 Layer 12.....	80
5.2.2.3 Platform III 3 B2	89
5.2.2.4 Platform III 3 B1	93
5.2.2.5 Platform II 1A.....	94
<i>5.2.3 Interpretation of the Middle Zhongjiagang region</i>	<i>97</i>
5.2.3.1 Dating of the Middle Zhongjiagang region.....	98
5.2.3.2 Particle size analysis of the T2621 profile	99
5.2.3.3 Site formation process of the profile T2621	101

5.2.3.4 Change in hydrology conditions and human activity in the Middle Zhongjiagang Watercourse.....	102
5.3 NORTH ZHONGJIAGANG REGION (T5020).....	104
5.3.1 <i>Field observation and stratigraphy of profile T5020</i>	104
5.3.1.1 The general stratigraphy and findings in the North Zhongjiagang Watercourse	104
5.3.1.2 Field description of profile T5020.....	105
5.3.2 <i>Results of soil micromorphological analysis in T5020</i>	108
5.3.2.1 Pre-occupation sediment.....	108
5.3.2.2 Platform III-2	112
5.3.2.3 Layer 10	115
5.3.2.4 Layer 9B.....	119
5.3.2.5 Layer 8.....	122
5.3.2.6 Layer 7.....	126
5.3.2.7 Layer 5.....	128
5.3.2.8 Layers 4 and 3.....	133
5.3.3 <i>Interpretation of the North Zhongjiagang Watercourse</i>	133
5.3.3.1 Radiocarbon chronology of the North Zhongjiagang Watercourse	133
5.3.3.2 Particle size analysis of the T5020 profile	136
5.3.3.3 Site formation processes of profile T5020.....	139
5.3.3.4 Change of hydrological conditions and human activity in North Zhongjiagang region	140
5.4 SUMMARY	142
CHAPTER 6: THE SETTLEMENT SITES OF LIANGZHU CITY	144
6.1 INTRODUCTION.....	144
6.2 THE SOUTHWEST MOJIAOSHAN ZONE (T0950)	144
6.2.1 <i>Field observation and stratigraphy of profile T0950</i>	145
6.2.2 <i>Results of soil micromorphological analysis in T0950</i>	149
6.2.2.1 Buried soil (Layer 15).....	149
6.2.2.2 Layer 14: Bottom layers of 'clay wrapped with grasses'	152
6.2.2.3 Layer 13.....	152
6.2.2.4 Layer 12.....	155
6.2.2.5 Layer 11.....	156
6.2.2.6 Layer 10.....	157
6.2.2.7 Layer 9.....	159
6.2.3 <i>Interpretation of the Southwest Mojiaoshan mound (T0950)</i>	160
6.2.3.1 Particle size analysis of the T0950 profile	160
6.2.3.2 Chronological sequence, soil formation process and human activity in the Southwest Mojiaoshan site (T0950).....	161
6.3 THE SOUTH ZHONGJIAGANG REGION (T3131).....	164
6.3.1 <i>Field observation and stratigraphy of profile T3131</i>	165
6.3.1.1 The general stratigraphy and findings in the South Zhongjiagang Region.....	165
6.3.2 <i>Results of soil micromorphological analysis in T3131</i>	169
6.3.2.1 Platform 8	169
6.3.2.2 Platform 7	172

6.3.2.3 Platform 6C	178
6.3.2.4 Platform 6B.....	182
6.3.2.5 Platform 6A.....	184
6.3.2.6 Platform 5-2	192
6.3.2.7 Platform 5-1	198
6.3.2.8 Platform 2	200
<i>6.3.3 Interpretation of the T3131 profile</i>	<i>203</i>
6.3.3.1 Radiocarbon chronology of the T3131 profile.....	203
6.3.3.2 Particle size analysis of the T3131 profile	204
6.3.3.3 Preliminary lipid analysis of the plant material in T3131 profile	205
6.3.3.4 Site formation process of profile T3131	208
6.3.3.5 Changes in hydrological conditions and human activity in the T3131 profile.....	214
6.4 SUMMARY	218
CHAPTER 7: SETTLEMENT SITES AND ANALOGUE PROFILES IN OUTER LIANGZHU CITY..	219
7.1 INTRODUCTION.....	219
7.2 OUTER CITY SETTLEMENTS OF LIANGZHU CITY.....	220
<i>7.2.1 Shiqianyu site</i>	<i>220</i>
7.2.1.1 Field description of the Shiqianyu site (T1812 and T1813)	220
7.2.1.2 Soil micromorphology analysis of the Shiqianyu site.....	222
7.2.1.3 Interpretation of the Shiqianyu profiles.....	240
<i>7.2.2 The South Jincun site.....</i>	<i>243</i>
7.2.2.1 Introduction	243
7.2.2.2 Results of soil micromorphological analysis in South Jincun site	244
7.2.2.3 Interpretation of the South Jincun profile	250
7.3 REFERENCE PROFILES FROM OUTER LIANGZHU CITY	253
<i>7.3.1 Huoxitang site</i>	<i>253</i>
7.3.1.1 Introduction	253
7.3.1.2 Results of soil micromorphological analysis in Huoxitang site	254
7.3.1.3 Interpretation of the Huoxitang profile	259
<i>7.3.2 North Tangshan profile.....</i>	<i>261</i>
<i>7.3.3 Dazhe profile</i>	<i>262</i>
7.3.3.1 Micromorphological observation	264
7.3.3.2 Results of bulk sedimentology of the Dazhe profile.....	264
7.4 SUMMARY	265
CHAPTER 8: DISCUSSION	266
8.1 INTRODUCTION.....	266
8.2 THE SEDIMENTARY AND HYDROLOGICAL HISTORY OF LIANGZHU CITY	266
<i>8.2.1 The pre-site sedimentary history of Liangzhu City.....</i>	<i>266</i>
<i>8.2.2 The sedimentation and hydrological history during the development of the Liangzhu culture.....</i>	<i>268</i>
<i>8.2.3 Post-Liangzhu depositional processes.....</i>	<i>269</i>
<i>8.2.4 Summary.....</i>	<i>270</i>
8.3 THE CONSTRUCTION AND OCCUPATION HISTORY OF LIANGZHU CITY.....	270

8.3.1	<i>The construction of mounds</i>	271
8.3.1.1	Direct soil borrowing from pre-site sediments	271
8.3.1.2	The 'clay wrapped with grasses' material	271
8.3.1.3	Processed soil material	273
8.3.1.4	Calclitic rock fragments	274
8.3.1.5	Summary	275
8.3.2	<i>The formation and exploitation of the local water systems</i>	276
8.3.2.1	The life history of the Zhongjiagang Watercourse.....	276
8.3.2.2	Water areas near the outer city settlements.....	277
8.3.2.3	Summary	278
8.3.3	<i>The occupation pattern of Liangzhu City</i>	278
8.3.4	<i>The modification and exploitation of local landscape</i>	280
8.4	THE COUPLING OF THE WATER, ENVIRONMENTAL AND CULTURAL PERIODISATION OF LIANGZHU CITY ...	282
8.4.1	<i>The early stage of the Early Liangzhu period (3300-3100 cal. BC)</i>	283
8.4.2	<i>The late stage of the Early Liangzhu period (3100-2900 cal. BC)</i>	284
8.4.3	<i>The early stage of the Late Liangzhu period (2900-2600 cal. BC)</i>	285
8.4.4	<i>The late stage of the Late Liangzhu period (2600-2300 cal. BC)</i>	286
8.4.5	<i>The Qianshanyang period (2300-2000 cal. BC)</i>	287
8.4.6	<i>The yellow silty clay layer</i>	288
8.4.7	Summary.....	289
8.5	FURTHER DISCUSSION	290
8.5.1	<i>Water, mound, and social complexity</i>	290
8.5.2	<i>The collapse of Liangzhu</i>	291
CHAPTER 9: CONCLUSION AND OUTLOOK		293
9.1	THE FORMATION OF THE EARLY CITY	293
9.2	THE ENVIRONMENT AND HUMAN INTERACTIONS.....	294
9.3	RECONSTRUCTING SOIL FORMATION PROCESSES IN AN ARTIFICIAL LANDSCAPE	296
9.4	OUTLOOK AND FUTURE WORK	298
BIBLIOGRAPHY		300
APPENDIX 1 LABORATORY PROTOCOLS OF BULK ANALYSIS AND THIN SECTION MAKING		321
APPENDIX 2 DETAILED MICROMORPHOLOGICAL DESCRIPTIONS		332
APPENDIX 3 RESULTS OF BULK ANALYSIS		419

List of figures

Figure 1.1 Distribution area of Liangzhu Culture and the location of Liangzhu City. .	6
Figure 2.1 The geomorphology of the Lower Yangtze River.....	17
Figure 2.2 The C-shape Liangzhu Basin and the distribution of Liangzhu sites in the basin (adapted from Liu <i>et al.</i> , 2020).....	18
Figure 2.3 Plan of the Liangzhu City	21
Figure 2.4 Layout and reconstruction of the water systems of the Liangzhu City	22
Figure. 2.5 Piers, bank protection materials and a roof model excavated from the suburbs of Liangzhu City	26
Figure 2.6 Construction materials and bank protection facilities found in Liangzhu City.....	30
Figure 2.7 Exquisite artefacts found in Liangzhu City	34
Figure 2.8 Paleo-topography of the southern Yangtze delta plain and major incised valleys of the Yangtze and Qiantang rivers (Adapted from Wang <i>et al.</i> , 2012).....	37
Figure. 2.9 Palaeogeographic map of the Tai Lake Plain since 5500 cal. BC (adapted from Chen <i>et al.</i> , 2018).	38
Figure 3.1 Soil micromorphology description guide (adapted from Macphail & Goldberg, 2017, 75).	48
Figure 3.2 The sampling positions of this thesis. The yellow spots locate the profiles that were sampled in 2017, and the red spots locate the profiles that were sampled in 2018.....	49
Figure 4.1 Site distribution map of the Liangzhu City region (modified from Jin, 2018b)	56
Figure 4.2 Reconstructed reservoir areas (Liu and Wang, 2018).....	57
Figure 4.3 a: Tiao River modelled by Jin (2018a); b: modelled flow system near Liangzhu City (Jin, 2018a); c: Tiao River modelled by Liu and Wang (2018); d: modelled flow systems near Liangzhu City (Liu and Wang, 2018).....	58
Figure 4.4 Modelled watershed and stream network of the Liangzhu Basin.....	60
Figure 4.5 Modelled water system near Liangzhu City (enlargement of Figure 4.4)..	61
Figure 4.6 a. inundated area below 5m; b. inundated area below 7m; c. inundated area below 10m; d. inundated area below 12m.	64
Figure 4.7 Model of inundation condition of the Tai Lake Plain and Hangjiahu Plain	65
Figure 5.1 Sampling positions of the North, Middle and South Zhongjiagang profiles.	67
Figure 5.2 Sampling positions and sediment sequences of Middle Zhongjiagang	

region.	69
Figure 5.3 Stratigraphy and sampling position of the T2621 profile.....	71
Figure 5.4 Slide scan and microphotographs from slide T2621 1, the numbers and lines in blue defines different units identified from this slide.....	74
Figure 5.5 Slide scan and microphotographs from slide T2621 2	75
Figure 5.6 Slide scan and microphotographs from slide T2621 3	77
Figure 5.7 Analytical results of pH, phosphorus, magnetic susceptibility, and carbon, total organic and calcium carbonate contents of profile T2621.	78
Figure 5.8 Slide scan and microphotographs from slide T2621 4	84
Figure 5.9 Slide scan and microphotographs from slide T2621 5	87
Figure 5.10 Slide scan and microphotographs from slide T2621 6	91
Figure 5.11 Slide scan and microphotographs from slide T2621 7	95
Figure 5.12 Slide scan and microphotographs from slide T2621 8	97
Figure 5.13 Particle Size Distribution Graph of T2621.	100
Figure 5.14 Percentage bar chart of the particle size of T2621.	101
Figure 5.15 Stratigraphy of the T5017, T5018, T5019 and T5020 excavation pits. Soil samples were taken from the T5020 profile.....	107
Figure 5.16 Slide scan and microphotographs from slide T5020 1	110
Figure 5.17 Analytical results of pH, phosphorus, magnetic susceptibility, and carbon, total organic and calcium carbonate contents of profile T5020.	111
Figure 5.18 Slide scan and microphotographs from slide T5020 2	114
Figure 5.19 Slide scan and microphotographs from slide T5020 3	116
Figure 5.20 Slide scan and microphotographs from slide T5020 4	118
Figure 5.21 Slide scan and microphotographs from slide T5020 5	120
Figure 5.22 Slide scan and microphotographs from slide T5020 6	123
Figure 5.23 Slide scan and microphotographs from slide T5020 7	125
Figure 5.24 Slide scan and microphotographs from slide T5020 8	130
Figure 5.25 Slide scan from slide T5020 9 and 10	131
Figure 5.26 Lithology of profiled LZ-N. Amended from Wang <i>et al.</i> 2017.....	135
Figure 5.27 Particle size distribution graph of T5020, the bold lines are mentioned in the context.	137
Figure 5.28 Percentage bar chart of the particle size of T5020.	138
Figure 6.1 a) the location of the T0950 profile and the reconstructed water area between Jiangjiashan and Mojiashan mounds based on multi-excavations since 2012	

(amended from Liu *et al.*, 2019a); b) four rows of woodpiles of Layer 8C; c) eastern wall of T0950 showing the cross section of Layer 8C composed of three rows of ‘clay wrapped with grasses’ using various soil materials. Excavation tools provide scale.147

Figure 6.2 Stratigraphy and sampling position of the T0950 profile..... 148

Figure 6.3 Slide scan and microphotographs from slide T0950 1 150

Figure 6.4 Analytical results of pH, phosphorus, magnetic susceptibility, and carbon, total organic and calcium carbonate contents of profile T0950..... 151

Figure 6.5 Slide scan and microphotographs from slide T0950 2 154

Figure 6.6 Slide scan and microphotographs from slide T0950 3 158

Figure 6.7 Particle size distribution graph of T0950. 161

Figure 6.8 Percentage bar chart of the particle size of T0950. 161

Figure 6.9 Stratigraphy of the T3132 and T3131 excavation pits, the blue rectangular shows the sampling position of the T3131 profile. 167

Figure 6.10 Analytical results of pH, phosphorus, magnetic susceptibility, and carbon, total organic and calcium carbonate contents of profile T3131..... 167

Figure 6.11 a. Stratigraphy identified in field and sampling positions of the T3131 profile..... 168

Figure 6.12 Slide scan and microphotographs from slide T3131 1 173

Figure 6.13 Slide scan and microphotographs from slide T3131 2 177

Figure 6.14 Slide scan and microphotographs from slide T3131 3 181

Figure 6.15 Slide scan and microphotographs from slide T3131 4 185

Figure 6.16 Slide scan and microphotographs from slide T3131 5 190

Figure 6.16 (continued) Slide scan and microphotographs from slide T3131 5..... 191

Figure 6.17 Slide scan and microphotographs from slide T3131 6 196

Figure 6.17 (continued) Slide scan and microphotographs from slide T3131 6..... 197

Figure 6.18 Slide scan and microphotographs from slide T3131 7 201

Figure 6.19 Particle size distribution graph of profile T3131 205

Figure 6.20 Percentage bar chart of the particle size of Profile T3131. 205

Figure 6.21 Histograms displaying the distribution and concentration of n-alkanes extracted from sediments. 208

Figure 7.1 Distribution map of profiles sampled outside Liangzhu City: 1. Shiqianyu site, 2 Huoxitang site, 3. South Jincun site, 4. North Tangshan profile, 5. Dazhe mountain profile..... 219

Figure 7.2 Stratigraphy and sampling position of the T1812 and 1813 profiles. 223

Figure 7.3 Slide scan and microphotographs from slides T1812 1 and 2 224

Figure 7.4 Analytical results of pH, phosphorus, magnetic susceptibility, and carbon, total organic and calcium carbonate contents of the Shiqianyu site.	225
Figure 7.5 Slide scan and microphotographs from slide T1812 3	227
Figure 7.6 Slide scan and microphotographs from slide T1813 4	233
Figure 7.7 Slide scan and microphotographs from slide T1812 5	234
Figure 7.8 Slide scan and microphotographs from slide T1813 6	235
Figure 7.9 Slide scan and microphotographs from slide T1813 7	239
Figure 7.10 Particle size distribution graph of the Shiqianyu profiles	241
Figure 7.11 Percentage bar chart of the particle size of the Shiqianyu profiles.....	241
Figure 7.12 Stratigraphy and sampling position of the South Jincun profile.	244
Figure 7.13 Slide scan and microphotographs from slide JCN 1	245
Figure 7.14 Analytical results of pH, phosphorus, magnetic susceptibility, and carbon, total organic and calcium carbonate contents of the South Jincun site.....	246
Figure 7.15 Slide scan and microphotographs from slide JCN 2	248
Figure 7.16 Slide scan and microphotographs from slides JCN 3 and 4	251
Figure 7.17 Particle size distribution graph of the JCN profile	252
Figure 7.18 Percentage bar chart of the particle size of the JCN profile	252
Figure 7.19 Stratigraphy and sampling position of the Huoxitang profile (left), North Tangshan profile (middle) and Dazhe profile (right).	254
Figure 7.20 Slide scan and microphotographs from slides HXT 1 and 2	255
Figure 7.21 Analytical results of pH, phosphorus, magnetic susceptibility, and carbon, total organic and calcium carbonate contents of the Huoxitang site.....	257
Figure 7.22 Slide scan and microphotographs from slide HXT 3	258
Figure 7.23 Particle size distribution graph of the Huoxitang profile	260
Figure 7.24 Percentage bar chart of the particle size of the Huoxitang profile	260
Figure 7.25 Analytical results of pH, phosphorus, magnetic susceptibility, and carbon, total organic and calcium carbonate contents of the North Tangshan site.	262
Figure 7.26 Percentage bar chart of the particle size of the North Tangshan profile.	262
Figure 7.27 Slide scan and microphotographs from slide DZ 1	263
Figure 8.1 Sketch of the construction components of a typical Liangzhu mound.....	274
Figure 8.2 Site formation process of the T2621 profile.....	282

List of tables

Table 4.1 Inundation area of the Liangzhu Basin under different elevations	64
Table 5.1 Radiocarbon dating of the Middle Zhongjiagang region.	99
Table 5.2 Radiocarbon dating of the North Zhongjiagang region and the LZ-N profile	134
Table 6.1 Radiocarbon dating of the T3131 profile and adjacent South Zhongjiagang Channel.	203
Table 6.2 n-alkane concentrations, average chain length (ACL), the carbon preference index (CPI) and Paq values from the sediment samples analysed.	207
Table 6.3 $\delta^{13}\text{C}$ and δD from the sediment samples.....	207
Table 6.4 Synthetic interpretation of the T3131 profile.....	212
Table 8.1 Results of bulk analysis of the pre-site samples.....	267

Acknowledgments

I would first like to express my sincere gratitude to my PhD supervisor Charly French for his patient guidance, support, and encouragement through each stage of this thesis. His expertise and enthusiasm in geoarchaeology, and his sincerity and kindness to myself and other people have greatly inspired me and have shown me what a good scholar and a good supervisor should be.

My colleagues from the Zhejiang Provincial Institute of Cultural Relics and Archaeology (ZPICRA) have provided tremendous help and support for my research and fieldwork in Liangzhu. I would like to thank LIU Bin and WANG Ningyuan for sharing their expertise and knowledge of Liangzhu research; CHEN Minghui, for providing me with valuable unpublished data and information about Liangzhu City and providing support for everything I needed in the field; and WANG Yonglei for patiently answering my questions and providing detailed excavation records for me. I would also like to thank WU Xin, SONG Shu, JI Xiang, ZHU Xuefei, YAN Kaikai, ZHU Yefei, WANG Shuai and WEN Yan for their help with collecting soil samples and with my everyday life at the Liangzhu Working Station. Working with them meant that my time in Liangzhu was both memorable and rewarding.

My heartfelt thanks also go to Dr ZHUANG Yijie for introducing me to geoarchaeology, for offering advice since my master's studies at UCL, and for helping me throughout the development of this thesis. I would also like to thank Prof. Colin Renfrew. During our two visits to Liangzhu, I learned a lot from his erudite and critical thinking.

During my time at the Charles McBurney Laboratory for Geoarchaeology, I received great support from the lab members. Dr Tonko Rajkovaca trained me in thin section manufacture, and his extreme kindness supported and encouraged me throughout my PhD. Dr Sean Taylor provided helpful advice with soil sampling and thin section

observation, Dr Natalia Égüez kindly conducted lipid analysis for the Liangzhu organic matter, Camilla Alday identified the bast fibres in the thin sections and shared her knowledge about bast fibre techniques, and Michael Lewis answered all my questions regarding Liangzhu pottery techniques. Other lab members, including David, Federica, Jeremy, Joanna, Malcolm, Menzi, Petros, and many others, also kindly shared their knowledge in their particular fields of expertise. In addition, David Redhouse trained me in GIS analysis and Laura Healy at the Physical Geography Laboratory of Cambridge hosted me for the sediment analysis. I am very grateful for all their support and for their knowledge-sharing.

This thesis has also benefited from many informal discussions with micromorphologists, particularly those who attended the International Working Group Meeting on Soil Micromorphology 2019 in Basel. I would particularly like to thank Dr Kristin Ismail-Meyer, Dr Hans Huisman and Dr David Brönnimann, who shared their experience in micromorphology interpretation and identified plant/bone remains in my thin sections.

This thesis is primarily funded by the Chinese Scholarship Council. The fieldwork and conference costs were supported by university and department fieldwork funding, with additional grants from the Dorothy Garrod Memorial Fund and Pillman Fund of Girton College. The cost of thin section production and sedimentological analysis was borne by the Charles McBurney Laboratory for Geoarchaeology. I am extremely grateful to these funding bodies for supporting this research.

My time in Cambridge has been one of the most wonderful experiences of my life. I am thankful to all the friends I met here, and to LIANG Shikang, in particular, who has been congenial company for me and who shared some of my most memorable days. I also cherished the joyful days I spent with other Girtonians, especially those days in Wolfson Court and Swirles Court with ZHANG Kexin and others. In addition, AN Ting,

SHANG Xue and the visiting scholars from the Needham Institute have been both good friends and knowledgeable peers during our academic discussions.

This thesis could not have been completed without the love and support of my family. I am grateful to my parents, LIAN Guopeng and YAN Liying, and my sister LIAN Huishan, for their unfailing love, care and support. Finally, my deepest gratitude goes to my beloved husband MA Tianyi. Thank you for encouraging and respecting me in all of my pursuits, for patiently listening to all the highs and lows of my PhD experiences, and for comforting and supporting me whenever I needed you. Thank you, with love.

Chapter 1: Introduction

1.1 General introduction

Water has been cited as a key factor in influencing the emergence of complex society and the development of early cities throughout the world. Liangzhu, one of the earliest ‘state’ society in East Asia dated from 3300 to 2300 BC, is characterised by its elaborate jade artefacts and hierarchical social structure. The centre of this culture is the 300 ha large Liangzhu City located in the Hangzhou Bay area where complex hydraulic systems and waterways have been discovered near large-scale man-constructed platforms (Liu and Wang, 2007; Renfrew and Liu, 2018) (Figure 1.1). Current evidence suggests that both hydrological and climatic changes may have directly influenced the vicissitude of this city (Long *et al.*, 2014; Wu *et al.*, 2014). However, how the construction and development of this city is related to the changing local hydrologic regime, and how water is related to the complexity of the Liangzhu Culture are interesting but little understood questions.

Focusing on the Liangzhu City and its nearby landscape, this study applied a series of geoarchaeological methods, namely soil micromorphology, bulk sedimentology and GIS-modelling, to investigate and model the long-term human-landscape relationship between Liangzhu City, its surrounding landscape and its hydraulic regime. GIS data were processed to reconstruct regional hydrological conditions. Soil profiles were sampled from the Zhongjiagang Watercourse inside Liangzhu City to understand the nature of the infillings and water sequences of the inner-city waterway throughout different stages of city development and its relationship with the near bank platform construction. Settlement sites inside Liangzhu City were studied to examine patterns and details of occupational sequences and their long-term relationship to the changes in

local hydrological regimes. A series of outer city settlements and profiles were also sampled to have a glimpse of the sedimentation processes, changes of hydrological condition, and interactions between human occupation and the local landscape at a regional scale.

This research aimed to reconstruct the sedimentary and hydrological history of Liangzhu City, and studied how Liangzhu people modified their local landscape and exploited near-water resources by reconstructing the formation process of canals and platforms of Liangzhu City. In this study, the occupation pattern of Liangzhu City was revealed, as well as major hydrological shifts and associated cultural responses being recognised and discussed. The changing water regime is considered as one of the most important factors influencing the formation, consolidation and the decline of the Liangzhu City. This study provides a unique opportunity to understand how an early city interacted with its local water regime, especially in an East Asian context that is relatively little known by world archaeologists.

1.2 Research questions

1.2.1 Water and the development of early cities

Water is one of the most important resources for human survival and also one of the most important factors influencing the formation, development and decline of early cities. The interaction between water and early cities has thus become a primary relationship which archaeologists need to understand.

On the one hand, the variation and fluctuation of hydrological conditions, influenced by climatic, eustatic and landscape conditions, has influenced the ebbs and flows of early cities around the world, either through extreme fluctuation of water conditions such as large flooding and drought events, or indirect impacts on the ecosystem,

agriculture, and land resources (Middleton, 2012; Weiss & Bradley, 2001 etc.). For instance in Southern Mesopotamia, regional eustatic and climatic changes that create productive habitats, flat and newly formed land resources, and high water table that promoted the efficient transport of goods, ideas and people and the formation of irrigation agriculture, facilitated the transition from small sedentary communities to early cities (Algaze, 2001; Kennett & Kennett, 2006 etc.). Moreover, the increased aridification and consequent decrease in agricultural productivity in the late 4th millennium BC may in part led to the collapse of Uruk society in northern Mesopotamia (Charles *et al.*, 2010; Kennett & Kennett, 2006; Weiss, 1997, 2000). In North Africa, the desertification of the Egyptian Sahara during the Holocene provoked stress on population in the Nile Valley and may have stimulated the rise of Egyptian civilization (Brooks, 2006; Malville *et al.*, 1998; Pennington *et al.*, 2019). In the Indus valley, the abandonment of urban centres is probably related to the drying climate caused by the weaken of Indian monsoon, which led to the drying up of lakes and a reduction of water supply to the urban centres, such that Indus settlements in different socio-ecological scenarios adopted diverse strategies to cope with this dramatic change (Angourakis *et al.*, 2020; Clift & Giosan, 2018; Petrie *et al.*, 2017 etc.). In highland Mexico and Andes, volatile climate and multidecadal drought caused by Intertropical Convergence Zone migration and changes in El Niño frequency are believed to be the direct cause of the societal decline in multiple sites such as Tiwanaku, Wari and the Mayan civilization (Chepstow-Lusty *et al.*, 1996; Binford *et al.*, 1997; Kennett *et al.*, 2012; Kennett & Marwan, 2015).

On the other hand, water management, especially irrigation, has long been argued as the catalyst for the formation of state society (Steward, 1955; Wittfogel, 1957, 1981). Although this hydraulic hypothesis has long been both criticised and modified by archaeologists (Adams, 1966, 1978; Butzer, 1976; Scarborough, 2003), the management of water is still considered as an important trigger that co-evolved with complex society (Zhuang & Altaweel, 2018). In early cities, the control of water was

vital for sustaining large populations, as settled farmers are strongly relied on sustainable water resources and persistent rainfall (Fagan, 1999; Kennett & Marwan, 2015). The control of water then became a method to secure and maintain power, both in the past and present (Scarborough, 2003; Holt, 2019 etc.). Societies in different regions and geographic settings adopted various water management strategies to cope with the local water regime, such as the canal and irrigation networks in Mesopotamia, the basin irrigation in Egypt, the manipulation of aguadas and the development of wetland field systems in Mayan times (Berking, 2018; Luzzadder-Beach *et al.*, 2016; Mays, 2010). The study of water management strategies and its relation to local geographic setting and cultural traditions may reflect the hierarchy, social organization and structure, and even the flow of population, goods, and ideas of a specific society.

Decades of archaeological work have demonstrated that the management of water in early civilizations around the world have shown a great variety and complexity in the techniques, scales and relationships to land, labour and social organization (Mithen, 2010; Lisa, 2002 etc.). Moreover, the sustainability and resilience of responses to environmental pressures of different societies are varied according to different local environment parameters from decline, reorganization, to expansion, and in some cases no obvious impact can be observed (Aimers & Hodell 2011; Dixit *et al.*, 2014 etc.). Correspondingly, not all major cultural changes had a climatic trigger (Anderson *et al.*, 2007). It can be seen that different geographic settings with their unique cultural traditions may react dissimilarly and develop various strategies and techniques to adapt and manage local water system, and thus create different pathways towards civilization. It is thus crucial to study the rise and fall of a specific early society in its local environmental context and its relationships to the changing water regime through its unique development history. This relationship between cultural history and water regime should be determined by thorough and comprehensive study of region cultural and technology traditions, geographic settings, socio-economy structures, and by the establishment of high resolution chronological, climatic, hydrological and

soil/sediment records (Maher *et al.*, 2011).

1.2.2 Liangzhu City in its regional context

In the past few decades, Liangzhu City, a walled city located in Southeast China that is believed to be one of the earliest cities in East Asia (3300-2300 cal. BC) was discovered and explored in some detail (Liu and Wang, 2007; Renfrew and Liu, 2018) (Figure 1.1). Currently, large-scale constructed earthen mounds, elite burials and hydraulic structures, involving about 10 million m³ of soil, with associated water systems have been found in the city (Liu *et al.*, 2019a, 2019b).

Liangzhu City is located in a C-shape basin within a low-lying and marshy environment. In the early Holocene, it is on the one hand susceptible to the fluctuation of sea water from the east, and on the other hand receiving river discharges from the Northern and Western mountainous areas inland, which makes it very vulnerable to local hydrological changes (Chen *et al.*, 2018; Liu *et al.*, 2018). Before the arrival of Liangzhu people, only a few Neolithic people had settled in this area because of the high sea level in this region. The retreat and stabilization of sea water since 7-6 kyr provided a newly formed, productive, open marsh environment suitable for long-term human occupation. This inhabitation of coastal margin after sea level stabilization is also widely seen in other areas around the world, such as in southern Mesopotamia and Peru (Day Jr. *et al.*, 2007, 2012; Kennett and Kennett, 2006). In this local freshwater marsh environment, Liangzhu people built gigantic anthropogenic structures such as dams, mounds and walls to adapt, utilize and control local water resources (Liu *et al.*, 2017). At the same time, a complex social structure, specific craftsmanship and unified ideological symbol appear, suggesting the complexity of this culture. The demise of Liangzhu city at around 2300 to 2000 cal. BC is also believed to be related to changes in the local hydrological regime (Long *et al.*, 2014; Wu *et al.*, 2014). This appears to have coincided with the global 4.2ka BP megadrought event (Weiss, 2017), but whether

and how this global scale pressure influenced Liangzhu society and City is not yet clear. What caused the change in hydrology? What were the scales and intensities of changes? Was it natural or human-induced? What were the long-term relationships between society and its hydraulic regime? How have human activities transformed their local landscape and made use of the local hydrological regime over time? All of these are important but currently unresolved questions. Therefore, to better understand the landscape history of Liangzhu City and the complexity of Liangzhu Culture, new evidence should be sought. In particular, more research should be undertaken to investigate the role of water control in the development of Liangzhu City, and brought together with different strands of evidence, such as from soil/sediment analyses, pollen study, archaeological findings, and the geomorphology survey of the region to further address these questions.



Figure 1.1 Distribution area of Liangzhu Culture and the location of Liangzhu City.

1.2.3 Research questions

This proposed study aims to investigate and model the relationships between the Liangzhu City site and its local environmental conditions set against the changing climatic regime, and especially to investigate the role of water in this floodplain location.

By applying geoarchaeological methods and approaches, this research aims to address the following issues: 1) the detailed sedimentation and hydrological history across the inner and outer parts of Liangzhu City; 2) the development history of Liangzhu City, including the construction and occupation techniques, strategy and history of the City; and 3) the long-term interactions between climate, hydrological conditions and cultural activities. Based on the results of these studies, this thesis will chart how the site and its people may have responded to environmental change, and discuss how water may have influenced the emergence of social complexity and even possibly led to the demise of Liangzhu City.

1.3 Research approaches

Geoarchaeology "involves the combined study of archaeological, soil and geomorphological records and the recognition of how natural, climatic and human-induced processes alter landscapes" (French, 2015, 1). Four scales of archaeological landscape contexts are involved in geoarchaeological study. The macro-scale concerns the land-use and landscape change of the region. The meso-scale or the immediate region of the site involves the land-use pattern and the position of the site in the landscape. The micro-scale is the area immediately around the site and deals with the use of space and human activities in the settlement context. The finest scale is the within-soil micro-environment and concerns mainly about the soil forming and transformation factors at work (French, 2003, 2015).

In this study, different approaches were adopted to answer research questions at these different scales. To be specific, in the macro- and meso-scales, fieldwalking, hand augering and GIS analysis were used to provide a wide general view of the site's location, siting, its relationship with local water systems, and the general stratigraphic sequences of the landscape. The soil micromorphological and associated physical and geo-chemical techniques are capable of studying the formation and modification of

sediment and occupation sequences for all scales. But for this study, these techniques were mainly adopted for the micro-scale and within-soil scale studies of site formation processes, changes of hydrology/sedimentary processes and long-/short-term stability and their immediate human response. It involves different types of sediment/soil encountered in Liangzhu City, including riverine sediments – to study their mechanics of flow and transport, the buried sediments – to examine the pre-site sedimentary and hydrological conditions, the occupation sequences – to investigate the occupation pattern and its relationship to local hydrological conditions, and the constructed layers – to analyse the techniques and strategies involved and their adaptation to local water regime. By combining these micro-to-macro scales of evidence, basic modelling of the landscape/site/cultural evolution of Liangzhu City became possible.

1.4 Thesis outline

This thesis begins with a comprehensive review of the geographical settings and climatic conditions of the southern Yangtze River Delta, with special emphasis placed on how Neolithic cultures before the Liangzhu may have adapted to the changing water regimes. This is followed by an account of the most up-to-date archaeological discoveries about Liangzhu City, including its layout, the major archaeological findings inside and outside the city, and the hydrological systems identified so far. Then the subsistence strategy and reflections of the social complexity of Liangzhu City is introduced. At the end of Chapter 2, the current progress on the environmental and sedimentation history of the Liangzhu City site is reviewed. To answer the research questions, Chapter 3 outlines the sampling strategy and geoarchaeological approaches employed in this study. The latter mainly includes the application of soil micromorphology, bulk sedimentology and GIS modelling analyses.

Chapter 4 first reviews the previous GIS research in Liangzhu City, and then presents the results of the GIS modelling of the river system around Liangzhu City and the

possible ranges of flooding under different depths of inundation.

Chapters 5 to 7 present the results of the micromorphological and sedimentological analyses of the profiles sampled from Liangzhu City. Chapter 5 focuses on the Middle and North Zhongjiagang profiles, aiming to provide a complete sedimentation and hydrological history of the inner area of Liangzhu City. Chapter 6 presents the geoarchaeological analysis of the Southwest Mojiaoshan and South Zhongjiagang sites, which studied the human occupation pattern and their relationships to the changes in local hydrological regimes in different areas of Liangzhu City. Chapter 7 focuses on the outer Liangzhu City profiles to investigate the relationships between human occupation and the local landscape from a regional perspective and to provide possible analogues for the Liangzhu City profiles and sequences.

Chapter 8 synthesises the results from Chapters 4 to 7 in order to provide a high-resolution record of the sedimentological and hydrological history of the area as well as the construction and occupation patterns of Liangzhu City. It then discusses the possible interactions between changing climate, hydrological conditions, and the development of the city. Next, the possible reasons for the eclipse of Liangzhu City are explored, and the relationships between water and social complexity are investigated.

Chapter 9 concludes with summaries of the implications of this study for a wider understanding of the emergence of complex society and human responses to a changing environment, and the importance of studying site formation processes more widely in archaeological research. Possible directions for future research are outlined at the end of this chapter.

Chapter 2: Environmental and Archaeological Context of the Liangzhu Culture and the Liangzhu City site

2.1 Introduction

The Neolithic period in China began in approximately 10,000 BC in the Middle and Lower Yangtze River (Cohen, 2014). After 6,000 years of development, Neolithic cultures¹ were widely and intensively developed from several centres including the Northern grassland region, the Yellow River Basin, the Yangtze River Basin, and the South China region (Zhang, 2001). Although different geographical units had unique pathways of development during the period from *c.* 3000 to 2000 BC, complex society with large-scale cities and a clear hierarchy had developed for example at Liangzhu (300 ha) in the Lower Yangtze River, Taosi (300 ha) and Shimao (425 ha) in the Middle Yellow River, and Chengtoushan (18.7 ha) in the Middle Yangtze River (Guo, 2007; He, 2013; Liu, 2014; Zhao, 2016). Subsequently by 1750 BC, the Shang Dynasty was established in the Middle Yellow River region, which marked the beginning of the mature state society of China.

Within this sequence of urban development, Liangzhu is one of the earliest complex societies in China that shows significant advances in the scale of settlement, craft technology and the exploitation of water. This chapter reviews the current understanding of the Liangzhu Culture and Liangzhu City archaeological records, and the existing environmental and sedimentation research from the Liangzhu City region,

¹The concept of 'Neolithic Culture' is used in this paper for the purpose of convenience. It refers to a group of contemporary and sympatric sites sharing a series of similarities including the making and decorating technique of pottery, ornaments, tools and houses, the rituals of burials as well as symbols such as totems and monuments.

before discussing the research debates and challenges surrounding the relationships between water and the development of the Liangzhu City site.

2.2 Liangzhu Culture

Liangzhu is located in the Lower Yangtze River region and was inhabited from 3300–2300 BC (Liu *et al.*, 2020). This section first outlines the physical geography and climate of the Lower Yangtze River region, and then briefly introduces the Neolithic cultures in this region to provide an overview of the trajectory of regional culture development and their relationships to the changing water regimes, prior to the introduction of the distribution and general characteristics of Liangzhu Culture.

2.2.1 Geographical context and climate of the southern Yangtze River Delta Plain

The study region is located in Eastern China (N28°45'–33°25', E118°20'–123°25') in a delta between two major rivers, the Yangtze, and the Qiantang. Based on current geomorphology, this delta can be further divided into three smaller plains: The Tai Lake, Hangjiahu and Ningshao Plains (Figure 2.1). However, in the early to middle Holocene, this delta was relatively isolated from nearby geographic features. In the north, the Ningzhen Mountains formed a natural barrier together with the Yangtze River. In the south, the Dongnan Hills, where the earliest Neolithic cultures of this region probably originated (ZPICRA and Pujiang, 2007), also became an impediment for prehistory people. Therefore, in Neolithic times, this region was more like a peninsula between the ancient estuaries of the Yangtze and the Qiantang (Liu, 2010).

The monsoon climate and the flat estuary landscape are the two main factors influencing the vegetation and hydrology of this region. Due to its closeness to the sea and its low elevation of about 3m above sea level (Ningbo, 2014), this estuary area is generally sensitive to sea-level fluctuations and regularly suffers from typhoons from

July to September. This area is in the subtropical monsoon climate zone and is characterised by mild winters and warm, humid summers. The duration and amount of precipitation is largely controlled by the intensity of the East Asian summer monsoon. The rain season normally continues from March to June and then August to September and the abundant precipitation may be exacerbated by rainstorms and storm surges that come with the typhoons, causing flooding and waterlogging in this poorly drained, flat estuary area. From mid-July to mid-August, the subtropical high predominates and causes high temperatures and drought.

Although floods and droughts are common in this estuary area, the seasonal rainfall, which is largely caused by the monsoon climate, also fosters the appearance of food production by providing a natural flood recession that encourages the growing of wild rice (White, 1995). The fertile, flat land in the delta area provided a solid foundation for human settlement and the development of agriculture.

2.2.2 The Neolithic cultures in the southern Yangtze River Delta Plain from 9000 to 3000 BC: An adaption history of the changing water regime

Since the early Holocene, the development trajectories of the prehistoric cultures in the southern Yangtze River Delta Plain were closely related to the geographical conditions and the changes in the hydrological regime (Chen and Wang, 1998). This section will briefly outline the changes in the environment and the development of the Neolithic cultures before the appearance of Liangzhu Culture.

2.2.2.1 The beginning of rice exploitation: The Shangshan Culture

After the Last Glacial Maximum (LGM) and Younger Dryas events, which happened in South China around 9100–8300 BC (Huang *et al.*, 2002), the climate of the Lower Yangtze River became increasingly mild, warm and humid (Zheng *et al.*, 2016; Zhu *et*

al., 2003). The higher temperatures contributed to a rise of sea level from -130 to -150m in LGM to -50m in 9000 BC and -15m in 6500 BC in the East China Sea (Xu *et al.*, 1997). Research shows that from 10,000 to 6000 BC, the difference in solar radiation between winter and summer was much greater than at present (Binford, 2001), and with the influence of the monsoon climate, the seasonality of the Lower Yangtze River increased, which may have fostered the appearance of storage and food production in this region (Chen, 2006).

During this period, there was basically no prehistoric settlement in the Tai Lake region due to the high sea level (Lin *et al.*, 1989). Most of the Neolithic sites were found on the south bank of the Qiantang River on the Ningshao Plain at relatively high altitudes. The earliest Neolithic culture that has been found in this region is the Shangshan Culture dating from *c.* 8000 BC to 6500 BC (ZPICRA and Pujiang Museum, 2007). This culture was distributed across the second terrace of the upstream Qiantang River (Figure 2.1) among a covering of evergreen broadleaf and coniferous mixed forest (Zheng *et al.*, 2016). The Shangshan were largely a hunter-gatherer society, with some possible early settlements (ZPICRA, 2007). Evidence from use-wear, residue analysis (Wang, 2016) and phytolith analysis (Zheng and Jiang, 2007) show that the Shangshan people began to collect and consume wild rice, with rice husks used as temper in pottery.

2.2.2.2 *Settlements in swampland: The Kuahuqiao and Hemudu Cultures*

At around 6500 BC, the Taihu Plain was still susceptible to marine flooding both in the spring and with storm tides, making it unsuitable for human settlement due to the high flood risk (Wang *et al.*, 2020). Neolithic settlements have only been found in the upland areas of the Ningshao Plain, which have been traced to the Kuahuqiao culture (6200 to 5000 BC) (Shu *et al.*, 2010; ZPICRA, 2004), who may be possible descendants of the Shangshan. The Kuahuqiao people (Figure 2.1) continued to cultivate rice on a small scale (Hu *et al.*, 2020; Jiang, 2013) and built their settlements on swampy land. A 5.6m-

long canoe with two paddles was preserved in one waterlogged site, which is the earliest canoe found in China (ZPICRA, 2004). From 5500 to 5000 BC, the sea level kept rising (Xiang, 2015). Geochemical and diatom analyses have shown that the Kuahuqiao and its surrounding areas were constantly influenced by seawater, and transgression by the sea might be the reason for the termination of settlement and cultivation of this culture (Innes *et al.*, 2009; ZPICRA, 2004; Zong *et al.*, 2007).

Since 7ka BP, the sea-water of the East China Sea has regressed, with the land around Tai Lake deposited. At the same time, the climate became milder and more moist and prehistoric peoples started to build their settlements on the downstream floodplain areas. During this period, there were two dominant Neolithic cultures in the Lower Yangtze River region: the Hemudu Culture on the Ningshao Plain (Figure 2.1), dating from 5000 to 3000 cal. BC, and the Majiabang Culture (Figure 2.1) who developed near Tai Lake and dated from 5100 to 3900 cal. BC (Wang, 2013).

Hemudu people also built their houses on swampy land. They used a form of rectangular longhouse (23*7 m) on stilts, raised about one metre off the ground to tackle the fluctuations in water level (ZPICRA, 2003a). Canoes, a bridge and a timber-framed well have also been found. The Hemudu people began to reclaim land for rice farming (Zheng *et al.*, 2009) together with acorn and aquatic plants such as the water chestnut and gorgon fruit (Fuller *et al.*, 2011). A transgressive layer dated at 4400–4300 cal. BC was found overlying the Hemudu layer at both the Tianluoshan (Figure 2.1) and Yushan sites (Figure 2.1), which may in part cause the demise of the Hemudu Culture (He *et al.*, 2018; Zheng *et al.*, 2012).

2.2.2.3 Settlements on dry land: The Majiabang and Songze Cultures

Majiabang (5100–3900 BC) and the following Songze culture (3900–3200 BC) (CPAM, 1992) were both distributed around the Tai Lake Plain (Figure 2.1). Majiabang people

started to build their dwellings on dry ground, while the Songze people lived mainly on artificially constructed mounds. The construction of these mounds requires engineering skills to work with earth materials, which was later inherited by Liangzhu people. During this period, the scale and techniques of rice farming further developed, with paddy fields with irrigation systems appearing (4280 cal. BC) at the Chuodun site, which is believed to be the earliest paddy fields known so far (Hu, 2013). Possible stone ploughs appeared around this time and were popularized during the Songze period (Wang, 2013b). Jade artefacts and preliminary social stratification developed in Majiabang period and were further intensified in the Songze period (Chen, 2018; Liu, 2019b). The development of the Majiabang and Songze cultures were also constrained by the hydrological conditions. According to the analyses of pollen, carbon isotope $\delta^{13}\text{C}$, magnetic susceptibility and Rb/Sr values, extreme low temperature and flooding events occurred in 4400 BC, 4000 BC and 3500 BC, which may have caused the interruptions in the Majiabang and Songze cultural layers (Zheng, 2005).

2.2.3 The distribution and characteristics of the Liangzhu Culture

In the Lower Yangtze River area, the change in hydraulic regime was a limitation as well as an impetus for the development of complex society. For over five thousand years, the prehistoric people in this region adapted and exploited the changing water environment by developing structures and techniques such as stilt houses, artificial mounds, bridges, canoes and wells, and making use of natural flood recessions to grow rice as well as moving their settlements from upstream basin positions to the wider floodplain area. During this process, the scale of food production, the population size, the scale of settlement, the technological level and the complexity of the society all increased, which provided a solid foundation for the appearance of Liangzhu.

Evidence of the Liangzhu culture (3300–2300 BC) was first discovered by SHI Xingeng in 1936 (Shi, 1938). This culture has inherited the techniques and tradition of rice

farming, the preference for jade artefacts and the tradition of living in man-constructed mounds from previous Majiabang and Songze cultures but showed a higher level of social complexity in every respect (which will be further elaborated in section 2.3). After 80 years of archaeological work, more than 600 sites distributed over an area of about 18,000 square kilometres of this cultural period have been found so far (Guo, 2014; Liu *et al.*, 2020). In general, most of the sites are concentrated in three regions (Qin, 2013). The first region was in the Tai Lake plain area (Figure 2.1), and the second was around the Hangjiahu Plain (Figure 2.1). In these two areas, early Liangzhu culture was developed and found to overly previous Majiabang and Songze cultural material. The third region, the so-called Liangzhu site complex, was located in a C-shape basin north to the Hangzhou Bay (Figure 2.2). Before the arrival of Liangzhu people, only a few Neolithic people had settled in this region because of the high sea level during the early Holocene (Qin, 2013). Since 3300 BC, this region became ideal for human occupation, and a walled city was constructed, with around 300 Liangzhu sites having been found so far (Liu *et al.*, 2020). This walled city, the so-called Liangzhu City was the centre of the entire Liangzhu Culture and is the main study objective of this PhD research.

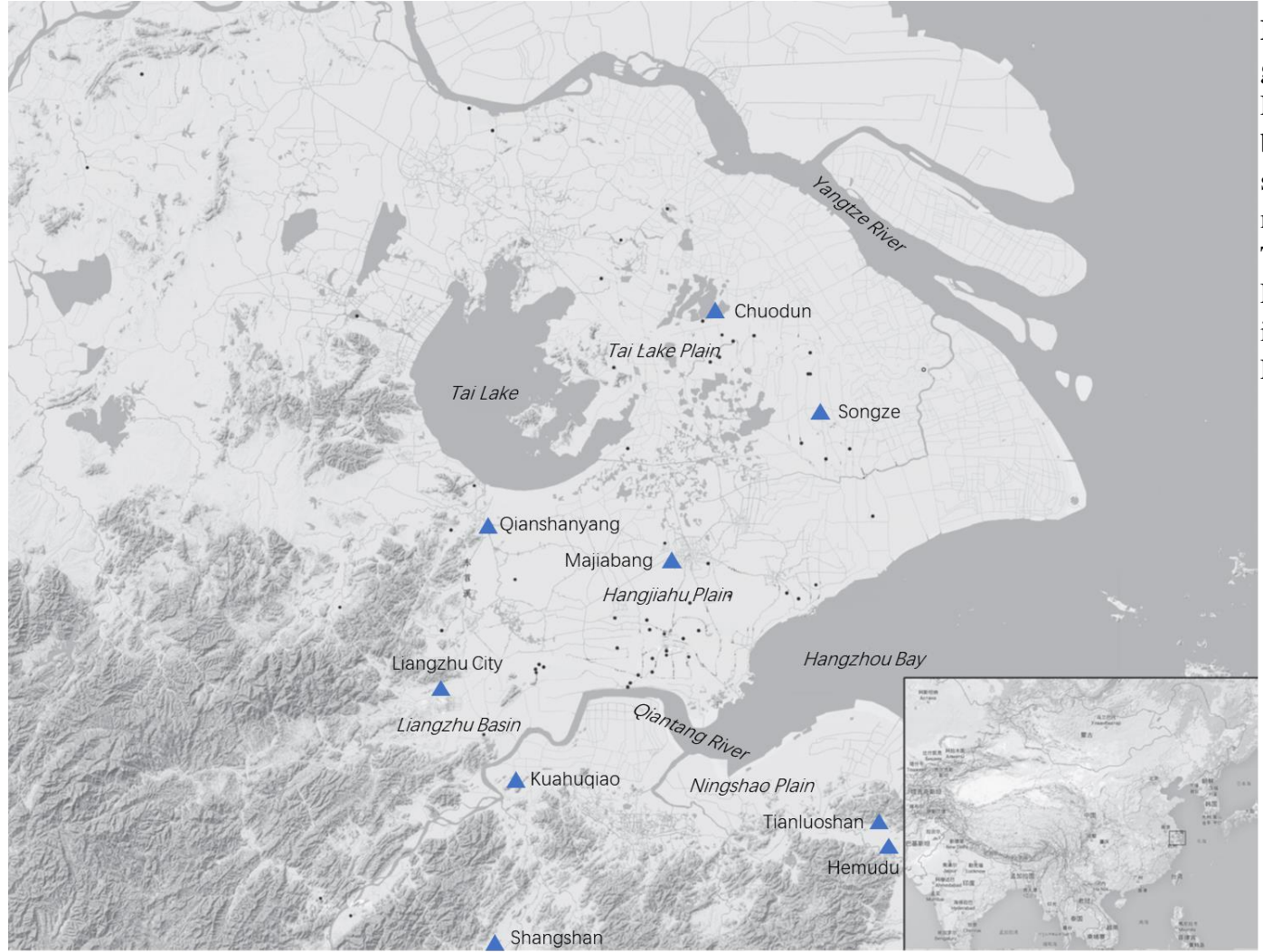


Figure 2.1 The geomorphology of the Lower Yangtze River. The blue triangles refer to the sites and Neolithic Cultures mentioned in this chapter. The black dots refer to Liangzhu period sites found in the region (adapted from Liu *et al.*, 2020)



Figure 2.2 The C-shape Liangzhu Basin and the distribution of Liangzhu sites in the basin (adapted from Liu *et al.*, 2020)

2.3 Liangzhu City site: The Emergence of Early State Society in China in 3000 BC

2.3.1 Introduction: Geographic Settings and Chronology

The Liangzhu City site (E119°56'41"~120°03'28", N30°22'36"~30°26'17") is located in a C-shaped basin (Figure 2.2) at an elevation of about 2 to 5 metres above sea level in the Pingyao and Liangzhu County of Yuhang District, Hangzhou City, China. For the convenience of future discussion, this basin will be referred to as the Liangzhu Basin in this thesis. To the west and north of this basin are the mountains and hills of West Zhejiang. These low mountains were mainly formed by volcanic eruptions during the Mesozoic era (Dong *et al.*, 2019). The major types of outcropping rocks are pyroclastic rocks (rhyolitic tuff, quartz tuff, and andesite), sedimentary rocks (sandstone, conglomerate, and mudstone), and hypabyssal intrusive rocks (ivernite). The terrain of this basin is higher in the west than in the east, with the streams and sediment from the mountains running eastward. East of the Liangzhu Basin is the Hangjiahu Plain, formed by overbank deposition from the Yangtze River. Generally speaking, this basin is relatively isolated with respect to nearby geographical units.

Nowadays, the Liangzhu Basin is densely covered with stream channels with a drainage density of 1.4 km/km² (ZPICRA, 2005b). Among all the streams, the East Tiao River is the largest and most important river in this basin currently flowing in a southwest to northeast direction into Tai Lake. At present, this river flows approximately 100 metres northwest of Liangzhu City at its closest point, although based on historical documents (Wu, 1987) and geographical evidence, the river used to flow south into the Palaeo-Qiantang valley during Neolithic times (Yan, 1987). However, beginning in the Eastern Han Dynasty (AD 25–220), the West Hangzhou Dam was built to protect Hangzhou City from being flooded by the East Tiao River, changing the direction of its course (Jin *et al.*, 2005). The survey from the Nature Museum of Zhejiang Province shows that

no large rivers were nearby at the time Liangzhu City was built in around 3000 BC (Jin *et al.*, 2005).

The earliest Neolithic remains found in the Liangzhu Basin can be dated back to the Majiabang (5100–3900 BC) and Songze (3900–3200 BC) periods, although very few locations have been found so far (Liu, 2019a). This region has been intensively occupied since the Liangzhu period and most sites are concentrated in the northern part of the basin (Figure 2.2). In general, the Liangzhu sites found in this region can be separated into five phases (Qin *et al.*, 2019): the early stage of the Early Liangzhu period (3300–3100 cal. BC), the late stage of the Early Liangzhu period (3100–2850 cal. BC), the early stage of the Late Liangzhu period (2850–2600 cal. BC), the late stage of the Late Liangzhu period (2600–2300 cal. BC) and the Qianshanyang period (2300–2000 cal. BC) – named after a recently discovered culture that succeeded the Liangzhu (Hou, 2016).

2.3.2 The layout and major archaeological findings of the Liangzhu City site

Liangzhu City consisted of dam systems, the city wall, burials, and inner-city and suburban settlements (Liu and Wang, 2014) (Figure 2.3). All of these were found on high ground, either on artificial mounds or natural low hills. In the early stage of the Early Liangzhu period (3300-3100 cal. BC), only a few settlement sites and burials are found in foot of natural low hills. The settlements mainly succeed the Majiabang and Songze period settlements in this area and were clustered around the foot of low hills (Figure 2.2). The major cluster is around the Daxiong Mountains, where near-water settlements (Miaoqian site) and dozens of early Liangzhu burials (Guanjintou site) with various delicate jade artefacts have been found (Zhao 2015; ZPICRA, 2005c). The late stage of the Early Liangzhu period is believed to be the ‘golden age’ of Liangzhu City with the construction of large settlement and/or ritual areas, dam systems and elite burials. In the early stage of the Late Liangzhu period, outer city settlements, such as

the Bianjiashan and Meirendi sites, formed a rectangular rim surrounding the Liangzhu City. The construction of the city wall also began during this stage, and the basic layout of Liangzhu City was completed during or slightly after this stage. During the late stage of the Late Liangzhu period, settlements both inside and outside the city kept expanding, and new settlement sites such as the Shiqianyu site 2km northeast of Liangzhu City have been found. Only a few archaeological remains from the Qianshanyang period have been found inside the city. In the following section, using the city wall as a segregation, the layout of Liangzhu City will be described based on the location inside or outside the city. The dam systems and channel systems of Liangzhu City will be introduced separately.

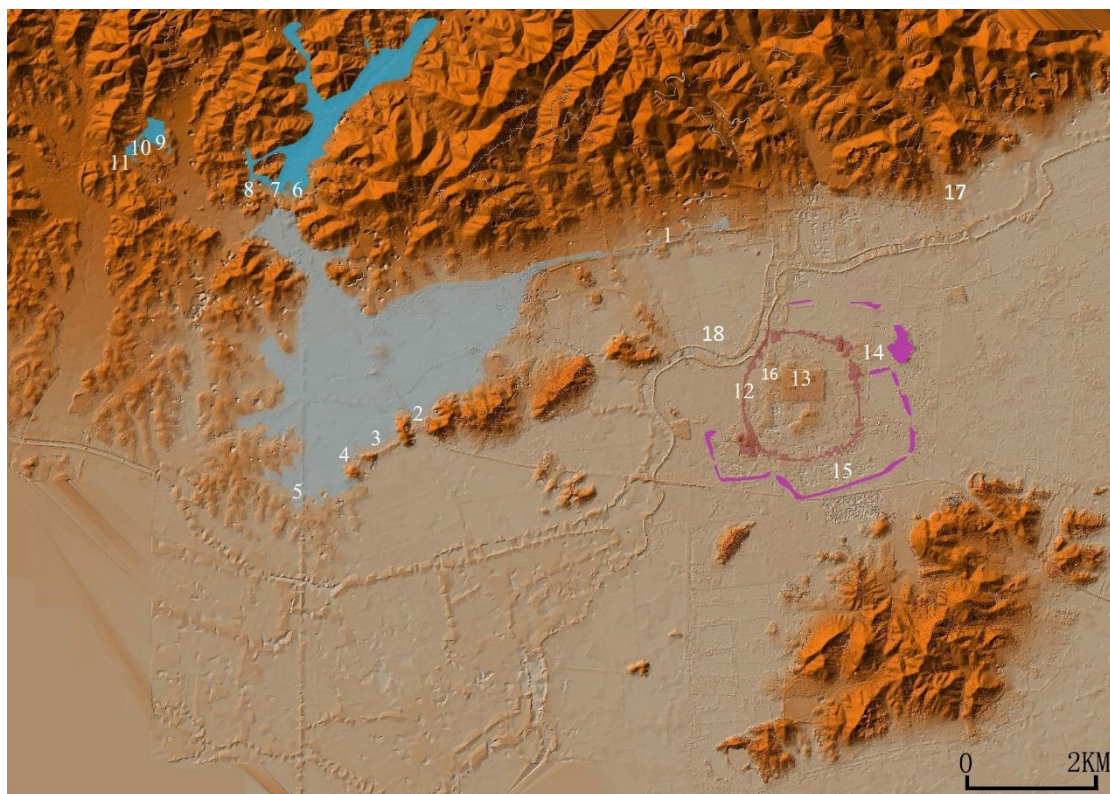


Figure 2.3 Plan of the Liangzhu City: 1 The Tangshan Dam, 2-5 Low dams, 6-11 High dams, 12 Liangzhu City wall, 13 Mojiaoshan mound, 14-15 Outer city settlements, 16 Fanshan cemetery, 17 Yaoshan cemetery, 18 Huiguanshan Cemetery (Courtesy of ZPICRA).

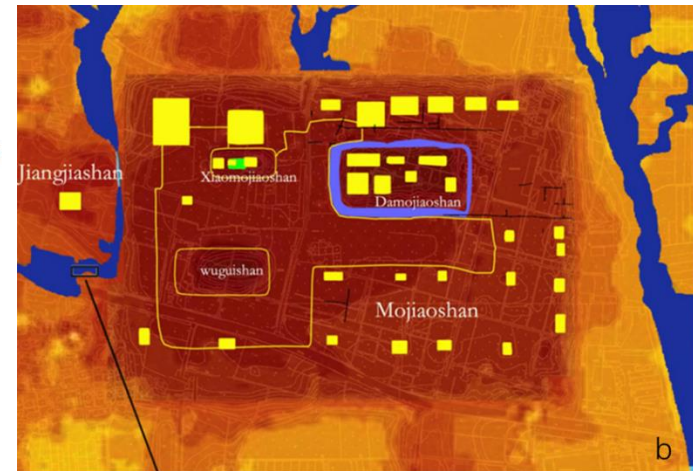
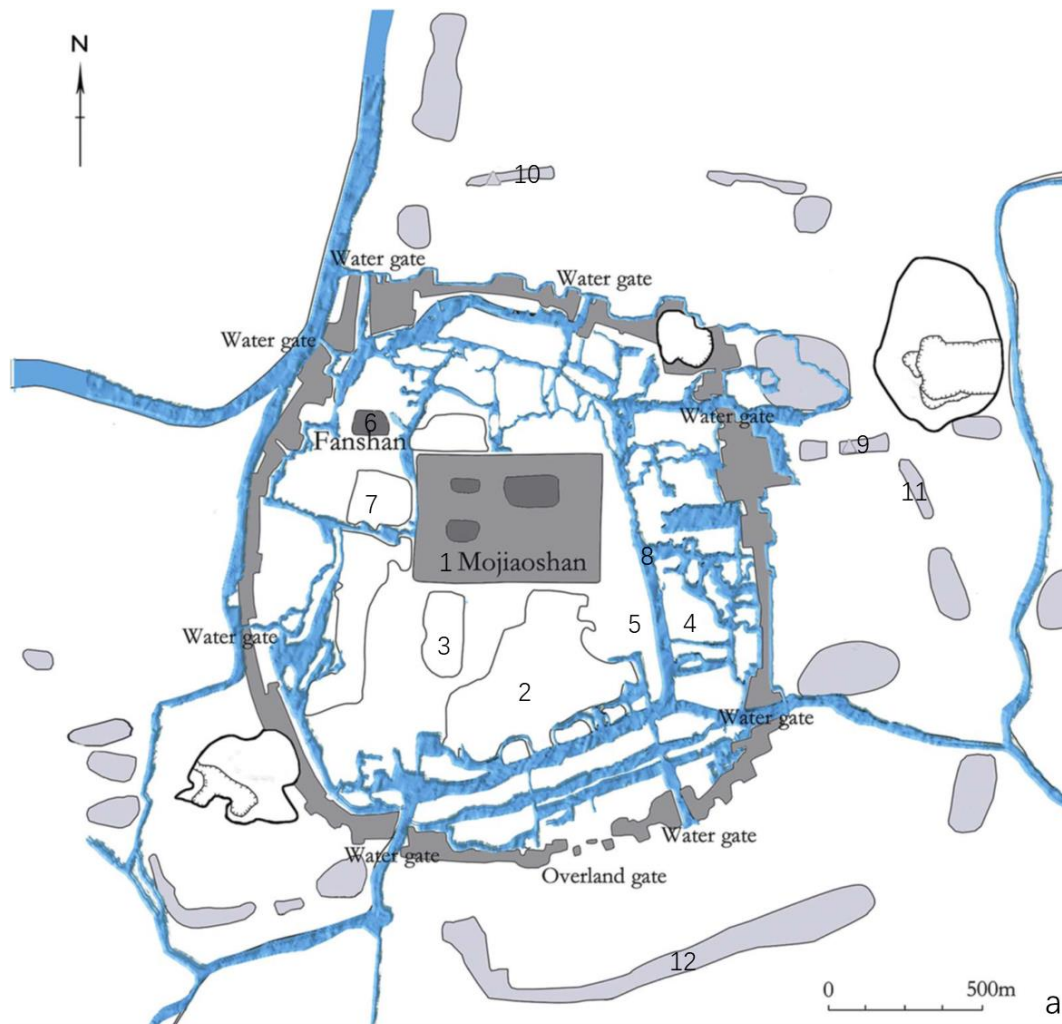


Figure 2.4 Layout and reconstruction of the water systems of the Liangzhu City; **a**: Liangzhu City sites mentioned in this chapter: 1 Mojiaoshan, 2 Huangfenshan, 3 Chizhongsi, 4 Zhongjiacun, 5 Lijiashan, 6 Fanshan, 7 Jiangjiashan, 8 Zhongjiagang Watercourse, 9 Meirendi, 10 Biandanshan, 11 Lishan, 12 Bianjiashan; **b**: DEM and current archaeological findings in the Mojiaoshan Mound. The blue refers to waterways and the yellow rectangle refers to building structures (Courtesy of ZPICRA).

2.3.2.1 Archaeological findings inside Liangzhu City

The inner part of Liangzhu City mainly comprised large settlements and burials in high mounds with channels between these high grounds (Figure 2.4).

The Mojiaoshan mound

In the centre of the city is the Mojiaoshan mound (3000-2840 cal. BC), which is considered the ‘palace’ of Liangzhu City. It is 670m long, 450m wide, 10m high and 29 hectares in size. This 10-m-high mound was mostly man-made, except for the western part, which incorporated the natural topography (Liu and Wang, 2014). Three smaller mounds were found on top of the Mojiaoshan mound. The largest Damojiaoshan mound (Figure 2.4b) is 15m in height, and on which large houses (palaces) and the remains of the biggest building with an area of 947m² have been found (Liu *et al.*, 2019a). Multiple layers of sand and clay paved the rest of the Mojiaoshan mound. The excavator recognized this as a ‘plaza’ and two lines of poorly-preserved house remains were found in this ‘plaza’ (Liu *et al.*, 2019a). On the edge of the Mojiaoshan mound, thick deposits of domestic refuse have repaved and raised the surface three times. Inside these deposits, a 600–700m² storage pit with a huge waste accumulation of rice (between 10,000 and 15,000 kg) has been found (Liu and Wang, 2013).

Other inner-city settlements

South of the Mojiaoshan mound is the Huangfenshan mound that is 24 hectares in size. This mound is believed to be a constructed ‘palace’ area similar to the Mojiaoshan mound but is currently unexcavated. Recently, remains of around 200,000kg of charred rice were found in the Chizhongsì site west of the Huangfenshan mound (Liu *et al.*, 2019a).

Using systematic augering, other mounds to the north and east of the Mojiaoshan mound have also been found, although these mounds are mainly smaller settlement sites or craft areas near channels/ditches (Liu *et al.*, 2019a). Currently, 37 mounds from the Early Liangzhu period have been identified. During the Late Liangzhu period, the occupation area expanded, small mounds merged into larger settlement areas, and 19 mounds were found. Possible jade/stone workshops and lacquer/wood workshops were

also found at the Zhongjiacun and Lijiashan sites, respectively (Liu *et al.*, 2019a).

Elite burials

The Fanshan and Jiangjiashan cemeteries were constructed on high ground and are located to the west of the Mojiashan site (Figure 2.4). The Fanshan cemetery (3300–2900 BC) was discovered in 1986 and contained more than three thousand jades from eleven tombs, making it the richest cemetery of the Liangzhu Culture (ZPICRA, 2005a). Among all the jade items, the *cong* and *yue* with elaborate ‘sacred human and animal’ motifs from Tomb M12 are particularly elaborate (Figure 2.7) (ZPICRA, 2005a). The Jiangjiashan cemetery south of the Fanshan has also been excavated recently, with fourteen burials and 582 pieces of jade artefacts being found. Elite and common people of all ages and genders were buried together in this cemetery. The excavator inferred, therefore, that the Jiangjiashan cemetery could have been a family cemetery (Liu *et al.*, 2019d).

The city wall

Earthen walls with stone foundations resembling city walls were confirmed in 2006–2007 by coring, surveying, excavation, and GIS recording techniques (Liu and Wang, 2016). The wall has a perimeter of about 7.5km and enclosed an area of 300 ha. The best-preserved part of the wall was 4m high and 40-60m wide at its base (Liu and Wang 2013). Like other walled sites in the Middle Yangtze River region, the wall had a wide base and a gentle slope, and so was not believed to have been defensible (Wen, 2011). Some scholars believe, therefore, that the city wall was used for flood prevention (ZPICRA, 2008). Nonetheless, residential remains have been found on top of the city wall (Liu and Wang, 2014) suggesting that the wall may have had multiple functions. Current dating suggests the city wall was inhabited between 2600 and 2300 BC (Qin *et al.*, 2019), but exactly when the city walls were constructed is still controversial, as it is difficult to date the construction material of the walls.

To counteract the swampy land, the wall was bedded by pebbles (Figure 2.6a) and was stacked with pure yellow clay or ‘clay wrapped with grasses’ (a construction material, described in section 2.3.2.3). Trench excavations in the sides of the walls have found a total of 29 ha of stonework, all for making the city walls (Wang *et al.*, 2019; Liu *et al.*,

2019b). A petrological study of these materials shows that the pebbles were derived from the foothills of the nearby mountains and were only transported a short distance (Lv *et al.*, 2015). Interdisciplinary research by Wang *et al.* (2019) revealed that the Liangzhu people may have worked in small groups to collect surface-accessible, hand-carried, 10–35cm stones from diverse sources which weighed around 5kg. These bedded pebbles were distributed continuously except for nine 10m–60m wide notches in the wall, which were identified as the gates of the city. Eight of the notches were identified as water gates because of the presence of ancient water channels discovered by coring. Only one land gate was found. The water gates were distributed two per each wall side with the only land entrance located in the south wall (Liu *et al.*, 2019b) (Figure 2.4).

2.3.2.2 Archaeological findings from the outer Liangzhu City

In 2010, by using GIS techniques together with coring and excavation, a series of residential remains surrounding the city walls, namely the Meirendi, Biandanshan, Lishan and Bianjiashan sites were confirmed as suburbs of Liangzhu City (ZPICRA, 2015a) (Figure 2.4). These remains were all located on 2-3m high, 40-50m wide, rectangular, artificial mounds constructed either on wetland or high ground (Liu *et al.*, 2019c). Elite burials and settlement clusters are also found within five kilometres of Liangzhu City. This section will introduce some of the most well-studied and well-dated sites from outer Liangzhu City.

The suburbs of Liangzhu City

The Bianjiashan site is a 1km long, 20-50m wide artificial mound south of the Liangzhu City. The site was constructed and occupied between 2900 and 2500 cal. BC (Qin *et al.*, 2019). Altogether, 66 commoner tombs were found near the occupation area, which was believed to be a residential area. Abundant human waste and utensils such as shell midden, animal fossils, pottery with elaborate carvings and symbols, exquisite lacquerware and stone artefacts were found. Additionally, and uniquely, a pier with 10m timber trestles as well as three wooden paddles were found, and over 150 timber piles and five rows of bamboo fencing had been constructed to protect the pier (ZPICRA, 2014) (Figure 2.5a). Other rarely seen artefacts were also discovered, such

as an earthen roof model of a Liangzhu period house (Figure 2.5c) and a vessel made from a human skull.



Figure. 2.5 Piers, bank protection materials and a roof model excavated from the suburbs of Liangzhu City; **a**: The pier with 10m timber trestle from the Bianjiashan site; **b**: wooden bank protection structure from the Meirendi site; **c**: earthen roof model from the Bianjiashan site (Photos courtesy of ZPICRA).

The Meirendi site is located east to the Liangzhu City. It is a 270m long, 30-60m wide rectangular mound built and occupied between 2900 and 2500 cal. BC (Qin *et al.*, 2019). This site is believed to have been constructed near and around a 30m wide canal, with the riverbanks protected by a complex wooden structure formed by pieces of wooden sleepers placed in a south-north direction at the bottom, overlain by beams in an east-west direction with standing wooden planks on top (Liu *et al.*, 2017) (Figure 2.5b).

Elite burial and possible ritual areas

The Yaoshan cemetery was found on the western slope of Dazhe Mountain 5km northeast of Liangzhu City, with 13 tombs and more than 2500 jade objects accompanying the burials (ZPICRA, 2003b). The Yaoshan site is 40 x19m in size, and shows a special structure: “Trenches were first dug out and the earth was compacted to form a concentric square structure with a red earthen platform inside, a square of trenches filled with greyish earth in the middle, and a gravel platform on the outside”

(Liu *et al.*, 2019a, 35-36). Tombs were then dug into the centre of these platforms. This earthen structure was believed to have a specific religious meaning and may have been used as a sacrificial place such as an altar (ZPICRA, 2003b). The organic matter at the Yaoshan site did not preserve well, so the dating of the Yaoshan tomb was determined according to the comparison of the typology of the pottery from the Miaoqian tomb that had ¹⁴C-dating data. The Yaoshan cemetery may have dated from approximately 3300 to 3000 BC, which would make it one of the earliest cemeteries of the Liangzhu culture (ZPICRA, 2003b).

The Huiguanshan cemetery was excavated in 1991. This cemetery was built on a natural, small hill 2km west of the Liangzhu City. Four tombs with more than 200 jade objects were found. The date of this cemetery is similar to Fanshan, and it also has ditches filled with grey clay like the Yaoshan cemetery. The excavator proposed that this could also have been an altar based on its similarity with Yaoshan (ZPICRA, 2001).

2.3.2.3 The control and exploitation of water of the Liangzhu City

The control, management and exploitation of water based on local topography is one of the most striking characteristics of Liangzhu City. This section will briefly outline the hydraulic system outside Liangzhu City, the channel systems inside the city walls, and the techniques developed for living near the water.

The hydraulic system

In the outer city, a series of engineering works for controlling the water were confirmed by the survey conducted from 2009 to 2013 (ZPICRA, 2015b). These water control-engineering features consist of high and low dam systems formed by 11 sections of artificial dams and natural hill features (Figure 2.3). Located in the Dazhe Mountain area, the high dam system (3100–2900 cal. BC) was located about 10km northwest of Liangzhu City. These dams were built between low hills, and by connecting these low hills two reservoirs about 25 to 30m and 35 to 40m above sea level were created. The low dam systems (2950–2850 cal. BC) consist of the 6.5km long and 5-8m high Tangshan dam site located at the north side of Liangzhu City, right under the foot of Dazhe Mountain (ZPICRA, 2008), and several smaller dams connecting the low hills

west of Liangzhu City. The middle part of the Tangshan site has parallel dams, which might be a buffer zone for the run-off from the Dazhe Mountain (Liu *et al.*, 2017). Late Liangzhu period burials and a jade workshop have been found on top of the eastern part of the Tangshan dam (Zhao, 2002), which may be supporting evidence for the dating of this site. These findings also indicate that the dam sites might have been multi-functional in Liangzhu times. Together, these dam systems created reservoirs with a total storage volume of c. 50 million cubic metres and occupied an area of 1.24ha (Liu *et al.*, 2017, 2020).

Some of the dams, particularly the lower dams, were built on marshy ground. A special building material, the so-called ‘clay wrapped with grasses’ (Figure 2.6b), was used as sandbags put on top of these swampy lands. Pure yellowish clay was then used as the main construction material for the dams (Liu and Wang, 2013). The normal size of a ‘clay wrapped with grasses’ is oval shaped, with a length of about 40cm and a weight of 4 to 5 kilos (Liu and Wang, 2013). Hundreds of ‘clay wrapped with grasses’ form a big block of ‘sandbags’ about 1m³ large. In a section of the Laohuling dam site, the boundary of different ‘sandbags’ can clearly be seen. Phytolith analysis shows that the grass used to wrap soil was identified as *Triarrhena lutarioriparia var. gracilior* (Chen, 2019). This plant is normally found near rivers, and on wetlands and mudflats. As the flowering and fruiting period of this plant is from September to December, it is believed that Liangzhu people made the clay wrapped with grasses in autumn or winter when the water level was low (Chen, 2019). Recent excavations within the city walls, Southwest Mojiaoshan mound and the Zhongjiagang region show that ‘clay wrapped with grasses’ were also abundantly used as a building material for artificial mounds and to fill in abandoned channels.

It is suggested that these dams were used not only as flood control systems but also acted as channels for shipping in winter, the water supply for Liangzhu City and irrigation for the paddy fields (ZPICRA, 2015b). However, more evidence and modelling is required to test these hypotheses.

The channel system of Liangzhu City

The coring of the entire Liangzhu City site was able to reconstruct the ancient channel system (Figure 2.4a). Moats in both the inner and outer city can be found in three of the four walls. Beside these moats along the walls, 51 canals were found inside Liangzhu City, with the total length of these waterways being more than 30km (Liu *et al.* 2017). These moats, together with the waterways connecting the inner city and the outer dam system, seem to suggest that Liangzhu City was a water city (Liu and Wang, 2013). The Liangzhu people may have utilised the interconnected reservoirs and channels to transport timber, stone or the ‘clay wrapped with grasses’ from nearby mountains to the city.

During 2015 and 2016, Zhejiang Provincial Institute of Cultural Relics and Archaeology (ZPICRA) excavated the Zhongjiagang Watercourse that flowing across the entire Liangzhu City. The watercourse is around 1km long, 18-80m wide and around 3m deep (Liu *et al.*, 2019a). This watercourse is one of the main research profiles of this PhD research, and its detailed stratigraphy will be introduced in Chapters 5 and 6.

Life near water: Raft and bank protection

Liangzhu people employed various techniques to adapt to the low-lying terrain and a dense network of waterways. The construction technique of ‘clay wrapped with grasses’ to provide a dry high ground has already been introduced. The pier and near-bank facility, involving a complex arrangement of wooden piles and planks, is best exemplified at the Bianjiashan and Meirendi sites (section 2.3.2.2). This section will outline some of the other techniques and strategies adopted for waterside living by the Liangzhu people.

Rafts and canoes have not yet been found in and around Liangzhu City but have been found at other Liangzhu sites. For example, a 7.35m long, 0.45m wide canoe that could carry a load of around 300kg was uncovered at the Maoshan site, and a 2.8m long, 0.6m wide bamboo raft was found at the Nanhu site (Wang, 2019).

Several types of bank-protection material were found in the Liangzhu City area including bamboo weaving material, wooden piles, combinations of bamboo weaving and wooden piles, and rows of planks – best exemplified at the Meirendi site (section

2.3.2.2) and the Middle Zhongjiagang area (Figure 2.6c). The excavation of the Lijiashan mound located on the western bank of the Zhongjiagang Watercourse revealed a well-preserved bank-protection material made with a combination of bamboo weaving and wooden piles (Figure 2.6d). The bamboo material was interwoven with 1–2.5 cm wide bamboo splits, forming long strips 50–90 cm wide. This woven bamboo was then hammered into the ground and clung to the bank, then timber piles were knocked in outside the bamboo at intervals of 30–40cm (Liu *et al.*, 2019a). Similar bank protection materials are widely seen along the Zhongjiagang Watercourse and at other Liangzhu near-bank settlements.



Figure 2.6 Construction materials and bank protection facilities found in Liangzhu City; **a**: bedded stones from the West City Wall site; **b**: a single unit of ‘clay wrapped with grasses’; **c**: wooden bank protection facility from Middle Zhongjiagang site; **d**: bank protection material made by the combination of bamboo weaving and wooden piles from Lijiashan site (Photos courtesy of ZPICRA).

2.3.3 Subsistence of Liangzhu City

2.3.3.1 Rice cultivation

The subsistence activities of the Liangzhu people relied largely on rice production and animal domestication (Wang, 2014). The examination of charred rice from the

Mojiaoshan site (Lian, 2015) shows that most of the rice was domesticated rice, *i.e.*, the *Oryza sativa Subsp. Japonica Temperate japonica group (syn. sinica)*, the Chinese *Jing*. Wild rice was also managed and harvested by Liangzhu farmers. A possible yield-optimizing harvesting strategy of the Liangzhu was proposed where the rice was harvested just before reaching maturity. The rice was then threshed, winnowed, and sieved in a clean state before storage. There is evidence of communal organization for the processing of rice; however, no rice paddy fields have currently been found in or near Liangzhu City. The nearest paddy fields were found at Maoshan about 30 km east of the city, where fire was widely used to increase soil nutrients and reduce weed cover. Intensive ploughing, deliberate fertilization and soil amendment have also been practised in rice cultivation. Higher levels of water management together with labour investment and technology innovations occurred on the Maoshan paddy fields (Zhuang, 2014). During the late Liangzhu period, the rice yield from the Maoshan paddy fields rose to 141kg/mu (=0.0667 hectares), which was very close to the yield of the Han dynasty (150-180kg/mu) two thousand years later (Zheng *et al.*, 2014).

2.3.3.2 *The diet of the Liangzhu*

A wide range of plant seeds and animal fossils were uncovered from Liangzhu City sites, which provide a general overview of the food structure of the Liangzhu people.

Most of the animal fossils found were subtropical mammals. The pig (*Sus scrofa* and *Sus scrofa domesticus*) was the most abundant animal fossil found in Liangzhu City, followed by deer (*Cervidae sp.*). Trace amounts of fossils from carnivores and primates, such as tigers and monkey, were also found. The large number of pigs and dogs found probably indicates that they were domesticated and also indicated a gradual development of pig breeding and a reduction in hunting activity (Wang, 2014). Less than 1% of the animal assemblages were birds, mainly those which resided near lake and wetland areas such as *Abster sp.*, *Cygnus sp.*, *Anas sp.* etc. A few freshwater reptile bones were also found, including carapaces from *Rafetus swinhoei*, which is one of the largest testudines on earth and is currently extinct in China. Most aquatic animals found were freshwater fish and molluscs. The only marine animal residues were a few shark teeth, which may have been exchanged or brought from another place (Matsui *et al.*,

2016; Song, 2019).

A variety of fruit seeds were found in Liangzhu City, including *Choerospondias axillaris*, *Amygdalus persica*, *Armeniaca mume*, *Armeniaca vulgaris*, *Prunus salicina*, *Vitis vinifera*, *Diospyros kaki* and *Cucumis melo*. Some of the fruit seeds show evidence of artificial selection and domestication, such as *Amygdalus persica*, *Cucumis melo* and *Lagenaria siceraria*. Only a few starch grains other than rice were found in Liangzhu City, which is suggestive of the reduced exploitation of wild staple food compared to the previous Hemudu Culture (Wu, 2019; Zheng *et al.*, 2019).

In summary, the Liangzhu people principally used domesticated pigs and rice as their main sources of food, and in the meantime acquired various wildlife as supplementary food sources. The fauna found mainly inhabit a freshwater wetland/lake environment, with a few forest animals also represented.

2.3.4 The social complexity of Liangzhu City

Some researchers have suggested that the Liangzhu Culture is the earliest early state society in East Asia (Renfrew and Liu, 2018). As the centre of the Liangzhu Culture, the complexity of Liangzhu City embodies the following four aspects.

City and landscape planning

As mentioned earlier, Liangzhu City has a clear layout, with the elite burials and ‘palace’ area in the centre and surrounded by encircled city walls and outer city settlements. From the centre to the rim the artificially built mounds decrease in height, which may imply a distinction in status (Liu *et al.*, 2020). Although these structures were constructed at several points that span more than 600 years (Qin *et al.*, 2019), they still reflect meticulous urban planning and possible central organisation. Additionally, the control and exploitation of water is conceptualised from the very beginning of the city planning, as indicated by the peripheral hydraulic system and channel systems inside Liangzhu City. These large-scale engineering features show that the Liangzhu people were adept at transforming and exploiting their local landscape.

Population and labour organization

With the development of rice cultivation, the Liangzhu population grew rapidly (Qin, 2013), which provided a solid foundation for the heavy construction of Liangzhu City. The current estimation is that around 22,900–34,350 people would have lived in the Liangzhu city region (Wang, 2019). According to Wang (2019), a total of 10 million m³ of soil and 100,000 m³ of stone was transported and used to build the Liangzhu city site and its dams. It may have taken 10,000 workers to continuously work for a minimum of seven to eight years to dig out, transport and build the mounds, which was an astonishingly large-scale construction task that would have needed a large labour force and time investment as well as effective social organization to accomplish.

Social stratification and craft specialization

Liangzhu society was highly stratified, which was reflected in the strict traditions of jade and pottery use found in the cemeteries (Qin, 2013). The richest tomb in Liangzhu City, the M12 in Fanshan, had more than 500 jade artefacts while the commoners' cemeteries often had no jade artefacts, with only pottery vessels buried with the dead. The different standard of burial goods indicative of different places in the hierarchy is a unified ideological feature of the whole of Liangzhu society (Song, 2008). Additionally, in the settlements occupied by the commoners on the outskirts of Liangzhu City, the living quarters were not separated from the burial areas. However, in the higher-ranking settlements inside Liangzhu City, specialized, artificially raised areas were built for the elite cemeteries (Fang, 2015). Throughout the whole Liangzhu city region, at least three tiers of settlements based on their scale have been identified (Chen, 2019; Wang, 2019).

There is also evidence of craftsmanship specialization, as jade, stone and wood workshops were found along the Tangshan Dam and the Zhongjiagang Watercourse inside Liangzhu City (Liu *et al.*, 2019a; Qin, 2013). Diverse forms of sophisticated fine crafts (Figure 2.7) were created under this specialization, with the jade craftsmanship being some of the most elaborate – unparalleled among the Neolithic jade cultures of China (Qin 2013; Rawson, 1995). Based on a study of jade workshops, Qin (2019) has revealed the labour divisions for both the production of different types of jade objects and the different stages of the production process.

Rituals and early writing systems

The belief system of Liangzhu City is mostly represented in the ‘sacred human and animal’ motif (Figure 2.7b). Variations or abbreviations on this motif have been seen in various jade artefacts from both Fanshan and other elite burials outside Liangzhu City, but all are highly consistent. This motif was believed to represent a deity/shaman or to represent the corporate community of the Liangzhu social unit (Renfrew and Liu, 2018). Additionally, evidence of altars and ritual activities such as human sacrifices has also been found, with most of the sacrifices believed to have been made for male elites (Zhao, 2001). Although a mature writing system was lacking in Liangzhu City, inscriptions on pottery suggest that possibly some forms of meaningful sentences were found and were believed to be an early form of ancient Chinese characters (Wang, 2013).

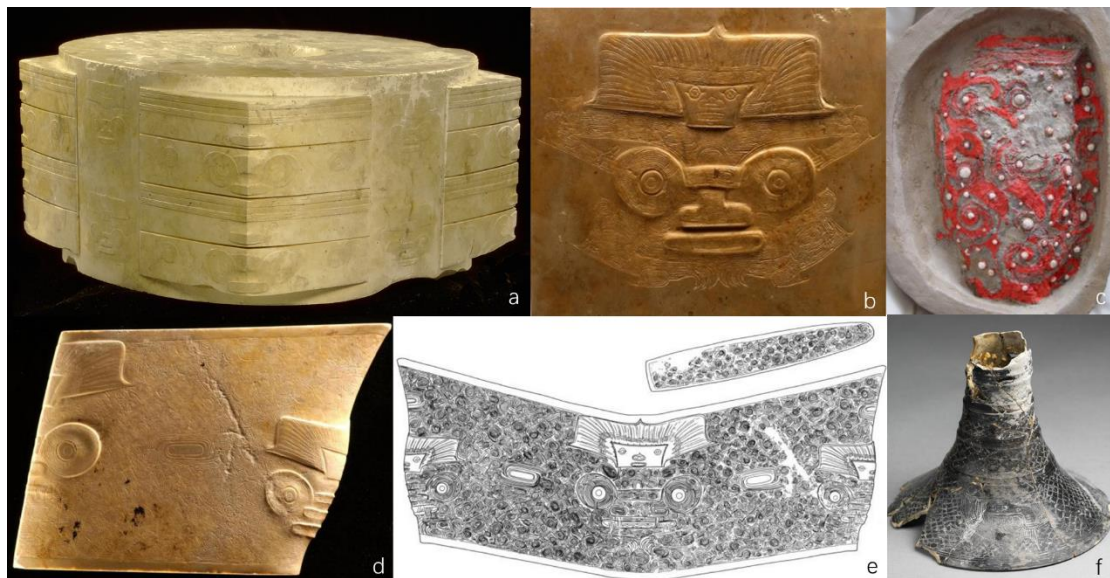


Figure 2.7 Exquisite artefacts found in Liangzhu City; **a**: jade *cong* from Fanshan M12 cemetery, 18cm in width, 8.9cm in height; **b**: enlargement of the ‘sacred human and animal’ motif from the jade *cong*; **c**: lacquerware inlaid with jade beads from Fanshan M12; **d**: jade *mao* (head of a sceptre) from Fanshan M12; **e**: detail of engravings on the jade *mao*; **f**: black pottery with delicate engravings from west City Wall (Photos courtesy of ZPICRA).

2.3.5 The decline of the Liangzhu

Despite being prosperous, Liangzhu City and its nearby settlement sites were abandoned around 2200 BC. This was the prelude to the collapse of the entire Liangzhu Culture. The subsequent late Neolithic cultures, the Qianshanyang (2400–2200 BC), Guangfulin (2200–1900 BC) and Maqiao (1900–1200 BC), show a clear decline in

social complexity and settlement scale (Shanghai, 2002a, 2002b; ZPICRA and Huzhou, 2014). Exactly how and why the Liangzhu collapsed is the subject of heated debate (Zhou and Zheng, 2000). Both environmental and cultural causes have long been argued about and among all the factors, hydrological changes (Long *et al.*, 2014; Wu *et al.*, 2014), unsustainable development of their theocratic society (Fu, 2008) and military defeats (He, 2002) have been regarded as the main reasons for the abandonment of the Liangzhu settlements. However, current archaeological evidence is neither sufficient nor valid enough to fully support the social collapse and foreign invasion hypothesis. In addition, recent sedimentological analysis does not support the assumption that a flash flood or a single marine flood had destroyed the entire City (Zong *et al.*, 2011). It will take further research to fully understand the causes and mechanisms that had led to the demise of Liangzhu.

2.4 The environmental and sedimentation history of the Liangzhu City site

In recent years, dozens of sedimentary cores have been studied around the Tai Lake and Hangzhou Bay area using particle size analysis, foraminifera, diatoms, pollen, environmental-magnetism properties, carbon, and nitrogen stable isotopes and AMS ^{14}C dating methods (Chen, 2017; Chen *et al.*, 2018; Liu *et al.*, 2018; Ma, 2012; Wang *et al.*, 2012 etc.). The results all showed that the sedimentation and hydrological conditions in the region had been strongly influenced by fluctuations in climate and sea-level since the LGM, which happened in southern China around 9100–8300 BC (Huang *et al.*, 2002). This section will highlight the current research progress of the pre-site, Liangzhu period and the post-Liangzhu sedimentation history in the Liangzhu Basin, along with the major climate fluctuation events influencing Liangzhu City, and relevant studies regarding soil properties and sources of soil/sediment in this region.

2.4.1 Sedimentation history of the Liangzhu Basin and southern Yangtze Delta

2.4.1.1 Basal geomorphology of the southern Yangtze Delta

By detailed studying of sediment cores from the southern Yangtze Delta, Wang *et al.* (2012) drew the Holocene isopach map of the southern Yangtze delta (Figure 2.8).

Three major terraces were identified. Terrace 1, located on the eastern edge of the delta, is later covered by 20-30m of Holocene sediments. Terrace 2, covered by 5-15m of sediments, is located in the northeast and southwest. Terrace 3 is covered by less than 5m of Holocene sediments. A 15-20m deep palaeo-incised valley that opens to the palaeo-Qiantang valley, the so-called Palaeo-Taihu valley, is identified near the foot of western mountainous area.

According to the study of sediment cores, the basement material underlying the Holocene sequence is either a palaeosol ('stiff mud') formed during the LGM (Chen *et al.*, 2008; Wang *et al.*, 2012) or gravelly sand fill in palaeo-incised river channels (Wang *et al.*, 2012). In the Early Holocene, the East China Sea experienced a rapid rising of sea level from 130-150m below sea level to 5m below present-day sea level (Xu *et al.*, 1997). The sedimentation process in this region is dominated by transgressive sediments, with minimal influence from the Yangtze and Qiantang rivers as the sediment carried by these rivers was mostly trapped at the apex of the river mouth, which was around 200 km west of the current shoreline (Hori *et al.*, 2001; Wang *et al.*, 2012). The early Holocene sequence deposited on Terrace 1 from around 8000-6000 cal. BC is a clayey silt from a tidal flat environment, successively overlain by soft shallow-marine muds and subtidal and intertidal silts (Zhao *et al.*, 2008; Wang *et al.*, 2012). The deposition in Terrace 2 starts from 6750-6650 cal. BC and is dominated by thick homogeneous muds of marsh and muddy tidal flat, followed by laminated subtidal and intertidal silts, and topped by brownish gray lacustrine clayey silt. In Terrace 3, the palaeosol was covered by brackish water marsh deposits from 5290 cal. BC (Wang *et al.*, 2012). Since 4000 cal. BC, as the sea-level stabilized, progradation of the Yangtze delta dominated the sedimentation progress, and the south Yangtze Delta gradually changed to a freshwater floodplain (Hori *et al.*, 2002; Wang *et al.*, 2012), providing suitable environment for large-scale human inhabitation in the delta.

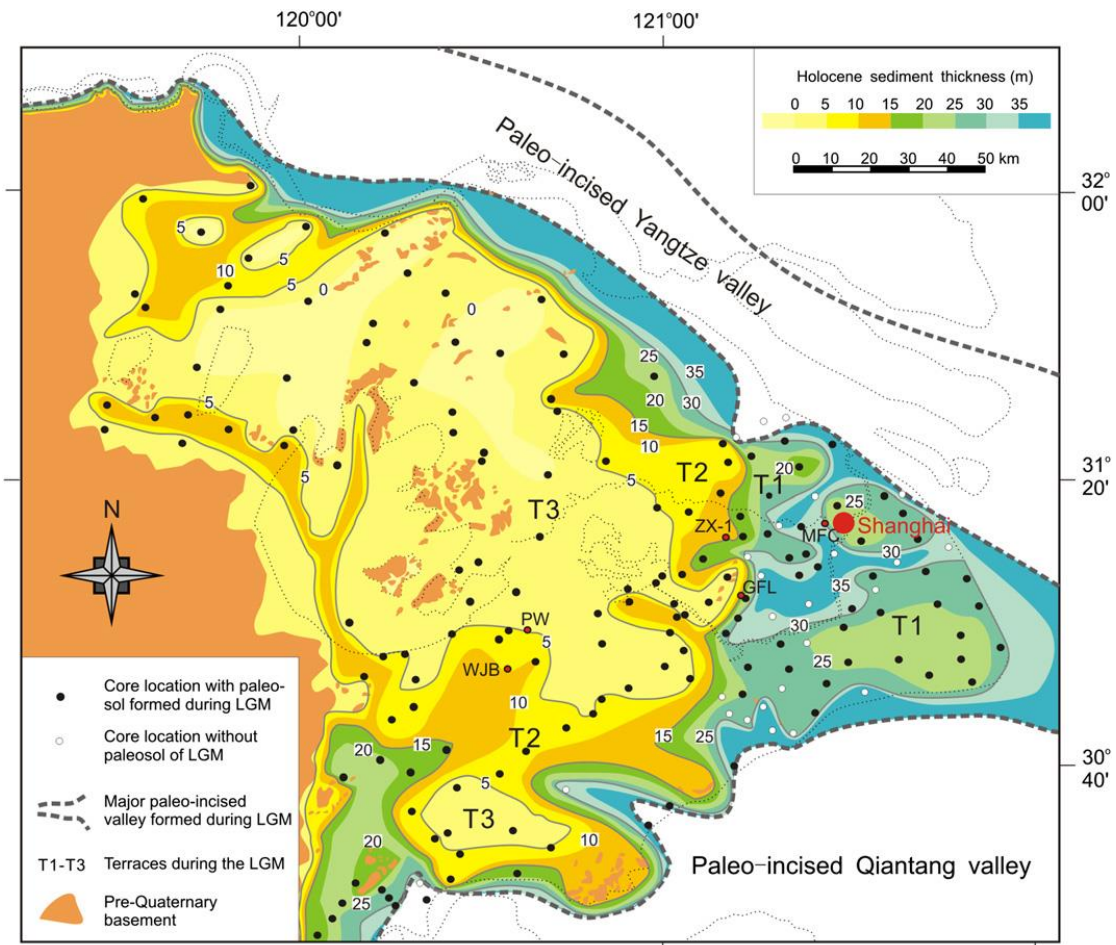


Figure 2.8 Palaeo-topography of the southern Yangtze delta plain and major incised valleys of the Yangtze and Qiantang rivers (Adapted from Wang *et al.*, 2012).

2.4.1.2 Sedimentation history of the Liangzhu Basin during the early Holocene

The Liangzhu Basin, located on the southwestern corner of the south Yangtze Delta, contains Holocene sequences with c. 20-25m thick tidal-influenced sediment, similar to Terrace 1 of the delta. To be specific, the palaeosol of the Liangzhu Basin is a grayish condensed mud interlayered with brownish clayey silt, formed due to strong pedogenesis during the LGM (Liu *et al.*, 2018; Qin *et al.*, 2008; Wang *et al.*, 2012). In the Holocene before 7000 cal. BC, the sediments in the Liangzhu region are yellowish clayey silts formed in a tidal-flat-channel complex. From 7000 cal. BC, the Basin was occupied by greyish silt and clay formed by a tributary channel with intense tidal influence. From 6500 to 5500 cal. BC, this region changes to a deep-water, high-salinity estuary environment with grey silty clay and laminations of sand-mud. A very high sedimentation rate (up to 2 cm yr⁻¹) has been identified and more than 14m of deposits aggraded within a thousand years (Chen *et al.*, 2018). Since 5500 cal. BC, the

sedimentation environment changes from sub-tidal to intertidal flat facies, with the sediments dominated by greyish clayey silt with fine silt laminations. Between 5000 and 4500 cal. BC, seawater penetration occurred again, and saltmarsh developed. Since 4500 cal. BC, persistent freshwater marsh formed due to seawater retreat and a strong Yangtze freshwater discharge (Chen *et al.*, 2018; Liu *et al.*, 2018).

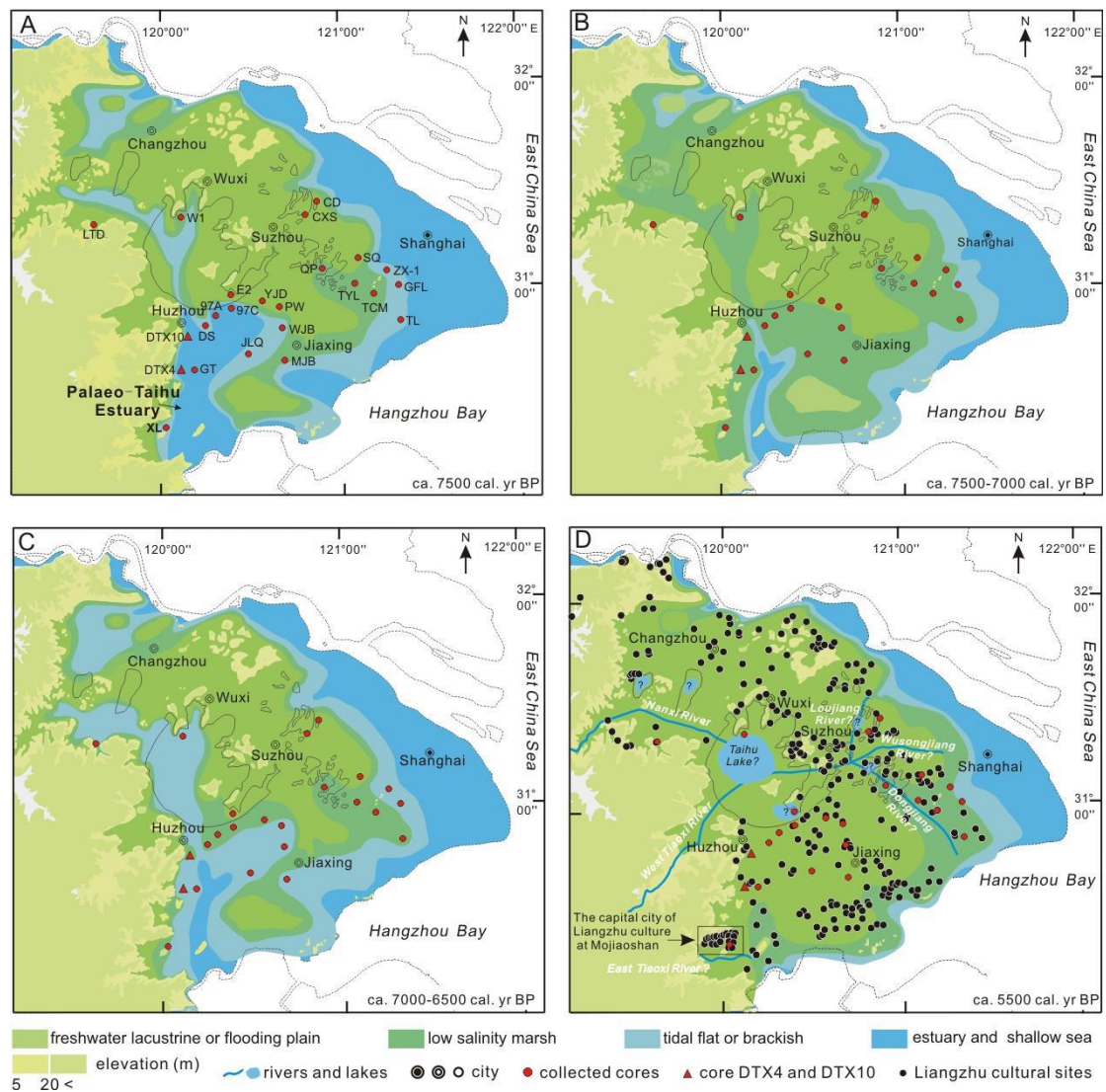


Figure. 2.9 Palaeogeographic map of the Tai Lake Plain since 5500 cal. BC (adapted from Chen *et al.*, 2018).

The geomorphology of the Palaeo-Taihu valley would also have had a significant influence on the development of Neolithic cultures in the Liangzhu Basin. When sea level rose from -18 to -4 m between 6600 cal. BC and 5300 cal. BC, the southern part of the Palaeo-Taihu valley became an estuary, allowing sea water from Hangzhou Bay to reach the central Taihu Plain (Hong, 1991; Wang *et al.*, 2012). This estuary continued

to exist in the Majiabang (5000–4000 cal. BC) and Songze (4000–3000 cal. BC) periods, and became a natural barrier for Neolithic people being able to live in the Liangzhu Basin (Figure 2.9) (Chen *et al.*, 2018; Liu *et al.*, 2018). After 3600 cal. BC, a dramatic shrinkage/closure of the Palaeo-Taihu Estuary occurred when the sea level was relatively stable. Only after this stage did Neolithic people enter and reside in the Liangzhu Basin.

2.4.1.3 Sedimentation during Liangzhu time

Since 3000 cal. BC onwards, the sea level was relatively stable with minor fluctuations (Chen & Stanley, 1998; Song *et al.*, 2013; Zong, 2004). In most of the natural profiles sampled in the Liangzhu Basin and southern Yangtze Delta, there is a hiatus between around 2350 cal. BC and 3600 to 5500 cal. BC, and a sharp sediment contact is observed (Chen *et al.*, 2018; Liu *et al.*, 2018). This depositional hiatus may form due to nondeposition and/or erosion and/or removal of sediment materials in the region (Wheeler, 1958). Further study should be conducted to understand the source of these sediments in Liangzhu cultural layers.

2.4.1.4 The demise of Liangzhu

Current research on microfossils shows that large scale marine flooding may not have been responsible for the abandonment of this region since 2000 cal. BC (Zong *et al.*, 2011). But it is interesting that clear evidence of storm surges and marine intrusion have been identified in the archaeological sites located on the southern bank of the Qiantang River in 4300 cal. BC and 2500 cal. BC (Tang *et al.*, 2019; Wang *et al.*, 2018). But the range of these extreme events, especially the storm surges in 2500 cal. BC, and their impacts on Liangzhu City site are currently unclear and require further study.

In the Liangzhu Basin and even the whole Tai Lake region, Liangzhu sediments were directly covered by an around one metre thick light yellowish clayey deposits. These were long considered to be related to massive flooding in the region and caused the collapse of the Liangzhu Culture (Zhang, 1998; Liu, 2019). However, recent dating shows that the date of this horizon is after 2000 cal. BC (Qin, 2019; Li, 2013), which

implies that it may not have directly caused the demise of Liangzhu. However, in order to better understand the change and correlation between climatic, geomorphological, and hydrological conditions of this region over a larger timescale, it is still necessary to study the genesis of this horizon in detail.

Current research using particle size, clay minerals, magnetic measurements and geochemistry indicates that this layer is a poorly sorted overbank deposit formed under low-energy hydrodynamics (Li, 2013; Song, 2012). Multiple magnetic minerals have contributed to the magnetic susceptibility of the layer, therefore suggest multi-flooding events instead of one (Li, 2013). The particle size gets coarser from the west to the east of the Liangzhu Basin and the yellow silty clay in the east contains chlorite and shows a similar Mg/Mn ratio with the sediment from the Yangtze River, which implies the influence of seawater in the east (Song, 2012). The comparison of the Sr-Nd isotopic compositions around the Liangzhu Basin demonstrated that this silty layer is a mixture of sediments from the East China Sea and the Qiantang River (Ji, 2016). Current evidence suggests that this layer is not formed by flash flooding or marine intrusion but is more relevant to impeded drainage in the region possibly due to a change in geomorphology near the estuary, creating a tidal backwater and retrogressive accumulation of the river system (Ji, 2016; Li, 2013; Song, 2012).

After 2000 cal. BC when this yellow silty clay horizon formed, the quiescence of human activity around the Tai Lake continued for more than a thousand years. Although Liangzhu was not directly destroyed by this event, its demise may be related to this regional trend of impeded drainage and silting-up processes that lead to a higher flood risk. Further studies are required to better understand how Liangzhu people responded to these changing hydrological conditions.

2.4.2 History of climate change since the LGM in the Liangzhu Basin

Research shows that since the LGM, the area became progressively warmer and wetter, reaching a peak at around 6000–3700 cal. BC, the so-called Holocene Climatic Optimum, and from 3700–3500 cal. BC onwards, the climate became progressively cooler and drier (Cheng, 2016; Lu, 2014; Zhang, 2017). Some scholars have proposed

that climate anomalies around 3500 cal. BC, namely the 5.5ka BP event, influenced the emergence of complex society in the Tai Lake region and other areas of China (Goldsmith *et al.*, 2017; Wang, 2019; Wu *et al.*, 2018). However, this cooling event does not appear to have influenced on the pollen data around Tai Lake (Li, 2014). How this cooling event may have had an impacts on the emergence of Liangzhu is currently unclear, and consequently further study is required to better understand its mechanism.

Based on detailed pollen, foraminifera, and particle size analyses around the Liangzhu Basin, small climate fluctuations over a centennial timescale were reconstructed from 3300 to 2000 cal. BC. In 3300 cal. BC, the climate was warm, the vegetation was dominated by evergreen and deciduous broadleaved mixed forests, and foraminifera characteristic of living in interactive marine and terrestrial deposits were present (Jin *et al.*, 2005; Liu *et al.*, 2014; Mo *et al.*, 2019; Wang *et al.*, 2017). In 3000 cal. BC, the warm period reached its peak with the temperature 1-2°C higher than at present. Foraminifera disappeared and littoral lacustrine sediments were indicated (Jin *et al.*, 2005). Around 2900 cal. BC, cooler and drier conditions were reflected in the pollen data from the Liangzhu Basin and the wider Lower Yangtze River region (Innes *et al.*, 2014; Wang *et al.*, 2017; Yi *et al.*, 2003, 2006) before the climate soon became slightly warmer and wetter from 2800 to 2500 cal. BC (Wang *et al.*, 2017). From 2500 to 2100 cal. BC, drier and cooler climate conditions with a concurrent reduction in rice cultivation were identified in the pollen profiles from Liangzhu City and the Maoshan site 20km east of Liangzhu City (Jin *et al.*, 2019; Wang *et al.*, 2017). From 2200 to 2000 cal. BC, the temperature of this region was 1°C to 2°C lower than at present, ferns flourished, and deciduous broadleaved forest became the dominant vegetation (Jin *et al.*, 2005). The weakening of the East Asian monsoon and continuous drying for 100–200 years is also reflected in the oxygen and carbon isotope data obtained from the analysis of stalagmites in Songya Cave, Zhejiang Province (Cui, 2019).

In general, Liangzhu City developed under a general trend of a colder and drier climate conditions starting from 3700–3500 cal. BC and was then affected by climate fluctuations with two major cooling events in 2900 and 2500 cal. BC.

2.4.3 Complexity of regional hydrological and sedimentation processes in the Liangzhu Basin

Due to the low elevation and the closeness to the coastline, the Liangzhu Basin is sensitive to eustatic, climatic and geomorphological changes in the Holocene. These factors may collectively or separately influence the hydrological conditions in this region and different stages may have different dominant factors. In addition, to what extent Liangzhu people managed and controlled their local water regime is not fully understood yet. Studies of what caused the change of hydrology, the scales and intensities of changes, and whether it was natural or human-induced are thus complicated and require detailed and thorough study of sedimentological, climatic, geomorphological and archaeological evidence.

Moreover, the sediment transport process in the Liangzhu Basin is highly complicated due to the frequent water and sediment exchange with the Qiantang estuary. Pre-site sediments in the Liangzhu Basin are mainly transgressive sediments from the southern Hangzhou Bay area (see discussion in 2.4.1), and provenance studies using geochemistry methods (Ji, 2016) also suggest that, instead of western mountainous areas, the cultural layers and post-Liangzhu yellow silty clay layer are mostly related to Qiantang, Yangtze, and East China Sea sediments. What is more, a significant amount of water and sediment were transferred into Hangzhou Bay, especially into the northern part, by the Yangtze River plume (Su, 1989; Du *et al.*, 2010; Fan *et al.*, 2012), which further complicated the situation. In the meantime, reworked old carbon from the Yangtze River caused by sediment storage and reworking along the dispersal path between headlands and the coasts (Chen & Stanley, 2000; Wang *et al.*, 2012) were then transported into the Hangzhou Bay area, and then into the Liangzhu Basin, which caused disruption to the radiocarbon dating of the sediment sequences.

These complexity in regional hydrological and sedimentation processes have caused difficulties and debates in the study of the formation, development and especially the causes of demise of Liangzhu Culture (Long *et al.*, 2014; Wu *et al.*, 2014 etc.). Therefore, new evidence should be sought, detailed study should be conducted on

sediment sequences of the Liangzhu Basin, especially during and post-Liangzhu period.

2.5 Characteristics of marine and freshwater sediment

Based on studies on sediment cores (Chen *et al.*, 2018; Wang *et al.*, 2018 etc.), the Liangzhu Basin has changed from an intertidal flat to an alluvial floodplain in around 4500 cal. BC. It is therefore worth and necessary to discuss the criteria for differentiating marine and freshwater sedimentation processes before the detailed analysis of the thin sections in the following chapters.

In general, newly formed estuarine salt marsh is dominated by well-laminated, well-sorted alternating humic clay and coarse silt to very fine sand size laminae. The coarse silt laminae are composed of quartz, calcite, fossil fragments and mica, with iron-impregnation of relict organic material (Macphail & Goldberg, 2017). Horizontally oriented detrital organic matter, often showing browning and iron-staining with occasional sodium carbonate impregnation are also found (Macphail & Goldberg, 2017). The pH value is generally slightly alkaline, ranging from 7.2 to 9.2 in the Yangtze estuarine and other salt marsh deposits around the world (Baumann *et al.*, 2015; Macphail & Goldberg, 2017; Yu *et al.*, 2018 etc.).

Whether Liangzhu City is influenced by seawater penetration or large-scale inundation of freshwater is still under heated debate. Therefore, it is also worth discussing the impact of the mutual transformation of freshwater and saline water conditions on soil/sediment/archaeological sites using some well documented case studies from Britain.

The marine inundation experiment in Wallasea (Boorman *et al.*, 2002; Macphail, 2009; Macphail *et al.*, 2010) provides an excellent analogue with which to understand the micromorphology and bulk sedimentology characteristics of agricultural soils formed based on reclaimed marine sediments. In Profile 1 at Wallasea, there was a change from salt marsh to arable land with the B horizon showing a massive and coarsely prismatic microstructure, and a composition of very coarse silt and clayey sediment with abundant textural pedofeatures. It is interesting that this sediment shows scarce molluscs,

macrofossils, poorly preserved foraminifera, low loss-on-ignition, low saltiness and specific conductance, which all suggest loss of diagnostic features of marine inundation during the reclamation (Macphail & Goldberg, 2017).

In terms of freshwater inundation, the Three Ways Wharf site was inundated by freshwater forming a 5-10cm clay layer, typified by the downwash of clay and amorphous sesquioxides forming clay void coatings and mottles in the lower layers (Macphail & Goldberg, 2017). The Thames valley that changed from a freshwater to river estuarine environment was marked by the inwash of calcitic silt into and over the peat layer (Macphail & Crowther, 2013). With respect of the change from mudflat sediment to freshwater inundation, the Boxgrove profile (Macphail & Goldberg, 2017) showed a coarse and fine bedded, fine laminated calcareous clay loams in the lower part of the profile (Unit 4b), with few bio-working and organic matter replaced by sesquioxides. These estuarine mudflat sediments were incompletely ripened and weathered into a soil (Unit 4c), with patches of calcitic sediment with relict laminae found (Unit 4c-1). The freshwater inundation layer on top (Unit 5a) shows non-calcareous clay and finely laminated, dusty clay void coatings.

In summary, these cases studies provide criteria for differentiating marine and terrestrial sedimentation processes and promoting the understanding of the mutual transformation between different hydrological regimes, which may serve as analogues with which to interpret the change of hydrological regimes in the Liangzhu profiles.

2.6 Unsolved research questions

Although archaeological excavations and research have revealed the general layout and features of Liangzhu City and quite a few studies have been conducted on the sedimentation history of the Liangzhu Basin, many questions remained unsolved. For example, what triggered the emergence of complex society in this region? Why did Liangzhu people select this particular area as their regional centre? Research by geologists focused on the natural sediments before and after Liangzhu, but exactly how Liangzhu people interacted with their local water regime and coped with climate fluctuations during the Liangzhu period is another matter. Also, although Liangzhu was

known as a water city, how did the current waterway systems form and function, and what were their flow characteristics? Moreover, climate and hydrological conditions had changed by the end stage of Liangzhu, and various events such as seawater penetration, cooling and drying of climate, and changing estuarine geomorphology have all occurred. To what extent and in what way these changing environmental factors influenced the development and eclipse of Liangzhu City is not yet clear.

In summary, the long-term relationships between Liangzhu society and its hydraulic regime and how human activities transformed the local landscape over time are still not clear. Therefore, new evidence should be sought and more research regarding the relationship between water and the development of Liangzhu City should be conducted in order to better understand the landscape history of Liangzhu City and the complexity of Liangzhu Culture.

2.7 Summary

The literature review presented in this chapter shows that the development of Liangzhu City was closely related to the changing water regimes. Before the arrival of Liangzhu people, only a few Neolithic people had settled in the Hangzhou Bay area because of the high sea level. The retreat of the water provided an open marsh environment in which Liangzhu people could construct their city. As a consequence of the local freshwater marsh environment, Liangzhu people built a gigantic anthropogenic structure with dams, mounds and walls to adapt, utilise and control the local water resources. During this process, Liangzhu showed a high level of social complexity. The demise of Liangzhu City may also relate to changes in the local hydrological regime in Hangzhou Bay area, making it potentially one of the most important factors influencing the development of Liangzhu City. Therefore, the interaction between water and Liangzhu City is the primary relationship archaeologists need to understand.

Chapter 3: Fieldwork and Methodology

3.1 Introduction

This study used geoarchaeological methods to investigate the human-landscape relationships of Liangzhu City and its surroundings. The geoarchaeological fieldwork was mainly conducted in the summer of 2017 and 2018 in both the inner and outer Liangzhu City sites. The fieldwork and sampling strategy is introduced in section 3.2. The samples collected were then analysed using soil micromorphology and other geo-science methods such as pH, magnetic susceptibility, loss-on-ignition, phosphate and particle size analyses in the University of Cambridge. GIS-modelling was also conducted to model the regional hydrological system and potential inundation conditions of the Liangzhu Basin under different circumstances (section 3.3).

3.2 Fieldwork and sampling strategy in the Liangzhu City site

To have a complete understanding of the changing hydrological and sedimentary environments of Liangzhu City, and to study the potential interactions between the construction of Liangzhu City and changing hydrological conditions, this research aimed to sample soil profiles that covered the whole history of occupation and formation of waterways in both the inner and outer parts of Liangzhu City.

3.2.1 *General working procedure*

This geoarchaeological research covers all four scales of archaeological landscape contexts. The macro and meso-scale geoarchaeological research started with communication with archaeologists from Liangzhu working station, who have systematically augered a wide range of areas outside Liangzhu City (data unpublished). This was followed by fieldwalking and hand augering, especially to the north of Liangzhu City, to understand the lateral, spatial and vertical variation of stratigraphic sequences of the Liangzhu landscape. GIS modelling of the East Tiao River drainage basin was also conducted to provide a macro-scale understanding of the regional water

regime.

Based on the general understandings of local landscape and combining soil/sediment analyses of previous research (section 2.4), this research selected nine representative profiles with which to study the Liangzhu landscape and its interaction with human activity in micro-and with-in soil scales. Five of the profiles are exposed sections associated with ongoing archaeological excavations and thorough artefact and environmental data retrieval. Four of profiles are hand augered that are representative of nearby stratigraphy sequences (section 3.2.2).

The study of these representative profiles starts with observation of the nature and type of boundaries and their lateral continuity between layers and horizons, along with the colour, structure and texture of the major layers. Next, the profiles were sampled across horizon boundaries. The samples were then brought back to the laboratory for higher level of observation, description and interpretation (Figure 3.1, this study mainly used the first two levels of observation). By these different levels of observation from field to microscopy, both micro- to macro-scale evidence was collected.

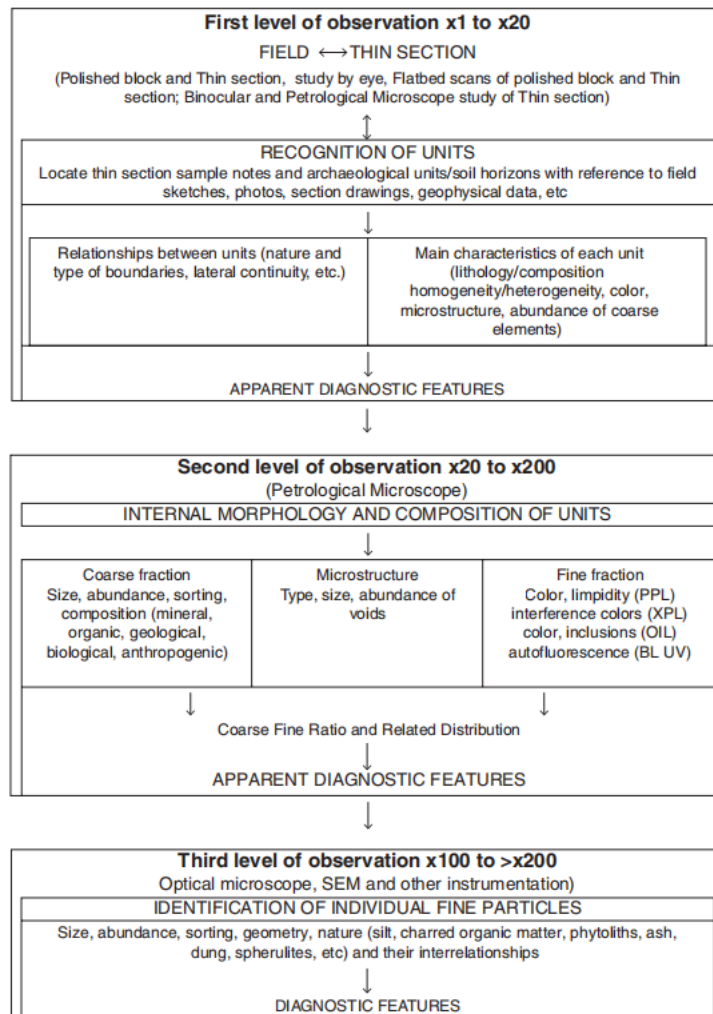


Figure 3.1 Soil micromorphology description guide (adapted from Macphail & Goldberg, 2017, 75).

3.2.2 Site selection

In the summer of 2017, large scale excavations took place inside Liangzhu City as part of the infrastructure project to create the Liangzhu City Heritage Park. The large exposure of archaeological profiles of the Zhongjiagang Watercourse revealed the whole water channel and associated near bank occupation areas and provided an excellent opportunity for geoarchaeological research. Three representative profiles from the Middle, North and South Zhongjiagang regions and one profile from Southwest Mojiaoshan site were then sampled. Profile T2621 from Middle Zhongjiagang area is located in the conjunction area of the Mojiaoshan mound and Zhongjiagang Watercourse, and covers the pre-Liangzhu deposits and early stage of mound construction of Liangzhu City (Figure 3.1, Location 1). Profile T0950 from

Southwest Mojiaoshan site represents the early stage of mound construction and occupation of the city (Figure 3.1, Location 2). Profile T3131 from South Zhongjiagang region is a near-bank mound area mainly occupied in the Late Liangzhu period (Figure 3.1, Location 3). The profile T5020 from North Zhongjiagang area is located in the centre of the Zhongjiagang Watercourse and covers the whole history of the water flow and post-Liangzhu deposits (Figure 3.1, Location 4).

In the summer of 2018, to better understand regional sedimentation processes, changes of hydrological condition, and interactions of human occupation and local landscape at a larger scale, five additional profiles were sampled north of Liangzhu City. It includes two settlement profiles, the Shiqianyu site (Fi. 3.1, Location 5) and South Jincun site (Figure 3.1, Location 6), and three relatively natural analogue profiles, which are the Huoxitang (Figure 3.1, Location 7), North Tangshan (Figure 3.1, Location 8) and Dazhe profiles (Figure 3.1, Location 9).

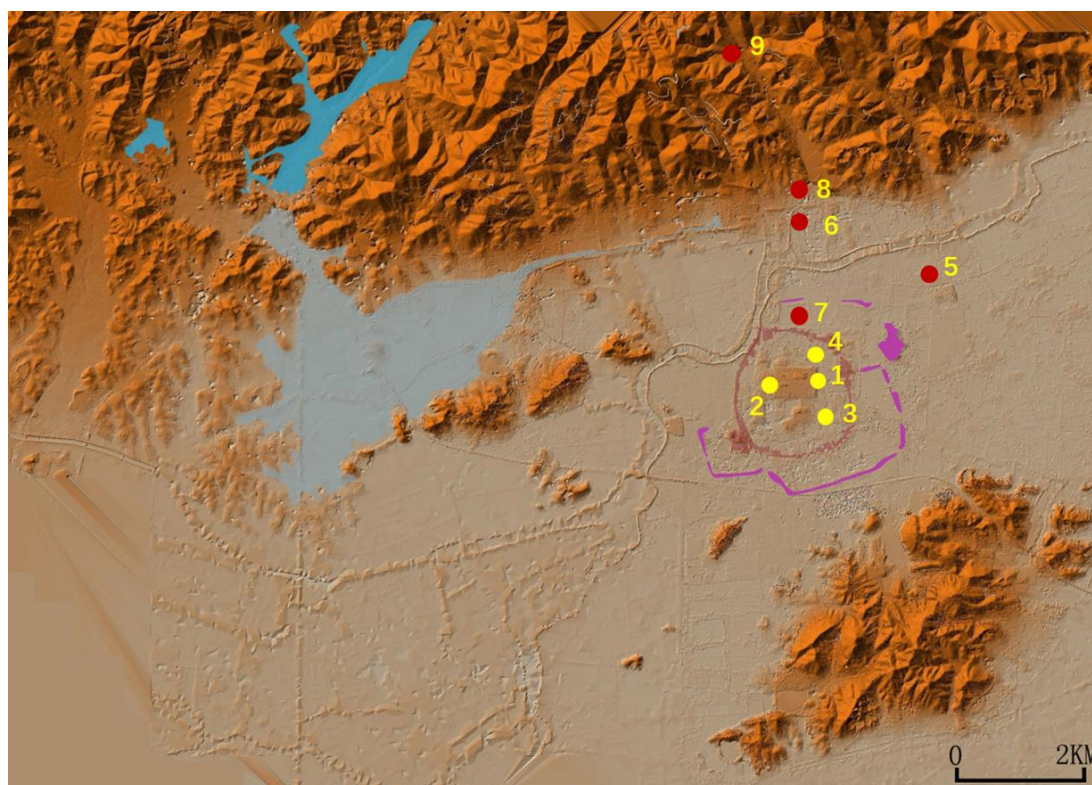


Figure 3.2 The sampling positions of this thesis. The yellow spots locate the profiles that were sampled in 2017, and the red spots locate the profiles that were sampled in 2018.

3.2.3 Sampling procedures

In the profiles that have ongoing excavations, such as the inner Liangzhu City profiles and the Shiqianyu site, the soil/sediment samples were directly collected from exposed sections. Most of these sections are the most typical and complete profiles available at the sites, and were also sampled for radiocarbon dating and other archaeological analyses. In the relatively natural analogue profiles and South Jincun site, the soil/sediment samples were extracted by hand augering.

The sampling procedures for micromorphology and loose bulk samples follow the protocols of the McBurney Laboratory for Geoarchaeology and the Department of Geography, University of Cambridge (see French, 2015, Apps. 1-3; www.geog.cam.ac.uk/facilities/laboratories/techniques/psd.html). Micromorphology samples 15*10*10cm in size were taken across horizon boundaries between layers by sharp trowels and were wrapped with clean non-woven gauze. Around 150g bulk samples were taken beneath and above the boundaries and were stored in clean plastic specimen bags. In total, 87 bulk samples and 55 intact soil blocks were collected for further laboratory analyses.

3.3 Methodology

The approach used in this thesis involved a combination of geoarchaeological methods, including bulk sedimentological, soil micromorphological and GIS modelling analyses. The GIS modelling aimed to present a wider regional view of the geomorphology and hydrological conditions of the Liangzhu Basin. The bulk sedimentological analysis should provide ‘unique insights into microfacies characterizations and interpretations into site formation processes’ (Macphail & Goldberg, 2017, 40). These new sets of information should be both complementary to and corroborated by features and observations obtained from the micromorphological analysis, and combined to suggest the changing nature of past environments as well as human impact and post-depositional processes at work.

3.3.1 Bulk Sedimentological Analyses

87 bulk samples taken from Liangzhu were analysed by bulk sedimentological methods, namely for pH, magnetic susceptibility (MS), total phosphate (P), total carbon (C) and calcium carbonate (CaCO₃) (using loss-on-ignition) and particle size analysis (PSA). The principles of these methods and the equipment used are introduced as follows:

3.3.1.1 pH Values

pH is the log of the hydrogen ion concentration (Bates, 1964). The pH of the soil will influence the preservation of materials. For instance, alkaline values tend to improve the preservation of bone and shell; acid values tend to preserve pollen and macrobotanical material, whereas neutral values tend to preserve most organic materials (Goldberg & Macphail, 2006). The analysis of pH provides a basic soil environment background for the results of other bulk analysis methods. A HI 8314 Portable pH/mV/°C metre from Hanna Instruments was used following the protocol of the McBurney Laboratory (Appendix 1).

3.3.1.2 Magnetic Susceptibility

Magnetic susceptibility surveys of soil test for the presence of magnetic iron-oxide minerals, and are commonly used in geoarchaeological analysis to indicate old land surfaces, trampled surfaces, and areas of burning or fire-related activities (Goldberg & Macphail, 2006). Changes in the oxidation condition of sites, as a result of the presence of anthropogenic features, cycles of wetting and drying, groundwater fluctuations and biological activities will also alter the magnetic susceptibility of soil (Sternberg, 2001). Magnetic susceptibility measurements can also reflect changes in the climate and environment over a longer time range (Maher and Thompson, 1999). A Bartington Instruments MS3 2B susceptibility metre with a low frequency sensor was used following the protocols of the McBurney Laboratory (Appendix 1).

3.3.1.3 Phosphate Analysis

Phosphates are believed to be markers of human occupation and activity and phosphate analysis is a basic geochemical technique that has been widely applied to archaeological

studies to detect domestic contexts (Holliday and Gartner, 2007). A HI 83200 Multiparametre Bench Photometre from Hanna Instruments was used following the protocol of the McBurney Laboratory to determine total phosphate values (Appendix 1).

3.3.1.4 Loss-on-Ignition

Loss-on-Ignition (LOI) is a useful method to measure the organic, carbon and calcium carbonate contents of sediments. Changes in the organic matter content of a profile may suggest the presence of former topsoils or middening for example, as well as changes in the extent and nature of human activities (Goldberg & Macphail, 2006). Calcium carbonate will occur naturally in calcareous and shell-rich soils, but may also be influenced by anthropogenic activities and changes in groundwater conditions (Macphail & Crowther, 2008).

The Loss-on-Ignition analysis was carried out in the Physical Geography Laboratory of the Department of Geography at the University of Cambridge under the supervision of Laura Healy (Senior Research Laboratory Technician) and following the protocols of the Physical Geography Laboratory (www.geog.cam.ac.uk/facilities/laboratories/techniques/psd.html; Appendix 1). The samples were dried at 105°C and then heated to 400°C, 480°C and 950°C. The percentages of water, calcium carbonate, carbohydrate, carbon and total organic, respectively, were then calculated.

3.3.1.5 Particle Size Analysis

Particle size analysis has been widely used to detect the components, sources and energy of sediments and their formation process, and can therefore provide a scenario indicative of a wider regional environmental framework for archaeological sites (Boggs, 2001; Catt, 1985; Goldberg & Macphail, 2006).

The particle size analysis was carried out in Physical Geography Laboratory of the Department of Geography at the University of Cambridge under the supervision of Laura Healy (Senior Research Laboratory Technician). The samples were pre-treated

to remove organic matters and a Malvern Mastersizer 2000 was used following the protocols (v1.3) of the Geography Laboratory (www.geog.cam.ac.uk/facilities/laboratories/techniques/psd.html; Appendix 1).

3.3.2 Soil Micromorphological Analyses

Soil micromorphology is an ‘extremely useful and all-encompassing technique’ (French, 2003, 47) to reveal detailed and subtle changes in the environment and sedimentation as well as indications of anthropogenic features (Goldberg & Macphail, 2006).

Fifty-five sample blocks were taken from Liangzhu and stored in the DEFRA Storeroom of the McDonald Institute for about four weeks before impregnation. In the initial preparation stage of the thin section making, the resin did not thoroughly infiltrate into the blocks due to the high clay and silt content of the Liangzhu samples, even under 48 hours of vacuum treatment. This study therefore adapted a new thin section preparation method developed by Dr Tonko Rajkovaca (Chief Technician of the McBurney Laboratory) to tackle this problem. Compared to the general protocol, an extra glass slide is added in the first mounting stage to protect the sample to create a glass/soil/glass ‘sandwich’, one side of which was then ground on the Brot thin section machine to a thickness of *c.* 30 microns. Sometimes, it was also necessary to undertake several extra mountings so as to reinforce the infiltration of resin. The detailed thin section making procedure can be found in Appendix 1.

The new method worked well for the silt/clay/organic-rich samples from Liangzhu. The slides were described using a Leica Laborolux 12 Pol S polarizing microscope and an Olympus fluorescence microscope, and photographed using a Q-Capture digital camera and software system. The description of the thin sections follows the descriptive system developed by Bullock *et al.* (1985) and Stoops (2003). Detailed descriptions of each slide are reported in Appendix 2.

3.3.3 GIS modelling

GIS is a very powerful technological tool for tackling archaeological problems (Conolly and Lake, 2006, 3). In particular for this thesis, the rapid development of software tools for hydrological modelling and the rapidly expanding availability of Digital Elevation Model (DEM) data have made the application of GIS for waterflow modelling much easier (Harrower, 2010).

This thesis used the ASTER GDEM (Version 3), which was newly released in 2019 with a resolution of around 30m as the base map. The hydrological modelling tools within ArcGIS software (version 10.5) were then used to model hydrological conditions at Liangzhu. The major workflow includes the ability to modify the anomalies of the DEM, define flow direction, produce flow accumulation, generate vector channel networks, and define flow catchments. The data of the current lake and river system around Liangzhu was obtained from the 1: 1,000,000 databases of the National Geomatic Center of China, and were then superimposed over the DEM of the area to better present the hydrological conditions of this region.

3.4 Summary

This thesis used an integrated geoarchaeological approach to analyse the stratigraphic complex from both the inner and outer areas of Liangzhu City. The results of GIS modelling will be introduced in Chapter 4. The results of soil micromorphological and bulk analyses will be presented in Chapters 5, 6 and 7.

Chapter 4: GIS modelling of the Liangzhu Region

4.1 Introduction

To have a general overview of the site distribution and hydrological conditions of the Liangzhu region, this chapter first introduces previous GIS research in this region, and then models the regional hydrological system and inundation conditions based on newly released Digital Elevation Map (DEM) and elevation data obtained from excavations.

4.2 Previous GIS modelling of the Liangzhu region

In recent years, a few GIS modelling studies have been conducted to investigate questions related to site distributions around Liangzhu City as well as the function of the dam systems and the reconstruction of the hydrological system around the Liangzhu Basin. Their results can be summarized as follows.

Spatial analysis of Liangzhu sites around Liangzhu City

The spatial analysis of Liangzhu sites around Liangzhu City were conducted using maps of different resolutions. Jin (2018a) and Liu and Wang (2018) have reconstructed the general topography around Liangzhu City using the DEM converted by 1:10000 topographic map. Jin (2018b) reconstructed the topography around Liangzhu City using a Digital Surface Model obtained from ALOS (AW3D standard product) with a horizontal resolution of approximately 5 metres (Figure 4.1). Using the GIS data, they have both modelled the field of vision, slope and aspect, and conducted site territorial analysis of the Mojiaoshan site. Their results show that 83.7% of the sites of Liangzhu City are located at an altitude of 0-10m, and 85.03% sites were distributed in flat areas with a gradient lower than 6°. Based on size areas and locations, there are five major clusters of site groups in this region, the Liangzhu City site groups, the Tangshan site groups north to Liangzhu City, the Yaoshan site group to the north-east of the city, the Shiqianyu site group east to the city, and the Miaoqian site group clustered around Daxiong Mountain (Figure 4.1). The Liangzhu City site group has the largest site areas and site numbers, and were constructed at the top of the watershed that has a slightly

higher terrain (Liu and Wang, 2018). The Tangshan site group clustered around the Tangshan dam site and contained important settlements such as Yaojiadun and Lucun that dated to the early stage of Early Liangzhu period. The Yaoshan site and Shiqianyu site groups show a relatively scattered site distribution. The Miaoqian site group shows a smaller individual site area but with a higher site density. It is interesting that there is a blank area of site distribution between these two site groups. This gap may be related to the palaeochannel flowing between these two areas (Jin, 2018a) (see below for discussion).

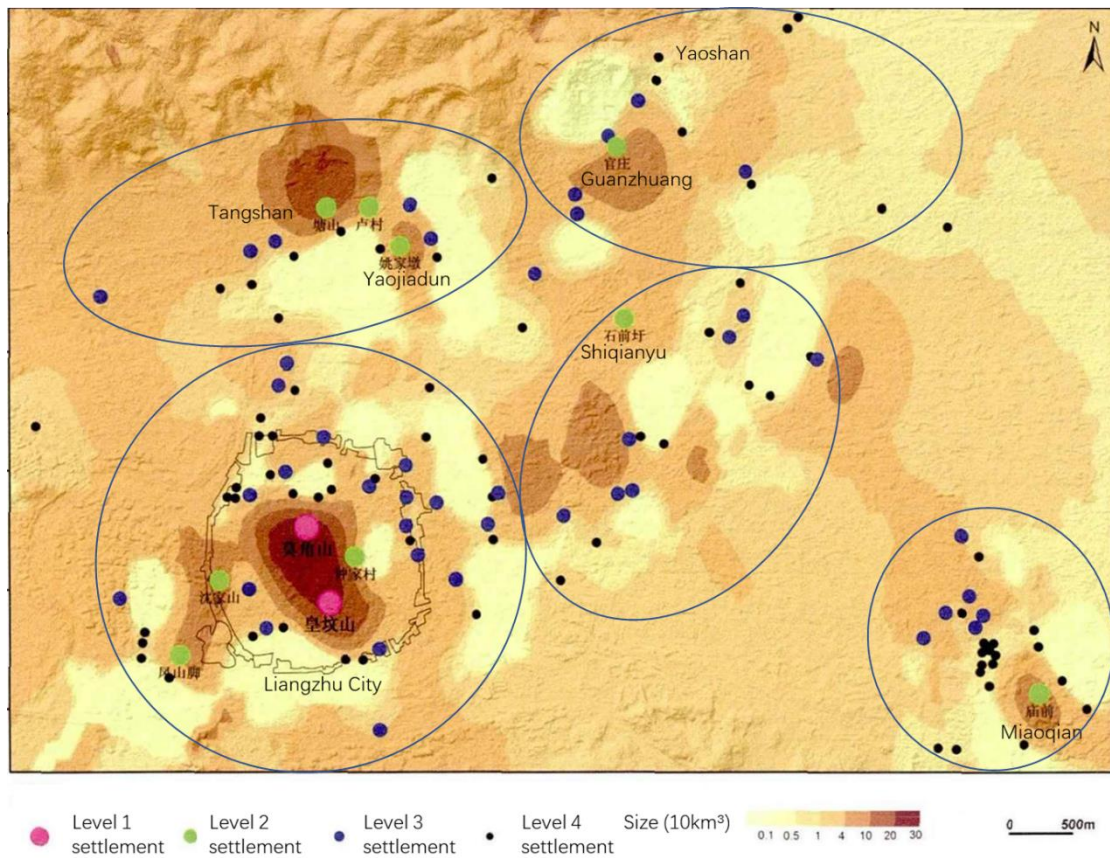


Figure 4.1 Site distribution map of the Liangzhu City region (modified from Jin, 2018b)

GIS analysis of the dam system

The dam system of Liangzhu City has also been modelled using the DEM converted from the 1:10000 topographic map (Liu and Wang, 2018) (Figure 4.2). The area enclosed by the Tangshan Dam and the Dazhe mountain (Figure 4.2, area A) may be used for water collection. The construction of the Tangshan Dam forced the water from the Dazhe mountain to flow from east to west, and drained into the lower dam reservoir area. The lower dam system (Figure 4.2, area B) forms a water area of 9.36 square

kilometres with a reservoir capacity of around 44 million m³. The high dam systems form two reservoirs (Figure 4.2, areas C and D) with a water area of 1.18 square kilometres and 0.83 square kilometres, and a reservoir capacity of 11.3 million m³ and 5.5 million m³, respectively (Liu and Wang, 2018). But currently, controversies still exist about whether these artificial mounds were functioned as dams in Liangzhu times, as the overflow spillway of the proposed dam systems have not been fully studied until now.

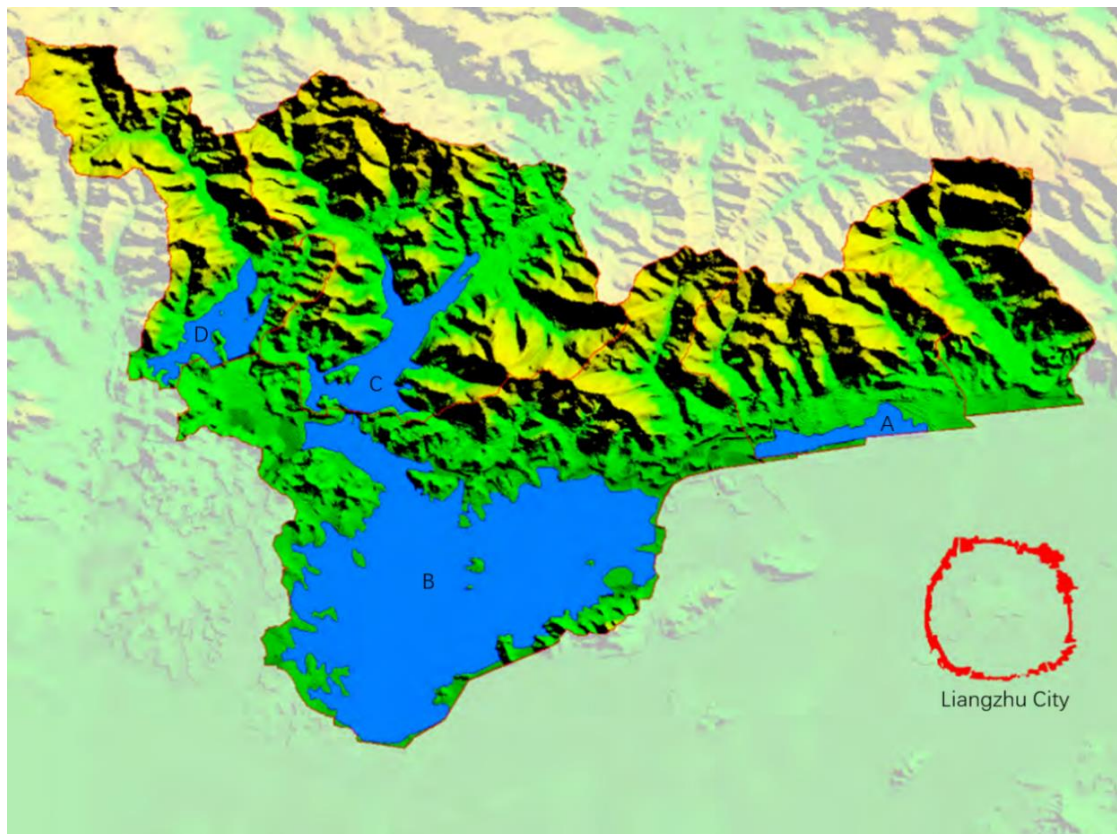


Figure 4.2 Reconstructed reservoir areas (Liu and Wang, 2018)

Model of the hydrological system of the Liangzhu Basin

Both Liu and Wang (2018) and Jin (2018a) have modelled the flow system of the Liangzhu Basin and its nearby area, but their results are slightly different. Jin (2018a) used ASTER GDEM data with a horizontal resolution of approximately 30 metres. The comparison between the modelled channel system flowing under natural conditions and the current water system of the region (Figure 4.3a) shows that under the current terrain, the rivers will flow from south-west to north and drain into the Tai Lake. The flow model of the Liangzhu Basin demonstrated that after the confluence of the north and middle Tiao River, the water flows south to Liangzhu City between the Bianjiashan site

and the Meirendi site, which may result in the blank area between Liangzhu City site clusters and the Miaoqian site clusters (Figure 4.3b).

In Liu and Wang’s research (2018), the flow system of the Liangzhu Basin was reconstructed using STRM data with a resolution of 90m, with the flow conditions near Liangzhu City reconstructed using the DEM converted to the 1:10000 topographic map. Probably due to the different selections of drainage basins and the different resolution of base maps, the modelled water systems of the Liangzhu Basin show a trend of water flowing east instead of north-east (Figure 4.3c), and the water mainly flows in a north-south direction near Liangzhu City with no waterway running south to Liangzhu City between the Bianjiashan and the Meirendi sites (Figure 4.3d).

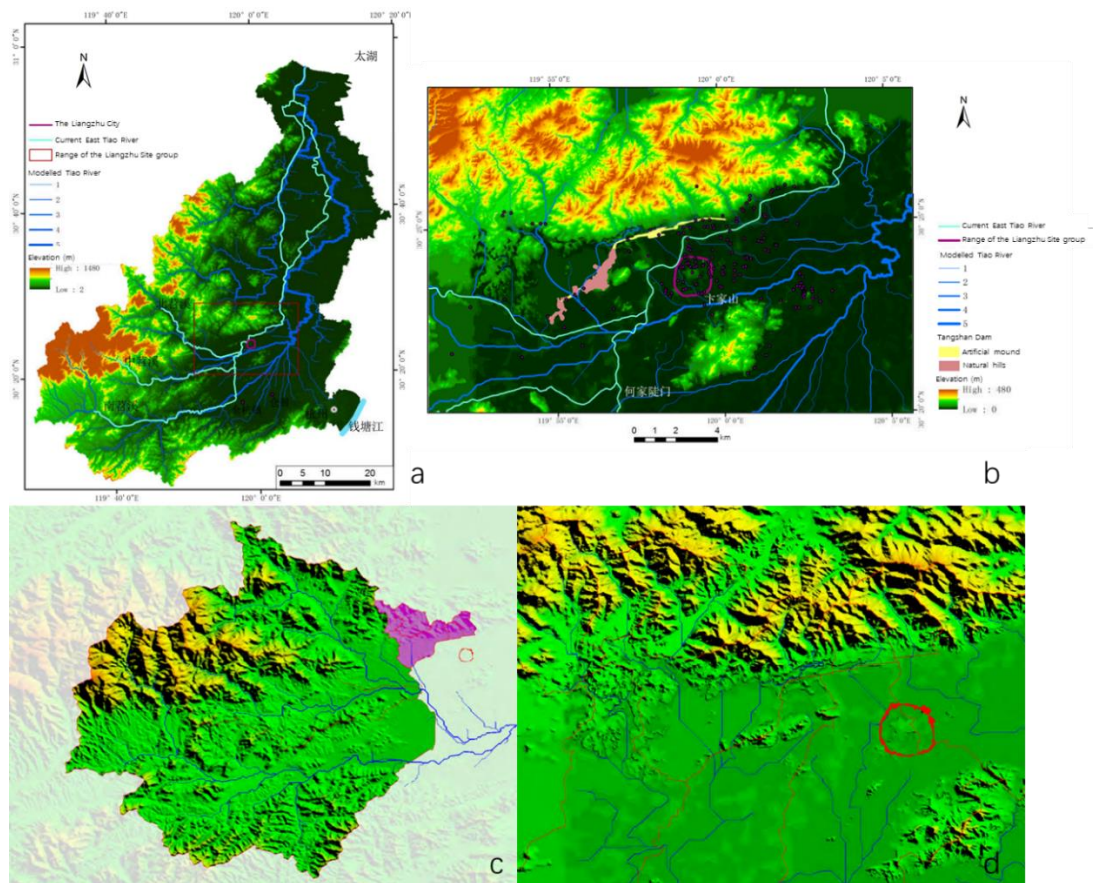


Figure 4.3 a: Tiao River modelled by Jin (2018a); b: modelled flow system near Liangzhu City (Jin, 2018a); c: Tiao River modelled by Liu and Wang (2018); d: modelled flow systems near Liangzhu City (Liu and Wang, 2018).

In general, basic spatial analysis and hydrological analysis have been conducted in Liangzhu City and the broader Liangzhu Basin. But disagreement about the detailed hydrological conditions near Liangzhu City still exist. Further studies are thus required.

4.3 Basic GIS Modelling of the Hydrological Condition of the Liangzhu Region

To better understand the changing hydrological regime of the Liangzhu region and provide a wider hydrological background for the study of Liangzhu City, two main hydrological analyses were conducted for this thesis: the first was to model the river system around Liangzhu City and the wider Liangzhu Basin, and the second was to simulate the range of flooding under different depths of inundation to investigate the potential relationship of seasonal flooding, river surface height and occupation levels. The ASTER GDEM (version 3) that was newly released in 2019 with a resolution of around 30m was used as the base map. ArcGIS software (version 10.5) was used to model the hydrological condition. The data of current lake and river obtained from the 1: 1,000,000 databases of the National Geomatic Center of China were then superimposed to better present the hydrological conditions of this region.

4.3.1 Modelled water system around Liangzhu region

After data processing using hydrological modelling tools provided by ArcGIS (v.10.5), the watershed and stream networks of the Tiao River were modelled (Figure 4.5). The modelled river network is slightly different to previous studies introduced above (Liu and Wang, 2018; Jin, 2018a). The upstream area of the modelled water system corresponds very well with the current Tiao River. However, instead of draining into the Tai Lake, the streams of the Liangzhu Basin under natural topographical gradients flow from south-west to north-east, and converge with other streams that afterwards drain into the Qiantang River.

Based on research on the palaeochannel and historical documents, the current watercourse of the Tiao River that flows from south to north may have been artificially diverted after the Eastern Han dynasty (AD 25-220) (Jin *et al.*, 2005). The location of the palaeochannel (Jin *et al.*, 2005) confirms that the ancient Tiao River was once flowing from west to east, which corresponds well with the modelled watercourse by GIS (Figure 4.4). It is speculated that the raising of the Qiantang Riverbank since the Middle Holocene, which is around 7-8m above sea level now, has significantly influence the hydrological system of the Liangzhu Basin and forced the Tiao River to

flow to the north (Jin *et al.*, 2005). However, the timing of the northward diversion of the Tiao River is not yet clear, and how it has impacted on the development of Liangzhu should be carefully examined in the future.

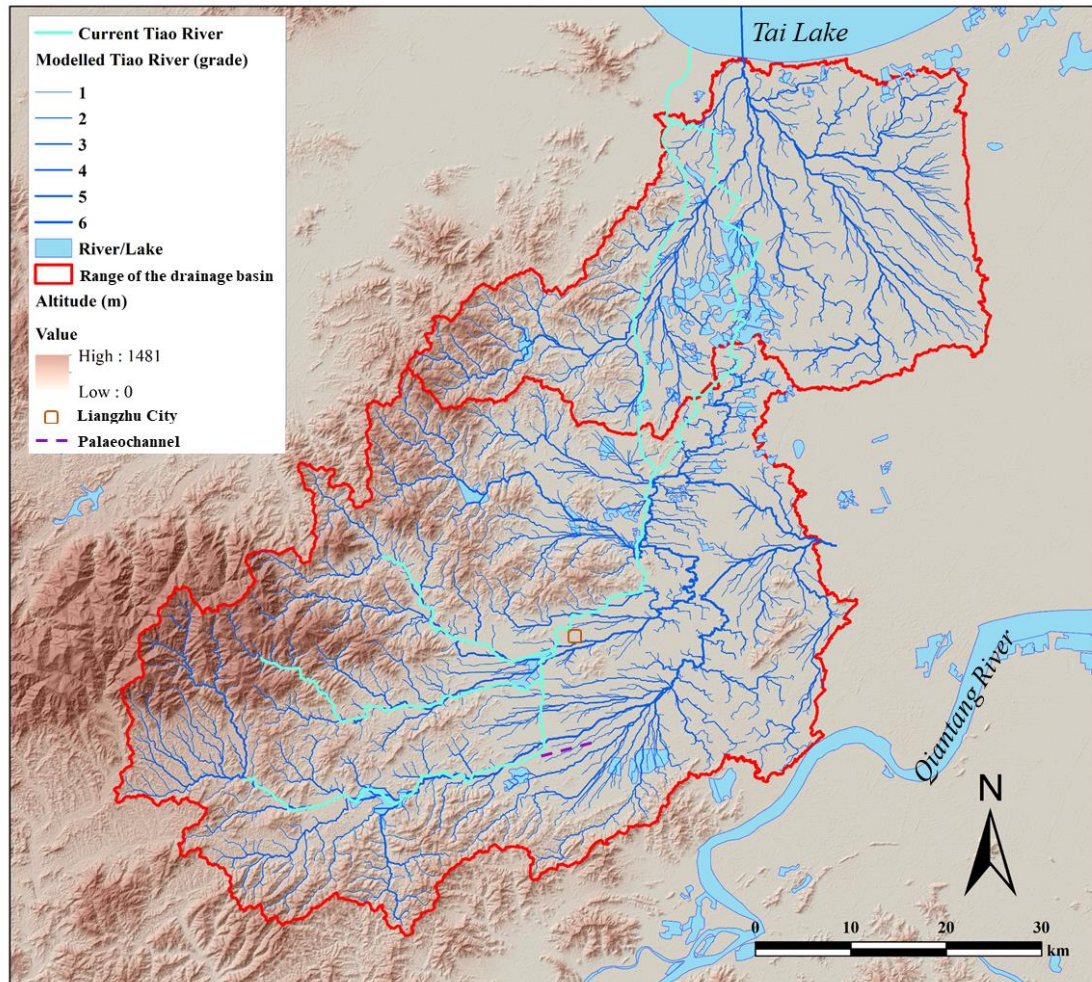


Figure 4.4 Modelled watershed and stream network of the Liangzhu Basin. Higher river grades mean higher number of tributaries converge into the river.

Compared to the current riverway that is heavily modified in historical times, the modelled waterway as indicated in the DEM may be closer to the stream network in Liangzhu times. In general, the modelled water system near Liangzhu City (Figure 4.5) corresponds well with the notches and water gates between raised artificial mounds, which may be spaces reserved for waterways. The small waterway in the north Liangzhu City corresponds well with the northern inner city canals, which implies that the inner city waterways may to some extent take advantage of natural watercourses. Based on the DEM, the water generally flows from west to east near Liangzhu City, which is also supported by archaeological findings that suggest that the palaeochannel

found in the outer city settlement site (the Shiqianyu site) northeast to Liangzhu City also flowed in a west-east direction (see Chapter 7).

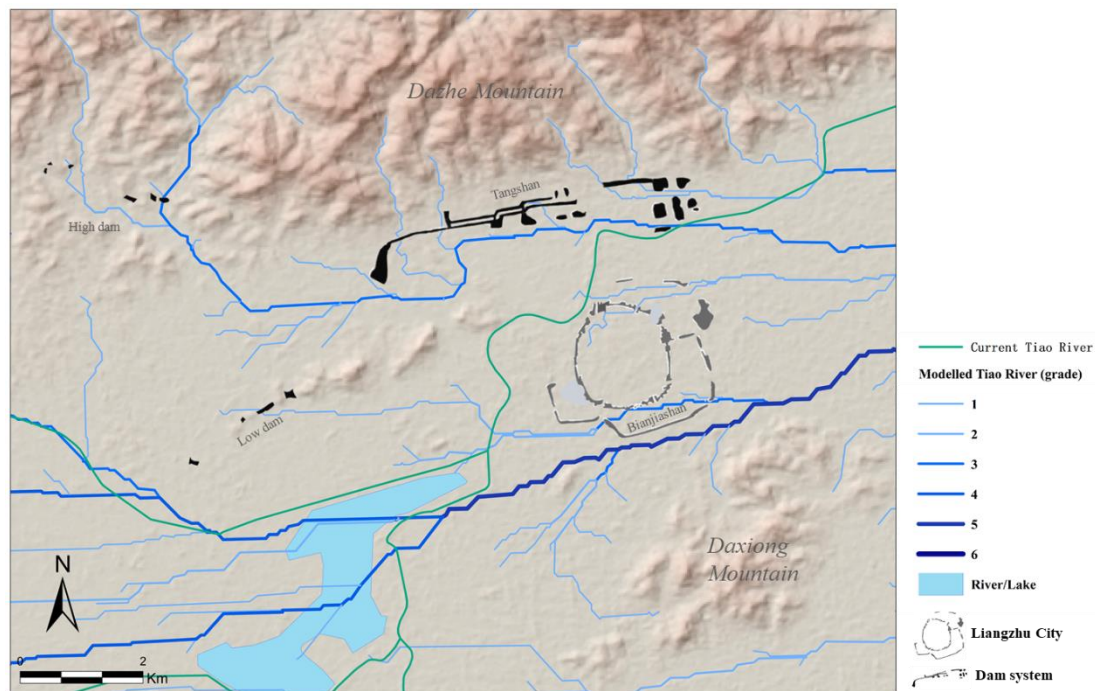


Figure 4.5 Modelled water system near Liangzhu City (enlargement of Figure 4.4)

The modelled flow system shows that there is a major riverway south to Liangzhu city, between the Bianjiashan site and Miaoqian site group. Augering survey also demonstrated that between the Bianjiashan site and Daxiong Mountains there are large areas of light yellowish silty clay and grayish silt possibly deposited under fluvial conditions (Zhao, 2013). The south-facing pier and paddles found at the Bianjiashan site (ZPICRA, 2014) also imply the existence of rivers or channels in the south. The construction of the outer city settlements that dated to 2850-2600 cal. BC was possibly constrained by the course of the river flowing south to Liangzhu City as the current inclined orientation of the Bianjiashan site may possibly represent the flow direction of the palaeochannel. In addition, the Liangzhu site group and the Miaoqian site group may be linked by this channel. The reason for the abandonment of the Bianjiashan site and the construction of the city walls at around 2600 cal. BC is not yet clear. But the range of the city wall is also constrained by local stream networks north and south of the city walls. The locating and study of the changing hydrological regime of the waterway running south to the south city wall and the Bianjiashan site may help to interpret how the layout of Liangzhu City was formed, and how the encircled artificial mounds shifted from the northwest-southeast outer city settlements to the north-south

city walls that were inhabited around 200 years later (Figure 4.5). Therefore, further research is required to better understand the formation process of this possible palaeochannel and its influence on the vicissitude of Liangzhu city.

Based on natural flow direction, the water coming from the Dazhe Mountains should converge and flow from west to east (Figure 4.5). The construction of the Tangshan dam does not seem to significantly change the major flow direction, but may divert some of the small streams of the Dazhe Mountain. The eastern Tangshan site may obstruct two small streams from the Dazhe mountain and formed a small reservoir as reconstructed by Liu and Wang (2018) (Figure 4.2). Another two small streams in the west may be forced to flow from east to west with the water then collected in the lower dam reservoir. It is interesting to note that based on the hydrological modelling, there are no major streams from the north to the middle part of the Tangshan dam. This part of the Tangshan dam, which is around 2km long, does not seem to hold-up water, rather they may more likely be settlement mounds situated parallel to the waterway that flows south to the Tangshan dam site. This may imply that the Tangshan dam has served several functions during Liangzhu times and different parts of the ridges may have different main functions.

In terms of the high dam system, it can be seen that most of the construction of the high dams avoids the main streams and only controlled small branches of the water flow. To understand how the construction of the high dam may have influenced or managed the local water system requires a DEM with higher precision and further study.

4.3.2 Reconstruction of regional inundation condition

Based on the ASTER GDEM Version 3 data, the overwhelming majority of the Liangzhu Basin have an elevation of above 3m, which in general agree with the elevation data measured during excavations. However, this elevation data only reflects the height of current land surfaces but not the land surfaces at Liangzhu times.

Based on excavation results (Liu *et al.*, 2019a, b, c) and elevation data collected during soil sampling, the elevation of different components of Liangzhu City can be

reconstructed. Around and inside Liangzhu City, the buried soils that existed before the occupation of Liangzhu people have an elevation of 0.3-1m, and channel deposits such as the Zhongjiagang Watercourse have an elevation of 1.8-2.3m. The elevation of the yellow silty clay layer that dated to around 2000 cal. BC is around 2-3m, whereas the average elevation of the outer city settlements are around 4-5m, with the extant highest point of the city wall at around 7m above sea level, and the Mojiaoshan mound at 12m above sea level. Unfortunately, as the DEM data can only reflect the terrain above 3m, most of the subtle changes of terrain and the potential rise and fall of the water heights in the associated canal and river systems of Liangzhu cannot be seen and analysed using current DEM data. Even so, it is still possible to model extreme flooding conditions and to see the range of inundation when the water table reached 3m, 5m, 7m and 12m, which represent the height of the yellow silty clay layer, the outer city settlement, the city walls and the Mojiaoshan mound, respectively.

4.3.2.1 Model of inundation condition of the Liangzhu Basin

Using the ASTER GDEM Version 3 data as a base map, the inundation condition of the Liangzhu Basin was modelled by the ArcGIS software (v. 10.5) (Table 4.1) using "without source flood" algorithm. The modelling shows that when the water table reached 5m, about 3.3% of the area below 20m would have been flooded, with the flooded areas concentrated in the southern part of the Liangzhu Basin (Figure 4.6a). This implies that when the water table reached the height of the outer city settlement, there was still sufficient exposed land available for occupation by the Liangzhu people. Meanwhile, the terrain in the north is generally higher and less susceptible to flooding than the south, which may help to explain why most Liangzhu sites were settled in the northern part of the basin. If the water table reached 7m, which is the height of the city wall, about 25.6% of the area below 20m would have been flooded (Figure 4.6b) with the inundated area spread all over the basin. This suggests that a substantial amount of land would have been unavailable in this situation. If the water table reached 12m, which is the height of the Mojiaoshan mound, about 81.9% of the area below 20m would have been inundated and the whole Liangzhu Basin would have been totally unsuitable for human occupation (Figure 4.6d).

It should be noted that this research only provides a simple model presenting the possible scenarios of influence of flooding at different scales and the utility of the artificial mounds constructed by Liangzhu people. To better understand the ancient landforms of Liangzhu City, a comprehensive survey and associated excavations around the Liangzhu City region are required to provide more detailed information about the palaeo-geomorphology and the distribution and scale of river systems present in the past.

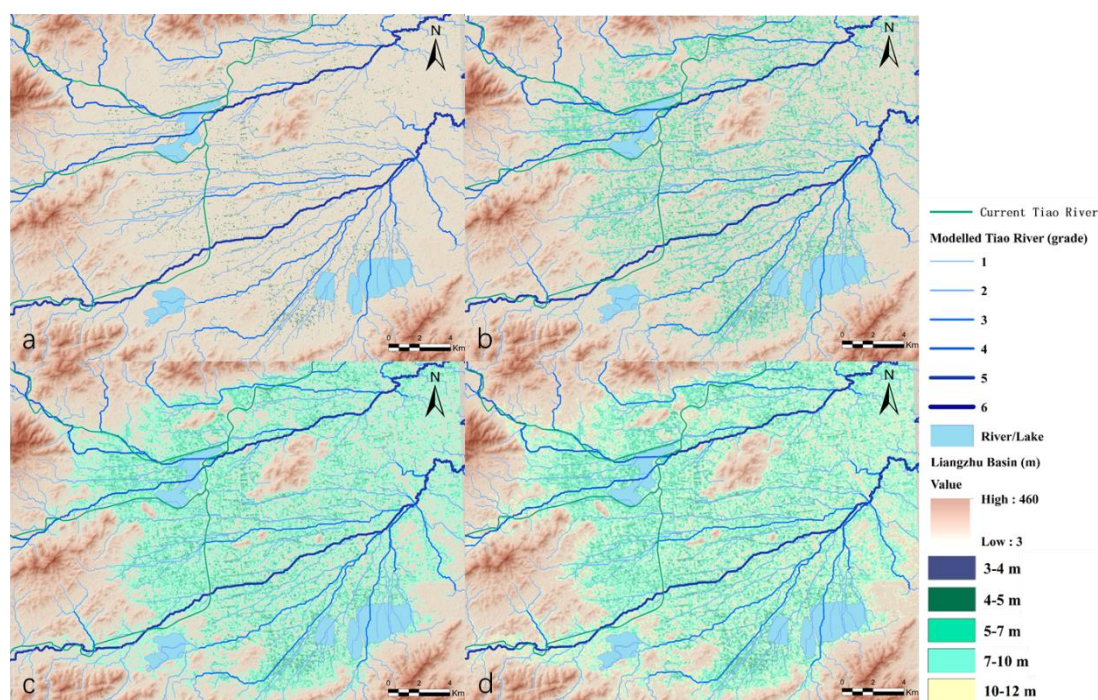


Figure 4.6 a. inundated area below 5m; b. inundated area below 7m; c. inundated area below 10m; d. inundated area below 12m.

Table 4.1 Inundation area of the Liangzhu Basin under different elevations

Elevation	Inundation area (km ²)	Percentage below 20m
<4m	0.2	0.4%
<5m	16.6	3.3%
<7m	128.5	25.6%
<10m	336.8	67.1%
<12m	411.1	81.9%
<20m	502	100%

The inundation condition of wider Tai Lake Plain and the Hangjiahu Plain is also presented here. It can be seen that the low-lying areas are mostly concentrated near the Tai Lake and the Qiantang River. The inundation of areas below 5m may not produce significant influences on human occupation as there is still substantial land available.

However, if the flooding reached 7m, this area would have been generally unsuitable for human occupation.

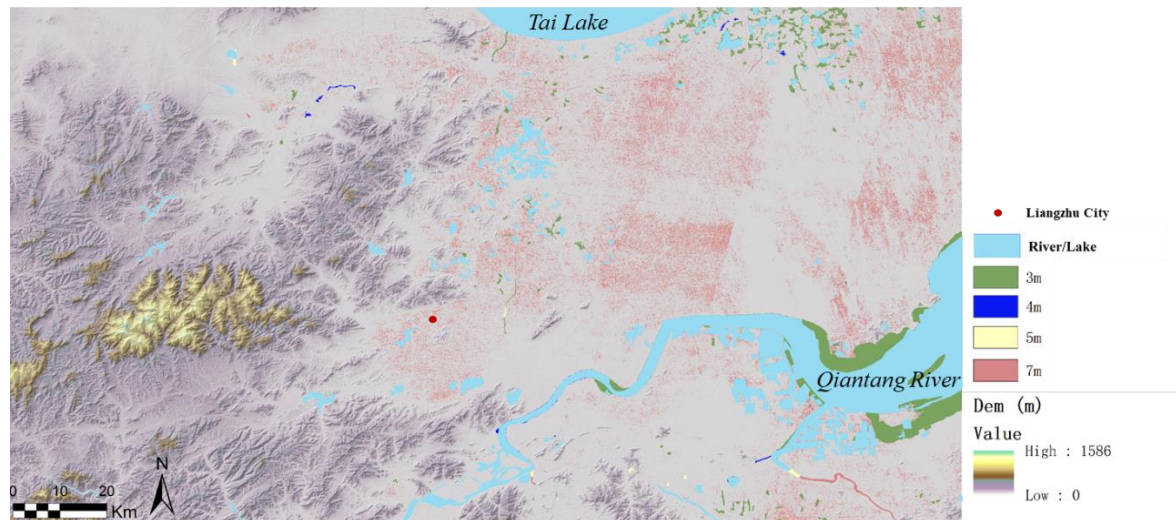


Figure 4.7 Model of inundation condition of the Tai Lake Plain and Hangjiahu Plain

4.4 Summary

The GIS modelling of the hydrological conditions of the Liangzhu Basin provide a broad context for the analysis of the hydrological regime of the Liangzhu City, and the modelling of stream network under natural conditions may give insights into the hydrological conditions during Liangzhu times.

The results of GIS modelling show that the Tiao River will flow from west to east and possibly drained into the Qiantang River under natural flow conditions. The reconstruction of the stream network near Liangzhu City indicates that there is a major channel flowing south to Liangzhu City with the inner city water system possibly taking advantage of natural channels. The Tangshan dam may to some degree divert streams from the Dazhe mountain in the north, but its main body may have been constructed mainly for settlement purposes. The construction of the high dam system only controlled small branches of the stream and its function and use-pattern require further studies. The inundation modelling of the Liangzhu Basin shows that under current terrain, if the water table reached the height of the outer city settlement, there would still have been enough exposed land surfaces for human occupation, especially in the north of the Liangzhu Basin. But if the water table reached 7m, which is the height of the city wall, the Liangzhu Basin and the wider Tai Lake region would have been

unsuitable for human occupation.

Limited by the precision of the DEM data and the change of the terrain from the past to present, this research is preliminary and only shows the general trend of river flow and inundation conditions. More factors and data should be considered and incorporated in any future studies.

Chapter 5: The Results of Soil Micromorphological and Associated Chemical and Physical Analyses in the Zhongjiagang region, Inner Liangzhu City

5.1 Introduction

Zhongjiagang Watercourse is one of the major waterways that crosses the whole Liangzhu City. It is in a north-south direction, about 1370m long, 18-80 metres wide and 3 metres deep. The discovery of this palaeochannel originated from the prospection project of the Liangzhu Ancient City by Shaanxi Longteng Company from 2011 to 2014. As part of the infrastructure project of the Liangzhu City Heritage Park, Zhejiang Provincial Institute of Cultural Relics and Archaeology conducted large-scale excavations to recover the whole watercourse and nearby occupation areas along the banks of the channel from 2015 to 2017 (Liu *et al.*, 2019a). For the convenience of discussion, the whole excavation areas, *i.e.*, the watercourse together with near bank excavation areas, were separated into three parts, which are North, Middle and South Zhongjiagang region. In the following discussions, the Zhongjiagang Watercourse refers to the waterway itself, the Zhongjiagang region refers to the waterway and activity areas found along the banks.



Figure 5.1 Sampling positions of the North, Middle and South Zhongjiagang profiles.

In June 2017, soil samples were collected from excavation pit T5020 in North Zhongjiagang region, T2621 in Middle Zhongjiagang region and T3131 in South Zhongjiagang region when the excavations were still ongoing (Figure 5.1). In these locations, samples for radiocarbon dating were also collected from the same layer in the same excavation pit and were analysed in the Archaeometry and Archaeological Dating Laboratory in Peking University, China and the Beta Analytic radiocarbon dating lab, USA. In the following discussions, dates are reported from the original publications (Qin *et al.*, 2019). All dates are calibrated using OxCal 4.3 (Reimer *et al.*, 2013) and the IntCal 13 calibration curve (Ramsey, 2019). Using methods introduced in Chapter 3, 25 micromorphology samples and 52 bulk samples in total were collected and analysed. In this chapter, the samples from the T2621 excavation pit will be elucidated first as it represents the earliest human occupation stage in the Liangzhu period near the watercourse, following by T5020, which represents the main filling up process of the Zhongjiagang Watercourse.

5.2 Middle Zhongjiagang region (T2621)

In the middle part of the Zhongjiagang region, the stream flows east to the Mojiaoshan mound (Figure 5.2). Accompanying the five stages of platform² building on the western bank, domestic refuse gradually filled up the channel. In the later period of Liangzhu Culture, the palaeo-channel in this section was nearly abandoned as the watercourse became filled with one-metre thick ‘clay wrapped with grasses’ and new surfaces made by interlacing sand and silty soil were constructed above it (ZPICRA, 2019) (Figure 5.2, Stage 4).

² A single stage of mound construction is referred to a platform in this thesis.

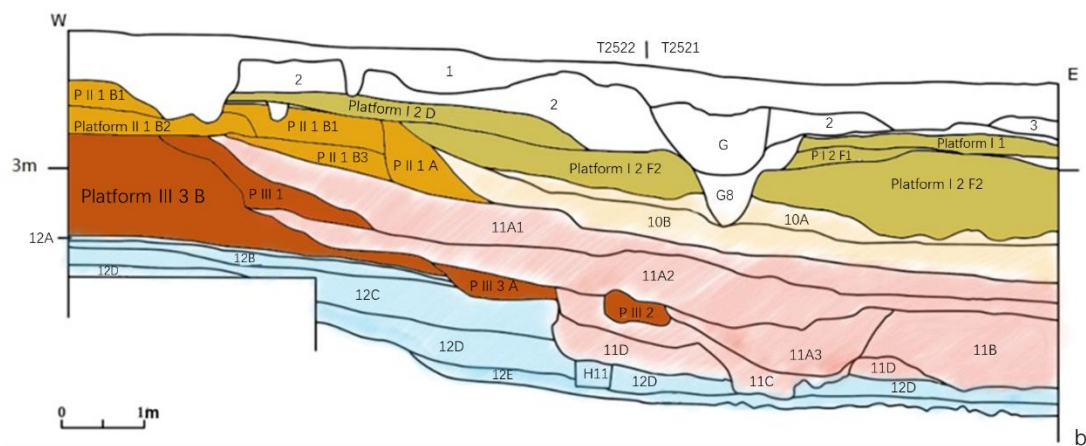


Figure 5.2 Sampling positions and sediment sequences of Middle Zhongjiagang region; **a**: position of Profile T2621; **b**: sketch of profile T2522-2521 showing the general stratigraphy of the Middle Zhongjiagang area. The solid colours refer to constructed platforms. The light colours refer to riverine and pre-site sediments. Different colours refer to different stages of deposition: Stage 1 is in blue (Layer 12), Stage 2 is in red (Platform III and Layer 11); Stage 3 is in yellow (Platform II and Layer 10); Stage 4 is in green (Platform I) (Courtesy of ZPICRA).

During the excavation in 2017, the south wall of the excavation pit T2621, located in the western bank of the channel next to the Mojiaoshan mound, provided a good profile with which to understand the pre-site condition and early stage mound building of this region. Accordingly, a total of eight micromorphology samples and 17 bulk samples were collected from each layer in profile T2621 (Figure 5.3).

5.2.1 Field observation and stratigraphy of profile T2621

5.2.1.1 The general stratigraphy and findings in the Middle Zhongjiagang region

Based on field observation and archaeological findings, the Middle Zhongjiagang region has been separated into five stages of mound construction and channel infilling by the excavator (Liu *et al.*, 2019a) (Figure 5.2). At the first stage, Platform IV was built, nine large timber components have been found in Layer 12 with very few other anthropogenic artefacts. At the second stage, Platform III was built on top of Platform IV. In this stage, Liangzhu people used blocks of ‘clay wrapped with grasses’ and grayish silty clay to fill the ancient channel and connect the west mounds with the east mounds. A beheaded stream was formed in the north. Layer 11 was then accumulated in this stagnant water. Pottery, stone artefacts and lacquerwares were found. At the third stage, Platform II is built on top of Platform III. Four timbers and a large amount of human remains were found in Layer 10, which is the waste accumulation during the use of Platform II. At the fourth stage, Platform I was built north to the Platform II with multiple sandy layers on top. Layer 9 was silted up in the Zhongjiagang channel. After that, a row of planks was built along the bank to protect the bank. The waste accumulation of Platform I, Layers 8, 7 and 6 were formed. At the fifth and final stage, the mound continues to expand to the north, Layers 5, 4 and 3 were formed with fewer artefacts found, and the cut off stream area continued to recede to the north (Liu *et al.*, 2019a).

5.2.1.2 Field description of profile T2621

Based on field observation and archaeological findings, the profile in T2621 shows four main layers and covers the first, second and third stage of mound construction in the Middle Zhongjiagang region (Figure 5.3). The field description of T2621 is introduced from top to bottom as follows:

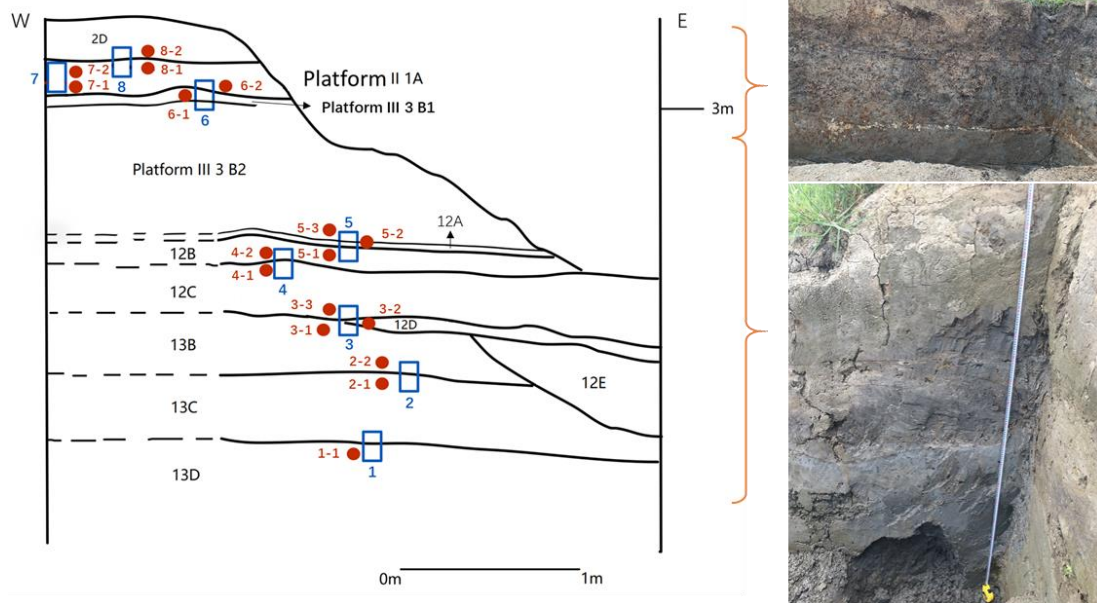


Figure 5.3 Stratigraphy and sampling position of the T2621 profile. The blue rectangles and numbers refer to the sampling positions and numbers of the soil micromorphology samples. The red dots and numbers refer to the sampling positions and numbers of bulk samples.

Platform III 1 A: Gray silty clay with a charcoal lens, few inclusions and common rusty mantels or streaks formed from amorphous sesquioxides. 0-10cm thick.

Platform III 3 B1: a thin layer of white sands. This sandy layer starts near the bank and extends into the Mojaoshan mound. The full distribution range of this layer has not yet been exposed.

Platform III 3 B2: Gray silty clay with a small amount of charcoal. The upper boundary is diffuse and wavy. 50-95cm thick.

Layer 12: Gray silty clay with wavy laminations and clear upper horizon boundary. Four sub-layers, 12A, 12B, 12C and 12D can be seen in this profile. 12A is 0-5cm thick, a loose brownish silty clay with fragments of charcoal, plant and pottery. 12B is 5-15cm thick, light gray silty clay. 12C is grayish brown, 25-35cm thick, loose, with no inclusions. 12D is 0-40cm thick, light gray with yellowish spots, with small amounts of charcoal, plant fragments and seeds. In adjacent excavation pits, three large wooden building components around four metres in length and 22 to 30cm in width have been found in Layer 12D.

Layer 13: Light brownish gray soil with clear upper horizon boundary. Whether this layer is natural or cultural cannot be identified from the field. This layer can be divided

into three sub-layers: 13A, 13B and 13C (see below for description).

The layer below Layer 13 was not excavated and sampled, and it is believed that these were pre-Liangzhu depositions.

5.2.2 Results of soil micromorphological analysis in T2621

Detailed descriptions of each micromorphology sample may be found in Appendix 2. Analytical results of the T2621 profile (Figure 5.3) will be introduced from the bottom to top layers below.

5.2.2.1 Layer 13

5.2.2.1.1 Introduction

In the preliminary stratigraphic division, Layer 13 was divided into three sub-layers by the excavator (Figure 5.3). During sampling in 2017, Layer 13 was sampled from the top and bottom of Layer 13A, the top and bottom of Layer 13B and the top of Layer 13C, which are shown in slide T2621 1, T2621 2 and the bottom of T2621 3. However, based on the soil micromorphology analysis, there is no substantial difference between Layers 13C, 13B and the bottom of 13A. The micromorphology feature of the main body of Layer 13 will be described based on slide T2621 1 and T2621 2. The top of Layer 13 will be described based on the bottom facies of slide T2621 3.

5.2.2.1.2 The main body of Layer 13: description of Slide T2621 1 and T2621 2

T2621 1 is very massive. It has a close porphyric coarse/fine related distribution. Its porosity is around 3-5%, most of the voids are 0.15 to 2mm wide, zigzag channels with irregular walls and vesicles 0.2-0.5mm in size. This fabric can be divided into 11 units and shows an alternating bedding of three facies (Figure 5.4):

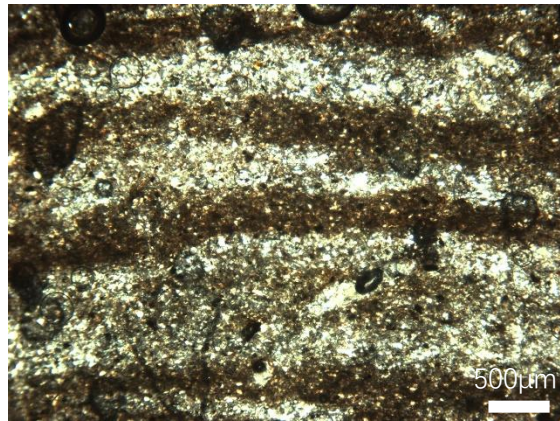
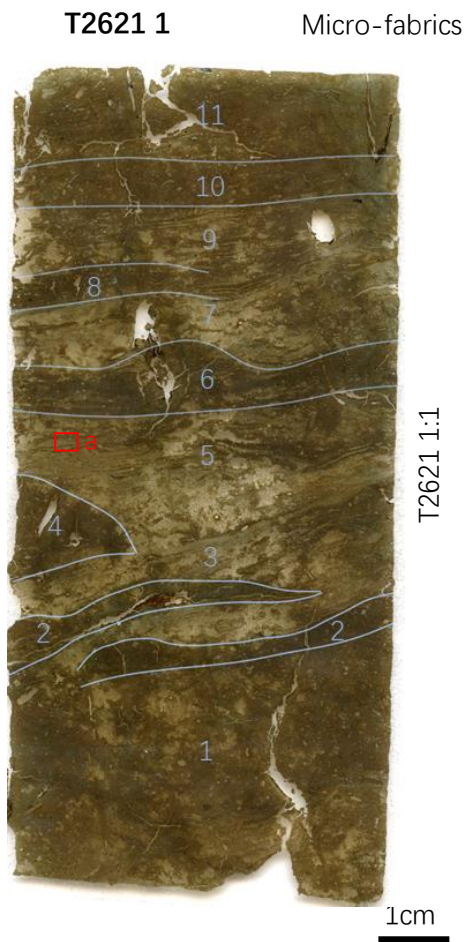
Facies 1 (Units 2/4/6/8/10): around 5mm to 1cm thick silty clay crusts composed of very compact yellowish brown (PPL) very fine silty clay mixed with randomly distributed very fine charcoal (1-2%) up to 63 microns (μm) in size. The groundmass

is undifferentiated. Only weak birefringence was observed, possibly due to the 'mask' of humic fine material. No obvious sorting of particles can be seen.

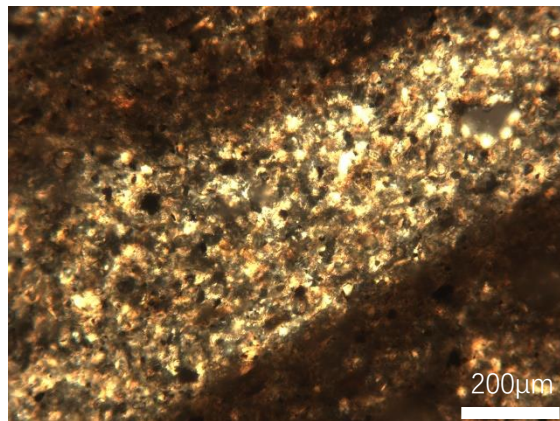
Facies 2 (Units 3/5/7/9): alternating very fine/coarse material, which is humic silty clay crusts with silt-size quartz (Figure 5.4). The humic silty clay crusts are similar to those seen in Facies 1 and are around 0.2mm thick. In some of the units, a fining upward process could be observed. The coarse material micro-layers are formed from well-sorted sub-angular coarse silt to fine sand-size quartz (60%), chlorite (5-10%), muscovite (2-3%), and calcium carbonate (3-5%), with a close porphyric c/f distribution and 70/30 c/f ratio (limit: 10 μ m). The coarse materials are weakly or very weakly oriented, and parallel to the fine materials. Most of the coarse fabric in Facies 2 has a stipple-speckled b-fabric with light yellow (PPL) dotted groundmass and weak birefringence, which may be due to the slightly greater thickness of the slide. In the thinner part of the slide, striated and weakly reticulate clay with moderate birefringence could be seen.

Facies 3 (Units 1/11): a massive version of the above two types of facies and shows poor-sorting. Loose aggregates of Facies 1 and rounded small clay aggregates possibly formed by bioturbation were found randomly accommodated in the groundmass. Segments of Facies 2 still preserve. Although difficult to identify, dense incomplete infillings of dusty silty clay material similar to the groundmass could be found.

Bioturbation including voids or fissures created by small fauna and root void was discovered over the whole slide. Thin hypo-coatings of dirty clay and hypo- and quasi-coating of amorphous sesquioxide impregnated organic matter with weak birefringence could be observed in most of the voids. A few vivianite crystals were observed in Unit 11 and a single case of pyrites spherulites was found near a void wall coated by dirty organic matter in Unit 9.



a: Alternating coarse and fine materials, XPL.



a: Mineral composition of the coarse laminations, XPL.

Figure 5.4 Slide scan and microphotographs from slide T2621 1, the numbers and lines in blue defines different units identified from this slide.

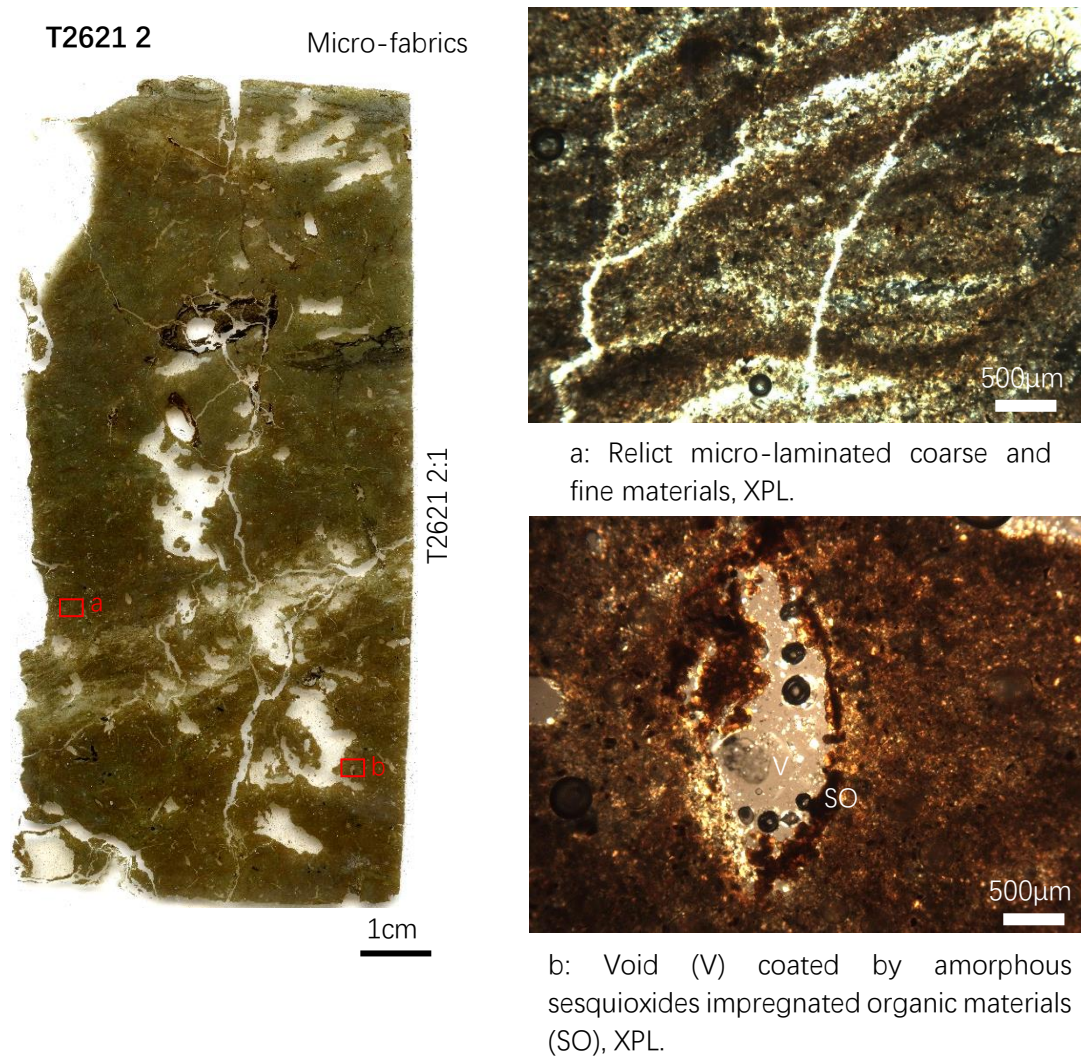


Figure 5.5 Slide scan and microphotographs from slide T2621 2

Slide T2621 2, which was sampled from the top of Layer 13B and the bottom of Layer 13A, is mainly composed of Facies 3 material (Figure 5.5). It has been heavily influenced by shrink-swell processes, linear channel infills of dusty clay and massive-type intercalations of fine fabric material from above layers have been found. More crystals of vivianite and calcium carbonate have been found. The primary microstructures are not preserved as well as in slide T2621 1, where secondary soil structures such as vertical channels and large root voids start to appear, which is suggestive of incipient soil formation process.

5.2.2.1.3 The top of Layer 13: description of the micro-fabric T2621 3:3

The groundmass of the top of Layer 13 (micro-fabric T2621 3:3) is mostly made up

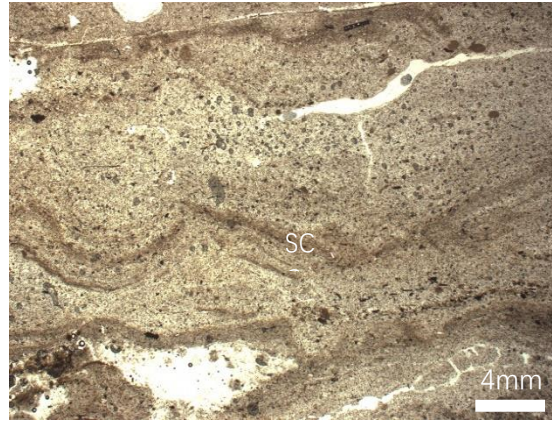
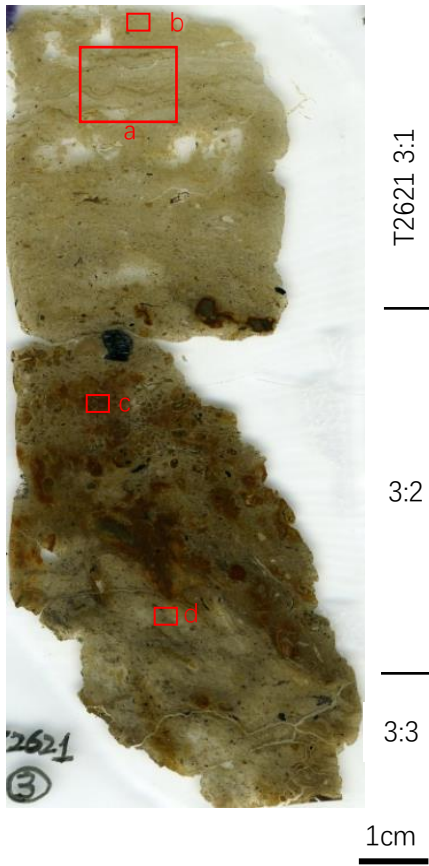
from coarse material similar to the coarse layer in Facies 2 materials with a trace amount of sand-size rock fragments (Figure 5.6). The c/f ratio is 75/25 (limit: 10 μ m), which is generally coarser than T2621 1 and 2. There are also occasional rounded clayey, dark brown soil fragments about 0.5 to 1mm in size and clusters of dirty micritic calcium carbonate nodules with diffuse boundary in the groundmass. A few pyrite spherulites have also been found.

The micromass is a mixture of light brown (PPL) dotted silty clay (15%), pale gray (PPL) micritic calcium carbonate (5-8%) and dark brown (PPL) aggregates of fine silty clay (5%), with less than 10% area stained by yellowish brown amorphous sesquioxides. The b-fabric is mixed by a stipple-speckled and a crystallitic b-fabric caused by the distribution of micritic calcium carbonates (Figure 5.6).

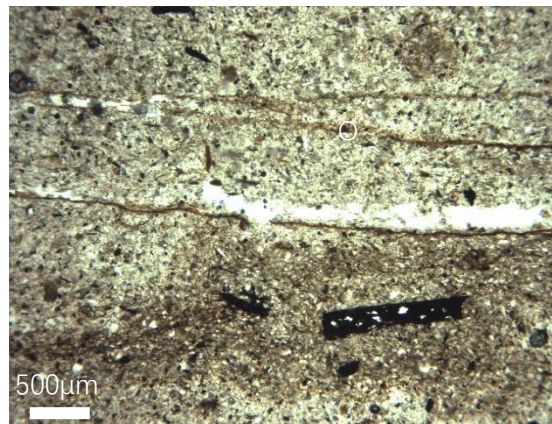
This fabric has a crack structure with 10% partially accommodated planar voids. This fabric is generally more oxidized with a few root voids and the subsequent impregnation of iron oxides observed. Calcium carbonate hypo-coatings can be observed in most voids, especially those close to the calcium carbonate nodules. No trace of illuviation of clay or fine organic matter has been found.

T2621 3

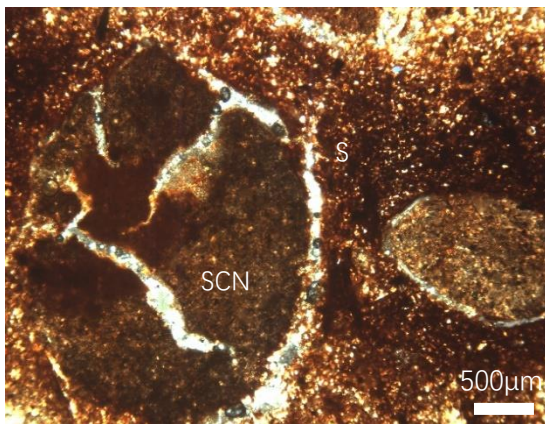
Micro-fabrics



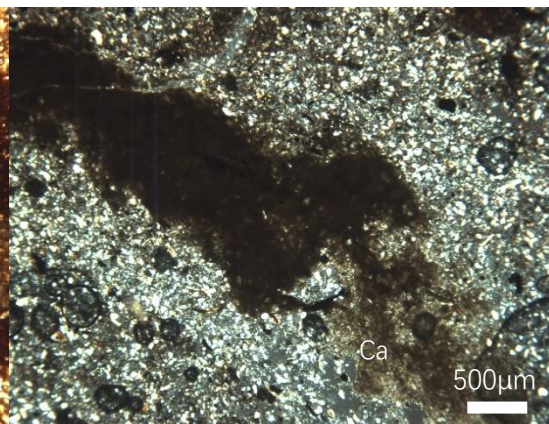
a: Fluctuating silty clay crusts (SCC) , XPL.



b: Laminated organic materials (O), PPL.



c: Rounded silty clay nodules (SCN) coated with sesquioxides (S), PPL.



d: Clusters of micritic calcium carbonate (Ca), XPL.

Figure 5.6 Slide scan and microphotographs from slide T2621 3

5.2.2.1.4 Results of bulk analysis and interpretation of Layer 13

Bulk analysis shows that the bottom of Layer 13 (bulk sample T2621 1-1) has a slightly alkaline pH, low content of P, organic matter and carbon, medium-low content of magnetic susceptibility, and medium-high calcium carbonate contents (Figure 5.7). As the sample elevations increase, the contents of pH, magnetic susceptibility, calcium carbonate, carbon and total organic show different levels of decreases (bulk samples T2621 2-1, 2-2 and 3-1), which may suggest the change of sedimentation environment in the mid-upper part of Layer 13. Combining bulk analysis results and the fact that except for some very fine soot, no anthropogenic artefacts and few disturbances of soil were found in soil thin sections or during excavation, it could be inferred that this layer is a natural layer with possible small-scale human activities observed.

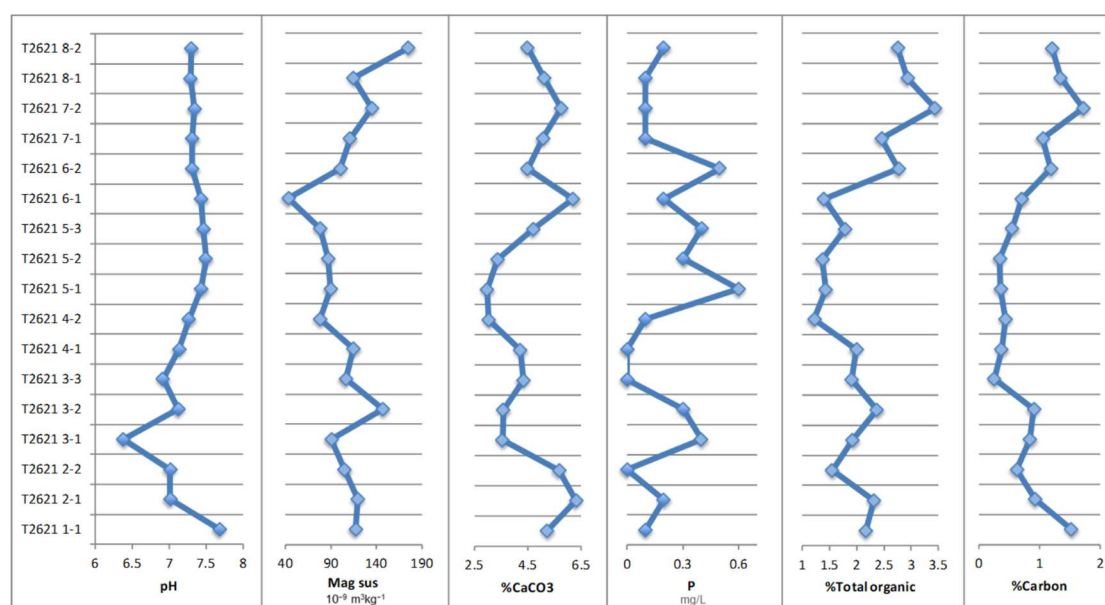


Figure 5.7 Analytical results of pH, phosphorus, magnetic susceptibility, and carbon, total organic and calcium carbonate contents of profile T2621.

In slide T2621 1, more than eighty micro-layers of silty clay crusts alternating with very fine quartz with humic silty clay (Facies 2) together with five 3-5mm thick layers of silty clay crusts (Facies 1) were found in the 12cm long thin section, most of which concentrate in the middle part of the slide. Based on micromorphology observation, all of these crusts are physical soil crusts, which are modifications of topsoil caused by physical perturbation, such as raindrop impact or sedimentation, resulting in the

development of a compacted surface layer with reduced porosity (Pagliai and Stoops, 2010). As a gradual fining upward process could be observed in some of the Facies 2 materials, combining alternating sub-millimetric coarse/fine material features, the humic silty clay crusts in Facies 2 are suspected to be depositional crusts, which are formed by lateral transport of fine particles at the surface (Bresson and Valentin, 1993; Pagliai and Stoops, 2010). Each of the fine crusts represents a fine exposed surface (Goldberg, 2000). The undisturbed and repeated occurrence of these exposed surfaces indicates that the build-up of sediment in this region is in a high frequency that does not provide enough time for soil development, and is under the constant influence of wet conditions in which no shrink-swell processes have happened. Together with the alkaline pH value and medium-high calcium carbonate content, the alternations of coarse and fine material in Facies 2 were most likely to have formed under a mudflat/intertidal flat environment.

As introduced before, Facies 3 is a massive version of Facies 1 and 2, and has been influenced by both bioturbation and shrink-swell processes. Shrink-swell processes caused by an alternating water level in clayey materials (Kovda and Mermut, 2010) have incorporated soil fabrics from above and caused big cracks to form in the soil profile which were later infilled by soil material from above and then coated by within-soil illuviated clay and organic matter. The various but discrete traces of fauna activity and plant growth indicate incipient soil development and regular wet-dry alternations in this unit.

In sum, the lower part of Layer 13, which is represented by slide T2621 1, has experienced alternating wet-dry conditions and incipient soil development in the bottom, then steady sedimentation under mudflat/intertidal flat condition in the middle part and finally switched back to alternating wet-dry conditions at the top of the slide.

In slide T2621 2 and the bottom of T2621 3, the appearance of more vivianite, infillings and bio-activities suggests that the layer has undergone greater bioturbation and shrink-swell processes. In the top of Layer 13, the clusters of micritic calcium carbonate with diffuse boundaries should be authigenic. These calcium carbonate nodules and hypo-coatings of voids may form due to the evaporation of calcium carbonate rich

groundwater, which may indicate surface exposure and drying (Durand *et al.*, 2010; Wieder and Yaalon, 1982). The absence of clay and fine material illuviation and the decrease of fine material content in the bottom of T2621 3 may imply that the dirty clay coatings in the T2621 1 and 2 were illuviated from this layer. These dirty clay coatings may come from a slurry of mixed, wet material (French, 2003; French *et al.*, 2009; Gebhardt, 1993), which suggest the input of soil material by a shallow, slow-moving soil-water slurry (Pagliai and Stoops, 2010). Together with the decrease of bulk data discussed above, the upper part of Layer 13 may be an accumulating alluvial floodplain.

In sum, the bottom of Layer 13 may be an undisturbed natural sediment formed under intertidal flat conditions. Towards the top of this layer, freshwater alluvial sedimentation environment dominates, soil formation process starts and a stable, exposed and relatively dry surface was formed.

5.2.2.2 Layer 12

5.2.2.2.1 Introduction

In the field, Layer 12 was divided into four sub-layers by the excavator (Figure 5.3). During soil sampling in 2017, Layer 12 was sampled from Layer 12D, the top and bottom of Layer 12C, the top and bottom of 12B, and Layer 12A, which are shown in the slide T2621 3 (middle and upper part), T2621 4 and T2621 5 (the bottom two fabrics). Based on soil micromorphology analysis, the groundmass of the sub-layers of Layer 12 are consistent and are generally similar to Layer 13. However, the hydrological conditions of this layer indicate several cycles of changes which led to changes in soil texture and colour during field observations. The detailed description and analysis of Layer 12 will be made following the stratigraphic division observed and recorded in the field.

5.2.2.2.2 Layer 12D

5.2.2.2.2.1 Description of micro-fabric T2621 3:2

Layer 12D is represented in the middle fabric of slide T2621 3 (Figure 5.6, micro-fabric T2621 3:2). It is heterogeneous with a coarse/fine ratio of 65/35 (limit: 10 μ m). The coarse component of the groundmass consisted mainly of well-sorted, fine silt-size, sub-angular to angular, single quartz grains with a small (5-10%) amount of muscovite and chlorite, and a few coarse sand-size rock fragments (1-2%). 60% of the fabric is moderately to heavily impregnated by reddish brown amorphous sesquioxides and the micromass is light brown to reddish brown (PPL, 40:60) with a stipple-speckled to micritic calcitic or crytallitic b-fabric (95:5). This layer has a massive structure with a few fissures. Most organic matter are amorphous, occasional root fragments and a few plant fragments of grasses can be identified. The orientation of the humified organic matter is mostly oblique or parallel to the surface. A piece of charcoal was found on top of this layer. There was also a substantial (30%) component of dark brown (PPL) rounded silty clay nodules commonly coated with reddish brown amorphous sesquioxides (Figure 5.6). These nodules are up to 8mm in size and are either mixed with micritic calcium carbonates or have incorporated vivianite crystals with weathered rims. A few 1-2mm clusters of fine Fe/Mn aggregates are also observed. Planar voids in the bottom of this layer separate Layer 13A with Layer 12D, which suggest changes of soil texture above and below.

5.2.2.2.2 Results of bulk analysis and interpretation of Layer 12D

This layer has a neutral pH, low content of carbon, total organic, phosphorus and calcium carbonate and a relatively high value of magnetic susceptibility (Figure 5.7). This high value of magnetic susceptibility may be influenced by the widely distributed oxidized Fe/Mn compounds. In this layer, the only evidence of possible human activity may be represented by the presence of a 5cm charcoal fragment observed in thin section. However, based on bulk analysis and micromorphology observation, the extent of human activity is quite low.

This layer has a distinctively common amount of silty and/or organic rich topsoil filling in the voids created by rooting, which were later surrounded by secondary amorphous iron oxides due to the oxidation and accumulation of Fe/Mn, which indicates a dry vegetational surface. The date of this layer is 3127-3007 cal. BC (52.6%; Beta-

509709) or 3331-3215 cal. BC (31.9%; Beta-509709) (Qin *et al.*, 2018 and section 5.2.3.1), preceding the great majority of human activity in or near Liangzhu City, which imply this dry surface is formed under natural process rather than human-induced activities such as dam construction or drainage. This dry surface may therefore have provided favourable conditions for human activity and occupation. Besides the charcoal observed in the thin section, archaeological finds including small amounts of charcoal, seeds, plant fragments and three large wooden building components from four metre in length and 22 to 30cm in width were also found in Layer 12D (Liu *et al.*, 2019a). Considered together these features may indicate the beginnings of human activity accompanied by the possible construction of large houses in nearby areas.

5.2.2.2.3 Layer 12C

Layer 12C is a grayish brown, 25-35cm thick layer with wavy laminations and no inclusions. This layer has been shown in micro-fabrics T2621 3:1 and 4:3.

5.2.2.2.3.1 Layer 12 C: Description of the micro-fabrics T2621 3:1 and 4:3.

The groundmass of Layer 12C from the bottom to the top is basically the same. This layer has an 80/20 c/f ratio (limit: 10 μ m) and a close porphyric c/f related distribution pattern. The coarse materials are composed by well-sorted silt-size and fine sand-size sub-angular quartz grains (80%) and 3-5% micas including muscovite, chlorite, and biotite, and a few very coarse sand-size volcanic rock fragments. Trace amounts of iron nodules and authigenic Fe/Mn micromass and a few rounded fragments of clayey soil fabrics are found randomly mixed in the groundmass. The organic components (5%) of this layer are mostly found as amorphous organic fine material with a weak trend of horizontal distribution in the middle and bottom part, and micro-laminated organic matter in the upper part. This layer has a massive microstructure with a few planar voids and 6% porosity, most of the voids are small root voids with remnant amorphous organic matter. The micromass is composed of a light yellow (PPL) fine material with a stipple-speckled to striated b-fabric. Trace amounts of micritic calcium carbonate were mixed in with the groundmass.

Alternation of coarse/fine materials were shown throughout this layer, which is similar to the Facies 2 fabric in T2621 1 (section 5.2.2.1.2). In the bottom of this layer (micro-fabric T2621 3:1) the sediment varies from a previous highly disturbed vegetation layer (Layer 12D) to less disturbed fabrics with clear horizontal wavy lamination in the upper part. Parallel striated clay mineral can be observed in the fine crusts. The coarse material is very weakly oriented. And then the upper part of this layer (micro-fabric T2621 4:3) exhibit a clear fining upwards and parallel oriented coarser layers (Figure 5.8). At the top of Layer 12C, the laminations were slightly disturbed.

5.2.2.3.2 Results of bulk analysis and interpretation of Layer 12C

This layer has a neutral pH, very low content of P, carbon and total organic, and slightly lower content of magnetic susceptibility and calcium carbonate (Figure 5.7), which in general suggests a low degree of human activity.

Based on micromorphology observation, the sediments transit from slightly bioturbated to undisturbed and then to back to slightly disturbed crusts. Although a few root voids have been found, the plant growing period should be ephemeral as most of the laminations have been left intact. During this process, the fining upward and oriented coarse material indicate that the hydrodynamic force has decreased, and these fine laminations are formed under a shallow water ponding environment (Karkanis & Goldberg, 2018). This layer could be a natural layer with no trace of human activity being observed.

5.2.2.4 Layer 12B

Layer 12B is 5-15cm thick, light gray silty clay. Based on the variation of hydrology and soil inclusions, this layer can be divided into four sub-units (Figure 5.8 and 5.9) and were named Unit 12B-1, Unit 12B-2, Unit 12B-3 and Unit 12B-4. The first two units were represented in the upper part of slide T2621 4 with diffuse boundaries. The remaining two units are located in the bottom part of slide T2621 5 with clear boundaries.

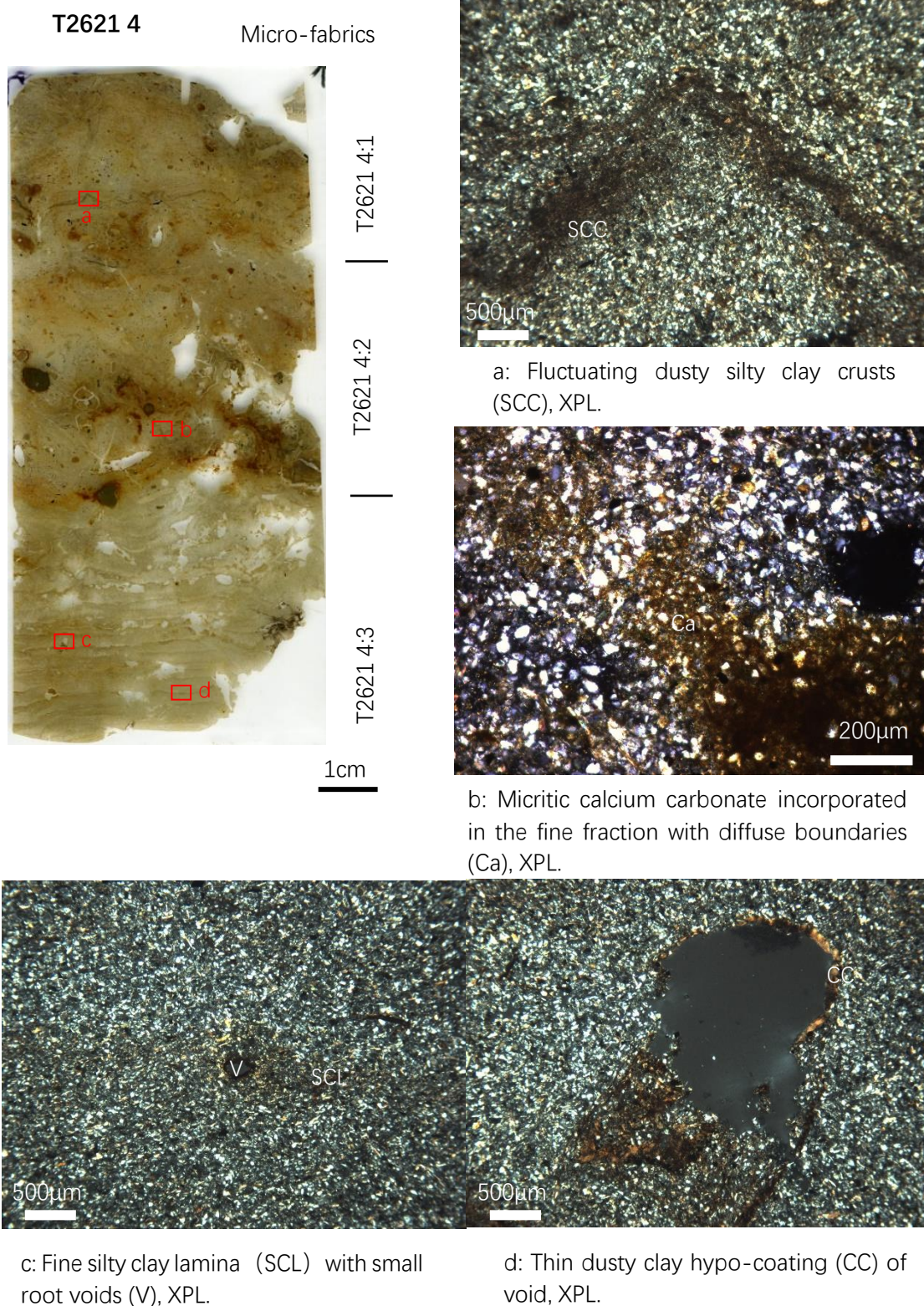


Figure 5.8 Slide scan and microphotographs from slide T2621 4

5.2.2.2.4.1 Units 12B-1 and 12B-2: Description of the micro-fabrics T2621 4:2 and 4:1

The first two units of Layer 12B have a very similar mineral composition with Layer 12C but are different in groundmass and pedofeatures. In Unit 12B-1 (Micro-fabric T2621 4:2), 10% micritic calcium carbonate is incorporated in the fine fraction and mostly seen as hypo-coatings and quasi-coatings of voids with diffuse boundaries (Figure 5.8b). The micromass is light yellow (PPL) with stipple-speckled to calcitic crystallitic b-fabric (90:10). 15% of the fabric is moderately to heavily impregnated by red (PPL) amorphous sesquioxides, mostly found around voids/silty clay aggregates with diffuse boundaries. A few humified amorphous tissue residues are randomly distributed throughout. This unit has a massive microstructure with a few root voids with remnant amorphous organic matter. A few complete dense infillings of brown (PPL) calcitic clayey or silty topsoil are found in root voids and are commonly coated by amorphous iron oxides (Figure 5.8). A few light brown (PPL), rounded fragments of clayey soil fabrics and trace amounts of thin hypo-coating of micro-laminated dusty clay around voids are observed.

Unit 12B-2 (Micro-fabric T2621 4:1) has a diffuse and faint boundary with the Unit 12B-1. It shows similar features with the Unit 12B-1 except that the groundmass of Unit 12B-2 contains less calcium carbonates and is less impregnated by amorphous sesquioxides. What is more, five to six layers of micro-laminated and slightly fluctuating dusty fine silty clay crusts appears again and occupies 5% of the fabric. The humified tissue residues (3%) are laminar distributed or found around root voids.

5.2.2.2.4.2 Unit 12B-3: Description of the micro-fabric T2621 5:4

The groundmass of this sub-layer is basically the same as Units 12B-2 and 12B-1, but is poorly sorted with a higher content of fine fraction (c/f: 70/30; limit: 10 μ m) and is very heterogeneously mixed with rounded clayey soil fragments and fragmented, thick, dark brown (PPL) dusty silty clay crusts, especially on the top of this sub-layer (Figure 5.9). A few small pieces of charcoal and shell were randomly mixed in the groundmass. The b-fabric is undifferentiated, probably due to the 'mask' of humified organic matter and a thicker slide thickness. The boundary between this layer and Unit 12B-4 is distinct (Figure 5.9).

5.2.2.2.4.3 Unit 12B-4: Description of the micro-fabric T2621 5:3

The groundmass of the top of Layer 12B is similar to the rest of Layer 12 introduced before, but with poorer sorting. This layer also has massive structure but with a few interconnected zigzag channels with slightly serrate void walls. The micromass is light brown with an undifferentiated b-fabric due to the 'mask' of humified organic matter. A few fragments of dark brown clayey organic topsoil, micro-charcoal and humified tissue residues were found randomly mixed in the groundmass.

In this layer, clear depletion of Fe/Mn in the groundmass can be observed. Iron-rich clay hypo-coating of voids with sharp and contrasted boundaries with the groundmass were commonly seen. The boundary between this layer to the above Layer 12A is very sharp with a slightly undulating shape (Figure 5.9). No obvious evidence of compression or trampling was observed.

5.2.2.2.4.4 Results of bulk analysis and interpretation of Layer 12B

Layer 12B has a slightly alkaline pH and a very low content of all other variables (Figure 5.7). Based on micromorphology observation and bulk analysis, although a few charcoals are mixed in the groundmass, this layer is generally a naturally formed layer.

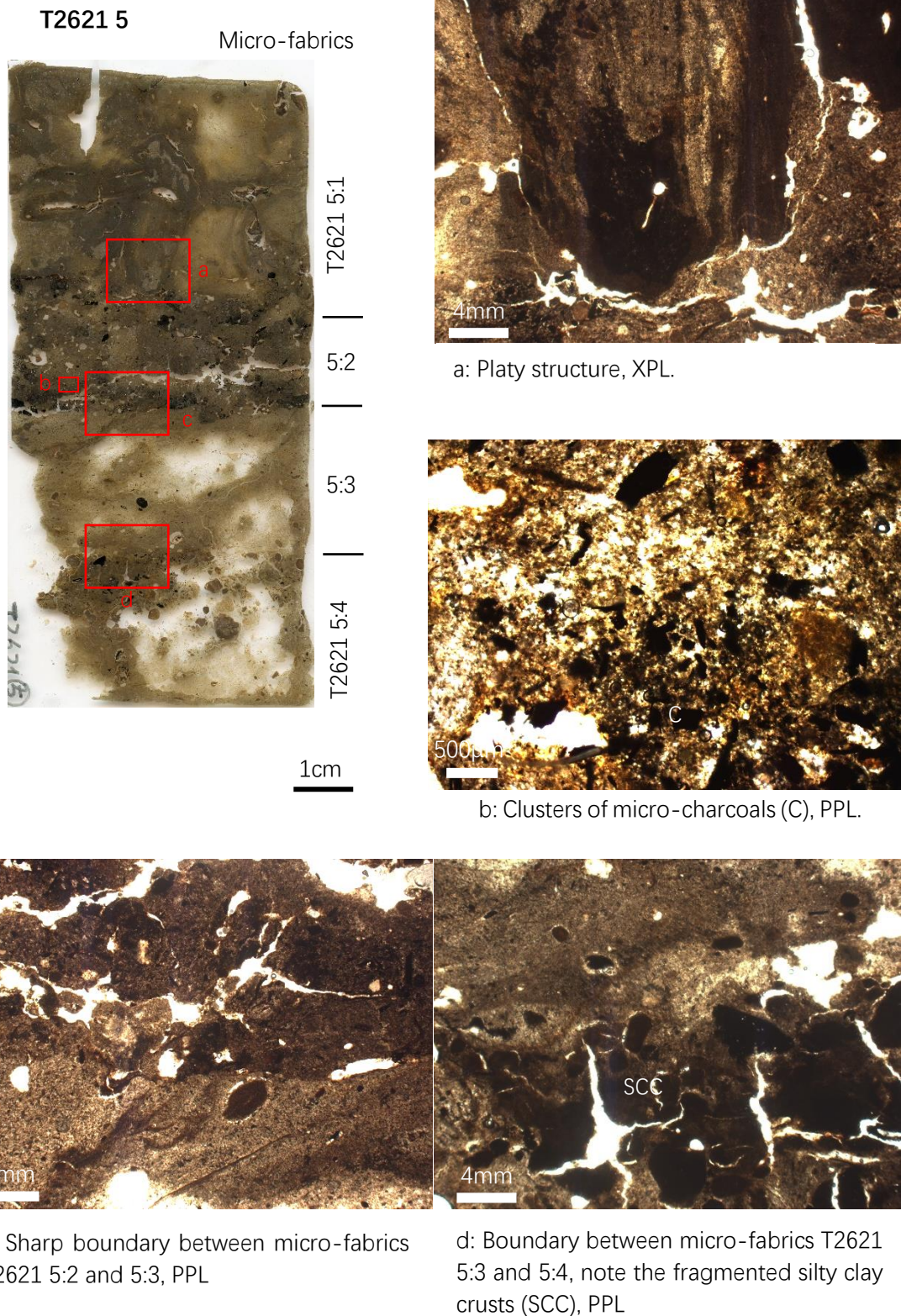


Figure 5.9 Slide scan and microphotographs from slide T2621 5

In Unit 12B-1, the sediments were deposited under slightly oxidized and dry conditions with bioturbation, and has a vegetation zone similar to Layer 12D. The transitional zone to Unit 12B-2 has a lower level of bioturbation and plant growth. Unit 12B-2 is under

the short-term influence of run-off which is similar to the bottom layer of 12C. Unit 12B-3 is highly bioturbated with dense vegetation growth. On top of this unit, a thick layer of silty clay crust was formed but was afterwards broken down into partially interconnected clods possibly due to drying and bioturbation. Unit 12B-4 is under the influence of periodic waterlogging again with less bioturbation. These features suggest that the hydrological condition of this layer has shifted from relatively dry conditions to wet surface and then back to a dry exposed surface and finally back to a slightly wet condition.

The top of Unit 12B-4 may be modified by human activity such as levelling or fetching of soil material, and the upper Layer 12A was directly dumped on the Unit 12B-4 (please refer to Section 5.2.2.2.5).

5.2.2.2.5 Layer 12A

This layer is about 3cm thick. In the field, this layer cannot be clearly identified due to the similarity of soil texture and colour caused by long-term water stagnation. This layer was found sandwiched by Layer 12B and Platform III 3 B2 (Figure 5.9).

5.2.2.2.5.1 Layer 12A: Description of the micro-fabric T2621 5:2

This layer is very heterogeneous and has mixed clusters of charcoal fragments (1 to 5mm in size) within the brown (PPL) very humic silty clay groundmass with an undifferentiated b-fabric (Figure 5.9). The groundmass has a similar mineral component to Layer 12B. Amorphous organic coarse and fine material, fresh plant tissue and amorphous iron replaced plant tissues are also randomly mixed in the sediment, including a discontinuous inclined bedding of humified plant residues that separates different soil fabrics. This layer has a channel and vesicular microstructure, a 5cm long, horizontal planar voids cut off the fabric and vesicles 1 to 3mm in size commonly seen in the groundmass. Very dusty silty clay hypo-coatings were widely found around voids. A concentric dirty clay and a few vivianite crystals with a weathered rim were observed in the upper part of this layer.

5.2.2.2.5.2 Results of bulk analysis and interpretation of Layer 12A

The results of bulk analysis of this layer is similar to Layer 12B (Figure 5.7). The random mixture of charcoal clusters, different orientations of organic matter and sharp boundaries between lower and upper layers indicate that this layer could be a heavily modified layer deliberately prepared and dumped by humans. The closely fitting clusters of charcoal and the appearance of vesicles and channels suggest that these materials were dumped when wet and then compacted. The cracks may form due to the rapid drying of this wet material.

5.2.2.2.6 Summary of Layer 12

All the four sub-layers of Layer 12 (Layers 12A, 12B, 12C and 12D), are represented in the T2621 profile. In the first three sub-layers (12B, 12C and 12D), at least three large dry-wet cycles can be identified through micromorphological observation. 12D is the first dry and exposed surface with direct evidence of human activity in profile T2621 because the charcoal fragment observed from thin section and the large timber components found in nearby excavation pits. 12C experienced long-term stagnation shown by the alternation between fining upward silty clay crust and fine sand-size quartz. In 12B, dry and wet sedimentation alternated back and forth. Although traces of human activity have been found, the sedimentation of these 35cm thick sub-layers were mainly influenced by natural forces such as rainfall events, alluvium floodplain deposition and/or channel infillings. The modification of the landscape in this location is still limited. However, Layer 12A, although being classified as a sub-layer of Layer 12 by the excavator, is more likely to be a man-made mound based on soil micromorphological observation and should be classified as a separate stratum.

5.2.2.3 Platform III3 B2

In the field, this layer is believed to be the second stage of a near-bank mound in the Middle Zhongjiagang Watercourse. The bottom of this mound was sampled close to the surface of a slope covered by grass, which is shown in the micro-fabric T2621 5:1. In the profile, more than 30cm long vertical cracks are found extending from the top of

the slope to the bottom of Platform III 3 B2, with yellow spotting near the root voids. The top of Platform III 3 B2 is represented in the micro-fabric T2621 6:3.

5.2.2.3.1 The bottom of Platform III 3 B2: Description of the micro-fabric T2621 5:1

This layer is a heterogeneous mix of two different soil materials with clusters of charcoal fragments (Figure 5.9). The first soil material (70% of the fabric) acts as groundmass and its coarse material and organic matter is similar to the soil material from Layer 12B. Its micromass has a similarly yellowish colour and stipple-speckle to randomly striated b-fabric. The clustered fragmented charcoal (2-3%) were randomly mixed in this soil material. 2-3% of humified very fine charcoal was also randomly mixed in with the groundmass with no orientation. The second soil material shows an inverted direction of iron impregnated clay laminations. This soil material is organic rich and its micromass is brownish in colour. Platform III 3 B2 in general has a massive microstructure with 3-5% chambers in the second soil material and a few vesicles in the matrix material. In these chambers, incomplete dense infillings of micro-laminated very dusty silty clay and small aggregates (0.5mm) of fine charred materials and clusters of crystalline vivianite were widely found. In the matrix soil material, depletion hypo-coatings of dusty silty clay around voids are commonly seen, with some impregnated by reddish yellow (PPL) amorphous sesquioxides.

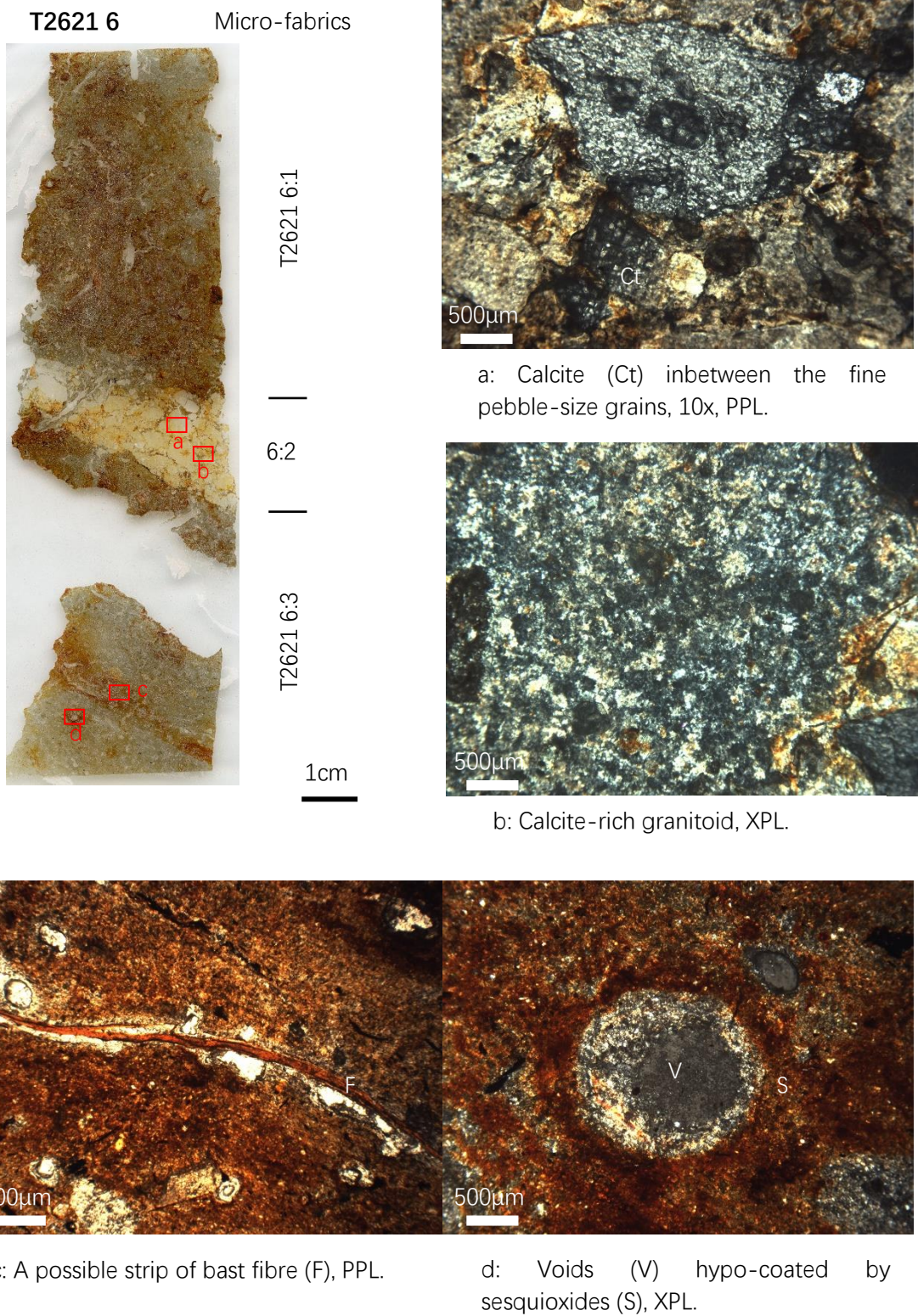


Figure 5.10 Slide scan and microphotographs from slide T2621 6

5.2.2.3.2 The top of Platform III3 B2: Description of the micro-fabric T2621 6:3

The groundmass of the top of Platform III3 B2 is very similar to the sediments from the channel infill, such as Layer 12B, with a trace amount of medium sand-size rock fragments. Around 60% of the groundmass is impregnated by amorphous iron oxides, which are more concentrated near the voids.

This layer has a weakly developed sub-angular blocky microstructure, partially accommodated planar voids, with vesicles 0.5 to 1mm in size and 5-8% porosity. In the iron-depleted groundmass, the micromass is light yellowish in colour with striated b-fabric. A few weakly laminated small charcoal fragments and a possible strip of bast fibre was found incorporated in the groundmass (Figure 5.10). Pedofeatures such as iron depleted hypo- and quasi-coatings of voids with diffuse boundaries and thin dusty clay quasi- and hypo-coatings of voids with high birefringence were commonly observed (Figure 5.10).

5.2.2.3.3 Results of the bulk analysis and interpretation of Platform III 3 B2

The bulk analysis shows that Platform III 3 B2 has a slightly alkaline pH, moderate content of P and low magnetic susceptibility, and low carbon, total organic and calcium carbonate components (Figure 5.7), which suggest a low degree of human activity.

The groundmass of the bottom of Platform III 3 B2 was a mixture of two different soil materials with charcoal clusters, probably all under saturated condition. The matrix material may be the natural sediment similar to Layer 12B. The clusters of charcoal are probably anthropogenic. These two materials are most likely artificially mixed and dumped by Liangzhu people, evidenced by close compaction between these two materials and random orientations of organic matter in the matrix. The second soil material may be later period or even contemporary organic topsoil fallen from long cracks formed due to the shrink-swell of the clay-rich matrix. The channels or chambers were also created due to the shrinkage of clay-rich material, which were later infilled by amorphous iron oxide impregnated illuviated clay material.

The top of Platform III 3 B2 was an exposed surface where plants grow, which produced root voids that were then filled with infillings and impregnated with secondary amorphous iron oxides. The depletion of the groundmass with iron hypo- and quasi-coatings of voids indicates the drainage of previously saturated horizons (Lindbo *et al.*, 2010). The matrix of this part does not show any obvious mixture of different soil material but is mostly made up of soil material similar to natural sediments in Layer 12B.

In sum, Platform III 3 B2 is a human-dumped layer using soil material from natural sediments probably from nearby older buried soils. The hydrological conditions have shifted from long-term wetness to relatively dry conditions at the top.

5.2.2.4 Platform III 3 B1

A layer of sands has separated the Platform III 3 B2 and Platform II 1A (Figure 5.3). The excavator named this layer as Platform III 3 B1, which is represented in the micro-fabric T2621 6:2.

5.2.2.4.1 Platform III 3 B1: Description of the micro-fabric T2621 6:2

This 2cm thick layer is sandwiched between Platform III 3 B2 and Platform III 1A and is very compact. This layer contains mainly 2-5mm whitish to light yellowish, very fine to fine gravel. Most of the gravels are granitoids with 30-40% calcite (Figure 5.10). Around 5% forsterite and a few calcites (Figure 5.10) were also observed in-between these granitoids. These rock fragments were commonly coated by red (PPL) silty clay moderate to heavily impregnated by sesquioxides with moderate to high birefringence and a parallel striated b-fabric.

5.2.2.4.2 Results of the bulk analysis and interpretation of Platform III 3 B1

The bulk sample T2621 6-1 was sampled from the Platform III 3 B1 and has a very low magnetic susceptibility and a relatively low content of phosphorus, carbon and total organic (Figure 5.7). However, the content of calcium carbonate is quite high in this

layer, which is coincident with the micromorphology observation. The low magnetic susceptibility suggests that this layer has not been burnt. These calcite-rich granitoids are similar to the local whitish marble widely mined in Hangzhou Region nowadays, which is named 'Hang Gray Marble' and is famous for its uniform grayish colour and fine texture (Zhang, 1994). Based on the size and angularity of these gravels, they are more likely to be collected from a nearby riverbed and have only been simply prepared as a kind of 'plaster' or paving stones.

5.2.2.5 Platform II 1A

Platform II 1A is believed to have been constructed during the third stage mound construction in the Middle Zhongjiagang. This layer is around 30cm thick. The bottom of this layer is presented in the top of slide T2621 6. The major part of this mound, with a short intercalation of carbon observed in field, is shown in slide T2621 7. The top of this layer is present in the bottom of slide T2621 8.

5.2.2.5.1 Platform IIIA: Description of the micro-fabrics T2621 6:1, 7:2, 7:1 and 8:1

From the bottom to the top of Platform IIIA, the composition of the sediments is generally similar. This layer is significantly coarser compare to previous layers. It is composed of clusters of sub-angular medium sand to very coarse sand-size rock fragments which occupies 25-35% of the sediment, and 45-60% silt and 15% clay with high birefringence (Figure 5.10, 5.11 and 5.12). A few very fine pebbles are also occasionally mixed in the groundmass. Most of the rock fragments are quartz and quartzite with a few feldspars, rhyolites and iron-rich volcanic rocks that are commonly seen in nearby mountainous areas. 40-70% of the groundmass is impregnated by reddish yellow (PPL) amorphous sesquioxides, unimpregnated part is light yellow (PPL). This layer has a stipple-speckled to random striated to porostriated b-fabric (60:30:10) and a single space to close porphyric c/f related distribution.

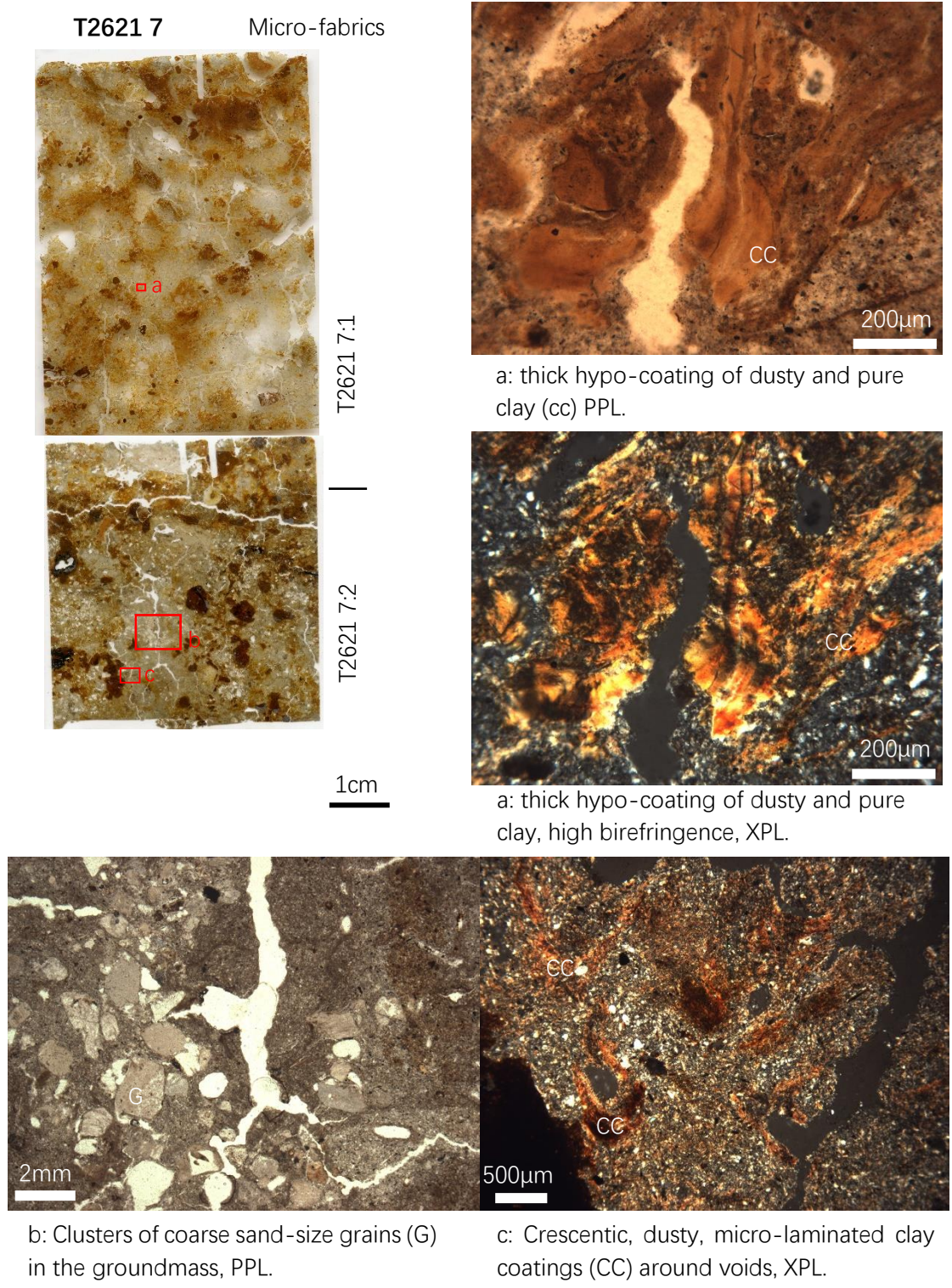


Figure 5.11 Slide scan and microphotographs from slide T2621 7

This layer has a moderately developed sub-angular blocky microstructure with partially accommodated channels and a few vesicles 0.5-1mm in size (8-10% porosity). A few randomly distributed dark brown to black amorphous organic fine material/micro-charcoal are also mixed in the groundmass. Secondary amorphous iron nodules with

both clear and diffuse boundaries are widely found, and depletion of the groundmass is clearly observed in the bottom of this layer. Textural pedofeatures are frequently observed (Figure 5.11 and 5.12). Around 1mm thick crescent dirty clay hypo-coatings with high birefringence and clear extinction band are widely found around voids. Compound clay coatings such as alternations of light grayish (PPL) and yellowish (PPL) clay in crescentic clay hypo- and quasi-coatings, crescentic dirty clay coatings in the bottom with link cappings of limpid clay were occasionally observed. A few bright orange (XPL), very limpid clays with very high birefringence and strong extinction were incorporated in the groundmass as fragments (0.2-1mm), infillings (0.1 to 1mm) and thin coatings of voids and grains.

It should be noted that, in the middle of slide T2621 7, a 1-2cm thick concentration of granitoid rich in calcite, which is similar to the Platform III 3 B1, was observed. On top of the rock fragments, a few thin laminations of fine material were observed, which may indicate levelling activity on top of these calcite-rich marbles. In the upper part of this layer, several pieces of daub 0.5 to 2.5cm in size were mixed in the sediment, and a layer of rotten wood was found (Figure 5.12).

5.2.2.5.2 Results of bulk analysis and interpretation of the Platform II 1A

From the bottom to the top of Platform III 1A, the magnetic susceptibility values gradually increased. The peak value at the top may be influenced by the daub mixed in the groundmass. The content of carbon and total organic also increased but are still lower than the average number of the Liangzhu region. The content of phosphorus is extremely low except the bottom of this layer. The calcium carbonate content is slightly higher than the average number (Figure 5.7).

Similar to Platform III 3 B2, the major part of Platform II 1A was composed of sediments very similar to channel infills, but mixed with rock fragments and coarse sand from nearby riverbed or mountainous area. The mixture of fragmented limpid clay in the groundmass may possibly be due to the physical modification of the sediments and strong shrink-swell process as indicated by the cross-striated and grano-striated b-fabrics. The alternation of dusty and clean clay coatings, the appearance of thick, clean

clay coating, and the vesicles microstructure produced by water or air escape denote the possible involvement of water during the preparation of this construction material. The widely observed secondary amorphous iron oxide component may also be related to plant growth and rooting due to the closeness to the surface.

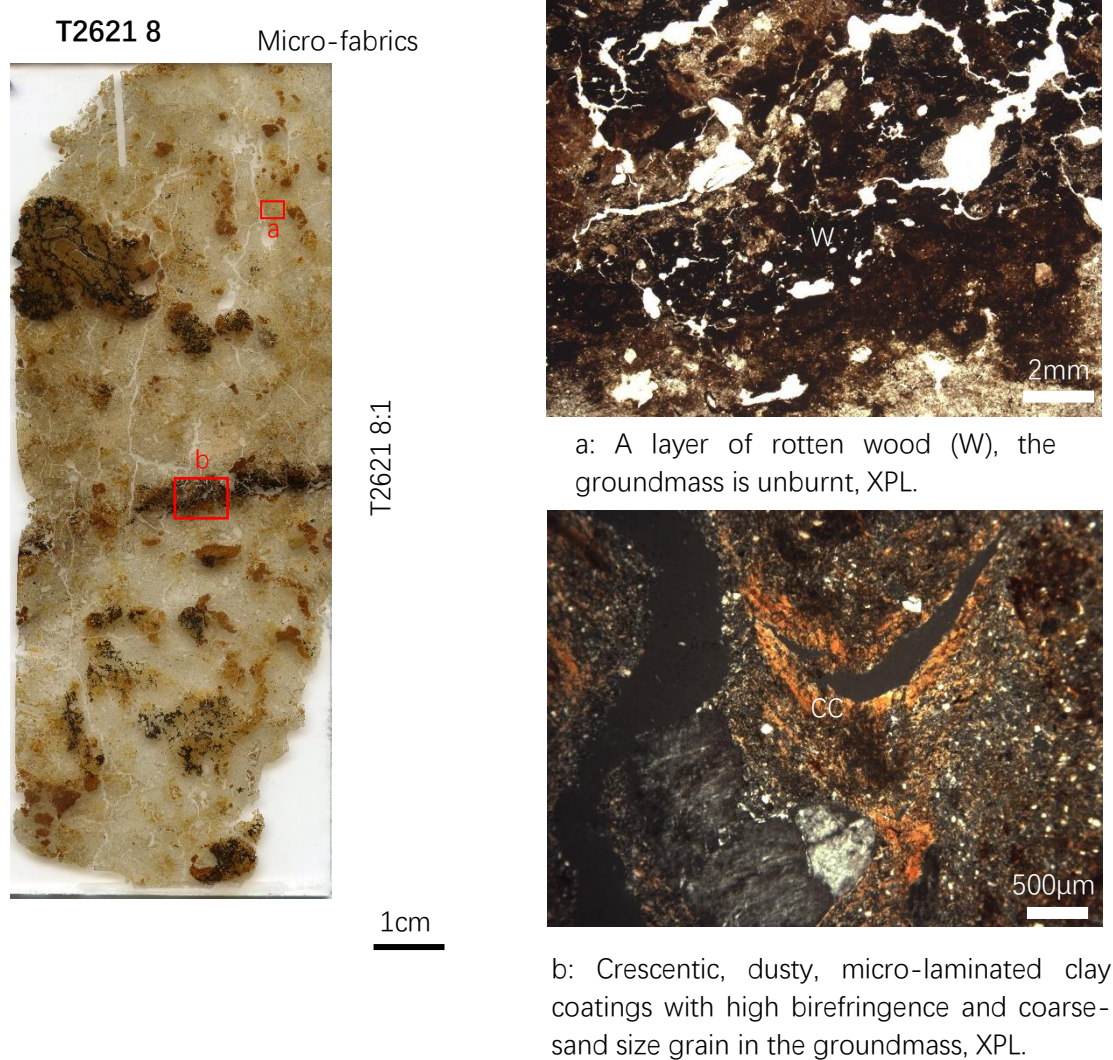


Figure 5.12 Slide scan and microphotographs from slide T2621 8

Generally speaking, Platform IIIA is a layer of man-made mounding material with the coarse sands deliberately mixed in, interrupted by 1-2cm thick, thin layer of calcitic granitoid.

5.2.3 Interpretation of the Middle Zhongjiagang region

In this section, the site formation processes observed in the Middle Zhongjiagang profile will be discussed based on the results of dating data, particle size analysis, soil

physical and chemical properties and soil micromorphology.

5.2.3.1 Dating of the Middle Zhongjiagang region

During the 2017 excavation, plant remains selected from flotation samples of T2621 and nearby excavation pits were sampled and dated in the Archaeometry & Archaeological Dating Laboratory in Peking University, China (Qin *et al.*, 2019). Unfortunately, samples from Layer 12D and Platform II did not provide useful dating data. Dating of Platform III and its associated rubbish layer provided the only directly available radiocarbon dating for profile T2621, and the results show that the construction of Platform III starts from 2993-2896 cal. BC (95.4%) or 2936-2904 cal. BC (68.2%) and ends in 2912-2841 cal. BC (95.4%) or 2903-2876 cal. BC (68.2%). Although there is no available dating in Platform II, the Platform I, which directly overlies Platform II, is dated from 2700 cal. BC, which provides a lower limit of date for Platform II. Therefore, it can be speculated that the construction period of Platform II is between 2850 cal. BC and 2700 cal. BC.

To further understand the dating of Middle Zhongjiagang region, plant remains from the Middle Zhongjiagang profiles were tested in the Beta-Analytic Radiocarbon Dating Laboratory in 2019 (Table 5.1, data from ZPICRA). A sample taken from the bark of the wooden structure from Layer 12D was dated to 3127-3007 cal. BC (52.6%; Beta-509709) or 3331-3215 cal. BC (31.9%; Beta-509709). Plant stem material from Platform III is dated to 3029-2904 cal. BC (89.8%; Beta-509710), which coincides with the pre-existing data from Peking University (Qin 2019). Wood material from layer 11A, which lies between Platform III and Platform II and is believed to be the waste accumulation during the use of Platform III, is dated to 3029-2904 cal. BC (89.8%; Beta-509714). The grass from Platform II is dated to 3115-2921 cal. BC (82.7%; Beta-509715), which is slightly earlier than Platform III and Layer 11 below it. Combining these with the results from the soil micromorphology analysis, these slightly earlier dates are probably due to the use of soil material from an earlier stratum in Platform II. The bamboo and tree leaf from Layer 10B, which directly overlies Platform II, are dated to 2874-2621 cal. BC (95.4%; Beta-509711) and 2814-2737 cal. BC (47.7%; Beta-509712). Combining the dating data from both Peking University and Beta-

Analytic, the date of Platform II should be around 2900-2800 cal. BC.

Table 5.1 Radiocarbon dating of the Middle Zhongjiagang region.

	Peking University		Beta-Analytic Lab		
	Calibrated date	Sampling position	2 σ (95.4%) Calibrated date	Sampling position	Lab No.
Stage 1	No data		(52.6%)3127-3007cal BC (31.9%)3331-3215cal BC (6.4%)2988-2931cal BC (4.6%)3186-3156cal BC	T2321-2322h14	Beta-509709
Stage 2	From 2936-2904BC (68.2%) or 2993-2896BC (95.4%) to 2903-2876BC (68.2%) or 2912-2841BC (95.4%)	Platform III and Layer 11	(89.8%)3029-2904cal BC (5.6%)3085-3064cal BC	T2421-2422 East Wall Platform III②A	Beta-509710
			(89.8%)3029-2904cal BC (5.6%)3085-3064cal BC	T2521-2522①A1	Beta-509714
Stage 3	No data		(82.7%)3115-2921cal BC (7.1%)3266-3236cal BC (5.0%)3321-3272cal BC (0.6%)3171-3163cal BC	T2723-2724 T1 Platform II②	Beta-509715
			(95.4%)2874-2621cal BC	T2421-2422⑩B	Beta-509711
			(47.7%)2814-2737cal BC (33.3%)2900-2848cal BC (14.5%)2731-2679cal BC	T2521-2522⑩B	Beta-509712
			No data		
Stage 4	2700-2500BC	Layer 9c/9a/7	No data		
Stage 5	2650-2500BC	Layer 4 and Pottery J1	(95.4%)2578-2457cal BC	Pottery J1	Beta-509717

Based on soil micromorphology observations, Layers 12 and 13 are indicative of natural sedimentation under the minor influences of human activity. Layer 13 should therefore be dated earlier than Layer 12, which is before 3127-3007 cal. BC (52.6%; Beta-509709) or 3331-3215 cal. BC (31.9%; Beta-509709).

In sum, in profile T2621, Layer 13 represents sediments accumulated through alluviation before the construction of Liangzhu City. Layer 12 represents the first stage of human activity in this region at around 3127-3007 cal. BC (52.6%; Beta-509709) or 3331-3215 cal. BC (31.9%; Beta-509709), which is slightly before the construction of the Mojiaoshan Mound that is dated to 3000-2800BC (Qin *et al.*, 2019). Platform III 3 B2 indicates the second stage of mound construction at Middle Zhongjiagang region at around 3000-2900 cal. BC. Platform II 1A represents the third stage of mound building at around 2900-2800 cal. BC.

5.2.3.2 Particle size analysis of the T2621 profile

17 samples from profile T2621 have been subjected to particle size analysis. Based on the different characteristics in the frequency histogram (Figure 5.13), these samples can be grouped into two major groups. The first group has a single peak, which generally indicates the good-sorting of particles in the soil material. The second group has multiple peaks, which suggests a more diverse set of sources of the soil material.

Generally speaking, the results of the particle size analysis coincide with the field and micromorphological observations, and provide more details about the relationships between each layer.

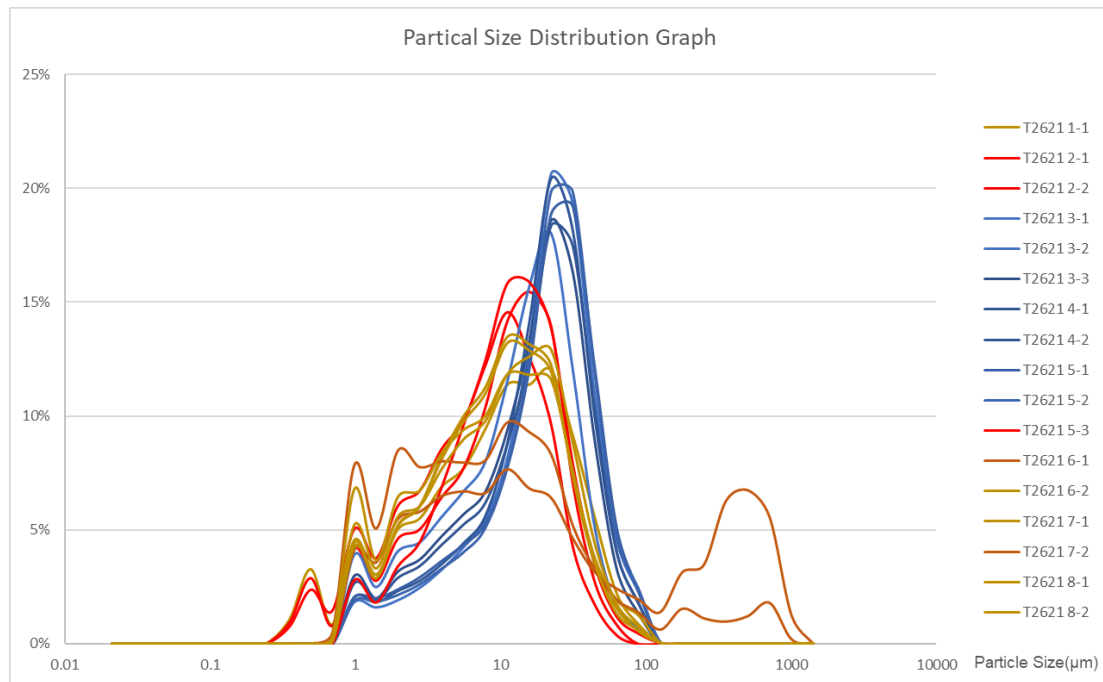


Figure 5.13 Particle Size Distribution Graph of T2621.

In the first group, two sub-groups can be further distinguished. The first sub-group has a high narrow peak with a D50 particle size of around 23 microns. This was seen in samples T2621 3-1, T2621 3-2, T2621 3-3, T2621 4-1, T2621 4-2, T2621 5-1, T2621 5-2, which were sampled from the top of Layer 13B, Layer 12D, 12C, 12B and 12A. These results indicate that excluding the impact of organic matter, Layer 12 and the top of Layer 13B have a similar well-sorted source material most likely from natural forces. The second sub-group has a wider single peak with a lower D50 particle size of around 11.6 microns and is constituted by samples T2621 2-1, T2621 2-2 and T2621 5-3, which are sampled from the top of Layer 13C, the bottom of Layer 13B and the bottom of Platform III 3 B2. This sub-group is less well-sorted, probably formed due to natural processes, and generally has a finer mean particle size compared to the first sub-group. The similarity in particle size between the bottom of Platform III 3 B2 and Layer 13C also support the observation from micromorphology that the construction of Platform III 3 B2 has used soil material from an older stratum nearby.

The second group has multiple peaks in the particle size distribution graph and is likely to have multiple sources of particles. All samples except one from the top of Layer 13D are from platform layers. Among these samples, samples T2621 6-1 and 7-2 were sampled from the stony layers of Platform III 3 B2 to Platform II 1A and therefore has obvious peaks from 100 to 1000 microns.

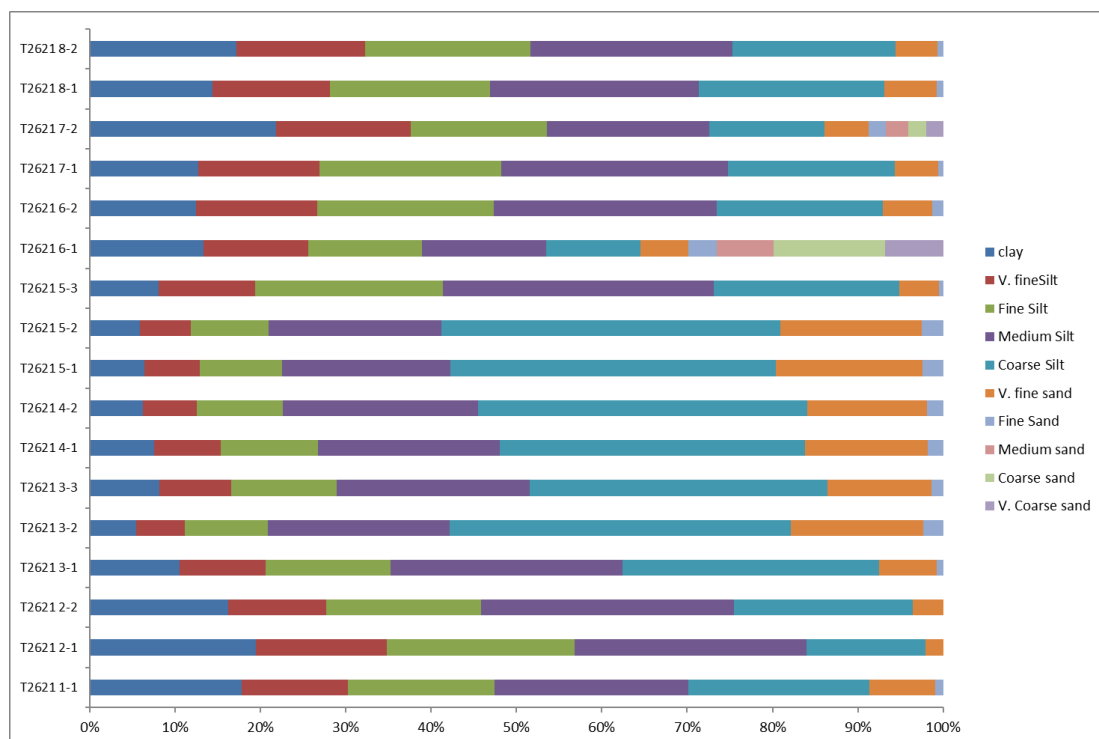


Figure 5.14 Percentage bar chart of the particle size of T2621.

The percent bar chart (Figure 5.14) shows that the T2621 profile is generally dominated by silt-size particles. Samples from Layer 12 show obvious decline in clay content and increase in very fine sand size particles, which suggest a higher sedimentation dynamic. In general, there is a major change of sedimentation environment from Layer 13 to Layer 12 and the platform layers are highly influenced by human activities as indicated by the variable content of sand-size material and the multi-peak distribution pattern.

5.2.3.3 Site formation process of the profile T2621

In summary, the sedimentation in profile T2621 can be divided into two parts. Layers below 12A are natural depositions, and Layer 12A and above are human-dumped layers.

Combining the dating results, particle size analysis and soil micromorphology analysis, the site formation processes of profile T2621 and Middle Zhongjiagang Watercourse can be reconstructed.

Before 3150 cal. BC, the Middle Zhongjiagang region was a low area of ground under intertidal flat conditions. The bottom of Layer 13 represents an accumulating floodplain formed under cycles of high frequency sediment build-up. In the middle part of Layer 13, the accumulation of the floodplain was still ongoing, but incipient soil formation began, and some secondary soil structure appeared at the same time. At the top of this layer, the soil texture starts to change under a stronger depositional energy, with hydrological conditions gradually changing from stagnant water to dryness and land exposure.

In around 3150 cal. BC, Layer 12D, a dry vegetation zone appears, which indicates a favourable period of soil formation and human activity. Evidence of human activities is represented by the presence of pieces of charcoal and pottery, and large wooden structures start to appear in the Middle Zhongjiagang Watercourse. However, the hydrological conditions soon change to being wet again. From 3150 to 3000BC, soil material under frequent wet-dry sedimentation cycles was deposited. In this period, at least two relatively dry and stable soil surfaces with vegetation growth has been observed in the thin section, but both of which had quickly changed back to wet conditions again.

In around or slightly before 3000 cal. BC, Layer 12A was dumped with wet soil material derived from a previous stratum, most likely from Layer 12B or 12C, and mixed with clusters of charcoal fragments. Following this was the construction of Platform III 3 B2 using soil material similar to Layer 13B. This began to form the top of Platform III 3 B2 in depositional conditions that were mostly dry. A layer of very fine pebble-size, calcite-rich marble fragments was sandwiched between Platform III 3 B2 and Platform III 1A. Platform II 1A was built between around 2900 to 2800 cal. BC using mixture of coarse and very coarse sand with soil material similar to Layer 13D.

5.2.3.4 Change in hydrology conditions and human activity in the Middle Zhongjiagang

Watercourse

T2621 is located in the junction between the Middle Zhongjiagang Watercourse and the Mojaoshan mound, which is sensitive to the change of water table in Zhongjiagang Watercourse. Based on the interpretation introduced above, profile T2621 underwent repeated wetting and drying cycles, indicating that human activity in this region was closely related to changes in the regional hydrological system.

Layer 13, which is representative of pre-Liangzhu sedimentation, formed under wet conditions weakly influenced by tidal actions. Although fine charcoal has been found mixed in the groundmass of the sediments, there is no direct evidence of human activity observed in Layer 13. The first human activity observed in the Middle Zhongjiagang profile is around 3150 cal. BC in Layer 12D, which is the first dry period observed in the profile. This dry exposed surface provided a favourable living situation for Liangzhu people, as large wooden components for house building have been found in Layer 12D, which suggests large-scale human occupation in this region before the construction of the Mojaoshan mound. This initial occupation probably failed as the dry vegetation zone was quickly covered by around 30cm of wet channel deposits. No trace of human activity has been found in this subsequent period. After two or three cycles of alternating wet-dry conditions, at around 3000 cal. BC, although the sedimentation in this region is still under the influence of water, Liangzhu people started the construction of large mound using local sediments with different components such as charcoal fragments and coarse sands, interspersed with calcite-rich, off-white, gravel layers. Considering that the dam system was dated to around 3000-2900 cal. BC (Qin *et al.*, 2019), its construction may partially relate to the necessity of having to control wetness in the Zhongjiagang region in order to make settlement use possible.

In sum, the Middle Zhongjiagang profile exemplified the close relationship between human activity and the changing hydrological conditions at an early stage of the development of Liangzhu City. At this early stage of the Middle Zhongjiagang profile, the appearance of a dry exposed surface supports the idea of human activity in this region. However, human activity is still largely constrained by local hydrological conditions at this time, because when the wetness increased, the Liangzhu people

abandoned this region. But from around 3000 cal. BC, Liangzhu people were actively modifying and transforming the local landscape regardless of the wetness in the Middle Zhongjiagang Watercourse. This implies a deliberate site selection and strong determination to transform the local hydrological regime to provide favourable living spaces.

5.3 North Zhongjiagang region (T5020)

In the North Zhongjiagang region, human occupation was found in man-built mounds on both banks, with abundant human waste such as human and animal bones, pottery sherds and stone artefacts present in the associated channel infillings. The excavations since 2015 mainly focused on the western bank and the major channel infillings (Figure 5.15). Current excavation progress shows that the west bank of the watercourse has been expanded multiple times, and the watercourse gradually narrows and is finally completely filled and out of use by the end of the Liangzhu culture at about 2300-2000 BC (Liu *et al.*, 2019a).

During the excavation season in 2017, the south wall of the excavation pit T5020, located in the central part of the channel, provided a representative profile with which to understand the nature of the infillings and water sequences of the channel as well as the hydrological conditions present at the end stage of Liangzhu. Therefore, 10 micromorphology samples and 21 associated bulk samples were systematically taken from each layer exposed in T5020 (Figure 5.16) to understand the sedimentation sequences and their formation processes.

5.3.1 Field observation and stratigraphy of profile T5020

5.3.1.1 The general stratigraphy and findings in the North Zhongjiagang Watercourse

At present, the data compilation of the excavations in the North Zhongjiagang region is still ongoing. The information in this section is thus compiled from the excavation records provided by the Zhejiang Institute of Cultural Relics and Archaeology.

Based on field observation and archaeological investigations, five stages of platform construction have been observed in the North Zhongjiagang Region (Figure 5.15). The mound construction materials are mainly composed of ‘clay wrapped with grasses’ (see section 2.3.2.3 for detailed explanation) and light gray silty clay mixed with coarse sands and burnt clay (daub). The earliest stage of mound construction was in the high ground where Platform V and IV were found, with Layer 12 inbetween (represented in excavation pit T5017, Figure 5.15). Five layers of grass/wood ash about 5cm thick appeared repeatedly in the bottom of the sub-layers of Platform IV, Layer 12 and Platform V. Layer 11 was found on top of Platform IV, which was then overlaid by Platform III-2. During this process, the mounds gradually expand towards the middle of the channel (represented in excavation pit T5018 and T5019, Figure 5.15) and most of Platform III-2 was directly stacked on top of the natural sediments. At the edge of Platform III-2, remains of wooden piles were recovered. The range of these revetment piles was 50.6 metres from north to south, with 21 wooden piles revealed in total. Bamboo weaving objects were found accompanying these piles and were found projecting into the ground. The two reported bamboo weavings were 10.25m and 6.7m long respectively, with a maximum residual height of 0.36m. Paving stones were found on top of Platform III-2, but the purpose of these stones is still under discussion. Platform II was constructed on top of Platform III-2 with 66 revetment piles along a length of 69 metres, and associated bamboo weaving found on the slope of the mound. A few wooden planks were found lying on top of Platform II. In addition, remnant grass paving features, possible grass mattings, have been found on the surfaces of Platform II and III-2. Platform I was laid on top of Platform II, with more than 120 revetment piles over a length of 103 metres, again with associated woven bamboo bank protection material observed on the slope of the terrace.

5.3.1.2 Field description of profile T5020

According to the excavation record, profile T5020 mainly reflects the nature of the infillings and water sequences of the channel sedimentation of the Late period of Liangzhu. In T5020, the bottommost Liangzhu deposition is Platform III-2, which is situated directly above the natural sediment sequence (Figure 5.15). Above this platform were four stages of riverine accumulation from the Late Liangzhu period,

which were then overlaid by post-Liangzhu and historical period sediments. The field descriptions of each layer from top to bottom are as follows:

Layer 3: Light yellowish. Song dynasty (AD 960-1279) accumulation. 0-55cm thick.

Layer 4: Grayish brown. Based on the pottery sherds found, this layer should be the remains of Eastern Zhou dynasty (770–256 BC). 20-30cm thick.

Layer 5: Yellowish-brown silt. This layer has been widely found in the Liangzhu region, which could be dated from the post-Liangzhu to Eastern Zhou periods (770-256 BC). Two sub-layers, Layer 5A and 5B were identified in the field. 72-80cm thick.

Layer 7 to 10: These are believed to be the infillings of the river, with abundant pottery and stone debris as well as organic matters found in the sediments. Based on pottery typology, this sequence is dated to the early stage of Late Liangzhu period (2850-2600 cal. BC).

Layer 7: Light grayish-brown silty clay. This is the last stage of river sediment accumulation in this profile. A few coarse sands, daub fragments and pottery sherds were found in this layer. 15-30cm thick.

Layer 8: Light grayish-brown silty clay. This depositional layer was found overlying Platform I in nearby excavation pits and was classified as the third stage of waste accumulation. A few pottery sherds were found. 0-45cm thick.

Layer 9B: Light grayish-brown silty clay. The layer was deposited on top of the Platform II in nearby excavation pits and was classified as the second stage accumulation by the excavator. 0-47cm thick.

Layers 10A, 10B and 10C: These layers were deposited above the Platform III and were classified as the first stage of channel fill. Pottery sherds, burnt soil and charcoal fragments were found in Layer 10A (light ash black). Plant fragments were found in Layer 10B and 10C (light greyish blue). 50-120cm thick.

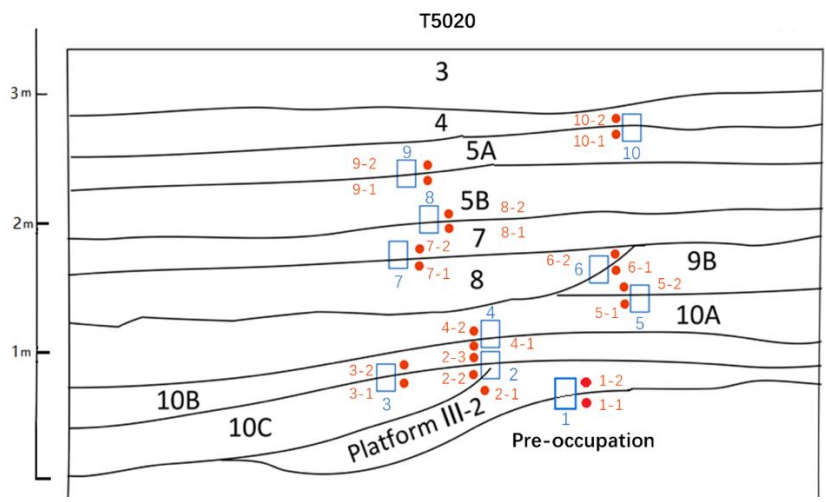
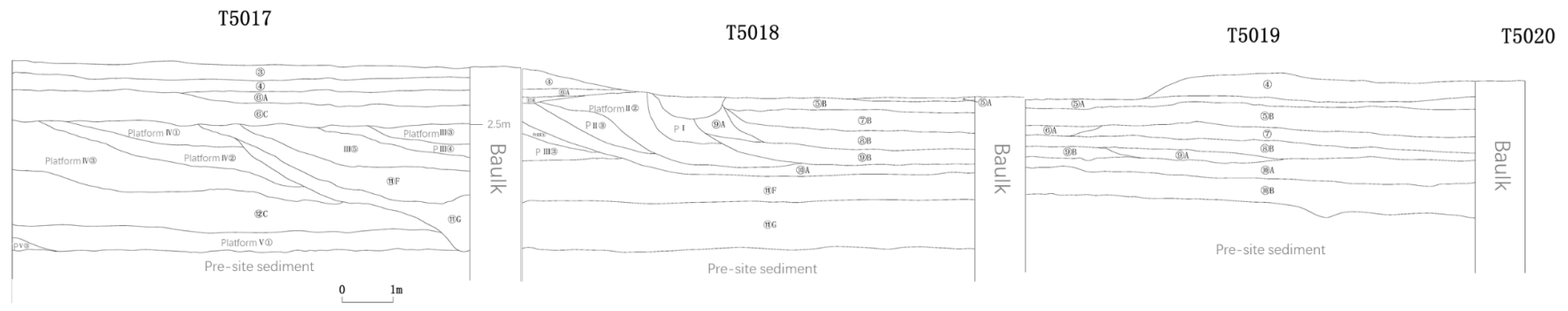


Figure 5.15 Stratigraphy of the T5017, T5018, T5019 and T5020 excavation pits. Soil samples were taken from the T5020 profile. The blue rectangles and numbers refer to the sampling positions and numbers of the soil micromorphology samples. The red dots and numbers refer to the sampling positions and numbers of bulk samples

PlatformIII-2: The base of this platform was built of blocks of 'clay wrapped with grasses' over a thickness of c. 30-50cm. Stone in different sizes, ranging from 10cm to 40cm in length, were laid on top of the platform and on its side-slopes. Between these stones, soil material was used to fill in and compact the platform and create a horizontal surface. On one side of the slope of this platform, one timber pile was found inserted obliquely into the pre-occupation sediment. Two more piles were found on top of and inserted into the platform. These piles are believed to be part of the platform protection facilities in North Zhongjiagang Watercourse. 0-80cm thick.

Pre-occupation sediment: Gray silty clay with some yellow spots. Identified as natural sediments in the field.

5.3.2 Results of soil micromorphological analysis in T5020

The detailed description of each micromorphology sample can be found in Appendix 2. Analytical results of the T5020 profile will be introduced from the bottom to top layers.

5.3.2.1 Pre-occupation sediment

5.3.2.1.1 Introduction

The pre-occupation sediment is represented in the lower part of slide T5020 1 (Micro-Fabric T5020 1:2, Figure 5.16). It is believed to be the natural sediments in the centre of the North Zhongjiagang Watercourse, and it is expected that this pre-occupation sediment will reflect some of the flow characteristics of the Zhongjiagang Watercourse before the construction of the mounds. This sediment is mainly composed of gray (2.5Y 5/1), homogeneous silty clay.

5.3.2.1.2 Pre-occupation sediment: description of micro-fabric T5020 1:2

The pre-occupation sediment (micro-fabric T5020 1:2) is brown (PPL), dotted mixture of very fine silty clay with moderate birefringence, micritic pale gray calcite (10%) and silt-size black organic punctuations (3%). It generally shows a reticulate to parallel striated and calcitic crystallitic (90:10) b-fabric. A few dusty silty clay crusts and

possible topsoil fragments with a higher content of organic matter were incorporated into the groundmass.

The sediment fabric evident in slide T5020 1 was separated into eight main pedes with sizes ranging from 2 to 3.5cm by channels of about 2-4mm wide. These cracks are extra-visible due to the slight shrinkage that occurred during the air drying process of the clay-rich soil samples (Figure 5.16).

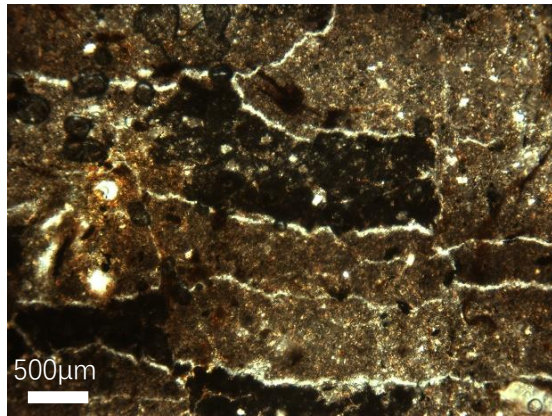
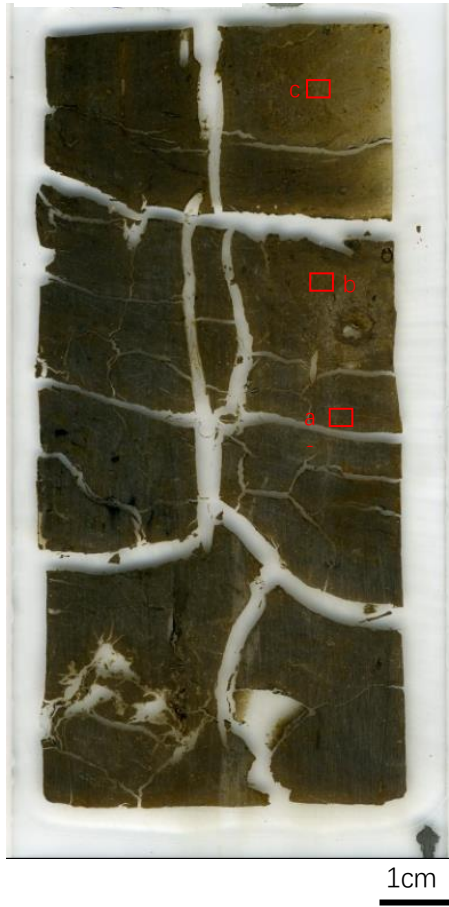
In the bottom four pedes, which is the pre-occupation sediment (micro-fabric T5020 1:2), sub-angular blocky microstructures were weakly developed with 17% porosity. Root voids and passages were commonly stained and coated with amorphous iron oxide (reddish yellow) replaced organic matter. Most organic matter were amorphous and horizontally oriented. Pyrite framboids were commonly seen near humified organic matter. Dusty striated clay with a high birefringence was incorporated in the groundmass as light yellowish streaks. The boundary between the pre-occupation sediment and Platform III-2 is very diffuse, with the exact the interface probably destroyed by the strong shrink-swell processes.

5.3.2.1.3 Results of bulk analysis and interpretation of the pre-occupation sediment

The bulk sedimentology results (Figure 5.17) indicate that this buried layer has a high magnetic susceptibility and calcium carbonate content, but a relatively low carbon and total organic content, and very low phosphorus content. The high magnetic susceptibility probably indicates an exposed surface (Allen & Macphail, 1987). And the high calcium carbonate content may form due to the drying and exposure of the old land surface where calcium-rich water has come up to the surface and precipitated as a drying event happened (Goffer, 2008, p. 416). This potential indicator was further confirmed by the observation from thin section analysis that micritic calcium carbonate silt-sized particles are distributed throughout and are concentrated in the pores (Figure 5.16).

Slide T5020 1

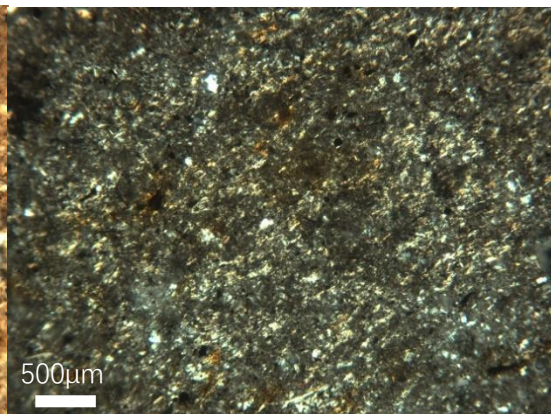
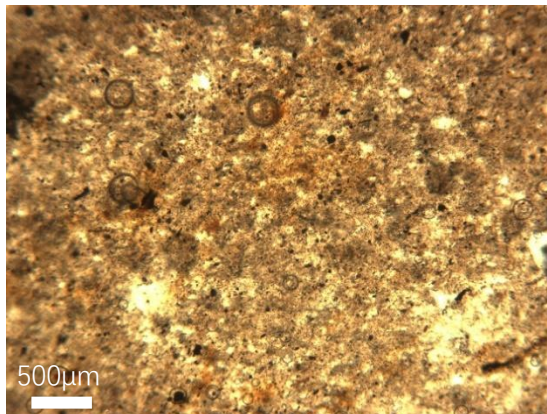
Micro-fabrics



a: Platy microstructure, XPL.



b: Clusters of humified organic matter, PPL.



c: Dotted groundmass mixed with silty clay and organic pigments, PPL (left); Straited b-fabric, XPL (right).

Figure 5.16 Slide scan and microphotographs from slide T5020 1

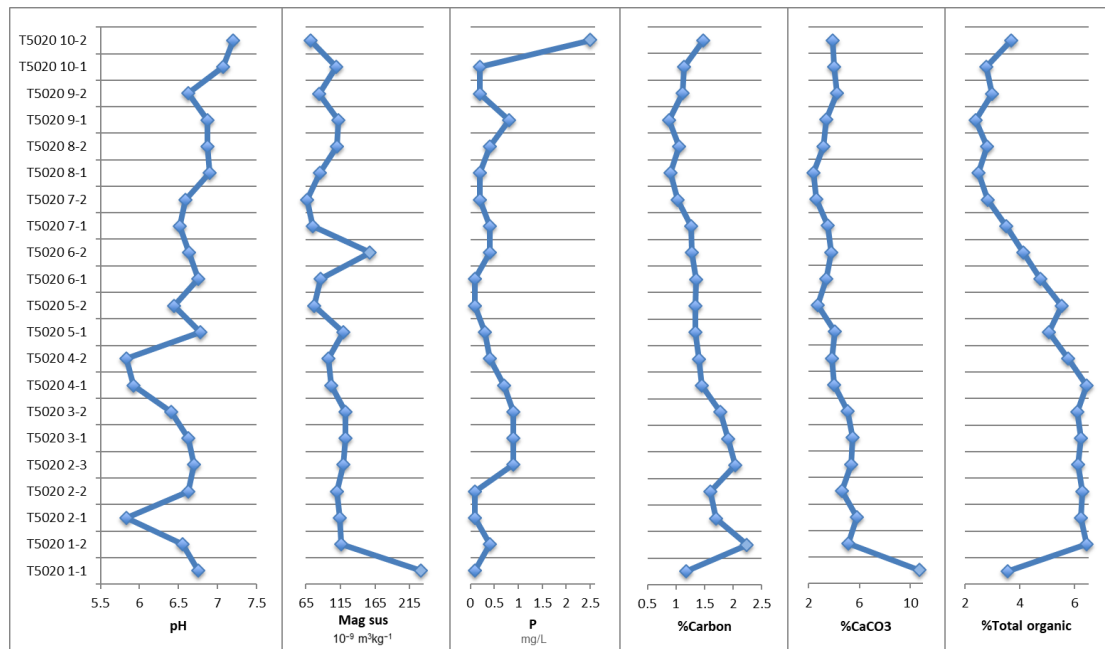


Figure 5.17 Analytical results of pH, phosphorus, magnetic susceptibility, and carbon, total organic and calcium carbonate contents of profile T5020.

This layer has an exceptionally high content of clay and very fine silt of more than 60%. Although tiny plain voids are commonly observed, very few vertical channels were seen in the layer, which means the high percentage of clays are not formed by illuviation. Also, the remnant laminations of dusty silty clay crusts indicate the repeated accumulation and strong drying out of fine material transported by slow-moving water. The weakly laminated organic matter, remnants of silty clay crusts and very fine particle size collectively point to alluvial deposits accumulating under a very gentle or even stagnant water environment. The organic punctuations could be anthropogenic origin, possibly due to the incorporation of charcoal dust from crop burning.

This alluvial sediment was then exposed and subject to drying, leading to the secondary precipitation and formation of silt-sized calcium carbonate. In the meantime, wetting and drying created conditions for strong shrink-swell processes which created fine planar voids in the silty clay fabrics (Figure 5.16) and incorporated topsoil fragments. The latter may come from lumps of soil falling into gaps produced by shrinking and swelling or might due to human or animal trampling. Repeat shrinkage and swelling also makes all material both well-mixed and compacted.

In sum, this pre-occupation sediment is indicative of the slow build-up of alluvial material containing aggregated fragments of A horizon material under repeated alternating conditions of water saturation and periodic drying with exposure stages.

5.3.2.2 Platform III-2

5.3.2.2.1 Introduction

This layer represents the third stage of platform construction evident in the North Zhongjiagang profile. The soil samples were taken from the edge of this platform (Figure 5.15). The bottom of this layer is shown in the upper part of slide T5020 1, and the top of this layer is represented at the bottom of slide T5020 2. The maximum thickness of this platform in excavation pit T5020 is 50cm.

5.3.2.2.2 Platform III-2: description of the micro-fabrics T5020 1:1 and 2:2.

The bottom part of Platform III-2 is presented in four well defined peds (Figure 5.16, micro-fabric T5020 1:1), which is similar to the pre-occupation sediment. Each ped has a sub-angular blocky to platy microstructure with around 14% porosity and a fine monic c/f distribution. The micro-fabric T5020 1:1 has a slightly coarser groundmass (c/f: 2/98; limit: 50 μ m) with the add-in of a small proportion (2%) of very fine sand-size quartz grains. A few clusters of highly fragmented humified organic residues (Figure 5.16) together with clusters of organic topsoil fragments were randomly mixed in the groundmass, and most of the organic material in the groundmass has various orientations. The fine fraction is light brown (PPL) dotted mixture of silt-size material (73%), highly birefringent clay material (25%), and organic pigments (3%) with a random striated b-fabric. Trace amounts iron impregnated clay hypo-coating with diffused boundaries are found around the voids. A few black manganese compounds are found as clustered pellets with diffuse boundary, nodules and hypo-coating of voids. Traces amounts of pyrite framboids are found near humified organic materials.

The top of the Platform III-2 (Figure 5.18, micro-fabric 2:2) has a coarser groundmass to the base of the platform and exhibits a different microstructure: interconnected

channels with slightly serrated walls with large vesicles 1-12mm in size, which creates a porosity of 15%. This fabric contains a heterogeneous mixture of topsoil aggregates (5%), characterised by humified organic matter, and a few charcoal and fine to medium sand-size rock fragments in the groundmass. The micromass is light yellow (PPL) dotted mixture of silty clay with high birefringence and light yellow interference colour, micritic calcium carbonate (5%), and organic pigments (3%), and shows stipple speckled to grano-striated to calcitic crystallitic (90:5:5) b-fabric. Pyrite framboids, reddish and diffuse iron oxide impregnated clay hypo-coatings, and remnant organic matter fragments are widely found around the voids. Fine dusty clay coatings and organic-rich silty clay infillings are commonly found in channels (Figure 5.18). Perpendicular laminar fine silty clay crusts were also found (Figure 5.18), which are similar to those observed in the bottom of Platform III③B2 in the Middle Zhongjiagang profile (see section 5.2.2.3.1). These have probably formed due to surface crusts falling into the long drying cracks during the shrink-swell of the clay-rich matrix.

The boundary between Platform III-2 and Layer 10 is very diffused, probably due to the influence of strong shrink-swell processes.

5.3.2.2.3 Results of bulk analysis and interpretation of the Platform III-2

Platform III-2 has a moderate magnetic susceptibility value and calcium carbonate content, high carbon and total organic content, and low phosphorus content (Figure 5.17). From the pre-occupation sediment to the top of Platform III-2, the pH values gradually decreased from 6.75 to 5.83, probably due to the increase of organic matter and the decrease of calcium carbonate content.

Due to high clay contents (more than 30%) and repeat wetting and drying in the Pre-occupation sediment and Platform III-2, the strong shrink-swell processes produce long cracks or channels that were later infilled by disorganised topsoil material, fragmented humic matter and surface crusts in dry conditions that were well-incorporated in the groundmass, as well as clay striae showing high birefringence.

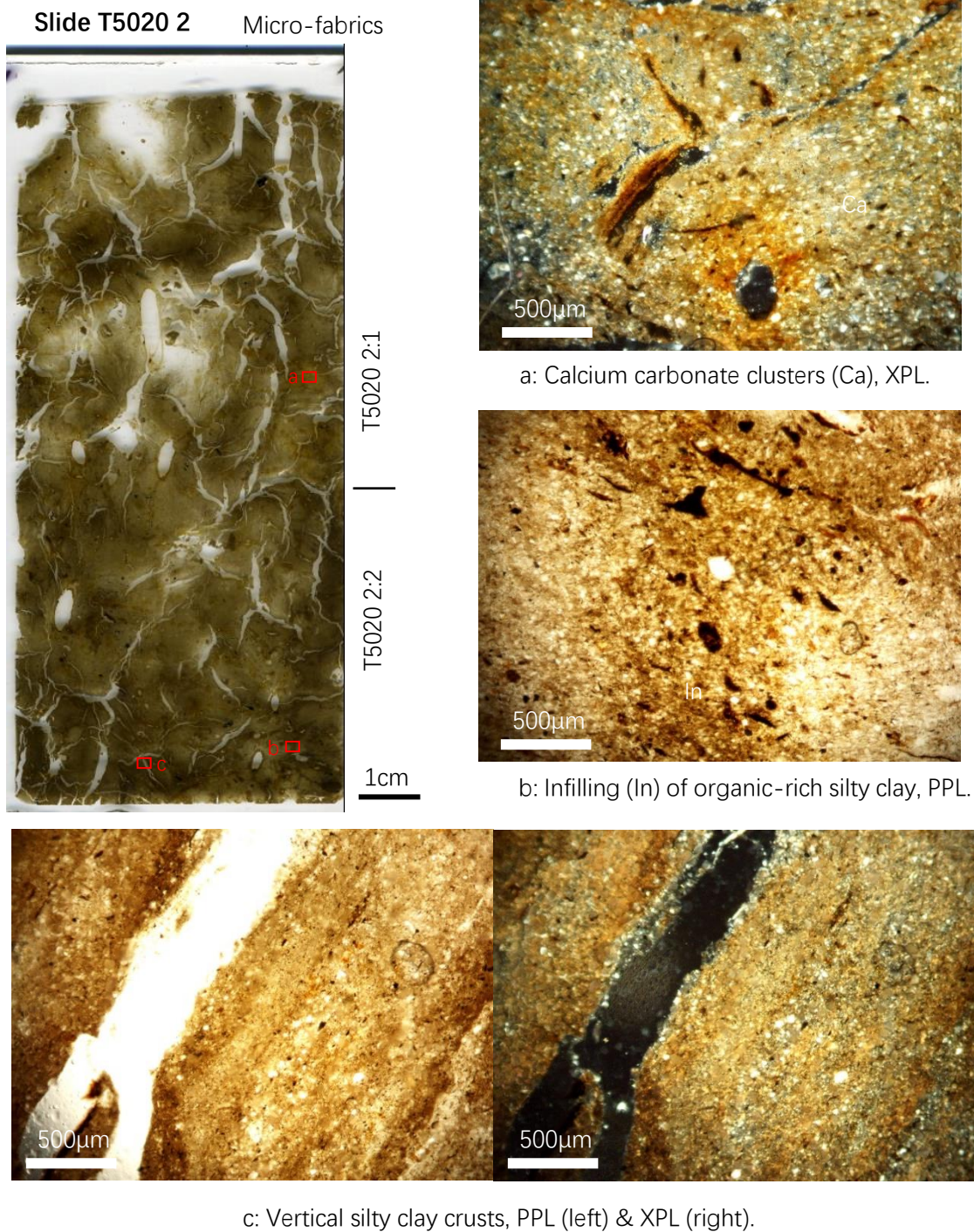


Figure 5.18 Slide scan and microphotographs from slide T5020 2

From field observation, the bottom of the Platform III-2 is believed to be constructed using blocks of ‘soil wrapped with grasses’. Based on the relatively high content of humified and disoriented organic matter, the clusters of topsoil fragments and highly fragmented organic matter, and the relatively low phosphorus and magnetic

susceptibility, the analysis of soil thin section supports the hypothesis that the bottom of Platform III-2 is made of artificially mixed, organic-rich, very fine silty clay without evidence of human occupation. The matrix of this layer is similar but slightly coarser than the pre-occupation sediment below, therefore, these soil materials may be collected from similar sediments nearby. The top of the Platform III-2 (Micro-fabric 2:2) is also heterogeneous and strongly influenced by shrink-swell processes. The commonly found topsoil aggregates and root voids indicate a certain degree of disruption by pedogenic processes and physical mixing possibly caused by human activities.

In sum, the Platform III-2 is an anthropogenic construct composed of organic-rich silty clay material, possibly the 'clay wrapped with grasses' material, with the top of this layer once an exposed surface with vegetation growth.

5.3.2.3 Layer 10

5.3.2.3.1 Introduction

In the field, Layer 10 was divided into three sub-layers: 10A, 10B and 10C. Sub-layer 10C is 40cm thick with no included archaeological artefacts. Nonetheless a few bones, including both human and animal bones, and a paddle have been found in Layer 10B, which is around 30cm thick in T5020. Layer 10A, which is around 50cm thick in T5020, contained burnt soil fragments, pottery sherds and a few pieces of fine charcoal. Based on micromorphological observation, Layer 10C and the bottom of Layer 10B are basically the same material and will be discussed together. The top of Layer 10B and Layer 10A will be described separately.

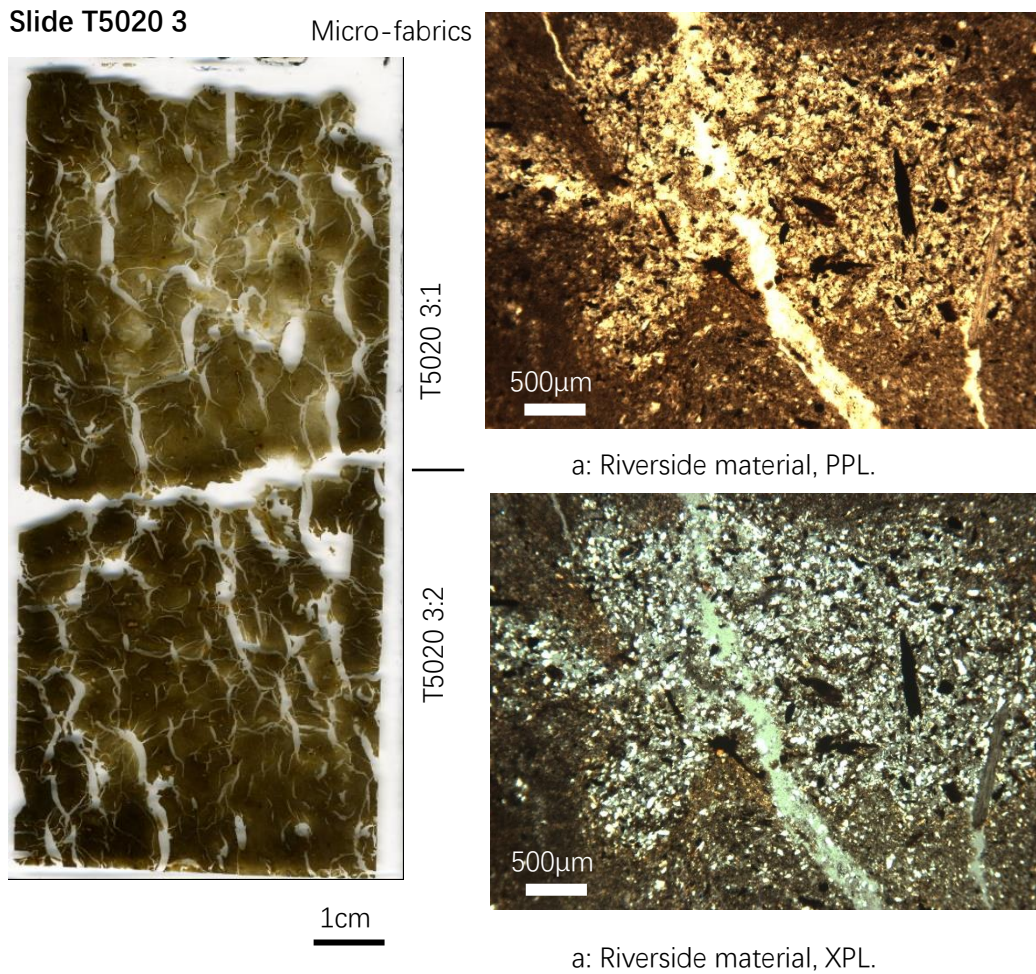


Figure 5.19 Slide scan and microphotographs from slide T5020 3

5.3.2.3.2 *Layers 10C and the bottom of 10B: Description of micro-fabrics 2:1, 3:2 and 3:1*

Layers 10C and the bottom of 10B (Figure 5.18 and 5.18, Micro-Fabrics T5020 2:1, 3:2, 3:1) generally have a similar groundmass, microstructure and pedofeatures to the top of Platform III-2, except for the presence of a few iron impregnated calcium carbonate clusters with diffuse boundaries that are distributed in the bottom of Layer 10C (Figure 5.18), and a few clusters of coarse silt/very fine sand-size quartz with a high content of disoriented organic matter that are mixed in the groundmass throughout Layers 10C and 10B (Figure 5.19). Around the voids, remnant root fragments, diffuse amorphous iron hypo-coating of small voids, amorphous iron impregnated dusty clay hypo-coating of large vesicles are commonly seen, features which are indicative of

alternating wet/dry conditions (Kühn *et al.*, 2010; Lindbo *et al.*, 2010). Micro-laminated silty clay crusts and vivianite crystals are still frequently observed, and point to stop/start illuviation of fines and periods of waterlogging (Pagliai and Stoops, 2010; Karkanis and Goldberg, 2010). In general, these features and the finely channelled, irregular structure (Figure 5.18 and 5.18) give the impression of having been puddled in saturated conditions with strong vertisol-like features (Kovda and Mermut, 2010; Lindbo *et al.*, 2010).

5.3.2.3.3 The top of Layer 10B: description of the micro-fabric T5020 4:2

The top of Layer 10B (Figure 5.20, micro-fabric T5020 4:2) exhibits a similar microstructure and groundmass to the previous layers, but with a higher content of clay (35%), clusters of coarse silt-size quartz with fragmented plant tissue, and vivianite crystals. Also, organic matters are weakly laminated, and thick, partially fragmented, dark brown, dusty silty clay crusts are widely found (Figure 5.20). Anthropogenic artefacts such as charcoal around 5mm in size are found lying obliquely on top of these crusts and a small sherd was found in one vertical crack (Figure 5.20).

5.3.2.3.4 Layer 10A: description of the micro-fabrics T5020 4:1 and 5:2

The transition from Layer 10B to 10A is indistinct. The groundmass of Layer 10A (Figure 5.20 and 5.20, micro-fabrics T5020 4:1 and 5:2) is a mixture of brown (PPL) dotted humic silty clay with 15% dark brown (PPL) fragmented dusty silty clay crusts and 3% amorphous organic fine material, and shows a stipple-speckled b-fabric. This layer is slightly coarser than previous sediments, with a c/f ratio of 7/93 (limit: 50µm). Organic matter in this layer is mostly inclined laminar, and 1-5mm-sized humified plant and charcoal fragments are more frequently observed than in previous layers.

This layer has a different microstructure compare to other sub-layers in Layer 10, which is a moderately separated platy structure. Amorphous iron compound hypo-coatings of voids with diffuse boundaries, aggregates of topsoil, and crystallized vivianites are occasionally seen. On top of Layer 10A (Figure 5.21, micro-fabric T5020 5:2), infillings of soil material from above Layer 9B are commonly seen in the vertical

channels. The boundary with Layer 9B is not very distinct.

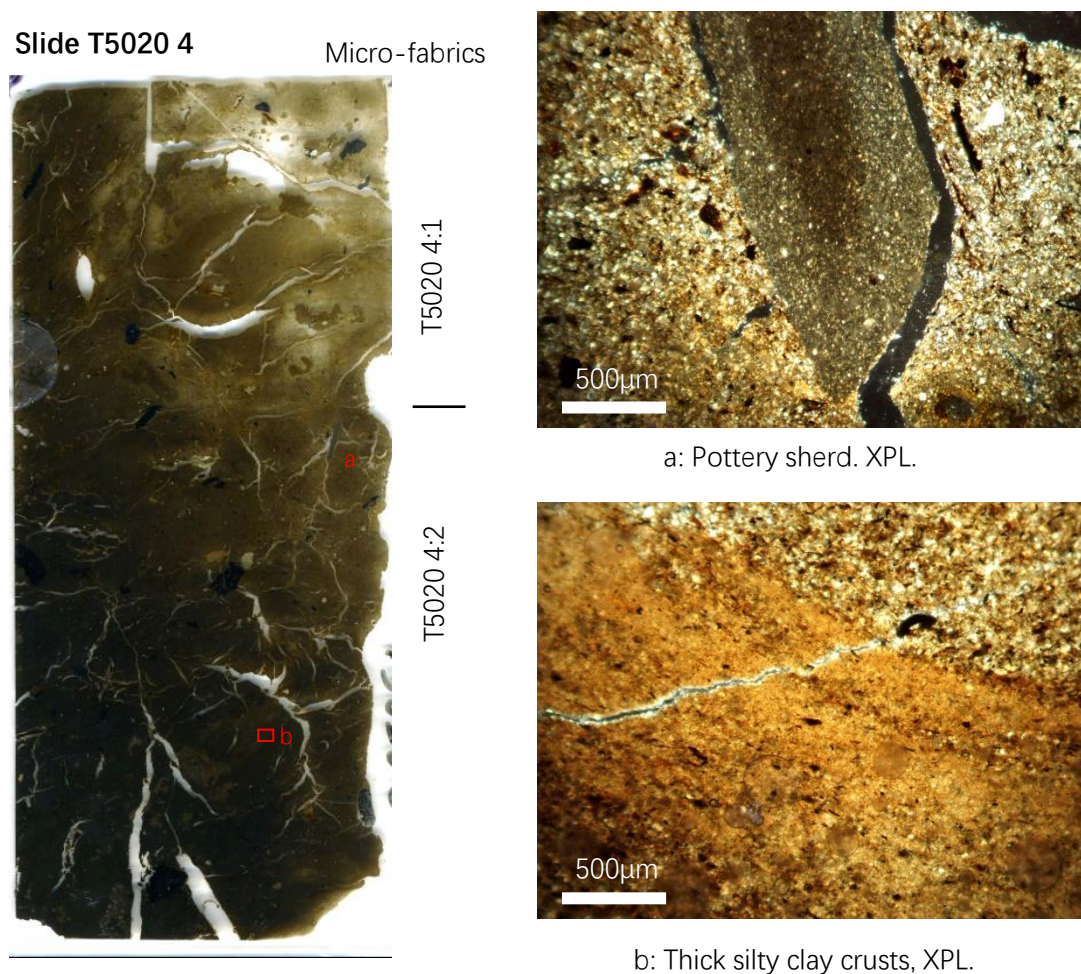


Figure 5.20 Slide scan and microphotographs from slide T5020 4

5.3.2.3.5 Results of bulk analysis and interpretation of Layer 10

From the bottom of Layer 10C to the top of Layer 10B, the pH value gradual decreases from 6.5 to 6 and then increases back to 7 in Layer 10A (Figure 5.17). The phosphorous content is higher in Layer 10B than other sub-layers (Figure 5.17). Generally, Layer 10 has moderate magnetic susceptibility and calcium carbonate content, and high organic matter and carbon content (Figure 5.17). The decrease of pH value might be related to the high organic matter content and relevant pedogenic process in Layer 10B. The increase of phosphorous content coincident with the increase of vivianite in Layer 10B and may be related to human waste or degradation of organic material (Karkanias & Goldberg, 2018).

Similar to the top of Platform III-2, the groundmass of Layer 10 has an alluvial origin. The clusters of organic matter-rich, coarse silt-size and very fine quartz sand (Figure 5.19) mixed in the groundmass is possibly from lake/riverside input or from fine soil eroded from the exploitation of the catchment and/or the winnowing of fine material at the water's edge by lapping and lateral washing. Commonly found root voids and rounded topsoil aggregates in the groundmass indicate that incipient soil formation processes had begun in Layers 10C and 10B. Also, the calcium carbonate clusters in the bottom of Layer 10C indicate possible dry phases in this alluvial sediment. In the upper part of 10B, anthropogenic artefacts begin to be mixed into the sediment. Importantly, the weakly laminated organic matter and thick silty clay crusts indicate a faster sedimentation rate under a shallow, slow-moving or even stagnant environment with repeat wetting and drying (Pagliai and Stoops, 2010). In Layer 10A, the input of coarser sediment material increases, which indicates a stronger depositional energy than layers below. The mostly oriented organic matter suggests that Layer 10A is less disrupted by soil formation processes, but the commonly found anthropogenic artefacts in Layers 10B and 10A suggest the intensification of human activity in this area.

In summary, Layer 10 built up under the processes of alluviation. Layer 10C indicates a weak depositional energy period with ephemeral dry phase and incipient soil formation. Layer 10B illustrates a shallow, quiet water environment with the beginning of the input of anthropogenic material. Layer 10A returns to constant wet conditions with stronger water motion.

5.3.2.4 Layer 9B

5.3.2.4.1 Introduction

Based on the stratigraphy in nearby excavation pits, Layer 9B, with a maximum thickness of 50cm in T5020, was found deposited on top of Platform II material (Figure 5.15), and was interpreted as the waste accumulation of the people living in Platform II. Burnt soils, charcoal and pottery sherds were found in this layer. The bottom of this layer is represented in the micro-fabric 5:1. Soil samples are also taken from the slope of this platform, which is represented in the micro-fabric 6:3.

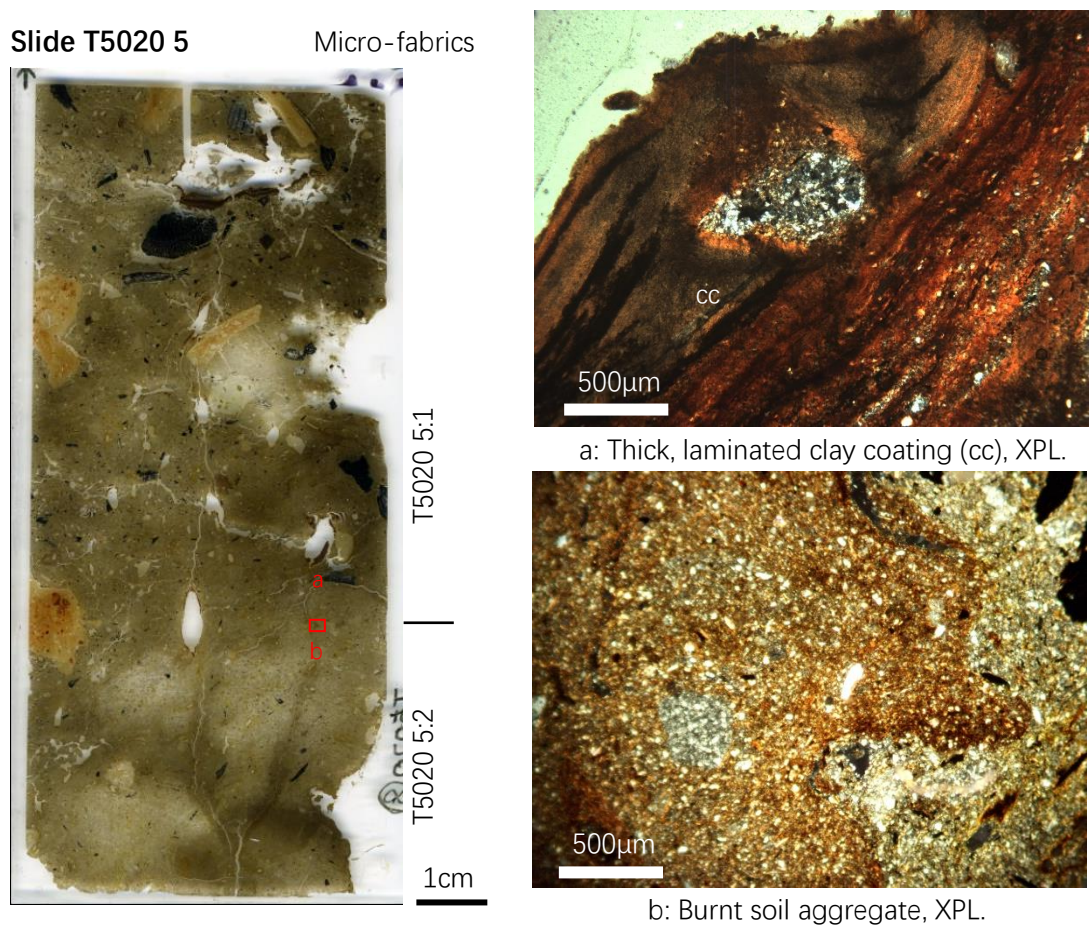


Figure 5.21 Slide scan and microphotographs from slide T5020 5

5.3.2.4.2 *Layer 9B: Description of micro-fabrics 5:1 and 6:3*

This layer is heterogeneous with a c/f ratio of 10/90 (limit: 50µm). The groundmass is mainly composed of light brown (PPL) dotted humic silty clay, mixed with rock fragments (5%) varying in size class from fine sand-size to pebble-size, charcoal fragments (5%) of 1-13mm in size, a few pottery sherds with sharp boundaries, and a few burnt soil aggregates (Figure 5.21). All clasts larger than coarse sand-size are disordered and floating in the fine matrix. The clay content increase from 10% to 20% from the bottom to top and the micromass shows a stipple-speckled to poro-striated (95:5) b-fabric.

The bottom part of this layer (Figure 5.21, Micro-fabric T5020 5:1) has a more massive microstructure with a few vertical channels and chambers. Also, the organic matter is disoriented, but laminar organic matter appears from the middle part of this layer. In

the middle of this layer, the number of anthropogenic clasts increase and a large chamber hypo-coated by dusty silty clay crusts with dozens of laminations was observed (Figure 5.21).

The top of Layer 9B, which is shown in micro-fabric T5020 6:3 (Figure 5.22), has a moderately developed angular blocky microstructure. Humic, silty clay soil aggregates were widely mixed in the groundmass. A few partially broken, thick silty clay crusts were found (Figure 5.22). A burnt topsoil fragment (Figure 5.22, 2cm in size), probably from adjacent dry lands, and a pottery sherd resting obliquely on the slope were observed. Vivianite crystals were widely found in the voids.

5.3.2.4.3 Results of bulk analysis and interpretation of Layer 9B

Layer 9B has a low magnetic susceptibility value, as well as low phosphorus and calcium carbonate contents, and medium carbon and total organic contents (Figure 5.17). All the values suggestive of human activities are low. Although many anthropogenic artefacts were found in this layer, this layer is not likely to be indicative of an occupation layer.

In the bottom of Layer 9B, the clay content is relatively low (10%) and the content of medium silt-size and coarser material is significantly higher than upper and lower layers. As there is no obvious increase of clay content in Layer 10A below, it could be speculated that this layer was constituted by a different source material from the Layer 10. Considering the disorganized grain orientation, it is likely that the bottom of Layer 9B is using soil material from somewhere else and was laid in this position by dumping or deliberate platform construction.

Starting from the middle part of Layer 9B, laminar organic matter starts to appear, which manifests the influence of water at this level. Combining the oriented organic matter and disoriented coarse materials, especially the pottery sherd with distinct and sharp angles, it can be surmised that the coarse materials such as charcoal and pottery sherds have not been transported far and were dumped into the sediments that were later covered by slow-moving water and associated fine material. The dumping action may

also produce the chambers between the large clasts (Karkanas & Goldberg, 2018, 141), which was later coated by thick, compound, dusty clay coatings. In the slope of Layer 9B, the appearance of silty clay crusts indicates the slowing down of hydraulic dynamics. The weakly developed soil structure and the broken-up silty clay crusts point to the drying-out of the previously wet fabric (Pagliai and Stoops, 2010), which indicates a stable surface for human activities such as the dumping of pottery sherds and burnt soil fragments from dry lands.

In sum, the bottom of Layer 9B should be a dumped or constructed platform which is later covered by slow-moving water with included anthropogenic material. This layer then dried-out and became more stable for human activity.

5.3.2.5 Layer 8

5.3.2.5.1 Introduction

Based on the stratigraphy in the nearby excavation pits, Layer 8, with a maximum thickness of 50cm in T5020, was found deposited on top of Platform I (Figure 5.15) and was interpreted as the waste accumulation of the people living in Platform I. A few pottery sherds were found in this layer.

5.3.2.5.2 Layer 8: Description of the micro-fabrics T5020 6:2, 6:1 and 7:2

The main body of Layer 8 is composed of a massive, 30-40% dusty silty clay, 50% silt-size and very fine sand-size quartz grains, 3% medium to coarse sand-size quartz and 5% black humified organic matter and fine charcoal fragments of 0.5-5mm in size. Trace amounts of coarse sand-size rock fragments are also seen. All these components were randomly mixed in the groundmass. The micromass is dense, light yellow (PPL) silty clay with a speckled to striated b-fabric. Vivianite crystals (8%) with weathered rims, as indicated by the optically isotropic, yellowish substance surrounding the vivianite crystals (Stoops and Delvigne, 1990), were distributed in the lower and middle part of this layer but were more concentrated in the middle part (Figure 5.22). The microstructure, pedofeatures and coarse material content change slightly from the

bottom to top of this layer.

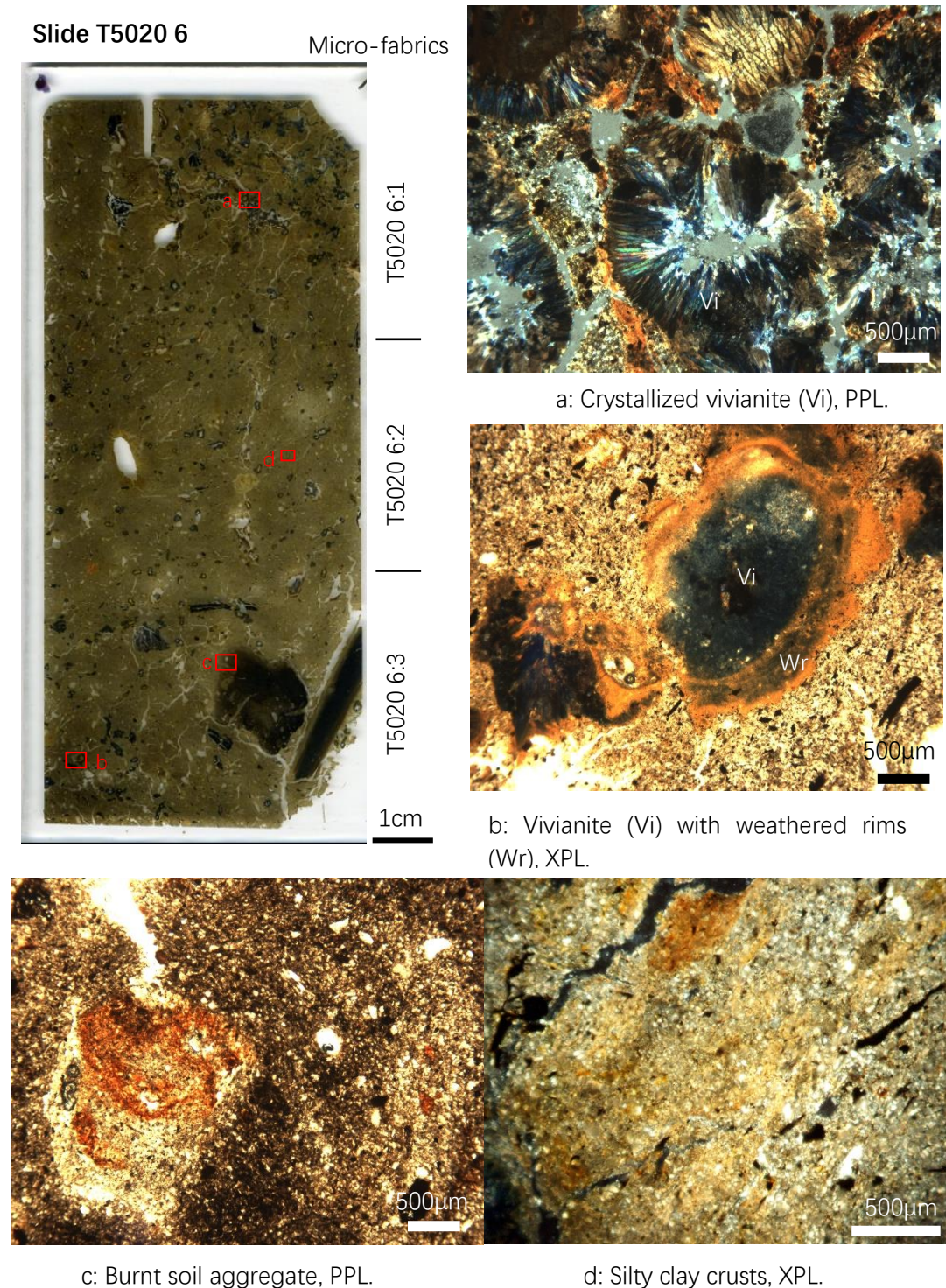


Figure 5.22 Slide scan and microphotographs from slide T5020 6

The bottom of Layer 8 (Figure 5.22, Micro-fabric 6:2) has a weakly-developed angular blocky structure with a porosity of 6%. Voids hypo-coated by dusty, high birefringence clay, some of which were impregnated and further quasi-coated by iron oxides, were

widely observed. Humified organic matter was weakly laminated. Laminations of fine silty clay crusts can be observed indistinctly.

The middle part of Layer 8 (Figure 5.22, Micro-fabric 6:1) has a moderately-developed angular blocky structure with a porosity of around 10%. More coarse sand-size grains and charcoal fragments were mixed in the groundmass. Thick, compound, dusty clay hypo-coatings, some of which were impregnated with iron-oxides, were widely observed around voids and channels. Small amorphous iron oxide mottles were seen around vivianite crystals (Figure 5.22). The majority of the organic component was randomly distributed.

Due to loss during slide making, only a small portion of the upper part of Layer 8 was preserved. The remaining part (Figure 5.23, micro-fabric 7:2) has a massive microstructure with 8% porosity formed by small fissure and root voids. Only a few fine organic matter fragments were present and were mostly randomly distributed, only a few exhibiting parallel orientations. The boundary between the top of Layer 8 and the overlying Layer 7 is distinct.

5.3.2.5.3 Results of bulk analysis and interpretation of Layer 8

Layer 8 has low phosphorus, calcium carbonate and total organic contents, medium carbon content and a slightly higher magnetic susceptibility value in the base of this layer (Figure 5.17). The higher magnetic susceptibility value is possibly because the sample position is above the slope of Platform 9B where anthropogenic materials such as burnt soil are scattered.

The groundmass of Layer 8 is composed of the commonly seen alluvial silty clay deposit in the Liangzhu area. In the basal part, the processes of accumulating alluvial plain were relatively well-preserved. In the middle part, input of anthropogenic material such as charcoal increased. The widely found vivianite crystals are probably related to the decay of organic substances in once waterlogged deposits (Karkanis & Goldberg, 2018). The thick, compound clay coating implies a repeat coming and going of slurry over the middle of this layer. In the meantime, the amount of passages increased,

together with the angular blocky structure, it can be speculated that the middle part of Layer 8 experiences a degree of pedogenesis and may have partly dried out. The small root voids and passages and the homogenized fabric in the upper part of Layer 8 indicate that incipient pedogenic processes also occurred.

In general, this layer is an accumulating alluvial deposit which subsequently experienced some short-term soil development and drying out, accompanied by the input of anthropogenic materials, although lesser than other layers, in the relatively stable surface.

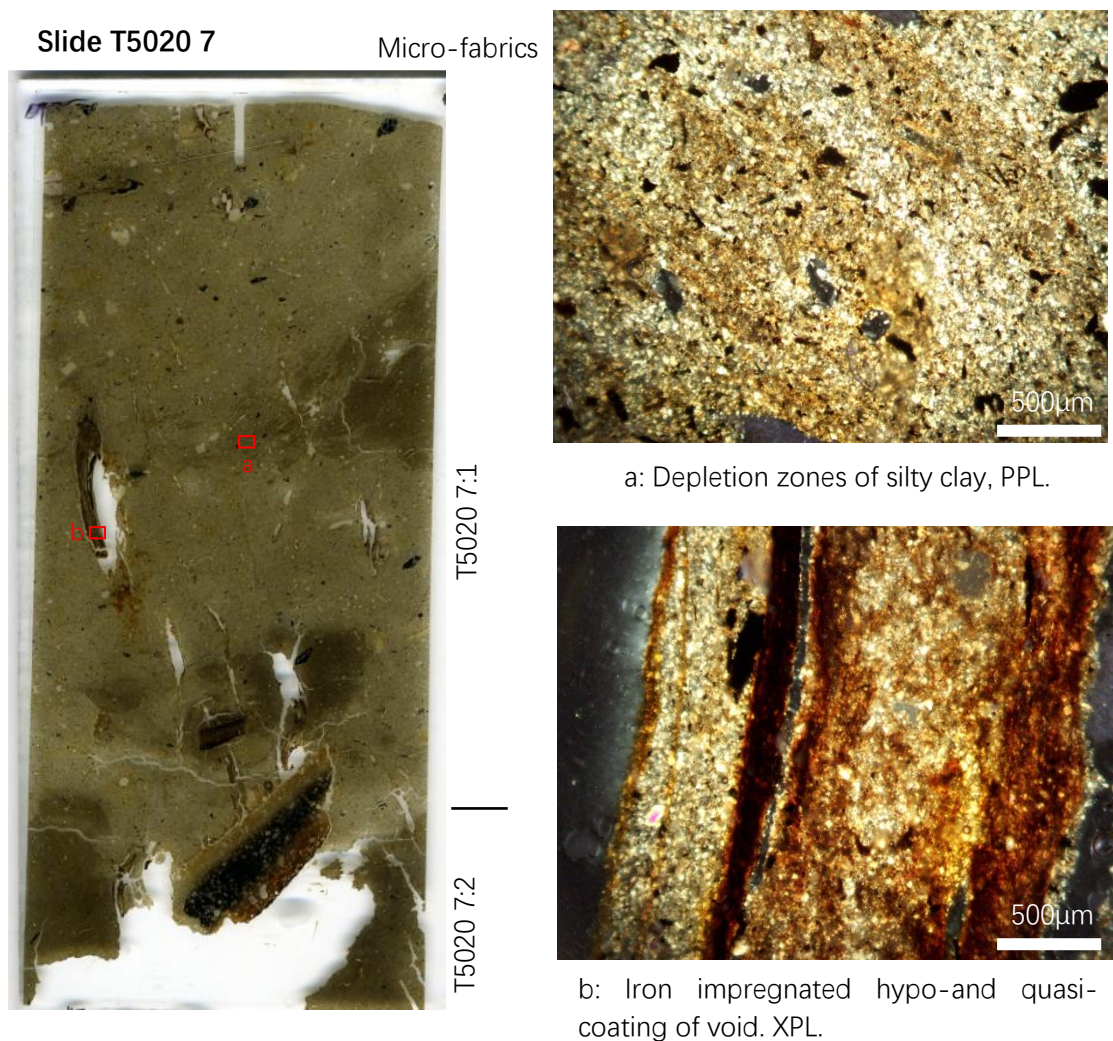


Figure 5.23 Slide scan and microphotographs from slide T5020 7

5.3.2.6 Layer 7

5.3.2.6.1 Introduction

Layer 7 is 25cm thick and is believed to represent the last stage river accumulation of the Liangzhu City. Coarse sand, burnt soil and pottery sherds were found during the excavation.

5.3.2.6.2 Layer 7: Description of microfabrics T5020 7:1, 8:6, 8:5 and 8:4

Although being classified as one single layer, Layer 7 can be separated into three major units based on soil micromorphological observations, and was named Unit 7-1, Unit 7-2 and Unit 7-3 from the bottom to top.

Unit 7-1 (Figure 5.23 and 5.23, Micro-fabrics 7:1 and 8:6) has a coarser material composition compared to previous river accumulation deposits. This unit has a c/f ratio of 10/90 (limit: 50 μ m). It is mainly composed of light grayish yellow (PPL) dotted silty clay with stipple-speckled b-fabric fine silty clay with a few very fine to coarse sand-size rock fragments. Charcoal fragments and dark humified organic matter 0.1-2mm in size occupies around 5% of the groundmass. A few larger charcoal pieces around 5mm in size and a few anthropogenic materials such as two pottery sherds inserted into the top of Layer 8 obliquely were found. This fabric has a massive microstructure with <5% porosity, although channels and passages produced by biogenic activities were commonly seen. The vertical root voids were commonly hypo- and quasi-coated by amorphous iron oxide compounds with diffuse boundaries (Figure 5.23). Around 20% lesser depleted zone of light brown (PPL) silty clay with a higher content of organic matter were observed (Figure 5.23).

Towards the top of Layer 7, there is a waste accumulation of burnt soil, charcoal, ashes, pottery sherds and rock fragments (Unit 7-2, Figure 5.24, Micro-fabric T5020 8:5). This unit is sloping with an angle of roughly 30 degrees and the lower contact with Unit 7-1 is slightly fluctuating. The poorly sorted coarse material, which occupies around 50-70% of the fabric, is dispersed within a finer fine to medium silt-size matrix and becomes

slightly coarser up-profile. Clusters of fine charcoal are commonly found inbetween the coarse materials (Figure 5.24). A root void disrupts this fabric, in which a thick iron impregnated dusty clay hypo-coating was formed. Laminated, sloping silty clay crusts (Figure 5.24) were observed covering this fabric.

On top of this slope, pebble-size rock fragments are found dispersed within Unit 7-3 (Figure 5.24, Micro-fabric T5020 8:4). The groundmass of this unit is the same as the basal unit (Figure 5.24, Micro-fabric T5020 8:3) of Layer 5B, but with coarse material input similar to the Unit 7-2. A detailed description of the groundmass of this fabric can be referred to Section 5.3.2.7.2.

5.3.2.6.3 Results of bulk analysis and interpretation of Layer 7

Layer 7 generally has a slightly acidic pH and low values of all other bulk analyses, which suggests a low level of human intervention in this layer.

Unit 7-1 is also an alluvial deposit similar to previous layers but as the grain size has slightly increased, a higher-energy stream flow is indicated. The depletion pedofeatures may suggest a long-term saturation of stagnant water (Lindbo *et al.*, 2010). The bioturbation evidence and the hypo- and quasi-coating of amorphous iron suggests the temporary shallow water or even an exposed land surface environment with vegetation growth and soil faunal activity.

Based on the slightly inclined, fluctuating lower contact, dispersed but poorly-sorted coarse material in the fine silty clay matrix, weakly grading upwards, and the long axis of pebble size material parallel to the slope direction, the Unit 7-2 on top can be identified as a debris flow (Karkanis & Goldberg, 2018), possibly bringing sediment from the nearby bank that contained relatively large amounts of anthropogenic materials and eroded the original surface of the Unit 7-1.

The groundmass of Unit 7-3 is the same as the overlying Fabric 1 of Layer 5B except that pebble-size rock fragments are found in the fine silty clay matrix. These rock fragments may slide or roll over the slope by gravity, with this process only stopping

when the contour dip zone was totally filled and levelled.

Compared to Layer 8, the energy of stream flow in Layer 7 has increased but was still subjected to bioactivities. In the top of this layer, a high-energy event happened as indicated by the input of coarser material by the debris flow. It is noteworthy that the debris flow deposition indicates either a less maintained riverbank or river floods or overland flows, or even both situations, which may imply some abandonment in this area. After the debris flow, prolonged fluvial deposition with a higher depositional energy dominated, a process which will be discussed in the next section.

5.3.2.7 Layer 5

5.3.2.7.1 Introduction

Layer 5 is believed to be indicative of the period of post-Liangzhu deposition and was divided into two sub-layers: 5B and 5A in the field. Layer 5B is 40cm-thick, light gray, and Layer 5A is 30cm thick, yellowish. A few pottery sherds are found in both sub-layers. These two sub-layers are represented in slide T5020 8, 9 and 10.

5.3.2.7.2 Layer 5B: Description of micro-fabrics T5020 8:3, 8:2, 8:1 and 9:2

Layer 5B can be further divided into four units based on the difference in groundmass and deposition structure, and were named Unit 5B-1, 5B-2, 5B-3, 5B-4 from the bottom to top, respectively.

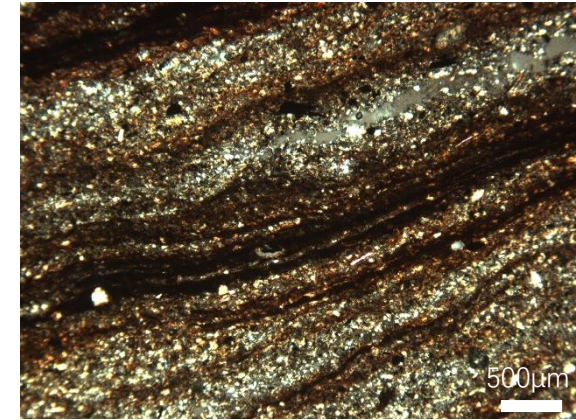
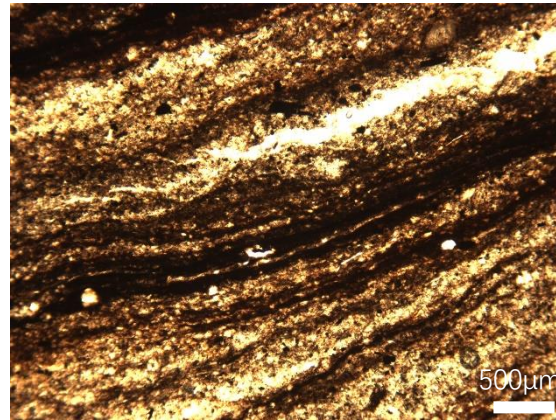
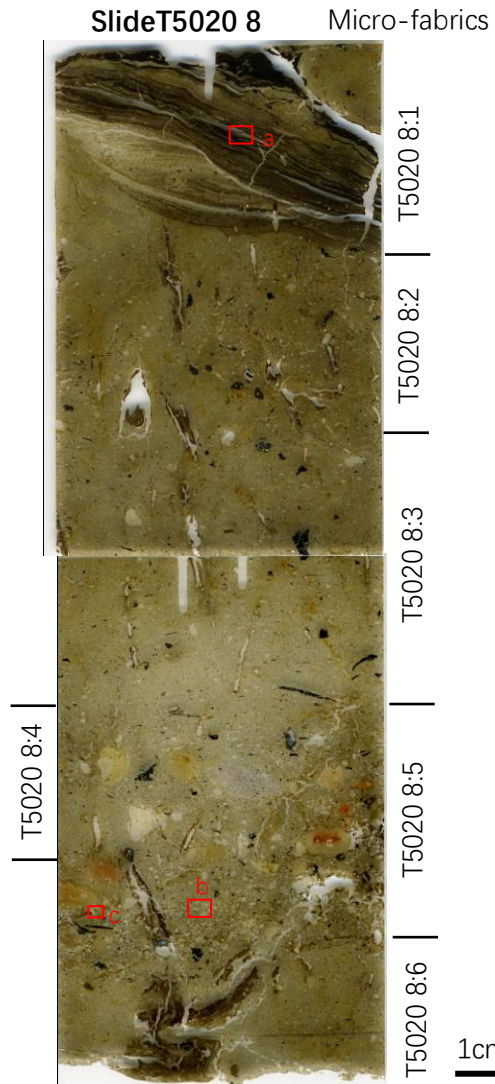
Unit 5B-1 (Figure 5.24, Micro-fabric T5020 8:3) has a c/f ratio of 10/90 (limit: 50 μ m) and is composed of 10% sub-angular to sub-rounded, medium to coarse sand-size rock fragments, 65% well-sorted, very weakly laminated, sub-angular to sub-rounded, coarse silt-size and very fine sand-size quartz, and 3-5% parallel laminated muscovite flakes. The micromass is light yellow (PPL) with a stipple-speckled b-fabric. Fine charcoal occupies around 5% of the groundmass and are parallel laminated. Vertical root voids and passages with no or very thin hypo-coatings of dusty clay frequently impregnated by the iron oxides are constantly observed in this fabric. Reddish mottles

of iron oxides appear and increase up-profile. A single case of pyrite framboids are found around root voids. Trace amounts of dusty silty clay aggregates are also mixed in the groundmass. Unit 5B-1 has a diffuse boundary with the Unit 5B-2 above.

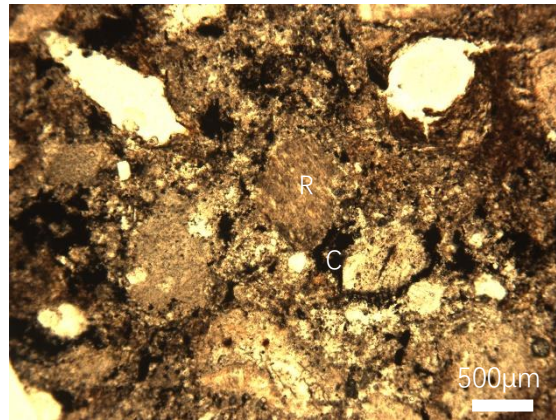
Unit 5B-2 (Figure 5.24, Micro-fabric T5020 8:2) has a similar but slightly finer groundmass with the Unit 5B-1. The fine charcoal and dark humified organic matter are randomly mixed in the groundmass. A few anthropogenic materials including a small piece of bone, a possible phytolith slag, and a few charcoal fragments 3-5mm in size are mixed in the unit. This unit has a weakly developed sub-angular blocky microstructure and a higher porosity of 8%. The root voids and passages are mostly vertical. Most of the root voids were hypo- and quasi-coated by iron oxide impregnated, crescentic, compound dusty and clean silty clays of various thicknesses. A few dense infillings of dusty clay are observed. A few vivianite crystals with yellowish weathered rims are found.

Unit 5B-3 (Figure 5.24, Micro-fabric T5020 8:1) is dominated by reddish-brown and brownish ironpan (Figure 5.24). The basal boundary of this fabric exhibits a concave shape, which may result from some truncation of shallow water flow. The bottom part of the fabric is dominated by slightly fluctuating, weakly fining upward, dusty, organic-rich, silty clay crusts interlaced with well-sorted, parallel laminated, sub-angular to sub-rounded, medium to coarse silt-size and very fine sand-size quartz grains. A few small root voids are found in the fine material laminations. From the middle of this fabric, more than fifty layers of reddish-brown laminations are interlaced with medium silt-size quartz similar to the bottom of this fabric and a few sand-size quartz grains. These laminations are a complex mix of both dusty silty clay crusts and amorphous iron oxide impregnated or replaced laminations of organic matter. The plant structure of these organic matter is completely lost due to their complete replacement by iron oxides.

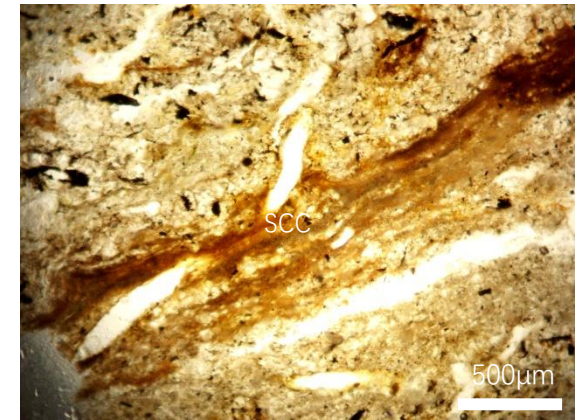
The upper part of this layer (Figure 5.25, Micro-fabric T5020 9:2) is similar to Unit 5B-2. In this part, reddish-yellow mottles of amorphous iron oxides, vivianite crystals in vertical root voids, and large infills of crescent layered dusty clay in root voids are commonly seen.



a: Reddish brown ironpan, PPL (left) & XPL (right)



b: Sand-size rock fragments (R) coated with fine charred (C) material, PPL.



c: Silty clay crusts (SCC) on top, PPL.

Figure 5.24 Slide scan and microphotographs from slide T5020 8

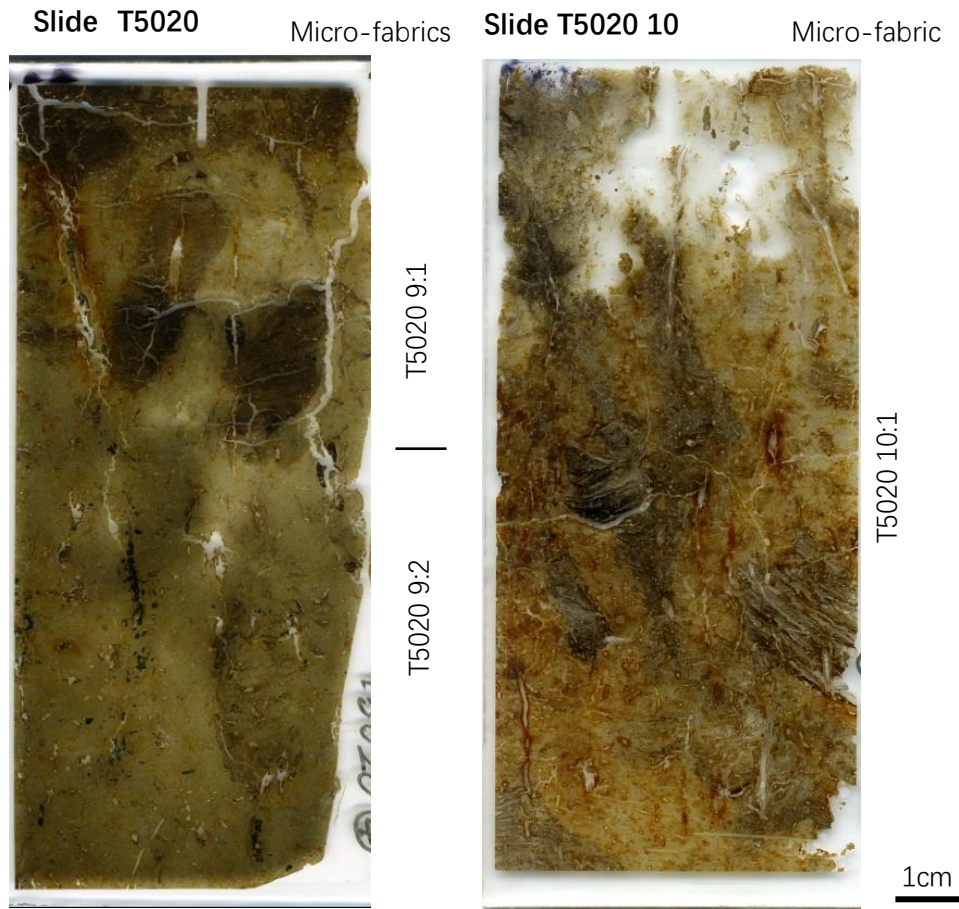


Figure 5.25 Slide scan from slide T5020 9 and 10

5.3.2.7.3 Layer 5A: Description of micro-fabrics T5020 9:1 and 10:1

Layer 5A (Figure 5.25, Micro-fabrics T5020 9:1 and 10:1) has a similar but slightly depleted groundmass compared to the Unit 5B-2. Also, soil development is more mature in this sub-layer with a moderately developed angular blocky structure, long vertical root voids subsequent filled by dusty, sometimes laminated, clay-rich infillings and hypo-coated by crescentic, highly birefringent clay.

In the upper part of this layer, the input of sub-angular sand-size materials increases. It is highly bioturbated and oxidized, with around 60% of the groundmass stained by reddish iron oxides.

5.3.2.7.4 Results of bulk analysis and interpretation of Layer 5

Layer 5 has low organic matter and carbon content, and slightly increased but still low calcium carbonate values (Figure 5.17). Sub-layer 5B has a moderate magnetic susceptibility and phosphorous content, which is slightly increased compared to previous layers due to the influence of iron-replaced organic matter. These values fall back again in sub-layer 5A.

In Layer 5B, Unit 5B-1, where the depositional energy is the strongest in the profile, is indicative of fluvial deposition that quickly accumulated such that it preserved most of its sedimentation structure. In Unit 5B-2, the depositional energy decreases with an increased fine material component. In addition, incipient soil formation processes are indicated by the weakly-developed sub-angular blocky structure and various root voids and passages. Under this relatively stable sedimentation environment, a few fine anthropogenic artefacts have been introduced to the groundmass. In the bottom of Unit 5B-3, the fine silty crusts suggest several stages of slow-moving water influx carrying very fine sediment, then drying and surface crusting, and possibly some truncation. These subtle flow changes to a standing water and then a dry surface environment have resulted in fine silty clay crusts being formed with the secondary amorphous iron oxide replacement of the organic matter component. The fine, plane-parallel, mineralized amorphous organic clay laminae demonstrate a deposition in a quiet and shallow water environment (Macphail & Goldberg, 2017), possibly near the riverbank. After this, there was renewed alluvial deposition with incipient soil formation.

Starting from Layer 5A, the soil formation become more mature, but with constant wet-dry alternation and more oxidation. On top of Layer 5A, the input of coarse material and greater bioturbation may indicate a more stable sedimentation environment favourable for human occupation.

In sum, the changing hydrological conditions in Layer 5 begin with relatively high energy fluvial deposition, then changes to a stable period with incipient soil formation, which was then eroded by rills, following by long-term inundation of stagnant water, and then back to fluvial deposition which is later covered by a more mature and oxidized soil.

5.3.2.8 Layers 4 and 3

These two layers are dated to the Eastern Zhou dynasty (770–256 BC) and Song dynasty (AD 960-1279) based on the pottery sherds found in field. These layers are represented in the top of slide T5020 10 (Figure 5.25). As these layers are not directly relevant to the Liangzhu Culture, the description and interpretation of them will not be discussed in detail here.

Generally speaking, the layers are indicative of a well-developed, oxidized B horizon with illuviated clay coatings of the channels formed due to the strong shrink-swell processes, rooting, and repeated wetting and drying. No or few anthropogenic influences have been observed except the high phosphorus content, which is possibly increased due to modern manuring in this area.

5.3.3 Interpretation of the North Zhongjiagang Watercourse

5.3.3.1 Radiocarbon chronology of the North Zhongjiagang Watercourse

Unfortunately, there is no direct dating in the excavation pit T5020. However, human bones found during the excavation of the North Zhongjiagang Watercourse in 2015 were dated using the AMS laboratory at the University of Tokyo, Japan. The bones selected were from Layers 10 and 12 from excavation pits T3822, T4222, T4251, T4520 and T4820, which are from the bottom part of the North Zhongjiagang Watercourse.

The dating is conducted by Qin *et al.* (2019) at the Archaeometry and Archaeological Dating Laboratory in Peking University, China. All dates are calibrated using OxCal 4.3 (Reimer *et al.*, 2013) and the IntCal 13 calibration curve (Bronk, 2019). The results indicate that the date of the human bones concentrates between 2900 and 2600 cal. BC (Qin *et al.*, 2019). Due to the continuity of layers and the consistency of the archaeological findings in these layers, it can be speculated that in profile T5020, Layer 10 and Platform III-2, which is sandwiched by Layers 10 and 12 in other excavation pits, are also dated between 2900 and 2600 cal. BC.

The dating of a profile 700m north to the excavation pit T5020 also provides some insights about the dating of the layers in T5020. Compared to profile T5020, this profile (LZ-N) has a similar but less complex stratigraphy. This profile was dug in a modern paddy field outside of the northern wall of Liangzhu City and has been studied by Mo *et al.* (2019) and Wang *et al.* (2017). Mo *et al.* (2019) used particle size analysis, X-Ray fluorescence, and pollen analysis while Wang *et al.* (2017) mainly used pollen and charcoal records in order to study the change in human-environment relationships in the middle-late Liangzhu period. As part of their research, they both dated the LZ-N profile (Table 5.2).

Table 5.2 Radiocarbon dating of the North Zhongjiagang region and the LZ-N profile

Layers	Calibrated Dates	Sampling Location	Altitude	Dating material	Dating Lab	Lab No.	Reference
Yellow-brown silt	1940BC(95.4%)	LZ-N	1.85m	Bulk organic matter	Peking University	BA08426L	Mo et al. 2019
Yellowish-brown silt	1690-1605BC	LZ-N	1.61m	Pollen Concentrates	Beta Analytic Inc	LZ-N-3	Wang et al. 2017
Yellowish-brown silt	2150-2025BC	LZ-N	1.59m	Pollen Concentrates	Beta Analytic Inc	LZ-N-4	Wang et al. 2017
Dark-gray clayed silt	2695-2565BC	LZ-N	1.29m	Charcoal	Beta Analytic Inc	LZ-N-7	Wang et al. 2017
Dark-gray clayed silt	2700-2570BC	LZ-N	1.07m	Pollen Concentrates	Beta Analytic Inc	LZ-N-6	Wang et al. 2017
Dark-gray clayed silt	2495-2455BC	LZ-N	1.07m	Charcoal	Beta Analytic Inc	LZ-N-8	Wang et al. 2017
Dark-gray clayed silt	3550BC(83.0%)	LZ-N	0.93m	Bulk organic matter	Peking University	BA08427L	Mo et al. 2019
Dark-gray clayed silt	2875-2615BC	LZ-N	0.89m	Charcoal	Beta Analytic Inc	LZ-N-9	Wang et al. 2017
Dark-gray clayed silt	2665-2550BC	LZ-N	0.73m	Charcoal	Beta Analytic Inc	LZ-N-10	Wang et al. 2017
Layers 10 and 12	2900-2600BC	North Zhongjiagang River:T3822, T4222, T4251, T4520, and T4820	0.37-1.3m	Human bones	University of Tokyo	Tka-19795, 19794, 19792, 19509, 195010, 19511	Qin et al. 2019

The LZ-N profile can be divided into four layers: topsoil, yellow-brown silt, yellowish-brown silt and dark-gray clayed silt (Figure 5.26). The yellow-brown silt and yellowish-brown silt equate to Layer 5 in T5020, as this is a sediment horizon covering the entire

Liangzhu region after the demise of Liangzhu Culture (see section 2.43). The dark-gray clayey silt layer is similar to the reduced, alluvial deposits, such as Layers 10, 8 and 7 in T5020. Mo *et al.* (2019) and Wang *et al.* (2017) both collected dating samples from yellowish-brown silt and dark-gray clayey silt layers. The dating of Mo *et al.* (2019) was based on AMS 14C dating of bulk organic matter while Wang *et al.* (2017) used AMS 14C dating on both charcoal and pollen concentrates that were believed to be free of old charcoal. Their dating results are summarised in Table 1, where it should be noted that the dating of pollen concentrates is believed to be slightly older than their actual age because of the introduction of pre-aged organic carbon in the fluvial setting (Wang *et al.*, 2017 and references therein). The results also suggest that the yellowish-brown silt was deposited at around 2000 cal. BC, and the dark-gray clayey silt was deposited between 2875 and 2455 cal. BC, which is slightly later than deposition of the Layers 10 and 12 in T5020.

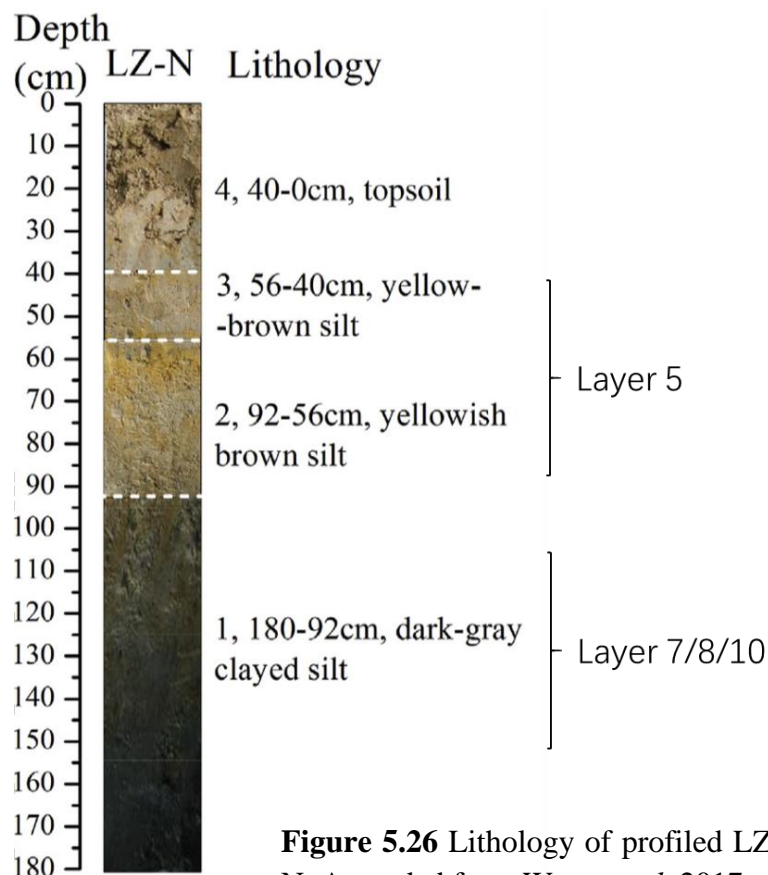


Figure 5.26 Lithology of profiled LZ-N. Amended from Wang *et al.* 2017.

Based on the above analyses, the chronology of the T5020 profile can be reconstructed. The pre-occupation layer was deposited before 2900 cal. BC; Layer 10 and Platform III-2 are dated to between 2900 and 2600 cal. BC; Layers 9B, 8 and 7 were formed between 2600 and 2000 cal. BC; Layer 5 was deposited after 2000 cal. BC; and the overlying Layer 4 was formed during the Eastern Zhou dynasty (770–256 BC) based on pottery typology. Notably, there is no direct radiocarbon dating for Layers 9B, 8 and 7, while no or only a few locations along the entire Zhongjiagang Watercourse have been dated to between 2500 to 2000 cal. BC so far. This gap in the record may be due to underlying layers being eroded under a higher-energy stream flow from Layer 5, or the decrease of human activity in the Liangzhu region during this period. The former hypothesis is not currently supported by the soil micromorphology analysis as no erosion has been observed between Layer 5 and the underlying Layer 7 in T5020. Therefore, more research and dating data are needed to better understand this apparent gap.

5.3.3.2 Particle size analysis of the T5020 profile

Altogether, 21 samples from profile T5020 have been subjected to particle size analysis. Based on the different characteristics in the frequency histogram (Figure 5.27), these samples can be separated into two major groups that reflect different deposition modes. The first group (blue lines in Figure 5.27) has a single peak, which generally indicates a good sorting of particles in the soil material, while the second group (green and red lines in Figure 5.27) has multiple peaks, which suggests a more diverse set of sources of the soil material. The change in particle size distribution of each sample is more clearly shown in Figure 5.28. Combining these two diagrams, the flow characteristics and change of particle size distribution of profile T5020 can be reconstructed.

The pre-occupation sediment, namely the top of Platform III-2, Layer 10C and the

bottom of Layer 10B (light green lines in Figure 5.27), have similar diverse sources of soil material, which is dominated by fine materials. From the pre-occupation sediment to the bottom of Layer 10B, the amount of clay material slightly decreases with a gradually increasing input of coarser material. The bottom of Platform III-2 (sample T5020 1-2) shows a slightly different multi-peak pattern with slightly coarser material dominant in the sediment. The top of Layer 10B (dark red line, sample T5020 4-1) shows a very low kurtosis with a very high percentage of clay material, which indicates the very poor sorting of the sediment. Based on micromorphological observation, this increase in clay content is largely due to the deposition of thick silty-clay crusts under a shallow and stable water environment. Layers 10A, 8 and the top of 9B (dark green lines in Figure 5.27) show a similar multi-peak distribution pattern with a higher mode than those samples in light green.

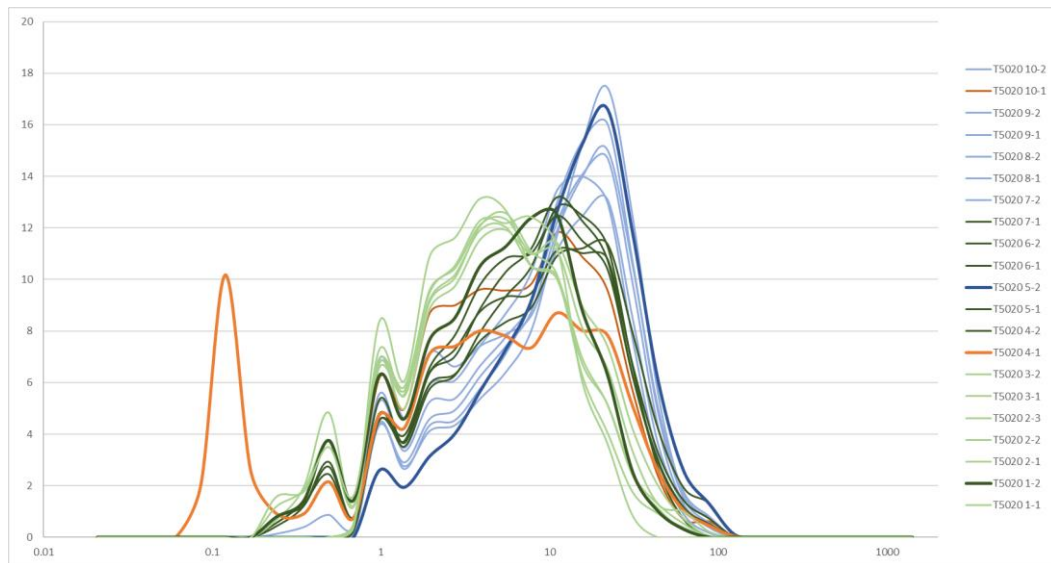


Figure 5.27 Particle size distribution graph of T5020, the bold lines are mentioned in the context.

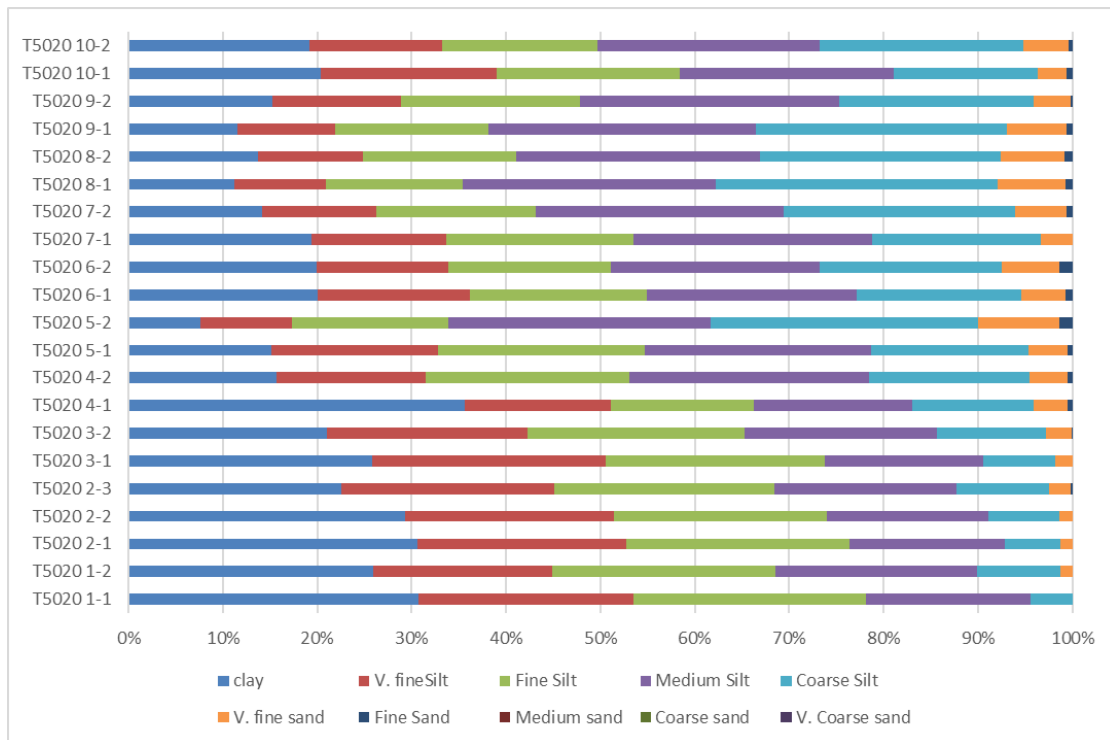


Figure 5.28 Percentage bar chart of the particle size of T5020.

The bottom of Layer 9B (sample T5020 5-2, blue line in Figure 5.27) presents a single-peak pattern and a relatively low clay content, which suggests a different, natural source material compared to the underlying sediments in the profile. It is interesting that the particle size of the bottom of Layer 9B is very similar to the bottom of Platform III^③B2 and Layer 13C in profile T2621, which suggests that the Layer 9B may have been constructed using soil material from an older stratum similar to the Platform III^③B2 (see section 5.2.2.3 and further discussion in Chapter 8). Layers 7, 5B and the bottom of 5A also have a similar single-peak pattern (blue lines in Figure 5.27) but with a slightly higher clay content. The debris flow fabric of Layer 7 is not represented in the particle size analysis as the sample was taken from the middle-upper part of Layer 7, and the pebble-size material was removed during sample processing. The top of Layer 5A returns to a multi-peak pattern (red lines in Figure 5.27) with an increase in clay content, which may be due to bioturbation and soil formation in this stable surface based on soil micromorphological observation (see section 5.3.2.7.3). The bottom of Layer 4 returns to a single-peak pattern.

In general, the particle size of profile T5020 gradually increases from bottom to top and probably represents low-energy alluvial sedimentation. The highest depositional energy of this profile appears to be in the bottom of Layer 9B, the top of Layer 7 and the bottom of Layer 5, which correlates with the soil micromorphology observations and the results of particle size analysis of LZ-N profile (Mo *et al.*, 2019).

5.3.3.3 Site formation processes of profile T5020

The T5020 profile represents the centre of the North Zhongjiagang Watercourse and part of the edges of the mounds. In general, the channel was a gradually accreting alluvial plain deposited by slow-moving and shallow water and was repeatedly interrupted by short-term drying and soil formation processes.

Before 2900 cal. BC, the pre-occupation sediment is a slow build-up of alluvium containing humic topsoil (Ah horizon material) aggregates, exhibiting alternating conditions of water saturation and periodic drying with phases of exposure. From 2900 to 2600 cal. BC, Platform III-2 was built-up by human action, possibly by ‘clay wrapped with grasses’, which was then covered by alluvium deposited in a shallow water environment. At the same time, alluvial deposition with some surface incipient soil formation and possible drying phases were observed in Layer 10C, alluvial deposition with a slightly faster sedimentation rate due to a slow-moving or even stagnant water environment were observed in Layer 10B, and a greater coarser material component, possibly resulting from higher water motion, was found in Layer 10A. From the upper part of the Layer 10B, the input of anthropogenic material begins. From Layers 10C to 10A, the sedimentation environment changes from constant wet-dry alternating conditions to permanently wet conditions.

After 2600 cal. BC, Layer 9B was either dumped or deliberately constructed using natural, coarser soil material possibly derived from an older stratum. Coarse material

such as charcoal and pottery sherds that had not been transported far were dumped into the sediment which was later covered by slow-moving water and associated fine material. The top of this layer dried out and was found to contain dumped material from dry land. In Layer 8, the accumulation of an alluvial floodplain continued with relatively short-term soil development. From the bottom to the top of Layer 8, the water environment showed a drying trend. However, wet conditions soon returned with an increase in water motion seen in the Unit 7-1 of Layer 7. In the end stage of Liangzhu, an overland flood happened as the debris flow containing the remains of human occupation from nearby mounds was deposited.

From 2000 cal. BC onwards, fluvial deposition with a higher-energy dominated. In Layer 5B, relatively high-energy fluvial deposits continued but were later weakened and stabilised with associated incipient soil formation. A shallow rill eroded the alluvium, followed by inundation with shallow, stagnant water with no disturbance from human or faunal activities. The sediment then shifted to alluvial deposits with higher levels of oxidation and mature soil development in Layers 4 and 3.

5.3.3.4 Change of hydrological conditions and human activity in North Zhongjiagang region

At the time the Liangzhu people arrived and occupied the North Zhongjiagang region, the region had a relatively stable surface but was subject to repeated wetting and drying episodes. The deposits were probably formed by slow-moving sheetwash while the constrained channelised flow of the Zhongjiagang Watercourse did not exist before 2900 cal. BC. This evidence correlated with the pollen data from the Liangzhu and wider Lower Yangtze River region which reflected a temperature drop and drier conditions since 2900 cal. BC, compared to the previous warm and humid climate (Innes *et al.*, 2014; Wang *et al.*, 2007; Yi *et al.*, 2003, 2006). Under the background of this cold, dry event, Platform III-2 was constructed and extended into the middle part

of the North Zhongjiagang Watercourse. This platform was actually quite thin, with a thickness of only 30-50cm. This demonstrated that at the time Platform III-2 was built, the groundwater table was low, such that a thinly constructed surface was sufficient.

However, wet ground conditions soon returned with Platform III-2 soon abandoned and subsequently affected by the influence of shallow and slow-moving water. The overlying Layer 10 showed a trend of increasing wetness with a greater depositional energy. Based on pollen data, this may relate to the recovery of warm and humid conditions from 2900 to 2700 cal. BC (Mo *et al.*, 2019). Specifically, in the bottom sub-layer 10C, the alluvium had accumulated under very weak water motion with occasionally dry conditions and was only slightly influenced by surface soil formation processes. In the middle of sub-layer 10B, the sediments accumulated quickly under shallow water with alternating wet and dry conditions. In the top of sub-layer 10A, the depositional energy increased and long-term wet conditions predominated. This is the stage when the northern part of the Zhongjiagang Watercourse was most properly functioning as a waterway.

Layer 9B accumulated on top of the Layer 10 under the continuous influence of shallow water. However, the slope of Layer 9B became dried out and exposed for a short period. The deposition of Layer 8 on top of this layer also showed a drying trend, which coincided with a decrease in the swampy conditions as indicated in the pollen analysis after 2500 cal. BC (Wang *et al.*, 2017). During this drying period, there was a clear decline in human activity, particularly in rice growing, as indicated by the decrease in *Gramineae* pollen of >38mm in size (Wang *et al.*, 2017). The gap in radiocarbon data between 2500 and 2000 cal. BC inside the Liangzhu City coincided with the formation of compound clay coatings in this layer. However, what happened during this relatively dry period and whether it influenced on the decline of Liangzhu Culture is still unclear.

In Layer 7, the stream flow energy shows a rapid rise. In the mid-upper part of Layer 7,

a small scale debris flow carrying stones and anthropogenic artefacts from nearby mound structure occurred, which indicates that part of the channel bank was probably affected by strong overland flow or even a flood. This flood event coincides with the date that Liangzhu City was abandoned, that is slightly before 2000 cal. BC. The high-energy stream flow extended into Layer 5B, which was then stabilised with a return of anthropogenic material and incipient soil formation processes. However, after a possible large rainfall event, a rill eroded the sediment and a completely ponded water environment dominated for a considerable period. In general, the evidence of suddenly increased of flow energy and overland flow in Layer 7 supports the hypothesis that the abandonment of Liangzhu City and Liangzhu Culture was related to flooding events. Moreover, the long-term wet conditions and absence of human activity in Layer 5 agree with wider regional scale sedimentation evidence that areas around the Tai Lake and Hangzhou Bay have been abandoned for more than a thousand years.

5.4 Summary

The Middle Zhongjiagang profile (T2621) exemplified the close relationship between human activity and the changing hydrological conditions at the early stage of the development of Liangzhu City. Before the arrival of Liangzhu people, the Middle Zhongjiagang region was under the influence of tidal action. At around 3100 cal. BC, a dry and exposed surface appeared and humans began living in the region. This short dry surface is soon covered by alternating wet-dry alluvial sediments, and the Liangzhu people abandoned this region. After two or three cycles of alternating wet-dry conditions, at around 3000 cal. BC, although the sedimentation in the region was still under the influence of water, Liangzhu people started constructing large mounds along the channel using local sediments adding with different components such as charcoal fragments and coarse sands, and interspersed with calcite-rich, off-white, gravel layers. This implies a deliberate site selection and a strong determination to transform the local hydrological regime to create favourable living conditions.

The North Zhongjiagang profile (T5020) provides an informative understanding of the lifecycle of the Zhongjiagang Watercourse, particularly in its terminal stage, as well as the hydrological conditions at the time that Liangzhu City was abandoned. Generally, the northern part of the Zhongjiagang Watercourse only functioned as a waterway intermittently, and the sphere of human activity reacted sensitively to the changes of local water conditions. When the climate was relatively dry at around 2900 cal. BC (Innes *et al.*, 2014; Wang *et al.*, 2007; Yi *et al.*, 2003, 2006), the channel was probably more similar to a drained swamp with intermittently exposed surfaces and a high clay content, and human activity expanding into this new space. When wet conditions returned, the channel functioned more like a slow-moving waterway with a high sedimentation rate, leading to a retreat in human activity space. After 2600 cal. BC, the hydrological conditions changed quickly from wet to dry as indicated by Layers 9B and 8, and the Liangzhu Culture began to decline (Wang *et al.*, 2017). The anthropogenic material found on top of Layer 8 implied that human occupation resumed for a short period but was soon covered by long-term fluvial deposition with greater and higher water action. Slightly before 2000 cal. BC, the bank and probably the whole Liangzhu City was unmanaged. From 2000 cal. BC onwards, although human activity returned for a short relatively stable period, the main theme of the times was a wide-scale stagnant and ponded water environment, which marked the complete demise of Liangzhu and its descendants in the region.

Chapter 6: The settlement sites of Liangzhu City

6.1 Introduction

Profiles T0950 and T3131 contained a number of lenses of occupation remains including burning, matting and dumping. The T0950 profile is taken from the Southwest Mojiaoshan mound, which is between Mojiaoshan mound itself, the central part of the Liangzhu City where large house remains were revealed, and Jiangjiashan mound where groups of elite burials were found (Liu *et al.*, 2019d). T3131 is taken from the South Zhongjiagang Region, which was believed to be related to craft production and the occupation of common people (Liu *et al.*, 2019a). This chapter will discuss these two profiles to provide a glimpse of human occupation and their relationship to the changes of local hydrological regimes in different areas of Liangzhu City.

6.2 The Southwest Mojiaoshan Zone (T0950)

Excavations since 2012 revealed that the Southwest Mojiaoshan Zone and generally the western part of the Mojiaoshan mound was a concave area with possible channel depositions between the Jiangjiashan and Mojiaoshan mounds (Figure 6.1a) (Liu *et al.* 2019). During the excavation in 2017, the T0950 profile provided a complete sedimentation sequence with which to understand the construction history of the Southwest Mojiaoshan Zone. The profile is mainly composed of two stages of well-preserved ‘clay wrapped with grasses’ construction, with associated wooden piles and bamboo mats (Figure 6.1b). Between these two stages of construction was a 10-20cm thick layer of charred material (Figure 6.2). The archaeological meaning of this burnt

material and whether it was *in situ* or not could not be adequately determined in field. The pottery found in these layers belonged to the Early Liangzhu period (roughly 3300–3000 cal. BC), and the dating of the charred material from the burnt layer is dated to 3000 cal. BC (personal communication from ZPICRA). The study of the T0950 profile from the Southwest Mojaoshan Zone aims to provide information regarding the construction history of a potential occupation zone and its relationship with potential changes in the local water regime in the early stages of the development of the central part of Liangzhu City.

6.2.1 Field observation and stratigraphy of profile T0950

During the excavation in 2017, three micromorphological samples and six bulk samples were taken (Figure 6.2). The soil sampling and analysis focus on the pre-site condition and the hydrological condition and human activity between the two stages of ‘clay wrapped with grasses’ construction. The field descriptions of each layer in T0950 are as follows:

Topsoil: A pond built in the historical period (date unsure, might be Eastern Han, AD 25-220) that destroyed the upper layer of the ‘clay wrapped with grasses’.

The upper layer of ‘clay wrapped with grasses’ (Layer 8C) is about 2-3m thick. The excavation exposed three rows of ‘clay wrapped with grasses’ materials surrounded by four rows of wooden piles (Figure 6.1b). A single piece of ‘clay wrapped with grasses’ material was 40 x 10 x 8 cm in size and collectively forms 2m³ large soil blocks. These ‘clay wrapped with grasses’ materials are made and transported from different places as indicated by the various colour of the soil materials. The excavator suggested that the wooden piles of about 1m in length were knocked in first, and then two rows of ditches in the sides were filled in with blocks of ‘clay wrapped with grasses’ materials, and the middle row was filled in last (Figure 6.1c).

Layer 9 is a small ditch filled with light gray (2.5Y 6/1) fine silty clay material. A few charcoal fragments and humified plant remains were found. Based on field observation, this ditch is believed to contain water flowing from the east (the direction of the Mojiaoshan mound) to the west.

Layer 10 is a light brownish gray (2.5Y 6/2) silt-size material overlying the burnt layer and was undercut by the Layer 9.

Layer 11 (2.5Y 3/1 very dark gray) is located in the north-eastern part of the excavation pit. It is about 20cm thick and is composed of a mixture of charred materials and charred seeds including rice, *Vitis*, and *Cucumis*, pottery sherds, ashes, burnt soils and burnt wall fragment with impressions of wooden strips preserved. The date of this layer is around 3000 cal. BC (personal communication from ZPICRA).

Layer 12 is a dark brownish, hardened layer below the charred materials. Lots of stems, coarse sands, charcoal, burnt soils and ash were found in this layer.

Layer 13 is a light greyish (2.5Y 6/1) silty clay overlying the 'clay wrapped with grasses' with distinct boundaries. It is mixed with light yellowish soil aggregates, which can be observed in field. Two micromorphology samples and four bulk samples were taken from the bottom of Layer 9 to the top of the Layer 13. The T0950 2 soil block was taken from the central part of the burnt material and the T0950 3 block focuses on the peripheral part of the burnt material.

The bottom layers of 'clay wrapped with grasses' (Layer 14) were about one metre thick. Two sub-layers can be identified by their sharp boundaries, but the boundary between each piece of 'clay wrapped with grasses' is indistinct.

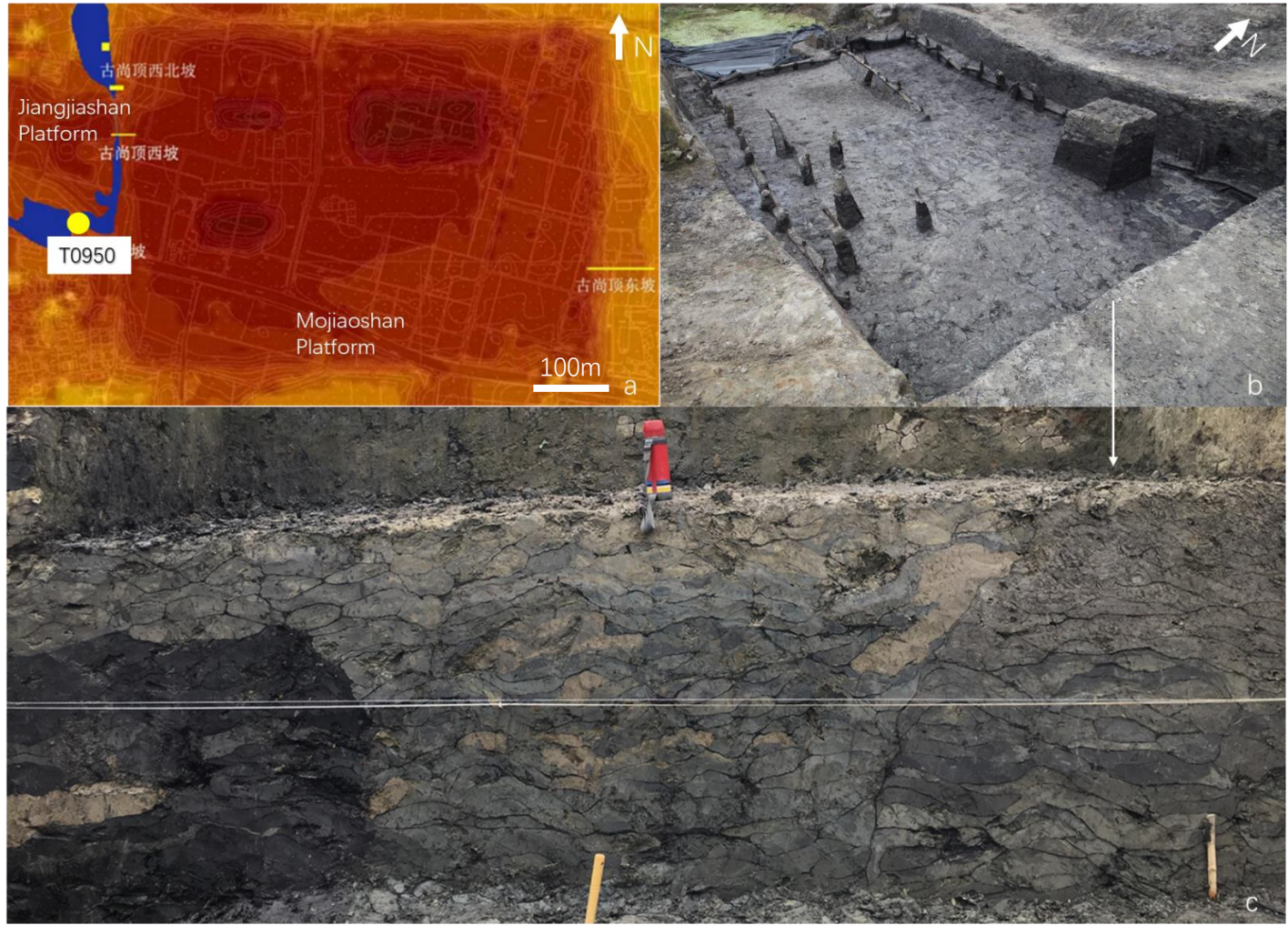


Figure 6.1 a) the location of the T0950 profile and the reconstructed water area between Jiangjiashan and Mojiashan mounds based on multi-excavations since 2012 (amended from Liu *et al.*, 2019a); b) four rows of woodpiles of Layer 8C; c) eastern wall of T0950 showing the cross section of Layer 8C composed of three rows of ‘clay wrapped with grasses’ using various soil materials. Excavation tools provide scale.

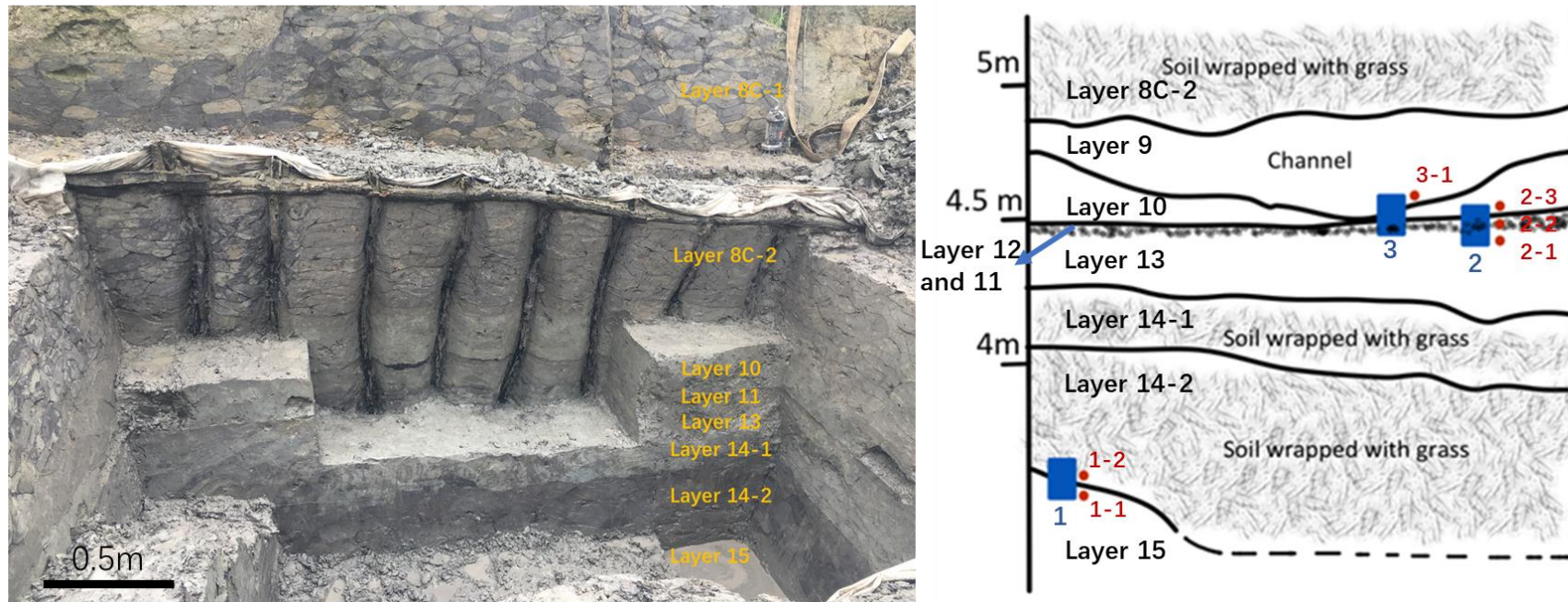


Figure 6.2 Stratigraphy and sampling position of the T0950 profile. The blue rectangles and numbers refer to the sampling positions and numbers of the soil micromorphology samples. The red dots and numbers refer to the sampling positions and numbers of bulk samples.

Buried soil (Layer 15): Gray (2.5Y 6/1) silty clay. One micromorphology sample and two bulk samples were taken from the boundaries of Layers 15 and 14.

6.2.2 Results of soil micromorphological analysis in T0950

6.2.2.1 Buried soil (Layer 15)

6.2.2.1.1 Micromorphological description of the micro-fabrics T0950 1:2 and T0950 1:3

The buried soil (micro-fabric T0950 1:3) has a c/f ratio of 2/98 (c/f limit: 50 μ m) and is dominated by light-brown (PPL) humic silty clay with a weakly reticulate-striated b-fabric. The microstructure is mainly massive with a few fissures, which creates 3% porosity. Trace amounts of very fine charcoal fragments are found. The organic matter (3%) is mostly humified and laminar. A few bluish vivianite crystals (3%) are also mixed in the groundmass. A few root voids with remnant organic matter are also observed. Occasional micritic calcium carbonate clusters with diffuse boundary are found around voids and nearby groundmass (Figure 6.3). Partially fragmented fine silty clay crusts are observed in the upper part of this layer (Figure 6.3). Overlying the silty clay crusts is a 1cm thick laminar calcrete zone (micro-fabric T0950 1:2) formed by the mixture of 70% of micritic calcium carbonate and 30% silty clay stained by humic organic matter or amorphous iron oxides (Fig 6.3).

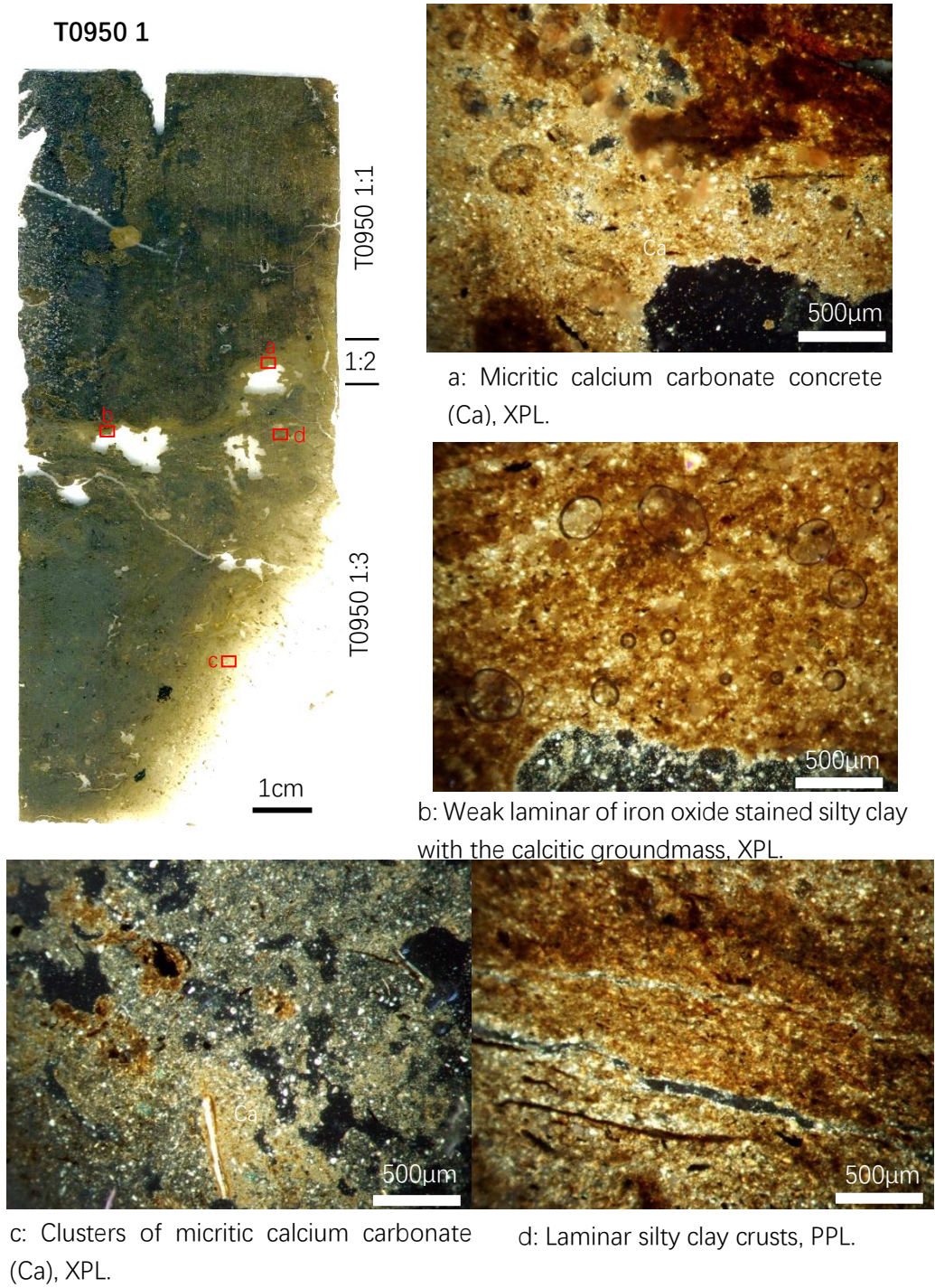


Figure 6.3 Slide scan and microphotographs from slide T0950 1

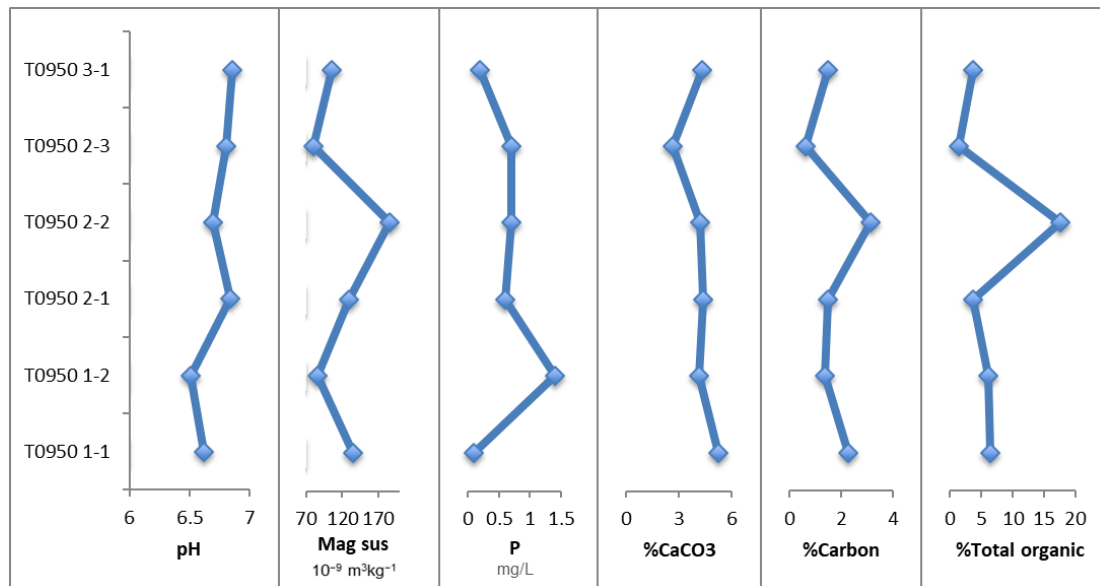


Figure 6.4 Analytical results of pH, phosphorus, magnetic susceptibility, and carbon, total organic and calcium carbonate contents of profile T0950.

6.2.2.1.2 Results of bulk analysis and interpretation of the buried soil

The bulk sedimentology results (Figure 6.4) indicate that the buried soil has a slightly acidic to neutral pH, moderate magnetic susceptibility, moderate total organic and calcium carbonate content, and very low phosphorus and carbon contents, which are all indicative of a low degree of human activity. The very fine sand, silt and clay dominated fabric of this layer suggest that it accumulated under a gentle water flow, probably as an overbank alluvial deposit, which is then subject to periodic drying leading to the formation of diffuse clusters of calcium carbonate. The silty clay crusts on top of this layer indicates a shallow, gentle, overland flow conditions with periodic surface drying (Pagliai and Stoops, 2010). The formation of laminar calcium carbonate crusts is suggestive of sharply reduced hydraulic conductivity of the soil by cementation (Durand *et al.*, 2010), which in the case of the T0950 profile, may be related to the construction of ‘clay wrapped with grasses’ layer (Layer 14) on top that caused the cementation.

6.2.2.2 Layer 14: Bottom layers of 'clay wrapped with grasses'

6.2.2.2.1 Micromorphological description of the micro-fabric T0950 1:1

This layer is composed of 95% humic dusty or silty clay with 5% sub-angular fine sand-size quartz. Humified organic matter (2-3%) is randomly mixed in. The micromass is generally a massive, reddish brown (PPL) speckled b-fabric form with a few planar fissures that create 2-3% porosity.

6.2.2.2.2 Results of bulk analysis and interpretation of the Layer 14

Layer 14 has a slightly acidic pH, very low magnetic susceptibility and carbon content, moderate total organic and calcium carbonate content, but a high phosphorus content, which may suggest some level of human intervention. This layer is identified as constructed 'clay wrapped with grasses' layer in field, using silty clay alluvial material.

6.2.2.3 Layer 13

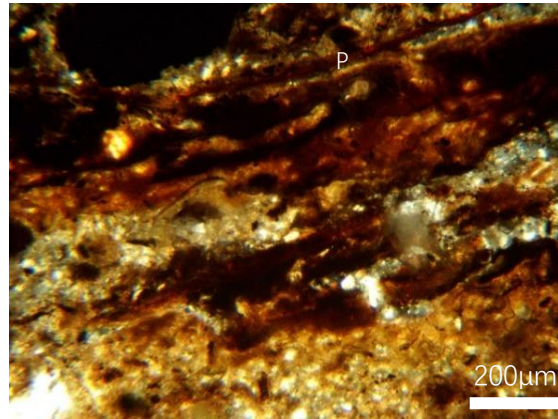
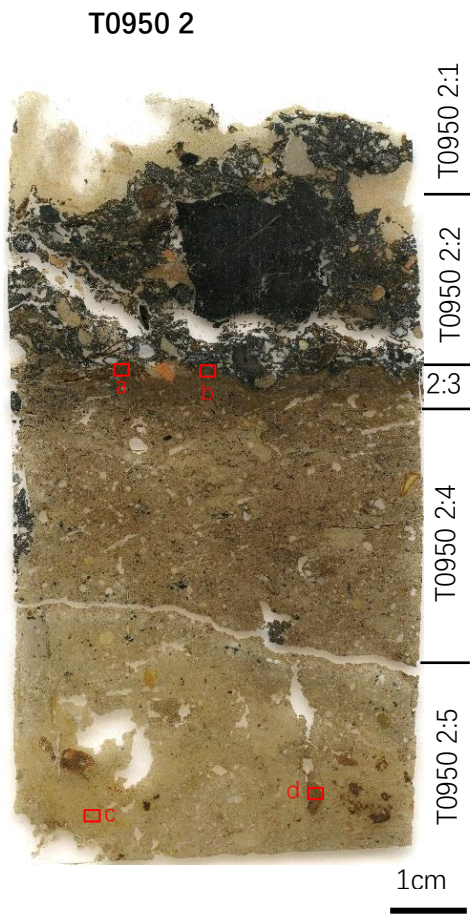
6.2.2.3.1 Micromorphological description of the micro-fabrics T0950 2:5 and T0950 3:5

Layer 13 is represented in the bottom part of slide T0950 2 and 3 (micro-fabrics T0950 2:5 and T0950 3:5). This layer has a massive microstructure and is generally a mixture of at least two different soil materials. The description here will be based on the micro-fabric observed in fabric T0950 2:5. The first material that occupies 70% of the fabric has a c/f ratio of 5/95 and is mainly composed of light yellowish (PPL) silty clay with yellowish interference colour and striated b-fabric and 5% sub-angular, very fine sand-size rock fragments. Iron mottles/nodules are widely and evenly distributed in the groundmass, occupying around 40% of this soil material (Figure 6.5). A few fine

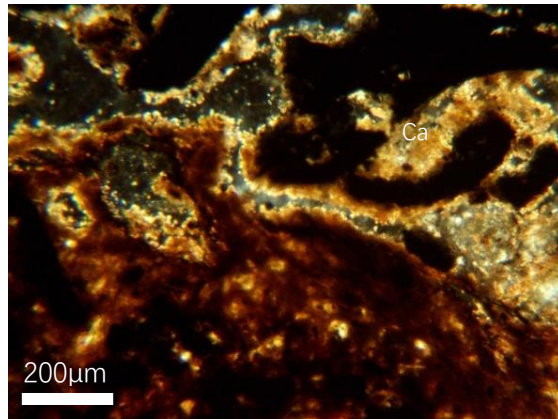
charcoal rich soil aggregates with potential calcium carbonate pseudomorphs of prismatic crystals are heterogeneously mixed in the groundmass (Figure 6.5). The second soil material is composed of 30% poorly sorted, sub-angular, fine to coarse sand-size rock fragments and 70% light brownish (PPL) silty clay with a striated b-fabric. Occasional reddish brown (PPL) micritic calcium carbonates lenses and aggregates are mixed in.

6.2.2.3.2 Results of bulk analysis and interpretation of the Layer 13

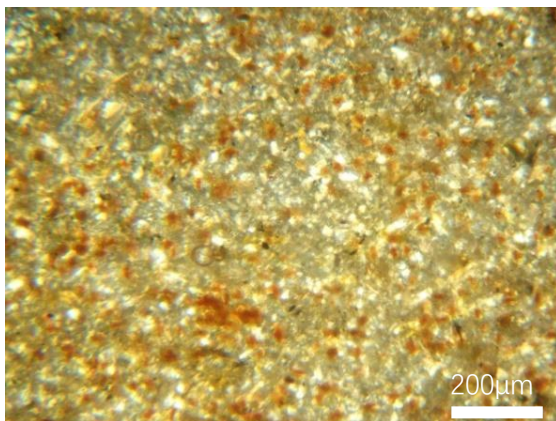
Layer 13 has a slightly increased pH, moderate magnetic susceptibility, phosphorus and calcium carbonate contents, and low total organic and carbon content, which is suggestive of a low degree of human activity. The low organic content and massive structure imply no or few pedogenic processes have occurred in this layer. The mixture of different soil aggregates, which is also macroscopically observed in field, may therefore be caused by human invention or disturbance in this layer. The particle size distribution of the first soil material of micro-fabric T0950 2:5 suggests alluvium as the origin of this sediment. The widely developed amorphous iron oxide mottles suggest the soil materials accumulated under relatively dry but alternating wet-dry conditions. The occasionally found aggregates of micritic calcium carbonate and charred material rich in calcium carbonate pseudomorphs of prismatic crystals may come from burning events.



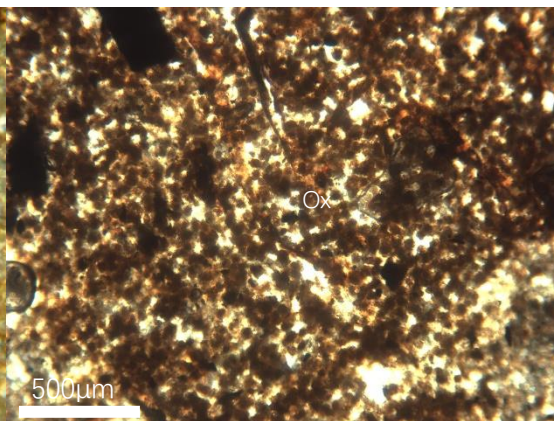
a: Reddened sediment with laminated plant material (P) and micritic calcium carbonate, XPL.



b: Reddened sediment and the micritic calcium carbonate (Ca) in-between charred material, XPL.



c: Iron oxide mottles in the groundmass, XPL.



d: Possible calcium carbonate pseudomorphs of oxalate (Ox), PPL.

Figure 6.5 Slide scan and microphotographs from slide T0950 2

Combined with the evidence of the archaeological context, this layer was disturbed, physically mixed and probably deliberately prepared by human activity by using dried alluvial material mixed with products of burning activity.

6.2.2.4 Layer 12

6.2.2.4.1 Micromorphological description of the Micro-fabrics T0950 2:4 and 2:3

Layer 12 is represented in the middle part of slide T0950 2 and 3, the description here will be based on micro-fabrics T0950 2:4 and 2:3 from slide T0950 2. The lower part of Layer 12 (Micro-fabric T0950 2:4) is a heterogenous mix of 65% brownish organic silty clay, 20% light yellowish silty clay, 10% sub-angular, poorly-sorted, sand-size rock fragments and 5% reddish brown (PPL) clay aggregates. These soil fabrics are generally planar and well compacted. The humified organic matter in the dark brown organic silty clay is mostly laminated and occupies around 15% of the groundmass. The light yellowish silty clay shows a striated b-fabric. This layer generally has a massive microstructure with a few vughy voids. A few fine charcoal, shell fragments, occasional burnt quartz and blueish vivianite crystals are randomly mixed in the groundmass.

On top of Layer 12 is a 0.5cm thick, reddened sediment (Micro-fabric T0950 2:3). It is heavily masked by micritic calcium carbonate (Figure 6.5), which creates a crystalline b-fabric in the brownish to reddish brown (PPL) micromass. Laminated humified and charred organic matter and potential bast fibres occupied around 15% of the groundmass.

6.2.2.4.2 Interpretation of the Layer 12

No bulk analysis data is available for this layer. The mixture of planar and compacted soil aggregates and the occasionally found fragments of occupation debris of the lower

Layer 12 suggests that this fabric could be dumped settlement-derived materials that have been trampled and compacted. The laminated organic matter (Figure 6.6) and potential bast fibres on top could be the remnants of matting materials. The reddened sediment and micritic calcium carbonate masked groundmass suggest that this fabric has been severely burnt and the micritic calcium carbonate may originate from the overlying charred material fabric (Layer 11). In summary, the micro-fabric T0950 2:3 could be a burnt occupational living surface.

6.2.2.5 *Layer 11*

6.2.2.5.1 *Micromorphological description of the Micro-fabric T0950 2:2*

Layer 11 is represented in the mid-upper part of slide T0950 2 and 3, and the description here will be based on micro-fabric T0950 2:2 from slide T0950 2 (Figure 6.5). This layer is a mixture of carbonized material including charred wood, stem, seed, a few ash lumps, burnt soil, soil aggregates, and small pottery fragments. Some of the highly broken-up charred material appears to be weakly laminated. Micritic calcium carbonate rich soil materials are found filling the gaps between the coarse components and are more concentrated in the lower part of this layer (Figure 6.5).

6.2.2.5.2 *Results of bulk analysis and interpretation of the Layer 11*

Layer 11 has a slightly acidic pH, high magnetic susceptibility, moderate phosphorus and calcium carbonate content, and very high organic and carbon content (Figure 6.4). The bulk sedimentology and soil micromorphology analysis both suggest that this layer is the product of a large burning event. The combination of reddened soil material in the upper part of Layer 12 and abundant charred material with no or few evidence of disturbance indicate that this burning event probably happened *in situ*. The widely found micritic calcium carbonates in the lower part of Layer 11 and the reddened

sediment of Layer 12 are suggestive of the solution and remobilization of ash overlying the charred material to the lower part of the burnt layer. Based on findings in field, Layer 12 is a mixture of fine occupational debris and potential house construction materials such as eight pieces of wall fragments with impressions of wooden branches are found. Further comprehensive archaeobotanical study of this layer may reveal the full picture of this occupation area. In summary, this layer could be interpreted as a *in situ* burnt area.

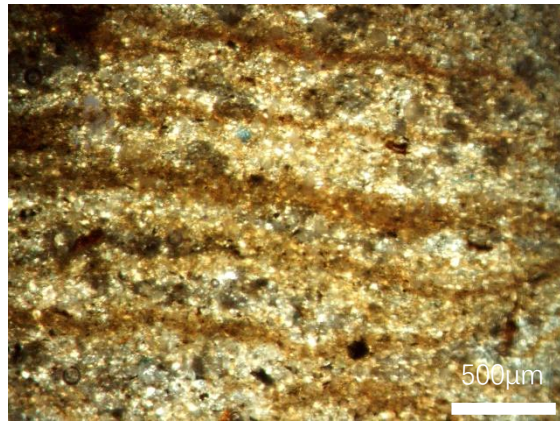
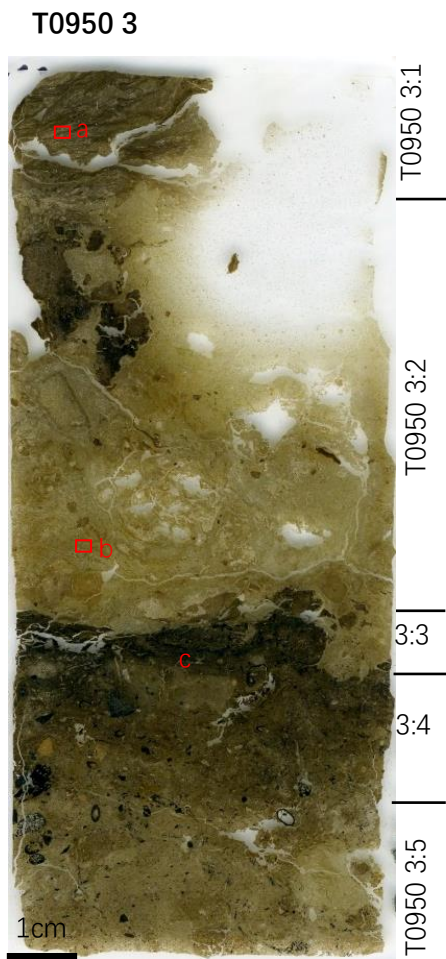
6.2.2.6 Layer 10

6.2.2.6.1 Micromorphological description of the Microfabric T0950 3:2

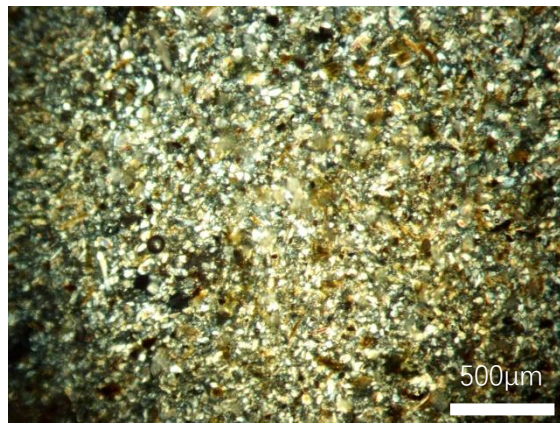
Layer 10 is represented in the upper part of slide T0950 2 and 3 with the description here will be based on micro-fabric T0950 3:2 from slide T0950 3. This layer covered the burnt layer with distinct and wavy boundary. It is composed of more than 70% well-sorted, sub-rounded coarse silt and fine sand material (Figure 6.6). Humic silty clay aggregates in various sizes are commonly found in the groundmass. Few fragments of dusty silty clay crusts with low interference colours are intermittently found.

6.2.2.6.2 Results of bulk analysis and interpretation of the Layer 10

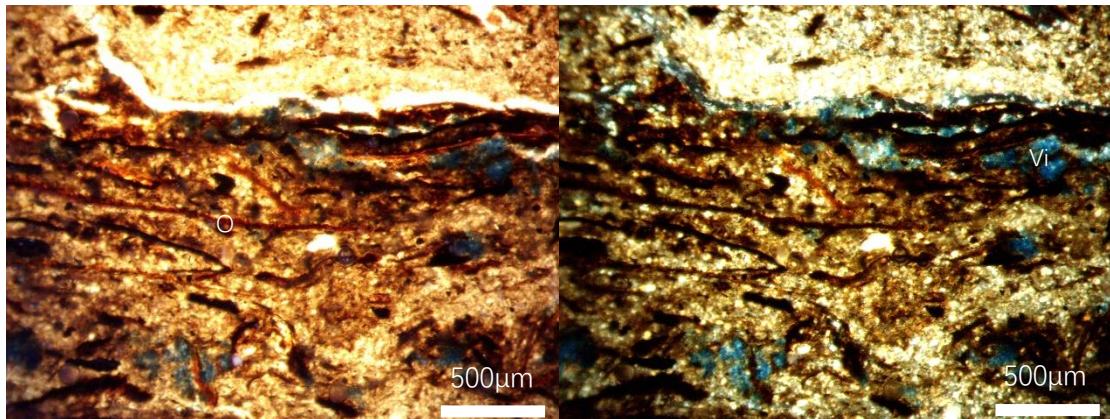
Layer 10 has a slightly increased pH, very low magnetic susceptibility, total organic and carbon contents, a low calcium carbonate content, and a moderate phosphorus content (Figure 6.4), which all signify a very low level of human activity. The very fine quartz sand/coarse silt particle size and the very low organic content are suggestive of a fine-grained wind-blown material accumulating under a dry (xeric) environment (Goldberg & Macphail, Chapter 6, 2006). The occasionally found silty clay crusts suggest irregular shallow, standstill water comes into the system but dries out quickly.



a: Silty clay crusts, XPL.



b: Groundmass composed of coarse silt size quartz and micas, XPL.



c: Lamina organic matter (O) in darkened sediment with vivianite (Vi) crystals, PPL (left) & XPL (right)

Figure 6.6 Slide scan and microphotographs from slide T0950 3

6.2.2.7 Layer 9

Layer 9 is identified as a ditch in the field and was the last layer sampled in this research. On top of this ditch, layers of ‘clay wrapped with grasses’ were found within constructed wooden frameworks (Figure 6.1).

6.2.2.7.1 *Micromorphological description of the Micro-fabric T0950 3:1*

Layer 9 is represented in the upper part of slide T0950 3 (Micro-fabric T0950 3:1). This layer is mostly composed of wavy micro-laminations of dusty silty clay interlaced with medium silt-size to very fine sand-size quartz (Figure 6.6). It exhibits a channel microstructure with 2-3% laminated, very fine charcoal mixed in. This fabric has a prominent and sharp lower boundary with Layer 10.

6.2.2.7.2 *Results of bulk analysis and interpretation of the Layer 9*

The pH of Layer 9 continues to increase slightly from below. This layer has medium-low magnetic susceptibility and calcium carbonate content, low phosphorus content, and slightly increased but still low total organic and carbon contents (Figure 6.4). The sedimentation structure is well-preserved and is suggestive of little or no distortion from human activity. The alternation of thick silty clay laminae with fine sandy silt laminae suggest slow-moving, low energy water conditions (Pagliai and Stoops, 2010) in the bottom of the Layer 9. This supports the hypothesis that this is a ditch flowing from the Mojiaoshan mound to the concave area between the Mojiaoshan and Jiangjiashan areas which is then eroded and has material transported away from Layer 10.

6.2.3 Interpretation of the Southwest Mojiaoshan mound (T0950)

6.2.3.1 Particle size analysis of the T0950 profile

Six samples from profile T0950 have been subjected to particle size analysis (Figures 6.7 and 6.8). Based on the different characteristics in the frequency histogram (Figure 6.7), these samples exhibit two major groups that reflect different deposition modes. The first group (green and red lines in Figure 6.7) includes samples T0950 1-2, 1-1 and 2-2 from Layers 15, 14 and 11, respectively. These samples have multiple peaks, which suggests a more diverse set of sources of the soil material. Based on micromorphological observations, Layer 15 has undergone various sedimentation processes, such as fluvial and stand-still water deposition, causing the diverse size classes observed. Layer 14 is a mixture of different soil materials and thus produces a similar multi-peak particle size pattern. Layer 11 shows a wider peak (red lines in Fig 6.7) with a significant input of coarser material in its tail, which may relate to the mixing of various anthropogenic materials in this layer.

The second group (blue lines in Figure 6.7) includes samples T0950 2-3, 2-1 and 3-1 from Layers 13, 10 and 9, respectively. These samples have a single peak distribution pattern, which generally indicates a good sorting of particles in the soil material. Layer 10 has a very narrow, high peak in the distribution pattern (dark blue lines in Figure 6.7), which suggests well-sorted, wind-blown material. This distribution pattern has not been seen in the other sampled profiles from Liangzhu City in this research. Layers 13 and 9 have a very similar single, relatively wide peak pattern (lighter blue lines in Fig 6.7). Combined with soil micromorphological analysis, this pattern is indicative of alluvial sediments.

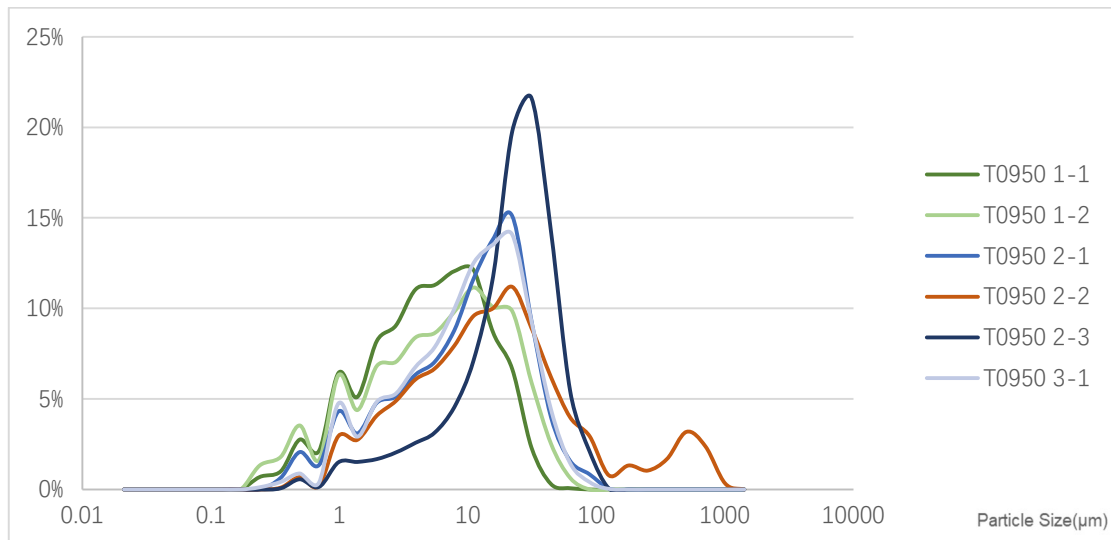


Figure 6.7 Particle size distribution graph of T0950.

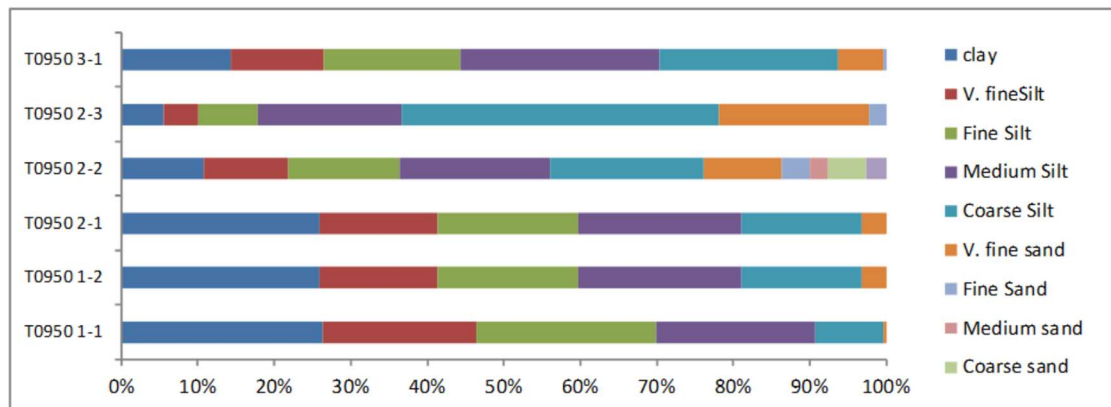


Figure 6.8 Percentage bar chart of the particle size of T0950.

6.2.3.2 Chronological sequence, soil formation process and human activity in the Southwest Mojiaoshan site (T0950)

6.2.3.2.1 Chronological sequence of profile T0950

Currently the only available radiocarbon dating of the T0950 profile is from the charred material from Layer 11, which is dated to 3000 cal. BC (personal communication from ZPICRA). Based on the pottery typology analysis (Liu *et al.*, 2019a), the pottery found in Layers 14 to 8C belong to the Early Liangzhu period (roughly 3300–3000 BC). Therefore, the construction and occupation of the Southwest Mojiaoshan site concentrates in the early stage of Liangzhu Culture, between 3300 and 3000 BC.

6.2.3.2.2 Soil formation process of profile T0950

Before the Liangzhu people arrived, the area was an old land surface (Layer 15) which underwent repeat wetting and drying. At the time the Liangzhu people constructed the ‘clay wrapped with grasses’ layer, the land surface was covered with a shallow, standing water. The ‘clay wrapped with grasses’ layer (Layer 14) overlying the buried soil was about 1m thick, without a wooden framework, and caused a sharp reduction in hydraulic conductivity and the formation of calcrete lamina between the buried soil and the constructed layer.

The construction of this site can be divided into two stages. As observed in the field, the first stages used organic rich dark gray soil material and the overlying second stage used light-grey soil material. On top of the ‘clay wrapped with grasses’ is Layer 13 which, based on micromorphological observation, could be disturbed, physically mixed and probably deliberately prepared by human activity by using dried alluvial material incorporating products left over from burning. The sediment above the alluvial deposits is possibly an occupation layer (Layer 12), which underwent repeated trampling, matting and mixing of different soil materials. In the upper part of Layer 12, the remnants of possible matting are better preserved and are shown as laminated organic matter in the thin sections. Above Layer 12, a large, *in situ* burning event occurred around 3000 cal. BC and produced strongly reddened sediments and thick charred remains. The ashes of this burning event were dissolved, translocated and re-precipitated in the lower part of the burnt remains. After this burning event, the site was immediately abandoned as wind-blown material with occasional cover of shallow water flow overlaid it (Layer 10), showing no or few interruptions from human activity. The dry aeolian sedimentation conditions coincided with the drying event happened at around 2900 cal. BC, as observed in other parts of Liangzhu City, such as at the North Zhongjiagang Watercourse (see section 5.3.3.4). However, after the 2900 cal. BC, the

wet conditions soon returned, and a channel with relatively higher stream flow energy eroded the wind-blown layer, which also corresponds with the change of local hydrological patterns observed in the North Zhongjiagang profile (see section 5.3.3.4). As the wet conditions continued, another stage of ‘clay wrapped with grasses’ about 3m thick with knocked-in wooden frameworks was constructed.

6.2.3.2.3 Interactions between the local hydrological condition and human activity in the Southwest Mojiaoshan site

During the Early Liangzhu period, the hydrological conditions were relatively wet, and the Liangzhu people actively modifying their living space by constructing layers of ‘clay wrapped with grasses’ to heighten their living spaces in response. On top of this constructed surface, Liangzhu people resided in this area and left traces of accumulated matting material and fine organic debris. After a large burning event around 3000 cal. BC, the site was abandoned and became covered by drier wind-blown material. It is interesting that the large, charred rice pit containing about 13 tonnes of grains that were believed to have been carbonised after two fires found in the eastern part of Mojiaoshan mound, is also dated to the later stage of the Early Liangzhu Period from 2940 to 2840 cal. BC (Liu *et al.*, 2014; Liu *et al.*, 2019a; Qin *et al.*, 2019). The correlation between the large-scale burning event between the east and the west Mojiaoshan and its relationship to the drier local environment, and the subsequent short-term abandonment of the occupation zone in Southwest Mojiaoshan and possibly the wider Liangzhu region is an interesting question that requires further research.

After wet conditions returned, Liangzhu people reappeared in the area and further constructed the ‘clay wrapped with grasses’ layer using a more advanced technique, as indicated by the construction of well-jointed wooden structures. These ‘clay wrapped with grasses’ materials provided a solid foundation for further occupation in the later stage of Liangzhu. Additionally, this forming of several stages of ‘clay wrapped with

grasses' implies that there are multiple phases of construction of the Southwest Mojiaoshan site.

In summary, during the Early Liangzhu Period, the dynamic sedimentation environment of the Southwest Mojiaoshan changed dramatically, with human activities such as mound construction, occupation, burning and abandonment shift. Profile T0950 provides a vivid example of the close relationships between the changes in human activity and the local hydrological conditions in the central part of Liangzhu City.

6.3 The South Zhongjiagang Region (T3131)

The South Zhongjiagang Region was excavated in 2015, 2016 and 2017. During the first two years of excavation, possible large-scale burnt living surfaces with abundant semi-products of jade and stone artefacts were found in the eastern bank of the South Zhongjiagang Watercourse, which suggest the presence of jade and stone workshops of Liangzhu City (Liu *et al.*, 2019a). Also, extensive areas of wooden piles and woven bamboo used for protecting the banks were found on the western bank of the South Zhongjiagang Watercourse. It is believed that this area had been intensively occupied by Liangzhu people and a large amount domestic garbage and organic matter from the occupation areas in both banks had filled up the South Zhongjiagang Watercourse (Liu *et al.*, 2019a).

In 2017, as part of the infrastructure project of the Liangzhu City Heritage Park, the excavations mainly focused on the infillings of the watercourse without disturbing the platform layers in the banks. Only a small section, excavation pit T3131, was exposed in order to understand the mound construction and occupation sequences of the western bank of the South Zhongjiagang Region. Studying this sequence aims to understand the patterns and details of the occupational sequences and to examine the long-term relationship between water and the occupation of Liangzhu City. During the excavation

in 2017, seven soil micromorphology samples and 14 bulk samples were taken from the southern wall of the excavation pit T3131 (Figure 6.11a).

6.3.1 Field observation and stratigraphy of profile T3131

6.3.1.1 The general stratigraphy and findings in the South Zhongjiagang Region

At present, the data compilation of the excavations in the South Zhongjiagang Region is still ongoing. The information in this section is thus compiled from the excavation records provided by the Zhejiang Institute of Cultural Relics and Archaeology.

The excavation in 2017 focused on the western part of the South Zhongjiagang Region, which included the accumulation of channel deposition of the South Zhongjiagang Watercourse (T3132), the successively accumulated or constructed west bank area (T3131), and the conjoining area in-between (Figure 6.9). For the purposes of protecting the occupational area, most of the western bank was not excavated except for test pit T3131.

In general, the channel infilling part (exemplified by excavation pit T3132, Figure 6.9) consists of eight major layers. The first three layers at the top are post-Liangzhu layers from modern times to the Zhou Dynasty (1046 to 256 BC) and were removed before the excavation. Layer 4 is the yellow silt layer covering the Liangzhu region after 2000 cal. BC (see section 2.4.3 for detail), and Layer 5 is dated to the end stage of the Late Liangzhu period between 2300 to 2200 cal. BC (Qin *et al.*, 2019) and contains pottery sherds from the Qianshanyang Period. The bottom three layers, Layers 6, 7 and 8, are dated to the early stage of the Late Liangzhu period from 2700-2500 cal. BC (Qin *et al.*, 2019). Large amounts of archaeological materials such as pottery sherds, charcoal, plant remains and burnt clay aggregates were uncovered from Layers 4 to 8.

Soil sampling and analysis focused on the mound accumulation area in the excavation pit T3131 (Figure 6.11a). It is located in the conjoining area of the channel infillings of South Zhongjiagang Watercourse and the occupational areas of the west bank. In this profile, several platforms from different periods were exposed. The excavator grouped the platforms into two stages: Platforms 2, 5 and 6 in the upper part were constructed in Stage II, which corresponds to the Late Liangzhu period (2700-2200 BC). Platforms 7 and 8 are constructed in Stage III, which corresponds to the early to middle Liangzhu period (3100-2700 BC, Figure 6.9b). Seven soil micromorphology samples and 14 associated bulk samples were taken from the boundaries of each platforms (Figure 6.11a). The field descriptions of each platforms of the T3131 profile from top to bottom are as follows:

Platform 2: Yellowish-brown silty clay mixed with burnt clay aggregates, charcoals and coarse sands.

Platform 5-1: Loose light gray silty clay. Burnt clay aggregates, charcoals and pottery debris were found.

Platform 5-2: Dark gray silty clay. Laminae of blackish plant remains were found.

Platform 6: Gray silty clay. A bedding of burnt soil and pottery sherd with abundant organic materials such as bamboo weaving material, charcoals, pig jaws and seeds etc. were found. Three possible sub-units - 6a, 6b and 6c (Figure 6.11a) were observed in the field, with soil samples also taken from the boundaries of these units.

Platform 7: Dark gray silty clay. Relatively pure with few large anthropogenic artefacts.

Platform 8: Dark gray silty clay. Relatively pure with few large anthropogenic artefacts.

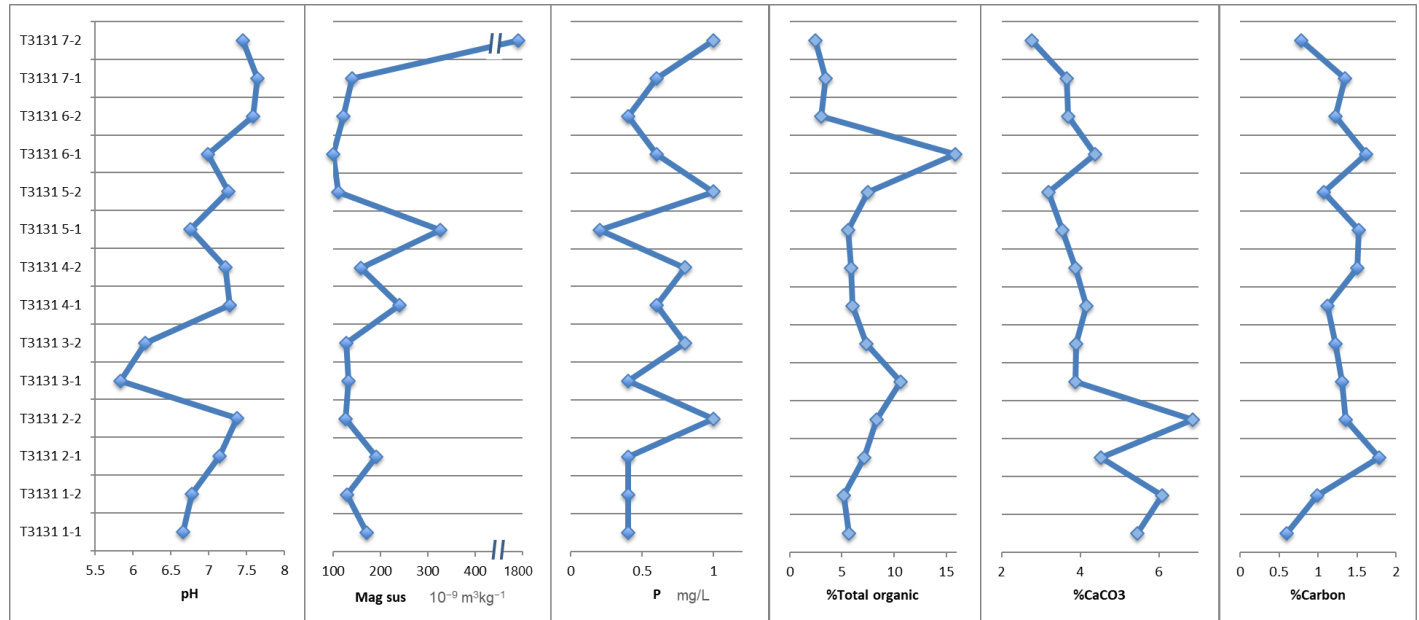
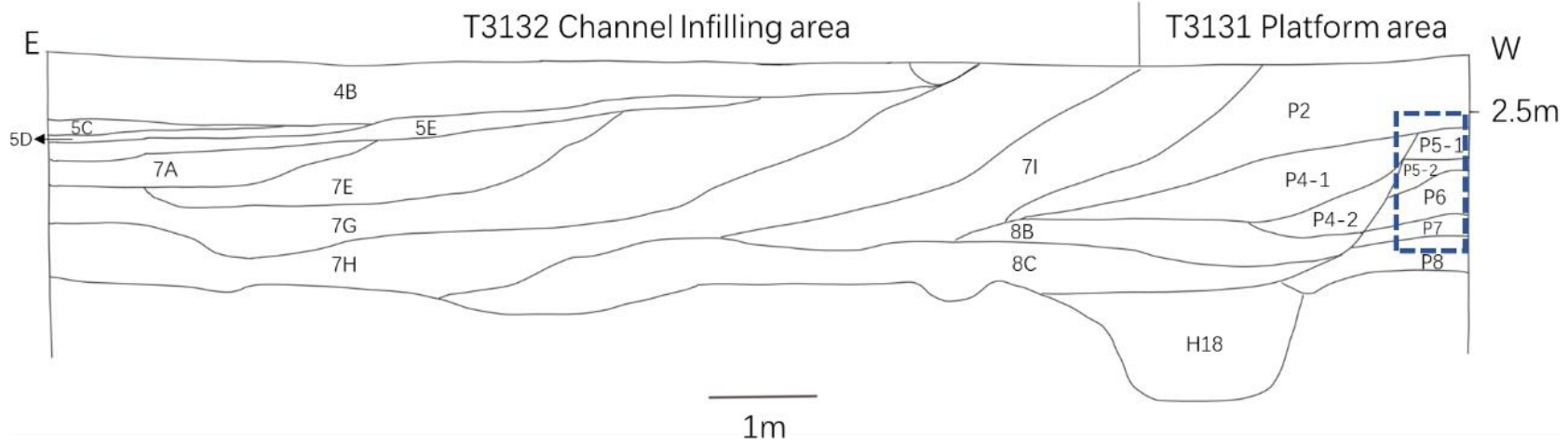


Figure 6.9 Stratigraphy of the T3132 and T3131 excavation pits, the blue rectangular shows the sampling position of the T3131 profile.

Figure 6.10 Analytical results of pH, phosphorus, magnetic susceptibility, and carbon, total organic and calcium carbonate contents of profile T3131.

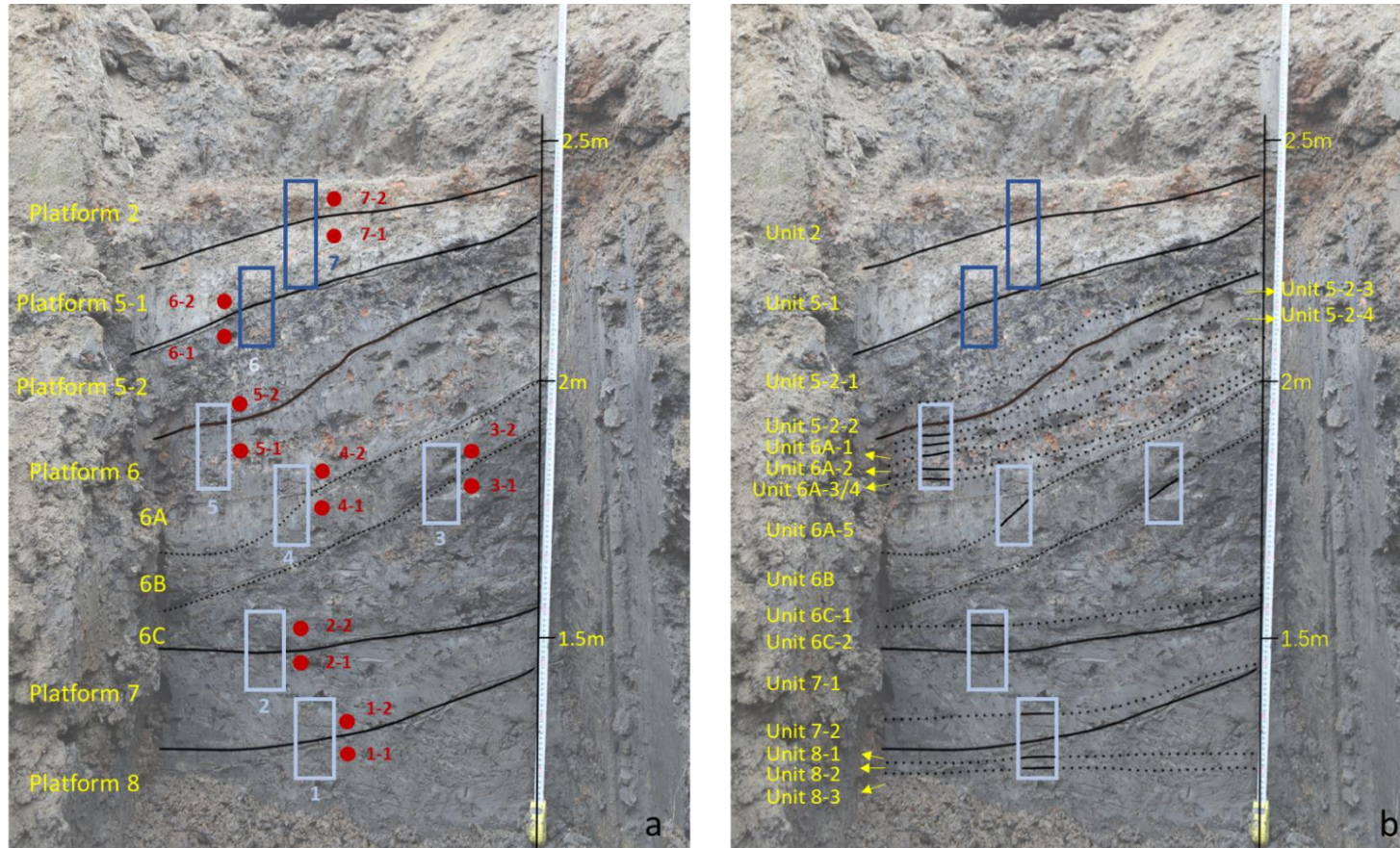


Figure 6.11 a. Stratigraphy identified in field and sampling positions of the T3131 profile. The blue rectangles and numbers refer to the sampling positions and numbers of the soil micromorphology samples. The red dots and numbers refer to the sampling positions and numbers of bulk samples; **b.** Units identified after micromorphological analysis. The full lines represent interface observed in field and under thin section, the dotted lines represent putative interfaces.

6.3.2 Results of soil micromorphological analysis in T3131

In the field, soil micromorphology samples were taken from the main stratigraphic horizon change zones (Figure 6.9b). After micromorphological observation, the macroscopically defined layers were further refined, and more sub-layers were identified. In this section, these sub-layers will be re-named using the unit system (Figure 6.11b, in yellow lettering). The comparison of these two classification systems is exemplified in Figure 6.11. The description and interpretation of the T3131 profile will generally follow the stratigraphy framework established in field, and within each platform, units identified under the microscope will be further elaborated. In addition, in this profile, sediment-derived units will be described as if it is a soil, with units mainly composed of various anthropogenic materials and rock fragments described based on the relative proportions of each component.

6.3.2.1 Platform 8

6.3.2.1.1 Introduction

This layer is the earliest mound material in the west bank of the South Zhongjiagang Watercourse. It is a dark grey silty clay with few large archaeological objects being found. Only the top of this platform was sampled, and three units from bottom to top can be identified: Unit 8-3 represented by Micro-fabric T3131 1:5, Unit 8-2 represented by Micro-fabric T3131 1:4, and Unit 8-1 represented by Micro-fabric T3131 1:3 (Figure 6.12).

6.3.2.1.2 Platform 8: description of the Micro-fabrics T3131 1:5, 1:4 and 1:3

Unit 8-3 (Micro-fabric T3131 1:5, Figure 6.12) in the bottom of the Platform 8 is mainly a very heterogeneous and random mix of anthropogenic materials, including 30% fine

pebble-size rock fragments, half of which are light yellowish (PPL) calcite-rich metamorphic rock fragments, 10% charcoal, 6% uncharred organic residues, 5% pottery sherds with sharp boundaries, 2% bast fibres and a few rounded soil aggregates. The fine sedimentary material in between, which occupies 30% of the fabric, is composed of poorly-sorted, sub-angular, fine to coarse sand and brownish (PPL) very humic calcareous silty clay incorporating 10% humified organic fine material (c/f 40/60, limit: 50µm). The humified organic matter masked most of the fine fabric and shows an undifferentiated b-fabric. Micritic calcium carbonate clusters with diffuse boundaries are commonly found. This fabric has a massive microstructure and most of the voids (3% porosity) are formed after the shrinkage or decay of organic matter. The boundary between Micro-fabrics 1:5 and 1:4 is distinct.

Unit 8-2 (Micro-fabric T3131 1:4, Figure 6.12) is 2cm thick and relatively homogeneous. It is mainly composed of brown (PPL) humic silty clay with 8% coarse sand-size and fine pebble-size rock fragments. This fabric has a massive structure with a few planar fissures (1% porosity). The groundmass has an undifferentiated b-fabric due to the 'mask' of humified organic matter. Charred or humified fine organic matter occupies 20% of the fabric and exhibits parallel laminae in the basal part, but has no orientation in the middle and upper parts. The boundary between Micro-fabrics 1:4 and 1:3 is distinct and wavy.

Unit 8-1 (Micro-fabric T3131 1:3, Figure 6.12) is a slope accumulation with a heterogeneous mixture of anthropogenic materials. It is the mixture of 30% sub-angular, coarse sand-size to fine pebble-size rock fragments, these rock fragments are mostly random but are weakly laminated and parallel to the slope direction in the upper part of this fabric; 30% sedimentary material is found in between the coarse clasts, which is composed of poorly-sorted, sub-rounded, fine to coarse sand-size mineral and rock fragments and dark brown (PPL) humic silty clay with a speckled to undifferentiated b-fabric (c/f 40/60, limit: 50µm); 5% uncharred organic residues; 5% burnt bones,

including fish bones and a reptile bone (Figure 6.12, David Brönnimann, per. comm.); 5% dark brown micritic calcium carbonate aggregates, which are possibly reworked ash lumps or plaster materials (Figure 6.12); 3% charcoal; 2% weakly laminated bast fibres; 1% burnt soil aggregate; a single piece of pottery sherds with sharp edges and a single piece of stone artefact. A few blueish vivianite crystals near burnt bone materials are found. This fabric is massive with 5% porosity, half of which are formed after the decay of organic matter and the other half are possibly formed due to their loss during thin section manufacture. The top of Unit 8-1 is sloping and has a distinct boundary with the Unit 7-2 (Micro-fabric T3131 1:2).

6.3.2.1.3 Results of bulk analysis and interpretation of Platform 8

The top of Platform 8 generally has a slightly acidic pH, high magnetic susceptibility, moderate phosphorus, total organic and calcium carbonate contents, and a low carbon content (Figure 6.10).

Unit 8-3 can be interpreted as a dumped layer based on the chaotic distribution of various anthropogenic materials. The pottery sherds with sharp boundaries imply these waste materials were dumped not far away from their original positions. The micritic calcium carbonate clusters in this fabric were possibly precipitated under natural conditions as they have diffuse boundaries and are relatively pure without the incorporation of charred material and imply an alternating wet-dry condition of this fabric (Durand *et al.*, 2010).

Unit 8-2 is likely to be an alluvial deposition based on the relatively homogenous composition and the fine particle size. The laminated organic matter in the bottom may demonstrate the undisturbed sedimentation process of this alluvial material. Starting from the middle part of the unit, the input of anthropogenic material increases, and the sedimentation structure is disturbed and not well preserved.

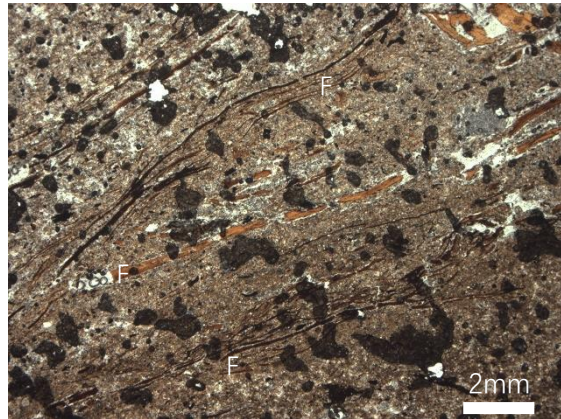
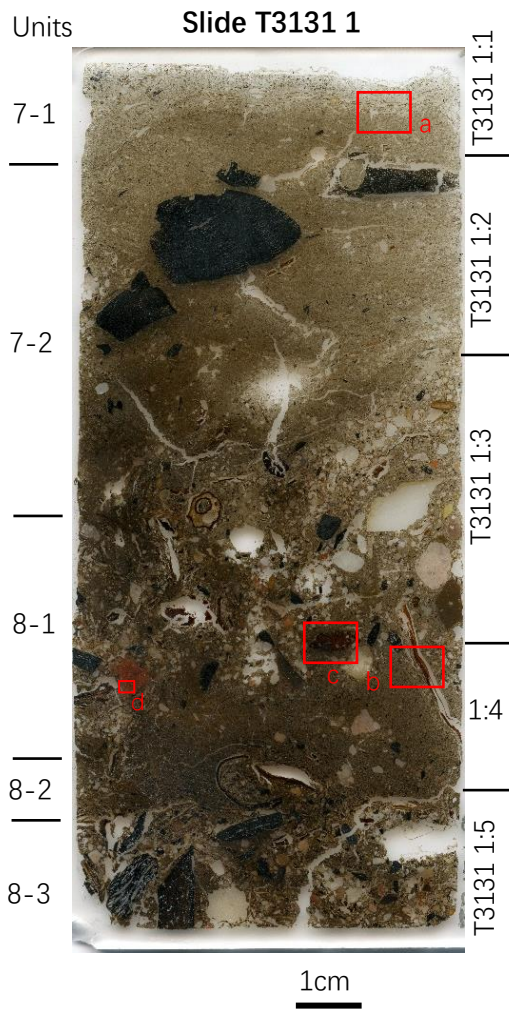
Similar to Unit 8-3, Unit 8-1 is a heterogeneous mixture of various anthropogenic materials. The upper part of this unit shows sorting and a sloping arrangement of coarse rock fragments parallel to the slope direction, which may be due to the rolling or sliding-down of material on the slopes by deliberate dumping (Karkanas & Goldberg, 2018). Vertical soft bast fibres are found traversing both units (Figure 6.12), suggesting that Unit 8-2 is likely to be soil materials coming with Unit 8-3, dumped as a whole. The undulating interface between these units may form due to self-compaction (Karkanas & Goldberg, 2018).

In general, the top of Platform 8 is dominated by the accumulation of two stages of dumped materials from nearby activity zones. The rich and various anthropogenic materials found imply intensive human occupation and activities on the western bank of the South Zhongjiagang Watercourse at this time. The hydrological condition is generally alternating wet-dry.

6.3.2.2 Platform 7

6.3.2.2.1 Introduction

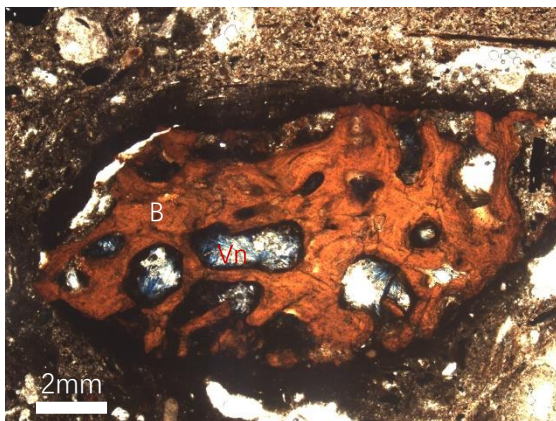
Platform 7 can be divided into two units from bottom to top: The Unit 7-2 represented by Micro-fabric 1:2 and Unit 7-1 represented by Micro-fabrics 1:1 and 2:3 (Figure 12 and 13).



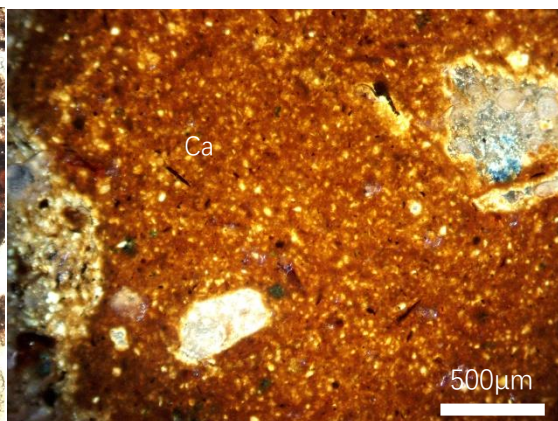
a: Two types of laminar bast fibres (F): thicker bright yellow in between the thinner brown bast fibres, PPL



b: Fragment of bast fibres (F) traversing Micro-fabric T3131 1:3 on the left and T3131 1:4 on the right, PPL



c: Burnt potential reptile bone (B) with vivianite (Vn) growth in voids, PPL



d: Calcitic soil aggregate, XPL

Figure 6.12 Slide scan and microphotographs from slide T3131 1

6.3.2.2.2 Platform 7: description of the Micro-fabrics T3131 1:2, 1:1 and 2:3

Unit 7-2 in the bottom of Platform 7 (Micro-fabric T3131 1:2) is composed of 15% charred material and fresh woody material 1-2cm in size and 15% poorly-sorted fine sand to fine pebble-size rock fragments dispersing within fine fractions. The fine matrix is light brownish (PPL) humic calcareous silty clay with a striated b-fabric. The charcoal fragments and tree roots have their long-axis parallel to the surface. Weakly laminated organic matter, especially bast fibres, are occasionally found in the groundmass. A few reddened clusters of micritic calcium carbonates are also observed. This fabric generally has a massive microstructure with a few fissures (2-3% porosity).

Unit 7-1 in the mid-upper part of Platform 7 (Micro-fabrics T3131 1:1 and 2:3) is mainly composed of dozens of parallel-bedded bast fibres with laminated charred materials and anthropogenic material inbetween these bast fibres in a humic silty clay groundmass. In the bottom part of this unit (Micro-fabric T3131 1:1), the fabric is dominated by 20% bedded bast fibres and humic silty clay with sparse anthropogenic inclusions. Two types of laminar bast fibres, laminae of thicker bright yellow (PPL) bast fibres in between the thinner brown (PPL) bast fibres are observed (Figure 6.12). As the bedding of bast fibres continues (Micro-fabric T3131 2:3, Figure 6.13), aggregates of reddened micritic/sparite calcium carbonates with diffuse boundaries (15%), charred materials (10%), pottery sherds (3%), burnt rock fragments, tree roots (3%), fine burnt bones (1%), a single piece of dry and burnt soil aggregates (1cm) coated with fine charcoals, and shell fragments (<1%) are unevenly scattered inbetween the laminated plant materials (20%). In addition, a few blueish vivianite crystals are incorporated in the groundmass and intact calcium carbonate pseudomorphs of plant remains are observed (Figure 6.13). This fabric generally has a weakly developed platy microstructure structure with 10% planar vegetal voids formed after the decay of organic matter. The bedding of bast fibres are more compacted in the mid-lower part of

Micro-fabric T3131 2:3 and gradually becomes less compacted with fewer but larger anthropogenic materials and laminated bast fibres in the mid-upper part of the Micro-fabric T3131 2:3. A 4cm long, 1mm thick wood plank demarcates Unit 7-1 and Unit 6C-2 above.

6.3.2.2.3 Results of bulk analysis and interpretation of the Platform 7

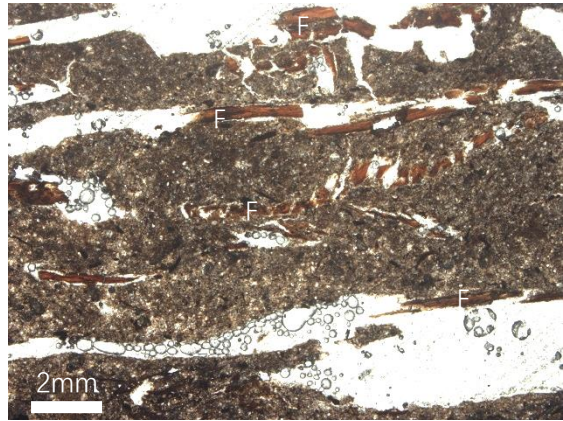
From bottom to the top of Platform 7, the pH increases from slightly acidic to neutral, the magnetic susceptibility values and carbon content rises from moderate to high, and the calcium carbonate content decreases from medium high to medium low. The phosphorus values and total organic content are generally moderate (Figure 6.10). These data generally suggest an increase and intensification of human activity from the bottom to the top of this platform.

The groundmass of Unit 7-2 in the bottom of Platform 7 is dominated by humic calcareous silty clay and is suggestive of alluvial sediment deposited under slow water motion. This unit generally shows no trace of trampling. The bast fibres are laminated but relatively loose and scattered, which is most likely to be introduced with the water flow. The large intact charcoal fragments and tree roots in this unit may be dumped from the nearby occupation area. The origins of the high calcium carbonate content and the occasionally observed reddened clusters of micritic calcium carbonate in this unit cannot be exactly determined now, but could be ash and possibly calcitic plaster material with the charred material from the nearby hearth, or formed due to the repeated drying of calcitic-rich water (Durand *et al.* 2010). In general, Unit 7-2 could be interpreted as alluvium deposited under shallow and slow water conditions with the input of occupational debris from nearby occupation areas.

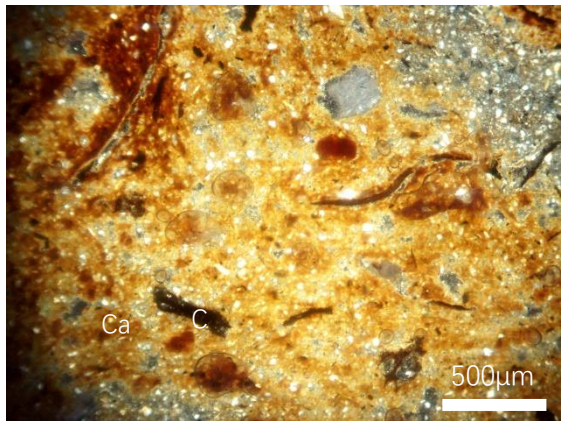
In Unit 7-1, the bedding of bast fibres in the lower part is cleaner with fewer anthropogenic inclusions (Figure 12). The middle of this unit is composed of more

compacted bast fibres with abundant archaeological materials from hearth remains such as shell and burnt mammal bones trapped inbetween these bast fibres, which suggests more intense trampling. Bast fibres showing twill-plaited patterns can also be seen clearly in the impregnated soil block and bulk samples of the Micro-fabric T3131 2:3 (Figure 6.13), which further proves that the bedded bast fibres observed in thin section are intact woven material. Lipid analysis of these bast fibres suggests that these are grasses that contain arundoin, a chemical compound commonly found in *sugarcane* (*Saccharum* spp.) and tropical tall grasses (*i.e.*, *Imperata cylindrica* and *Austroderia* spp.) (Nishimoto *et al.*, 1965; Jacob *et al.* 2005; see section 6.3.3.3 for further explanation). Inbetween the bast fibres, the intact calcium carbonate pseudomorphs of plant tissue structure may be remnants of ash (Canti and Brochier, 2017). When reaching the top of this unit, repeated overlying of matting material is still observed but with longer intervals between each layer. The size of charred materials has increased and are less fragmented. Rounded burnt soil coated with fine charred materials may be rolled over from nearby dry land. This evidence indicates that dumped remains gradually came to dominate the sediments, and that the living surfaces are less well maintained. In general, the Unit 7-1 represents an *in situ* living floor with intensive human activities such as trampling, burning and repeated superimposition of matting materials.

In summary in Unit 7-2, the wet-dry alternating conditions continue, with this unit deposited under slow water motion with the input of occupational debris from the nearby human occupation zone. In Unit 7-1, Liangzhu people occupied this location intensively as indicated by *in situ* matting, which implies the relatively dryness of this near bank area. When reaching the top of the Unit 7-1, the living floor is less well maintained, probably suggesting a retreat of human activity towards drier land nearby.



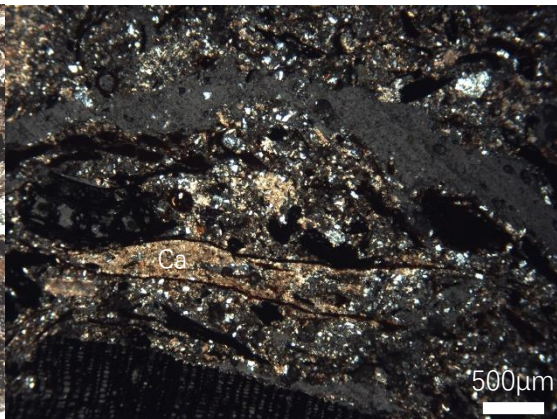
a: Bast fibre (F) laminar with planar voids, the bast fibres in the middle are twisted, PPL. 5.8



b: Cluster of micritic calcium carbonate (Ca) incorporating fine charred materials (C), XPL



c: Laminated bast fibres (B), charred (C) and humified plant remains (H) with planar voids (B) (V), PPL.



d: Calcium carbonate (Ca) pseudomorphs after plant structure, XPL.



Plan view of twill plaited matting material from the impregnated block of T3131 2:3.

Figure 6.13 Slide scan and microphotographs from slide T3131 2

6.3.2.3 Platform 6C

6.3.2.3.1 Introduction

Similar to Platform 7, Platform 6C can also be divided into two units from bottom to top: Unit 6C-2 is represented by Micro-fabric T3131 2:2 and Unit 6C-1 is represented by the Micro-fabrics T3131 2:1 and 3:2.

6.3.2.3.2 Platform 6C: description of Micro-fabrics T3131 2:2, 2:1 and 3:2

Unit 6C-2 (Micro-fabric T3131 2:2, Figure 6.13) is similar to the Unit 7-2 in Platform 7. It is composed of archaeological inclusions (30%) disperse within a finer matrix (70%) composed of 15% poorly sorted fine to coarse sand-size rock fragments and yellowish brownish (PPL) humic calcareous silty clay with a striated b-fabric. The coarse archaeological inclusions include 10% randomly oriented charcoal fragments with various sizes from 1mm to 2.5cm, 8% unevenly distributed sparitic calcium carbonate clusters and a 2cm long, elongated cluster of iron impregnated micritic calcium carbonate incorporating fine charred materials, 8% mostly laminated humified organic matter and bast fibres, 2% various burnt and unburnt soil lumps, <1% fine burnt bone fragments, and <1% shell fragments. This unit has a massive structure with 8% porosity formed by root voids, fissures and soil lost during section making. Some of the root voids contain remnant organic matter, and some are coated with amorphous iron impregnated clay material and pyrite framboids. Trace amounts of blueish vivianite crystals near decayed organic matter are also found.

Unit 6C-1 (Micro-fabric T3131 2:1 and 3:2, Figure 6. 13 and 6.14) is mainly composed of dozens of parallel-bedded bast fibres with laminated charred materials and anthropogenic material inbetween these bast fibres in a groundmass similar to Unit 6C-2. In Micro-fabric T3131 2:1, the bottom of Unit 6C-1, the bedded bast fibres are

overlain with compacted soil material with a parallel striated b-fabric. Planar vegetal voids are created around the bast fibres and this micro-fabric shows a moderately developed platy microstructure (Figure 6.13). In the Micro-fabric T3131 3:2, the mid-upper part of Unit 6C-1, the bedding of bast fibres continues but are more disturbed by anthropogenic inclusions and ‘exotic’ soil aggregates. It is composed of mostly laminated and compacted anthropogenic material such as rounded, mostly burnt soil aggregates with diverse groundmass and sizes that are commonly coated with fine charred materials (40%), bast fibres (10%), charred material in various size (8%), burnt bone fragments (5%), fresh wood material (3%) and phytolith slags (<1%). Various types of poorly-sorted fine sand to fine pebble-size rock fragments occupies 15% of the fabric. It is noteworthy that a yellowish brown (PPL), optically isotropic, phosphate-rich aggregate with imprints of various organic matter fragments or phytoliths is found (Figure 6.14), which is possibly a coprolite. Evidence of fresh wood material broken *in situ* are also observed (Figure 6.14). This unit generally has a weakly-developed platy microstructure formed after the decay of organic matter around organic matter (15% porosity). The fine matrix inbetween the coarse anthropogenic inclusions are dark brownish (PPL) humic silty clay with a stipple to striated b-fabric. Unit 6C-1 has a distinct and sloping interface with the upper Platform 6B.

6.3.2.3.3 Results of bulk analysis and interpretation of the Platform 6C

From Unit 6C-2 to Unit 6C-1, the pH values drop dramatically from slightly alkaline to acidic (7.37 to 5.84), the content of phosphorus and calcium carbonate decreases from high to medium, and the total organic content increases from medium to high. These units generally have moderate to low magnetic susceptibility values and moderate carbon contents (Figure 6.10).

Unit 6C-2 shows a pattern of charred material dispersing within finer groundmass, which is similar to the Unit 7-2 but with higher input of archaeological remains. The

calcium carbonate lumps observed in Unit 6C-2 have a diffuse boundary and some of which have incorporated fine charred materials, which possibly imply the anthropogenic origin of these calcium carbonates. Combining the widely found large charcoal pieces, they could be the remains of ash which have experienced a certain degree of dissolution, but were preserved due to the suitable slightly alkaline pH value in this unit. The ash together with the large charcoal pieces may indicate the dumping of hearth remains from nearby living areas in this location. The enrichment with phosphorus also supports the suggestion of a high input of organic waste remains from human activity (Middleton, 2004). In general, similar to the Unit 7-2, this unit could be interpreted as an alluvium deposited under shallow and slow water with the input of occupational debris from nearby settlement areas, but nonetheless represents a weakening of direct human activity in this location.

Unit 6C-1 is dominated by layered bast fibres and various archaeological materials, which represent the return of direct human occupation in this location. The matting in the bottom is relatively clean with few inclusions and disruption from human activity, which is similar to the bottom part of Unit 7-1. The mid-upper part of this unit is a heavily trampled floor sequence with intensive human activity indicated by the compacted, laminated matting material, as indicated by the planar orientation but random distribution of soil aggregates and archaeological remains, and the *in situ* breakage of fresh woody material. The refuse trapped between the matting materials are probably mainly kitchen remains as it is mainly composed by fuel materials, burnt bone fragments and phytolith slugs that indicate a relatively high temperature (Cant and Brochier, 2017). The coprolite observed is likely to be human based on its amorphous, yellowish brown colour (PPL), optically isotropic, and its relatively fine matrix without coarse bone or clastic mineral material (Brönnimann *et al.*, 2017; Karkanas & Goldberg, 2018). The autofluorescence of coprolites may be lost in the waterlogged conditions (Brönnimann *et al.*, 2017). Due to the single appearance of a coprolite in thin section, this coprolite could be brought-in by occasional foot traffic.

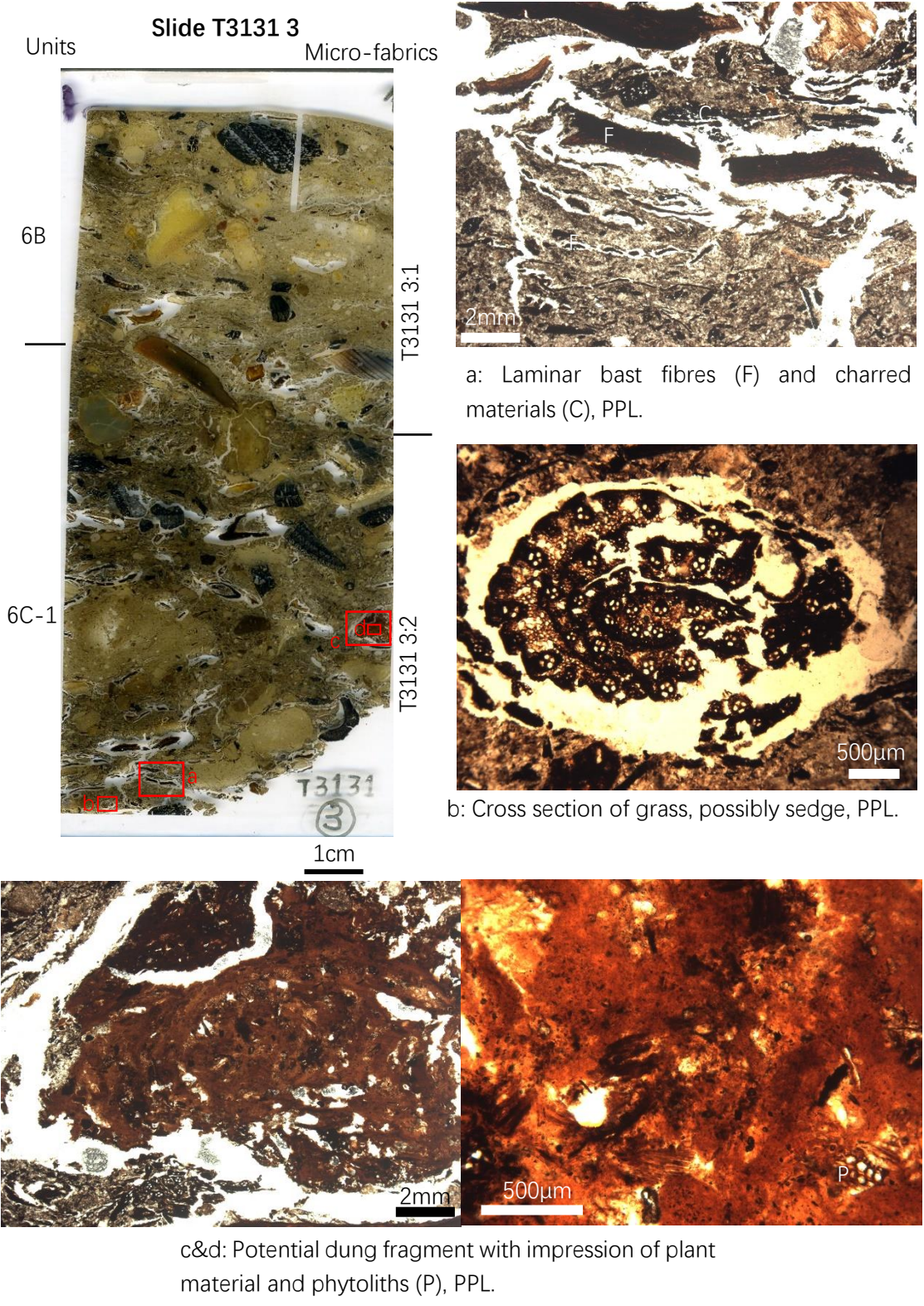


Figure 6.14 Slide scan and microphotographs from slide T3131 3

In summary, similar to the Platform 7, Platform 6C demonstrates a change from dumped archaeological remains in alluvial deposits to a trampled and intensively occupied floor sequence. The floor sequence is cleaner and more intact in the bottom part, and the mid-upper part is more disturbed with introduction of various archaeological remains.

6.3.2.4 Platform 6B

6.3.2.4.1 Introduction

In the field, Platform 6B is inclined with a dip angle of 20-30° (Figure 6.11). Only one unit, Unit 6B was identified under the microscope. It is represented in the upper part of slide T3131 3 (Micro-fabric T3131 3:1) that is closer to the western bank, and the bottom of slide T3131 4 (Micro-fabric T3131 4:2) that is closer to the South Zhongjiagang Watercourse (Figure 6.11). The coarse inclusions of these two micro-fabrics are different and will be discussed separately.

6.3.2.4.2 Platform 6B: description of Micro-fabrics T3131 3:1 and 4:2

The Micro-fabric T3131 3:1 that is near to the western bank is mainly composed of poorly-sorted pebble size materials (50%) dispersed within a finer matrix (50%). The coarse inclusions include randomly distributed rounded pebble size rock fragments (20%), soil aggregates with diverse groundmass (20%) and charcoal fragments (10%). A few burnt bone fragments (2%) and a 2cm large pottery sherd obliquely inserted into the top of Unit 6C-1 are also found. The fine matrix is mainly composed of poorly-sorted sub-angular to sub-rounded sand and humic silt. The amount of amorphous fine organic material is less than the Platform 6C, which creates a light brownish (PPL) colour. Light yellowish (PPL) limpid clay with bright yellowish interference colour are

occasionally (5%) found as small aggregates and grano-coatings of rock fragments. This fabric generally has a weakly developed platy microstructure with 10% planar vegetal voids. The sediment in the bottom 2cm is more compacted and the organic material and pottery sherd are mostly laminated. Laminae of fine charcoal rich, humic silty clay similar to the fine matrix in Unit 6C-1 are occasionally (5%) intercalated between the coarse materials.

The Micro-fabric T3131 4:2 that is near to the South Zhongjiagang Watercourse is less compacted and incorporates fewer anthropogenic remains. The groundmass has a similar fine fraction with the Micro-fabric T3131 3:1 and finer and better sorted coarse mineral components. The anthropogenic inclusions are reddened, possibly burnt aggregates (3-7mm, 10%) mixed with a calcium carbonate rich groundmass and fine charred material, charcoal fragments in various size (5%), various rounded burnt soil aggregates (5%), fresh wood fragments (3%), a single piece of highly degraded, 5mm large, rounded pottery sherd, and a bimodal 'paste' that is a mixture of very fine silty clay and angular sand-size rock fragments (Fig 6.15). The organic matter is generally randomly oriented, but laminae of horizontal oriented organic matter appear at intervals. The soil material trapped inbetween these organic beddings shows a darker colour with finer particle sizes and are weakly laminated. This micro-fabric generally has a massive microstructure with 5% fissures and vughs near organic materials.

6.3.2.4.3 Results of bulk analysis and interpretation of the Platform 6B

The results of bulk sediment analysis show different characteristics in Micro-fabric 3:1 and 4:2 (Figure 6.10). The Micro-fabric 3:1 has an acidic pH value, moderate magnetic susceptibility, carbon and calcium carbonate contents, and medium high phosphorus and total organic contents. The Micro-fabric 4:2 has a slightly alkaline pH value, high magnetic susceptibility, and medium carbon, calcium carbonate, phosphorus and total organic contents. The increase in pH and magnetic susceptibility in Micro-fabric 4:2

may be related to the introduction of burnt calcium carbonate materials (Macphail *et al.*, 2004; Macphail & Goldberg, 2017: Chapter 10).

In general, Micro-fabrics 3:1 and 4:2 from Unit 6B have a similar sedimentation pattern of coarse archaeological material dispersing within fine matrix with the Units 6C-2 and 7-2, which is suggestive of dumped archaeological material in alluvial deposits. The Micro-fabric 3:1 was sampled closer to the bank area and contained higher amounts of archaeological materials with stronger influences of trampling and compaction. The Micro-fabric 4:2 is closer to the channel area. The groundmass is finer, better sorted and contained fewer and lesser organized archaeological remains, which imply a stronger influence of fluvial conditions in this location. The regularly observed laminated organic material and compression of soil material are suggestive of periodic trampling on the possibly wet surface. What has not been seen in previous layers is a bimodal paste for pottery or plaster making.

In summary, Platform 6B contains various archaeological remains dumped from nearby occupation zones. The wet conditions prevail, and this location appears to be on the edge of the human activity zone but still constantly visited by Liangzhu people.

6.3.2.5 Platform 6A

6.3.2.5.1 Introduction

In the field, Platform 6A is inclined with a dip angle of 10-30° (Figure 6.11). This platform can be divided into five units from bottom to top: Unit 6A-5 represented by Micro-fabrics T3131 4:1 and 5:8, Unit 6A-4 represented by Micro-fabric T3131 5:7, Unit 6A-3 represented by Micro-fabric T3131 5:6, Unit 6A-2 represented by Micro-fabric T3131 5:5, and Unit 6-1 represented by Micro-fabric T3131 5: 4.

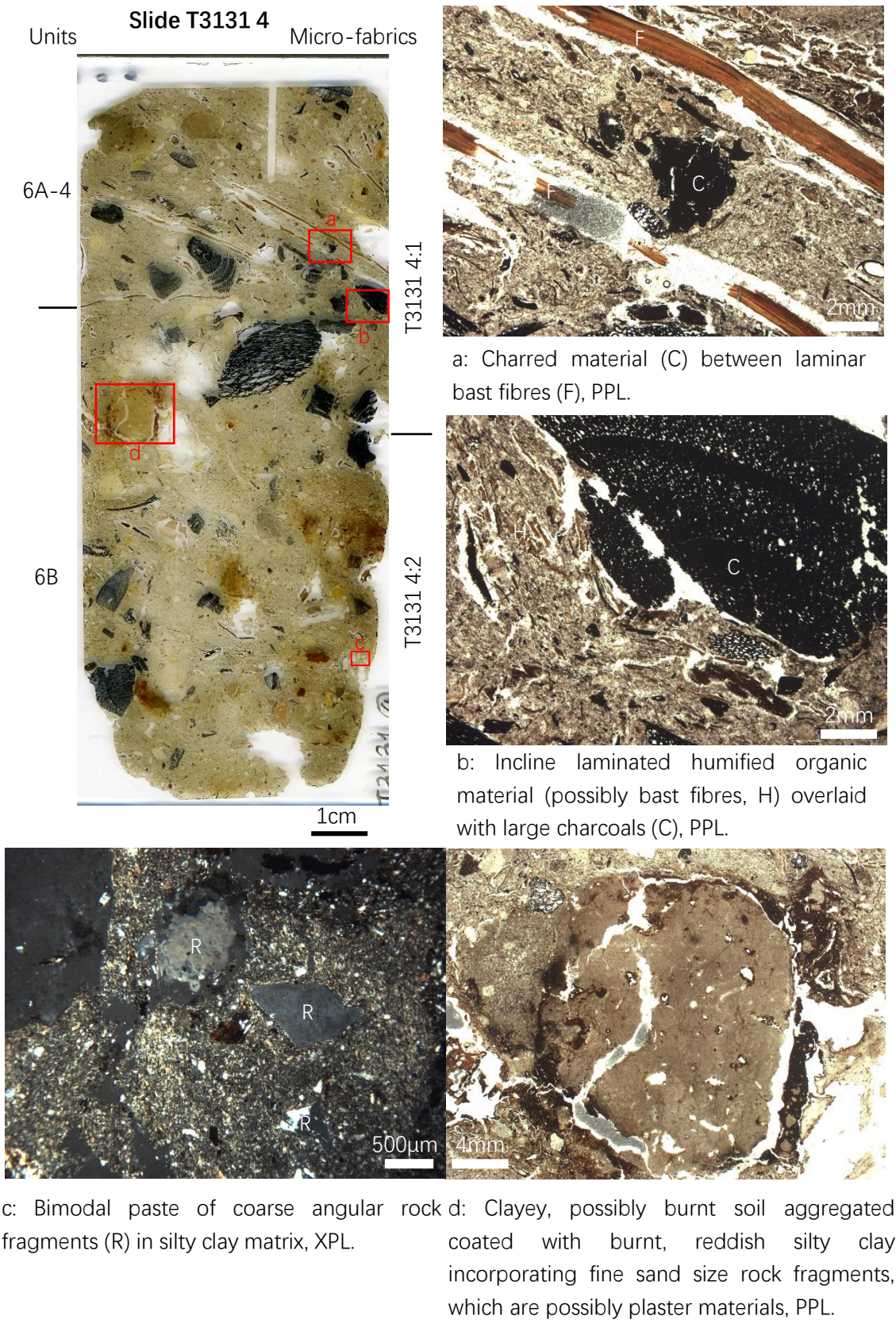


Figure 6.15 Slide scan and microphotographs from slide T3131 4

6.3.2.5.2 Platform 6A: description of Micro-fabrics T3131 4:1, 5:8, 5:7, 5:6, 5:5, and 5:4

Unit 6A-5 has a similar but slightly coarser groundmass with the Unit 6B. This unit generally has a weakly developed platy structure formed after the decay of organic matter (8-10% porosity). In the bottom of this unit (Micro-fabrics T3131 4:1) are laminae of obliquely laminated large, charred wood fragments, which are covered by several sloping beddings of bast fibres (Figure 6.15). The soil material, fine charred material and humified plant tissues inbetween or underlying these bast fibres are compacted and parallel to the slope direction (Figure 6.15). On top of the organic beddings, a variety of soil aggregates, rock fragments and a few fragmented charred materials are distributed horizontally or obliquely. The top of this unit (Micro-fabric T3131 5:8) is rich in compacted, fragmented and parallel-laminated humified plant tissues and amorphous organic fine material, charcoal fragments and fresh woody plant remains. A few rounded soil aggregates and sand-size rock fragments are also mixed in.

Unit 6A-4 (Micro-fabrics T3131 5:7) is 2cm thick and has distinct boundaries and a contrasting groundmass with the lower units (Figure 6.16). It has a c/f ratio of 70/30 (c/f 10 μ m) and is dominated by moderately-sorted coarse silt size quartz. Only a few amorphous organic matter fragments (3%) and little or no charcoal fragments are found. This unit has a massive structure with 5% accommodated planar voids with serrated walls. The fine fraction is light yellow (PPL) humic silty clay with a random striated b-fabric. A few intercalations of dusty, clay rich silty clay with a parallel striated b-fabric are found. Several rounded soil aggregates are mixed in the fabric. Above this unit is the 1cm-thick Unit 6A-3 (Micro-fabric T3131 5:6). This unit has the same groundmass with the Unit 6A-4 but incorporates horizontally laminated humified plant tissues (including 1/3 bast fibres), fine charred materials, rounded soil aggregates, and fine bone fragments that in total occupies more than 30% of the fabric.

Unit 6A-2 (Micro-fabric T3131 5:5) is 3cm thick and has a highly separated granular microstructure with 40% voids caused by both loss during thin section making and the open structure of the aggregates. The granules are loose, slightly inclined, fine to medium-pebble size, chaotic material composed of various rounded burnt soil aggregates commonly coated with fine charred materials or clay coatings (40%), rock fragments in various types and sizes (10%), rounded, highly degraded pottery sherds (10%), and fresh woody plant material (7%). Soil material (10%) composed of poorly-sorted, sub-angular, fine to coarse sand-size rock fragments, and light brown (PPL) humic silt clay with speckled to undifferentiated b-fabric (c/f 40/60, limit: 50µm) incorporating bast fibres and humified plant tissues (8%) and a trace amount of phytoliths are concentrated in the bottom of this unit. Thick, compound clay coatings consist of alternating dark brown (XPL), dusty and light yellow (XPL) limpid clay materials with high birefringence are widely found coating the coarse clasts (Figure 6.16).

Unit 6A-1 (Micro-fabric T3131 5:4) are dominated by crudely bedded, planar oriented, well compacted coarse clasts (60%) in a fine matrix (40%) composed of poorly sorted sub-angular, fine to coarse sand-size rock fragments and light brown (PPL) humic silty clay (c/f: 40/60, limit: 50µm) with a speckled to undifferentiated b-fabric. The coarse clasts are mainly elongated, laminar, soil aggregates (25%) comprised by well-sorted, weakly laminated, sub-rounded, very fine to fine sand-size rock fragments and light yellow (PPL) silty clay with striated b-fabric (c/f: 50/50, limit: 50µm), laminated organic matter including humified plant tissues and bast fibres (15%, Figure 6.16), sub-rounded fine pebble-size rock fragments (10%), fresh woody plant materials (8%), fine charcoals (5%), and two small pottery sherds with sharp boundaries (5%). This layer has a weakly separated platy microstructure with 10% planar voids. A thin lamina of very dusty silty clay inbetween coarse clasts is found in the upper part of this fabric. A layer of bast fibre demarcates Unit 6A-1 from the overlying Unit 5-2-4.

6.3.2.5.3 Results of bulk analysis and interpretation of the Platform 6A

Unit 6A-5 (Bulk Sample 4-2, Figure 6.10) has a slightly alkaline pH value, medium high phosphorus and carbon contents, moderate magnetic susceptibility values and total organic contents, and medium low calcium carbonate contents. The bulk sedimentology in general suggests a moderate level of human activity.

Unit 6A-5 shows similar laminated, compacted laminae of charcoals, bast fibres and soil aggregates with Units 6C-1 and 7-1, which suggests a trampled floor sequence containing abundant occupational debris. However, the micromass of this unit contains lesser fine charred or humic organic material and therefore shows a lighter soil colour. This may be due to the change of space of use that produce a cleaner floor surface or the change of sedimentation environment that contains or preserves fewer organic matter. What is more, the amount of archaeological objects in this unit is also lesser than in Units 6C-1 and 7-1. Considering the sloping arrangement of this unit, this unit could indicate the periphery of occupation areas, or the possible slope of a large platform.

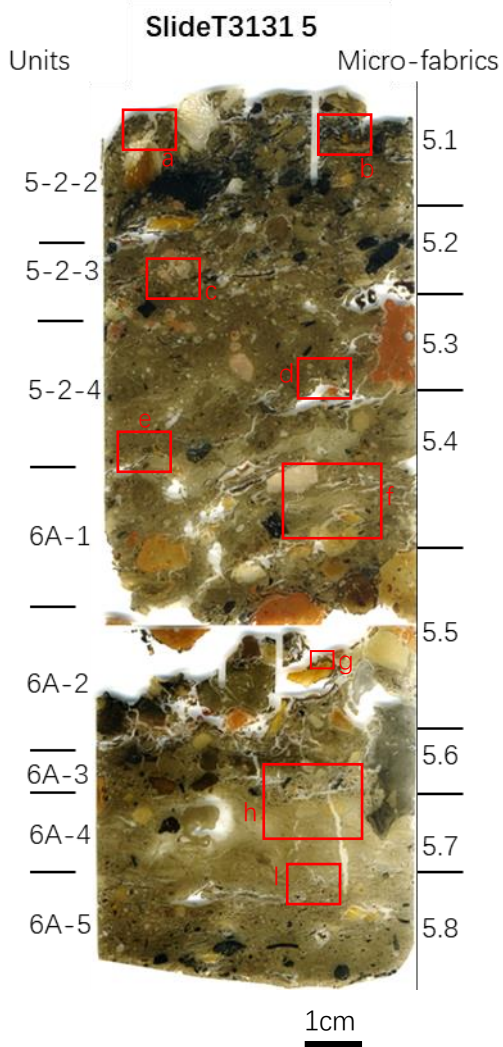
In Units 6A-4, 6A-3, 6A-2, and 6A-1 (Bulk Sample 5-1, Figure 6.10), the pH value is slightly acidic, the total organic content is moderate, and the calcium carbonate content is medium-low. The magnetic susceptibility value and carbon content are relatively high, which may be related to the burnt materials. But the phosphorus content is extremely low, which may imply a low-level of direct living activities represented in these units.

Unit 6A-4 was not noticed in the field, consequently its distribution range is unclear. In the thin section, this unit shows a contrasting groundmass with the units below and above. The dominant coarse silt particle size, low organic content and the homogenous arrangement of soil particles are suggestive of fine grained, wind-blown material (Goldberg and Macphail, 2006: Chapter 6). The root voids and rounded soil aggregates

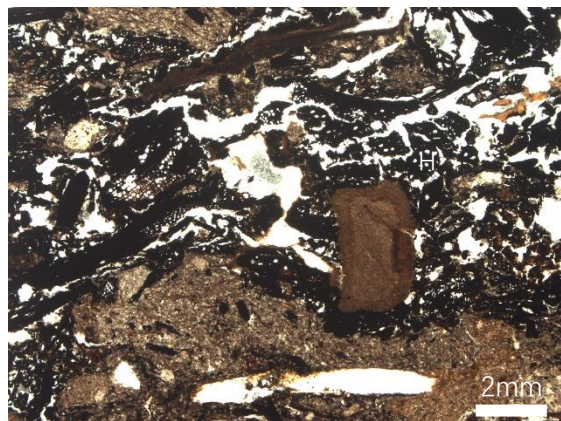
may imply an incipient soil formation process. This layer could be a natural wind-blown material with incipient pedogenesis, which may mark a short hiatus of human activity. However, considering its location in a heavily modified terrain by human activity and the thin thickness of only 2cm, this layer could also be dumped soil materials fetched from dry higher ground, similar to those from Micro-fabrics T0950 2-1 and 3-2 (Section 6.2.2.6). Limited by the scope of thin section analysis, the nature of this unit cannot be determined; further investigation is needed to comprehensively understand its formation process.

Unit 6A-3 contains laminar fine occupational debris and organic materials, which are suggestive of trampling and possible occupation activities on top of the Unit 6A-4. These laminae are directly overlaid by Unit 6A-2, a 3cm thick sediment composed of loose, chaotic, mostly burnt soil aggregates, which is possibly dumped in dry conditions. The thick coating of clay material in the voids created by the loose clustering of the dumped materials suggests an open environment with repeated comings and goings of water coverage on top of the dumped materials. The alternation of pure limpid and dusty clay coatings may suggest the rhythmic alternation of clean rain-splash and overland slurry with surface slaking (Courty *et al.*, 1989). The rounded clasts coated with very fine charcoal and clay material on the top of this unit form the ‘rolling pedofeatures’ (Angelucci and Zilhão, 2009), which suggest rolling of these materials from a nearby activity zone.

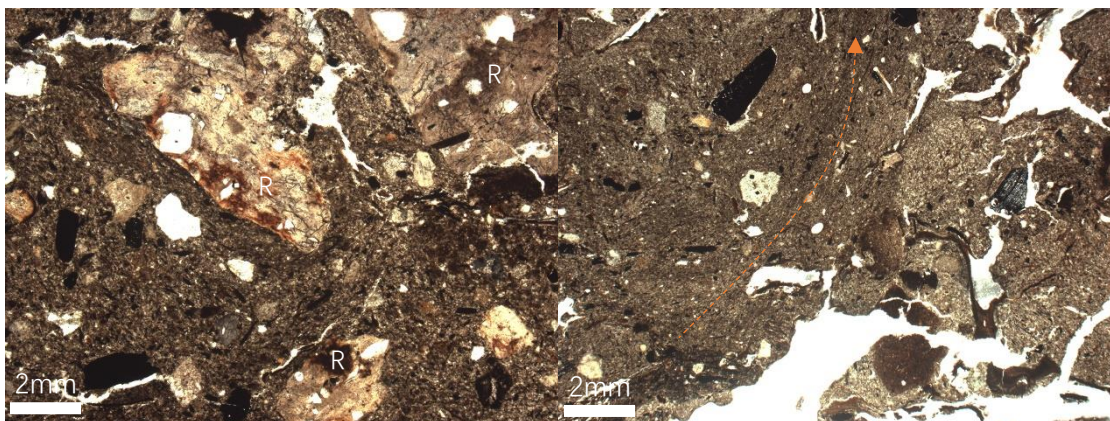
Unit 6A-1 is dominated by compacted, elongated, slightly inclined soil aggregates, laminated organic materials and occupational debris, which are suggestive of intensive trampling and the bringing-in of ‘exotic’ soil materials by human activity in this possible living surface. The thin lamina of very dusty silty clay found in the upper part of this unit indicates an open-air sedimentation environment of this unit.



a: *In situ* fragmented burnt bones (B), PPL



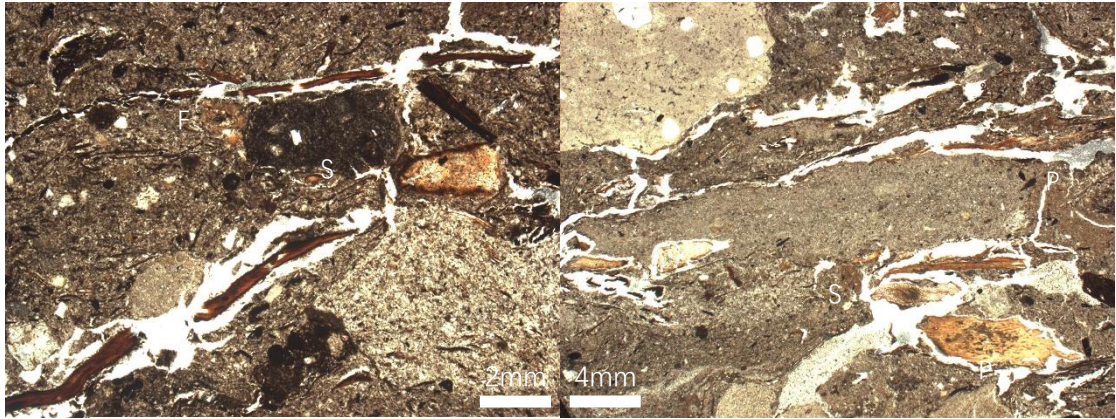
b: Lamina of humified grass materials (H), PPL



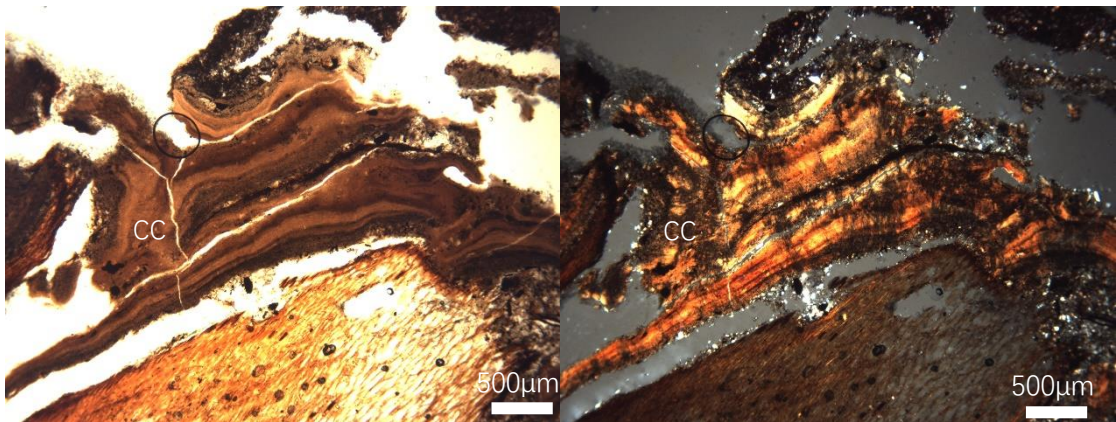
c: Crudely bedded, rock fragments (R), possibly heated, PPL

d: Conjunction between two soil aggregates, note the changing of orientation of the plant material, PPL.

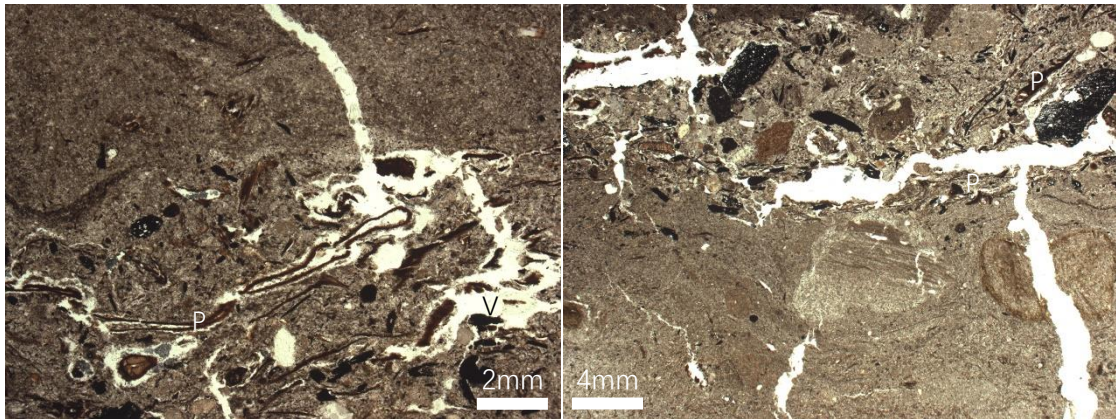
Figure 6.16 Slide scan and microphotographs from slide T3131 5



e and f: Laminar bast fibres (F) and plant material (P) between elongated soil aggregates (S), PPL.



g: Thick, compound clay coating (CC) showing alternations of limpid and dusty clay materials, PPL (left) and XPL (right)



h: Interface of Micro-fabrics T3131 5:7 (upper) and 5:8 (bottom). Note the homogenous groundmass in the upper part and the laminated plant tissues (P) creating plant voids (V) in the lower part, PPL.

i: Interface of Micro-fabrics T3131 5:6 (upper) and 5:7 (lower). Note the laminated plant tissues (P) and fine occupational debris in the upper part, PPL.

Figure 6.16 (continued) Slide scan and microphotographs from slide T3131 5

In summary, Unit 6A-5 could be a trampled surface on the slope of the occupation area on the west bank of the South Zhongjiagang Watercourse. Unit 6A-4 could be a dumped layer using up-land soil materials or a natural wind-blown material with incipient pedogenesis, with the top of this unit exhibiting possible trampling, and then was overlain by loosely dumped and rolled-over burnt soil materials in open-air conditions (Unit 6A-2). Unit 6A-1 could be a heavily trampled, open-air living surface.

6.3.2.6 Platform 5-2

6.3.2.6.1 Introduction

Platform 5-2 was characterised by a high content of black plant materials in the field. Based on micromorphology analysis, this platform can be divided into four units from bottom to top: Unit 5-2-4 is represented by Micro-fabric T3131 5:3, Unit 5-2-3 by Micro-fabric T3131 5:2, Unit 5-2-2 by Micro-fabric T3131 5:1, and Unit 5-2-1 by Micro-fabric T3131 6:2.

6.3.2.6.2 Platform 5-1: Description of microfabrics T3131 5:3, 5:2, 5:1, and 6:2

Unit 5-2-4 (Micro-fabric T3131 5:3, Figure 6.17) is the intermixing of two different soil materials: Sediments 1 and 2. Sediment 1 occupies 80% of the fabric. The main inclusions are sub-angular to sub-rounded sand-size quartz and fine pebble-size rock fragments and brown (PPL) humic silt clay with undifferentiated to speckled b-fabric (c/f: 40/60; limit: 50µm). The humified plant tissues and amorphous fine organic material (15%) of this material are mostly laminated, but when reaching the conjunction places between the two soil materials, the organic materials become vertically laminated. Sediment 2 is mainly comprised of a reddish, highly degraded pottery sherd and its surrounding soil aggregates. In the voids around this pottery sherd and the voids between the two materials, infillings and coatings of very dusty clay material are

observed. Some of the coatings show alternations between dusty and limpid clay material.

Unit 5-2-3 (Micro-fabric T3131 5:2, Figure 6.16) is mainly composed of crudely bedded, reddened, coarse sand to pebble-size rock fragments (40%) with laminar humified plant tissues and bast fibres (10%), rounded soil aggregates (10%), lenses of humified/charred blackish brown grass material (5%), identified based on its 'skull' shaped vascular bundles (Ismail-Meyer, 2017), and charcoal (5%) in a groundmass similar to the Sediment 1 of Unit 5-2-4. This unit has a weakly separated platy microstructure with 10% planar voids.

Unit 5-2-2 (Micro-fabric T3131 5:1) is dominated by lenses of blackish plant material (30%), reddened, coarse sand to pebble-size rock fragments (20%), rounded soil aggregates (15%), charcoals (10%), fresh woody material (5%) in a groundmass similar to Unit 5-2-3. The lenses of blackish plant material are located in the lower part of the fabric, their cell structures are brownish, which suggests humification instead of charring (Figure 6.16). On top of the plant beddings, several burnt, highly calcined bone fragments are observed, some of which show evidence of *in situ* breakage (Figure 6.16). This unit has a weakly separated platy microstructure with 10% porosity. Around the coarse clasts and voids, compound coatings of limpid, orange (XPL) clay with high birefringence and dusty clay coatings incorporating very fine charcoal can be observed.

Unit 5-2-1 (Micro-fabric T3131 6:2) is a mixture of 35% lenses of black, humified and charred plant material, 25% fine silty clay (Sediment 1), 20% light reddish brown (PPL) soil aggregates (Sediment 2), 10% rock fragments, 5% pottery sherds and 5% pedofeatures. In the bottom of this fabric are 5-25mm large, light reddish brown (PPL), possibly burnt soil aggregates (Sediment 2) commonly coated with fine charred material. Sediment 1 material, which is homogeneous and composed of sub-angular, very fine to fine sand-size quartz grains and light yellow (PPL) silty clay with a striated

b-fabric with few or no organic inclusions (c/f: 30/70; limit: 50µm), is found overlying the Sediment 2 soil aggregates and as rounded to elongated aggregates and groundmass between the lenses of organic material. One-third of the Sediment 1 material is possibly burnt. Thick, micro-laminated, partially fragmented, reddish yellow (XPL) dusty silty clay with high birefringence has filled in the gaps between the soil aggregates and humified plant material in the lower part of the fabric (Figure 6.17). In the mid-upper part of this fabric, the blackish, humified grass material identified based on the widely seen scattered vascular bundles (Figure 6.17) similar to the Unit 5-2-2 are laminated *in situ*. On top of the laminated grass is a mixture of laminar and compacted humified plant materials (Figure 6.17), burnt and unburnt sand-size rock fragments, elongated Sediment 2 aggregates, charcoal fragments (5%), platy woody material (3%), phytolith slags, and two pieces of pottery sherds. Occasional thin, dusty, light yellowish clay coatings with high birefringence are found inbetween the laminated plant material. This unit generally has a massive microstructure with 5% planar vegetal voids formed after the decay of organic material.

6.3.2.6.3 Results of bulk analysis and interpretation of the Platform 5-2

Units 5-2-4, 5-2-3 and 5-2-2 (Bulk Sample 5-2, Figure 6.10) have a slightly alkaline pH, high phosphorus contents, moderate total organic and carbon contents, and medium-low magnetic susceptibility values and calcium carbonate contents.

In Unit 5-2-4, the intermixing of two different soil material implies that this unit could be deliberately constructed or prepared. The micro-laminated dusty clay coating in the voids suggest an open space environment with repeated coverings with clean water flow and soil-water slurry. In a similar groundmass, crudely bedded reddened burnt rocks that were possibly constructed or brought by traffic from nearby hearths are widely found in Unit 5-2-3.

Unit 5-2-2 exhibits fine bedding mixed with charcoal, humified grasses, burnt bone fragments and fresh plant tissues. Although abundant burnt materials were found, the groundmass of this unit shows no evidence of burning under the microscope, which is further supported by the medium-low magnetic susceptibility value of this unit. The burnt materials may be dumped here and were later trampled as indicated by the *in situ* fractures of burnt bones and the weakly separated platy microstructure.

Unit 5-2-1 (Bulk Sample 6-1, Figure 6.10) has a slightly acidic pH value, significantly high total organic content, medium high carbon, medium calcium carbonate and phosphorus contents. It is interesting that the magnetic susceptibility value of this unit is the lowest of the T3131 profile, and the % carbon does not grow in pace with the % total organic content, which both support the micromorphological observation that most part of this unit is unburnt and the dark plant materials are uncharred. The lipid analysis of blackish plant material collected from this unit by Natalia Égüez in the Archaeological Micromorphology and Biomarkers (AMBI Lab), Universidad de La Laguna, Spain, further confirms that these black plant materials are grasses that contain arundoin (see section 6.3.3.3 for further explanation). The dark brown to black colour is common for grass material under the microscope (Ismail-Meyer, 2017) and forms due to humification.

Slide T3131 6

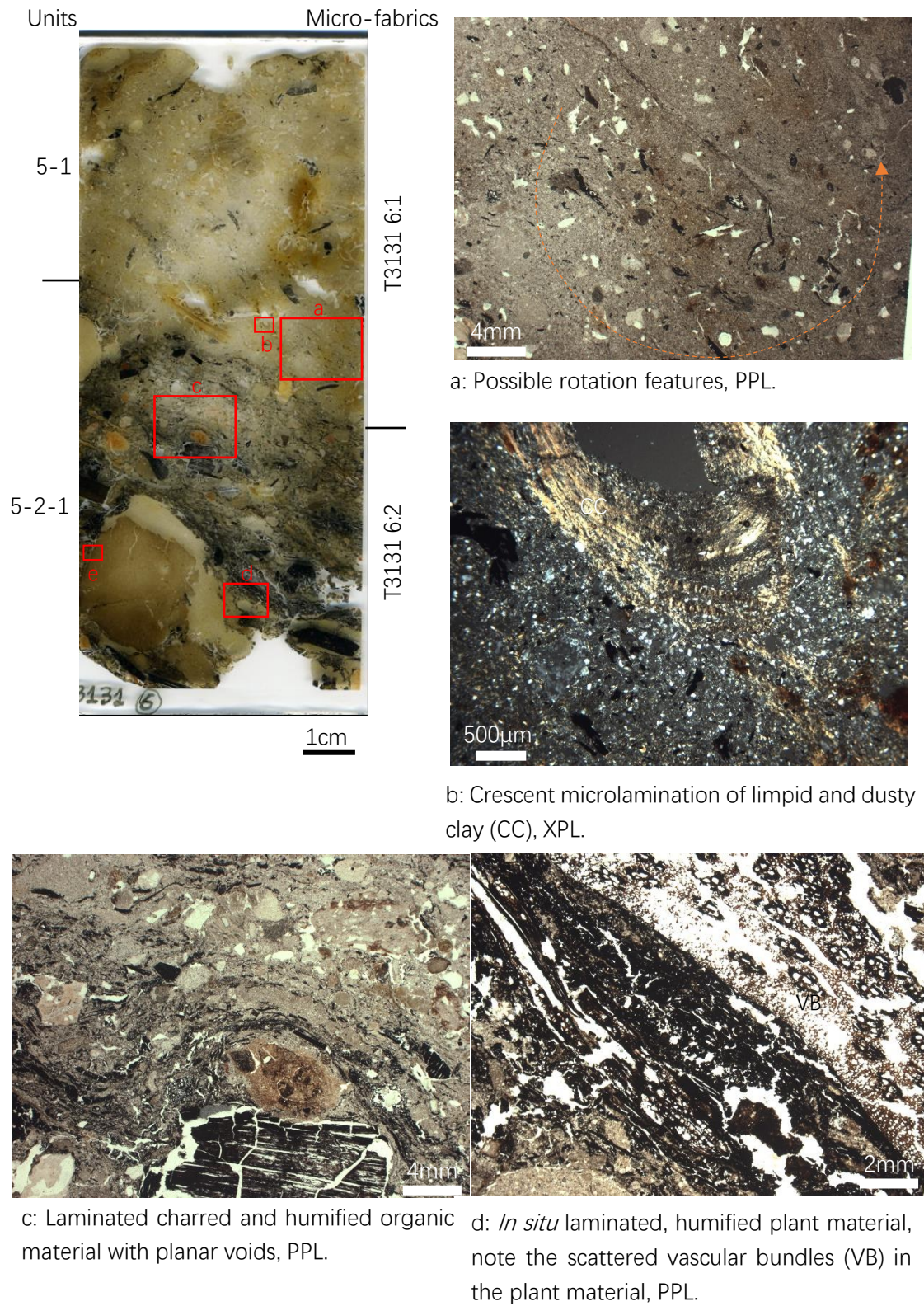
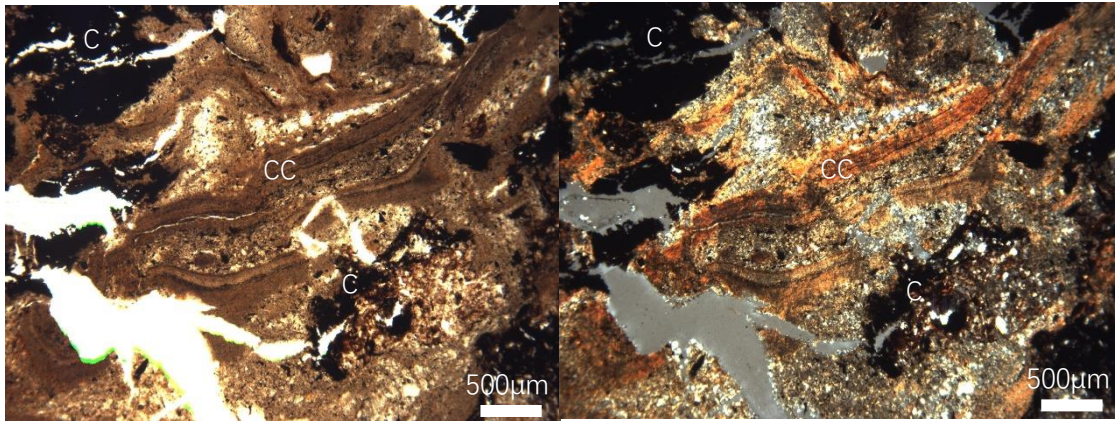


Figure 6.17 Slide scan and microphotographs from slide T3131 6



e: Microlamination of dusty clay coating (CC) in-between charred materials, PPL and XPL

Figure 6.17 (continued) Slide scan and microphotographs from slide T3131 6

In the bottom of Unit 5-2-1, large, possibly burnt, soil aggregates coated with fine charred materials are mixed in. In field observation, these soil aggregates could be seen by eye and are widely mixed in this unit. The grass bedding covering these soil aggregates are inter-connected and are likely to be bedded *in situ*. The use of easily accessed grasses instead of woven bast fibre may imply the expedient use of the grass material. These grass beddings are intensively trampled, mixed in with compacted, light yellow silty clay aggregates that are different from the groundmass of previous units. Occasionally found charcoal and trace amounts of phytolith slag may come from nearby hearth remains. Widely found thick, micro-laminated clay coatings from Unit 5-2-2 to Unit 5-2-1 suggest that these units are deposited under open-air conditions. This unit in general is a heavily trampled, open-air living surface with repeatedly lain matting with grass materials.

In summary, the lower part of the Platform 5-2 is a deliberately constructed surface incorporating fine burnt rock fragments. On top of this, this location was covered by grass matting, which provided an open-air activity surface for Liangzhu people, on which heavily trampled occupational debris and burnt soil aggregates accumulated.

6.3.2.7 Platform 5-1

6.3.2.7.1 Introduction

In Platform 5-1, only one unit, Unit 5-1, was identified. The lower part of this unit is presented in the Micro-fabric 6:1, and the upper part is shown in Micro-fabric 7:2. Daub, charcoal and pottery debris were observed in this unit in field.

6.3.2.7.2 Platform 5-1: Description of the Micro-fabrics 6:1 and 7:2

This unit is mainly the heterogeneous mixture of various coarse inclusions in a light yellow (PPL) limpid silty clay groundmass with high birefringence and a random to grano-striated b-fabric. In the lower part of this layer (Micro-fabric 6:1), the coarse inclusions include 25% sub-angular to sub-rounded sand-size rock fragments, 10% rounded soil aggregates, 3% burnt bone fragments (Figure 6.18), 3% clusters of fine charcoal rich soil materials. All of these inclusions are randomly mixed in with the groundmass in random orientations. Soil aggregates in the bottom of this unit have a similar groundmass with the fine fraction of this fabric but are 'cleaner' and more clayey. The lower part of this unit has a vesicular microstructure with 10% irregular vesicles (Figure 6. 18). Various textural pedofeatures are observed, including light yellow (XPL) crescentic coatings and hypo-coatings of juxtaposed limpid and dusty clay of voids with a high birefringence (Figure 6.17), and reddish yellow (XPL) micro-laminated intercalations of dusty silty clay. A possible rotational feature is noted in the lower part of this unit (Figure 6.17).

In the mid-upper part of this unit (Micro-fabric 7:2), there is a higher amount (40%) of sand-size rock fragments and some of which appear as aggregations. 25% of the fabric is stained by amorphous iron oxides and shows a reddish brown colour (PPL). Rounded, burnt, clayey soil aggregates of a larger size (2-12mm) are also more frequently seen.

A few clusters of fine charcoal are also observed. A platy, half charred, wood material is observed in the mid-upper part of this layer. The middle part of this unit has a weakly developed sub-angular-blocky microstructure, which gradually shifts to a prismatic microstructure in the upper part with 10% voids created by accommodated, short, planar voids and partially accommodated, vertically aligned, planar voids. The textural pedofeatures in the upper part are fewer and are dominated by amorphous iron impregnated clay intercalations and hypo-coating of voids. Hypo-coatings and depletion quasi-coatings of amorphous iron oxides are commonly seen in the voids and channels.

6.3.2.7.3 Results of bulk analysis and interpretation of the Platform 5-1

Platform 5-1 has a slightly alkaline pH, moderate magnetic susceptibility, carbon and phosphorus, medium low calcium carbonate and low total organic contents, which generally suggest a low level of human activity.

In Platform 5-1, the heterogeneous mixture of coarse inclusions such as clustered rock fragments, fine bone fragments, various rounded soil aggregates in the structureless silty clay groundmass is suggestive of physical mixing and possibly deliberate preparation of the soil material by human activity. The potential rotation features indicate possible kneading processes during their preparation (Friesem *et al.*, 2014). The widely found dusty silt and clay coatings, the smooth vesicles and vughs produced by water or air escape denote the possible involvement of water during the preparation of this construction material. And the soil aggregates that have a similar but cleaner matrix with the groundmass may be the product of insufficient slaking. The upper part of the Platform 5-1 is moderately stained by reddish brown amorphous iron oxides, which may be due to long-term surface exposure and the input of burnt material in the overlying layers (see section 6.3.2.9).

It is interesting that the groundmass of this construction material is firstly found in the underlying Unit 5-2-1 in a cleaner and purer state, and is very different from the humic silty clay micromass in previous units. Based on the correlation between the fine material in Units 5-2-1 and 5-1, the grass bedding in the Unit 5-2-1 could have formed synchronously with the construction of Unit 5-1 and could be interpreted as a temporary surface for the preparation of the construction material. It is likely that this soil material for construction was brought-in from other sources and when it was fetched, it was a very clean and pure silty clay as shown in Unit 5-2-1 in some of the soil aggregates in the lower part of this layer. It was then prepared near this location by slaking and mixing with coarse sand-size rock fragments. Bone fragments and fine charred material from nearby hearth area might be incorporated during this process.

In summary, the Platform 5-1 is a deliberately constructed horizon using light yellow silty clay material with the addition of coarse sand-size rock fragments as temper and the incorporation of fine occupational debris.

6.3.2.8 Platform 2

6.3.2.8.1 Introduction

This layer is the uppermost Liangzhu period platform of this profile. It is a yellowish-brown silty clay mixed with burnt daub, charcoal and coarse sands. Only one unit, Unit 2, was identified. The lower part of this unit is presented in the Micro-fabric T3131 7:1.

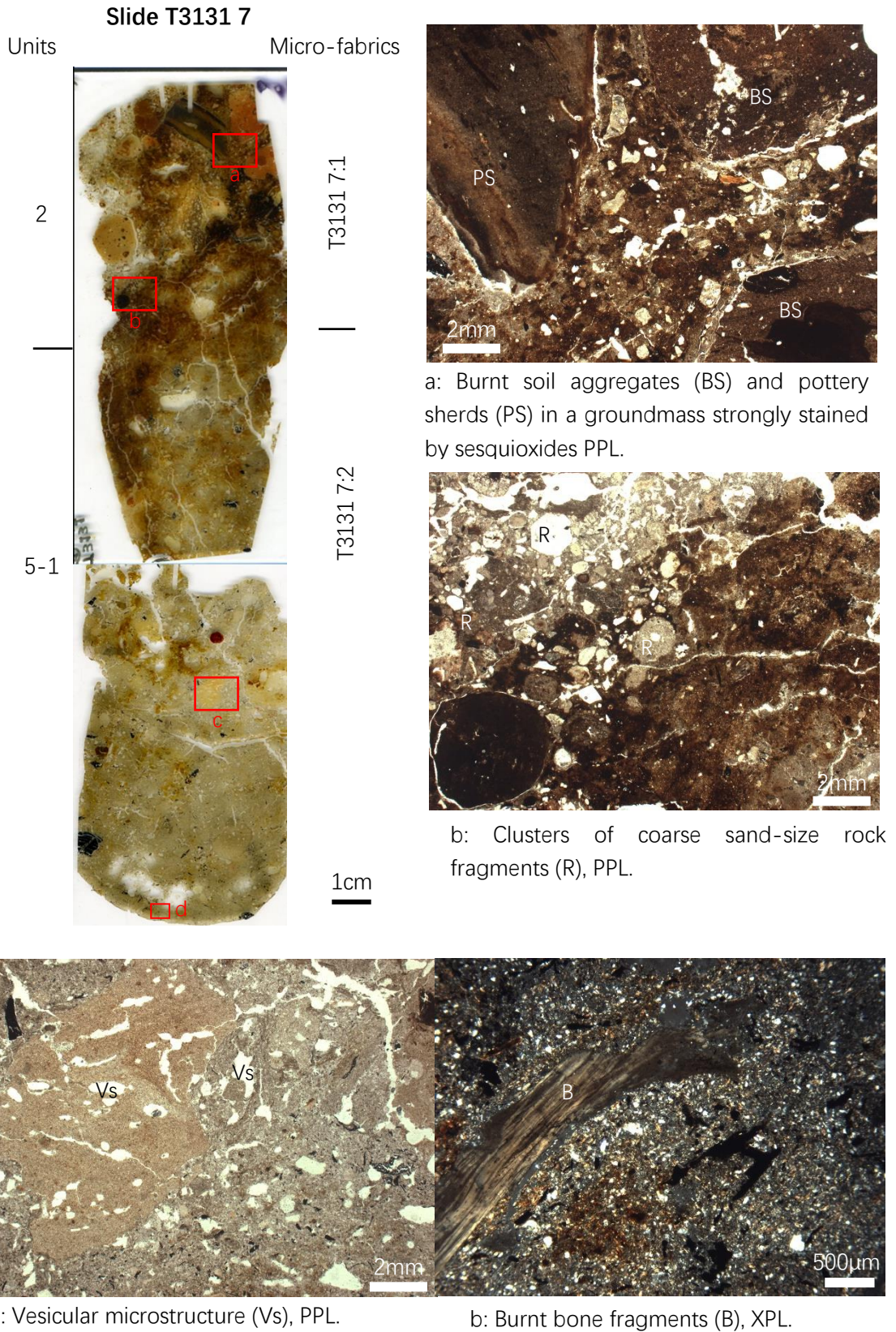


Figure 6.18 Slide scan and microphotographs from slide T3131 7

6.3.2.8.2 Platform 2: description of the Micro-fabric T3131 7:1

This unit is a very heterogeneous mixture of coarse inclusions in a coarse silt-size matrix heavily stained by amorphous iron/manganese oxides (Figure 6.18). The coarse inclusions occupied around 50% of the groundmass and are composed of frequently found, clustered, angular to sub-angular, sand-size and fine pebble-size rock fragments, three rounded burnt clay aggregates (daub), two slightly degraded pottery sherds, common rounded soil aggregates, a few fine charred materials and a trace amount of fine bone fragments. The mineral composition of the fine matrix is very similar to the groundmass in Platform 5-1. 80% of the fine matrix is impregnated by reddish brown to black (PPL) amorphous iron and manganese oxides and the remaining 20% is light yellow (PPL) with a striated b-fabric. This unit generally has a moderately developed prismatic microstructure with 5% partially accommodated planar voids and 3% irregular small vughs. Pedofeatures are dominated by amorphous iron and manganese oxides staining around the voids and channels.

6.3.2.8.3 Results of bulk analysis and interpretation of Platform 2

Platform 2 has a slightly alkaline pH, extremely high magnetic susceptibility value that is ten times higher than the average level in this profile, a high phosphorus content, and low total organic, carbon and calcium carbonate contents, which in general points to intensive human activity and possible intensive oxidation events. The widely found burnt archaeological remains such as pottery sherds and daub in this layer may be transported and probably intentionally added-in as indicated by their degraded rounded to sub-rounded shape and the clustering and wide distribution of these materials observed in field. Although this unit was heavily stained by amorphous iron/manganese oxides, the groundmass was not burnt based on micromorphology observation. These iron/manganese oxides that have diffuse boundaries may be translocated from the burnt remains and precipitated under oxidizing/drying conditions. Although the

iron/manganese oxides masked most of the sedimentation features of this layer, the clustered rock fragments found in this layer are indicative of a similar constructed layer such as in Platform 5-1.

In summary, this layer could be a constructed layer mixed with abundant burnt archaeological materials.

6.3.3 Interpretation of the T3131 profile

6.3.3.1 Radiocarbon chronology of the T3131 profile

In 2017, three sets of plant remains from Platforms 7, 6 and 5 from excavation pit T3131 were collected for radiocarbon dating at the Archaeometry and Archaeological Dating Laboratory in Peking University, China (Qin *et al.*, 2019). In the following discussions, dates are reported from the original publications (Qin *et al.*, 2019). All dates are calibrated using OxCal 4.3 (Reimer *et al.*, 2013) and the IntCal 13 calibration curve (Ramsey, 2019). The results (Table 6.1) show that Platform 7 is dated to 2896-2778 cal. BC (68.2%) or 2903-2705 cal. BC (96.4%), Platform 6 is dated to 2910-2890 cal. BC (68.2%) or 2921-2880 cal. BC (96.4%), and Platform 5 is dated to 2618-2468 cal. BC (68.2%) or 2851-2347 cal. BC (96.4%). Based on these data, the dates of the Platform 8 and Platform 2 can be inferred, with Platform 8 deposited before 2900 cal. BC and Platform 2 constructed after 2600 -2450 cal. BC.

Table 6.1 Radiocarbon dating of the T3131 profile and adjacent South Zhongjiagang Watercourse. The dating is conducted by Qin *et al.* (2019) at the Archaeometry and Archaeological Dating Laboratory in Peking University, China. All dates are calibrated using OxCal 4.3 (Reimer *et al.*, 2013) and the IntCal 13 calibration curve (Bronk, 2019).

Sampling position	Calibrated dates (68.2%)	Calibrated dates (96.4%)	Dating material	Dating Lab	Lab No.

T3131 Platform 7	2896-2778	2903-2705	Plant remains	Peking University	BA170953
T3131 Platform 6	2910-2890	2921-2880	Plant remains	Peking University	BA170951
T3131 Platform 5	2618-2468	2851-2347	Plant remains	Peking University	BA170955
T3332 7H	2561-2471	2571-2464	Plant remains	Peking University	BA170950
T3332 7G	2622-2498	2835-2488	Seed	Peking University	BA170943
T3232 7G	2836-2575	2859-2497	Plant remains	Peking University	BA170946
T3332 7A	2618-2494	2831-2480	Wood	Peking University	BA170945

6.3.3.2 Particle size analysis of the T3131 profile

Altogether, 14 samples from the T3131 profile were subjected to particle size analysis. The majority of the samples showed similar multi-peak patterns on the frequency histogram (blue lines in Figure 6.19), which suggests a diverse set of sources for the soil material. The two exceptions are the T3131 4-1 and T3131 5-1 samples. The T3131 4-1 sample shows a single-peak pattern (red line in Figure 6.19), which was sampled from the top of Unit 6B (Micro-fabric T3131 4:2), with the particle size analysis agreeing with the microscopic observations that the sediment was deposited under weak water motion and was relatively well-sorted. The T3131 5-1 sample also shows a slightly different multi-peak pattern to the other samples (green lines in Figure 6.19). It was sampled from the upper part of Layer 6A where units that have various groundmass (Micro-fabrics T3131 5:4, 5:5, 5:6, 5:7 and 5:8) were identified under the microscope. The mixture of these various soil materials may be the cause of the differences in the particle size distribution patterns.

The percent bar chart (Figure 6.20) shows that the T3131 profile is generally dominated by silt-size particles. Bulk samples from the bottom of this profile, namely T3131 1-1, 1-2, 1-3, 1-4 sampled from Units 8, 7 and the bottom of Unit 6C, have a higher content

of clay, which may imply a different source of soil material than for the other bulk samples. Generally, this profile has been strongly influenced by human activity as indicated by the variable content of sand-size material and the multi-peak pattern shown in Figure 6.19.

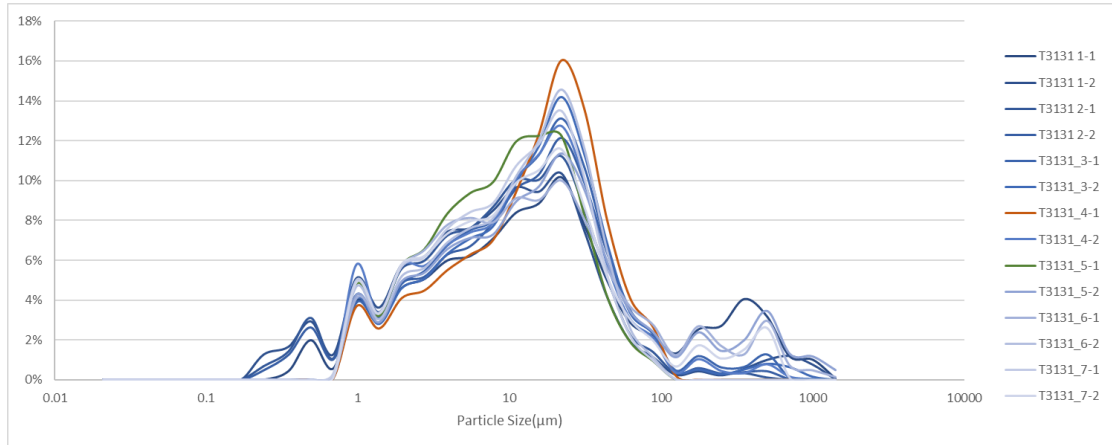


Figure 6.19 Particle size distribution graph of profile T3131

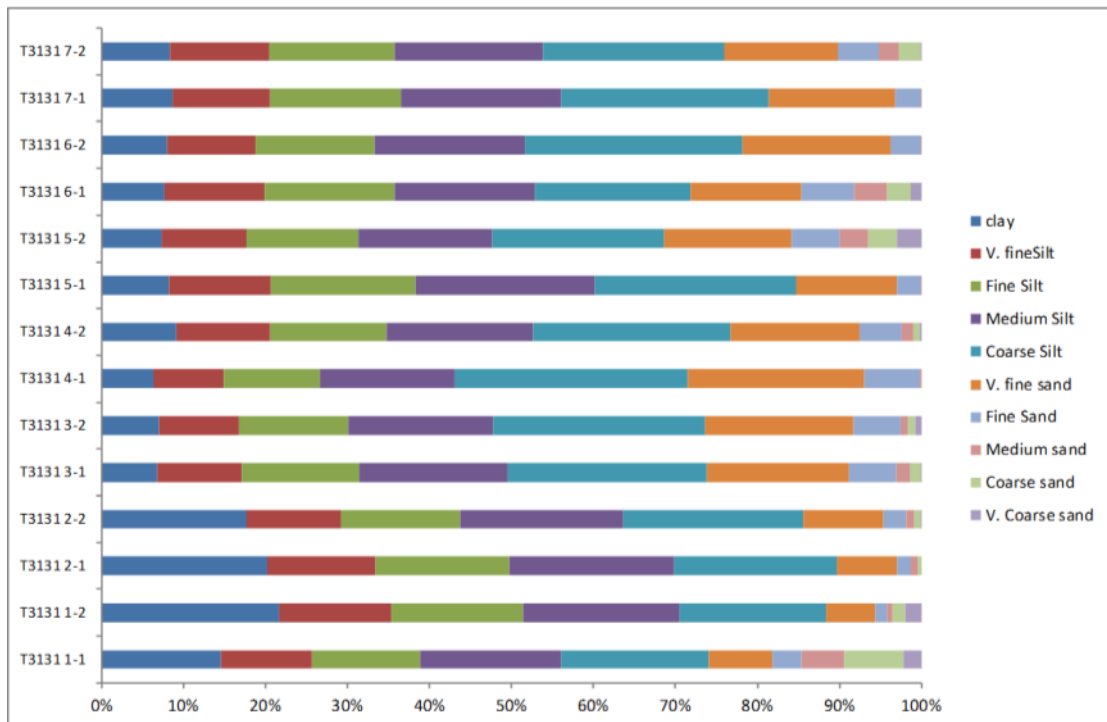


Figure 6.20 Percentage bar chart of the particle size of Profile T3131.

6.3.3.3 Preliminary lipid analysis of the plant material in T3131 profile

To better understand the nature of the bast fibres and the layered possible grass material

found in the T3131 profile, two soil and plant samples from the T3131 profile and one control sample from the base of T2621 profile were selected for lipid and isotope analyses at the Archaeological Micromorphology and Biomarkers (AMBI Lab), Universidad de La Laguna, Tenerife.

The first sample, T3131 2-1, was taken from the intact twill plaited bast fibres from the Micro-fabric T3131 2:3 (Figure 6.13). The second sample, T3131 6-1, was taken from the black, bedded organic material from the Micro-fabric T3131 6:2 (Figure 17). The control sample was taken from microfabric T2621 1:1 from the base of profile T2621, which is a pre-site, natural accumulated alluvium with little or no human intervention based on the micromorphology analysis (see section 5.2.2.1). The sample processing and analysis was conducted by Natalia Égüez.

The results (Figure 6.21, Table 6.2, 6.3) suggest that the samples found in T3131 2-1 and T3131 6-1 are C3 grasses that contained arundoin, a compound commonly found in the plant species belonging to *sugarcane* (*Saccharum* spp.) and tropical tall grasses (*i.e.*, *Imperata cylindrica* and *Austroderia* spp.) (Nishimoto *et al.*, 1965; Jacob *et al.*, 2005). The grass species in these two samples are almost identical and also completely different from the control sample. Common tall grasses used to extract bast fibres such as *Arundo donax*, *Imperata cylindrica*, and *Phragmites australis* are either C4 plants or do not contain arundoin (Ohmoto *et al.*, 1970; Brook, 1989). So far, the only weaving material that is a C3 plant, contains the arundoin triterpenoid and grows near Liangzhu is from the sub-family of *Bambusoideae* (Ohmoto *et al.*, 1970; Neto and Guerra, 2019). Considering that bamboo strips were also widely used for bank protection, it is highly likely that Liangzhu people extensively exploited bamboo for different tasks. In particular, the stems may have been processed to extract bast fibres for mat weaving (as in the Units 7-1 and 6C-1), and the leaves and stems may have been directly laid to provide temporary activity surfaces (as in the Unit 5-2-1). However, it should be noted that bamboo may not be the only grass material Liangzhu people used to produce

textiles, more specific analyses of other textile remain found inside Liangzhu City are required to further address this question.

Table 6.2 n-alkane concentrations, average chain length (ACL), the carbon preference index (CPI) and Paq values from the sediment samples analysed. * denotes compounds which were detected but in quantities below the limit of quantification.

Sample	T2621	T3131_2	T3131_6
Total n-alkane (in µg/g sample)	0.17	0.89	0.65
ACL	28.16	29.16	30.00
CPI	4.03	4.01	6.04
Paq	0.15	0.89	0.07
Arundoin		*	*

Table 6.3 $\delta^{13}\text{C}$ and δD from the sediment samples. Values are expressed in per mil (‰). Error reports standard deviation. * indicate that there were not peaks detected.

Sample	T2621	T3131_2	T3131_6
$\delta^{13}\text{C}$			
C₂₉	-23.91±0.4	-28.37±0.2	-27.27±0.1
C₃₁	-24.24±0.5	-27.00±0.1	-23.27±0.5
δD			
C₂₉	*	-396.51±1	-371.32±3
C₃₁	*	-371.07±3	-379.23±4

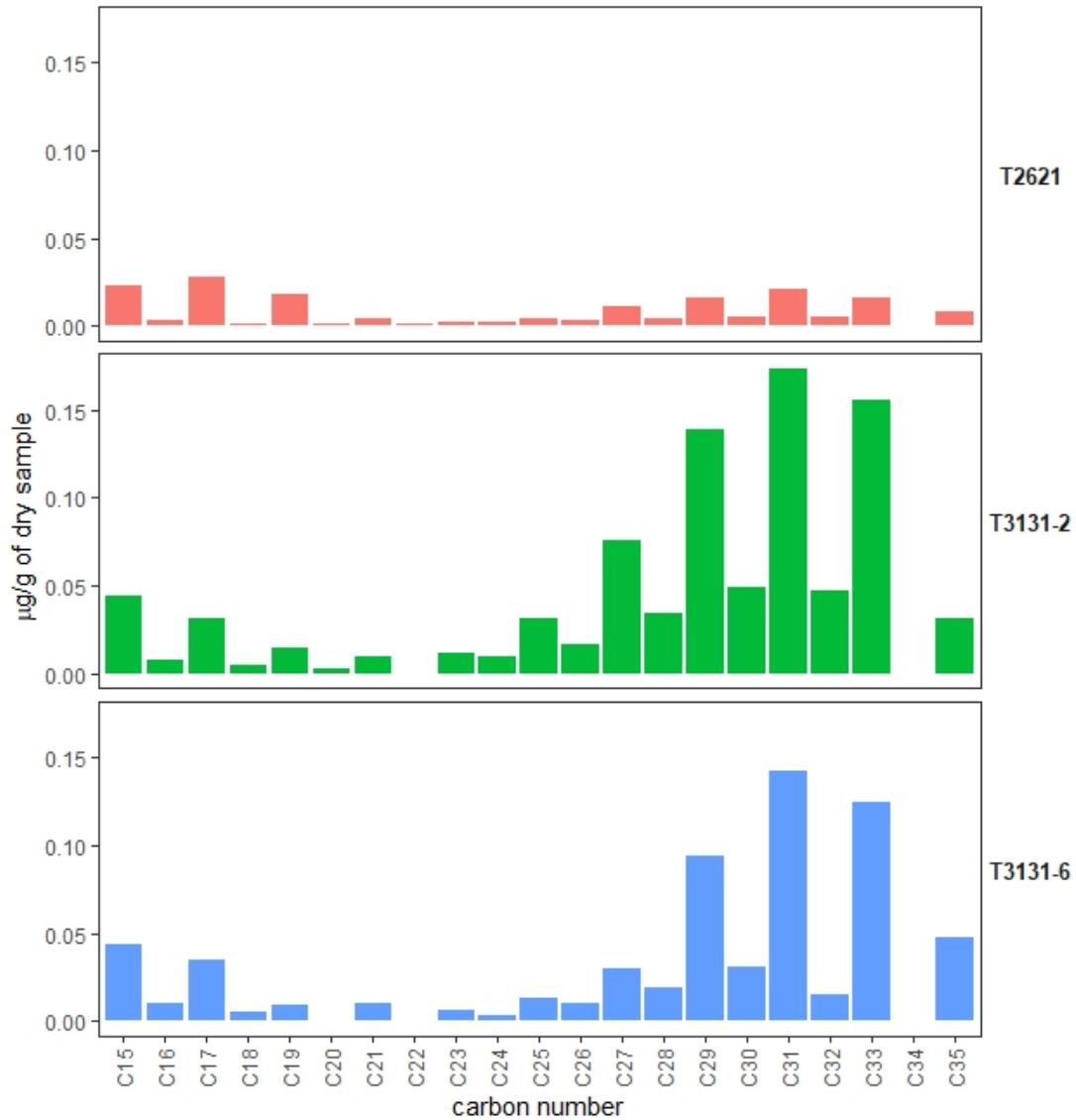


Figure 6.21 Histograms displaying the distribution and concentration of n-alkanes extracted from sediments. IS: 5a-androstane. The x-axis represents the alkane carbon chain length and the y-axis represents the concentrations given in µg per g of dry sediment (µg/g).

In summary, the repeatedly found laminae of bast fibres and blackened organic materials in profile T3131 consist of the same grass material, most likely from *Bambusoideae*, which was used for matting and/or thatching.

6.3.3.4 Site formation process of profile T3131

Based on the soil micromorphology analysis, profile T3131 is generally a near-water

human occupation area showing a repetitive occurrence of dumped occupational debris and construction materials.

To better understand the formation of this occupation floor site, the Passive, Reactive, Active Zone model developed by Gé *et al.* (1993) and Courty *et al.* (1994), was adopted based on both soil micromorphology and bulk sedimentology interpretation (Table 6.2). The Passive Zone refers to an accumulation of sedimentary material with little mechanical affect by trampling, such as sedimentary layer, surface soil horizon, dumped waste, ground raising deposits, prepared floors and floor coverings, etc. (Courty *et al.* 1994; Gé *et al.* 1993). In the case of the T3131 profile, it is mostly represented by construction material and various dumped material different in the arrangement of coarse inclusions, e.g., anthropogenic materials dispersing within finer matrix or loosely packed, and types of inclusion, such as hearth remains or rock fragments. The Reactive Zone is mainly the fragmentation of the Passive Zone material due to trampling and incorporates micro-artefacts brought in by foot traffic (Macphail & Goldberg, 2017). The Reactive Zone in T3131 profile is not always prominent, probably due to the direct covering of matting material on the Passive Zones and will therefore be discussed together with the Active Zone if it cannot be clearly identified. The Active Zone is characterised by large amounts of well-sorted archaeological micro-artefacts formed by homogenisation and compaction from human activities (Courty *et al.*, 1994; Gé *et al.*, 1993; Macphail & Goldberg, 2017). In T3131, this zone is demonstrated by elongated, densely compacted micro-aggregates and various micro-artefacts between layered, mostly intact matting material with sub-horizontal fissures. In general, a cycle of Passive Zone, Reactive Zone and Active Zone can be regarded as one phase of occupation. In combination with dating data, field observations, micromorphology observations and bulk sedimentology analysis, it is suggested that a total of seven phases of occupation can be discerned from the T3131 profile (Table 6.2).

Units 7-2, 8-1, 8-2 and 8-3 can be recognised as Passive Zones with different forms of

expression. Together with Unit 7-1, which was identified as a Reactive to Active Zone, these units were grouped as the Phase 1 occupation. The date of the Passive Zones of the Phase 1 occupation was around or slightly before 2900 cal. BC and the Reactive and Active Zones were around 2900 cal. BC. Unit 8-3 in the base was a dumped layer full of chaotic archaeological material formed under alternating wet-dry conditions, followed by a thin layer of possible dumped alluvial deposits in Unit 8-2, which was again covered by a pile of chaotic, dumped archaeological material with a sloping upper interface. This pile of debris was overlaid by a gradually accumulating alluvial deposit deposited under a gentle flow that contained abundant dumped charred materials. Dumping normally occurs on the periphery of activity areas (Binford, 1978). The appearance of the dumped layers with various components generally suggests that in around or slightly before 2900 cal. BC, this location was a largely unmanaged area near the activity zones. These dumped units intentionally or unintentionally provided a solid foundation for human activity and occupation on top, such as Unit 7-1. The bottom of Unit 7-1 is dominated by intact, *in situ* matting material with few anthropogenic inclusions. The middle part of this unit is composed of intact matting material with abundant occupational fine debris in between. The *in situ* burning activity may have happened on top of these mats and based on the micro-lamination and regular succession of micro-aggregates and bast fibres, these mats may have been constantly maintained by clearing and re-surfacing (Gé *et al.*, 1993). The upper part of this unit was a trampled Active Zone with various fragmented matting materials, occupational fine debris and rounded soil aggregates.

The Phase 2 occupation was composed of Units 6C-2 that were recognised as a Passive Zone, and Unit 6C-1 that was identified as a Reactive to Active Zone. This phase was also dated to around 2900 cal. BC and these two units basically mirrored the Phase 1 occupation. In the bottom of Units 6C-2 was composed of dumped hearth remains in alluvial deposits, the middle was composed of laminae of 'clean' intact matting materials, and the upper part contained heavily trampled, fragmented matting materials,

occupational debris and soil aggregates.

The Phase 3 occupation was represented by Unit 6B, which was recognised as a Passive Zone, and Unit 6A-5, which was identified as a Reactive to Active Zone. Unit 6B contained various archaeological remains either swept or dumped from a nearby occupation zone into an alluvial sediment. Wet conditions prevailed in this unit, and the location appears to be on the edge of the inhabited area and was constantly visited by Liangzhu people. Unit 6A-5 was composed of heavily trampled charred material in the bottom, followed by intact, inclined matting materials with mixed-in fine occupational debris. The top consisted of trampled fine occupational debris in an alluvial derived matrix. Again, this phase was dated to around 2900 cal. BC.

The Phase 4 occupation was represented by the Units 6A-4 and 6A-3. Unit 6A-4 was a dumped or natural aeolian sediment, which could be classified as a Passive Zone. If confirmed by future excavations and investigations, Unit 6A-4 could perhaps be indicative of a short hiatus of human activity at this location sometime between 2900 cal. BC and 2600 cal. BC. Unit 6A-3 was a disrupted and trampled version of Unit 6A-4 that contained abundant occupational fine debris and could be classified as a Reactive Zone. In general, this phase represents a short period of human activity in either a prepared or natural sedimentary layer.

The Phase 5 occupation was composed of Unit 6A-2, which was recognised as a Passive Zone, and Unit 6A-1, which was identified as a Reactive to Active Zone. Unit 6A-2 was mainly composed of loosely-packed burnt soil aggregates rolled over and/or dumped from a nearby activity zone and deposited in a dry, open space environment with repeated coverings of clean and slurry water flow. Unit 6A-1 consisted of a mixture of intensively trampled, elongate, 'exotic' soil materials and occupational fine debris. This phase of occupation may have taken place sometime between 2900 to 2600 cal. BC.

Table 6.4 Synthetic interpretation of the T3131 profile

Unit	Micro-fabric	Brief soil micromorphology interpretation	Brief summary of bulk sedimentology	Unit types	Occupation Phases
Unit2 (Platform 2)	T3131 7:1	Constructed layer: mixture of abundant burnt archaeological materials	Very high Mag sus, high P, low %total organic, %Carbon and % CaCO ₃	Passive Zone	Phase 7
Unit 5-1 (Platform 5-1)	T3131 7:2 and 6:1	Constructed layer: mixture of fine silty clay and coarse sand-size rock fragments	Low %total organic, moderate all other elements	Passive Zone	
Unit 5-2-1 (Platform 5-2)	T3131 6:2	Heavily trampled, open-air living surface with repeated matting of grasses material	High %total organic and %Carbon, moderate all other elements High P, medium-low % CaCO ₃ , moderate all other elements	Active zone	Phase 6
Unit 5-2-2 (Platform 5-2)	T3131 5:1	Dumped and trampled occupational debris and grass matting material		Active zone	
Unit 5-2-3 (Platform 5-2)	T3131 5:2	Crudely bedded burnt sand-size rocks, either constructed or brought by traffic		Reactive zone	
Unit 5-2-4 (Platform 5-2)	T3131 5:3	Constructed layer: kneading of different soil materials		Passive Zone	
Unit 6A-1 (Platform 6A)	T3131 5:4	Intensive trampling and bring-in of exotic soil materials by human activity in possible living surfaces	High Mag Sus and %Carbon, Low P, moderate all other elements	Reactive to Active zone	Phase 5
Unit 6A-2 (Platform 6A)	T3131 5:5	Loosely-packed dumped burnt soil aggregates		Passive Zone	
Unit 6A-3 (Platform 6A)	T3131 5:6	Trampling and incorporation of micro-artefacts		Reactive Zone	Phase 4
Unit 6A-4 (Platform 6A)	T3131 5:7	Dumped or natural aeolian sediment		Passive Zone	
Unit 6A-5 (Platform 6A)	T3131 5:8 and 4:1	Trampled floor sequence containing intact layers of bast fibres and abundant occupational debris		High P and %Carbon, moderate all other elements	Reactive to Active zone

Unit 6B (Platform 6B)	T3131 4:2 and 3:1	Dumped archaeological material in alluvial deposits	Medium high Mag Sus, moderate all other elements	Passive Zone	
Unit 6C-1 (Platform 6C)	T3131 3:2 and 2:1	Trampled and intensively occupied floor sequence with intact woven bast fibres and abundant occupational debris	High %total organic, moderate all other elements	Reactive to Active zone	Phase 2
Unit 6C-2 (Platform 6C)	T3131 2:2	Alluvium deposited under shallow and slow water with input of occupational debris from nearby occupation areas.	High P and % CaCO ₃ , medium high %Carbon, moderate all other elements	Passive Zone	
Unit 7-1 (Platform 7)	T3131 2:3 and 1:1	Trampled and intensively occupied floor sequence with intact woven bast fibres and abundant occupational debris	High %Carbon, medium high Mag sus, moderate all other elements	Reactive to Active zone	Phase 1
Unit 7-2 (Platform 7)	T3131 1:2	Alluvium deposited under shallow and slow water with input of occupational debris from nearby occupation areas	High % CaCO ₃ , moderate all other elements	Passive Zone	
Unit 8-1 (Platform 8)	T3131 1:3	Inclined dumped layer containing large amount of burnt anthropogenic materials.	Medium high Mag sus and % CaCO ₃ , low %Carbon, moderate all other elements	Passive Zone	
Unit 8-2 (Platform 8)	T3131 1:4	Alluvial deposition, possibly dumped			
Unit 8-3 (Platform 8)	T3131 1:5	Dumped archaeological materials			

(Table 6.2, continued)

The Phase 6 occupation took place between 2600 and 2450 cal. BC. This phase included Units 5-2-4, 5-2-3, 5-2-2 and 5-2-1. Unit 5-2-4 in the bottom was a constructed layer made from the kneading of at least two different soil aggregates and could be regarded as a Passive Zone. Unit 5-2-3 has a similar groundmass to Unit 5-2-4 but contained crudely bedded, burnt, sand-size rocks that may have been deliberately mixed in or brought in by traffic; this unit could be considered as a Reactive Zone. Unit 5-2-2 contained laminae of grass material that had been overlain by charcoal and burnt bones in a groundmass similar to the units below. These archaeological materials had possibly been trampled, so this unit could be regarded as an Active Zone. Unit 5-2-1 was a heavily trampled, open-air living surface with repeated grass matting material, which can also be regarded as an Active Zone. The groundmass of this unit is similar to the Phase 7 occupation above, and the use of fresh grasses as bedding may provide a short-lived living surface for the preparation and construction of Unit 5-1 above it.

Shortly after or contemporary with 2600-2450 cal. BC was the Phase 7 occupation, which was composed of Units 5-1 and 2 that could both be seen as a Passive Zone. Unit 5-1 was a constructed layer using very clean and pure silty clay brought-in from other sources that were probably prepared near this location by slaking and mixing of coarse sand material. During the preparation process, bone fragments and fine charred material were incorporated from a nearby hearth. The pattern of mixing coarse sand material in a silty clay matrix to construct platforms is similar to the construction layers in the Middle Zhongjiagang profile (see section 5.2.5) and could be a paradigm commonly used in Liangzhu City. Unit 2 was dominated by abundant, burnt and moderately degraded archaeological materials with a similar groundmass to Unit 5-1. These burnt archaeological materials may have been deliberately brought in as a temper to increase the hardness of the construction material. These constructed layers provided a solid activity surface for human occupation, but unfortunately most of the activity surfaces were not preserved due to post-depositional disturbance probably since historical times.

6.3.3.5 Changes in hydrological conditions and human activity in the T3131 profile

The T3131 profile is located on the western bank of the South Zhongjiagang Watercourse. It was generally on the periphery of main human occupation zone and was sensitive to changes in local hydrological conditions. Based on the difference in groundmass and the dating results, the occupation and construction of this mound can be divided into three main stages.

The first stage includes Phases 1, 2 and 3, which all show a similar pattern of dumped materials in alluvial deposits covered by regularly maintained occupation floors that accumulated in a relatively dry condition. Considering that no breaks in deposition were seen in the soil micromorphological observations, a continuous, relatively fast accumulation in around 2900 cal. BC can be inferred (Qin *et al.*, 2019). This stage starts with at least 7 cm of dumped archaeological materials. These dumped materials seem to be dumped as a whole as secondary refuse (Schiffer, 1978), which imply this location was at first an unmanaged area near activity areas. Then this profile is covered by 3-5cm alluvium deposited under shallow and slow water conditions with the input of occupational debris from nearby occupation areas. Regularly maintained and heavily trampled occupation floors containing repeat matting made of interwoven, twill-plaited grasses mixed with occupational fine debris then occurred, which showed an expansion of direct activity zones and the intensive exploitation of this low-lying area.

The repeated appearance of alluvial deposits and activity surfaces imply an unstable hydrological condition in this area, which supports the current dating results that the low dam systems were constructed after 2900 cal. BC (Qin *et al.*, 2019). Liangzhu people seems to directly occupy the low-lying grounds with a relatively low groundwater table at a relatively low altitude of only 1.5m a.s.l and retreat when wet conditions arrived. What caused this fluctuation and whether it is related to human management of local water resources is as yet unclear. In addition, whether there is a canalized channel or river near the site in early Liangzhu period is also obscure, as bank

protection facilities only appears in the Late Liangzhu period, and only Late Liangzhu period artefacts were found in the South Zhongjiagang channel. More geoarchaeological work in the region is required to further address this question.

The use of grass mats may be a simple but effective method with which to cope with this unstable water table as it may help to provide a dry, flat surface for human activity near the water's edge. The duration of the occupation and abandonment are difficult to estimate. It could be seasonal, related to the seasonal rise and fall of the nearby waterway, but most likely annually based on the thickness of the alluvial layers of 3-7cm, and the occupational accumulations of more than 7cm with more than ten layers of mats observed.

The second stage is dominated by Phase 4 and 5. There is no direct dating for this stage, but based on the dates of the upper and lower layers could be between 2900 to 2600 cal. BC. Phase 4 represents an ephemeral activity surface on top of dry aeolian sediment. Current dating analysis suggests that there may be a 100-150 year hiatus of human activity indicated in the whole Zhongjiagang channel between 2850 and 2700 cal. BC (Qin *et al.*, 2019). This 1.5cm thick aeolian sediments could perhaps be indicative of a short hiatus of human activity at this location if confirmed by future excavations and investigations. In Phase 5, probably due to the increase in sedimentation height, the dumped materials were placed in an open space under dry conditions followed by repeated coverings of clean and muddy water flows. Intensive open-space occupational activity then returned on top of the dumped units.

In the last stage, Phases 6 and 7 were synchronously constructed in around 2600-2450 cal. BC. The Passive Zones of these phases were dominated by constructed soil materials, including the kneading of different soil materials, layering of burnt soil aggregates, and mixing of fine gravels, water, burnt daubs and fine silty clay materials. The construction of these various soil materials is probably indicative of the active

enlargement of occupation area and the modification of the local landscape by Liangzhu people. This mound expansion is also commonly seen in other locations of Liangzhu City during the Late Liangzhu period (Liu *et al.*, 2019a). The Active Zone is dominated by layered fresh grasses in a relatively dry and open space. These grasses were heavily trampled and interlaced with hearth remains such as burnt bones and charcoal fragments. Although the same grass material as the first stage mattings was used, these grasses were most likely exploited for short-term occupation.

From the Early to Late Liangzhu period, the Passive Zone material shows a trend of formalization from natural alluvial floodplain accumulation and randomly dumped human waste to meticulous prepared construction materials. This change may be an active response to the fluctuating water table and is also related to the expansion of mounds into previous wetland areas both inside and outside Liangzhu City, such as in the Shiqianyu site east to Liangzhu City and the Bianjiashan site south to the city (Zhejiang, 2014).

In summary, profile T3131 located on the western bank of the South Zhongjiagang, represents a near-water human occupation area showing a repetitive occurrence of dumped occupational debris and construction materials interlaced with activity surfaces. At around 2900 cal. BC, this area is a near-bank area with alternating wet-dry hydrological conditions. Liangzhu people did not actively modify the landscape. They repeatedly occupied this area during dry periods and retreated when the regional water area enlarged. Between 2900 and 2600 cal. BC, there was a transitional stage with short periods of occupation on top of aeolian sediment and dumped burnt materials. After 2600 cal. BC, the Liangzhu people actively expanded their living area by constructing man-made mounds. This profile in general is formed due to sequential buildings and deposits from human activities and settlements, its formation process is similar to the artificial mounds or 'tells' widely found around the world (Matthews, 2017). Nonetheless, this near-water settlement has its unique and complex sequence of

formation process, as well as a dynamic relationship between the changing hydrological conditions and human activities.

6.4 Summary

Using an integrated set of geoarchaeological methods, this study has revealed how the Liangzhu people interacted with and adapted to local hydrological conditions and their occupation pattern of living near water by using mats and constructing platform structures. By combining soil micromorphological and bulk sedimentological analyses, at least six intact activity surfaces have been recognised in the T3131 profile based on the presence of intact matting materials and the trampling of anthropogenic fine debris. The 'Passive-Active' occupation pattern was then adopted to describe the long-term rhythm of occupation, abandonment and construction in this artificial landscape highly modified by Neolithic people. This research thus provides the first detailed study of Neolithic floor sequences in east China. The study of the T0950 profile has revealed dramatic change of sedimentation environment of the Southwest Mojiashan and may benefit the study of the occupation patterns of Liangzhu society, particularly for the Early Liangzhu period, and the environmental and cultural changes happened in the critical transition from early to late Liangzhu period. Importantly in addition, the lipid and isotope analyses of the grass material shed light on how Liangzhu people exploited grass materials, especially bamboo, for both long-term and short-term living purposes.

Chapter 7: Settlement sites and analogue profiles in outer Liangzhu City

7.1 Introduction

Besides Liangzhu City, hundreds of smaller settlement, burial and dam sites dated from the early to late Liangzhu period have been found in a region of 50 km² around the site (Liu, 2019). To better understand the regional sedimentation processes, changes of hydrological condition, and interactions of human occupation and local landscape in a larger scale, soil profiles for soil micromorphology and bulk sedimentology analysis were sampled north of Liangzhu City, including two settlement profiles – the South Jincun site and the Shiqianyu site – and three relatively natural analogue profiles, namely the Huoxitang, North Tangshan and Dazhe profiles (Figure 7.1).

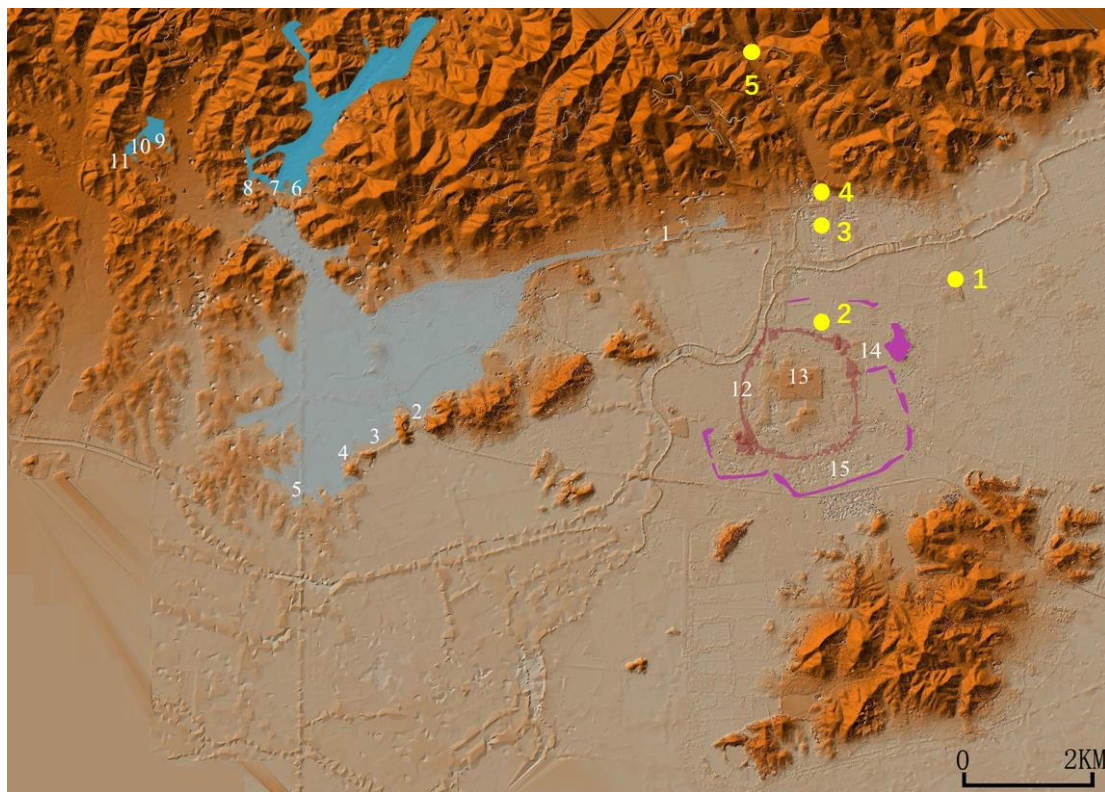


Figure 7.1 Distribution map of profiles sampled outside Liangzhu City: 1. Shiqianyu site, 2 Huoxitang site, 3. South Jincun site, 4. North Tangshan profile, 5. Dazhe mountain profile

7.2 Outer City settlements of Liangzhu City

The settlements in outer Liangzhu City are normally found as strip-shaped mounds 3-5m above sea level and around 1-2m above surface ground with a length of 200-350m and a width of 30-100m (Liu *et al.*, 2019c). Most settlements were occupied in the Late Liangzhu period, between 2900–2500 cal. BC (Qin *et al.*, 2019), with marshlands and shallow water bodies between each mound. To gain a general idea of the hydrological conditions and the living strategies in the broader Liangzhu City region, two profiles were taken from the outer city settlements in 2018. The first profile was sampled from the Shiqianyu site north-east of the Liangzhu City during the rescue excavation (Figure 7.1, site 1). The second profile was sampled by hand augering from the Jincun site north of Liangzhu City (Figure 7.1, site 3).

7.2.1 Shiqianyu site

7.2.1.1 Field description of the Shiqianyu site (T1812 and T1813)

The Shiqianyu site is around 2km north-east of Liangzhu City. It is formed by two successively constructed platforms: Platforms I and II. In the bottom is the Platform II constructed on top of the pre-occupation layers and a possible channel deposit (Layer 5). Two sub-units have been identified in this platform. A thin layer of black organic material is found at the interface of the Platform II and Platform I. Platform I can be separated into four sub-units, and remains of ‘clay wrapped with grasses’ soil blocks are identified. A simple wooden coffin of a Liangzhu person was found in the middle of the Platform I (excavation data provided by ZPICRA).

When sampling during the rescue exaction in 2018, no one section exposed the complete sedimentation sequence. Therefore, soil samples were collected from two

adjacent excavation pits, T1813 and T1812, to have a full understanding of the soil formation process and pre-site hydrological conditions. The T1813 profile shows the sequence of successively deposited Platforms II and I on top of the channel deposits (Figure 7.2). The T1812 profile shows the sequence of the sub-units of Platform I that overlie the channel deposit and the pre-occupation sediments (Figure 7.2). In total, seven soil micromorphology samples and twelve bulk samples were taken above and below the boundaries of each layer. The field descriptions from top to bottom of profile T1812 and T1813 are as follows:

Profile T1812:

Platform I-1: Brown (2.5Y 3/2) silt loam with blocky structure that contains abundant pottery sherds and charcoal. Calcium and iron nodules are widely found.

Platform I-2: Very dark gray (5Y 3/1), compact constructed layer that contains abundant pottery sherds and charcoal.

Platform I-3: Constructed layer built by brown (2.5Y 3/2) 'clay wrapped with grasses' that has a blocky soil structure and contains large amounts of fresh organic matter.

Platform I-4: This sub-unit is not clearly seen in the field. It is a light brown silt loam that contains a few pottery sherds and fine charcoal.

Layer 5: Very dark gray (5Y 3/1) silt loam. A few pottery sherds and organic materials are found. This layer is believed to be a palaeochannel deposit.

Pre-occupation sediment 1: Very dark gray (5Y 3/1) silty clay loam with weak microlaminations. A few fine charcoal are found.

Pre-occupation sediment-2: Very dark gray (10YR 3/1) silt clay loam with weak microlaminations. This sediment is pure with few inclusions.

Profile T1813:

Platform I-1: the same as T1812 (not sampled).

Platform I-2: This platform is believed to be built by 'clay wrapped with grasses' that contains abundant fresh organic matter and exhibits a blocky soil structure. Between

Platforms I-2 and II-2 is an organic rich layer showing a black colour (5Y 2.5/1).

Platform II-2: Black (5Y 2.5/1) silty clay with a few charcoal inclusions. This layer is relatively homogeneous and is believed to be constructed by 'clay wrapped with grasses'. Charcoal and pottery sherds are found in this layer.

Layer 5 and Pre-occupation sediment: the same as profile T1812 (not sampled).

7.2.1.2 Soil micromorphology analysis of the Shiqianyu site

7.2.1.2.1 Pre-occupation sediment 2

7.2.1.2.1.1 Introduction

Two soil samples were collected from the buried soil of the Shiqianyu site to understand the pre-occupation condition in the outer Liangzhu City area. The first one (slide T1812 1) was taken from 0.3m below sea level by hand augering and the other one (slide T1812 2) was sampled from 0.25m above sea level.

7.2.1.2.1.2 Pre-occupation sediment 2: description of Micro-fabrics T1812 1:1 and 2:1

Micromorphology observation shows that there is no substantial change of sedimentation process from -0.3m to 0.25m above sea level in the T1812 profile. The sediments are all very homogenised, calcium carbonate rich, very fine silty clay with a few humified tissue residues (Figure 7.3). The description here will be based on the Micro-fabric T1812 1:1.

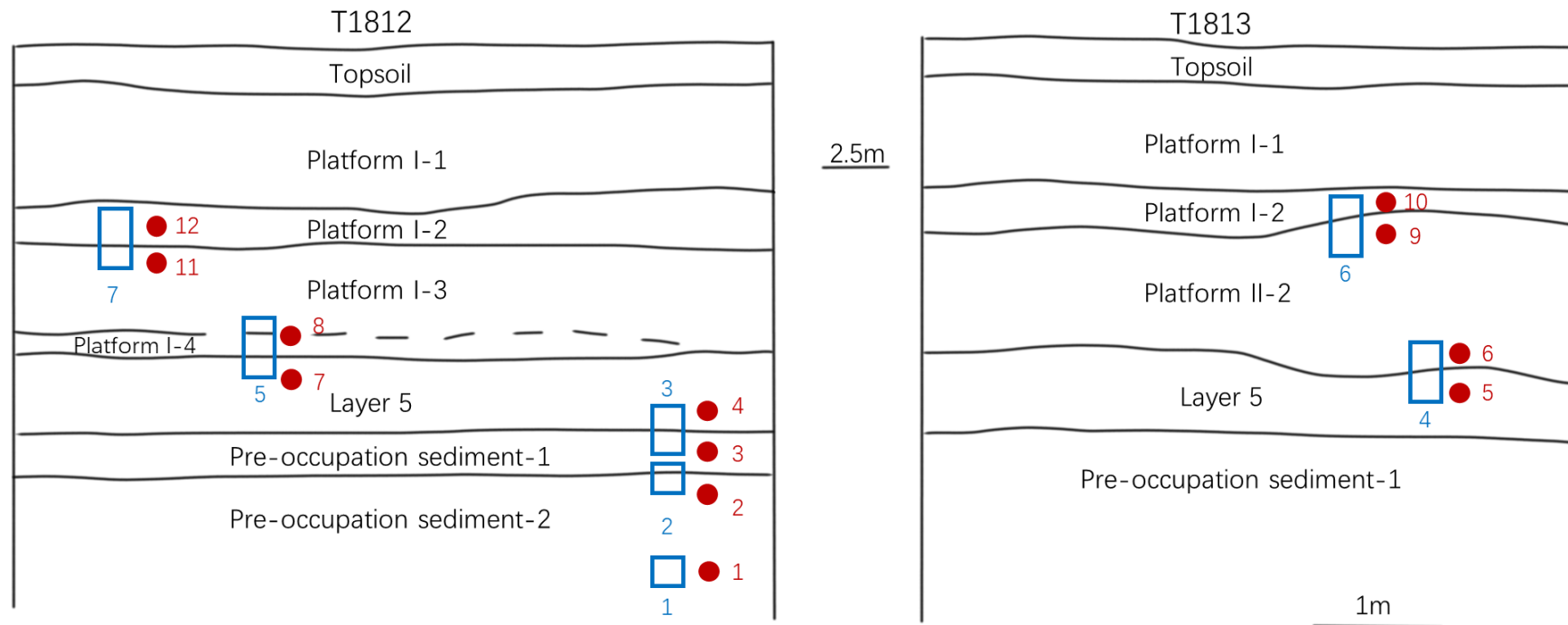
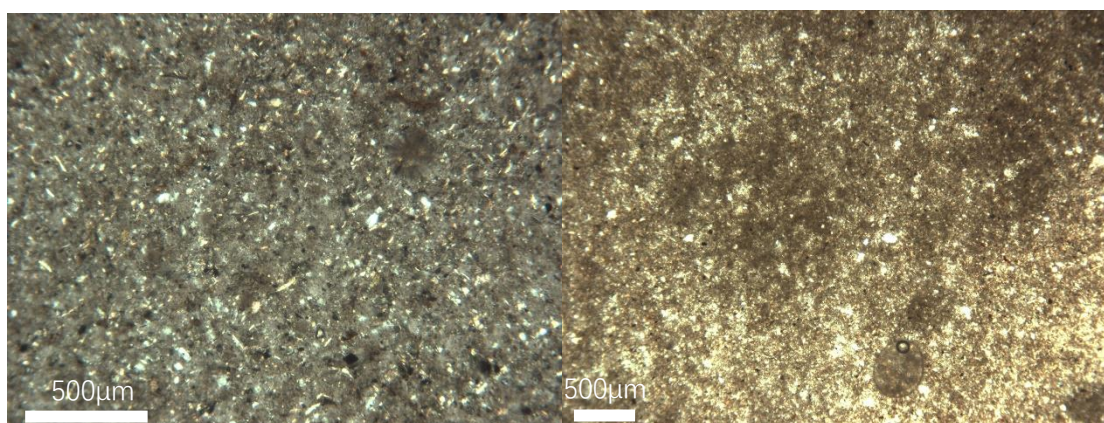
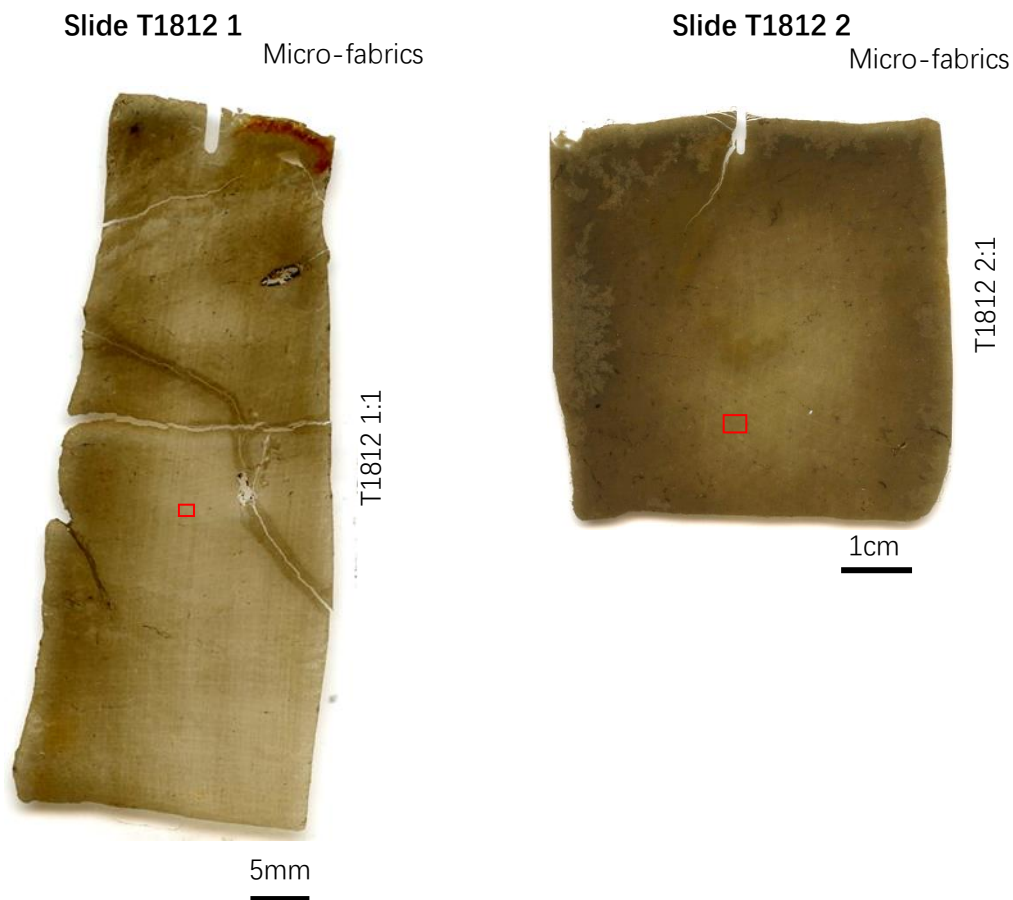


Figure 7.2 Stratigraphy and sampling position of the T1812 and 1813 profiles. The blue rectangles and numbers refer to the sampling positions and numbers of the soil micromorphology samples. The red dots and numbers refer to the sampling positions and numbers of bulk sample.



T1812 1:1 Calcareous silty clay groundmass, XPL.

T1812 2:1 Calcareous silty clay groundmass, XPL

Figure 7.3 Slide scan and microphotographs from slides T1812 1 and 2

The pre-occupation sediment generally has a c/f ratio of 2/98 (limit: 50µm). The groundmass is composed of well-sorted, sub-rounded, very fine sand-size quartz (2%) and light yellow (PPL) calcitic silty clay with moderate birefringence and a reticulate-striated to micritic calcitic crystalline b-fabric. This sediment contains a few dark brown humified and amorphous fine organic matter and has a massive microstructure

with a few channels. These channels are partially (1/4) infilled by finer silty clay with serrated void walls. On top of Micro-fabric 1812 1:1, alternating micro-laminations of fine silty clay and calcium carbonate rich fine silt material are observed. A trace amount of black manganese compound is incorporated in the groundmass and a few pyrite framboids are found around the humified organic matter. A few clusters of micritic calcium carbonate with diffuse boundaries are also found.

7.2.1.2.1.3 Results of bulk analysis and interpretation of Pre-occupation sediment 2

As shown in Figure 7.4 (Bulk samples T1812 1 and 2), this sediment generally has a slightly alkaline pH of 7.78 and 7.84, which are the highest of all the bulk samples of the Liangzhu region. The high magnetic susceptibility value and calcium carbonate content, very low phosphorus content and the lack of anthropogenic materials imply a low level of human activity in this layer and the natural origin of the high magnetic susceptibility and calcium carbonate content. This layer generally has a medium-low total organic content, together with the undisturbed sedimentation structure, implies a very fast sedimentation rate. The carbon content has slightly increased from bottom to top, which may demonstrate the increase of human activity at the end stage of this layer.

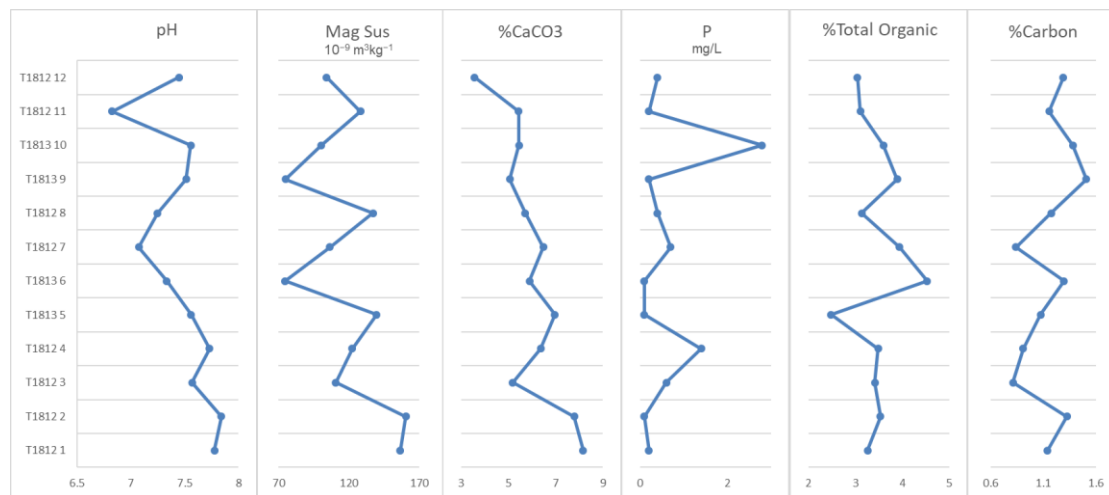


Figure 7.4 Analytical results of pH, phosphorus, magnetic susceptibility, and carbon, total organic and calcium carbonate contents of the Shiqianyu site.

Based on the well-sorted particle size and the alternation of fine silty clay and calcium carbonate rich silty clay, the pre-occupation sediment (from -0.3m to 0.25m) can be identified as a gradually deposited alluvium or more likely an intertidal flat sediment

based on the slightly alkaline pH, high magnetic susceptibility value, evenly distributed calcium carbonate and fast sedimentation rate. Similar sedimentation characteristics have been seen in other pre-site sediments of the Middle Zhongjiagang region (section 5.2) and South Jincun site (section 7.2.2), which may all reflect the intertidal flat/coastal river valley wetland environment before the arrival of Liangzhu people.

7.2.1.2.2 Pre-occupation sediment 1

7.2.1.2.2.1 Introduction

In the field, this pre-occupation sediment was identified as a separate unit to the pre-occupation sediment 2 because it contained fine charcoal. This layer is present in the Micro-fabric T1812 3:3.

7.2.1.2.2.2 Pre-occupation sediment-1: description of the Micro-fabric T1812 3:3

This sediment is composed of moderate-sorted, sub-rounded very fine to fine sand-size quartz in a light grayish yellow (PPL) humic, calcareous fine silty clay micromass with a low birefringence and a stipple-speckled to striated b-fabric (c/f: 5/95; limit: 50 μ m). Compared to the Pre-occupation sediment 2, the groundmass is slightly coarser and the amount of calcium carbonate crystals in the groundmass has significantly decreased. Also, the humified organic matter are laminated and infrequently seen, and a trace amount of very fine charcoal and a few fine silty clay soil aggregates are found. This sediment has a massive microstructure with a few channels (1% porosity). Dusty silty clay crusts in various thicknesses that alternate with coarse silt size material are widely seen in the lower part of the fabric. The silty clay crusts are mostly fragmented in the mid-upper part of the fabric.

7.2.1.2.2.3 Results of bulk analysis and interpretation of Pre-occupation sediment-1

Compared to the Pre-occupation sediment 2, the Pre-occupation sediment-1 shows a sharp decrease of pH, magnetic susceptibility, calcium carbonate and carbon contents, a moderate rise of phosphorus content and a stable total organic content (Figure 7.4,

Bulk sample T1812 3). The increase of phosphorus content together with the fine charred material found in the field (although not reflected in both bulk analysis and micromorphological observation) demonstrate the introduction of human activity in this area. The abrupt decrease of other bulk data has taken place within 5cm of deposition, which may imply a rapid change of sedimentary environment from Pre-occupation sediment 1 to Pre-occupation sediment 2.

The widely found dusty silty clay crusts and laminated organic material indicate the input of soil material by shallow, slow-moving slurry (Pagliai and Stoops, 2010). The coarser particle size indicates a slightly stronger deposition energy, which all suggest an alluvial sedimentary environment.

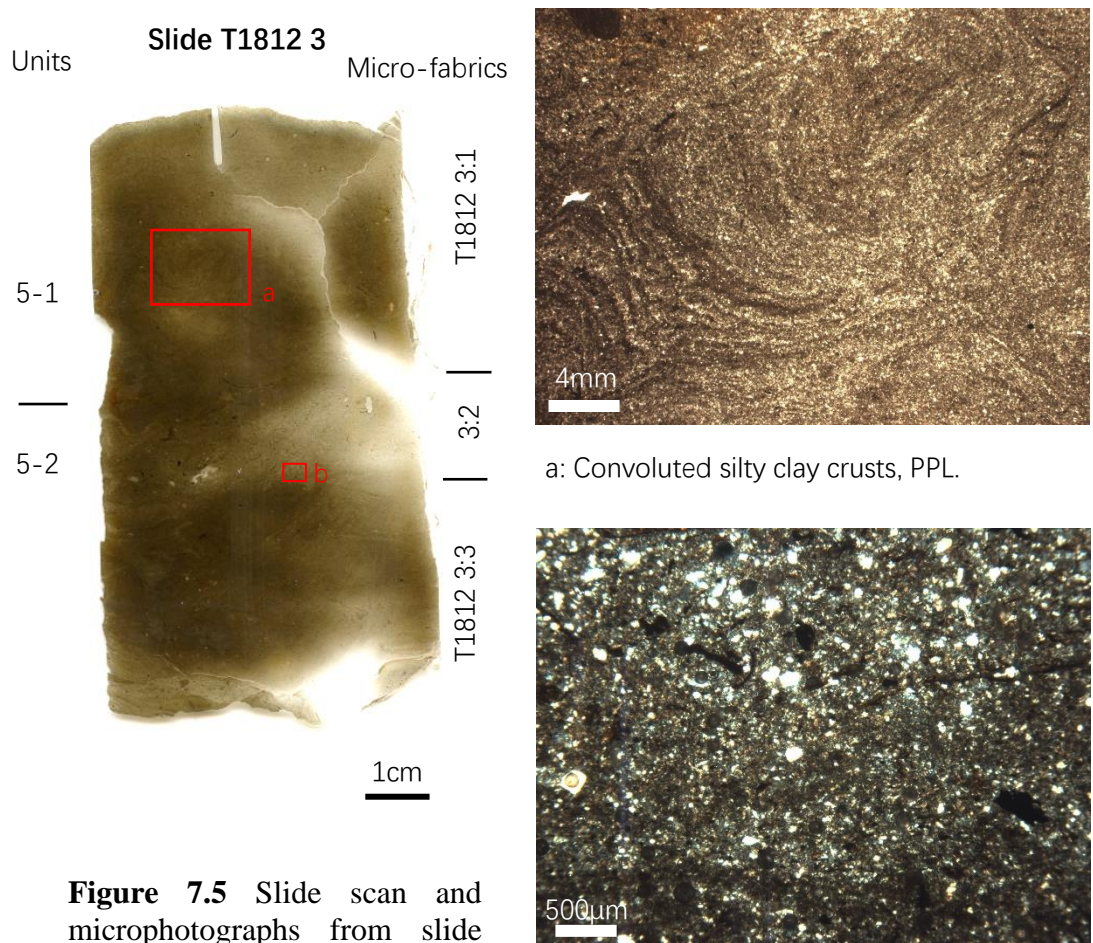


Figure 7.5 Slide scan and microphotographs from slide T1812 3

a: Convoluted silty clay crusts, PPL.

b: Interface of T1812 3:3 and 3:2, note the coarser particle size in the upper part, XPL.

In sum, from Pre-occupation sediment 2 to Pre-occupation sediment 1, the sedimentary

environment changes from periodically exposed intertidal flat to an accumulating alluvial plain. This change may have provided a suitable environment for soil formation and plant growth. Human occupation and the extent of human activity may also increase during this process.

7.2.1.2.3 Layer 5

7.2.1.2.3.1 Introduction

Layer 5 is identified as a palaeochannel flowing in a west-east direction in field. A few pottery sherds and organic materials were revealed from this layer. The bottom of Layer 5 is represented in the Micro-fabrics T1812 3:2 and 3:1. The upper part of Layer 5 is shown in Micro-fabrics T1813 4:2 and T1812 5:5.

7.2.1.2.3.2 Layer 5: description of the Micro-fabrics T1812 3:2, 3:1, 5:5 and T1813 4:2

Two sub-units have been identified in the bottom of the Layer 5. The Unit 5-2 overlying the Pre-occupation sediment 1 is a 2cm thick, coarser silty clay material with higher content of humified organic matter (Micro-fabric T1812 3:2, Figure 7.5). It is composed of poorly-sorted, angular to sub-angular, very fine to medium sand-size quartz and light grayish yellow (PPL) humic silty clay micromass with a low birefringence and a stipple-speckled to striated b-fabric (c/f: 20/80; limit: 50µm). Above it, the sediment returns to fine calcitic silty clay with a secondary sedimentary structure of convoluted laminations of dusty silty clay crusts (Unit 5-1, Microfabric T1812 3:1, Figure 7.5). A few vertical, partially accommodated channels with serrated walls are formed. In Unit 5-1, micritic calcium carbonate is evenly distributed in the groundmass and shows a stipple-speckled to micritic calcitic crystallitic b-fabric. A cluster of micritic calcium carbonate with diffuse boundaries, a few manganese nodules incorporated in the groundmass and around voids, and a few humified and amorphous fine organic matter are observed.

In excavation pit T1813, the top of Layer 5 (Micro-fabric 4:2) is mainly comprised of

very fine, light brownish (PPL) humic silty clay with a moderate birefringence and a reticulate striated b-fabric with a c/f ratio of 2/98 (limit: 50 μ m, Figure 7.6). A few soil aggregates composed of organic rich fine silt-size materials are randomly mixed in. A few vivianite crystals and stains of red amorphous iron oxides are found. Micro-fabric 4:2 shows a strongly developed angular-blocky structure with a porosity of 20% formed by accommodated, interconnected planar voids and fissures.

The top of Layer 5 in excavation pit T1812 (Micro-fabric 5:5) is formed by deformed silty clay crusts similar to those in Unit 5-1 in the bottom and is covered by thick laminations of very fine silty clay similar to the Micro-fabric T1813 4:2. Light reddish yellow (PPL) stain of amorphous iron oxides as quasi-coatings of voids and mottles are commonly seen in the groundmass. Trace amounts of manganese nodules near voids and humified organic materials are observed.

7.2.1.2.3.3 Results of bulk analysis and interpretation of Layer 5

The bottom of Layer 5 has a slightly alkaline pH, moderate magnetic susceptibility value and calcium carbonate content, and medium-low total organic and carbon contents (Figure 7.4, Bulk sample T1812 4). The phosphorus content is moderately high, which imply the appearance of human activity in this area.

Unit 5-2, which is the transition from Pre-occupation sediment 2 to Layer 5, shows a short increase of particle size that is suggestive of a higher stream flow energy in the alluvial system. The accumulation of alluvial material under repeated wetting and drying conditions soon returns as indicated by the repeatedly deposited dusty silty clay crusts that are deformed with convoluted features (Unit 5-1). The convoluted laminations are formed due to the increase of pore pressures, partially liquification and dewatering processes (Dzulynski and Smith, 1963; Töro and Pratt, 2015 and reference therein). It is commonly seen in rapidly deposited, newly-formed, saturated soft-sediments (Allen, 1982) and are also observed in tidal bores from nearby Qiantang Estuary (Fan *et al.*, 2012). In this unit, the deformed features may be caused by the fast sedimentation of alluvial material in Layer 5 and/or high pressure from overlying constructed soil materials.

The top of this layer in profile T1813 has a medium-high magnetic susceptibility value and calcium carbonate content, moderate carbon content, and low phosphorus and total organic contents (Figure 7.4, Bulk sample T1813 5), which generally indicate little or no interventions from human activity. The top of Layer 5 in profile T1813 shows a very high content of clay, which is suggestive of deposition under a very quiet, shallow, ponding environment. The occasional found silt-size soil aggregates could have been flushed into the system by rainfall events. Repeated wetting and drying and exposure of the land surface then happened as indicated by the widely seen clay striations produced by strong shrink-swell process (Kovda and Mermut, 2010), the evenly distributed micritic calcium carbonates in the groundmass, and the moderately high magnetic susceptibility value (Durand *et al.*, 2010).

The top of Layer 5 (Micro-fabric 5:5) in profile T1812 has a moderate magnetic susceptibility value and calcium carbonate content, medium-high total organic, medium-low phosphorus content, and low carbon contents (Figure 7.4, bulk sample T1812 7). The bottom of this fabric is the continuation of alluvium deposited under repeated wetting and drying with deformed features. It was then covered by relatively thin silty clay crusts formed under a very quiet, ponded environment similar to those observed in profile T1813.

Layer 5 in general is an aggrading alluvial plain formed under shallow and slow-moving hydrological conditions. Similar to the top of Layer 10B in the North Zhongjiagang Watercourse (section 5.3.2.3), the thick silty clay crusts indicate a fast sedimentation rate under a ponded environment with repeated wetting and drying (Pagliai and Stoops, 2010). Compared to Profile 1812, the excavation pit T1813 has a thicker silty clay layer and was located in a more central place of ponding.

7.2.1.2.4 Platform II-2

7.2.1.2.4.1 Introduction

In the field, Platform II-2 was shown in the profile T1813 (Figure 7.2). The bottom of

Platform II-2 is represented in the Micro-fabric T1813 4:1 and the top is represented in Micro-fabric T1813 6:3.

7.2.1.2.4.2 Platform II-2: description of Micro-fabrics T1813 4:1 and 6:3

The bottom of Platform II-2 has a distinct interface with lower Layer 5 and is an unevenly but well-incorporated mixture of four different soil materials. The first material (Sediment 1) acts as a groundmass and is a light brown (PPL) calcareous humic silty clay with low birefringence and a stipple-speckled to striated b-fabric (c/f: 5/95; limit: 50 μ m). The second material (Sediment 2) is slightly coarser and less humic. It is composed of well-sorted, sub-rounded, very fine sand-size quartz and light grayish yellow (PPL) calcareous silty clay with high birefringence and a random to parallel striated b-fabric (c/f: 10/90; limit: 50 μ m). Sediment 3 is a dark brown (PPL) very humic silty clay soil aggregates (c/f: 5/95; limit: 50 μ m) rich in finely fragmented humified and charred organic matter. The fourth material is the light yellow, clay-rich soil material from the Micro-fabric T1813 4:2 in Layer 5. These four materials and a few sand-size mineral grains are randomly mixed together. This layer generally has a moderately developed prismatic structure with a few vertical planar voids and fissures (10% porosity). Thin dusty clay hypo-coatings around voids are occasionally found.

The top of Platform II-2 (Micro-fabric T1813 6:3) is similarly composed of four different soil materials but slightly varied in the component ratio of the soil materials. The microstructure exhibits a mixture of moderately developed sub-angular blocky and vesicular structure (20% porosity). The vesicles have smooth voids and shows water/gas escaping features (Figure 7.8). Intercalations of limpid and dusty micro-layers of clay with high birefringence and thin hypo-coatings of yellow (in XPL) limpid and orange (in XPL) dotted clay with a high birefringence are occasionally observed around voids (Figure 7.8).

7.2.1.2.4.3 Results of bulk analysis and interpretation of Platform II-2

Platform II-2 has a slightly alkaline pH, medium-high carbon, moderate calcium carbonate, very low magnetic susceptibility and phosphorus contents, which in general

suggest very low degree of human intervention (Bulk Sample T1813 6 and 9, Figure 7.4). The bulk samples of the bottom of this platform have the highest total organic content in the profile, which implies the introduction of organic material probably from the grasses wrapping the soil materials.

The heterogeneous mixture of different soil aggregates observed from thin section agrees with the observation in the field that this layer is constructed by 'clay wrapped with grasses' using various sources of soil materials. Based on micromorphology observation, Platform II-2 has used soil materials from the top of the Layer 5 (Sediment-4 of Micro-fabric T1813 4:2) and incorporated soil aggregates with a high organic matter content (Sediment-3 in Micro-fabric T1812 4:1) that were possibly from topsoil, which are both locally available.

It is interesting that the top of Platform II-2 has a vesicular microstructure. The vesicle feature suggests when water enters the soil system, the escape of air is probably hindered by the sealing crusts (Evenari *et al.*, 1974). Research also demonstrates that vesicles can be formed simply by the wetting of dry soils (Dietze *et al.*, 2012). The appearance of vesicular microstructures in the top of Platform II-2 suggests that the soil material was once dried and with the water coming into the soil material, the air was trapped due to the hindrance of bedded grass and/or another layer of construction material overlaid it. The involvement of water was also indicated by the rhythmic alternation of limpid and dusty clay coatings, which is suggestive of an exposed surface with repeat wet-dry alternations. Also, the various textural intercalations may form due to the slaking of disturbed soil of this mound raising material (Macphail & Goldberg, 2010).

In summary, Platform II-2 is a constructed layer. The bottom may be mainly constructed by 'clay wrapped with grasses' using locally available soil materials. The upper material may be an exposed surface with repeated wet-dry alternations, which were then covered by another layer of construction material.

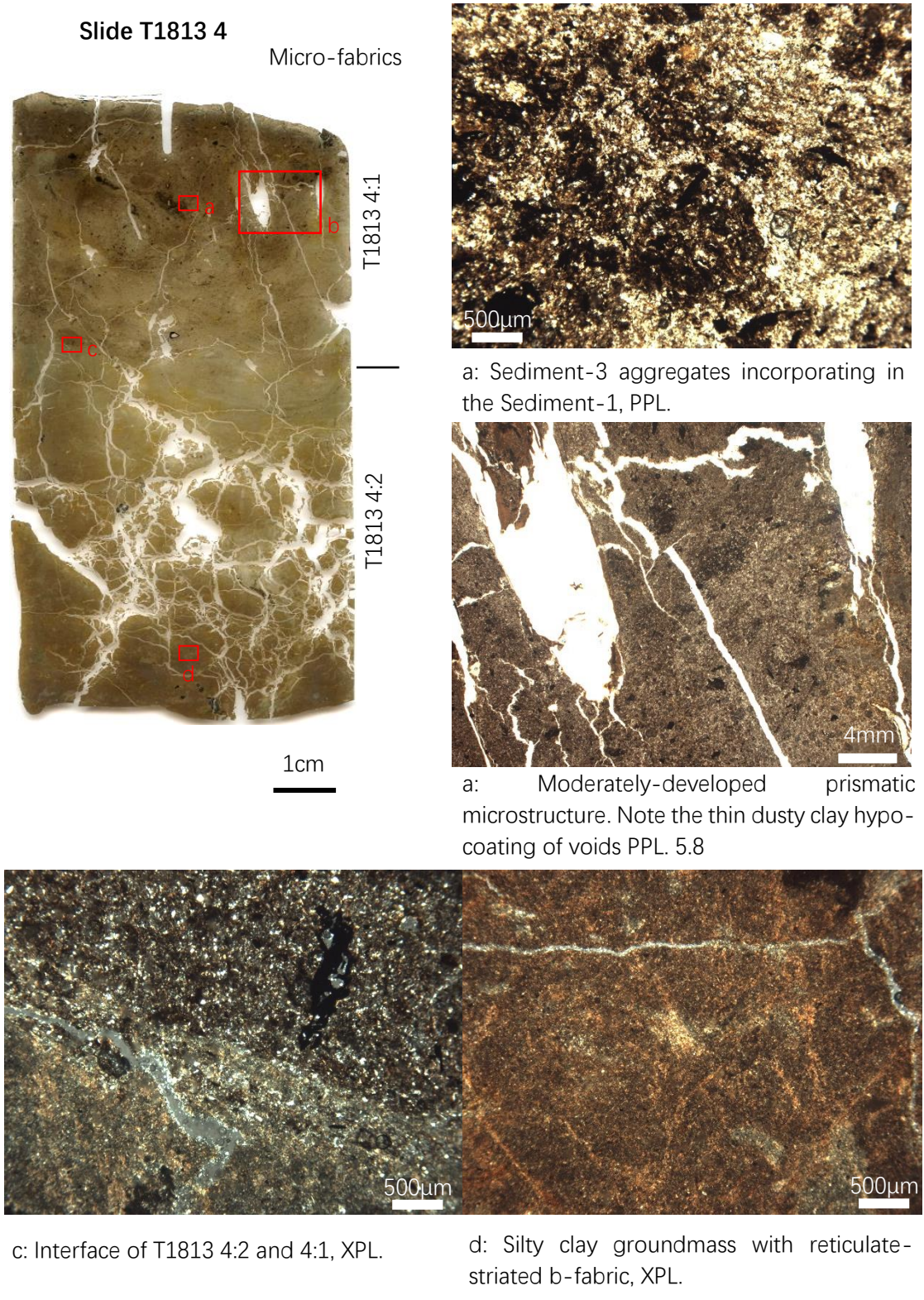
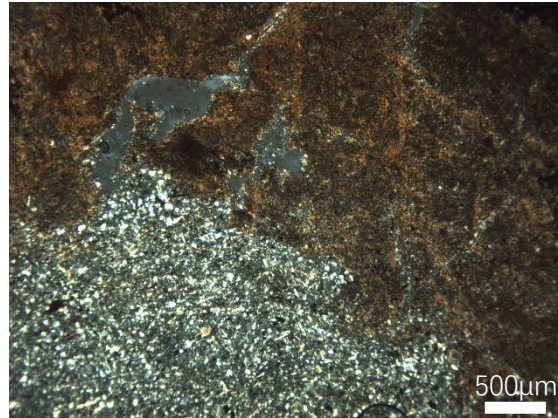
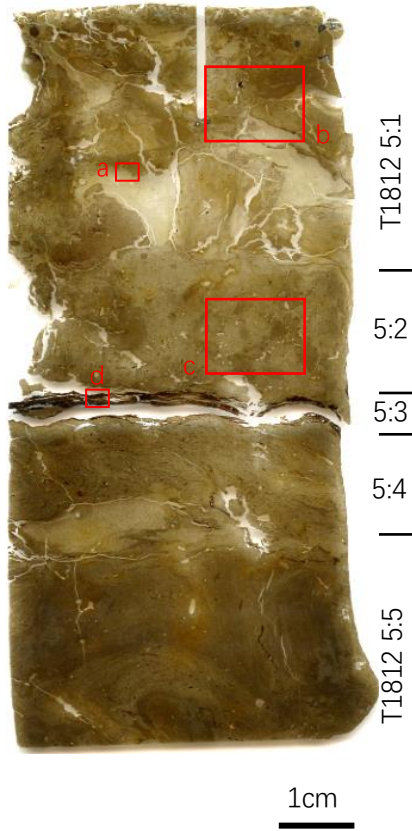


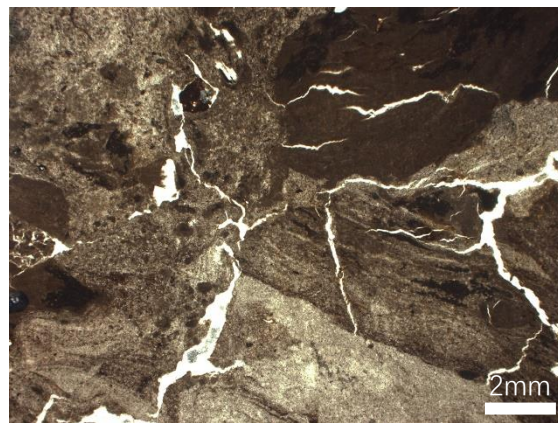
Figure 7.6 Slide scan and microphotographs from slide T1813 4

Slide T1812 5

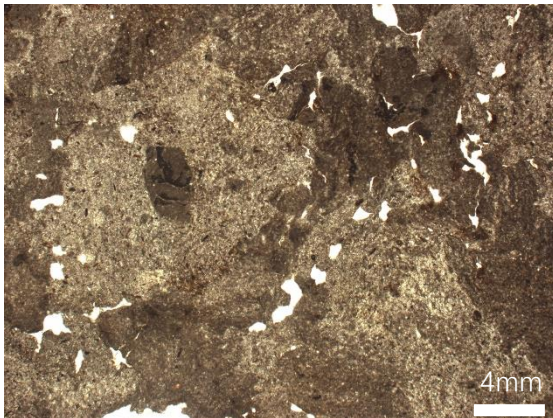
Micro-fabrics



a: Well-incorporated Soil aggregates -3 (lower left) and Soil aggregates -2 (upper right), XPL.



b: Mixture of different soil materials, PPL.



c: Fragmented humic fine silty clay soil aggregates in the groundmass. Note the vesicular microstructure. PPL.

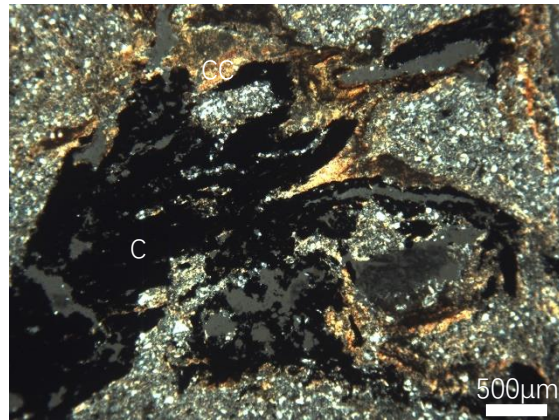
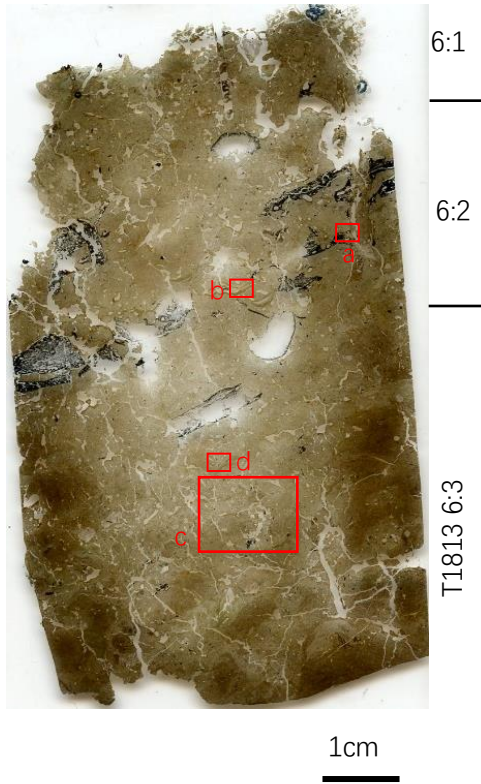


d: Laminated organic material interlaced with very fine silty clay, XPL.

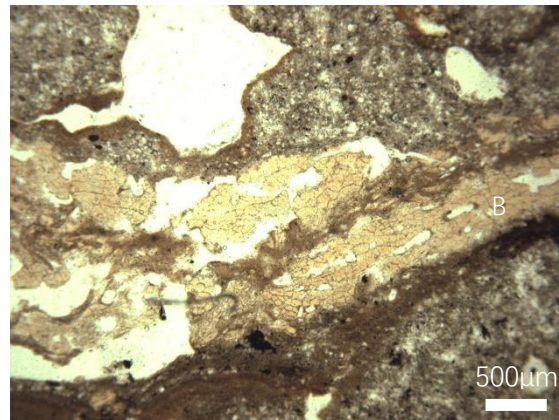
Figure 7.7 Slide scan and microphotographs from slide T1812 5

Slide T1813 6

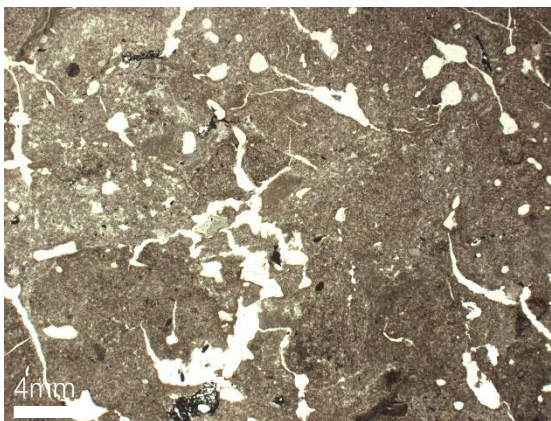
Micro-fabrics



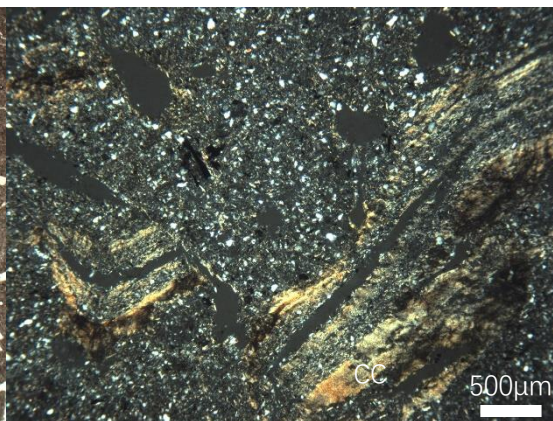
a: Charcoal (C) partly degraded by humification and coated with high birefringence clay (CC), XPL.



b: Bone fragments (B) coated with dusty silty clay, PPL.



c: Vesicular microstructure. PPL.



d: Micro-laminated limpid and dusty clay coatings (CC) with high birefringent. Note the possible shear deformation feature. XPL.

Figure 7.8 Slide scan and microphotographs from slide T1813 6

7.2.1.2.4.4 Platform I in Profile T1812

7.2.1.2.4.4.1 Platform I-4: description of Micro-fabrics T1812 5:4, 5:3 and 5:2

In the field, Platform I-4 was not clearly observed, therefore no bulk sample was collected from this unit. However, under the microscope, three sub-units of Platform I-4 are identified. The sub-unit in the bottom (Micro-fabric T1812 5:4) is composed of moderately well-sorted, sub-rounded to sub-angular, very fine to fine sand-size quartz and light grayish yellow (PPL) humic silty clay with a moderate birefringence and a parallel striated b-fabric (c/f: 15/85; limit: 50 μ m). Laminar dark brown humified and amorphous fine organic matter and fragmented fine dusty silty clay crusts near these organic materials are frequently observed. This fabric has a massive microstructure with 5% horizontal planar voids. Soil aggregates composed of coarse silt-size and very fine sand-size quartz and light yellow (PPL) silty clay (c/f 40/60, limit: 10 μ m) with fewer fragmented humified organic materials were horizontally laminated in the bottom and occupy 20% of the fabric.

In the middle are dozens of laminated, humified organic residues with light brown (PPL) dusty, very fine silty clay with moderate birefringence filled in the interspaces (Micro-fabric T1812 5:3, Figure 7.7). Above it is a 2cm thick, heterogeneous layer composed of highly fragmented silty clay crusts and fragmented fine silty clay soil aggregates with irregular boundaries in a light grayish yellow (PPL) humic silty clay groundmass with a random striated b-fabric. A small proportion (3%) of the micromass was stained a light reddish yellow due to impregnation with amorphous iron oxides. This fabric contains a few randomly distributed dark brown humified and amorphous fine organic matter fragments and has a vesicular microstructure with 5% porosity.

7.2.1.2.4.4.2 Interpretation of the Platform I-4

Based on the moderately well-sorted fine silty clay particle size, laminated humified organic matter, and frequently seen fragmented silty clay crusts, the bottom of this platform is an alluvial sediment similar to Layer 5 that underlies it. But this sub-unit also contains laminar silt-size soil aggregates, which may have been flushed in by

rainfall events and indicate a higher depositional energy compared to the previous Layer 5 sediment. This sub-unit is generally naturally formed and could be deposited synchronously with Platform II-2 as seen in Profile T1813.

The laminae of organic materials in the middle are most likely introduced or placed there by human activity based on the sharp contrast with lower and upper layers. The accumulation of fine material in between these organic materials denotes a shallow ponding environment. The sediment above has a similar groundmass with the bottom unit. However, its original soil structure is destroyed, the highly fragmented silty clay crusts and aggregates are most likely physically mixed by human activity. This sub-unit also has a vesicular microstructure. This evidence generally suggests a constructed soil material made with water and stirring in with soil, possibly sourced from a nearby stratum.

In summary, Platform I-4 demonstrates a change from alluvial deposition to a ponding environment with the layered accumulation of organic material, and then the constructed layer using soil material from the previous stratum.

7.2.1.2.4.4.3 Platform I-3 and I-2: description of Micro-fabrics T1812 5:1, 7:2 and 7:1

The bottom of Platform I-3 (Micro-fabric 5:1) has a distinct interface with lower fabrics. It is a combination of at least four different types of soil aggregates (Figure 7.7). These soil aggregates are closely compacted. Soil aggregates 1 is a light brown (PPL) fine silty clay (c/f 30/70, limit:10 μ m) with lamination of silty clay crusts (30% of the soil aggregate). Some of aggregates have vertical laminated silty clay crusts, which may suggest the inversion of original deposition positions. Soil aggregates 2, a yellow (PPL) very fine silty clay with striated b-fabric and high birefringence (c/f 5/95, limit:10 μ m), is similar to the T1813 4:2 Micro-fabric in Layer 5. Soil aggregates 3, a light yellow (PPL) silty clay, is very similar to the groundmass of Unit 5-1 of profile T3131 (a constructed layer using soil material from exotic resource, see Section 6.3.2.8). Soil aggregates 4 is a brown (PPL) humic silty clay with a high content of humified amorphous fine material (c/f 50/50, limit:10 μ m). This fabric generally has a fissured microstructure with 10% unaccommodated fissures between the soil aggregates. A few

vivianite crystals are found in the upper part of the fabric.

The top of Platform I-3 (Micro-fabric 7:2) and the bottom of Platform I-2 (Micro-fabric 7:1) are the oxidized versions of the Platform II soil material observed in profile T1813 (see section 7.2.1.2.4), with around 50% of the groundmass is heavily stained by orange (PPL) amorphous iron oxides (Figure 7.9). A thin lamina of dusty (orange in XPL) silty clay crusts with high birefringence demarcates these two platforms (Figure 7.9). These units generally have a complex microstructure of moderately developed sub-angular blocky and vesicular structure with accommodated peds.

7.2.1.2.4.4 Results of bulk analysis and interpretation of the Platform I-3 and I-2

From bottom to the top of Platform I-3, the pH value drops from neutral to slightly acidic. Platform I-3 generally has a very low phosphorus content, moderate low % total organic, moderate % carbon and % CaCO₃, which all suggests a low degree of human activity. The moderately high magnetic susceptibility of this platform may be influenced by the high content of amorphous sesquioxides in the fabric. Platform I-2 has a low content of all the bulk sample values (Figure 7.4).

Platforms I-3 and I-2 are both constructed layers using various locally available soil materials. It is interesting that the Soil aggregates 3 from the bottom of Platform I-3 was not seen in previous stratum and is similar to the groundmass of the constructed layer of profile T3131 (section 6.3.2.8), which is suggestive of using soil materials from other sources. The thin dusty silty crust between the Platform I-3 and I-2 indicates a short land exposure and covering of overland flow between the two construction stages.

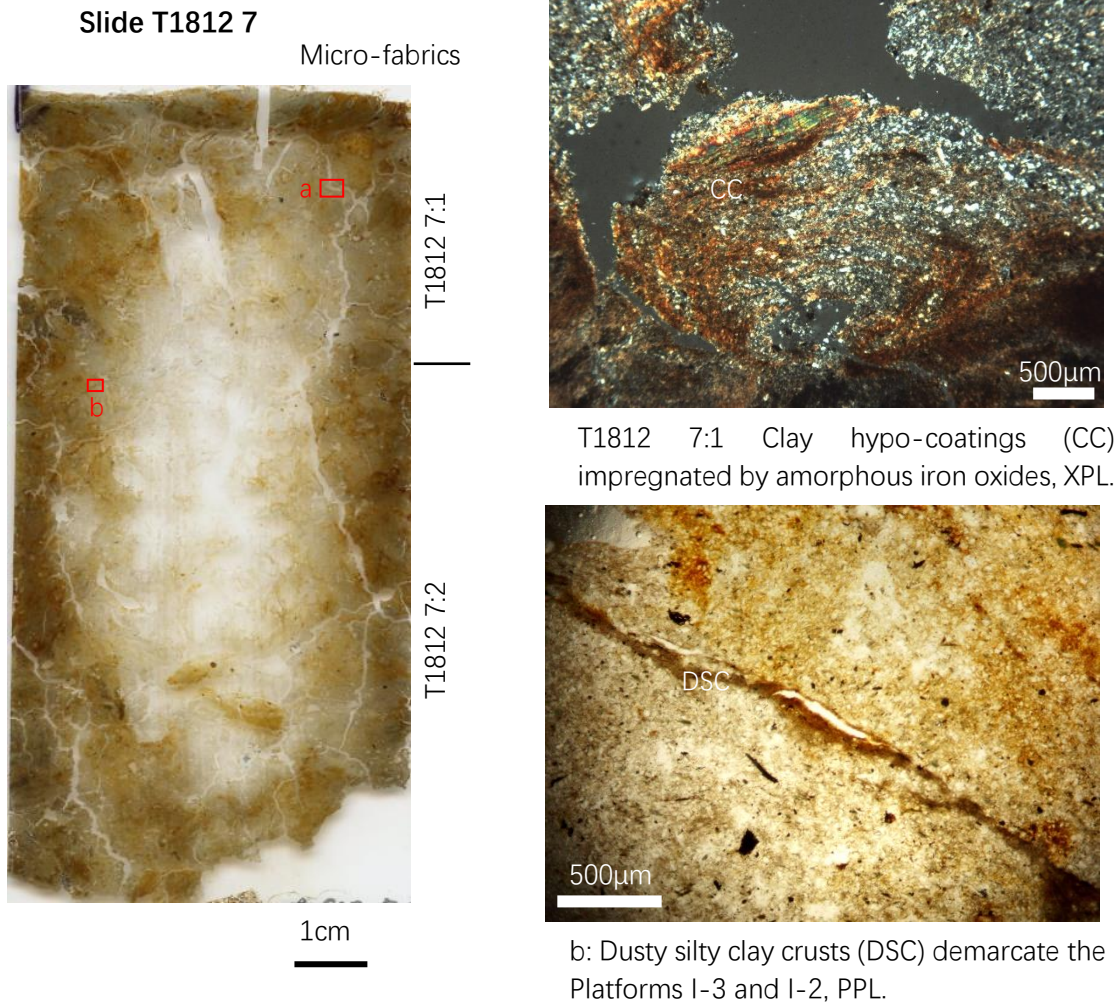


Figure 7.9 Slide scan and microphotographs from slide T1813 7

7.2.1.2.4.5 Platform I-2 in Profile T1813

In profile T1813, Platform I-2 is overlying Platform II-2. The bottom of this layer is an inclined (30°) layer of black, humified grass materials (Micro-fabric T1813 6:2) with a thin lamina of fragmented bone material (Figure 7.8). The groundmass and soil microstructure inbetween and overlying (Micro-fabric T1813 6:1) the organic material is generally similar to the top of Platform II-2. Textural pedofeatures such as crescent hypo-coatings and intercalations of alternating dusty and limpid clay with high birefringence, and hypo-coatings of thin limpid yellow (in XPL) or dotted orange (in XPL) clay with high birefringence are frequently found around voids and the grass materials (Figure 7.8).

The Platform I-2 of profile T1813 has a very high phosphorus content and a relatively

high carbon content (Figure 7.4, Bulk sample T1813 10), which suggest a high extent of human activity in this layer. Similar to the Unit 5-2-1 of the T3131 profile (section 6.3.2.6), this open-air matting of grass materials may function as a temporary activity surface and demarcates Platforms II and I. Crescent hypo-coatings, intercalations and coatings of alternating dusty and limpid clay are more frequently seen around the voids and grass materials, which is suggestive of repeated coverings of clean rain splash and overland slurry (Courty *et al.*, 1989).

7.2.1.3 Interpretation of the Shiqianyu profiles

7.2.1.3.1 Particle size analysis of the Shiqianyu profiles

Most of the soil samples collected from Shiqianyu show a single peak distribution pattern (blue and green lines in Figure 7.10). The two exceptions are samples T1813 9 and 10 from the bottom of Platform I-2 and the top of Platform II-2 in profile T1813 that have a multi-peak or wide peak pattern (yellow lines in Figure 7.10), which based on micromorphological observation have showed evidence of grass bedding and associated human activities. Among the single peak samples, the samples shown in green lines (T1812 1, 2 from the pre-occupation layers and T1812 12 from Platform I-2) have a narrower peak, suggesting better sorting.

In general, the soil samples from the Shiqianyu site show very similar particle sizes, composed of about 20% clay, 75-80% silt and 1-5% sand (Figure 7.11). This similarity supports the observation under the microscope that the platforms of the Shiqianyu site were constructed using locally available soil materials.

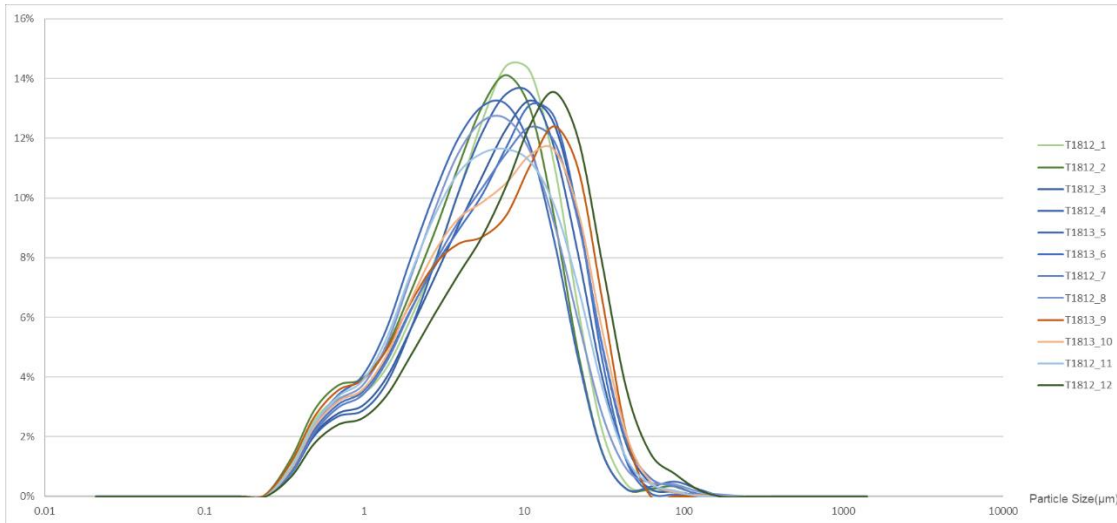


Figure 7.10 Particle size distribution graph of the Shiqianyu profiles

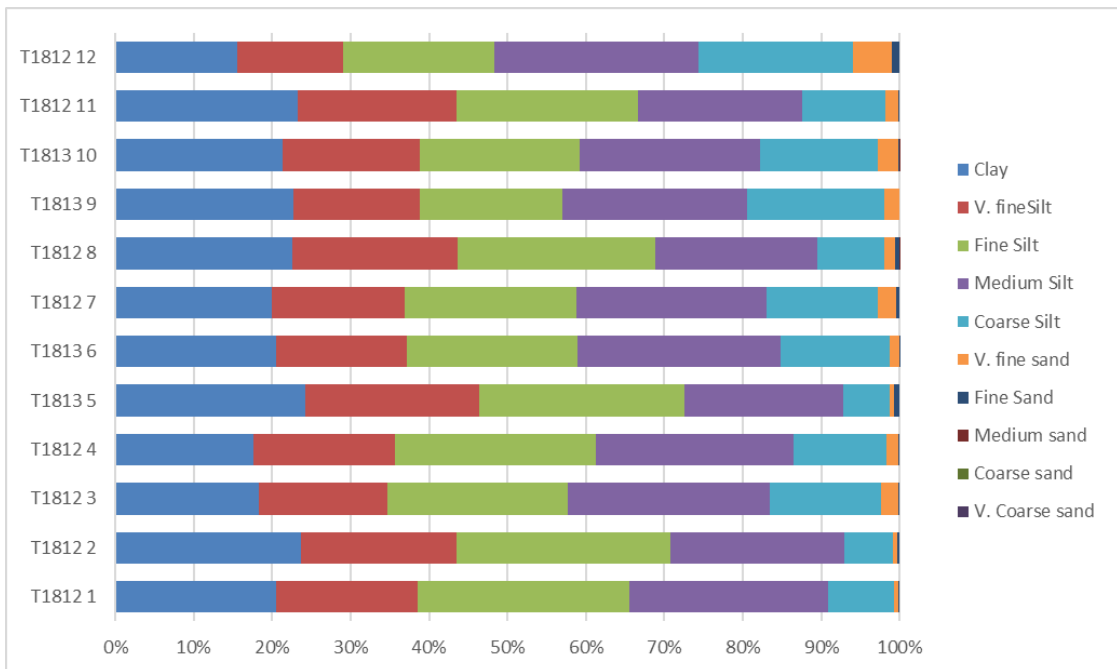


Figure 7.11 Percentage bar chart of the particle size of the Shiqianyu profiles

7.2.1.3.2 Site formation process of the Shiqianyu profiles

Currently no radiocarbon dating is available for the Shiqianyu site. However, based on pottery typology, Platforms I and II of the Shiqianyu site are inferred to have been constructed in the late stage of the Late Liangzhu period from c. 2600-2300 BC (Chen Minghui, per. comm.).

Before Liangzhu people occupied this area, from Pre-occupation sediment 2 to Pre-

occupation sediment 1 (-0.3m to 0.25m above sea level), the sedimentation environment changed from periodically exposed intertidal flat to an accumulating alluvial plain. The transition from Pre-occupation sediment 2 to Layer 5 (Unit 5-2) showed a short increase in depositional energy. However, Layer 5 is generally indicative of an aggrading alluvium floodplain formed under shallow, slow-moving and even ponding hydrological conditions that contained a few anthropogenic materials, which indicates the beginning of human activity in nearby area.

In Profile T1813, Layer 5 may have experienced a longer term of ponding. Platform II-2 was constructed using at least four different soil materials that were stacked directly onto a relatively wet surface. The bottom of this platform may have been mainly constructed by 'clay wrapped with grasses' using locally available soil materials. The soil materials in the upper part of the layer may have been processed by possibly adding water, stirring and mixing with different soil materials, before being dried and piled up. An open-air grass bedding with a few archaeological remains was laid on top of the Platform II-2, which indicates a short period of occupation before the next stage of platform construction.

In Profile T1812, synchronous to Platform II, the alluvial conditions continue with a higher depositional energy as indicated by the flushed-in laminar, silt-size soil aggregates. Laminae of organic tissues were then introduced or placed there by humans, with the shallow ponding continuing as seen in the fine material that accumulated inbetween these organic materials. On top of the organic laminae are layers of constructed materials that belong to Platform I. The bottom layer used a mixture of soil material from the previous alluvial horizon. Platforms I-3 and Platform I-2 were mainly constructed by various locally available soil materials. A few 'exotic' soil materials similar to those from Profile T3131 were also used in Platform I-3.

In summary, the Shiqianyu site is a man-made mound constructed in a previously marshy region, which may reflect the expansion of settlement area in the late stage of the Late Liangzhu period. The analysis of the pre-site sediments from -0.3 to 0.3m above sea level demonstrates the rapid shift of intertidal to alluvial conditions before the arrival of Liangzhu people within a few centimetres of deposition. In the Early to

Middle Liangzhu period, this area was largely an unmanaged wetland area that incorporated trace amounts of anthropogenic materials. The two stages of platform construction exploited nearby soil materials and may have changed the local landscape, similar to the case in Middle Zhongjiagang site. The construction technique, pattern and the use of grass beddings are similar but simpler compared to the inner city settlement sites, such as the layers constructed in the Late Liangzhu period in profiles T3131 and T2621.

7.2.2 The South Jincun site

7.2.2.1 Introduction

The South Jincun site is located between the Tiao River and the Tangshan Dam. After an extensive survey and small-scale trial excavations, abundant Early to Middle Liangzhu period mounds and settlements (3300-2900 BC) were found in this area (Zhao, 2002, Liu *et al.*, 2020). One profile (JCN) was sampled from the central part of this settlement area (Figure 7.1) in order to have a preliminary understanding of the stratigraphy and site formation process here. The JCN profile is around 3.5m above sea level with four readily identifiable stratigraphic units.

The stratigraphy from top to bottom are as follows:

Unit 1: 0-30cm below ground surface, topsoil material.

Unit 2: 30-130cm below ground surface, very dark grayish brown (2.5Y 3/2) silt, possible Liangzhu period mound construction material.

Unit 3: 1.3-2m below ground surface, very dark brown (10YR 2/2) silty clay, possible Liangzhu period channel deposits.

Unit 4: 2m below ground surface, very dark gray (5YR 3/1) silt, pre-site sediment.

Four soil micromorphology samples and associated bulk samples were taken from the top of Unit 4, the bottom of Unit 3, the transition between Unit 3 and Unit 2 and the bottom of Unit 2 (Figure 7.12).

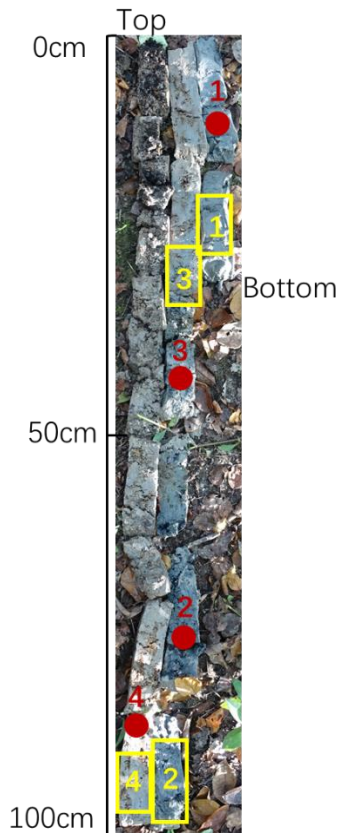


Figure 7.12 Stratigraphy and sampling position of the South Jincun profile. The blue rectangles and numbers refer to the sampling positions and numbers of the soil micromorphology samples. The red dots and numbers refer to the sampling positions and numbers of the bulk samples.

7.2.2.2 Results of soil micromorphological analysis in South Jincun site

7.2.2.2.1 Unit 4

7.2.2.2.1.1 Micromorphological description of the Micro-fabric JCN 1:1

Unit 4 shows a rhythmic bedding of alternating coarse (Facies 1) and fine (Facies 2) laminae that do not grade into each other (Micro-fabric JCN 1:1, Figure 7.13). The coarse laminae (Facies 1) are composed of weakly laminar, well-sorted, sub-rounded, coarse silt-size to very fine-sand size minerals, including 50% quartz, 20% micas, 20% dark brown heavy mineral and 10% calcium carbonate, and a few light yellow (PPL) silty clay with undifferentiated b-fabric (c/f: 95/5; limit: 10 μ m). The fine laminae (Facies 2) are mainly brown (PPL) humic silty clay crusts with varied thicknesses and incorporate a few laminar, dark brown, humified and amorphous fine organic matter.

The coarse and fine laminae are mostly horizontally laminated, but occasional cross-stratification is also observed (Figure 7.13). Occasional thin laminae of medium silt-size, black (PPL and XPL) heavy mineral were also found (Figure 7.13). This unit generally has a platy microstructure with 5% partially accommodated, horizontal planar voids.

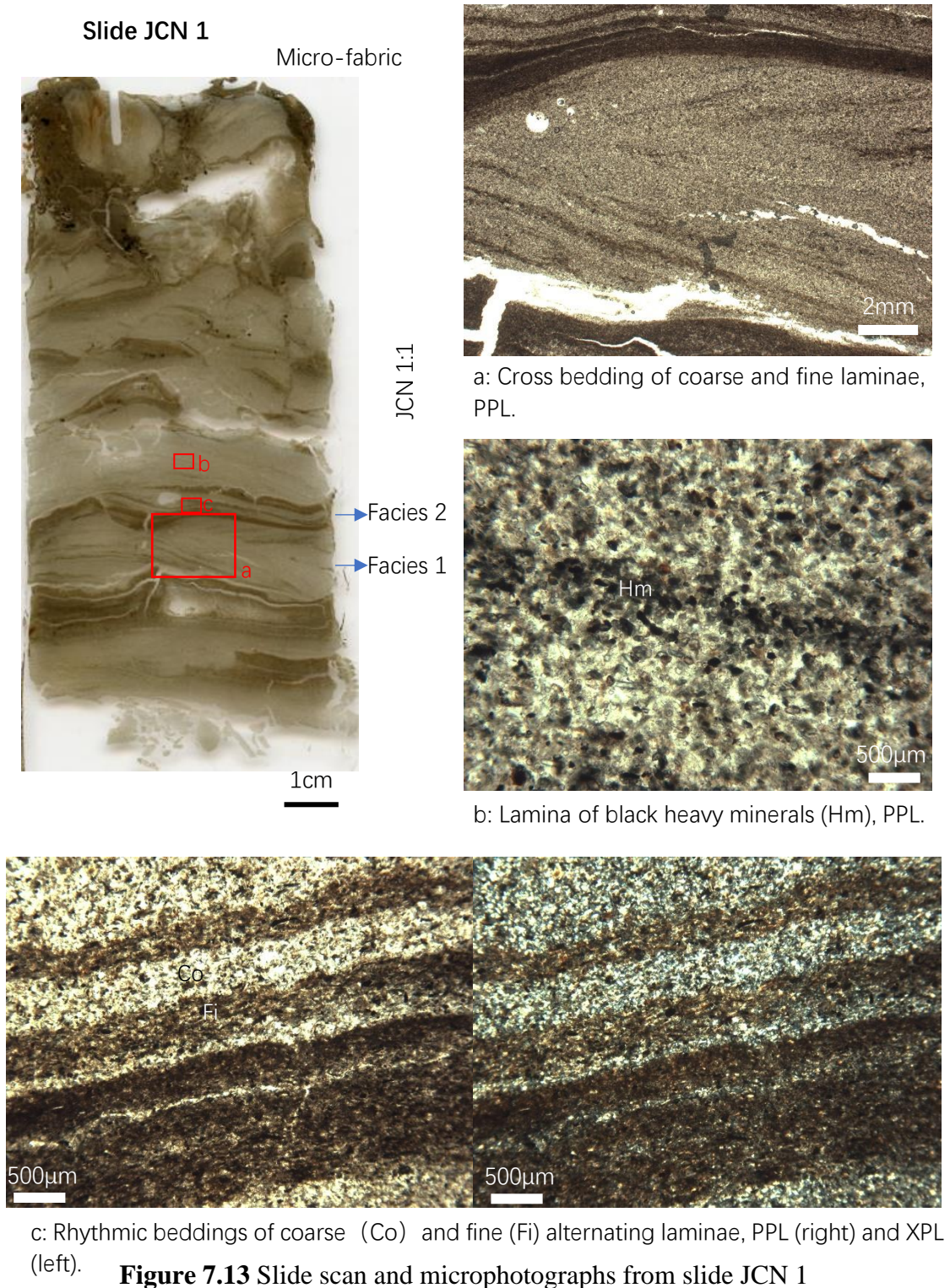


Figure 7.13 Slide scan and microphotographs from slide JCN 1

7.2.2.2.1.2 Results of bulk analysis and interpretation of the Unit 4

As shown in the Figure 7.14 (Bulk sample JCN 1-1), Unit 4 has an alkaline pH of 7.71, which is one of the highest pH values of all the Liangzhu samples. The magnetic susceptibility and % CaCO₃ are also high and the phosphorus content is medium. The contents of total organic and carbon are very low, and together with the well-preserved sediment structure suggest no soil pedogenesis and a high sedimentation rate. In the micromorphology samples, this unit shows rhythmically alternating, well-sorted coarse silt and fine clay laminae, which is the result of alternating periods of current activity and quiescence (Karkanis & Goldberg, 2018). The micromorphological observation and bulk data collectively point to a sediment deposited under repeated alternation of high- and low-energy depositional process in an alkaline and calcium carbonate rich environment, which is most likely a mudflat/intertidal flat near the estuary. The occasional cross beddings, which are extensively shown in aeolian, fluvial and shallow marine deposits (Karkanis & Goldberg, 2018), are the results of the migration of waves and ripples. The thin laminae of heavy minerals may be concentrated by the sea-wave sorting mechanism (Cascalho *et al.*, 2020 and references therein). In general, Unit 4 presents a well-preserved pre-Liangzhu sediment formed in an intertidal flat condition.

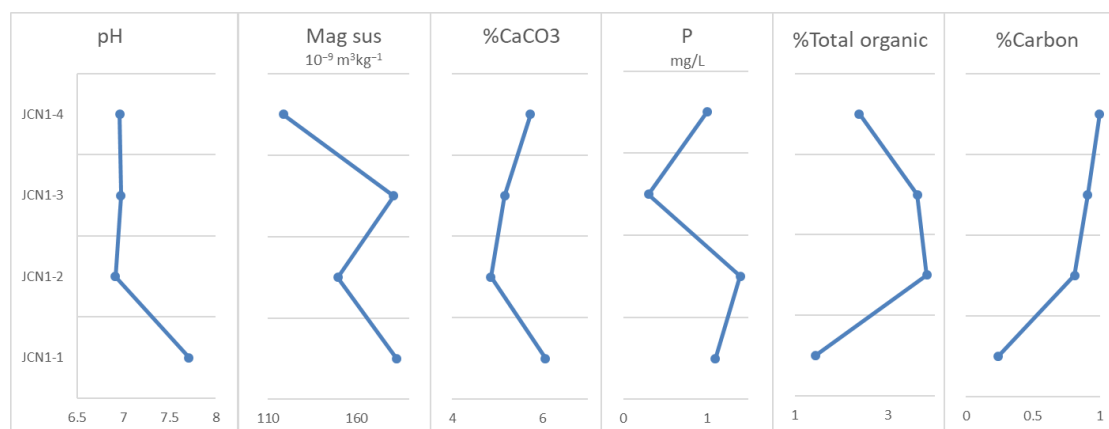


Figure 7.14 Analytical results of pH, phosphorus, magnetic susceptibility, and carbon, total organic and calcium carbonate contents of the South Jincun site.

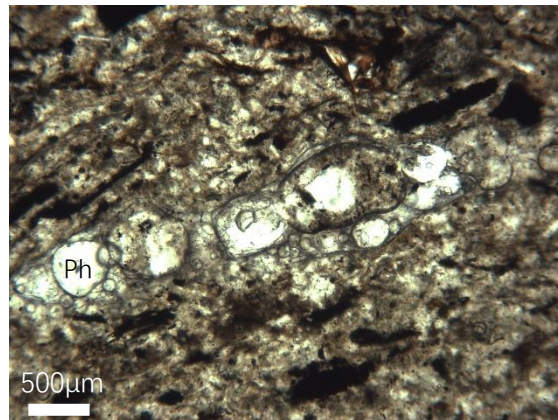
7.2.2.2.2 Unit 3

Unit 3 is believed to be an Early Liangzhu period channel containing abundant archaeological remains. Soil samples were collected from the bottom of this unit.

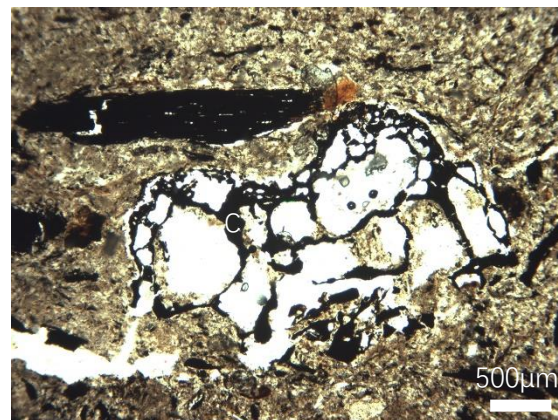
7.2.2.2.2.1 Micromorphological description of the micro-fabrics JCN 2:3, 2:2 and 2:1

Three sub-units can be identified from the bottom of this unit. The lower sub-unit (Micro-fabric JCN 2:3) is composed of 15% moderate-sorted, sub-angular to sub-rounded, very fine to fine sand-size quartz, 5% sub-angular coarse sand-size to fine pebble-size rock fragments and 80% light brown (PPL) humic silty clay with moderate birefringence and a randomly striated b-fabric. Light brown to black, humified organic residues and amorphous organic fine material are frequently found in random to parallel laminae in the groundmass. One-fourth of these organic materials are possible bast fibres (C. Alday, pers. comm.). A few fine charcoal, fine burnt bone fragments and pottery debris are also mixed in. This fabric has a massive microstructure with 2% partially accommodated fissures and 2% voids formed after the decay/shrinkage of organic material.

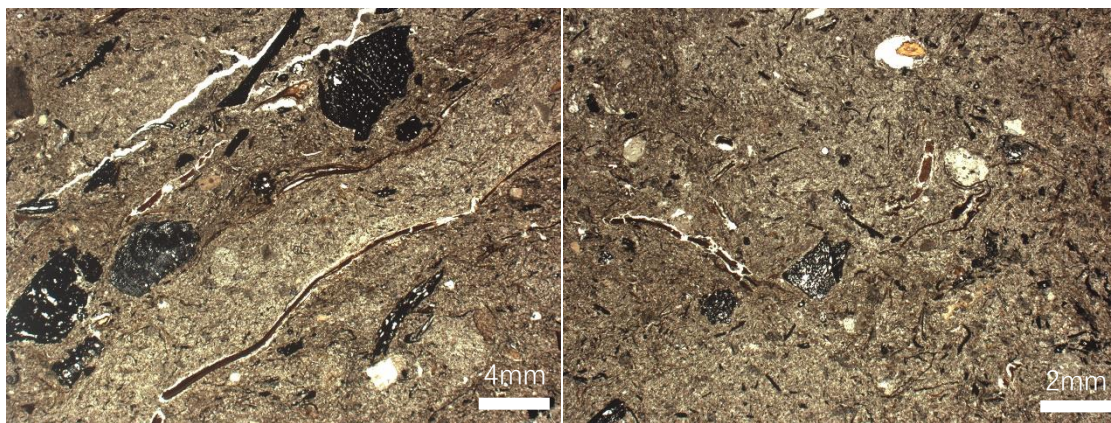
Two intact layers of bast fibre covered the Micro-fabric JCN 2:3 (Figure 7.15). On top of these bast fibres are 0.5cm thick compacted laminae rich in horizontally laminated fine charcoal and fragmented bast fibres (Micro-fabric 2:2). The upper sub-unit (Micro-fabric JCN 2:1) has a similar coarse fraction with the JCN 2:3, but the fine fraction is less humic with a parallel to random striated b-fabric. Charcoal fragments are commonly seen and are mostly horizontally laminated. Laminae of very fine charred materials are found in the upper part of the fabric. Light brown to black, humified organic residues and amorphous organic fine material (10%) are parallel laminated, and one fourth of which are fragmented bast fibres. This fabric contains abundant anthropogenic materials from kitchen remains, including burnt bone fragments, phytolith slugs and fat-derived char (Figure 7.15). This fabric has a platy microstructure with 5% partially accommodated horizontal planar voids. Small, rounded, 'clean', fine silty clay soil aggregates mainly composed of sub-angular silt size minerals are commonly seen in the upper part of the fabric.



a: Phytolith slags (Ph), PPL.



b: Fat-derived char (C), note the vesicles with varying sizes and small radiating cracks, PPL.



c: Laminated bast fibres and compacted fine charred material on top, PPL.

d: Randomly distributed fine charred material in a humic silty clay groundmass, PPL.

Figure 7.15 Slide scan and microphotographs from slide JCN 2

7.2.2.2.2 Results of bulk analysis and interpretation of the Unit 3

Unit 3 has a neutral pH, high phosphorus, total organic and carbon, and medium high magnetic susceptibility and calcium carbonate contents (Figure 7.14), which combining the hearth remains observed under the microscope, is suggestive of intensive human activity, especially cooking, in this unit.

The bottom of this unit is composed of fine alluvial sediments widely seen in the Liangzhu region with a few fine anthropogenic remains, which is similar to the Micro-fabrics T3131 4:2 and 3:1 from Profile T3131 and could be regarded as a Passive Zone for human activity. The overlying intact bast fibres and the compacted lamina containing fragmented and horizontally laminated archaeological remains are suggestive of matting and possible trampling on the activity surface and could be interpreted as a Reactive Zone. The upper sub-unit with abundant laminated charred materials, including the fine charcoal, burnt bones, phytolith slags and fat-derived char, together with the 'exotic' soil aggregates, is indicative of intense human activity of cooking, dumping, trampling and bringing in of material by foot traffic, and could be seen as an Active Zone. In summary, the Unit 3 probably represents an occupational floor sequence similar to the early phases of the T3131 profile (Section 6.3).

7.2.2.2.3 Unit 2

In the field, Unit 2 was inferred as mound construction materials. Soil samples are taken from the transitional place of Unit 3 and 2 (Micro-fabric JCN 3:1) and mid-lower part of the Unit 2 (Micro-fabrics JCN 4:1).

7.2.2.2.3.1 Micromorphological description of the Micro-fabrics JCN 3:1 and 4:1

Under the microscope, Micro-fabric JCN 3:1 and 4:1 have similar structure, groundmass and pedofeatures (Figure 7.16), the description of the Unit 2 will be based on Micro-fabric JCN 3:1. This fabric is composed of 15% moderate-sorted, sub-rounded, very fine to fine sand-size quartz, 15% sub-angular coarse sand-size to fine pebble-size rock fragments and 70% light brown (PPL) humic silty clay with moderate

birefringence and random striated b-fabric (c/f limit: 50 μ m). Half of the micromass is stained by red (PPL) amorphous sesquioxides as nodules and mottles. A few clusters of fine charred materials are randomly mixed in the groundmass. This fabric has a moderately developed sub-angular blocky microstructure with partially accommodated peds and channels and associated vughs that create 5% porosity. Dusty clay hypo-coatings of voids and grano-coating of soil aggregates and rock fragments are rarely seen. Rounded, 'clean' soil aggregates mainly composed of sub-angular silt size minerals are commonly mixed in the groundmass.

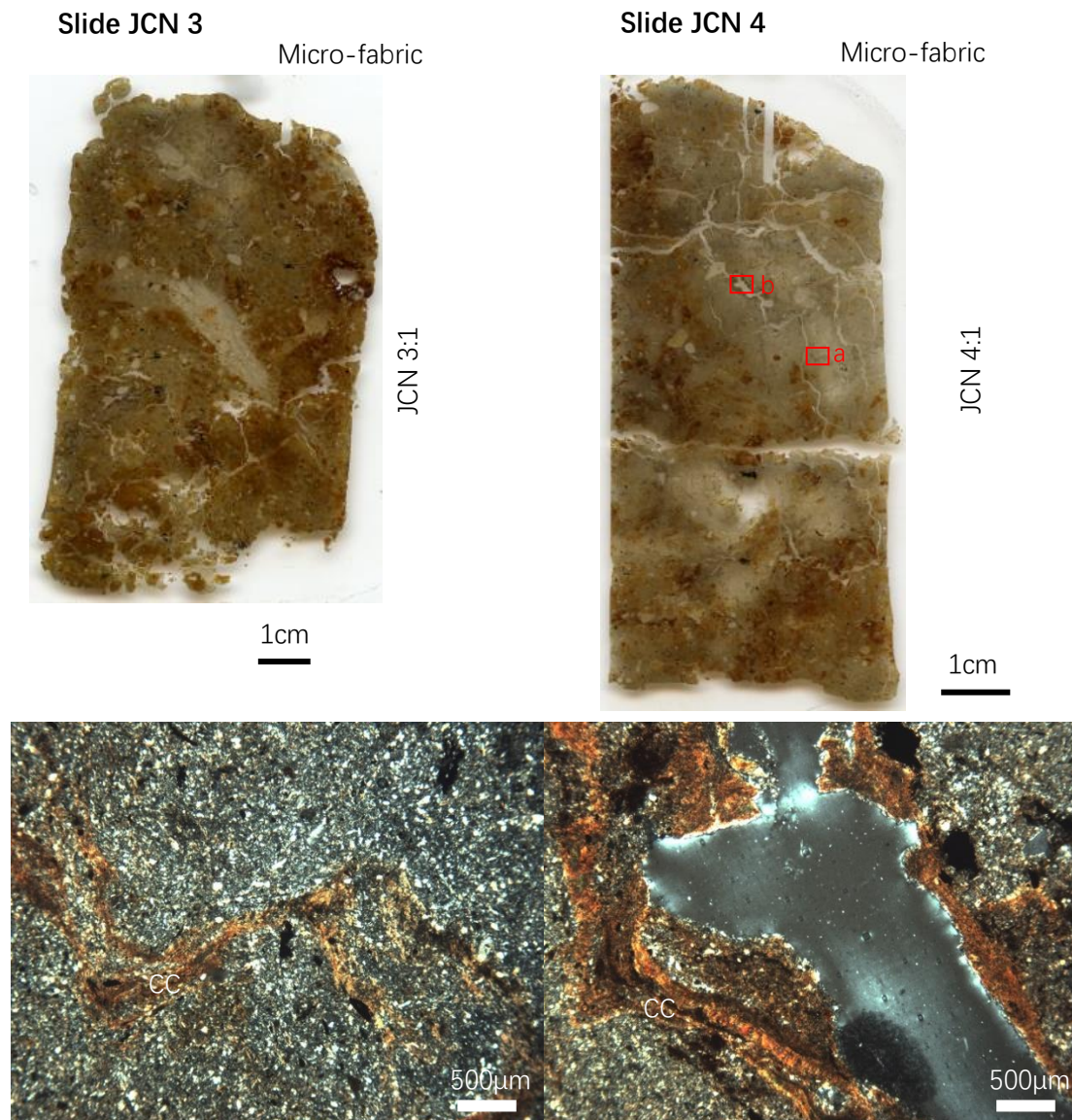
The Micro-fabric JCN 4:1 from the mid-lower part of Unit 2 has a higher content of textural pedofeatures and some show alternations of micro-laminated dusty and limpid clay (Figure 7.16). Depletion hypo-coating of dusty silty clay are also commonly seen.

7.2.2.2.3.2 Results of bulk analysis and interpretation of the Unit 2

Unit 2 has a neutral pH, moderate magnetic susceptibility, high phosphorus, carbon and calcium carbonate and medium-low total organic contents (Bulk sample JCN 4, Figure 7.14). Although in the micromorphology sample, this unit does not show an obvious mixture of various soil materials or aggregating coarse rock fragments as at the mounds identified in the other Liangzhu site, such as Platform 2 of profile T3131 and Platform II of Shiqianyu site, the heterogeneous mixture of coarse sand-size rock fragments and fine charred material, the less humic micromass and commonly found clay illuviation features are all share characteristics of man-constructed mounds in Liangzhu region. Unit 2 therefore could also be interpreted as constructed mound.

7.2.2.3 Interpretation of the South Jincun profile

The bulk sample from Unit 4 shows a single peak distribution pattern (green lines in Figure 7.17), which indicates good sorting and single source of sediment. The particle size is dominated by coarse silt and fine sand-size material (Figure 7.18). The rest of the samples have multi-peak patterns (blue lines in Figure 7.17), which suggest a diverse set of sources of soil material which are dominated by silt-size material, with slight variations in clay and sand content (Figure 7.18).



a: Stress deformed clay illuviation coatings (CC), incorporated in the groundmass, XPL. b: Dusty and limpid clay hypo-coatings of voids, XPL.

Figure 7.16 Slide scan and microphotographs from slides JCN 3 and 4

Based on previous research conducted in this region, the Jincun site contains archaeological remains dated to the early period of Liangzhu Culture (3300-2900 BC) (Chen Minghui, per. comm.), which are represented in Units 3 and 2 of this profile. Unit 4 in the lowermost part of this profile, is the pre-occupation sediment. Based on the micromorphological and bulk sedimentology analyses, it is an intertidal flat/mudflat deposit that has a higher sedimentation energy and is very different to the other units. The Unit 3 is an occupation floor sequence similar to the early phases of the T3131

profile, which is composed of alluvium deposits that contain randomly distributed fine charred materials (Passive Zone), a matting area overlaid with trampled, fragmented micro-artefacts (Reactive Zone), and trampled occupational fine debris mainly from kitchen remains (Active Zone). Unit 2 is probably a deliberately prepared and constructed layer containing fine charred material. In general, the South Jincun site demonstrated a sedimentation sequence of pre-site occupation, alluvium deposits, occupational floors and a constructed mound. This profile could be used as an analogue profile for the inner city settlement profiles.

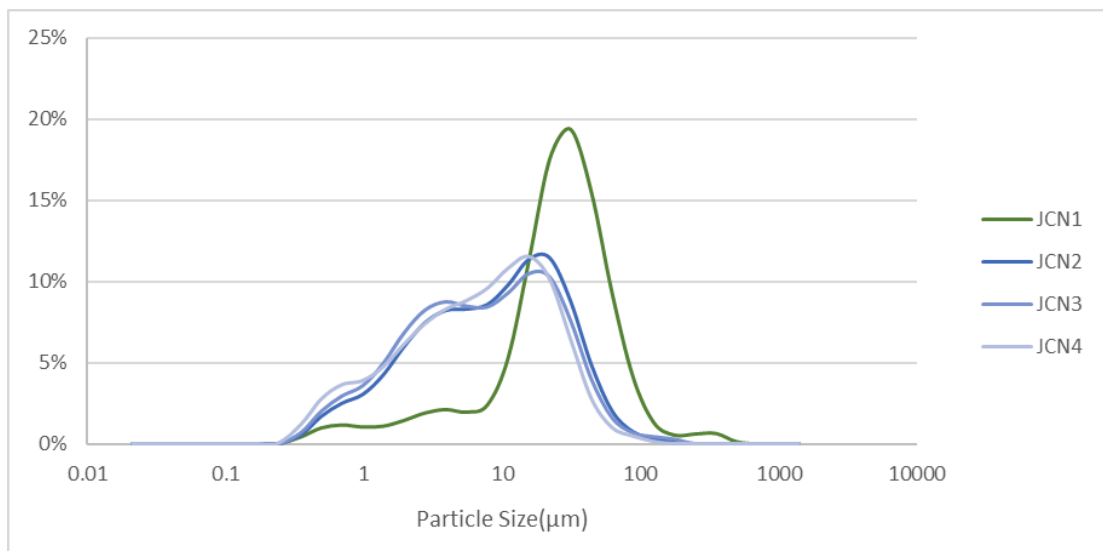


Figure 7.17 Particle size distribution graph of the JCN profile

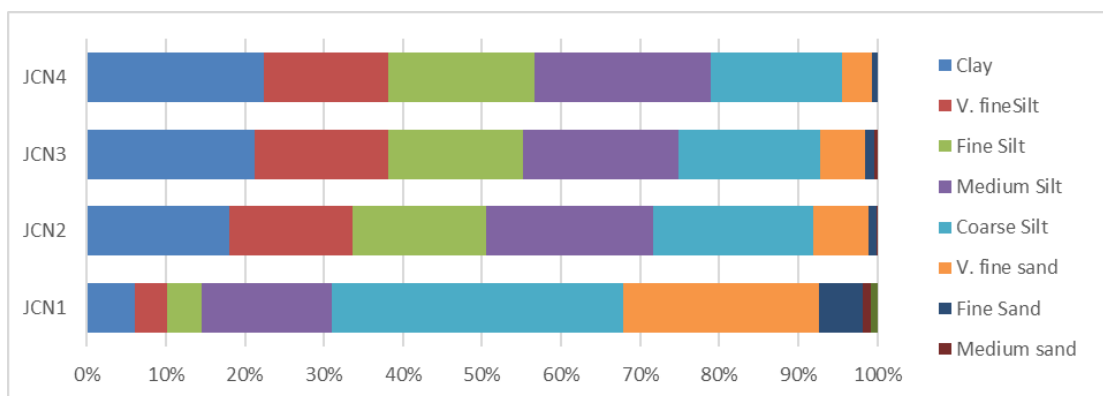


Figure 7.18 Percentage bar chart of the particle size of the JCN profile

7.3 Reference profiles from outer Liangzhu City

To understand Liangzhu City at a regional scale, soil samples were taken by hand augering north of the Liangzhu City from the Huoxitang (HXT) site near the North City Gate, the paddy field profile north to the Tangshan Dam (TSB), and a small stream in the Dazhe Mountain (DZ) (Figure 7.1). No dating is available for these sample locations. This section will briefly introduce the results of soil micromorphological and bulk sedimentological analysis at these locations to give a broader understanding of the sedimentation conditions of the Liangzhu region and provide some reference geological context for the Liangzhu City sites.

7.3.1 Huoxitang site

7.3.1.1 Introduction

The Huoxitang site is located on the western bank of the north water gate of Liangzhu City (Figure 7.1, site 2), which is around ten metres to the north of the Liangzhu City. The current ground surface of the Huoxitang is around 3m above sea level. By using hand augering, three metres of soil/sediment sequence were recovered (Figure 7.19).

Four stratigraphic units can be identified in this profile:

Unit 1: 0-50cm below ground surface, topsoil material.

Unit 2: 50-150cm below ground surface, brown (10YR 4/3) silt.

Unit 3: 1.5-1.9m below ground surface, olive brown (2.5Y 4/3) silty clay.

Unit 4: 1.9-3m below ground surface, very dark gray (5Y 3/1) silty clay.

Three soil micromorphology samples were taken from the bottom of Unit 4, the boundary between Units 4 and 3, and the boundary between Units 3 and 2. Four bulk samples were taken from the bottom and upper part of Unit 4, the upper part of Unit 3 and the lower part of Unit 2 (Figure 7.19).

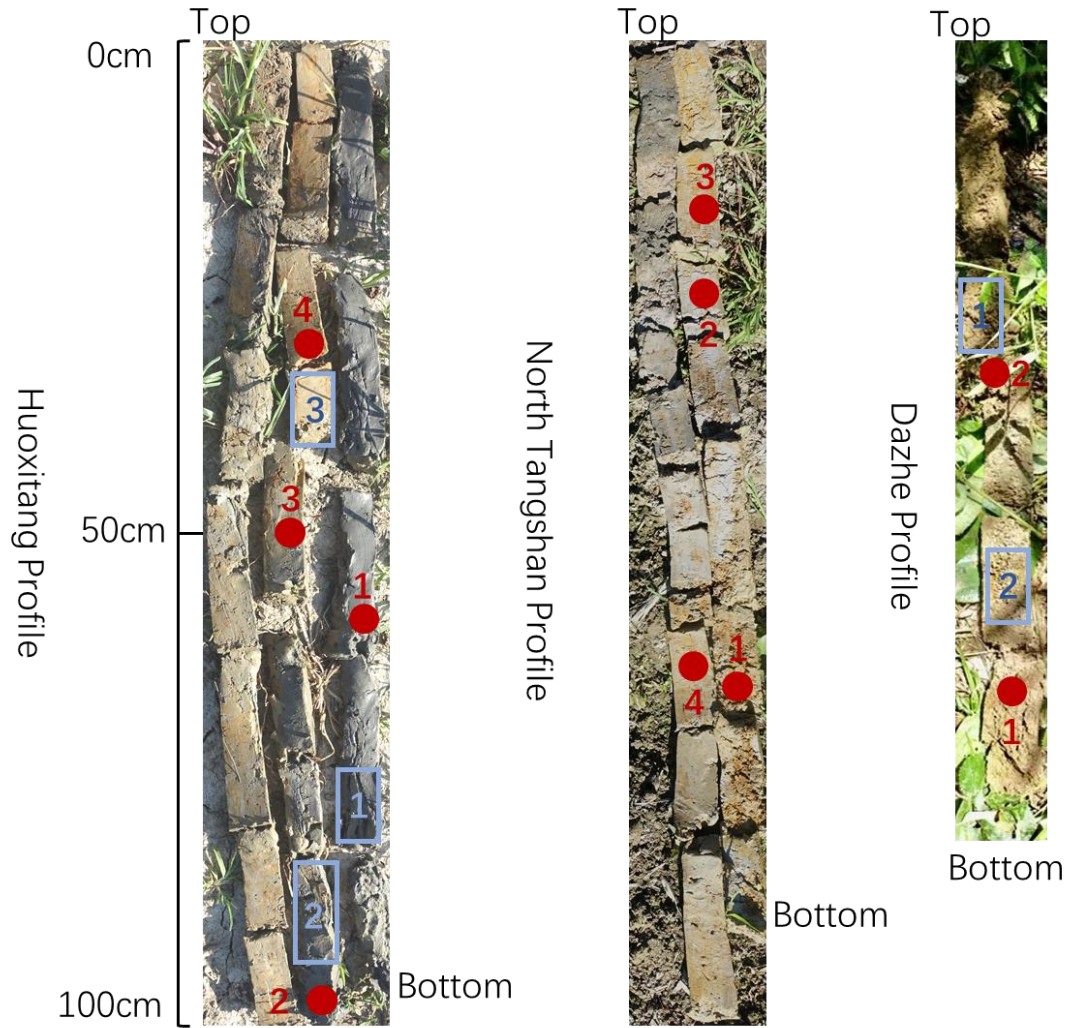
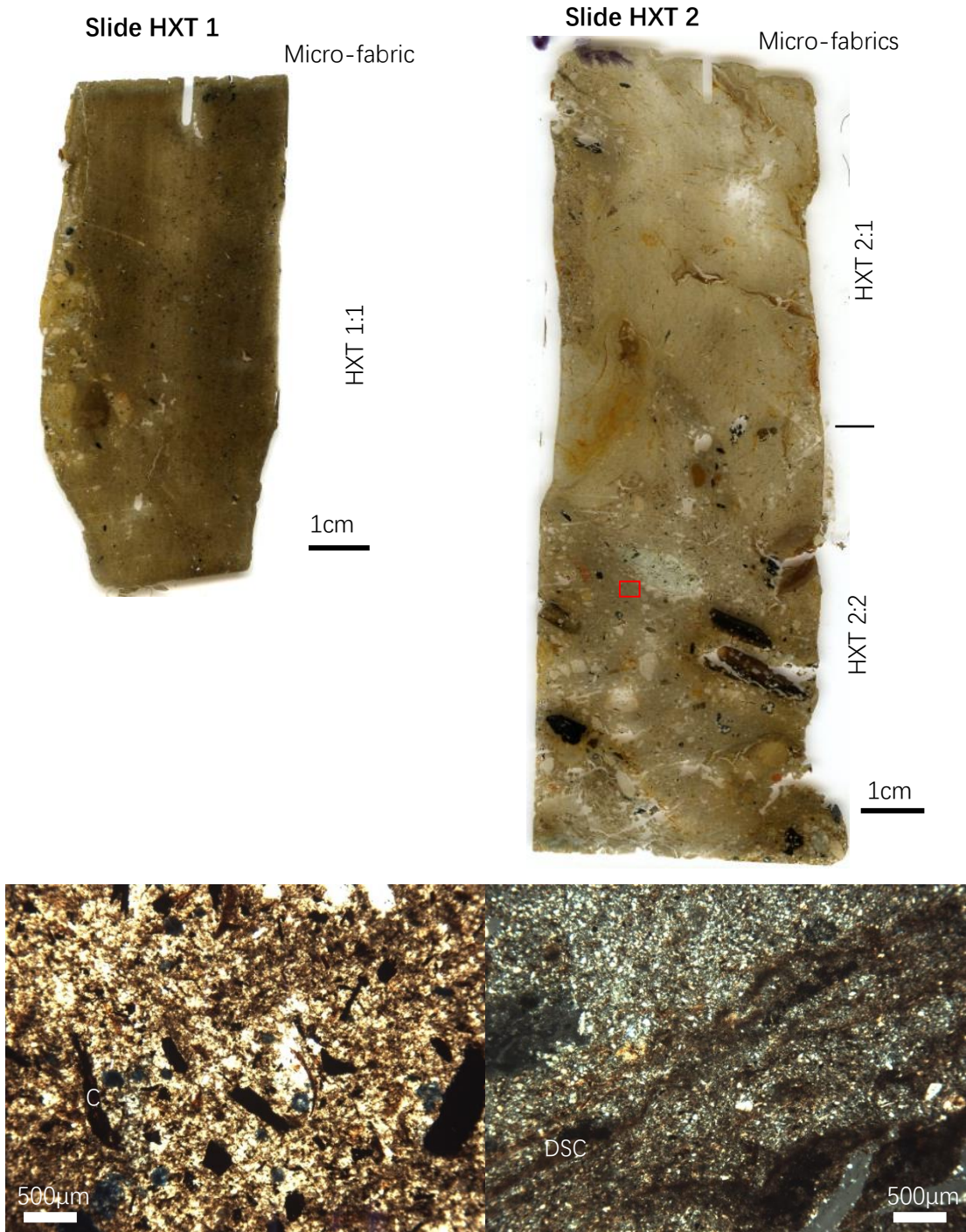


Figure 7.19 Stratigraphy and sampling position of the Huoxitang profile (left), North Tangshan profile (middle) and Dazhe profile (right). The blue rectangles and numbers refer to the sampling positions and numbers of the soil micromorphology samples. The red dots and numbers refer to the sampling positions and numbers of bulk sample.

7.3.1.2 Results of soil micromorphological analysis in Huoxitang site

7.3.1.2.1 Unit 4

Micromorphology samples were collected from the mid-lower part and the top of the Unit 4, which are represented in Micro-fabrics HXT 1:1 and 2:2.



HXT 1:1 Randomly distributed fine charred (C) material in humic silty clay groundmass, PPL

HXT 2:2 Very dusty silty clay crusts (DSC), XPL

Figure 7.20 Slide scan and microphotographs from slides HXT

The mid-lower part of Unit 4 (Micro-fabric HXT 1:1) is mainly composed of poorly-sorted, sub-angular, very fine to fine sand-size quartz and brown (PPL) humic silty clay

with a low birefringence and a stipple-speckled to undifferentiated b-fabric (c/f: 10/90; limit: 50 μ m). A few very fine dark brown to black humified organic residues and amorphous organic fine material and trace amounts of very fine charred material are randomly distributed in the groundmass. This unit has a massive microstructure (1% porosity). A few aggregates of vivianite crystals are randomly incorporated in the groundmass.

The top of this layer (Micro-fabric HXT 2:2) has a coarser particle size with a c/f ratio of 30/70 (limit: 50 μ m). The coarse component consisted mainly of moderate-sorted, sub-rounded, very fine to fine sand-size quartz and sub-angular coarse sand-size to fine pebble-size rock fragments. The micromass is composed by light grayish brown (PPL) humic silty clay with a moderate birefringence and a parallel to random striated b-fabric. A few humified organic residues and charred materials are randomly distributed in the groundmass (Figure 7.20). Three pottery sherds were horizontally laminated. This layer generally has a massive structure with a few irregular vughs and fissures (9% porosity). A few micro-laminated, thin dusty clay crusts with a low birefringence and reddish brown interference colour are embedded in the groundmass. Trace amounts of yellow (PPL) staining of amorphous iron oxides and vivianite crystals are observed. Various soil aggregates are incorporated in the groundmass (4-5% of the fabric).

The bottom of Unit 4 (Bulk sample HXT 1, Figure 7.21) has a neutral pH and a medium-low carbon content. The medium-high magnetic susceptibility, calcium carbonate, total organic and phosphorus contents indicate possible influences from human activity. But in the thin section, no bioturbation or intervention from humans are observed. This layer is generally a very fine alluvium accumulated under a very weak depositional energy and waterlogged condition.

The top of Unit 4 (Bulk sample HXT 2, Figure 7.21) has a slightly acidic pH, medium magnetic susceptibility, calcium carbonate, carbon, and total organic contents, and a low phosphorus content. The bulk data suggests relatively low extent of human activity. But based on micromorphological observation, the top of Unit 4 contains abundant anthropogenic materials such as pottery sherds, various soil aggregates and charred materials. The silty clay crusts indicate periodic shallowing and possible drying of the

water, and with vivianite crystals suggesting a change from waterlogged to rapidly drying conditions (Karkanis and Goldberg, 2010). The top of Unit 4 in general is a shallow water area with the input of archaeological remains from nearby activity zones.

In summary, in the early stage of Unit 4, this area is an undisturbed slow-moving or static water area with human activity nearby. In the end stage, this unit is still a shallow water area that was disrupted by more intensive human activities.

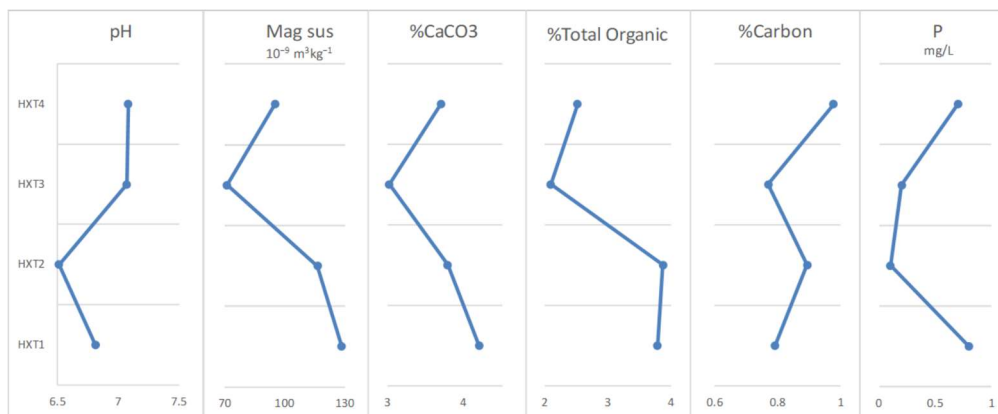


Figure 7.21 Analytical results of pH, phosphorus, magnetic susceptibility, and carbon, total organic and calcium carbonate contents of the Huoxitang site.

7.3.1.2.2 Units 3 and 2

Soil samples were collected from the bottom of Unit 3 and the lower part of Unit 2. Based on micromorphological observation, Unit 3 (Micro-fabric HXT 2:1) and Unit 2 (Micro-fabric HXT 3:1) are very similar and will be discussed together here. The description is based on Micro-fabric HXT 3:1.



Figure 7.22 Slide scan and microphotographs from slide HXT 3

Units 2 and 3 are a yellowish silty clay with a c/f ratio of 20/80 (limit: 50µm). The coarse component consisted mainly of moderately-sorted, sub-angular, very fine to fine sand-size quartz and a small proportion (2%) of sub-rounded coarse sand-size rock fragments. The micromass is mainly light yellow (PPL) silty clay with a moderate birefringence and a stipple-speckled to random striated b-fabric. 15% of the micromass is stained by reddish yellow (PPL) amorphous sesquioxides as mottles, vertical fine striations and hypo-coatings of voids. A few very fine charred materials embedded in the groundmass and iron-impregnated organic residues near voids are found. This fabric generally has a massive microstructure with a few vughs and fissures (5%

porosity). Occasional limpid to dotted clay hypo-coatings of voids with a high birefringence and orange interference colour, and dusty clay hypo-coatings of voids with low to moderate birefringence and dull red interference colour are observed.

These two units generally have a neutral pH, low magnetic susceptibility, calcium carbonate and total organic contents (Bulk samples HXT 3 and 4, Figure 7.21). The carbon and phosphorus contents have increased from low to moderate from Unit 3 to Unit 2. The bulk data in general suggests a low influence of human activity, especially in the Unit 3.

Unit 3 has a distinct and clear interface with the underlying Unit 4 and are generally post-Liangzhu sediments that show a sudden decrease of human activity. This direct change may be due to erosion of possible transition layers or the rapidly change in sedimentation conditions. In general, Units 3 and 2 are still typical alluvial deposits in the Liangzhu region with a slightly coarser particle size and are less humic, which denotes a higher depositional energy. These units are under long-term saturation and with the effect of rooting that caused mottling and vertical fine striations of amorphous sesquioxides (Lindbo *et al.*, 2010). The later are relict roots that were replaced with amorphous sesquioxides.

7.3.1.3 Interpretation of the Huoxitang profile

The bulk samples of the Huoxitang profile generally show a single peak pattern and are suggestive of good sorting with single source of the soil material (Figure 7.23). The bulk sample from the top of Unit 3 exhibits a coarser particle size with better sorting (green line, Figure 7.23), which may suggest an increase of depositional energy. The sorting and particle size then reduce in the bottom of Unit 2 (Bulk sample HXT 4, Figure 7.23 and 7.23), which may imply unstable sedimentation conditions in these two units.

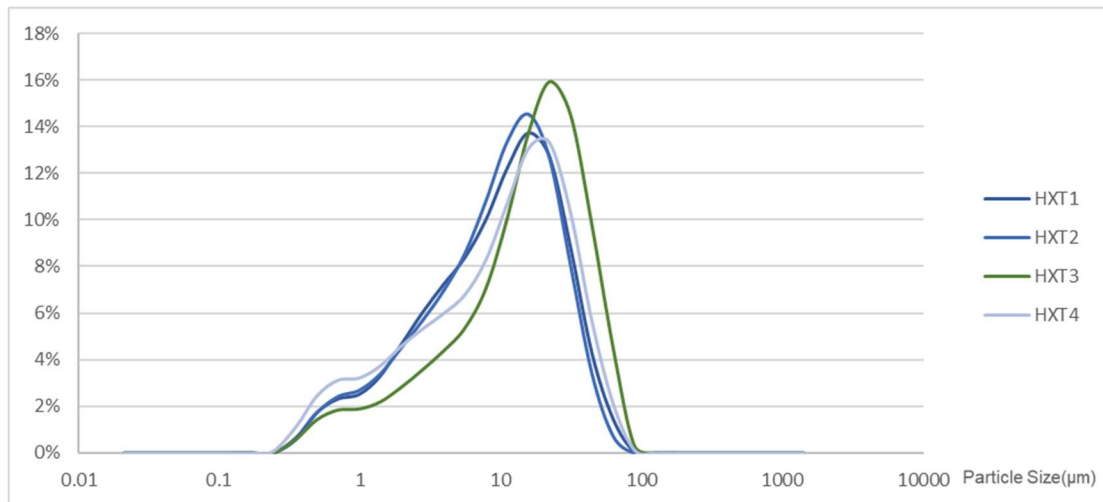


Figure 7.23 Particle size distribution graph of the Huoxitang profile

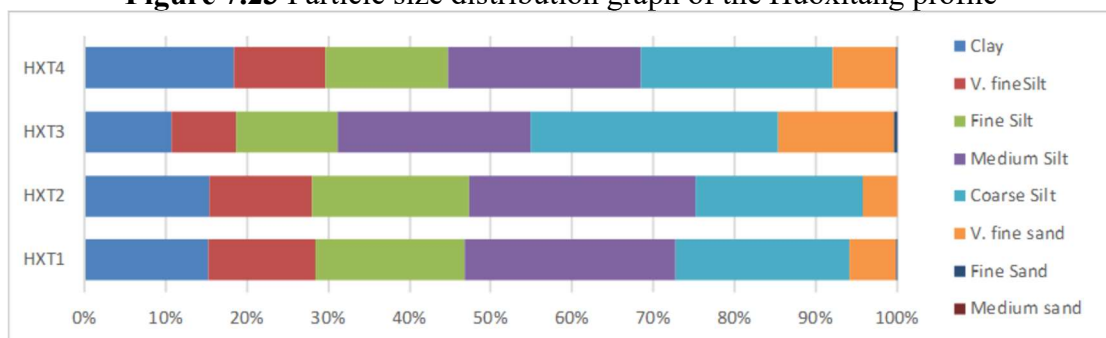


Figure 7.24 Percentage bar chart of the particle size of the Huoxitang profile

Currently no radiocarbon data is available for the Huoxitang profile. Its chronology sequence can be speculated from the nearby LZ-N profile studied by Mo *et al.* (2019) and Wang *et al.* (2017), which is near to the Huoxitang profile (see section 5.4.3.1 for details). Units 2 and 3 in Huoxitang are representative of the post-Liangzhu sediment horizon (2000 cal. BC) covering the whole Liangzhu region after the demise of Liangzhu Culture. Unit 4 consists of alluvial deposition during and/or before the Late Liangzhu period (2900-2300 cal. BC).

In summary, the Huoxitang area has long been an area of water ponding with more than one metre of fine humic silty clay material having accumulated. Abundant archaeological remains were introduced in the end-stage of Unit 4, which was then directly covered by light yellow silty clay with a slightly higher depositional energy. The water energy may reach the peak at the top of Unit 3 and decline in the bottom of Unit 2; this trend is similarly shown from Layers 5B to 5A of the T5020 profile (section 5.4.2.7). The Huoxitang profile may provide a comparable outer city, Late and post-Liangzhu period profile for the T5020 profile in the North Zhongjiagang region and

could give insights for the demise of the Liangzhu Culture.

7.3.2 North Tangshan profile

This profile was sampled from a paddy field 20-30m north of the Tangshan Dam (Figure 7.1) in order to understand the sedimentation conditions inside the dam area and the possible impact of dam construction. The sampling position was around 7m above sea level and two metres of sediment were retrieved by hand augering (Figure 7.19). Below is a brief summary of the field stratigraphy:

0-50cm: grayish yellow topsoil.

60-110cm: brown to yellowish brown (10YR 4/3 and 5/4) silt. Bulk samples TSB 4 and 3 are sampled from the top and bottom of this layer.

120-150cm: dark grayish brown (10YR 4/2) silt with Fe mottles, could be influenced by gleying. Bulk sample TSB 2 is collected from the top of this layer.

160-200cm: dark yellowish brown (10YR 4/6) silt with high content of Fe nodules. Bulk sample TSB 1 is sampled from the top of this layer.

Below 200cm: gravels.

The North Tangshan profile is a modern paddy soil developed under repeated alternating wet-dry conditions. The bulk sedimentology data could be used as a modern analogue for the Liangzhu samples. In North Tangshan profile, soil samples have a stable, slightly alkaline pH value. The content of total organic, carbon and calcium carbonate in the soil is lower than for the Liangzhu period sediments, but gradually increased upward. The particle size of the bulk samples was generally fine silty clay with 20%, 75% silt and 5% sand. The exception was the TSB 3 sample that had a larger input of sand-size material, a very high magnetic susceptibility and moderate levels of phosphorus, which implies the possible influence of human activity.

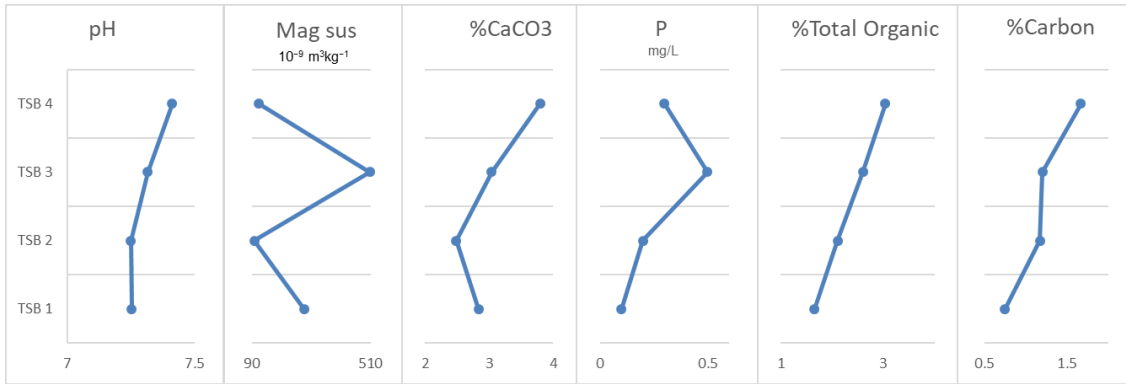


Figure 7.25 Analytical results of pH, phosphorus, magnetic susceptibility, and carbon, total organic and calcium carbonate contents of the North Tangshan site.

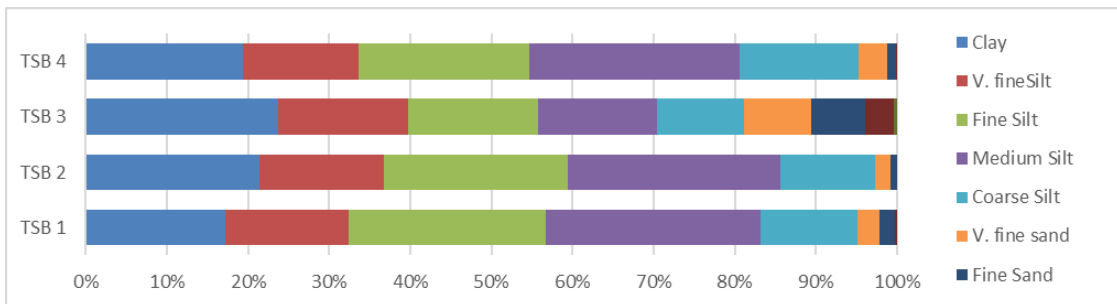


Figure 7.26 Percentage bar chart of the particle size of the North Tangshan profile.

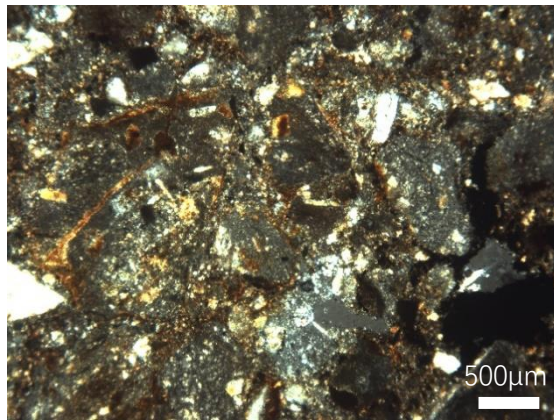
7.3.3 Dazhe profile

To better understand the geological context and regional rock/mineral composition in nearby mountainous areas and to provide a modern analogue for the Liangzhu City samples, samples were taken from the northern Dazhe Mountain area, a wooded area about five metres west of the bank and upstream of the Tangshan gully (DZ profile, Figure 7.1),

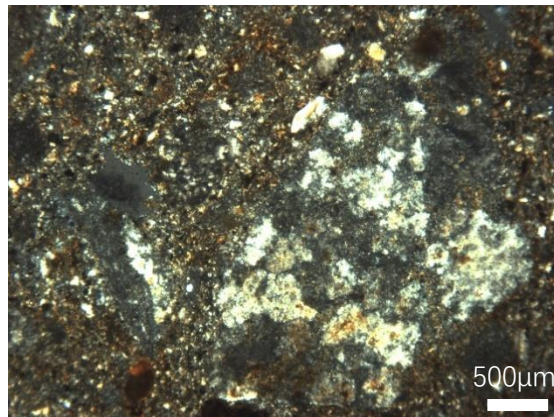
The DZ profile can be divided into two units (Figure 7.19): the first 10cm is topsoil, from 10 to 70cm is dark yellowish brown (10YR 3/4) river sand that contains small mollusc shells; and sediments below 70cm are bedrock or gravel layer. Two micromorphological and associated bulk samples were taken from this profile: sample DZ1 was taken from soil 60cm below the surface and DZ2 is taken from 30cm below the ground.

Slide DZ 1

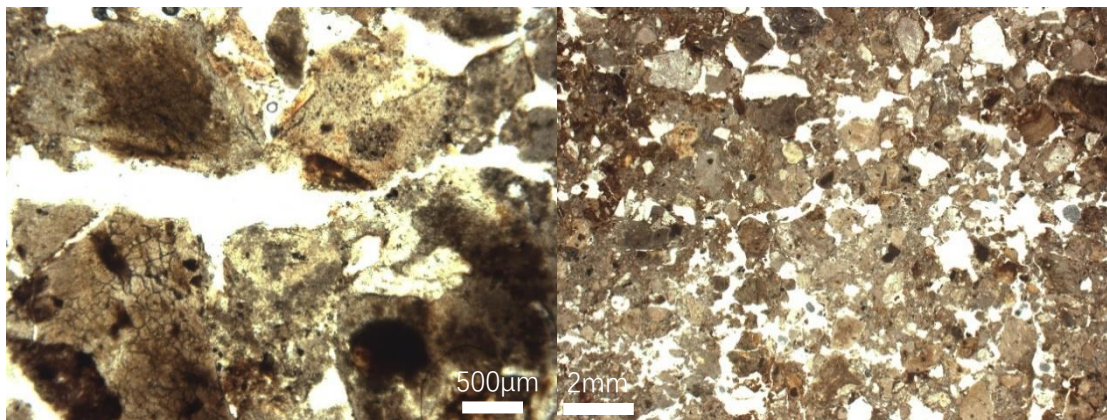
Micro-fabric



DZ 1:1 Rock fragments with infillings and coatings of clay minerals, XPL.



DZ 1:1: Calcite rich granitoid, XPL.



DZ 1:2 Darken rock fragments, note the release of dark brown Fe compounds, PPL.

DZ 1:2 Moderately separated granular microstructure with compound packing voids, PPL.

Figure 7.27 Slide scan and microphotographs from slide DZ 1

7.3.3.1 *Micromorphological observation*

Micromorphological observation shows that DZ1 and DZ2 have similar features. The description here will be based on the DZ1 sample. The sediment is a sandy loam with a c/f ratio of 70/30 (limit: 50 μ m) and a chitonic-gefuric related distribution. The coarse component mainly consisted of poorly-sorted, sub-rounded to sub-angular very fine to fine pebble-size rock fragments. The rock fragments show a variety of types, including quartz grains, orthoclase, calcite rich granitoid (Figure 7.25), and minerals that shows deformation features. Some of the rock fragments are altered/weathered with the release of dark brown Fe compounds and show a dark brown to black colour (Figure 7.25).

The micromass is a mixture of light yellow (PPL) silty clay with a grano-striated to stipple-speckled b-fabric and reddish yellow (PPL) amorphous sesquioxides. Some of the silty clay fabric is found as bright yellow, less oriented clayey aggregates (5%), grano-coatings and infillings in the cracks of the rock fragments, which may be the product of mineral weathering (Figure 7.25). The amorphous iron oxides are commonly found as nodules, including one concentric nodule, and grano-coatings inbetween the coarse rock fragments, which denotes repeated wet-dry alternations or fluctuation in groundwater tables (Lindbo *et al.*, 2010). This sediment generally has a moderately separated granular microstructure with 15% compound packing voids (Figure 7.25). Trace amounts of dark brown humified or charred very fine amorphous organic fine material are found.

7.3.3.2 *Results of bulk sedimentology of the Dazhe profile*

The bulk sedimentology analysis shows that the sediments from the Dazhe profile are relatively acidic, with a pH value of around 5.5. The calcium carbonate (2.62%), phosphorus (0.35 mg/L), total organic (2.19%) and carbon (0.87%) contents are all relatively low. The value of magnetic susceptibility is extremely low, with an average value of 1.13 SI, which may due to the porous soil structure, acidic pH, long-term water-saturated condition, low organic content and little or no soil forming processes (Blundell *et al.*, 2009).

In general, sediments from the Dazhe profile represent the natural accumulation of river sand under incipient weathering. The mineral types shown in the Dazhe profile demonstrate the commonly weathering products of the early Cretaceous intrusive and volcanic rocks of the Dazhe mountains (Wang *et al.*, 2020) and could be the source of the coarse sand-size rock fragments commonly seen in the sediments of the Liangzhu City.

7.4 Summary

This chapter presented the results of soil micromorphological and sedimentological analyses of profiles sampled from the outer Liangzhu City. The Shiqianyu profile is a man-made mound constructed in a previously marshy region, which may reflect the expansion of settlement area in the late stage of the Late Liangzhu period. The Jincun site reflects a sequence of intertidal flat/mudflat deposits, alluvium deposits, occupational activity surfaces and constructed mounds, and may be representative of the Early Liangzhu occupation pattern north of the contemporary Liangzhu City. The Huoxitang site represents an area of long-term ponding with the input of waste archaeological remains from nearby settlement areas; this change in depositional energy of this profile is similar to the North Zhongjiagang profile. The North Tangshan profile and the Dazhe profile present the natural sedimentary conditions north of Liangzhu City. In general, studying these profiles may contribute to the investigation of the relationships between human occupation and the local landscape from a regional perspective, and provide possible analogues for the Liangzhu City profiles and sequences.

Chapter 8: Discussion

8.1 Introduction

Based on the results of bulk sedimentology, GIS modelling and soil micromorphology, this chapter will begin by discussing the sedimentary and hydrological history of Liangzhu City, before discussing how the Liangzhu people modified their local landscape and exploited the near-water resources by constructing canals and mounds. Their relationship to the local water regime will then be analysed, followed by a synthesis of the associated occupation pattern of Liangzhu City. Finally, the interactions between the changing climate, hydrological conditions and the development of Liangzhu City are discussed in chronological order. The possible reasons for the eclipse of Liangzhu City are also explored, along with the relationships between water and social complexity.

8.2 The sedimentary and hydrological history of Liangzhu City

By integrating the research of previous scholars and the results of the soil analysis introduced in Chapters 5, 6 and 7, the sedimentary and hydrological history of Liangzhu City can be reconstructed. The pre-site conditions of Liangzhu City are represented by the Middle Zhongjiagang site (section 5.2), the Shiqianyu site (section 7.2.1) and the Jincun site (section 7.2.2); the changes in sedimentation and the hydrological conditions in the Early Liangzhu period are represented by the Middle Zhongjiagang (section 5.2) and the Southwest Mojiaoshan (section 6.2) profiles, and the conditions in the Late Liangzhu period are represented by the North Zhongjiagang (section 5.3) and Shiqianyu (section 7.2.1) profiles. These main periods of change and activity are discussed individually below.

8.2.1 The pre-site sedimentary history of Liangzhu City

Previous studies have argued that since 5500 cal. BC, the Liangzhu Basin has changed from being dominated by sub-tidal facies to intertidal flat facies, with the sediments

dominated by greyish clayey silt with fine silt lamination (Chen *et al.*, 2018; Liu *et al.*, 2018). During soil sampling for this PhD research, this greyish sediment was also widely seen in the pre-site sediment sequences in both inner and outer Liangzhu City, namely at the Middle Zhongjiagang site, the Shiqianyu site and the Jincun site. The sampled elevation was between -0.3 to 1.5m above sea level. In general, these soil samples exhibited similar bulk sedimentological characteristics with an alkaline pH, medium to high levels of calcium carbonate and magnetic susceptibility content, and low phosphorus and organic content (Table 8.1). Under the microscope, there is rhythmic bedding of alternating well-sorted coarse silt and humic silty clay crusts that do not grade into each other. This structure is better preserved in the Jincun and Middle Zhongjiagang sample (JCN 1, Figure 7.13 and T2621 1, Figure 5.4), with occasional cross beddings and thin laminae of heavy minerals, which collectively imply the presence of a slightly alkaline mudflat/intertidal flat near the estuary. This estuarine environment would be unsuitable for permanent human habitation due to the unstable sedimentary environment and its susceptibility to seawater influx.

Table 8.1 Results of bulk analysis of the pre-site samples

Sample Number	Depth (m)	pH	Mag sus ($10^{-9} \text{ m}^3\text{kg}^{-1}$)	CaCO ₃ %	P (mg/L)	Total Organic %	Total Carbon %
T2621 1	1.12	7.68	116.9	5.21	0.1	2.16	1.53
JCN 1	1.5	7.71	183	6.06	1.1	1.46	0.24
T1812 1 and 2	-0.3-0.25	7.81	158.5	7.97	0.15	3.4	1.23

Just before the arrival of Liangzhu people, this area transitioned from an intertidal flat to a low-lying alluvial plain formed by freshwater deposition. From 1.12 to 1.41m above sea level in the Middle Zhongjiagang Region (section 5.2), the pH value was shown to decrease rapidly. Similarly, from -0.3 to 0.25m above sea level at the Shiqianyu site (section 7.2.1), the soil samples show distinct reductions in pH, magnetic susceptibility and calcium carbonate content, and an increase of phosphorus content, which in combination imply the shift from alkaline conditions to the introduction of freshwater into the sedimentary system.

8.2.2 The sedimentation and hydrological history during the development of the Liangzhu culture

Human intervention is responsible for most of the formation processes observed at the sites both inside and outside Liangzhu City during the Liangzhu Culture period (see discussion in section 8.3). Nonetheless, as the studied profiles of this thesis are commonly close to waterways and are sensitive to the change of local hydrological conditions, the meticulous studying of these soil profiles can still provide a high-resolution record of the sedimentation and hydrological history of Liangzhu City.

In the early stage of the Early Liangzhu period (3300-3100 cal. BC), the Liangzhu City region can be characterized as an alluvial floodplain receiving water and soil material from the nearby mountainous areas through very gentle flow and/or overbank standstill water conditions. At this stage, the hydrological conditions gradually changed from stagnant water to dryness and then land exposure. This process is clearly reflected in the base of Layer 13 of the Middle Zhongjiagang profile where an accumulating floodplain developed under cycles of high frequency build-up, with the mid-upper part of this layer exhibiting incipient soil formation processes suggestive of a slowing or brief halt in the aggradational floodplain dynamic. At around 3150 cal. BC, the first dry and exposed surfaces with the evidence of plant growth were identified in the Middle Zhongjiagang region (Layer 12D of profile T2621). However, this dry surface was quickly covered by around 30cm of alternating wet-dry channel deposits that dated from 3150 to 3000 cal. BC. Within this period, there were at least two relatively dry and stable soil surfaces where plant growth has been observed; however, both of these periods were short-lived, the wetter conditions soon returned.

At around 3000 to 2900 cal. BC, the sedimentation reflects a drying trend. At the Southwest Mojiaoshan site, dry wind-blown materials were found directly overlying the occupation floors abandoned at around 3000 cal. BC. In the North Zhongjiagang region, the low-lying areas around 0.5m above sea level were exposed and subjected to alternating conditions of water saturation and periodic drying with phases of exposure.

But since 2900 cal. BC, wet conditions in the sedimentation environment soon returned

and continued until about 2600 cal. BC. At the Southwest Mojiaoshan site, a palaeochannel was observed to down-cut through the aeolian deposits, which probably marked the return of wet conditions. In the North Zhongjiagang region (Layer 10 of profile T5020), the low-lying areas were filled by slow moving water and showed a trend of increasing wetness with a greater depositional energy. Specifically, in the bottom sub-layer 10C, the alluvium appears to have accumulated under very slow and shallow water conditions, occasionally exhibiting dry conditions with weak influence of surface soil formation processes. In the middle sub-layer 10B, the sediments quickly accumulated under shallow water with alternating wet and dry conditions. In the top sub-layer 10A, the depositional energy increased and long-term wet conditions again predominated.

After 2600 cal. BC, the accumulation of an alluvial floodplain continued under a drying trend of sedimentation. Short-term soil development began in what had previously been channel deposits. By the end stage of Liangzhu, wet sedimentation conditions returned with an increase in stream flow energy, and a high-energy hydrological event happened as the debris flow containing human occupation remains from nearby platforms was deposited (see Layer 7 of profile T5020).

8.2.3 Post-Liangzhu depositional processes

The yellowish silty clay layer superimposed on the Liangzhu layers was long considered to be related to massive flooding in the region, leading to the collapse of Neolithic cultures around the Tai Lake region (Liu, 2019; Zhang, 1998). Previous studies proposed that this layer was a poorly sorted overbank alluvial deposit formed under weak depositional energy conditions (Li, 2013; Song, 2012). By conducting a detailed study of the transitional process from the end-stage Liangzhu to post-Liangzhu sediments (mainly the Layer 7 to Layer 5 of the North Zhongjiagang profile), this research has revealed the changes in sedimentation process and the dynamics that occurred.

The results of micromorphological and bulk sample analyses suggest that the high-energy stream flow that occurred in the end-stage of Liangzhu extended into the post-

Liangzhu depositional sequence, dated to around 2000 cal. BC. This high water movement was then weakened and stabilised coincident with a return of incipient soil formation processes and evidence of anthropogenic material inclusions, which in general imply a drying trend. However, after a possible large hydrological event, small channel erosion then occurred, and a ponded water environment then predominated for a considerable period. After that, the depositional energy decreased with an increase in soil formation processes. Above the yellowish silty clay layer, the input of coarse material and greater bioturbation indicated a more stable sedimentation environment favourable for human occupation. Overlying this yellowish silty clay layer, the sediment that was dated to Eastern Zhou dynasty (770–256 BC) then shifted to becoming alluvial deposits that became more oxidised with mature soil development.

8.2.4 Summary

In the Liangzhu region, the sedimentary environment shifted from intertidal flats to freshwater alluvial floodplains with the occasional input of aeolian loess deposited on the higher ground. The hydrological conditions changed from being constantly wet in pre-site times to alternating wet-dry conditions at about 3300 to 3100 cal. BC, then to relatively dry at around 3000 cal. BC, wet from 2900 to 2600 cal. BC, back to relatively dry from 2600 to 2300 cal. BC, before returning to wet conditions with a possible flooding event at around 2200 to 2000 cal. BC. In the post-Liangzhu sediments, the yellowish silty clay layer appears to have been influenced by two major flooding events, the first reflecting the relatively high-energy stream flow continuing from the end-stage of Liangzhu and the second being indicative of regional ponding events.

8.3 The construction and occupation history of Liangzhu City

Integrating the results of the GIS and soil analyses introduced in Chapters 4, 5, 6 and 7, this section reconstructs the construction and occupation history of Liangzhu City, including reconstructions of how the mounds were constructed, the forming and exploitation of local water systems, and the occupation patterns near the rivers of the day.

8.3.1 The construction of mounds

One of the most distinctive features of Liangzhu is that the overwhelming majority of the Liangzhu sites, including both cemeteries and occupation areas, were found on artificially raised ground (Fang, 2015; Qin, 2013). These ubiquitous high-ground mounds may have been a deliberate strategy to tackle the soft and wet land surfaces of the Liangzhu region. The construction techniques and strategies of artificial mounds are thus a good starting point for understanding the development of Liangzhu City. Several types of construction materials and techniques were identified during this study, and their main micromorphology and bulk characteristics have been summarised based on their construction sequences from bottom to top.

8.3.1.1 Direct soil borrowing from pre-site sediments

At the base of most mounds, there is a c. 2-20cm thick, heterogeneous layer composed of well-mixed but disorganised micro-charcoal and highly fragmented soil aggregates (commonly organic topsoil) with irregular boundaries in a humic silty clay groundmass. Based on the comparison of particle size with other sediments of the profiles, this layer is interpreted as a former organic topsoil or pre-site sediment that has been physically transformed by human activity. This direct exploitation of soil materials was found at both the North City Wall and the Shiqianyu settlement and was best exemplified in the Middle Zhongjiagang profile where sequential soil borrowing from nearby pre-site sediments was observed and an inverted stratigraphic sequence was present that exhibited the deposition of older pre-site sediments overlying younger pre-site sediments (section 5.2.2.2.5 and 5.2.2.3). This exploitation of nearby pre-site sediments was both expedient and easy to operate. This material is commonly functioned as a cushion course (Figure 8.1) and may have helped to provide a flat surface for the subsequent stacking of construction components. This process may also have altered the terrain and geomorphology of the surrounding landscape (see section 8.3.2).

8.3.1.2 The 'clay wrapped with grasses' material

The 'clay wrapped with grasses' material has only been found in Liangzhu cultural

deposits and was widely used in the city wall, the dam systems, the Mojiaoshan mound and mounds near channels. The material was commonly used in the basal part of earthen structures where it was directly stacked on wet surfaces or placed on the substrates made by the first soil introduced above (Figure 8.1). Hundreds of 'clay wrapped with grasses' would form a big block of 'construction module' about 1m³ in size. In most cases these construction modules could be easily seen in the field during excavations (section 2.3.2.3 and Figure 6.1). Based on bulk analysis, this material had a slightly acidic pH in general, moderate to high total organic content, low to moderate magnetic susceptibility, and moderate calcium carbonate content. The carbon and phosphorus values are variable, probably due to the different degrees of influence from human activity.

Under the microscope, the 'clay wrapped with grasses' material encountered in this study showed different characteristics and can be divided into two types. The first type was mainly seen at the Shiqianyu site, from Platform I-3 of profile T1812 and Platform I-2, II-2 of profile T1813. Its main characteristic is the unevenly but well-incorporated mixture of several different soil materials with a few sand-size mineral grains. It has a moderately developed prismatic structure or fissured microstructure with a few vertical planar voids and fissures (with 10% porosity).

The second type, represented by Layer 14 of profile T0950 and Platform III-2 of profile T5020, does not show an obvious mixture of different soil materials under the microscope. The groundmass of this type is generally massive and brown (PPL), with a dotted mixture of humic silt-size material (>70%), highly birefringent clay material (>20%), and a small proportion (2-5%) of sub-angular fine sand-size quartz. A few (3%) clusters of highly fragmented humified organic residues with random orientations were also mixed-in, which could be the only possible criteria for discrimination.

Most of the sources of the 'clay wrapped with grasses' would have been available locally. For instance, Platform II-2 of profile T1813 used soil materials from the pre-site sediment at the Shiqianyu site and incorporated soil aggregates with a high organic matter content that were possibly from existing topsoil, which are both locally available. Occasional exotic sources were also observed. For example, the soil aggregates-3 of

the bottom of Platform I-3 of profile T1812 were not seen in previous strata and are similar to the groundmass of the constructed layer of the South Zhongjiagang profile.

The use of the 'clay wrapped with grasses' material may have had two major functions. On the one hand, the adding of grass material may have helped to bind the wet earth and to maintain the structure's shape, reduce cracking, and increase the tensile strength of the structure (Keefe, 2012, 57-58; Saxton, 1995). On the other hand, the sandbags formed by hundreds of single 'clay wrapped with grasses' were combined into similar sizes and were believed to be convenient for transportation, representing the carrying capacity of a raft (Wang, 2019).

8.3.1.3 Processed soil material

The processed soil material is mainly found in the upper layers of the Middle and South Zhongjiagang profiles, *i.e.*, Platform IIIA of profile T2621 and Platforms 5-1 and 2 of profile T3131. Based on micromorphological and bulk analyses, this material could be divided into two layers.

The bottom layer is the heterogeneous mixture of silty clay, clusters of sand-size rock fragments (25-35%), and a few (3-5%) included anthropogenic materials such as fine burnt bone fragments. The layer in general has a complex microstructure of moderately developed subangular blocky and vesicular microstructure. Various textural pedofeatures such as dusty to limpid clay coatings around the voids and grains and as intercalations are widely observed. In the South Zhongjiagang profile, soil clasts similar to the groundmass and a potential rotation features were still preserved, which implies insufficient slaking of the soil material and possible kneading during preparation (section 6.3.2.8).

The upper layer further incorporated highly degraded pebble-size burnt daub and pottery sherds, thus showing a red colour in field. This addition of burnt material may have given a better quality to the activity surface, and/or may have had yet unknown ritual or aesthetic meanings.

This material commonly had a slightly alkaline pH, mid-low carbon and total organic content. The magnetic susceptibility was much higher in the upper layer due to the inclusion of burnt materials. The phosphorous and calcium carbonate contents were variable, depending on the inclusion of different anthropogenic materials. In general, a process flow of preparing sand-size mineral grains, burnt clays and pottery sherds and silty clay material, adding water, physical mixing (stirring), and kneading can be reconstructed.

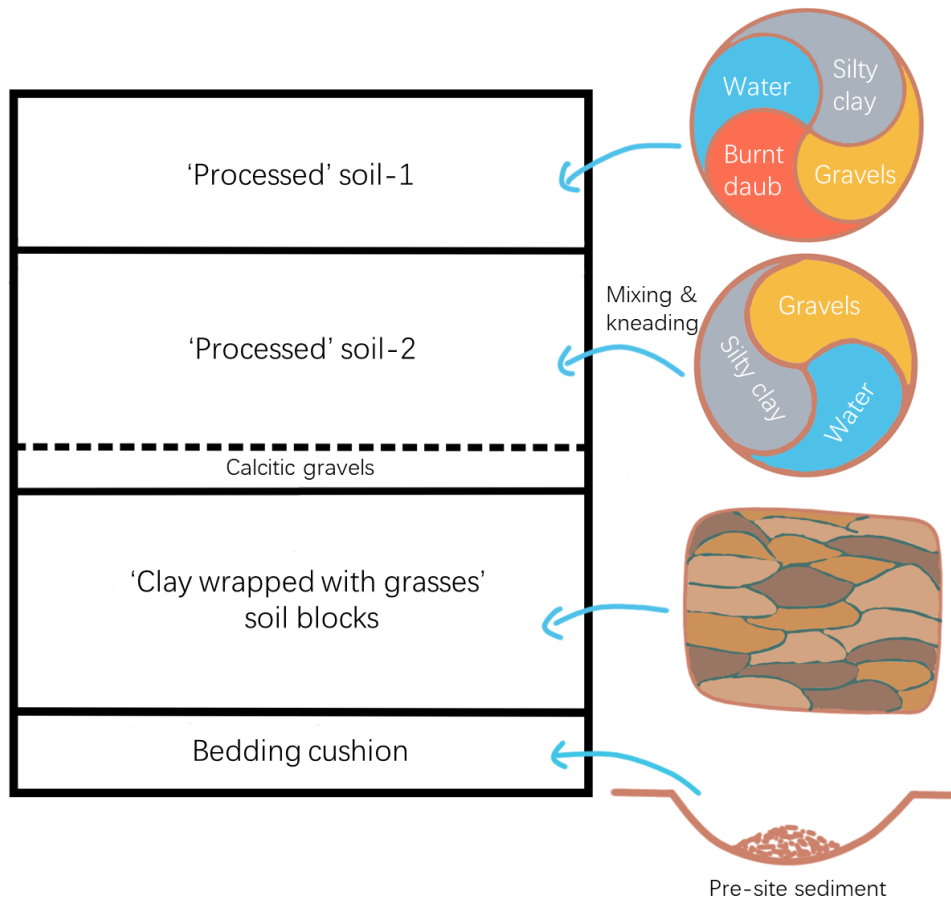


Figure 8.1 Sketch of the construction components of a typical Liangzhu mound

8.3.1.4 Calcitic rock fragments

In the Middle Zhongjiagang Watercourse, there was a 2cm thick layer composed of white, compact, fine pebble size calcitic granitoids (Platform III 3 B1 of profile T2621, section 5.2.2.4). This layer shows a uniform white colour and a mineral composition that suggests it was most likely intentionally selected from a riverbed, and perhaps, therefore, has ritualistic or aesthetic significance. However, both the micromorphological and bulk analyses indicate a low level of human activity in this

layer, so these calcitic grains may have only been simply prepared for mound construction. In Platform IIIA of profile T2621, a similar 1-2cm thick concentration of calcitic granitoids was also found. A few thin laminations of fine material were observed on top of these rock fragments, which may indicate simple levelling activity on top of these calcite-rich marbles.

8.3.1.5 Summary

Liangzhu people have used different techniques and construction materials to construct their mounds. The sites both inside and outside Liangzhu City share similar principles in terms of raw material selection and construction sequences (Figure 8.1). This common pattern shows how people, through time, learned and deployed multiple earthen engineering techniques, and are evidence of remarkable intellectual skills.

Generally speaking, the basal part of the mound commonly makes use of local materials, follows the principle of proximity and is relatively rough and simple. The ‘clay wrapped with grasses’ material is a unique construction method created by the Liangzhu and was expedient for transportation and soil amelioration. The wide use of this construction material at various Liangzhu sites suggests that the production and use of this material may have been standardised. The material preparation in the upper part is more exquisite. It involved a concoction of different raw materials and the collection and selection of a specific admixture for soil amelioration and possible ritual and/or aesthetic purposes. This carefully prepared construction material has only currently been observed inside Liangzhu City, which may imply some kind of differential between the inner and outer city settlements, as yet not understood.

As a pivotal part of the living of Liangzhu people, the building of mounds involved thorough consideration, planning and organisation before construction. Their choice of raw materials and methods of construction were well adapted to local resources and conditions. The study of these materials in this thesis demonstrates that the Liangzhu people had a well-developed and consistent concept and knowledge of raw material acquisition, selection, processing and transportation, as well as the sequence and thicknesses of materials to use and the selection of construction methods.

8.3.2 The formation and exploitation of the local water systems

Currently, the total length of the waterways found inside Liangzhu City is more than 30km (Liu *et al.*, 2017), and the moats together with the river channel connecting the inner city and outer dam system appear to make Liangzhu City a water city (Liu *et al.*, 2014). Studying the formation process and flow characteristics of the water systems is therefore crucial to understanding how Liangzhu people exploited these systems in the past.

8.3.2.1 The life history of the Zhongjiagang Watercourse

The Zhongjiagang Watercourse is an important part of the inner-city water system of Liangzhu City. Based on current investigation, it flowed through the whole Liangzhu city in a north-south direction. The flow characteristics of this river were represented by profiles T2621 and T5020 from the Middle and North Zhongjiagang region, which cover the entire life history of the Zhongjiagang Watercourse.

Based on the soil micromorphology analysis (see Chapter 5), the 1km long north-south Zhongjiagang Watercourse is likely to be an artificial river formed as a consequence of Liangzhu people borrowing earth to construct their mounds. Firstly, the pre-site sediments in both the Middle and North Zhongjiagang areas were composed of alternating wet-dry exposed land surfaces with no constrained watercourses in evidence. Only in Liangzhu times did riverine deposition appear. Secondly, the soil study of the Middle Zhongjiagang region (see sections 5.2 and 8.3.1, Figure 8.2) shows that Liangzhu people had probably borrowed earth from a nearby older stratum to create the foundations for their mounds. Shallow pit cuts in the nearby pre-site sediments that were afterwards superimposed by riverine deposition also side with this argument (Figure 5.2). This combination of evidence suggests that at least in the Middle Zhongjiagang Region, the river channel was formed in contemporary association with the construction process of the nearby mounds (Figure 8.2). Thirdly, another supporting point is that the natural stream networks near Liangzhu City are overwhelmingly oriented in a west-east direction based on GIS modelling (see Chapter 4). Zhongjiagang

Watercourse may possibly also have functioned as a canal to connect the natural west-east flowing streams from the north and south.

In the Middle Zhongjiagang region, riverine deposits only continued to form from around 3000 to 2800 cal. BC (Layers 11 and 10, Figure 5.2) and became filled up during the last stage of platform construction in this area (Figure 8.2). In the North Zhongjiagang region, the fluvial deposits were mainly concentrated in Layer 10, which is dated to 2900 to 2600 cal. BC. The micromorphological and particle size analyses of Layer 10 reveal that the Zhongjiagang Watercourse has a generally slow water motion but fast sedimentation accumulation rate of fine particles, but with the sedimentary dynamics slightly increasing from the bottom to the top of Layer 10. Although dominated by fluvial deposition, occasional land exposure and vegetation growth can still be observed under the microscope, which implies the occasional lower water level of the Zhongjiagang Watercourse. From 2600 cal. BC onwards, soil formation processes start to appear in the North Zhongjiagang Region, which suggests the gradual disappearance of the Zhongjiagang Watercourse. The vanishing of this canal may have occurred under the influence of a drier climate at around 2500 cal. BC and/or human changes of the local environment yet unknown (see section 8.3.4 for discussion and references), in combination with slow water motion and a fast sedimentation rate, and the lack of river dredging. At around 2000 cal. BC, high-energy hydrological events occurred, human activities ceased, and the Zhongjiagang Watercourse disappeared as an alluvial yellowish silty clay covered the whole region.

8.3.2.2 Water areas near the outer city settlements

In the outer Liangzhu City area, settlements were also commonly found accompanied with water areas. The excavations and soil sampling at the Shiqianyu site revealed that the channel near the settlement area is oriented in a west-east direction, which coincides with the modelling in GIS (Chapter 4, Figure 4.5). The current soil analysis of the Shiqianyu site demonstrates that their mounds were built on top of alternating wet-dry wetlands and the construction of mounds may have also exploited nearby soil materials and may have changed the local landscape by artificially creating low-lying wetlands or channels.

8.3.2.3 Summary

Current geoarchaeological research suggests that a certain amount of channels/moats in Liangzhu City were dug artificially, particularly those in a north-south direction, and the earth dug out may have been used as construction material for nearby mounds. This is best exemplified by the Zhongjiagang Watercourse, which was the main moat flowing through the Liangzhu City. It appears as Liangzhu people started to construct their mounds using nearby soil material. The depressions caused by soil removal were then transformed into canals to connect the water systems from the north and the south. This artificial river generally exhibited a slow flow velocity and shallow water depth, and became quickly silted up in the Middle Zhongjiagang region. This canal existed for longer in the North Zhongjiagang region but still became silted up with the demise of Liangzhu.

8.3.3 *The occupation pattern of Liangzhu City*

The identification and descriptions of activity surfaces in Liangzhu sites are usually restricted to the macroscopic observation of macro-artefacts, such as posts, beams and stones left in place. However, due to the frequent borrowing and transformation of soil materials, it is sometimes difficult to determine in field whether the artefacts were left *in situ*, let alone identifying the micro-facies related to human living. Based on the detailed study of the soil formation processes and micro-artefacts left in place, this thesis identified and studied the micromorphological characteristics of the floor sequences of the Liangzhu settlements, which was the first trial of this kind in this site and this region.

In this study, floor sequences were identified in the Southwest Mojiaoshan profile (section 6.3.2) and the South Jincun profile (section 7.2.2) but were best exemplified in the South Zhongjiagang profile (section 6.3.3). The micromorphological and bulk analyses indicate that the floor sequence of the Liangzhu City region can be described using the 'Active-Reactive-Passive Zone' model (after Courty *et al.*, 1994; Gé *et al.*, 1993; Macphail & Goldberg, 2017). In Liangzhu City, the Passive Zone used various

materials as the bedding course with little mechanical affect by trampling, such as dumped archaeological materials, alluvial/aeolian sediments, and constructed layers made by kneading together different soil materials (Figure 8.1). The mound construction material discussed in section 8.3.1 could generally be regarded as the Passive Zone of the floor sequences. The Reactive Zone is characterised by a mixture of construction material and micro-artefacts presumably brought-in by people traffic. The Active Zone is characterised by elongated, densely compacted micro-aggregates and various well to moderate sorted micro-artefacts between layered, mostly intact matting material with sub-horizontal fissures, which are formed by homogenisation and compaction from human activities. The matting material of intact woven bast fibres has been identified as grasses (*Poaceae*), most likely from *Bambusoideae* (section 6.3.3.3).

In addition to the continuous occupation sequences, layers of unprocessed plant matting were commonly found between different layers of mound construction materials during the excavation of the inner and outer Liangzhu City, such as in the North Zhongjiagang region, the South Zhongjiagang region and the Shiqianyu site. The plant matting was normally black, around 5-10cm thick, and with the size range from 80cm long, 40cm wide to 270cm long, 150cm wide (ZPICRA, per. comm.). Based on soil micromorphological and bulk analyses of Platform I-2 of Profile T1813 at the Shiqianyu site and Unit 5-2-1 of profile T3131 at the South Zhongjiagang site, this slightly inclined, layered, black plant material was identified as *in situ* grasses stems and leaves, most likely from *Bambusoideae*, which is similar to the woven bast fibres commonly found in the activity surfaces of Liangzhu City. Micro-artefacts such as fine bone fragments, micro-charcoal, phytolith slag and fine pottery debris were also mixed in and probably intensively trampled. Various clay coatings and textural intercalations were found in-between the grasses and artefacts, which generally imply an open-air matting incorporated with various hearth remains. The use of easily accessible grasses instead of woven bast fibres may imply the expedient use of the grass material. In addition, this layer commonly has the same groundmass as the construction material above, which may imply that it formed synchronously with the platform above. This open-air matting of fresh grass materials is thus interpreted as a temporary activity surface between the stages of platform construction.

The detailed study of site formation process of the selected profiles also contributed to the understanding of the occupation and expansion pattern of Liangzhu City mounds. Generally speaking, between 3000 and 2900 cal. BC, only several large mounds were constructed in Liangzhu City, *i.e.*, the Mojiaoshan and Huangfenshan mounds. Houses with meticulously prepared wall and matted surface were constructed and inhabited on top of these mounds (T0950 profile). Besides these carefully constructed mounds, Liangzhu people also directly occupied low-lying areas by repeatedly overlying bamboo mats on top of dumped layers and alluvial sediments (exemplified by the T3131 profile), and retreat to high grounds when the water level rises. After 2900 cal. BC, there is a reduce of human activity in the Mojiaoshan mound, marked by the large fire event and subsequent covering of aeolian sediments in the T0950 profile, and even across the whole Liangzhu City, indicated by the gap of radiocarbon dating in the artefacts found from the Zhongjiagang Watercourse (Qin *et al.*, 2019) and the possible aeolian sediment covering previous activity surfaces in the T3131 profile. After this event, the Mojiaoshan Mound was heightened: the west Mojiaoshan was raised by ‘clay wrapped with grasses’ with well-jointed wooden structures and the east Mojiaoshan was heightened by the carefully prepared ‘processed’ soils. Similar ‘processed’ soils were used in the South Zhongjiagang region and Bianjiashan site to heighten the mounds (ZPICRA, 2014) in a slightly later period. From 2600 to 2200 cal. BC, expansion of mounds towards previous waterways and/or wetland areas was observed from both inside, *e.g.*, Middle and South Zhongjiagang regions, and outside Liangzhu City, *e.g.*, Meirendi site, Bianjiashan site, and Shiqianyu site. In the Meirendi Site, the mound structures were enlarged dozens of times within a short period (ZPICRA, 2015a), which imply the rapid increase of population that cause the enormous demand for housing and living areas. In general, the pattern of mound construction and expansion are generally similar across Liangzhu City, with the Mojiaoshan Mound always ahead of other regions and were constructed with the best materials and the most sophisticated technology.

8.3.4 The modification and exploitation of local landscape

Based on this research, it is apparent that Liangzhu people heavily modified and

managed their local landscape (Figure 8.2). To set up a new settlement, Liangzhu people initially constructed high ground mounds situated on previous alternate wet-dry, flooded/ exposed land surfaces. During this process, depressions formed around the mounds as Liangzhu people excavated the soil from nearby pre-site sediments. These depressions together with the construction of dam systems and the exploitation of natural waterways were then interconnected to form a channel system connecting Liangzhu City with settlements outside the city and in the northern mountainous areas. Consequently, this channel system may have in return benefited and made easier the transportation and allocation of mound construction materials such as ‘clay wrapped with grasses’ soil blocks, river sand and calcitic rock fragments. Mounds and canals thus become a strongly interlinked feature of the Liangzhu cultural landscape.

The occupation on top of the mounds and near the canals extensively exploited the near-water resources. Besides the consumption of freshwater wetland/lake fauna as introduced in section 2.3.3.2, one of the most distinctive features of Liangzhu City was the use of wetland grass material, especially the *Bambusoideae*. This plant material was used for different tasks. In particular, the stems may have been processed to extract bast fibres for mat weaving, and the leaves and stems may have been directly laid to provide temporary activity surfaces.

In addition, different areas of Liangzhu City showed different characteristics of occupation and construction. In the centre of the city, the Middle Zhongjiagang region next to the Mojiaoshan mound had been constructed on top of former wetlands and used processed soil materials and selected off-white calcitic gravel, which suggests occupation after construction and careful planning before the engineering took place (Figure 8.2). In the South Zhongjiagang area, floor sequences were found in the near-bank area and were later covered by processed soil material, which implies that there was some occupation before construction and that the activity surfaces were improved in the later period. The Shiqianyu site was also constructed on top of wetland, but the building material was less exquisite compared to the Middle Zhongjiagang profile. These inter-site variability in building techniques and occupation sequences support previous observations that there may have been hierarchical differences between the inner and outer city settlements and that the Middle Zhongjiagang region and

Mojiaoshan mound were more carefully planned and constructed compared with other sites and may have been the most important region in the city (Liu *et al.*, 2017).

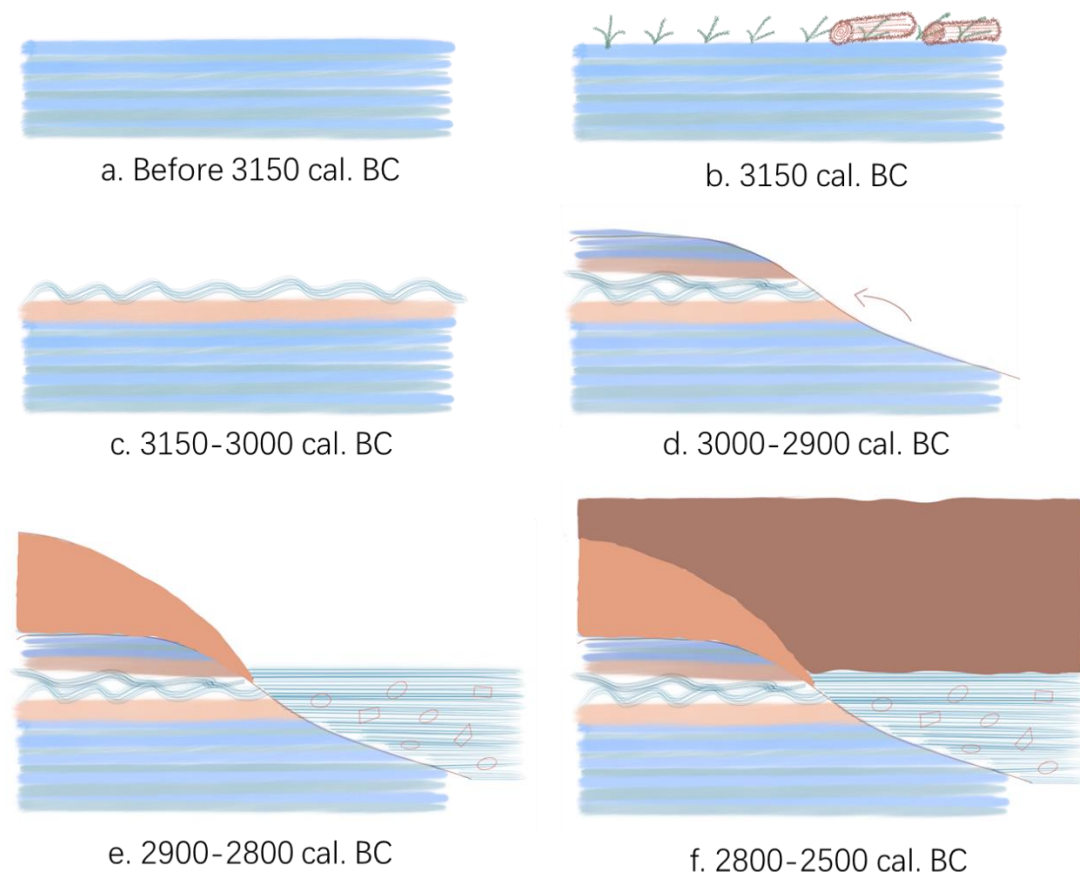


Figure 8.2 Site formation process of the T2621 profile. a. intertidal flat conditions; b. first dry vegetation phase; c. wet-dry sedimentation cycles; d. construction of platform areas using nearby soil materials; e. forming of the Zhongjiagang Watercourse and heighten of the Mojaoshan Mound; f. heighten of Mojaoshan Mound and the complete filled up of the Middle Zhongjiagang Watercourse

8.4 The coupling of the water, environmental and cultural periodisation of Liangzhu City

Based on the summary sequence of sedimentation and hydrological history, and the construction and occupation characteristics of Liangzhu City, this section will investigate the chronological development of Liangzhu City and its relationship with the local hydrological regime, and wider evidence of environmental change in the region. The discussion will use the framework of both the cultural periodisation proposed by Qin *et al.* (2019) (section 2.3.1) and the climate and hydrological changes

identified in this study.

8.4.1 The early stage of the Early Liangzhu period (3300-3100 cal. BC)

From 3300 to 3100 cal. BC, the current range of Liangzhu City was probably largely unoccupied based on currently available data, although a few Liangzhu settlement sites and burials have been found at the foot of natural low hills and close to major rivers in the Northern Liangzhu Basin. At this time the Liangzhu City area generally is still under the change from a stagnant wetland area to drier exposed land influenced by the stable sea-level, dramatic shrinkage/closure of the Palaeo-Taihu Estuary, progradation of Yangtze delta, and the cooling and drying trend of the Tai Lake region since 3700-3500 cal. BC (Chen *et al.*, 2018; Cheng, 2016; Liu *et al.*, 2018; Lu, 2014; Wang *et al.*, 2018; Zhang, 2014).

The first dry layer identified in this research is Layer 12D of the Middle Zhongjiagang profile, which was dated to about 3150 cal. BC and contained the first traces of human activity observed inside the current area of Liangzhu City. In the upper part of Layer 12D, large wooden structures and pieces of charcoal and pottery appeared, which implies Liangzhu people's efforts to construct large dwellings near the Middle Zhongjiagang area. The choice of the Middle Zhongjiagang region and the nearby Mojaoshan region as the one of the earliest places for residence may possibly be due to the relatively high altitude of this region. Based on recent coring and test excavations, before the Mojaoshan mound was constructed, the western part of the Middle Zhongjiagang area used to be a low-lying hill around 6-10m above sea level in the west and 0-2m above sea level in the east (Liu *et al.*, 2019a). The Fanshan cemetery to the west of the Middle Zhongjiagang region is around 12.4m above sea level and was also began to be used at around 3150 cal. BC (Qin *et al.*, 2019).

It is clear that the beginning and expansion of human activity in the area of Liangzhu City is related to the drying and exposure of the previous wetland area and the formation of a stable land surface near the Middle Zhongjiagang low hills. However, the hydrological conditions soon change to being wet again, with soil material being deposited under frequent wet-dry sedimentation cycles. When this happened, Liangzhu

people would have abandoned the Middle Zhongjiagang area and may possibly have retreated to higher ground areas.

8.4.2 The late stage of the Early Liangzhu period (3100-2900 cal. BC)

From around 3100 to 3000 cal. BC, the land surfaces of Liangzhu City were subject to alternating wet-dry conditions. It is believed that some of the high dams may have been constructed during this phase (Qin *et al.*, 2019), marking the beginning of large-scale water management at Liangzhu City.

At about 3000 cal. BC, although the sedimentation was still under the influence of water, large-scale mound constructions had started at the western and southern parts of Mojiaoshan mound. In the Southwest Mojiaoshan site, Liangzhu people constructed around a 1m thick 'clay wrapped with grasses' layer. On top of it, an activity surface with fragments of clay wall was observed. The Middle Zhongjiagang mound to the east of Mojiaoshan as well as the low dam system had also started construction. Associated with the construction of mounds, the inner city water system connecting both the canals and the natural waterway had started to form. The creation of the dam and water control systems inside Liangzhu City may have been a reaction and solution to counter the persistently alternating wet-dry conditions affecting the city. The development of these water systems also fostered the transportation of raw materials around Liangzhu City.

Between 3000-2900 cal. BC, the temperature dropped, and the climate became drier as compared to the previous warm and humid conditions (Innes *et al.*, 2014; Wang *et al.*, 2007; Yi *et al.*, 2003, 2006). In this stage, large scale firings were found in both the Southwest and East Mojiaoshan sites. At the Southwest Mojiaoshan site, the activity surfaces were covered by an *in situ* 20cm thick horizon of charred materials dated to around 3000 cal. BC that contained wall fragments, which was then overlaid by 50cm of aeolian sediment. At East Mojiaoshan, a large charred rice pit containing about 13 tonnes of grains dated to 2940–2840 cal. BC was found (Liu *et al.*, 2014; Liu *et al.*, 2019a; Qin *et al.*, 2019). All of these deposits imply that large-scale firings may have happened on the Mojiaoshan mound, and human activity briefly ceased. It should be noted that the pottery and jade assemblages before and after 2900 cal. BC also show

obvious changes, which divided the early and late Liangzhu period (Fang, 2020; Chen Minghui, per. comm.). Whether there is linkage between burning of houses and a granary, the dry climate conditions, and the cultural changes is not yet clear. Further studies are required to investigate whether this change is related to internal or external conflicts between communities at that time.

Besides the Mojiaoshan mound, mound construction started to expand in both the North and South Zhongjiagang areas. Under the drier climate, the low-lying areas of the North Zhongjiagang region became more like a drained swamp with intermittently exposed surfaces and a high clay content, and human activity expanding into this new space. The platform (Platform III-2 of profile T5020) which was then constructed was quite thin, with a thickness of only 30-50cm, implying that there was a lower groundwater table in this location, such that a thin constructed surface was sufficient for human activities to take place. In the South Zhongjiagang region, direct activity zones were found in near-bank areas. The repeated occurrence of dumped materials in alluvial deposits on top of the regularly maintained occupation floors that accumulated in relatively dry conditions illustrates the dynamic relationship between the periodic rise and fall of the water levels and the abandonment and occupation of this near-bank area.

8.4.3 The early stage of the Late Liangzhu period (2900-2600 cal. BC)

After 2900 cal. BC, the Liangzhu profiles studied in this research all show the return of wet conditions. Based on pollen data, this may relate to the resumption of warm and humid conditions from 2900 to 2700 cal. BC (Mo *et al.*, 2019). Whether this change is also related to the construction of dam systems is yet unclear and further study of the dam is required.

In the centre of Liangzhu City, the second stage of mound construction began at both the West and East Mojiaoshan mounds. In the Southwest Mojiaoshan site, a channel with relatively high stream flow energy eroded the wind-blown layer, before a 3m thick 'clay wrapped with grasses' layer with knocked-in wooden frameworks was constructed. In the Middle Zhongjiagang region east to the Mojiaoshan mound, the mound was constructed using fine calcitic pebbles and processed soil material

composed of a mixture of sand, silty clay and burnt daubs.

In the North Zhongjiagang region, the previous edges of mound were covered by 1m thick fluvial deposits suggesting an increased wetness and depositional energy from bottom to top. In the South Zhongjiagang region, the near-bank occupation area shows a retreat of human activity. In both cases, this implies the expansion of water areas. In addition, there were a variety of bank protection materials found in the North, Middle and South Zhongjiagang regions, which suggest that the Zhongjiagang Watercourse may have been well maintained at this stage (section 2.3.2.3 and Liu *et al.*, 2019a).

At the same time, the outer circle of settlements such as Bianjiashan and Meirendi were constructed and occupied. Various bank protection materials were also found in these sites (Liu *et al.*, 2019a). Additionally, the walls surrounding Liangzhu City may have also begun construction in this stage (Qin *et al.*, 2019) along with the moats both inside and outside the walls. All elements of Liangzhu City, including the Mojiaoshan mound, the mounds along the North and South Zhongjiagang region, the outer circle settlements, the city walls and the Miaoqian site groups which clustered around the Daxiong Mountain and possibly the dam systems, may all have been connected by waterways. These interconnected waterways may, in turn, have supported the engineering and construction of Liangzhu City. In general, this is the stage at which Liangzhu City can be best described as a ‘water city’.

8.4.4 The late stage of the Late Liangzhu period (2600-2300 cal. BC)

During this stage, the sedimentary environment analysed in this research shows a drying trend. Comparison of Dongge Cave $\delta^{18}\text{O}$ and atmospheric $\Delta^{14}\text{C}$ suggest that there was a small monsoon intensity peak and warm event driven by increasing solar activity from 2600 to 2400 cal. BC (Stuiver, 1998; Wang *et al.*, 2005). The pollen analyses also indicate a decrease of swampy conditions and drier and cooler climate conditions after 2500 cal. BC (Jin *et al.*, 2019; Wang *et al.*, 2017).

In the North Zhongjiagang region, the sediments overlying the fluvial deposits were influenced by soil formation processes and periodic drying. In the Middle and South

Zhongjiagang regions, there was a large-scale expansion of mounds into previous near bank and watercourse areas (Liu *et al.*, 2019a). Additionally, Liangzhu people began occupying previous wetland areas further away from Liangzhu City, such as at the Shiqianyu site. At the same time, the wall areas surrounding Liangzhu City were extensively occupied.

In general, under these drying trend, Liangzhu people actively expanded their sphere of activity by constructing mounds inside and outside the city. The waterways inside the city then gradually became silted up and/or were proactively filled up by Liangzhu people. The dam systems outside Liangzhu City showed no traces of human activity at this stage (Qin *et al.*, 2019), and may have already been abandoned.

8.4.5 The Qianshanyang period (2300-2000 cal. BC)

Archaeological findings suggest that around 2300-2000 cal. BC, the Zhongjiagang Watercourse and the city walls were still occupied and filled with abundant domestic waste (Liu *et al.*, 2019a). However, elite burials were not so commonly found at this stage, and the pottery had declined in quality and the types showed obvious influences from other Neolithic cultures such as the Qianshanyang culture and the Longshan culture that flourished in the Northern Yellow River basin. A cultural change seemed to have taken place (Liu, 2019b).

In terms of climate, the pollen data suggests a continuous trend of cooler and drier conditions during this stage (Jin *et al.*, 2019; Wang *et al.*, 2017). Notably, around the 4.2ka BP time there is the global cooling and drying event (Weiss, 2016). In the Zhejiang area this probably manifested itself as a weakening of the East Asian monsoon and continuous drying conditions (Cui, 2019).

However, in contrast to the drying climate, the depositional energy of this stage was raised. Moreover, at the end of this stage, a debris flow occurred in the North Zhongjiagang region, which indicates that part of the channel bank was probably affected by strong overland flow or even a flood event. These 10-20cm thick coarse-grain layers were also widely found in other areas of Liangzhu City, such as the Eastern

Wall, the Shagang site near the Meirendi site etc. (pers. comm. from Yijie Zhuang). This evidence strongly suggests that slightly before 2000 cal. BC, the bank and probably the whole of Liangzhu City was unmanaged.

This unconformity of climate and hydrological conditions implies that there are other factors influencing the enhancement of water motion in the city. This could relate to a wider deforestation process and associated water and soil loss in the northern mountainous area. However, current analysis of the profiles sampled from the northern Tangshan dam (section 7.3.2) shows no trace of colluvial deposits or an increase in particle size at this end stage of Liangzhu. A more probable cause may have been the narrowing of the riverbed caused by the continuous expansion of mound areas since the late stage of the Late Liangzhu period (2600-2300 cal. BC). Further GIS modelling based on accurate calculations of mound areas and channel capacity should be undertaken to further address this question.

8.4.6 The yellow silty clay layer

After 2000 cal. BC, Liangzhu City and wider Tai Lake region was covered by the yellow silty clay layer, which based on pollen and clay mineral analyses was formed under warm and humid sedimentary conditions (Li, 2013; Wang *et al.*, 2017). Archaeological findings show that although most parts of Liangzhu City were abandoned, there was still sporadic human activity around the Tai Lake region during this period, which was known as the Maqiao Culture (1900-1200 cal. BC). This culture was less complex compared to Liangzhu, and showed more cultural factors influenced by central China (Cao, 2010; Shanghai, 2002a).

The micromorphological analysis of this study suggests that the yellow silty clay layer began with a relatively high depositional energy. With the drying and stabilisation of sediment, sporadic human activity can then be observed. However, a quiet, ponded environment that lasted for a considerable period soon appeared, which may indicate the expansion of water areas and a relative hiatus of human activity inside Liangzhu City. The analysis of this thesis supports the opinion that the yellow silty clay layer was not formed by flash flooding or marine intrusion (Li, 2013; Ji *et al.*, 2016; Song, 2012),

but is more relevant to long-term, multiple processes of gentle water covering the region as an overbank alluvial flood deposit associated with a high groundwater table. The cause of regional ponding may possibly due to the enclosure of the Palaeo-Taihu Estuary (Yu, 2016) and the tidal backwater and retrogressive accumulation of the river system that caused the raising of the terrain near the Qiantang Estuary (Song, 2012; Xu, 1995). This change may have also caused the diversion of the East Tiao River, and further aggravated the process of paludification. Other factors such as a stable high sea level would have exacerbated the problem by keeping groundwater tables high and hindering drainage (Zong, 2011). Further GIS modelling of the changing geomorphology near the Qiantang Estuary and detailed study of the enclosure of the Palaeo-Taihu Estuary may shed more light on what caused the formation of this ubiquitous yellow silty clay layer.

8.4.7 Summary

The development trajectory of Liangzhu City is closely related to major environmental and hydrological shifts since around 3500 cal. BC and human transformation of local landscape may also in turn influence the local hydrological condition. In the early stage of the Early Liangzhu period, the Liangzhu people began to occupy the dry and exposed land near the Mojiaoshan area. As wet conditions return, Liangzhu people soon retreated to higher ground. In the late stage of the Early Liangzhu period, to tackle the fluctuating groundwater tables, Liangzhu people started the construction of dam systems and actively transformed and managed their local landscape by forming an occupation pattern of raised high-ground with associated artificially dug moats. At around 2900 cal. BC, under a drier climate, large-scale fire events appear to have happened in the Mojiaoshan area, which may have been related to cultural changes that divided the early and late period of Liangzhu Culture. The North and South Zhongjiagang regions also started to be occupied in this phase. In the early stage of the Late Liangzhu period, a warm and humid climate recovered with the construction of mounds inside and outside the city and the formation of interconnected water systems, making Liangzhu City a ‘water city’. In the late stage of the Late Liangzhu period, a dry environment predominated, and Liangzhu people intensively expanded their settlements onto previous wetland areas. The water systems were then largely

backfilled and abandoned. The Qianshanyang period is featured by an increase of depositional energy under a dry and cool climate. The non-managed riverbank together with the impact from central Chinese cultures both suggest the decline of Liangzhu Culture. After 2000 cal. BC, although there were still a few sporadic human activities in this region, Liangzhu City became generally unoccupied and constantly covered by shallow, still floodwater.

8.5 Further discussion

8.5.1 Water, mound, and social complexity

After the marine tides receded, what appeared in front of Liangzhu people was a new and unoccupied plain with abundant freshwater and food resources in the marshes and fertile soil derived from volcanic rocks that was favourable for human occupation. However, the alternating wet-dry land surfaces limited the potential for the enlargement of settlements, particularly in the early stage of the Early Liangzhu period as exemplified by the Middle Zhongjiagang profile.

As introduced in section 8.3.1, the construction of mounds on top of wet land surfaces commonly required several stages of building and the use of different techniques. Simply using clayey pre-site sediments was insufficient as the sediment was too soft and wet to keep its structure and shape. The construction of raised high grounds then required careful planning, heavy labour input and time investment as well as effective social organisation to collect, transport and process the raw material. Under these circumstances, division of labour became necessary, a power centre may have appeared to oversee the centralised allocation of existing land and food resources, as well as to plan and determine the location and scale of new mounds, and the command and dispatch of raw materials and human resources for the engineering of the new mounds. In addition, a higher mound requires a much higher labour input. Based on current GIS modelling (section 4.3.2), the constructed mounds of 7m in height were sufficient to withstand flooding that covered up to one-fourth of the Liangzhu Basin. The construction of any mounds higher than 7m may have been largely for symbolic rather than practical purposes. The construction and occupation of high-ground areas, such as for the Fanshan and Yaoshan burials and the Mojaoshan and Huangfenshan mounds,

may then have become a symbol of high social status.

In summary, the changing hydrological regime and the limited dry land surfaces may have confined settlement enlargement of Liangzhu in its early phase. However, these limitations may in turn have fostered the formation of a stratified society. As Liangzhu people mastered the techniques to tackle this problem, they actively transformed and modified their local landscape, with Liangzhu City situated on raised high-grounds along with associated, well-developed water networks constructed. These large-scale combined construction of mounds, dam and water system, together with the elaborate artefacts such as jade and lacquerware found inside the city, all suggest that Liangzhu can be thought of as possibly the earliest early state-society in East Asia (Renfrew and Liu, 2018).

8.5.2 The collapse of Liangzhu

Based on current geoarchaeological research, the abandonment of Liangzhu City is directly related to the increase of depositional energy and the ponding conditions that affected the region from about 2000 cal. BC. However, the decline of Liangzhu Culture may have begun much earlier. In around 2300 cal. BC or even earlier, Liangzhu City appears to have been less well maintained, craft production shows a decline in quality, and the cultural characteristics had come under the influence of cultures from central China. The environmental and cultural changes between 2600 to 2300 cal. BC may then become the key period from which to understand the fading of Liangzhu Culture.

Some scholars have proposed that storm surges and an increased risk of coastal flooding occurred in around 2500 cal. BC and that these factors were responsible for the decline of Liangzhu (Tang *et al.*, 2019; Wang *et al.*, 2018, 2020). The storm event observed at the Yushan site that was located on the southern bank of the Qiantang River is believed to have been particularly strong, and it eroded away a previous peat layer and formed a sand ridge (Wang *et al.*, 2018). Palynological studies around Liangzhu City also suggest a reduction in rice cultivation and possibly an interruption in human occupation at 2500 cal. BC (Jin *et al.*, 2019; Wang *et al.*, 2017). However, the soil analyses undertaken in this research indicate that no catastrophic flooding took place

between 2600 to 2300 cal. BC inside Liangzhu City. On the contrary, the sedimentary environment was relatively dry, the water systems were largely backfilled or abandoned, and the mound areas had expanded rapidly in both the inner and outer parts of Liangzhu City. This study thus strongly suggests that Liangzhu City was not directly affected by wider regional storm events.

A possible explanation for the marine inundation of the shoreline sites and the increase in the population of Liangzhu City may be that around 2500 cal. BC the coastal areas were unsuitable for human living, and the coastal residents may have migrated to the Liangzhu Basin, out of the area that was susceptible to marine flooding. Rice cultivation may also have been influenced by the drier climate and the reduction of swampy land over the longer-term, and may therefore have experienced crop failures during the inundation events. Thus, this decline in rice cultivation may have potentially weakened the economic basis of Liangzhu society (Liu *et al.*, 2017). In addition, the convergence of different communities in Liangzhu City may have fostered the change in pottery and jade production and styles, and caused difficulties for the administration and allocation of resources in Liangzhu City.

Overall, the current geoarchaeological studies around Liangzhu City and wider Tai Lake and Qiantang River regions are probably insufficient to absolutely interpret the causes and processes of the decline of Liangzhu. Nonetheless, this research has provided some strong clues and suggestions to pursue in the future. In order to better understand this important change in the late stage of the Late Liangzhu period, more detailed studies should be carried out concerning the changes in food sources and supply, pottery and jade assemblages, the flow of groups, and the sphere of influence of the coastal flooding events.

Chapter 9: Conclusion and outlook

Focusing on Liangzhu City and its surrounding landscape, this study applied a series of geoarchaeological methods to investigate and model the long-term human-landscape relationships between Liangzhu City, its surrounding landscape and its hydraulic regime. The GIS analysis has modelled the stream network under both natural and inundation conditions under different depths of water (Chapter 4). The soil micromorphological and sedimentological data from the inner and outer Liangzhu City profiles have revealed the sedimentological and hydrological histories as well as the interactions between the changing environment, the hydrological conditions and the development of Liangzhu City (Chapters 5-8). Based on these results, this chapter summarises the implications of this study for a wider understanding of the emergence of complex society and human responses to changing environmental conditions. It then considers the importance of studying site formation processes for wider archaeological research. At the end of this chapter, the outlook and directions for future research are outlined.

9.1 The formation of the early city

Based on meticulous soil micromorphological sedimentological analyses, this study provided a vivid case study of how the early Liangzhu City developed and thrived in a challenging environment, and how the earliest known city in East Asia was constructed by taking advantage of previously disadvantageous water conditions. In the early stage of Liangzhu, the development of the city was restricted by the local water regime as this occurred during the transition from the previous brackish water intertidal flat to a freshwater alluvial environment. There is no doubt that the fluctuating water table limited the enlargement of settlement in the Liangzhu area. However, Liangzhu people soon managed to deal with the environmental constraints and create innovative responses by actively managing and controlling the local landscape. Combining the study of near-bank profiles, this thesis has revealed the process by which Liangzhu people actively transformed local landscapes by constructing mounds using various materials and techniques, and forming new waterways at the same time. In addition, by investigating the Zhongjiagang Watercourse, this study has provided detailed

information about how and when the inner city waterways formed and then went into decline, and presents comprehensive information regarding the flow characteristics of this important inner city canal. A scenario of raised high-ground with associated artificially dug moats has been indicated. As discussed in the preceding chapters (see section 8.5.1), the social complexity of Liangzhu was enhanced and evolved during the process of dealing with the challenging water environment. The study of Liangzhu City has exemplified the complex relationship between early city water management and land, labour and social organisation, and acts as a valuable exemplar for the understanding of water, early city and social complexity combined.

9.2 The environment and human interactions

This study has demonstrated that the development of Liangzhu City was closely related to changes in local environment and that a combination of factors has influenced the environment of the Liangzhu area and relevant human responses. Since the fourth millennium BC, the stabilisation of sea-level and the retreat of seawater in the Hangzhou Bay area most probably caused the dramatic shrinkage/closure of the Palaeo-Taihu Estuary after 3600 cal. BC (Chen *et al.*, 2018; Liu *et al.*, 2018), which then provided substantial available land for human occupation. Liangzhu Culture thrived in this marshland area as discussed in section 9.1. During this process, the development of the city was closely related to regional climatic and hydrological conditions and changes, such that human activity areas retreated during wet periods whereas there was large scale expansion of mound areas in the corresponding dry periods. The changes in water regime since 2300 cal. BC may have significantly influenced the longevity of Liangzhu City. The depositional energy of the channel deposits in Liangzhu City showed an increase since 2300 cal. BC. Significantly, the cold and dry 4.2 ka BP event did not seem to significantly change this process. The long-term inundation that had occurred since 2000 cal. BC hindered human activity in the region, and this regional ponding with freshwater may have been triggered by the rise of the terrain near the Qiantang Estuary (section 8.4.6). In summary, the change of environment in this region during the fourth millennium BC was favourable to human occupation, and that from 3300 to 2300 cal. BC, the Liangzhu society co-evolved and well-adapted to these environmental and hydrological changes. However, since 2300 cal. BC, hydrological changes have significantly hindered the development of Neolithic settlements. This

illustrates that compared to climatic change, the hydrological conditions affected by regional geomorphology changes seem to have been more influential to the survival and development of Neolithic societies around the Hangzhou Bay area than anything else.

In addition, this thesis has recognised some important points in time where significant cultural shifts appear to have occurred under the influence of a combination of climatic, hydrological and cultural factors. The first was around 2900 cal. BC when firing events in the Mojaoshan mound, a dry climate event, and changes in pottery and jade styles occurred. Currently the scale of the fire events and the cause of the cultural shift are not clear; more archaeological evidence should be sought to address these questions. The second was around 2300 cal. BC, which signified the decline of Liangzhu Culture. Although what exactly triggered the decline is not yet clear (see discussion in section 8.5.2), this study has provided important evidence with which to understand the process. Based on the geoarchaeological study, no major flooding events had occurred between 2600 and 2300 cal. BC, and Liangzhu City continued to be occupied until 2000 cal. BC or slightly later. The sea invasion and crop failure events that probably occurred at around 2500 cal. BC (Jin *et al.*, 2019; Wang *et al.*, 2017, 2018, 2020) thus may not have had significant and direct effects on Liangzhu City. Besides, the GIS modelling of inundation conditions also showed that even if the groundwater table had reached around 2m in height above the contemporary ground surface, which is the height of the outer circle of settlements, there would still have been enough exposed land surfaces for human occupation and agriculture to take place. This evidence collectively suggests that past natural hazards may not have been so dramatic and catastrophic for Liangzhu City and that the decline of Liangzhu may have been a more prolonged process. Nonetheless, the changing hydrological conditions around the region may have weakened the economic basis of Liangzhu society. New evidence about the change of subsistence in Liangzhu society should be sought and carefully examined to understand the extent and scale of this influence.

Above all, this thesis has provided a detailed sequence of hydrological and environmental changes and corresponding human responses in Liangzhu City and its immediate hinterland from 3500 to 2000 cal. BC. The proxies established could be used

as a cornerstone for the study of other Neolithic sites around the Hangzhou Bay and Lower Yangtze region. Additionally, the human responses to the environmental shifts in the Liangzhu region could provide a unique perspective with which to understand the interaction between environment and human activity during this critical period of state society emergence, and may resonate with current questions surrounding the human response to climatic and environmental change.

9.3 Reconstructing soil formation processes in an artificial landscape

This thesis has reconstructed soil and built environment formation processes at several different types of Liangzhu sites which cover the whole life history of Liangzhu City. They include natural riverine deposits (T5020, section 5.3), constructed mounds (T2621 and T1812, sections 5.2 and 7.2.1), *in situ* occupation sequences (T3131, section 6.3), and sites that have been influenced by both geogenic, hydrological and anthropogenic inputs and formation processes (T0950, section 6.2).

The results show that the Liangzhu profiles, particularly the mound areas, have been frequently reworked. This reworking of sediments caused many difficulties for layer and horizon interpretations in the field. For example, the base of the mound which utilised near-by sediments are commonly found directly stacked on pre-site sediments and display very similar soil properties to the buried soil underneath. Although they have different functions, these two layers may be classified as sub-units of the same layer, e.g., in the Layer 12A sediment of profile T2621. Furthermore, this inversion of sediments may cause confusion in the interpretation of the radiocarbon dating results. For instance, in the Middle Zhongjiagang profile, the radiocarbon dating of the Platform III and II from bottom to top is 3029-2904 cal. BC and 3115-2921 cal. BC (section 5.2.3.1). This apparent inversion of dates in the mound areas may be due to the re-use of construction materials from an earlier stratum. Due to frequent soil borrowing and use of exotic soil materials, the direct dating of mound areas is not commonly reliable. To know the construction time of mounds, it may be more authentic to date the waste accumulation during the use of mounds rather than the mounds themselves. The definite identification of the formation processes evident in these reworked layers may thus avoid misinterpretations of subsequent artefact and fauna analyses, and is thus

crucial to the understanding of the archaeological records and chronological sequences.

In addition, detailed micromorphological and sedimentological studies have enabled the recognition of site formation process in the fill, floor, and mound sequences. In the field, it is not easy to distinguish between constructed mounds and accumulated occupation remains because archaeological remains may have been dumped and/or act as part of the construction materials of the mounds. For instance, profile T3131 was regarded in the field as a mound with dumped human waste, but with meticulous examination under the microscope, at least six intact activity surfaces have been recognised based on the presence of intact matting materials and the trampling of anthropogenic fine debris (section 6.3). This research thus provides the first detailed study of Neolithic floor sequences in east China. The floor sequences found at Liangzhu share similar characteristics with many occupation surfaces observed elsewhere around the world and could be described using models widely applied in tell site studies (Macphail & Goldberg, 2017, 342).

Before this study, the raised mounds widely found in Liangzhu and wider Lower Yangtze River area were commonly recognised as being substructures of buildings or grave mounds and have not been fully studied nor understood by both Eastern and Western scholars (Du and Wang, 2010). This research provides a preliminary understanding of the site formation process of the mound structures of Liangzhu. The results show that they were formed under different anthropogenic agencies and processes: some were constructed as the sub-structure of occupation areas, e.g., the Middle Zhongjiagang and Shiqianyu profiles, and some were formed due to sequential buildings and deposits from activities and settlement, e.g., the South Zhongjiagang profile. The latter has similar formation processes to the artificial mounds or 'tells' widely found around the Middle East, Pakistan, Eastern and Southern Europe and Central Asia (Matthews, 2017). With more studies being conducted in the Liangzhu region, future comparable studies could be conducted of the landscape and formation processes compared between the large earthen mound sites such as Harappan Indus civilisation in South Asia (Petrie *et al.*, 2017), early cities in Mesopotamia (Matthews and Postgate, 1994; McMahon, 2020 etc.) and the high-ground structures in Liangzhu, as well as the study of the cultural and environmental parameters that enable early

urbanism.

Another finding of this thesis that may benefit future archaeological analyses is that intact activity surfaces could be found between the stages of mound construction. Currently, most of the house remains and activity surfaces on top of the high ground areas were either disturbed or had vanished because of the continuous use of these mounds in historical times. This has largely limited the research of Liangzhu occupation patterns, house structures and functional divisions of occupation areas. Based on the research presented in this thesis, intact activity surfaces composed of layers of fresh grasses and even long-term floor sequences with house remains, such as in the Southwest Mojiashan site, were found inbetween stages of mound construction. The recognition and study of these *in situ* activity surfaces may benefit the study of the occupation patterns of Liangzhu society, particularly for the Early Liangzhu period.

Above all, this thesis has demonstrated the potential of combining soil micromorphological techniques of analysis in conjunction with bulk sedimentological analyses for reconstructing soil formation processes and identifying different types of human activity under a landscape that was highly modified by Neolithic people. The study of this thesis thus has far-reaching implications for archaeological research around the Tai Lake region and other large earthen mound archaeological sites around the world.

9.4 Outlook and future work

This research has provided some strong clues and suggestions to pursue in future studies. As suggested in the preceding discussions (section 8.4 and 8.5.2), the causes and effects of the major cultural shifts of Liangzhu society are not yet completely clear. More detailed studies should be carried out concerning the changes in food sources and supply, pottery and jade assemblages, the flow and interaction between different communities, and the sphere of influence of the regional climate and flooding events.

The closing of the Palaeo-Taihu Estuary and the associated geomorphological changes near the Qiantang Estuary seems to be significant to the change of water regime in the

Liangzhu Basin. The process of this change and its influences on Liangzhu City should be further studied and modelled by detailed geoarchaeological surveys and analyses near the Qiantang Estuary, combined with GIS modelling using DEM data with a higher resolution. In addition, what caused the unconformity of climatic and hydrological conditions in the Qianshanyang stage of Liangzhu City and whether it is related to regional geomorphology change is not yet clear. Land-use patterns in the northern mountains should be investigated and further GIS modelling based on accurate calculations of mound areas and channel capacity should also be undertaken to further address this question.

Importantly, as a crucial part of Liangzhu water system, the dam system outside Liangzhu City was not studied in detail in this thesis due to time limitations. Although current GIS modelling (Chapter 4) has provided suggestions about the watershed management capability of the dam systems, how the dam systems actually functioned is still obscure. Further geoarchaeological work should be conducted both the outside and within the dam systems to determine how the construction of these artificial mounds in specific locations may have altered the regional water flow characteristics and depositional processes.

In summary, many important questions about Liangzhu Culture and Liangzhu City remained unsolved. Further studies focusing on the wider landscape and regional geomorphological changes are necessary to address these issues.

Bibliography

Adams, R. M. (1971) *The evolution of urban society: early Mesopotamia and prehistoric Mexico*. Chicago: Aldine Publishing Company.

Aimers, J. and Hodell, D. (2011) Drought and the Maya, *Nature*, 479(7371), 44–45. doi: 10.1038/479044a.

Algaze, G. (2001). Initial Social Complexity in Southwestern Asia: The Mesopotamian Advantage. *Current Anthropology*, 42(2), 199–233. <https://doi.org/10.1086/320005>

Allen, J. R. L. (ed.) (1982) Soft-Sediment Deformation Structures, in *Developments in Sedimentology*, 343–393. Amsterdam: Elsevier. doi: 10.1016/S0070-4571(08)71019-7.

Allen, M. J. and Macphail, R. I. (1987) Micromorphology and magnetic susceptibility studies: their combined role in interpreting archaeological soils and sediments, in Fedoroff, N., Bresson, L. M. and Courty, M-A. (ed.) *Soil Micromorphology*. Paris: Plaisir, 669–76.

Anderson, D.G., Maasch, K.A., Sandweiss, D.H., and Mayewski, P.A. (2007) Climate and culture change: Exploring Holocene transitions, in Anderson, D.A., Maasch, K.A., and Sandweiss, D.H. (eds.) *Climate Change and Cultural Dynamics: A Global Perspective on Mid-Holocene Transitions*. Amsterdam: Elsevier Press.

Angelucci, D. E. and Zilhão, J. (2009) Stratigraphy and formation processes of the Upper Pleistocene deposit at Gruta da Oliveira, Almonda karstic system, Torres Novas, Portugal, *Geoarchaeology*, 24(3), 277–310. doi: 10.1002/gea.20267

Angourakis, A., Bates, J., Baudouin, J.-P., Giesche, A., Ustunkaya, M. C., Wright, N., ... Petrie, C. A. (2020). How to ‘downsize’ a complex society: An agent-based modelling approach to assess the resilience of Indus Civilisation settlements to past climate change. *Environmental Research Letters*, 15(11), 115004. <https://doi.org/10.1088/1748-9326/abacf9>

Atahan, P., Itzstein-Davey, F., Taylor, D., Dodson, J., Qin, J., Zheng, H. and Brooks, A. (2008) Holocene-aged sedimentary records of environmental changes and early agriculture in the lower Yangtze, China, *Quaternary Science Reviews*, 27(5–6), 556–570.

Bates, R. G. (1964) *Determination of pH: theory and practice*. New York, London, Sydney: John Wiley & Sons Inc.

Baumann, H., Wallace, R.B., Tagliaferri, T. *et al.* (2015) Large Natural pH, CO₂ and O₂ Fluctuations in a Temperate Tidal Salt Marsh on Diel, Seasonal, and Interannual Time Scales, *Estuaries and Coasts*, 38, 220–231. <https://doi.org/10.1007/s12237-014-9800-y>

Berking, J. (Ed.) (2018) *Water Management in Ancient Civilizations*. Berlin: Edition Topoi.

- Binford, L. R. (1978) Dimensional Analysis of Behavior and site Structure: Learning from an Eskimo Hunting Stand, *American Antiquity*, 43(3), 330–361. doi: 10.2307/279390.
- Binford, L. R. (2001) *Constructing Frames of Reference: An Analytical Method for Archaeological Theory Building Using Hunter-Gatherer and Environmental Data Sets*. Berkley: University of California Press.
- Binford, M., Kolata, A. L., Brenner, M., Janusek, J., Seddon, M., Abbott, M., and Curtis, J. (1997) Climate variation and the rise and fall of an Andean civilization. *Quaternary Research* 47, 235–248.
- Blundell, A., Dearing, J. A., Boyle, J. F. and Hannam, J. A. (2009) Controlling factors for the spatial variability of soil magnetic susceptibility across England and Wales, *Earth-Science Reviews*, 95(3–4), 158–188. doi: 10.1016/j.earscirev.2009.05.001.
- Boggs, S. (2001) *Principles of sedimentology and stratigraphy*. Upper Saddle River: Prentice Hall.
- Boorman, L., Hazelden, J., and Boorman, M. (2002) New salt marshes for old salt marsh creation and management, in Eurocoast (ed.) *Littoral 2002, The Changing Coast*. Portugal: EUCC, 35-45.
- Bresson, L.-M. and Valentin, C. (1993) ‘Soil surface crust formation: contribution of micromorphology’, in Ringrose-Voase, A. J. and Humphreys, G. S. (eds) *Developments in Soil Science*. Amsterdam: Elsevier, 737–762. doi: 10.1016/S0166-2481(08)70460-4.
- Brooks, N. (2006). Cultural responses to aridity in the Middle Holocene and increased social complexity. *Dark Nature: Responses of Humans and Ecosystems to Rapid Environmental Changes*, 151(1), 29–49. <https://doi.org/10.1016/j.quaint.2006.01.013>
- Bullock, P. (ed.) (1985) *Handbook for soil thin section description*. Albrighton: Waine Research Publ.
- Butzer, K. W. (1976) *Early hydraulic civilization in Egypt: a study in cultural ecology*. Chicago: University of Chicago Press.
- Cao, J. (2010) Rethinking of Maqiao Culture, *Kaogu*, 11, 58–70. (In Chinese)
- Cascalho, J., Costa, P. J. M., Gelfenbaum, G., La Selle, S. and Jaffe, B. (2020) Selective sediment transport during Hurricane Sandy on Fire Island (New York, USA): Inferences from heavy-mineral assemblages, *Journal of Sedimentary Research*, 90(3), 269–285. doi: 10.2110/jsr.2020.12.
- Catt, J. A. (1985) Soil particle size distribution and mineralogy as indicators of pedogenic and geomorphic history: examples from the loessical soils of England and Wales, in K. S. Richards, R.R. Arnett and S. Ellis. (ed.) *Geomorphology and Soils*. London: George Allen & Unwin, 202–218.

- Charles, M., Pessin, H. & Hald, M.M. (2010) Tolerating change at Late Chalcolithic Tell Brak: responses of an early urban society to an uncertain climate, *Environmental Archaeology*, 15:2, 183-198, DOI: 10.1179/146141010X12640787648892
- Chen, M. H. (2018) The pathway to social complexity in Circum-Tai Lake region and Sumer region, *Southern Relics*, 1, 77–88. (In Chinese)
- Chen, Q., Li, C., Li, P., Liu, B., Sun, H. (2008) Late Quaternary palaeosols in the Yangtze delta, China, and their palaeoenvironmental implications, *Geomorphology*, 100, 465-483.
- Chen, S. Q. (2006) The adaptation of the transition of hunter-gatherer in China's late Pleistocene, *Acta Anthropologica Sinica*, 25(3), 195–207. (In Chinese)
- Chen, T. (2017) *Mid- to late Holocene hydrology changes in the south Taihu area of the Yangtze delta plain, China, and its relationship to the development of Neolithic cultures*. Doctoral Dissertation. East China Normal University.
- Chen, T., Ryves, D. B., Wang, Z., Lewis, J. P. and Yu, X. (2018) Mid- to late Holocene geomorphological and hydrological changes in the south Taihu area of the Yangtze delta plain, China, *Palaeogeography, Palaeoclimatology, Palaeoecology*, 498, 127–142. doi: 10.1016/j.palaeo.2018.03.012.
- Chen, X. G. (2019) The research report of the ‘clay wrapped with grasses’ material of Liangzhu sites, in Zhejiang Provincial Institute of Cultural Relics and Archaeology (ed.) *A comprehensive study of Liangzhu Ancient City*. Beijing: Cultural relics publishing house, 420–422. (In Chinese)
- Chen, Z. Y. and Wang, Z. H. (1998) The Neolithic period in Tai lake: water and the development of culture, *Science* (2), 29–32. (In Chinese)
- Cheng, L. (2016) *Study recorded by sedimental carbon and oxygen isotopes of Beihuqiao (Bhq) Core in Zhejiang, China*. Masters Dissertation. Zhejiang Normal University. (In Chinese)
- Chepstow-Lusty, A. J., Bennett, K. D., Switsur, V. R., and Kendall, A. (1996) 4000 years of human impact and vegetation change in the central Peruvian Andes – with events paralleling the Maya record? *Antiquity* 70, 824–833.
- Cohen, David J. (2014) The Neolithic of Southern China, in Colin Renfrew and Paul Bahn. (ed.) *The Cambridge World Prehistory*. Cambridge: Cambridge University Press, 765–781.
- Clift, P.D. and Giosan, L., (2018) Holocene evolution of rivers, climate and human societies in the Indus basin, in Zhuang, Y. and Altaweel, M. (eds.) *Water Societies and Technologies from the Past and Present*. London: UCL Press, 17-39. doi:10.14324/111.978191157693.
- Committee for Preservation and Artifact Management of Shanghai (1992) The 1987 excavation of the Songze site in Qingpu, Shanghai, *Kaogu*, 3, 204–219. (In Chinese)

- Conolly, J. and Lake, M. (2006) *Geographical Information Systems in Archaeology*. Cambridge: Cambridge University Press. doi: 10.1017/CBO9780511807459.
- Courty, M. A., Goldberg, P. and Macphail, R. (1989) *Soils and micromorphology in archaeology*. Cambridge: Cambridge University Press.
- Courty, M.-A., Goldberg, P. and Macphail, R. (1994) Ancient people - lifestyles and cultural patterns, *Proceedings of International Soil Science Society*, 6, 250–269.
- Cui, T. (2019) *Late holocene paleoclimatic and paleoenvironmental evolutions recorded by stalagmite from the songya cave, Zhejiang province*. Masters Dissertation. Zhejiang Normal University. (In Chinese)
- Day, J. W., Gunn, J. D., Folan, W. J., Yáñez-Arancibia, A., and Horton, B. P. (2007) Emergence of complex societies after sea level stabilized. *EOS Transactions, American Geophysical Union* 88,169–170.
- Day, J. W., Gunn, J. D., Folan, W. J., Yáñez-Arancibia, A., and Horton, B. P. (2012) The Influence of Enhanced Post-Glacial Coastal Margin Productivity on the Emergence of Complex Societies, *The Journal of Island and Coastal Archaeology*, 7:1, 23-52. doi: 10.1080/15564894.2011.650346
- Dixit, Y., Hodell, D. A. and Petrie, C. A. (2014) Abrupt climate change and the decline of Indus urbanism, *Geology*, 42, 339–342.
- Dong, C. W., Lv, Q., Ma, X. X., Gu, H. Y., Zhou, C. (2019) The rock types and sources of rock of the bedding stones of the Liangzhu city walls, in Zhejiang Provincial Institute of Cultural Relics and Archaeology (ed.) *A comprehensive study of Liangzhu Ancient City*. Beijing: Cultural relics publishing house, 397–410. (In Chinese)
- Du, J. J. and Wang, G. F. (2010) Some questions in the study of mound graves, *Southern Relics*, 4, 120–132. (In Chinese)
- Du, P., Ding, P. and Hu, K. (2010) Simulation of three-dimensional cohesive sediment transport in Hangzhou Bay, China, *Acta Oceanol. Sin.*, 29, 98-106. <https://doi.org/10.1007/s13131-010-0028-9>
- Durand, N., Monger, H. C. and Canti, M. G. (2010) Calcium Carbonate Features, in Stoops, G., Marcelino, V., and Mees, F. (eds) *Interpretation of Micromorphological Features of Soils and Regoliths*. Amsterdam: Elsevier, 149–194. doi: 10.1016/B978-0-444-53156-8.00009-X.
- Dzuynski, S. and Smith, A. J. (1963) Convolute lamination, its origin, preservation, and directional significance, *Journal of Sedimentary Research*, 33(3), 616–627. doi: 10.1306/74D70ED4-2B21-11D7-8648000102C1865D.
- Evenari, M., Yaalon, D. H. and Gutterman, Y. (1974) Note on soils with vesicular structure in deserts, *Z. Geomorphol*, 18(2), 162–172.

Fagan, B. (1999) *Floods, Famines, and Emperors: El Niño and the Fate of Civilizations*. New York: Basic Books.

Fan, D., Cai, G., Shang, S., Wu, Y., Zhang, Y. and Gao, L. (2012) Sedimentation processes and sedimentary characteristics of tidal bores along the north bank of the Qiantang Estuary, *Chinese Science Bulletin*, 57(13), 1578–1589. doi: 10.1007/s11434-012-4993-6.

Fang, X. (2015) The hierarchy of jade using in Liangzhu culture, *Popular Archaeology*, 5, 58–64. (In Chinese)

Fang, X. M. (2020) A controlled fine craft: Jade production techniques in the Liangzhu culture, in Liu, B., Qin, L., and Zhuang, Y. (eds) *Liangzhu culture: society, belief and art in Neolithic China*, London: Routledge.

French, C. (2015) *A handbook of geoarchaeological approaches for investigating landscapes and settlement sites*. Oxford: Oxbow Books.

French, C. A. I. (2003) *Geoarchaeology in Action: Studies in Soil Micromorphology and Landscape Evolution*. London: Routledge.

French, C., Sulas, F. and Madella, M. (2009) New geoarchaeological investigations of the valley systems in the Aksum area of northern Ethiopia, *Catena*, 78(3), 218–233. doi: 10.1016/j.catena.2009.02.010.

Friesem, D. E., Karkanias, P., Tsartsidou, G. and Shahack-Gross, R. (2014) Sedimentary processes involved in mud brick degradation in temperate environments: a micromorphological approach in an ethnoarchaeological context in northern Greece, *Journal of Archaeological Science*, 41, 556–567. doi: 10.1016/j.jas.2013.09.017.

Fu, Y. G. (2008) Developed society and growing holdback: the reason for the swift decline of Liangzhu Culture, *Southeast Culture*, 5, 6–9. (in Chinese)

Fuller, D. and Qin, L. (2010) Declining oaks, increasing artistry, and cultivating rice: the environmental and social context of the emergence of farming in the Lower Yangtze Region, *Environmental Archaeology*, 15(2), 139–159.

Fuller, D., Qin, L., Zhao, Z., Zheng, Y., Leo-Aoi, H., Chen, X. and Sun, G. (2011) Archaeobotanical Analysis at Tianluoshan: Evidence for wild-food gathering, rice cultivation and the process of the evolution of morphologically domesticated rice, in Peking University and Zhejiang Provincial Institute of Cultural Relics and Archaeology (ed.) *Integrated studies on the natural remains from Tianluoshan*. Beijing: Cultural Relics Publishing House, 47–96. (In Chinese)

Gé, T., Courty, M.-A., Matthews, W. and Watez, J. (1993) Sedimentary formation processes of occupation surfaces, in Goldberg, P., Nash, D.T., and Petraglia, M. D., (eds.), *Formation Processes in Archaeological Contexts*. Monographs in World Archaeology No. 17: Madison, Wisconsin, Prehistory Press, 149–163.

Gebhardt, A. (1993) Micromorphological evidence of soil deterioration since the mid-

Holocene at archaeological sites in Brittany, France, *The Holocene*, 3(4), 333–341. doi: 10.1177/095968369300300405.

Goffer, Z. (2008) *Archaeological Chemistry*. New York: John Wiley & Sons.

Goldberg, P. (2000) Micromorphology and site formation at Die Kelders Cave I, South Africa, *Journal of Human Evolution*, 38(1), 43–90. doi: 10.1006/jhev.1999.0350.

Goldberg, P. and Macphail, R. I. (2006) *Practical and Theoretical Geoarchaeology*. Somerset: Wiley.

Goldsmith, Y., Broecker, W. S., Xu, H., Polissar, P. J., deMenocal, P. B., Porat, N., Lan, J., Cheng, P., Zhou, W. and An, Z. (2017) Northward extent of East Asian monsoon covaries with intensity on orbital and millennial timescales, *Proceedings of the National Academy of Sciences*, 114(8), 1817–1821. doi: 10.1073/pnas.1616708114.

Guo, M. J. (2014) The macroscopic study on the settlements of Liangzhu Culture, *Archaeological Report*, 1, 1–32. (in Chinese)

Guo, W. M. (2007) The build of the moat and wall of Chengtoushan site and its settlement change, *Southern Relics*, 2, 70–82. (in Chinese)

Harrower, M. J. (2010) Geographic Information Systems (GIS) hydrological modeling in archaeology: an example from the origins of irrigation in Southwest Arabia (Yemen), *Journal of Archaeological Science*, 37(7), 1447–1452. doi: 10.1016/j.jas.2010.01.004.

He, K., Lu, H., Zheng, Y., Zhang, J., Xu, D., Huan, X., Wang, J. and Lei, S. (2018) Middle-Holocene sea-level fluctuations interrupted the developing Hemudu culture in the lower Yangtze River, China, *Quaternary Science Reviews*, 188, 90–103. doi: 10.1016/j.quascirev.2018.03.034.

He, N. (2002) The discussion of applying historical literature in archaeological research, *Huaxia Archaeology*, 1, 206–111. (in Chinese)

He, N. (2013) The Longshan period site of Taosi in Southern Shanxi Province, in Underhill, A. P. (ed.) *A companion to Chinese archaeology*. Hoboken: John Wiley & Sons Inc.

Holliday, V. and Gartner, W. (2007) Methods of soil P analysis in archaeology, *Journal of Archaeological Science*, 34(2), 301–333.

Holt, E. (ed.) (2019) *Water and Power in Past Societies*. New York: State Univ of New York Pr.

Hong, X. Q. (1991) The formation and evolution of the Tai Lake, *Marine Geology and Quaternary Geology*, 1991, 4, 87–99. (in Chinese)

Hori, K., Saito, Y., Zhao, Q., Cheng, X., Wang, P., Sato, Y., Li, C. (2001) Sedimentary facies and Holocene progradation rates of the Changjiang (Yangtze) delta, China, *Geomorphology*, 41, 233–248.

Hori, K., Saito, Y., Zhao, Q., Wang, P. (2002) Evolution of the coastal depositional systems of the Changjiang (Yangtze) River in response to late Pleistocene Holocene sea-level changes, *Journal of Sedimentary Research*, 72, 884-897.

Hou, N. N. (2016) *A study on the Qianshanyang Culture*. Masters Dissertation. Jilin University. (in Chinese)

Hu, L., Chao, Z., Gu, M., Li, F., Chen, L., Liu, B., Li, X., Huang, Z., Li, Y., Xing, B. and Dai, J. (2013) Evidence for a Neolithic Age fire-irrigation paddy cultivation system in the lower Yangtze River Delta, China, *Journal of Archaeological Science*, 40(1), 72–78.

Hu, X. (2013) *Research on geomorphic and sedimentary basis for the Neolithic Liangzhu City within the Hangjiahu Plain*. Masters Dissertation. East China Normal University. (In Chinese)

Hu, Y., Zhou, B., Lu, Y., Zhang, J., Min, S., Dai, M., Xu, S., Yang, Q. and Zheng, H. (2020) Abundance and morphology of charcoal in sediments provide no evidence of massive slash-and-burn agriculture during the Neolithic Kuahuqiao culture, China, *Plos One*. 15(8), p. e0237592. doi: 10.1371/journal.pone.0237592.

Huang, J. H. *et al.* (2002) Study on High-Resolution Carbon, Oxygen Isotope and Trace Element Records and Paleoclimate from Heshang Cave, the Middle Reach of the Yangtse River, *Acta Sedimentologica Sinica*, 20(3), 442–446. (In Chinese)

Innes, J. B., Zong, Y., Chen, Z., Chen, C., Wang, Z. and Wang, H. (2009) Environmental history, palaeoecology and human activity at the early Neolithic forager/cultivator site at Kuahuqiao, Hangzhou, eastern China, *Quaternary Science Reviews*, 28(23–24), 2277–2294. doi: 10.1016/j.quascirev.2009.04.010.

Innes, J. B., Zong, Y., Wang, Z. and Chen, Z. (2014) Climatic and palaeoecological changes during the mid- to Late Holocene transition in eastern China: high-resolution pollen and non-pollen palynomorph analysis at Pingwang, Yangtze coastal lowlands, *Quaternary Science Reviews*, 99, 164–175. doi: 10.1016/j.quascirev.2014.06.013.

Issar, A. S. and Zohar, M. (2007) *Climate Change: Environment and History of the Near East*. New York: Springer Berlin Heidelberg.

Jacob, J., Disnar, J.-R., Boussafir, M., Spadano Albuquerque, A. L., Sifeddine, A. and Turcq, B. (2005) Pentacyclic triterpene methyl ethers in recent lacustrine sediments (Lagoa do Caçó, Brazil), *Organic Geochemistry*, 36(3), 449–461. doi: 10.1016/j.orggeochem.2004.09.005.

Ji, X. (2016) *The geochemistry and provenance of the sediments of Liangzhu sites and their implications on the collapse of Liangzhu civilization*. Masters Dissertation. Nanjing University. (In Chinese)

Jiang, L. P. (2013) The Early Neolithic Age of the Qiantangjiang Basin and Its Cultural Lineage, *Southeast Culture*, 6, 44–53. (In Chinese)

- Jin, T. (2018a) *Study on the human and land relationship in Liangzhu period based on GIS*. Masters Dissertation. China University of Geosciences (Beijing). (In Chinese)
- Jin, X. (2018b) *Study on the spatial pattern of settlement sites supported by GIS in Liangzhu ancient city, Zhejiang province*. Masters Dissertation. Nanjing University. (In Chinese)
-
- Jin, X. S. *et al.* (2005) Paleo-environment research about the Liangzhu site Groups in Yuhang District, in Zhejiang Provincial Institute of Archaeology (ed.) *Liangzhu sites Group*. Beijing: Cultural relics publishing house. (In Chinese)
- Jin, Y., Mo, D., Li, Y., Ding, P., Zong, Y. and Zhuang, Y. (2019) Ecology and hydrology of early rice farming: geoarchaeological and palaeo-ecological evidence from the Late Holocene paddy field site at Maoshan, the Lower Yangtze, *Archaeological and Anthropological Sciences*, 11(5), 1851–1863. doi: 10.1007/s12520-018-0639-1.
- Jonas Berking (ed.) (2010) *Water Management in Ancient Civilizations*. Berlin: Edition Topoi.
- Karkanias, P. and Goldberg, P. (2010) Phosphatic Features, in Stoops, G., Marcelino, V., and Mees, F. (eds) *Interpretation of Micromorphological Features of Soils and Regoliths*. Amsterdam: Elsevier, 521–541. doi: 10.1016/B978-0-444-53156-8.00023-4.
- Karkanias, P. and Goldberg, P. (2018) *Reconstructing Archaeological sites: Understanding the Geoarchaeological Matrix*. Hoboken; Chichester, West Sussex: Wiley Blackwell.
- Keefe, L. (2012) *Earth Building: Methods and Materials, Repair and Conservation*. London: Routledge.
- Kennett, D.J. and Kennett, J.P. (2006) Early state formation in Mesopotamia: sea levels, shorelines, and climate change, *J. Island Coast. Archaeol.* 1, 67–99. doi:10.1080/15564890600586283
- Kennett, D.J. and Marwan, N. (2015) Climatic volatility, agricultural uncertainty, and the formation, consolidation and breakdown of preindustrial agrarian states, *Phil. Trans. R. Soc. A* 373, 20140458. <http://dx.doi.org/10.1098/rsta.2014.0458>
- Kennett, D.J. *et al.* (2012) Development and disintegration of Maya political systems in response to climate change, *Science* 338, 788–791. doi:10.1126/science.1226299
- Kovda, I. and Mermut, A. R. (2010) Vertic Features, in Stoops, G., Marcelino, V., and Mees, F. (eds) *Interpretation of Micromorphological Features of Soils and Regoliths*. Amsterdam: Elsevier, 109–127. doi: 10.1016/B978-0-444-53156-8.00007-6.
- Kühn, P., Aguilar, J. and Miedema, R. (2010) Textural Pedofeatures and Related Horizons, in Stoops, G., Marcelino, V., and Mees, F. (eds) *Interpretation of Micromorphological Features of Soils and Regoliths*. Amsterdam: Elsevier, 217–250. doi: 10.1016/B978-0-444-53156-8.00011-8.

- Li, B. (2014) *Environmental evolution of eastern Taihu Plain during the Holocene achieved by Pingwang core*. Doctoral Dissertation. Nanjing University.
- Li, C. (2013) *Research on the environmental archaeology of the Yujiashan site in Hangjiahu Plain*. Masters Dissertation. East China Normal University. (In Chinese)
- Lian, H. R. (2015) *Rice harvesting, processing, storage and charring at Mojiaoshan site, Liangzhu Culture*. Masters Dissertation. University College London.
- Lin, J. X., Zhang, S. L., Qiu, J. B. *et al.* (1989) Quaternary marine transgressions and paleoclimate in the Yangtze River Delta region, *Quaternary Research*, 32(3), 296–306.
- Lindbo, D. L., Stolt, M. H. and Vepraskas, M. J. (2010) Redoximorphic Features, in Stoops, G., Marcelino, V., and Mees, F. (eds) *Interpretation of Micromorphological Features of Soils and Regoliths*. Amsterdam: Elsevier, 129–147. doi: 10.1016/B978-0-444-53156-8.00008-8.
- Liu, B. (2019a) The construction of Liangzhu City, in Zhejiang Provincial Institute of Cultural Relics and Archaeology (ed.) *A comprehensive study of Liangzhu Ancient City*. Beijing: Cultural relics publishing house, 59–68. (In Chinese)
- Liu, B. (2019b) The vicissitude of Liangzhu and climate, in Zhejiang Provincial Institute of Cultural Relics and Archaeology (ed.) *A comprehensive study of Liangzhu Ancient City*. Beijing: Cultural relics publishing house, 300–305. (In Chinese)
- Liu, B., Zhao, Y., Chen, M. H., Yan, K. K., Wang, Y. L., Zhu, Y. F., Song, S. (2019a) Archaeological findings inside the city, in Zhejiang Provincial Institute of Cultural Relics and Archaeology (ed.) *A comprehensive study of Liangzhu Ancient City*. Beijing: Cultural relics publishing house, 136–199. (In Chinese)
- Liu, B., Wang, N. Y., Chen, M. H. (2019b) Archaeological findings of the city walls, in Zhejiang Provincial Institute of Cultural Relics and Archaeology (ed.) *A comprehensive study of Liangzhu Ancient City*. Beijing: Cultural relics publishing house, 102–135. (In Chinese)
- Liu, B., Wang, N. Y., Zhao, Y., Yan, K. K., Chen, M. H. (2019c) Archaeological findings outside the city, in Zhejiang Provincial Institute of Cultural Relics and Archaeology (ed.) *A comprehensive study of Liangzhu Ancient City*. Beijing: Cultural relics publishing house, 200–235. (In Chinese)
- Liu, B., Chen, M. H., Zhu, Y. F., Song, S. (2019d) Elite burials inside the city, in Zhejiang Provincial Institute of Cultural Relics and Archaeology (ed.) *A comprehensive study of Liangzhu Ancient City*. Beijing: Cultural relics publishing house, 69–101. (In Chinese)
- Liu, B., Qing, L., and Zhuang, Y. J. (eds) (2020) *Liangzhu Culture: Society, Belief, and Art in Neolithic China*. 1st edn. London: Routledge. doi: 10.4324/9781315151014.
- Liu, B. and Wang, N. Y. (2014) Findings of Archaeological Survey of Prehistoric City

- at Liangzhu During 2006-2013, *Southeast Culture*, 238(2), 31–38 (in Chinese)
- Liu, B. and Wang, N. Y. (2016) The use of digital methods in large archaeological sites: the example from Liangzhu, *China Cultural Relics*, 2, 25–29. (In Chinese)
- Liu, B., Wang, N., Chen, M., Wu, X., Mo, D., Liu, J., Xu, S. and Zhuang, Y. (2017) Earliest hydraulic enterprise in China, 5,100 years ago, *Proceedings of the National Academy of Sciences*, 114(52), 13637–13642. doi: 10.1073/pnas.1710516114.
- Liu, H. W. (2010) The closeness of geographical region and the synthesis of regional culture: based on the geographical elements of the prehistory culture development in Tai Lake region, *Archaeology and Relics*, 3, 32–37. (In Chinese)
- Liu, J. G. and Wang, H. (2018) A study of water control engineering outside of the ancient Liangzhu City supported by spatial analysis techniques, *Jiangnan Archaeology*, 4, 111–116. (In Chinese)
- Liu, Y. (2014) *Environmental change of Hangzhou Bay coast since the Mid Holocene - a highlight to the formation of Liangzhu City complex*. Doctoral Dissertation. East China Normal University. (in Chinese)
- Liu, Y., Ma, C., Fan, D., Sun, Q., Chen, J., Li, M. and Chen, Z. (2018) The Holocene Environmental Evolution of the Inner Hangzhou Bay and Its Significance, *Journal of Ocean University of China*, 17(6), 1301–1308. doi: 10.1007/s11802-018-3562-2.
- Liu, Y., Sun, Q., Thomas, I., Zhang, L., Finlayson, B., Zhang, W., Chen, J. and Chen, Z. (2015) Middle Holocene coastal environment and the rise of the Liangzhu City complex on the Yangtze delta, China, *Quaternary Research*, 84(3), 326–334. doi: 10.1016/j.yqres.2015.10.001.
- Long, T., Qin, J., Atahan, P., Mooney, S. and Taylor, D. (2014) Rising waters: New geoarchaeological evidence of inundation and early agriculture from former settlement sites on the southern Yangtze Delta, China, *The Holocene*, 24(5), 546–558. doi: 10.1177/0959683614522309.
- Lu, W. (2014) *Characteristics of pollen assemblage and climate change in holocene at the BHQ core, Pingyao, Zhejiang*. Masters Dissertation. Zhejiang Normal University. (In Chinese)
- Lucero, L. J. (2002) The Collapse of the Classic Maya: A Case for the Role of Water Control, *American Anthropologist*, 104(3), 814–826. doi: 10.1525/aa.2002.104.3.814.
- Luzzadder-Beach, S., Beach, T., Hutson, S., & Krause, S. (2016) Sky-earth, lake-sea: Climate and water in Maya history and landscape, *Antiquity*, 90(350), 426–442. doi:10.15184/aqy.2016.38
- Lv, Q., Dong, C., Xu, H., Wang, N., Liu, B., Ma, X., Gu, H., Zhou, C. and Wu, W. (2015) The morphological characteristics and source of the bedding-stones from Liangzhu city wall, *Huaxia Archaeology*, 2, 79–88. (In Chinese)

Ma, C. (2012) *The evolution of environment and geomorphology during the Holocene of the East Tiao creek plain, Hangzhou Zhejiang provinces and its linkage with the Neolithic Civilization*. Masters Dissertation. East China Normal University. (In Chinese)

Macphail, R. I. (2009) Marine inundation and archaeological sites: first results from the partial flooding of Wallasea Island, Essex, UK., *Antiquity Project Gallery*, antiquity.ac.uk/projgall/macphail/.

Macphail, R. I., and Crowther, J. (2013) Appendix B: Soil micromorphology Tables, in Bates, M., and Stafford, E. (eds.) Thames Holocene. *A Geoarchaeological Approach to the Investigation of the River Floodplain for High Speed 1, 1994–2003*, 191-200.

Macphail, R. I. and Goldberg, P. (2010) Archaeological Materials, in Stoops, G., Marcelino, V., and Mees, F. (eds) *Interpretation of Micromorphological Features of Soils and Regoliths*. Amsterdam: Elsevier, 589–622. doi: 10.1016/B978-0-444-53156-8.00026-X.

Macphail, R. I. and Goldberg, P. (2017) Occupation surfaces and use of space, in *Applied Soils and Micromorphology in Archaeology*. 1st edn. Cambridge: Cambridge University Press. doi: 10.1017/9780511895562.

Macphail, R. I., Cruise, G. M., Allen, M. J., Linderholm, J. and Reynolds, P. (2004) Archaeological soil and pollen analysis of experimental floor deposits; with special reference to Butser Ancient Farm, Hampshire, UK, *Journal of Archaeological Science*, 31(2), 175–191. doi: 10.1016/j.jas.2003.07.005.

Macphail, R.I. and Crowther, J. (2008) Soil micromorphology, chemistry and magnetic susceptibility, in M. Leivers and C. Moore (ed.) *Archaeology on the A303 Stonehenge Improvement*. Wessex Archaeology: Salisbury.

Macphail, R. I., Allen, M. J., Crowther, J., Cruise, G. M., and Whittaker, J. E. (2010) Marine inundation: effects on archaeological features, materials, sediments and soils, *Quaternary International*, 214, 44-55.

Maher, B. A. and Thompson, R. (eds) (1999) *Quaternary Climates, Environments and Magnetism*. Cambridge: Cambridge University Press.

Maher, L., Banning, E., and Chazan, M. (2011) Oasis or Mirage? Assessing the Role of Abrupt Climate Change in the Prehistory of the Southern Levant, *Cambridge Archaeological Journal*, 21(1), 1-30. doi:10.1017/S0959774311000011

Malville, J.M., Wendorf, F., Mazar, A.A., Schild, R. (1998) Megaliths and Neolithic astronomy in southern Egypt. *Nature* 392, 488–491.

Mao, L. J. *et al.* (2007) Environmental Change since Mid-Pleistocene Recorded in Shangshan Archaeological site in Zhejiang, *Acta Geographica Sinica*, 63(3), 293–300. (In Chinese)

Matsui, A., Kiguchi, D., Matsusaki, T., Eda, M., Maruyama, M., Liu, B. & Wang, N. (2016) Animal remains unearthed from the Meirendi locus of Liangzhu site,

in Matsui, A. & Kiguchi, D. (ed.) *The origin and diffusion of livestock and poultry in Neolithic East Asia: new zooarchaeological evidence from China*. Nara: Nara National Research Institute for Cultural Properties, 51–53

Matthews, W. (2017) Tells, in Gilbert, A. S. (ed.) *Encyclopedia of Geoarchaeology*. Dordrecht: Springer Netherlands, 951–972. doi: 10.1007/978-1-4020-4409-0_148.

Matthews, W., and Postgate, J. N., with, Payne, S., Charles, M. P., and Dobney, K., (1994) The imprint of living in a Mesopotamian city: questions and answers, in Luff, R., and Rowley Conwy, P. (eds.), *Whither Environmental Archaeology?* Oxford: Oxbow Books, 171–212.

Mays, L. (ed) (2010) *Ancient Water Technologies*. Dordrecht: Springer.

McMahon, A. (2020) Early Urbanism in Northern Mesopotamia, *Journal of Archaeological Research*, 28(3), 289–337. doi: 10.1007/s10814-019-09136-7.

Middleton, W. D. (2004) Identifying chemical activity residues on prehistoric house floors: A Methodology and rationale for multi-elemental characterization of a mild acid extract of anthropogenic sediments, *Archaeometry*, 46(1), 47–65. doi: 10.1111/j.1475-4754.2004.00143.x.

Middleton, G. D. (2012). Nothing Lasts Forever: Environmental Discourses on the Collapse of Past Societies. *Journal of Archaeological Research*, 20(3), 257–307. <https://doi.org/10.1007/s10814-011-9054-1>

Mithen, S. (2010) The domestication of water: water management in the ancient world and its prehistoric origins in the Jordan Valley, *Philosophical Transactions of the Royal Society A: Mathematical, Physical and Engineering Sciences*, 368(1931), 5249–5274. doi: 10.1098/rsta.2010.0191.

Mithen, S. and Black, E. (2011) *Water, Life and Civilisation: Climate, Environment and Society in the Jordan Valley*. Cambridge: Cambridge University Press. doi: 10.1017/CBO9780511975219.

Mo, D. W., Jin, Y. X., Shi, C. X. (2019) Report of environmental study of Liangzhu city and its surrounding zones, in Zhejiang Provincial Institute of Cultural Relics and Archaeology (ed.) *A comprehensive study of Liangzhu Ancient City*. Beijing: Cultural relics publishing house, 378–396. (In Chinese)

Ningbo Institute of Archaeology. (2014) *Juzhang City: excavation and probing report*. Beijing: Science Press. (In Chinese)

Nishimoto, K., Ito, M., Natori, S. and Ohmoto, T. (1965) The structure of arundoin, the triterpene methyl ether from *Imperata cylindrica* var. *Media* and *Arundo conspicua*, *Tetrahedron Letters*, 6(27), 2245–2251. doi: 10.1016/S0040-4039(00)70366-2.

Pagliai, M. and Stoops, G. (2010) Physical and Biological Surface Crusts and Seals, in Stoops, G., Marcelino, V., and Mees, F. (eds) *Interpretation of Micromorphological Features of Soils and Regoliths*. Amsterdam: Elsevier, 419–440. doi: 10.1016/B978-0-

444-53156-8.00019-2.

Peng, Y. (2013) *Characteristics of climate around 4.0ka BP and its impacts on the collapse of Liangzhu Civilization in the Taihu Lake Region*. Masters Dissertation. East China Normal University. (In Chinese)

Pennington, B.T., Hamdan, M.A., Pears, B.R. and Sameh, H.I. (2019) Aridification of the Egyptian Sahara 5000–4000 cal BP revealed from x-ray fluorescence analysis of Nile Delta sediments at Kom al-Ahmer/Kom Wasit, *Quaternary International*, 108-118. doi:10.1016/j.quaint.2019.01.015.

Petrie, C. A., Singh, R. N., Bates, J., Dixit, Y., French, C. A. I., Hodell, D. A., Jones, P. J., Lancelotti, C., Lynam, F., Neogi, S., Pandey, A. K., Parikh, D., Pawar, V., Redhouse, D. I. and Singh, D. P. (2017) Adaptation to Variable Environments, Resilience to Climate Change: Investigating Land, Water and Settlement in Indus Northwest India, *Current Anthropology*, 58(1), 1–30. doi: 10.1086/690112.

Qin, L. (2013) The Liangzhu Culture, in Underhill, A. (ed.) *A companion to Chinese Archaeology*. Hoboken: John Wiley & Sons Inc.

Qin, L. (2019) The formation of Liangzhu City: Preliminary chronological study, in Zhejiang Provincial Institute of Cultural Relics and Archaeology (ed.) *A comprehensive study of Liangzhu Ancient City*. Beijing: Cultural relics publishing house, 335–377. (In Chinese)

Qin, L. (2020) Power and belief: Reading the Liangzhu Jade and society, in Liu, B., Qin, L., and Zhuang, Y. (eds) *Liangzhu culture: society, belief and art in Neolithic China*, London: Routledge.

Qin, J., Wu, G., Zheng, H., and Zhou, Q. (2008) The palynology of the first hard clay layer (late Pleistocene) from the Yangtze Delta, China, *Review of Palaeobotany and Palynology*, 149 (1), 63-72.

Rawson, J. (1995) *Chinese jade: from the Neolithic to the Qing*. London: Published for the Trustees of the British Museum by British Museum Press.

Renfrew, C. and Liu, B. (2018) The emergence of complex society in China: the case of Liangzhu, *Antiquity*, 92(364), 975–990. doi: 10.15184/aqy.2018.60.

Robert McC. Adams (1978) Strategies of Maximization, Stability, and Resilience in Mesopotamian Society, Settlement, and Agriculture, *Proceedings of the American Philosophical Society*, 122(5), 329–335.

Saxton, R. H. (1995) The Performance of Cob as a Building Material, *The Structural Engineer*, 73(7), 111–115.

Scarborough, V. L. (2003) *The Flow of Power: Ancient Water Systems and Landscapes*. Santa Fe: SAR Press.

Shanghai Municipal Commission for the Preservation of Ancient Monuments (2002)

Maqiao: Report on Excavation between 1993 and 1997. Shanghai: Shanghai Fine Arts Publisher. (in Chinese)

Shanghai Museum. (2002) The excavated report on the Neolithic site GUANG FU LIN, Songjiang, Shanghai during 1999-2000. *Kaogu*, 10, 31–48 (in Chinese).

Shi, X. G. (1938) *Liangzhu*. Hangzhou: Zhejiang Province Education Department Press. (In Chinese)

Shu, J., Wang, W., Jiang, L. and Takahara, H. (2010) Early Neolithic vegetation history, fire regime and human activity at Kuahuqiao, Lower Yangtze River, East China: New and improved insight, *Quaternary International*, 227(1), 10–21.

Song, B., Li, Z., Saito, Y., Okuno, J., Li, Z., Lu, A., Hua, D., Li, J., Li, Y. and Nakashima, R. (2013) Initiation of the Changjiang (Yangtze) delta and its response to the mid-Holocene sea level change, *Palaeogeography, Palaeoclimatology, Palaeoecology*, 388, 81–97. doi: 10.1016/j.palaeo.2013.07.026.

Song, J. (2008) The use and hierarchy of jade in Liangzhu culture, *The bulletin of the Shanghai Museum*, 371–381.

Song, S. (2019) A summary of current studies on animal remains unearthed from Liangzhu sites, in Zhejiang Provincial Institute of Cultural Relics and Archaeology (ed.) *A comprehensive study of Liangzhu Ancient City*. Beijing: Cultural relics publishing house, 426–440. (In Chinese)

Song, X. (2012) *Research on the yellowish silt sediments of Late Liangzhu Culture in the Southwest Hangzhou-Jiaxing-Huzhou Plain*. Masters Dissertation. East China Normal University. (In Chinese)

Stanley, D.J., Chen, Z.Y. (2000) Radiocarbon dates in China's Holocene Yangtze delta: record of sediment storage and reworking, not timing of deposition, *Journal of Coastal Research*, 16, 1126-1132.

Sternberg, R.S., (2001) Magnetic properties and archaeomagnetism, in Brothwell, D.R., and Pol-lard, A.M. (ed.) *Handbook of archaeological sciences*. Chichester: John Wiley & Sons, Ltd.

Steward, J. H. (1955) *Irrigation Civilizations: A Comparative Study; a Symposium on Method and Result in Cross-cultural Regularities*. Social Science Section, Department of Cultural Affairs, Pan American Union.

Stoops, G (2003) *Guidelines for Analysis and Description of Soil and Regolith Thin Sections*. Madison: Soil Science Society of America.

Stoops, G. and Delvigne, J. (1990) Morphology of Mineral Weathering and Neoformation. II Neoformations**International Training Center for Post-Graduate Soil Scientists-Ghent Publication n° 89/010, in Douglas, L. A. (ed.) *Developments in Soil Science*. Amsterdam: Elsevier, 483–492. doi: 10.1016/S0166-2481(08)70363-5.

- Stuiver, M., Reimer, P. J., Bard, E., Beck, J. W., Burr, G. S., Hughen, K. A., Kromer, B., McCormac, G., Van Der Plicht, J. and Spurk, M. (1998) INTCAL98 Radiocarbon Age Calibration, 24,000–0 cal BP, *Radiocarbon*, 40(3), 1041–1083. doi: 10.1017/S0033822200019123.
- Su, J. L., Wang, K.S. (1989) Changjiang River plume and suspended sediment transport in Hangzhou Bay, *Continental Shelf Research*, 9(1), 93–111.
- Tang, L., Shu, J., Chen, J. and Wang, Z. (2019) Mid- to late Holocene vegetation change recorded at a Neolithic site in the Yangtze coastal plain, East China, *Quaternary International*, 519, 122–130. doi: 10.1016/j.quaint.2018.12.031.
- Törő, B. and Pratt, B. (2015) Characteristics and Implications of Sedimentary Deformation Features in the Green River Formation (Eocene) in Utah and Colorado, *Utah Geological Association Guidebook*, 44, 371–422.
- Wang, H. (2013) The date of the origination of the chinese characters seen from the comparison of the oracles bone and bronze inscriptions and the archaeological materials: Also on the word-forming pottery marks of Liangzhu culture and the date of the chinese characters, *Acta Archaeologica Sinica*, 3, 283–296. (In Chinese)
- Wang, J. J. and Jiang, L. P (2016) The use-wear and residue analysis of stone tools from Shangshan site, *Southern Relics*, 3, 117–121. (In Chinese)
- Wang, N. Y. (2019) The construction technique and engineering research of the Liangzhu City, in Zhejiang Provincial Institute of Cultural Relics and Archaeology (ed.) *A comprehensive study of Liangzhu Ancient City*. Beijing: Cultural relics publishing house, 285–299. (In Chinese)
- Wang, S., Ge, J., Kilbourne, K. H. and Wang, Z. (2020) Numerical simulation of mid-Holocene tidal regime and storm-tide inundation in the south Yangtze coastal plain, East China, *Marine Geology*, 423, 106–134. doi: 10.1016/j.margeo.2020.106134.
- Wang, X., Mo, D., Li, C., Yu, S.-Y., Xue, B., Liu, B., Wang, H. and Shi, C. (2017) Environmental changes and human activities at a fortified site of the Liangzhu culture in eastern China: Evidence from pollen and charcoal records, *Quaternary International*, 438, 189–197. doi: 10.1016/j.quaint.2017.05.001.
- Wang, Y. (2014) Analysis of paleo diet and skeletal pathology of Liangzhu culture tombs from the Guangfulin site, *Southern Relics*, 2, 177–180. (In Chinese)
- Wang, Y. L. (2013) *A Research on the Archaeological Cultures of Circum-Taihu Lake Plain during the Majiabang Period*. Masters Dissertation. Shandong University. (In Chinese)
- Wang, Y., Cheng, H., Edwards, R. L., He, Y., Kong, X., An, Z., Wu, J., Kelly, M. J., Dykoski, C. A. and Li, X. (2005) The Holocene Asian Monsoon: Links to Solar Changes and North Atlantic Climate, *Science*, 308(5723), 854. doi: 10.1126/science.1106296.

Wang, Z., Ryves, D. B., Lei, S., Nian, X., Lv, Y., Tang, L., Wang, L., Wang, J. and Chen, J. (2018) Middle Holocene marine flooding and human response in the south Yangtze coastal plain, East China, *Quaternary Science Reviews*, 187, 80–93. doi: 10.1016/j.quascirev.2018.03.001.

Wang, Z., Zhuang, C., Saito, Y., Chen, J., Zhan, Q. and Wang, X. (2012) Early mid-Holocene sea-level change and coastal environmental response on the southern Yangtze delta plain, China: implications for the rise of Neolithic culture, *Quaternary Science Reviews*, 35, 51–62. doi: 10.1016/j.quascirev.2012.01.005.

Weiss, H. (1997) Late third millennium abrupt climate change and social collapse in west Asia and Egypt. In Dalfes, H. N., Kukla, G., and Weiss, H. (eds.) *Third Millenium BC Climate Change and Old World Collapse, NATO ASI, Series I, Global Environmental Change, Vol. 49*. Springer: Berlin, 711–723.

Weiss, H. (2000) Beyond the Younger Dryas: Collapse as adaptation to abrupt climate change in ancient west Asia and the eastern Mediterranean. In Bawden, G., and Reyecraft, R. M. (eds.) *Environmental Disaster and the Archaeology of Human Response, Anthropological Papers No. 7, Maxwell Museum of Anthropology*. Albuquerque: NM, 75–98.

Weiss, H. (2016) Global megadrought, societal collapse and resilience at 4.2-3.9 ka BP across the Mediterranean and west Asia, *Past Global Change Magazine*, 24(2), 62–63. doi: 10.22498/pages.24.2.62.

Weiss, H., and Bradley, R. S. (2001) What drives societal collapse? *Science* 291, 609–610.

Wen, L. (2011) *Study about the prehistory wall-sites in Middle Yangtze River*. Masters Dissertation. Nanjing Normal University. (In Chinese)

Wheeler, H.E. (1958) Time stratigraphy, *AAPG Bulletin*, 42, 1047-1063.

White, J. C. (1995) Modeling the Development of Early Rice Agriculture: Ethnoecological Perspectives from Northeast Thailand, *Asian Perspectives*, 34(1), 37–68.

Wieder, M. and Yaalon, D.H. (1982) Micromorphological fabrics and developmental stages of carbonate nodular forms related to soil characteristics, *Geoderma*, 28(3-4), 203–220.

Wittfogel, K. A. (1957) *Oriental despotism: a comparative study of total power*. New Haven: Yale University Press.

Wu, L., Zhu, C., Zheng, C., Li, F., Wang, X., Li, L. and Sun, W. (2014) Holocene environmental change and its impacts on human settlement in the Shanghai Area, East China, *Catena*, 114, 78–89. doi: 10.1016/j.catena.2013.10.012.

Wu, W. T. (1983) Holocene Palaeogeography along the Hangzhou Bay as constructed on the basis of Neolithic cultural remains, *Acta Geographica Sinica*, 38(2), 113–127.

(In Chinese)

Wu, W. T. (1987) Some problems about the geography vicissitude in Hangzhou, *Historical Geography*, 5, 176–184. (In Chinese)

Wu, W., Zheng, H., Hou, M. and Ge, Q. (2018) The 5.5 cal ka BP climate event, population growth, circumscription and the emergence of the earliest complex societies in China, *Science China Earth Sciences*, 61(2), 134–148. doi: 10.1007/s11430-017-9157-1.

Wu, X. (2019) A preliminary analysis of the plant remains unearthed from Zhongjiagang Watercourse, Liangzhu City, in Zhejiang Provincial Institute of Cultural Relics and Archaeology (ed.) *A comprehensive study of Liangzhu Ancient City*. Beijing: Cultural relics publishing house, 441–445. (In Chinese)

Xiang, Y. H. (2015) Regional water environment and the change of Neolithic cultures in Zhejiang, *Zhejiang Academic Journal*, 4, 44–52. (In Chinese)

Xu, G. R. et al. (1997) *On a building model of late Permian reefs in the central Yangtze River Area*. Wuhan: China University of Geosciences Press. (In Chinese)

Xu, R. Y. (1995) The formation and change of Qiantang river system, *Zhejiang Geology*, 11(2), 40–49. (In Chinese)

Xu, Y., Yao, S., Soetaert, K., Fan, X. (2020) Effects of salt marsh restoration on eukaryotic microbenthic communities in the Yangtze Estuary, *Mar Ecol Prog Ser*, 638, 39–50. <https://doi.org/10.3354/meps13242>

Yan, L., Li, M. T., Sun, Q. and Chen, Z. Y. (2014) Palaeoclimatic and environmental changes since the Mid-Holocene in the Hangzhou Bay and their possible impacts on the evolution of Liangzhu Culture, *Journal of Lake Sciences*, 26, 322–330. doi: 10.18307/2014.0220.

Yan, Q. S. and Huang, S. (1987) The change of the deposition environment of Hangjiahu Plain in Holocene, *Acta Geographica Sinica*, 42(1), 113–127. (In Chinese)

Yi, S., Saito, Y. and Yang, D.-Y. (2006) Palynological evidence for Holocene environmental change in the Changjiang (Yangtze River) Delta, China, *Palaeogeography, Palaeoclimatology, Palaeoecology*, 241(1), 103–117.

Yi, S., Saito, Y., Zhao, Q. and Wang, P. (2003) Vegetation and climate changes in the Changjiang (Yangtze River) Delta, China, during the past 13,000 years inferred from pollen records, *Quaternary Science Reviews*, 1501–1519.

Yu, X. (2016) *The investigation of provenance in the Hangjiahu Plain during the Middle and Late Holocene*. Masters Dissertation. East China Normal University. (In Chinese)

Yunfei, Z. (2009) Rice fields and modes of rice cultivation between 5000 and 2500 BC in east China, *Journal of Archaeological Science*, 36 (12), 2609–2616.

- Zhang, F. F. (2003) "Hang Gray" marble: Geological Features of the seam limestone layer, *Geological Architectural Materials*, 12, 43–46. (in Chinese)
- Zhang, L., Chen, Z. Y., Liu, Y., *et al.* (2014) The emergence of the ancient city Liangzhu with large-scale hydrological development in the Yangtze Delta and its bearings on environmental geography, *Scientia Sinica Terrae*, 44(5), 957–966. (in Chinese)
- Zhang, M. H. (2004) Flooding was responsible for the sudden demise of Liangzhu culture, *Jiangnan Archaeology*, 1, 62–64. (in Chinese)
- Zhang, Q., Zhu, C., Liu, C. L., Jiang, T. (2004) Environmental change of Yangtze Delta since 7000BP, *Acta Geographica Sinica*, 59(4), 534–542. (In Chinese)
- Zhang, X., Dalrymple, R. W. and Lin, C. M. (2018) Facies and stratigraphic architecture of the late Pleistocene to early Holocene tide-dominated paleo-Changjiang (Yangtze River) delta, *GSA Bulletin*, 130(3–4), 455–483. doi: 10.1130/B31663.1.
- Zhang, Y. X. (2017) *Environmental and vegetation history variabilities archived by pollen-spore of the drill core Beihuqiao2 in Hangjiahu Plain during the Mid-Late Holocene, China*. Masters Dissertation. Zhejiang Normal University. (In Chinese)
- Zhang, Z. H. (2001) The distribution pattern of the Neolithic sites in China, *Southern Relics*, 1, 50–53. (In Chinese)
- Zhao, H. (2016) The progress and significance of the excavation of Shimao site in Shannxi Province, *Weekly of China's Cultural Relics*, 3, 8–23. (In Chinese)
- Zhao, H., Wei, J. (2002) The discovery and research on the walled sites on Neolithic China, *Ancient Civilizations*, 1, 1–34. (In Chinese)
- Zhao, Y. (2001) The human sacrifice in Liangzhu, *Southern Relics*, 1, 32–37. (In Chinese)
- Zhao, Y. (2002) The survey of Liangzhu site Groups in Yuhang District, *Cultural Relics*, 10, 47–56. (In Chinese)
- Zhao, Y. (2015) Uncover the Daxiong Mountain and Guanjintou site--pursuing the origin of Liangzhu Civilization, *Public Archaeology*, 7, 19–25.
- Zhao, B., Wang, Z., Chen, J., Chen, Z. (2008) Marine sediment records and relative sea level change during late Pleistocene in the Changjiang delta area and adjacent continental shelf, *Quaternary International*, 186, 164-172.
- Zhejiang Provincial Institute of Cultural Relics and Archaeology, (2001) The second excavation report of Huiguanshan Cemetery, Liangzhu Culture, *Wenwu*, 12, 36–40. (In Chinese)
- Zhejiang Provincial Institute of Cultural Relics and Archaeology, (2003a) *Hemudu*.

- Beijing: Cultural relics publishing house. (In Chinese)
- Zhejiang Provincial Institute of Cultural Relics and Archaeology, (2003b) *Yaoshan*. Beijing: Cultural relics publishing house. (In Chinese)
- Zhejiang Provincial Institute of Cultural Relics and Archaeology, (2004) *Kuahuqiao*. Beijing: Cultural relics publishing house. (In Chinese)
- Zhejiang Provincial Institute of Cultural Relics and Archaeology, (2005a) *Fanshan*. Beijing: Cultural relics publishing house. (In Chinese)
- Zhejiang Provincial Institute of Cultural Relics and Archaeology, (2005b) *Liangzhu sites Group*. Beijing: Cultural relics publishing house. (In Chinese)
- Zhejiang Provincial Institute of Cultural Relics and Archaeology, (2005c) *Miaoqian*. Beijing: Cultural relics publishing house. (In Chinese)
- Zhejiang Provincial Institute of Cultural Relics and Archaeology, (2008) The 2006-2007 excavation of Liangzhu ancient city in Yuhang County, Hangzhou, *Kaogu*, 7, 3–10. (In Chinese)
- Zhejiang Provincial Institute of Cultural Relics and Archaeology, (2014) *Bianjiashan*. Beijing: Cultural relics publishing house. (In Chinese)
- Zhejiang Provincial Institute of Cultural Relics and Archaeology. (2015a) The detection of the periphery of Liangzhu city and the excavations on Meirendi and Biandanshan, *Kaogu*, 1, 14–29 (in Chinese)
- Zhejiang Provincial Institute of Cultural Relics and Archaeology. (2015b) The surveys and research on the water control engineering on the periphery of the Liangzhu ancient city, *Kaogu*, 1, 3–13 (in Chinese)
- Zhejiang Provincial Institute of Cultural Relics and Archaeology and Huzhou Museum, (2014) *Qianshanyang: a report on the third and fourth excavations of the site*. Beijing: Cultural relics publishing house. (In Chinese)
- Zhejiang Provincial Institute of Cultural Relics and Archaeology and Pujiang Museum (2007) The excavation report of Shangshan site in Pujiang County, Zhejiang, *Kaogu*, 9, 7–18. (In Chinese)
- Zheng, C. G. (2005) *Environmental archaeology on the temporal-spatial distribution of culture sites in Taihu Lake area during 7~4 ka BP*. Doctoral Dissertation. Nanjing University. (In Chinese)
- Zheng, H., Zhou, Y., Yang, Q., Hu, Z., Ling, G., Zhang, J., Gu, C., Wang, Y., Cao, Y., Huang, X., Cheng, Y., Zhang, X. and Wu, W. (2018) Spatial and temporal distribution of Neolithic sites in coastal China: Sea level changes, geomorphic evolution and human adaption, *Science China Earth Sciences*, 61(2), 123–133. doi: 10.1007/s11430-017-9121-y.

- Zheng, L. B., Hao, X. D., Zhuo, B., Liu, Y. L., Wang, X. L., Zhu, L. X., Yu, X. B., Zhang, Y. J. (2016) Holocene palaeoenvironment evolution and human activity of the Hemudu-Tianluoshan sites in Yuyao of Zhejiang Province, *Journal of Palaeogeography*, 18(5), 879–894. (In Chinese)
- Zheng, Y., Chen, X. and Ding, P. (2014) Studies on the archaeological paddy fields at Maoshan site in Zhejiang, *Quaternary sciences*, 34, 85–96.
- Zheng, Y. F., Chen, X. G., Zhao, Y., Wang, N. Y., Liu, B. (2019) A report of the plant remains unearthed from Bianjiashan and Meirendi sites, in Zhejiang Provincial Institute of Cultural Relics and Archaeology (ed.) *A comprehensive study of Liangzhu Ancient City*. Beijing: Cultural relics publishing house, 445–472. (In Chinese)
- Zheng, Y., Sun, G. and Chen, X. (2012) Response of rice cultivation to fluctuating sea level during the Mid-Holocene, *Chinese Science Bulletin*, 57(4), 370–378. doi: 10.1007/s11434-011-4786-3.
- Zheng, Y.F., Jiang, L.P., (2007) Remains of ancient rice unearthed from the Shangshan site and their significance, *Chinese, Kaogu*, 9, 19–25. (In Chinese)
- Zhongyuan Chen and Stanley, D. J. (1998) Sea-Level Rise on Eastern China's Yangtze Delta, *Journal of Coastal Research*, 14(1), 360–366.
- Zhou, H., Zheng, X. M. (2000) The impact of environmental changes on the development of prehistoric civilization: the decline of the ancient Liangzhu Culture in the southern plain of Yangtze River Delta, *Journal of East China Normal University (Natural Science)*, 4, 71–77. (In Chinese)
- Zhu, C., Song, J., You, K. Y. *et al.* (1996) Formation of the cultural interruptions of the Maqiao site in Shanghai, *Chinese Science Bulletin*, 41(2), 148–152. (In Chinese)
- Zhu, C., Zheng, C. G., Ma, C. M. *et al.* (2003) On the Holocene sea-level highstand along the Yangtze Delta and Ningshao Plain, East China, *Chinese Science Bulletin*, 48(24), 2672–2683. (In Chinese)
- Zhuang, Y., Ding, P. and French, C. (2014) Water management and agricultural intensification of rice farming at the late-Neolithic site of Maoshan, Lower Yangtze River, China, *The Holocene*, 24(5), 531–545.
- Zhuang, Y. and Altaweel, M. (eds.) (2018) *Water Societies and Technologies from the Past and Present*. London: UCL Press.
- Zong, Y. (2004) Mid-Holocene sea-level highstand along the Southeast Coast of China, *Quaternary International*, 117(1), 55–67. doi: 10.1016/S1040-6182(03)00116-2.
- Zong, Y., Chen, Z., Innes, J. B., Chen, C., Wang, Z. and Wang, H. (2007) Fire and flood management of coastal swamp enabled first rice paddy cultivation in east China, *Nature*, 449(7161), 459–462. doi: 10.1038/nature06135.
- Zong, Y., Innes, J., Wang, Z. and Chen, Z. (2011) Mid-Holocene coastal hydrology

and salinity changes in the east Taihu area of the lower Yangtze wetlands, China, *Quaternary Research*, 76(1), 69–82.

Appendix 1 Laboratory protocols of bulk analysis and thin section making

1. pH Protocol

OPERATIONAL GUIDE

INITIAL PREPARATION

The meter is supplied complete with a 9V battery. Remove the battery compartment cover on the back of the meter, install the battery while paying attention to its polarity.

Always remove the electrode protective cap before taking any measurements. If the electrode has been left dry, soak the tip in HI 70300 storage solution for half an hour to reactivate it. Connect the pH electrode to the DIN connector on the top of the instrument.

Turn the meter ON by pressing the ON/OFF key.

TAKING pH MEASUREMENTS

To take a pH measurement simply submerge the electrode tip (at least 4cm/1½") into the sample to be tested.

Select the pH mode. Shake briefly and wait a couple of minutes for the reading to stabilize. The display will show the pH value automatically compensated for temperature variations.

In order to take accurate pH measurements, make sure that the instrument has been calibrated for pH before use.

If measurements are taken in different samples successively, it is recommended to rinse the electrode thoroughly to avoid cross-contamination. After cleaning, rinse the electrode with some of the sample to be measured.

TAKING ORP MEASUREMENTS

Connect the ORP electrode to the DIN connector on the top of the meter.

To enter the "mV" mode (ORP, Oxidation Reduction Potential) turn the instrument ON and press the mV key.

To take the mV measurement of a sample submerge the ORP electrode tip (at least 4 cm/1½") into the solution to be tested. Wait a few minutes for the reading to stabilize.

TAKING TEMPERATURE MEASUREMENTS

Turn the instrument ON, press the °C key and allow the reading to stabilize.

pH CALIBRATION

For greatest accuracy, frequent calibration of the instrument is recommended. The instrument should be recalibrated for pH:

- whenever the pH electrode is replaced
- at least once a month
- after testing aggressive chemicals
- where extreme accuracy is required

PREPARATION

Pour small quantities of pH7.01 (HI 7007) and pH4.01 (HI 7004) buffer solutions into two clean beakers.

For accurate calibration use two beakers for each buffer solution, the first one for rinsing the tip of the electrode, the second one for calibration. In this way contamination of the buffers is minimized.

To obtain accurate readings, use pH7.01 (HI 7007) and pH4.01 (HI 7004) buffers if you are going to measure acidic samples, or pH7.01 (HI 7007) and pH10.01 (HI 7010) for alkaline measurements.

If you need to calibrate the meter to NIST standards, use pH6.86 (HI 7006) instead of pH7.01 and pH9.18 (HI 7009) instead of pH10.01.

PROCEDURE

- Connect the pH electrode and switch the meter ON.
- Remove the protective cap from the electrode, rinse the tip with some pH7.01 solution, then immerse the electrode into a pH7.01 buffer solution; stir gently and wait a couple of minutes for thermal equilibrium to be reached.

Note: the electrode should be submerged approximately 4 cm (1½") into the solution.

- Press the °C key to display the temperature of the buffer (e.g. 20°C).
- Press the pH key to read pH values. Stir gently and wait for a couple of minutes.
- Adjust the STD trimmer on the lower left of the front panel until LCD shows the pH value at the noted temperature.

- Rinse and immerse the pH electrode in pH4.01 or pH10.01 buffer (2nd calibration point) and stir gently.
- Wait a couple of minutes and adjust the SLOPE trimmer on the lower right of the front panel until the LCD shows the pH value at the noted temperature.



The pH calibration is now complete.

pH VS. TEMPERATURES

TEMP °C	pH VALUES		
	4.01	7.01	10.01
0	4.01	7.13	10.32
5	4.00	7.10	10.24
10	4.00	7.07	10.18
15	4.00	7.04	10.12
20	4.00	7.03	10.06
25	4.01	7.01	10.01
30	4.02	7.00	9.96
35	4.03	6.99	9.92
40	4.04	6.98	9.88
45	4.05	6.98	9.85
50	4.06	6.98	9.82
55	4.07	6.98	9.79
60	4.09	6.98	9.77
65	4.11	6.99	9.76
70	4.12	6.99	9.75

BATTERY REPLACEMENT

When the battery becomes weak, the meter displays a blinking additional decimal point on the left side of the LCD.

When the low battery indicator appears only a few hours of battery life is remaining. A low battery level may also result in unreliable measurements. It is recommended to replace the battery immediately.

Unscrew the 3 screws on the back of the meter, remove the battery cover and replace the battery while paying attention to its polarity.

Replacement must only take place in a non-hazardous area using an alkaline 9V battery.

ACCESSORIES

- HI 1217D Double junction, gel filled pH-electrode with built-in temperature sensor, DIN connector and 1 m (3.3') cable
- HI 3618D Platinum ORP-electrode with built-in temperature sensor, DIN connector and 1 m (3.3') cable
- HI 4619D Gold ORP-electrode with built-in temperature sensor, DIN connector and 1 m (3.3') cable
- HI 7004M pH 4.01 buffer solution, 230 mL bottle
- HI 7007M pH 7.01 buffer solution, 230 mL bottle
- HI 7010M pH 10.01 buffer solution, 230 mL bottle
- HI 70300M Storage solution, 230 mL bottle
- HI 7061M General cleaning solution, 230 mL bottle
- HI 7091M Reducing pretreatment solution, 230 mL bottle
- HI 7092M Oxidizing pretreatment solution, 230 mL bottle
- HI 731326 Calibration screwdriver (20 pcs)
- HI 76405 Electrode holder

CE DECLARATION OF CONFORMITY



2. Magnetic Susceptibility

Magnetic Susceptibility is a good and potentially non-destructive method of analysis which can give an initial look inside the core this can be measured in two ways. Either discrete samples can be placed in pots, weighed and the magnetic susceptibility per unit weight measured, or readings can be taken along a core measuring the fluctuations in magnetic susceptibility for a constant volume.

Equipment

- Bartington magnetic susceptibility metre.
- Either, pot (discrete sample) coil or a (core) reader attachment.
- Plastic pots and lids (if using discrete samples).
- Recording sheet appropriate to method.
- Booked bench space to use the equipment in!

Preparation of Discrete Samples

- Sediment samples are put into 10 cm³ plastic pots so that the pot is full to the top, and weighed. An average weight of empty pots is taken to subtract from the full pot weight. The pots are labelled with permanent marker pen.
- Samples are put in a drying oven overnight at no higher than 35 degrees C - take care not to melt the plastic pots!
- The samples are then removed from the oven, the lids fastened on and the dry weights recorded.

4. The magnetic susceptibility metre is set up and zeroed, it may take some time for the metre to stabilise so it is worth setting up the machine half an hour before you start taking readings. Any large metal objects such as metal trays, watches or belt buckles should be kept away from the metre.

Analysis of Discrete Samples

The readings are taken as follows:

1. The machine beeps at regular intervals (15.01 sec.). At the first beep the sample hole is empty and the value noted (A).
2. The sample is then lowered into the hole and the second beep value ignored as this covers the time whilst the pot was being placed into position.
3. The third and fourth beep values are recorded (B & C) the sample is then removed.
4. The fifth beep is ignored and the sixth beep value recorded (D). The values recorded measure a background magnetic field before and after the sample value.
5. The next sample is then measured in the same way.
6. When a routine is established there is usually enough time to move samples so that blank value D can become blank value A for the subsequent sample. Taking these two readings allows compensation to be made for natural drift in the earth's magnetic field.
7. As a final reading an empty pot is measured.
 - Top tip - now empty the sample into a sediment tube and use for particle size analysis.

Calculation

The magnetic susceptibility of a sample is calculated in the following way:

$$\frac{(B+C)}{2} - \frac{(A+D)}{2}$$

dry weight of sample

3. This gives the magnetic susceptibility of the sample in SI units /g dry weight.
4. Then the magnetic susceptibility value for the empty pot is subtracted to allow for the magnetic properties of the sample pot, to give a final value.

3. Phosphate Analysis Protocol

Methodology for Phosphate and Phosphorus using the Colorimetre

Sample preparation:

1. Grind and sieve out <2mm fraction of soil sample
2. Weigh out 1g of <2mm soil
3. Add to 100ml of distilled water; mix well; wait 5 minutes
4. Filter off liquid using a filter cone

Sample measurement:

5. Turn on colorimetre
6. Select Method menu, Select Phosphate (or Phosphorus)
7. Pour 10ml of liquid from step 4 into cuvette, and replace cap
8. Place in colorimetre, aligning the white and blue dots
9. Press the zero key; the display will show “-0.0-“
10. Remove the cuvette
11. Add 10 drops of Molybdate reagent A

12. Add one sachet of reagent B, and shake gently
13. Place cuvette in colorimetre
14. Press Timer, wait and press Read; the instrument should display the results in mg/l of phosphate (PO₄ 3-)
15. Press Chem Frm key to convert the measurement to mg/l of phosphorus (P)
16. Wash out cuvette with water and repeat.

4. Loss-on-Ignition Protocol

Equipment

- Balance - 2 or 3 decimal place, eg. in 1g, 10% accuracy = 0.1g, 1% accuracy = 0.01g, 0.1% accuracy = 0.001g
- Crucibles of an appropriate size for the samples - differently numbered
- Desiccator - with purple silica gel, if white put in 105°C oven for 6 hours to dry out.
- Drying oven - Must be booked in advance!
- Heat proof gloves.
- Muffle Furnace - capable of up to 1000oC - Must be booked in advance!
- Tongs.
- Trays & stack - capable of withstanding 1000oC.
- Volumetric Sampler.

If you have large batches of samples, using a Sartorius balance connected to a pc is a useful way to speed up collection of data.

Protocol (%water, bulk density, %organic, %calcium carbonate, %silicate residue)

- Clean dry, numbered porcelain crucibles are weighed empty.
- Approximately 1g of wet sediment is placed in the crucible, and the wet weight recorded. If bulk density of the sample is required a calibrated 1 cm³ brass volumetric sampler should be used and the sample should be weighed, allowing mass per unit volume to be calculated.
- Crucibles should then be placed on trays, the tray rack may be required if large numbers of samples are being processed.
- The samples are dried for 6 hours (until constant weight is achieved) usually overnight at 105oC in either the Drying Oven or Muffle Furnace. Remove trays carefully using the heat proof gloves. Use tongs to place crucibles in desiccator until they reach a temperature at which they can be handled safely. The desiccator prevents the absorption of water from the atmosphere and therefore weight gain. Then weigh samples again.
- The samples are transferred to a muffle furnace then heated to 550oC for at least six hours (overnight), the furnace should then be reduced to ~100oC, when this temperature has been reached samples should be allowed to cool in a desiccator to a temperature at which they can be safely handled, then weighed.
- The samples are then returned to the furnace and heated to 950oC for at least six hours (overnight) the furnace should then be reduced to ~100oC, when this temperature has been reached samples should be allowed to cool in a desiccator to a temperature at which they can be safely handled, then weighed.

Results

- The weight loss when the samples are dried at 105 oC (wet weight - dry weight) represents of the amount of pore-water held within the sample. The percentage of water should be expressed as a proportion of the wet weight. If the volume of the sample taken is known then the "Bulk Density" can be calculated from

this, expressed as weight of sample per unit volume, e.g. g/cm³ (g cm⁻³).

- The weight loss between 105 and 550°C as a percentage of the total original dry sample weight is the % organic material. This probably also includes water loss from clay minerals, this is likely to be a insignificant addition.
- The weight loss between 550 and 950°C is representative of the amount of CO₂ released from the sample. This can be used to calculate the amount of CaCO₃ present in the sample by using the ratio between the molecular weights, expressed as a percentage of the total original dry sample weight this is the % carbon.

Calculation (molecular weights in brackets)

- Ca (40.08) + C (12.01) + O₃ (3 x 16.00) = CaCO₃ (100.09)
- C (12.01) + O₂ (2 x 16.00) = CO₂ (44.01) Removed between 550 - 950 °C
- Ca (40.08) + O (16.00) = CaO (56.08) Remains in sample
- So to calculate the quantity of CaCO₃ the weight of CO₂ lost must be multiplied by a factor to account for the CaO remaining in the sample.
- CaCO₃ (100.09) / CO₂ (44.01) = 2.274
- So the part of the sample that is represented by the CaO is 2.274 times that of the known CO₂.
- So to calculate the quantity of CaCO₃ in a sample the weight lost between 550 - 950 °C must be multiplied by 2.274.
- The weight of the residue remaining after 950°C, minus the adjustment for carbon, as a percentage of the total original dry sample weight is expressed as the % silicate residue.

% Coal

When analysing samples for CCRU a slightly different method is used. The samples are prepared as above, and dried at 105°C, but then heated to 400°C and 480°C instead of 550 and 950°C. This distinguishes between organic matter, and coal.

5. Particle Size Analysis - Malvern Mastersizer protocol

50ml plastic tubes should be used, they should be clean and numbered with permanent marker. *

A lump of sediment approx. 1-5g is put in the bottom of the tube. If samples have been processed for magnetic susceptibility then this sample is used for particle size analysis.

Each tube is topped up with 4.4% sodium pyrophosphate (wear gloves and glasses when handling) and put in a water bath at 90°C for approximately three hours, stirring once with a glass rod.

The samples are removed from the water bath and centrifuged at 3500 rpm for 13 minutes. It is important to use the scales to balance the tubes, topping up with water if necessary.

The tubes are then removed from the centrifuge and the liquid decanted off.

Samples are now ready for the Malvern.

Switch on the power, check the drain tubes are in the sink and switch on the water supply (tap). Open the Mastersizer software on the PC.

The sample suspension unit uses glass beakers filled with tap water to present the

sample to the laser sizer. The pump rate and ultrasonic stir can both be set on the unit. Fill a beaker 4/5 full with water and lower the stirring head into place. The laser sizer automatically checks the water in the bath, measures the background and so on. When this is complete, you will have a background reading of the obscuration value of clean tap water. If this is below 1% it is now OK to add the sample.

Before adding the sample, mix it on the whirlimixer. It is important to ensure all the sample is moving freely in a vortex within the tube and that there are no lumps of clay stuck to the bottom of the tube.

A few drops of the sample should be added to the beaker with a pipette from the tube on the whirlimixer so all the particles are evenly mixed and distributed. Check the obscuration value given on the screen. An ideal value is 15%, between 10 - 20% is acceptable. If the value is too low, add another drop or two of sample, if it is too high add more water using the fill switch to dilute the sample. Analysis of the sample will proceed when the correct value is maintained for 6 seconds. When analysis has finished and the graph is plotted, drain the sample in the sink and rinse the unit three times with beakers of clean water to flush the sample away, ensuring that no particles are left. You are now ready for the next sample.

The data is automatically saved during analysis. The data and a statistical summary can be exported to an Excel file, and pdf files of the individual analyses can be made.

When analysing samples for coastal samples a slightly different preparation method is often used.

The samples are stirred to counteract settling during transit. 2-3 tablespoons of sediment are put into labelled 250ml beakers. Use two sandbaths in a fume cupboard on heat setting 2. Put the beakers onto the sandbath, ensuring they are well spaced to avoid contamination, about 15 beakers can be put on each sandbath. Pour 30% hydrogen peroxide into each beaker covering the sediment (wear lab coat, gloves and glasses when handling). Have wash bottles of meths (IMS) to hand, to control frothing of the sediments by squirting a small amount into the beaker. When the frothing has subsided then turn the sand baths up to 6 or 7. Pour more hydrogen peroxide onto the samples and control with meths. When all the organic material has been oxidised and there is no more frothing turn the heat off and leave to cool. Cover the sample with water to keep moist. Continue with analysis on Malvern as above.

6. Thin section making procedures

Edited by Prof. Charles French and Dr. Tonko Rajkovaca

Introduction

Large thin sections of soils and sediments and archaeological materials are made in the basement lab B5 of the West Building (or WB B5) of the Department of Archaeology, Downing site, University of Cambridge, under the supervision of Tonko Rajkovaca (Geoarchaeology Chief Research Technician). Risk assessments, protocols, emergency

procedures, and procedures for the importing, storing and handling of soils from non-EU countries are posted on the door of the WB B5 lab, and will be given to each person who is to undertake thin section production by the Chief Research Technician responsible prior to any lab work taking place. No lab work will be allowed out of normal business hours, nor unaccompanied by the Chief Research Technician.

Samples are collected from the field, and brought to the laboratory for drying by air, or acetone replacement (if waterlogged samples). The samples are then impregnated with crystic polyester resin, and stored to cold-cure in a ventilated cabinet for up to one month. When the resin has set, the samples are moved to an oven to be hard-cured with low heat. After the blocks have cooled, they are then sawed and cut to a desired size for the next stage of thin-section production using the Brot multi-plate grinder. The following illustrated, step-by-step guide sets out how to make a thin section of a soil/sediment block sample.

The WB B5 lab is equipped with one large ventilated cabinet, one large standing fume-cupboard, one fan-assisted standing oven, one vacuum chamber/oven, one Perspex-surround sawing unit, two multi-plate Brot grinding machines and Buehler bench-top thin-section equipment.

All products used in the production of thin-sections are solvent-based and flammable. It is lab policy that all chemical and resin preparation must be confined within a fume-cupboard. Under the guidance of the University Fire Officer, there are spillage kits, a fire-bin for flammable lab waste, one fire blanket, and the appropriate fire extinguishers in the laboratory. A First Aid Kit and Eyewash supplies are available within WB B5.

Collection and Drying of Samples

Protective Measures: All Persons working with soil, sediment, or archaeological materials should wear a lab coat in the laboratory, and vinyl or nitrile gloves if necessary.

1. Soil, sediment, and/or archaeological samples are taken from the field and brought into the lab.
2. Samples are set in open trays or plastic boxes with appropriate field markings, and cut open with scissors or a razor blade to reveal enough surface to allow air drying. Special care should be taken not to disturb the original composition and structure.
3. site designations and section orientation/profile are checked on the blocks, and written on the outside of the containers. Arrows can be added as an indication of the top of the profile, and where the block should be cut for thin-sectioning.
4. The samples are then placed on the shelves in the lab for a period of up to a month to remove moisture before impregnation. If samples arrive from the field wet, water will have to be removed by acetone replacement. See separate protocol
5. After 4-6 weeks time, the samples are taken from the shelves and placed in the oven for a final drying period, at about 35 degrees C.

6. The next step is impregnation.

Impregnation

Protective Measures: It is mandatory for all persons impregnating with resin to wear a lab coat and nitrile gloves, and work within the fume-cupboard. Safety glasses, and face-masks must be worn as additional personal protection equipment when transferring samples to the vacuum chamber, and the ventilated curing storage cupboard.

Before you start the impregnation process, make sure that you record the sample contextual details, drying times and impregnation recipe in the blue impregnation A4 folder.

1. Impregnation mixes may vary depend on the soil, sediment, and/or archaeological material type and structure. The standard mix for impregnation is 1800ml of resin, poured into a graduated plastic decanter. The colour of the resin is a clear light blue, and special attention should be given to the expiry date. All resin must be used within the shelf-life of the product, or the impregnation and cure will be poor.
2. Add 200ml of acetone to the resin to increase the viscosity. The amount of acetone needed is depend on the density, structure, and composition of the material. The acetone must be slowly folded and stirred into the resin until it disappears and amalgamates with the resin.
3. Add 1.0ml of Methyl Ethyl Ketone (MEKP), the catalyst for hardening the resin, by pipette and stirred until thoroughly mixed with the resin-acetone mix. This should take 3 to 5 minutes, and an immediate colour change from blue to green should take place. Any gloves that become contaminated with MEKP must be discarded into a sealed plastic bag, and new gloves put on to protect against potential chemical burn.
4. The samples previously placed in the oven overnight (at c. 35C) for drying, are taken to the fume cupboard for impregnation while still warm. No more than eight plastic containers should be used in each impregnation session.
5. Check that all the air bubbles in the resin from mixing have settled out, and then slowly pour around and down the inside of the container to prevent disturbance, fully immersing the samples.
6. The samples are left to infiltrate with resin by capillary rise for up to an hour within the fume cupboard. The resin level should be monitored, and further topped up if it should drop below the original immersion mark. Place the date of impregnation on the outside of the container. This will act as an aide in monitoring the length of the curing time.

7. A facemask and goggles must be worn when transferring samples to the vacuum chamber. After capillary rise, the samples are placed within the vacuum chamber, and slowly brought to 12 to 28 mercury vacuum, or until bubbles can be seen to gently evacuate from the samples. The samples are left under pressure for an initial 24-hour period.
8. After 24 hours, a second, top-up, resin mixture is prepared. After releasing the vacuum, the samples are taken from the chamber and placed in the fume cupboard. They are topped-up, and completely re-immersed in the resin, and then placed back into the vacuum chamber for a further 24 hour period, using the same 12 to 28 mercury vacuum pressure as before.
9. After the final vacuum, the samples are taken from the chamber and placed in the ventilated curing storage cupboard. Curing takes place over at least a month to six weeks, or until the blocks are completely hardened. Periodic checks should be made on the resin level in the containers, and topping-up carried out if needed.
10. The resin and MEKP used for impregnation must be stored in the ventilated curing storage cupboard after use. Beakers and associated impregnation equipment are wiped clean with acetone and tissue. The MEKP graduated cylinder must be rinsed with at least 30ml of acetone and all consequent liquid stored in the Toxic Waste Winchester. Any tissue or contaminated gloves used in the cleaning of MEKP must be disposed of separately, and placed in sealed plastic bags. All lab waste from the impregnation process is disposed of in the blue/black fire-bin. This is collected monthly for appropriate incineration.
11. After the samples have hardened, they are subjected to a final curing in the oven at 50 degree C for a 24-48 hour period.
12. The next step is sawing the blocks for thin-sectioning.

Sawing of Samples

Protective Measures: All persons using the large saw must wear a lab coat, plastic apron, rubber gloves, sleeve protectors, and ear protectors. As additional protection eye goggles or glasses, and cotton masks are available. No researcher is allowed to use the large saw unless monitored by the Chief Research Technician or laboratory director.

1. The main switches for the saw and extractor fan are turned on, and the silt- box is topped up with fresh water. Extra care is taken to hose out the drainage tray, so that all wastewater from sawing will run away smoothly to the silt-box. Any adjustments to the water spray feeding the saw blade must be made before beginning to saw the samples. **No person should ever attempt to saw samples without the saw blade being fed with water.**
2. The hardened resin blocks are brought to the sawing sled, and the plastic container is cut to separate the samples. Slow, even pressure is used to push the sawing sled with the container to the blade. The saw should be allowed to pull the block through at an even pace; extra force will cause friction problems.

3. Before making an actual cut to the block, note which face of the block is wanted for thin-sectioning. Decide the best way to cut down the block to obtain the needed sample slice, and proceed to cut the block with a plan.
4. Final sample slices should be at least 4-5mm thick. It is better to cut a thicker slice, than to cut a slice too thin to run on the thin-section machine. Ideally, two sample slices should be cut from every block for backup in the thin-sectioning process.
5. A small notch should be cut on the top of each sample slice to indicate which side of the slice is up in section.
6. The cut block, with sample slices are laid upright on newspaper, within the fume cupboard to dry. When completely dry, the sample slice needed for thin-sectioning is selected, and the face crossed and labeled with a permanent marker. The block is re-marked if needed, and put in a sealed bag with site designations.
7. When sawing is finished, care should be taken to hose out residual soil and resin. Wash off and wipe down the sawing sled and Perspex guards. Turn off the main switches for the saw.
8. Clean off all protective clothing worn whilst sawing. If the rubber gloves and plastic sleeves used are in good condition, they can be rinsed with water and hung to dry for the next use. Cotton masks and plastic aprons should be thrown away, and renewed when sawing again. Ear guards, and eye goggles or glasses for sawing must be safely stored away for next use in the laboratory.

Thin-Section Grinding of Soil Samples

Protective Measures: All students, staff, and researchers undertaking the preparation and grinding of soil samples must wear a lab coat, and nitrile gloves. Safety glasses, plastic aprons, cotton masks, and respirators are available if needed.

1. Sample slices are selected in groups of three (there are three slots on the mounting head of the thin-section machine), usually of the same size and width.
2. The slices are temporarily mounted to glass slides. The mounting mixture is 20ml of Polyester Crystic Resin, with .07ml of MEKP. Special care must be taken to wipe the thin-section face clean with acetone, in order to remove any remnant oil or dust before applying the resin. Resin is poured in small amounts onto the slice face, and spread thinly and evenly with a wooden mixing stick. A clean glass slide is then placed on top of the resin slice laid on the press. Pressure is applied on the press, and the slices are allowed to set and cure on the glass slides over a 24-hour period.
3. The machine is turned on at the wall and set to manual. On this setting, the mounting head should be rotated and wiped clean. Each slot should be liberally squirted with clean oil to remove dust and fine particles. The glued slices/slides are then placed on the mounting head, with the aid of oil squirted on the back of the glass slides. Each slice/slide should be pressed firmly into the slot, and pushed up and down to

check that it is held fast to the plate by the capillary vacuum of the oil.

4. The machine is set to automatic, and goes through a coarse wheel grinding process. As soon as all outward markings have been ground away on the slice faces, the machine is stopped. The grinding wheel is changed to a finer grade, and the machine is set to proceed grinding until a fine finish/polish is accomplished on all the slices.
5. The machine is set back to manual, and the slices/slides are taken off the machine, and set face down on a tissue to dry. They are then removed from the glass slide with a palette knife or Stanley blade, and acetone if necessary to soften the super-glue.
6. All oil from machining is wiped from the slices with blue toweling, and they are re-labelled on the rough face. They are then placed on a drying rack, and a cool/warm hair-dryer is used to blow remnant oil out of the slices. Periodic cleaning of the slices with acetone helps lift the oil during the drying-out process.
7. As soon as most oil has been removed from the slices, they can be permanently mounted to prepared, finely polished glass slides. The mounting mixture is 20ml of Polyester Crystic Resin, with .07ml of MEKP. Special care must be taken to wipe the thin-section face clean with acetone, in order to remove any remnant oil or dust before applying the resin. Resin is poured in small amounts onto the slice face, and spread thinly and evenly with a wooden mixing stick. A clean glass slide is then placed, polished face to sample, on top of the resin slice laid on the press. Pressure is applied on the press, and the slices are allowed to set and cure on the glass slides over a 24-hour period.
8. The slices/slides are then taken from the press, and remnant resin cleaned off the glasses back and sides with a Stanley blade, acetone and toweling.
9. The permanently mounted slices/slides are put in their original order back onto the sectioning machine, and the same process of coarse and fine grinding takes place to achieve finished micron-width thin-sections.
10. The thin-sections are taken from the machine, and all oil is wiped away. Hand-finishing may be needed to achieve the right over-all micron thickness for microscope analysis. Silicon Carbon sandpaper's, of assorted grades, can be used with some oil to obtain a finished section.
11. The finished thin-sections are thoroughly cleaned with acetone, and a glass cover slip is applied with the same resin mix used for permanent mounting. A spray cover is also available to seal the finished thin-sections. (Note that if you intend to do micro-probe work on the thin section, the slide should not be cover-slipped at this stage.)
12. Special care should be taken to store thin-sections properly, either in sealed plastic containers, or in a laboratory reference drawer in foam slots. Periodically, the slides should be maintained and cleaned with acetone.

Note: about half of the Liangzhu samples were made following the general protocol

introduced above. In samples of high content of clay and silt material, the resin cannot thoroughly infiltrate into the blocks. These samples were under special treatments: 1) an extra glass slide is added in the first mounting stage (procedure 2) to protect the sample to create a glass/soil/glass 'sandwich', one side of which was then ground away on the Brot thin section machine; 2) repeat procedures 7-9 if necessary to reinforce the infiltration of resin.

Appendix 2 Detailed micromorphological descriptions

T2621 8



T2621 8:1

Micro-fabric	Micromorphological Description	Interpretation
T2621 8:1 Upper Platform II 1A	<p><i>Thickness:</i> 13cm. <i>Lower boundary:</i> none.</p> <p><i>Structure and porosity:</i> similar to T2621 7:1.</p> <p><i>Mineral components and groundmass:</i> similar to T2621 7:2, except for a lower degree (40%) of impregnation from amorphous sesquioxides, and a lower content (15%) of clustered medium to coarse sand size rock fragments.</p> <p><i>Organics:</i> 2% randomly distributed dark brown to black amorphous organic fine material/micro-charcoal, <0.5mm; a layer of rotten wood, 8mm thick, 3cm long, in the middle of the fabric.</p> <p><i>Artefacts:</i> burnt clay daubs, 0.5 to 2.5cm in size, 10% of the fabric.</p> <p><i>Pedofeatures: Textural:</i> 1) dusty clay quasi- and hypo-coatings of voids, high birefringence, bright yellow (XPL), 0.1-0.5mm thick, 3% of the fabric; 2) crescentic, dusty, micro-laminated clay coatings and infillings, 0.2-0.5mm thick, high birefringence with clear extinction bands, bright yellow (XPL), 1% of the fabric; <i>Amorphous and cryptocrystalline:</i> 1) 40% of the groundmass slightly to moderately impregnated by reddish yellow (PPL) amorphous sesquioxides, mostly seen as nodules (<5mm) with distinct boundaries and amorphous impregnative mottles.</p>	<p>Constructed layer: mixture of burnt daubs, rock fragments, water, and a layer of rotten wood in a silty clay matrix.</p>

Slide thickness: 40µm, even,
no loss

T2621 7



T2621 7:1



T2621 7:2

Slide thickness: 40µm, even,
no loss

Micro-fabric	Micromorphological Description	Interpretation
T2621 7:1 Middle Platform II 1A	<p><i>Thickness:</i> 9.5cm. <i>Lower boundary:</i> distinct, clear.</p> <p><i>Structure and porosity:</i> the same as T2621 7:2, except for a higher porosity of 10%;</p> <p><i>Mineral components:</i> <i>CF limit:</i> 50µm; <i>CF ratio:</i> 35/65; <i>coarse fraction:</i> 25% moderate-sorted, angular to sub-angular, medium to fine pebble sand-size rock fragments, 0.2-12mm, clustered, most are granitoid, sandstone, quartz and feldspars grains and volcanic rock fragments rich in heavy mineral; 10% moderately sorted, very fine sand size quartz, sub-angular to sub-rounded, 50-100µm, mostly randomly distributed in the groundmass, 1/3 are unevenly clustered; <i>fine fraction:</i> 45% silt; 20% clay with high birefringence.</p> <p><i>Groundmass:</i> 60% of the groundmass impregnated by reddish yellow (PPL) amorphous sesquioxides, unimpregnated part is light grayish yellow (PPL); stipple-speckled to random striated to porostriated to granostriated b-fabric (50:30:10:10); <i>CF related distribution:</i> single space to close porphyric.</p> <p><i>Organics:</i> 3% randomly distributed dark brown to black amorphous organic fine material/micro-charcoal, <0.5mm; 1% root fragments around voids, heavily impregnated by sesquioxides, <1mm.</p> <p><i>Pedofeatures:</i> <i>Texture:</i> 1) a 1-2cm thick concentration of granitoid rich in calcite. a few thin laminations of fine material were observed on top; 5% of the fabric; 2) bright orange (XPL), very limpid clays with very high birefringence and strong extinction were incorporated in the groundmass as fragments (0.2-1mm), infillings (0.1 to 1mm) and thin (0.1-0.3mm) coatings of voids and grains, 5% of the fabric; 3) dusty clay quasi- and hypo-coatings of voids, high birefringence, bright yellow to orange (XPL), 0.1-0.5mm thick, 3% of the fabric; <i>Amorphous and cryptocrystalline:</i> 1) 60% of the groundmass moderately impregnated by reddish yellow (PPL) amorphous sesquioxides, mostly seen as nodules (<5mm) with distinct boundaries and amorphous impregnative mottles.</p>	<p>Constructed layer: mixture of rock fragments, water, and a thin concentration of granitoid rich in calcite in a silty clay matrix.</p>

<p>T2621 7:2 Lower Platform II 1A</p>	<p><i>Thickness:</i> 5cm. <i>Lower boundary:</i> none.</p> <p><i>Structure and porosity:</i> moderately developed sub-angular blocky and vesicular microstructure, the peds are accommodated, 1-2cm large; 5% vesicles, mostly <2mm large, random; 3% planar voids, partially accommodated, smooth to slightly serrated walls, <4cm long.</p> <p><i>Mineral components, groundmass and organics:</i> the same as T2621 6:2, except for a higher content (25%) of clustered medium to coarse sand size rock fragments and a low degree of amorphous sesquioxide impregnation (50%).</p> <p><i>Pedofeatures: Texture:</i> 1) dusty clay quasi- and hypo-coatings of voids, high birefringence, bright yellow to orange (XPL), 0.1-0.5mm thick, 3% of the fabric; 2) crescentic, dusty, micro-laminated clay coatings around voids, 0.2-0.5mm thick, high birefringence with clear extinction band, bright yellow to orange (XPL), 2% of the fabric; <i>Amorphous and cryptocrystalline:</i> 1) 50% of the groundmass moderate to heavily impregnated by reddish yellow (PPL) amorphous sesquioxides, mostly seen as nodules (<10mm) with distinct boundaries.</p>	<p>Constructed layer: mixture of rock fragments, and water in a silty clay matrix.</p>
---	--	--

T2621 6



Slide thickness: 40µm, even,
no loss

T2621 6:1

6:2

T2621 6:3

Micro-fabric	Micromorphological Description	Interpretation
<p>T2621 6:1 Bottom Platform II 1A</p>	<p><i>Thickness:</i> 4.5-6cm. <i>Lower boundary:</i> distinct, clear.</p> <p><i>Structure and porosity:</i> weakly developed sub-angular blocky and vesicular microstructure, the peds are accommodated, 1-2cm large; 5% vesicles, mostly <2mm large, random; 3% planar voids, partially accommodated, smooth to slightly serrated walls, <3cm long.</p> <p><i>Mineral components:</i> <i>CF limit:</i> 50µm; <i>CF ratio:</i> 25/75; <i>coarse fraction:</i> 15% moderate-sorted, angular to sub-angular, medium sand-size rock fragments, 200-400µm, clustered, most are granitoid, sandstone, quartz and feldspars grains; 10% moderately sorted, very fine sand size quartz, sub-angular to sub-rounded, 50-100µm, mostly randomly distributed in the groundmass, 1/3 are unevenly clustered; <i>fine fraction:</i> 60% silt; 15% clay with high birefringence.</p> <p><i>Groundmass:</i> 70% of the groundmass impregnated by reddish yellow (PPL) amorphous sesquioxides, unimpregnated part is light yellow (PPL); stipple-speckled to random striated to porostriated b-fabric (60:30:10); <i>CF related distribution:</i> single space to close porphyric.</p> <p><i>Organics:</i> 2% randomly distributed dark brown to black amorphous organic fine material, <0.5mm; 1% root fragments around voids, heavily impregnated by amorphous sesquioxides, <1mm.</p> <p><i>Artefacts:</i> none.</p> <p><i>Pedofeatures:</i> <i>Texture:</i> 1) thin (0.1-0.2mm) clay quasi- and hypo-coatings of voids, high birefringence, bright yellow to orange (XPL), 2% of the fabric; 2) crescentic, dusty, micro-laminated clay coatings around voids, 0.2-0.5mm thick, high birefringence, bright yellow (XPL), 1% of the fabric; <i>Depletion:</i> 1) iron depleted features around voids, 1-3mm thick; <i>Amorphous and cryptocrystalline:</i> 1) 70% of the groundmass moderate to heavily impregnated by amorphous reddish yellow (PPL) amorphous sesquioxides.</p>	<p>Constructed layer: mixture of rock fragments, and water in a silty clay matrix.</p>

<p>T2621 6:2 Platform III 3 B1</p>	<p><i>Thickness:</i> 2cm. <i>Lower boundary:</i> prominent, sharp. <i>Structure and porosity:</i> single grain structure with a chitonic c/f distribution. <i>Components:</i> CF limit: 50µm; CF ratio: 90/10; coarse fraction: whitish to light yellowish (PPL), very fine to fine gravel, 2-5mm; most of the rock types are granitoid with 30-40% calcite, with around 5% forsterite and calcites; fine fraction: red (PPL) silty clay moderate to heavily impregnated by amorphous sesquioxides, moderate to high birefringence, bright orange (XPL), parallel striated b-fabric, coated the rock fragments.</p>	<p>Constructed layer using simply prepared calcite-rich granitoids.</p>
<p>T2621 6:3 Upper Platform III 3 B2</p>	<p><i>Thickness:</i> 2.5cm. <i>Lower boundary:</i> none. <i>Structure and porosity:</i> weakly developed sub-angular blocky, the peds are accommodated, 1-2cm large; 3% planar voids, partially accommodated, slightly serrated walls, <2cm long; 2% vesicles, <3mm large, random. <i>Mineral components:</i> CF limit: 50µm; CF ratio: 5/95; coarse fraction: 4% very fine sand, 50-80; 1% medium sand-size rock fragments, 200-400; fine fraction: 75% silt, 20% clay, high birefringence. <i>Groundmass:</i> 60% of the groundmass impregnated by reddish yellow (PPL) amorphous sesquioxides, unimpregnated part is light yellow (PPL); stipple-speckled to striated b-fabric (60:40); CF related distribution: open porphyric. <i>Organics:</i> 3% weakly laminated micro-charcoal, mostly <1mm; a possible strip of bast fibre, 2cm long. <i>Pedofeatures:</i> Textural: 1) thin (0.1-0.2mm), dusty clay quasi- and hypo-coatings of voids, high birefringence, bright yellow to orange (XPL), 1%; Depletion: 1) iron depleted hypo- and quasi-coatings of voids with diffuse boundaries, 20%; Amorphous and cryptocrystalline: 1) 60% of the groundmass moderately impregnated by amorphous reddish yellow (PPL) amorphous sesquioxides, mostly seen as hypo- and quasi-coating of voids and replacement of organic material, more heavily impregnated around voids;</p>	<p>Constructed layer using silty clay material; exposed surface.</p>

T2621 5



Slide thickness: 30-50µm, uneven, moderate loss

Micro-fabric	Micromorphological Description	Interpretation
T2621 5:1 Bottom Platform III 3 B2	<p><i>Thickness:</i> 4cm. <i>Lower boundary:</i> none.</p> <p><i>Structure:</i> this fabric is the heterogeneous mix of two different soil materials (Fabrics 1 and 2); <u>Fabric 1</u>, 70% of the groundmass: fine silty clay composed by 10% very fine sand, 20% coarse silt and 70% dotted silty clay, the groundmass is light yellow (PPL) with a random striated to stipple-speckle b-fabric; <u>Fabric 2</u>, 30% of the fabric: a 3cm large humic, brown (PPL) very fine silty clay material showing perpendicular micro-laminated fine silty clay crusts.</p> <p><i>Porosity:</i> 5% chambers and vesicles, 2-10mm.</p> <p><i>Organics:</i> 2% dark brown humified and amorphous fine organic matter, randomly mixed in the groundmass, <0.5mm, and as root remnants of voids, 0.5-1mm, commonly replaced by reddish yellow (PPL) amorphous sesquioxides; 2% micro-charcoal randomly mixed in the groundmass.</p> <p><i>Artefacts:</i> none.</p> <p><i>Pedofeatures: Textural:</i> 1) Incomplete dense Infillings of micro-laminated very dusty silty clay and small aggregates (0.5mm) of fine charred materials in the voids, 5% of the fabric; <i>Depletion:</i> 1) depletion hypo-coating of brown (PPL) dusty silty clay around voids, 30% of the fabric; <i>Crystalline:</i> 1) coatings of vivianite crystals in the voids, 3% of the fabric; <i>Amorphous and cryptocrystalline:</i> 1) 8% of the groundmass weakly impregnated by amorphous reddish yellow (PPL) amorphous sesquioxides, mostly found as hypo- and quasi-coating of voids and replacement of organic material.</p>	Constructed layer, mixture of two different soil materials with charcoal clusters
T2621 5:2 Layer 12A	<p><i>Thickness:</i> 2.5cm. <i>Lower boundary:</i> prominent, sharp.</p> <p><i>Structure and porosity:</i> channel and vesicular microstructure; a 5cm long, horizontal planar voids cut off the fabric, unaccommodated with serrated walls, 5% of the fabric; 5% vesicles, 1-3mm in size.</p>	Constructed layer, modified and dumped when wet by

	<p>This micro-fabric is heterogeneous mixed of various closely compacted components: <u>Fabric 1</u>, 65% of the fabric: brown (PPL) very humic silty clay, mineral size <20µm, undifferentiated b-fabric, 3% dark brown to black humified amorphous tissue residues, 0.2-0.5mm; <u>Fabric 2</u>, 15% of the fabric: similar to Fabric 1 but is less humic and slightly coarser; <u>Fabric 3</u>, 15% of the fabric: very humic silty clay aggregates with more than 60% fragmented micro-charcoal, 1 to 5mm in size; 3% sub-angular, medium sand-size rock fragments, random; 2% humified tissue residues, <3mm, including a discontinuous inclined bedding of humified plant residues that separates different soil fabrics.</p> <p><i>Pedofeatures: Textural:</i> 1) very dusty silty clay hypo-coating of voids, 0.2-0.5mm thick, <1% of the fabric; 2) a concentric very dusty clay nodule, 2mm; <i>Crystalline:</i> 1) <1% vivianite crystals with a weathered rim, 1-2mm.</p>	human activities.
T2621 5:3 Layer 12B-4	<p><i>Thickness:</i> 2.5cm. <i>Lower boundary:</i> distinct, sharp.</p> <p><i>Structure and porosity:</i> massive; 25% slide loss; 2% interconnected, zigzag, partially accommodated channels with slightly serrated void walls, <3cm long; 1% root voids, <1mm.</p> <p><i>Mineral components and groundmass:</i> the same as T2621 4:1, except for a darker colour and an undifferentiated b-fabric due the thicker slide thickness.</p> <p><i>Organics:</i> 3% dark brown humified tissue residues and micro-charcoal, <1mm, randomly mixed in the groundmass or around root voids.</p> <p><i>Artefacts:</i> none.</p> <p><i>Pedofeatures: Amorphous and cryptocrystalline:</i> 1) 3% of the groundmass weakly impregnated by amorphous reddish yellow (PPL) amorphous sesquioxides, mostly found as hypo- and quasi-coating of voids; <i>Depletion:</i> 1) the soil material near channels and voids has a higher content of fine silty clay content, 30% of the groundmass is depleted probably due the loss of fine material during thin section making; <i>Fabric:</i> 1) 5% dark brown (PPL), rounded fragments of clayey soil fabrics, mostly <1mm, with</p>	Natural sediment under periodic waterlogging.

	moderate birefringence, randomly mixed in the groundmass.	
T2621 5:4 Layer 12B-3	<p><i>Thickness:</i> 2.5cm. <i>Lower boundary:</i> none.</p> <p><i>Structure and porosity:</i> massive; 60% slide loss; 3% fissures around fragmented soil fabrics, <1cm long.</p> <p><i>Mineral components and groundmass:</i> the same as T2621 4:1, except for:</p> <ol style="list-style-type: none"> 1) a thicker slide thickness and therefore shows darker, brown (PPL) colour and an undifferentiated b-fabric; 2) a higher content (30%) of fine fraction. <p><i>Organics:</i> 3% dark brown humified tissue residues, <1mm, random in the groundmass or around root voids and 1% charcoal fragment (<1mm), both are more concentrated in the upper part; single case shell fragment, 0.5mm.</p> <p><i>Pedofeatures: Textural:</i> 1) fragmented, thick (5-10mm), dark brown (PPL) dusty silty clay crusts on top of the fabric, 5% of the fabric; <i>Fabric:</i> 1) 10% dark brown (PPL), rounded fragments of clayey soil fabrics, all size <5mm, mostly concentrated in the upper part of the fabric.</p>	<p>Bioturbated surface with dense vegetation growth; on top is a layer of partially interconnected silty clay crust caused by drying and bioturbation.</p>

T2621 4



Slide thickness: 40µm, even, no loss

Micro-fabric	Micromorphological Description	Interpretation
T2621 4:1 Layer 12B-2	<p><i>Thickness:</i> 3cm. <i>Lower boundary:</i> faint, diffuse.</p> <p><i>Structure and porosity:</i> massive; 3% root voids with remnant amorphous organic matter, 2-8mm; 2% fissures, <3cm long.</p> <p><i>Mineral components:</i> the same as T2621 3:1.</p> <p><i>Groundmass:</i> light brown (PPL); <i>b-fabric:</i> mostly stipple-speckled, striated in the clayey soil fabrics; <i>CF related distribution:</i> close porphyric.</p> <p><i>Organics:</i> 3% humified tissue residues, laminar or around root voids, <3mm.</p> <p><i>Artefacts:</i> none.</p> <p><i>Pedofeatures: Textural:</i> 1) micro-laminated, slightly fluctuating, dusty fine silty clay crusts, 0.1-0.3mm thick, weak birefringence, 5% of the fabric; 2) thin (0.1-0.2mm) hypo-coating of micro-laminated dusty clay around voids, <1%; <i>Amorphous and cryptocrystalline:</i> 1) 10% of the groundmass weakly impregnated by amorphous reddish brown (PPL) sesquioxides; <i>Fabric:</i> 1) 5% light brown(PPL), rounded fragments of clayey soil fabrics, mostly <1mm, with moderate birefringence, randomly mixed in the groundmass.</p>	Natural alluvium sediment formed under shallow ponding condition with short-term influence of run-off.
T2621 4:2 T2621 4:3 Layer 12B-1	<p><i>Thickness:</i> 4cm. <i>Lower boundary:</i> distinct, clear.</p> <p><i>Structure and porosity:</i> massive microstructure with vesicles and fissures; 5% slide loss; 3-5% root voids with remnant amorphous organic matter, some were further infilled by topsoil, 4-10mm; 2% fissures, 0.5-3cm.</p> <p><i>Mineral components:</i> the same as T2621 3:1, except for 10% micritic calcium carbonate were incorporated in the fine fraction.</p> <p><i>Groundmass:</i> light yellow to red (PPL); stipple-speckled to calcitic crystallitic b-fabric (90:10); <i>CF related distribution:</i> close porphyric.</p> <p><i>Organics:</i> 3% light brown (PPL) humified amorphous tissue residues, mostly <2mm,</p>	Alluvial sediments deposited under slightly oxidized and dry conditions with bioturbation.

	<p>one 7mm long plant residues, randomly distributed.</p> <p><i>Artefacts:</i> none.</p> <p><i>Pedofeatures: Textural:</i> 1) thin (0.1-0.2mm) hypo-coating of micro-laminated dusty clay around voids, <1%; 2) 5% complete dense infillings of brown (PPL) calcitic clayey or silty topsoil in root voids, commonly coated by amorphous iron oxides, 2-5mm, random;</p> <p><i>Crystalline:</i> 1) pale gray (PPL) micritic calcium carbonates as hypo-coating and quasi-coating of voids with diffused boundaries, <2mm thick, 5% of the fabric; <i>Amorphous and cryptocrystalline:</i> 1) 15% of the fabric moderately to heavily impregnated by red (PPL) amorphous sesquioxides, mostly found around voids/silty clay aggregates with diffuse boundaries; 2) <1% small clusters (0.2-0.5mm) of black manganese pellets, hypo-coating around voids or randomly incorporated in the groundmass; <i>Fabric:</i> 1) 5% light brown(PPL), rounded fragments of clayey soil fabrics, <0.5mm, with moderate birefringence, randomly mixed in the groundmass.</p>	
T2621 4:3 Upper Layer 12C	<p><i>Thickness:</i> 4cm. <i>Lower boundary:</i> none.</p> <p>Structure and porosity: massive; 10% chambers caused by slide loss; 2% small root voids with remnant amorphous organic matter, 1-2mm.</p> <p>This fabric shows an alternation of coarse/fine materials. The coarse material is the same as the coarse fraction of T2621 3:1; the fine material occupies 25% of the fabric and is horizontally laminated, slightly wavy, 0.5-1mm thick, dusty silty clay crusts with a weak birefringence, parallel striated b-fabric, and exhibits a clear fining upwards texture. At the top of this fabric, the laminations were moderately disturbed.</p> <p><i>Organics:</i> the same as T2621 3:1.</p> <p><i>Pedofeatures: Amorphous and cryptocrystalline:</i> 1) 5% of the fabric weakly impregnated by reddish yellow sesquioxides.</p>	Alluvium sediment formed under shallow water ponding environment.

T2621 3



Slide thickness: 40µm, even, no loss

T2621 3:1
|
3:2
|
3:3

Micro-fabric	Micromorphological Description	Interpretation
T2621 3:1 Lower Layer 12C	<p><i>Thickness:</i> 5cm. <i>Lower boundary:</i> none.</p> <p><i>Structure and porosity:</i> massive; 3% chambers formed due to slide loss; 2% horizontal fissures, 1-2cm long; 1% small root voids with remnant amorphous organic matter, 1-2mm.</p> <p><i>Mineral components:</i> <i>CF limit:</i> 10µm; <i>CF ratio:</i> 80/20; <i>Texture:</i> 15% sand, 75% silt, 10% clay; <i>Coarse fraction:</i> 80% well-sorted, coarse silt to very fine sand size (30-80µm) minerals, most are sub-rounded single quartz grains, with 3-5% micas, random in the mid-lower part, weakly banded in the upper part; 1-2% medium sand-size rock fragments, sub-angular, 200-400µm; <i>Fine fraction:</i> 20% silty clay as small aggregates and thin crusts.</p> <p><i>Groundmass:</i> light yellow (PPL); stipple-speckled to striated b-fabric in silty clay aggregates, parallel striated in silty clay crusts, grano-striated around voids; <i>CF related distribution:</i> close porphyric.</p> <p><i>Organics:</i> 3% amorphous organic fine material, 2% fine charcoal, both are 0.2-1mm, weakly laminar in the middle and bottom part, laminated in the upper part.</p> <p><i>Artefacts:</i> none.</p> <p><i>Pedofeatures: Textural:</i> 1) horizontal wavy laminations of thin (0.2-0.5mm), dusty silty clay, concentrated in the upper part, weak birefringence, 10% of the fabric; <i>Amorphous and cryptocrystalline:</i> 1) 5% of the fabric weakly impregnated by reddish yellow amorphous sesquioxides; <i>Fabric:</i> 1) 5% rounded fragments of clayey soil fabrics, around 0.5mm in size, with moderate birefringence, randomly mixed in the groundmass; 2) aggregates of dark brown organic topsoil, 0.3-0.5mm, <2%, random.</p>	Alluvium sediment formed under shallow water ponding environment; slightly bioturbated.
T2621 3:2 12D	<p><i>Thickness:</i> 3cm. <i>Lower boundary:</i> distinct, clear.</p> <p><i>Structure and porosity:</i> massive structure with a few fissures; 2-3% voids around organic</p>	Dry vegetational surface with a

	<p>materials, 5-10mm long.</p> <p><i>Mineral components: CF limit:</i> 10µm; <i>CF ratio:</i> 65/35; <i>Texture:</i> 20% sand, 75% silt, 5% clay; <i>coarse fraction:</i> well-sorted, coarse silt to very fine sand size, sub-rounded single quartz grains 60%, 30-80µm; 3-5% coarse silt-size micas, 20-50µm; 1-2% medium sand-size rock fragments, sub-angular, 200-400µm; <i>Fine fraction:</i> 25% very fine to moderate silt; 5% micritic calcium carbonates; 5% clay.</p> <p><i>Groundmass:</i> light brown to reddish brown (PPL, 40:60); stipple-speckled to micritic calcitic cryptallitic b-fabric (95:5); <i>CF related distribution:</i> close porphyric.</p> <p><i>Organic:</i> 5% fragmented, humified, amorphous organic fine material and tissue residues, >0.1mm all size class, mostly oblique or parallel laminar; a piece of charcoal on top of the fabric, 5mm.</p> <p><i>Artefacts:</i> none.</p> <p><i>Pedofeatures: Amorphous and cryptocrystalline:</i> 1) 60% of the fabric moderately to heavily impregnated by reddish brown sesquioxides, generally seen around silty clay nodules and have diffuse boundaries; 2) 2% clusters (2mm) of black manganese pellets;</p> <p><i>Fabric:</i> 1) 30% dark brown (PPL) rounded silty clay nodules commonly coated with reddish brown amorphous sesquioxides, some of the nodules are mixed with micritic calcium carbonates, some have incorporated vivianite crystals with weathered rims (1-2mm), various size from 0.5-8mm, randomly distributed; 2) topsoil fragments with microlaminated silty clay crusts, 2-3mm, random, 1%.</p>	<p>few archaeological finds on top.</p>
<p>T2621 3:3 Upper Layer 13</p>	<p><i>Thickness:</i> 3cm. <i>Lower boundary:</i> none.</p> <p><i>Structure and porosity:</i> Crack structure; 10% planar voids, mostly horizontal, zigzag, smooth wall, partially accommodated.</p> <p><i>Mineral components: CF limit:</i> 10µm; <i>CF ratio:</i> 75/25; <i>CF related distribution:</i> close porphyric; <i>Texture:</i> 10% sand, 80% silt, 10% clay; <i>Coarse fraction:</i> well-sorted sub-angular coarse silt to very fine sand-size quartz (73%), 20-100µm, random; 2% medium</p>	<p>Alluvial sediment with short-term dryness and surface exposure.</p>

	<p>sand size rock fragments 200-500µm, random; <i>fine fraction</i>: 15% light brown (PPL) dotted silty clay; 5-8% pale gray (PPL) micritic calcium carbonate, clustered with diffuse boundaries; 5% dark brown (PPL) aggregates of fine silty clay; stipple-speckled to micritic crystallitic b-fabric.</p> <p><i>Organics</i>: 3% dark brown humified tissue residues, 0.5-2mm.</p> <p><i>Artefacts</i>: none.</p> <p><i>Pedofeatures: Amorphous and cryptocrystalline</i>: 1) 10% of the slide weakly impregnated with reddish-yellow amorphous sesquioxides; 2) <1% pyrite spherulites;</p> <p><i>Fabric</i>: 1) rounded clayey, dark brown soil fragments, 0.5 to 1mm, 5% of the fabric. 2) rounded aggregates of very dark brown topsoil, 0.-2mm, 3% of the fabric.</p>	
--	--	--

T2621 2



T2621 2:1

Micro-fabric	Micromorphological Description	Interpretation
T2621 2:1 Middle Layer 13	<p><i>Thickness:</i> 12cm. <i>Lower boundary:</i> distinct, clear.</p> <p><i>Structure and porosity:</i> massive with channels; 10% voids formed due to slide loss; 5% root voids, most with remnant organic residues, 0.5-1mm; 3% vertical channels, smooth to slightly serrated, partially accommodated, <5cm long, 0.5-2mm wide; 3% passages, 0.3-1mm.</p> <p><i>Mineral components:</i> same as Facies 3 of T2621 1:1, except for slightly higher calcium carbonate content of 5%.</p> <p><i>Organics:</i> 2% dark brown humified tissue residues around voids, 0.5-2mm; very fine charcoal mixed in the groundmass, <1%, 0.1-0.5mm.</p> <p><i>Artefacts:</i> none.</p> <p><i>Pedofeatures: Textural:</i> 1) linear channel infills of dusty clay and massive-type intercalations of fine fabric material from above layers, 1-2cm thick, 10% of the fabric; <i>Crystalline:</i> 1) vivianite crystals, 0.5-1mm, 1%; <i>Amorphous and cryptocrystalline:</i> 1) 10% of the slide weakly impregnated with reddish-yellow amorphous sesquioxides, commonly seen as hypo-coatings and complexed with organic residues.</p>	Accumulating alluvium platform with sediment inputs from dusty slurry.

Slide thickness: 30-600µm, uneven, minor loss

T2621 1



T2621 1:1

Slide thickness: 30-50µm, uneven, no loss

Micro-fabric	Micromorphological Description	Interpretation
T2621 1:1 Bottom Layer 13	<p><i>Thickness:</i> 12 cm. <i>Lower boundary:</i> none.</p> <p><i>Structure and porosity:</i> massive; 3% root voids, mostly with remnant organic material, 0.2-3cm long, mostly vertical; 3% channels, unaccommodated, straight, serrated walls, 0.5-4cm long; 3% vesicles and passages, 0.5-1mm.</p> <p>This fabric can be divided into 11 units and shows an alternating bedding of three facies: Facies 1, Facies 2, and Facies 3, which is a massive version of the combination of the first two facies.</p> <p>Facies 1 (Units 2/4/6/8/10), 20% of the fabric: around 5mm to 1cm thick silty clay crusts composed by very compact yellowish brown (PPL) very fine silty clay mixed with randomly distributed very fine charcoal (1-2%) up to 63µm in size, very weak birefringence, undifferentiated b-fabric.</p> <p>Facies 2 (Units 3/5/7/9): alternating very fine/coarse material, which is humic silty clay crusts with silt-size quartz. The humic silty clay crusts are similar to those seen in Facies 1 and are around 0.2mm thick with occasional fining upward.</p> <p>The coarse material layers: <i>CF limit:</i> 10µm; <i>CF ratio:</i> 70/30; <i>CF related distribution:</i> close porphyric; <i>Texture:</i> 10% sand, 80% silt, 10% clay; <i>Coarse fraction:</i> well-sorted sub-angular coarse silt to fine sand-size (20-100µm) quartz (60%), chlorite (5-10%), muscovite (2-3%), calcium carbonate (3-5%), weakly or very weakly oriented and parallel to the fine materials; fine fraction: 15% light yellow (PPL) dotted silty clay with weak birefringence and stipple-speckled b-fabric.</p> <p>Facies 3 (Units 1/11): a massive version of the above two types of facies and shows poor-sorting. Randomly mixture of loose aggregates of Facies 1, rounded small clay aggregates, and segments of unit 2 still preserves.</p> <p><i>Organics:</i> 2% dark brown humified tissue residues around voids, 0.5-1mm; very fine charcoal mixed in the groundmass, <2%, 0.1-0.3mm;</p>	<p>Top: wet-dry alternation with incipient soil development;</p> <p>Middle: steady sedimentation under mudflat/intertidal flat condition;</p> <p>Bottom: wet-dry alternation and incipient soil development. at the top</p>

	<p><i>Artefacts:</i> none.</p> <p><i>Pedofeatures: Textural:</i> 1) thin (0.2-0.5mm) hypo-coatings of dirty clay and hypo- and quasi-coating of iron oxide impregnated organic matter with weak birefringence around voids, <2%; 2) dense incomplete infillings of dusty silty clay material, 4/5 of the channels were filled, in Unit 1; <i>Crystalline:</i> 1) vivianite crystals, 1-2mm, <1%, in Unit 11; 2) a single case of pyrites spherulites near a void wall coated by dirty organic matter in Unit 9.</p>	
--	---	--

T5020 10



T5020 10:1

Slide thickness: 40µm, even, minor loss.

Micro-fabric	Micromorphological Description	Interpretation
T5020 10: 1 Lower part of Layer 4 and upper part of Layer 5A	<p><i>Thickness:</i> 13cm. <i>Lower boundary:</i> none.</p> <p><i>Structure and porosity:</i> moderately well-developed sub-angular to columnar blocky; 15% zone of groundmass lost during thin section making; 5% vertical root voids, 1-2mm wide; 3% channels, <5cm long, 0.2-2mm wide, accommodated, weakly serrated.</p> <p><i>Mineral components:</i> CF limit: 50µm; CF ratio: 5/95; Texture: 20% clay, 75% silt, 5% sand; <i>Related distribution:</i> open porphyric; <i>Coarse fraction:</i> 5% sub-angular fine to medium sand-size rock fragment, 50-500µm, random; <i>Fine fraction:</i> the groundmass is the mixture of 40% medium to coarse silt and 15% light gray (PPL) dotted fine silty clay with stipple-speckled b-fabric; 35% dark reddish brown (PPL) humic silty clay as infillings; 5% clay coatings; 80% of the micromass stained by amorphous sesquioxides;</p> <p><i>Organics:</i> 2% black/dark brown humified/charred tissue residues, 0.2-0.5mm, random.</p> <p><i>Artefacts:</i> none.</p> <p><i>Pedofeatures: Textural:</i> 1) 35% infillings of crescent, laminated, dusty clay in root voids, 2-5cm large, brown to red (XPL); 2) 5% limpid to slightly dusty clay with high birefringence as hypo-coatings (0.5-2mm) around voids and dense complete infillings (0.2-0.5mm), frequently impregnated by the iron oxides, red interference colour, , 5% of the fabric; <i>Amorphous and cryptocrystalline:</i> 1) 80% of the slide impregnated with reddish-yellow amorphous sesquioxides, 20% of the sesquioxides are hypo-and quasi-coating of voids and show stronger impregnations.</p>	<p>Clay-rich soil material suggestive of a well-developed, oxidized B horizon with abundant clay infills and coatings. Probably repeated illuviation indicative of frequent water saturation and drying episodes</p>

T5020 9

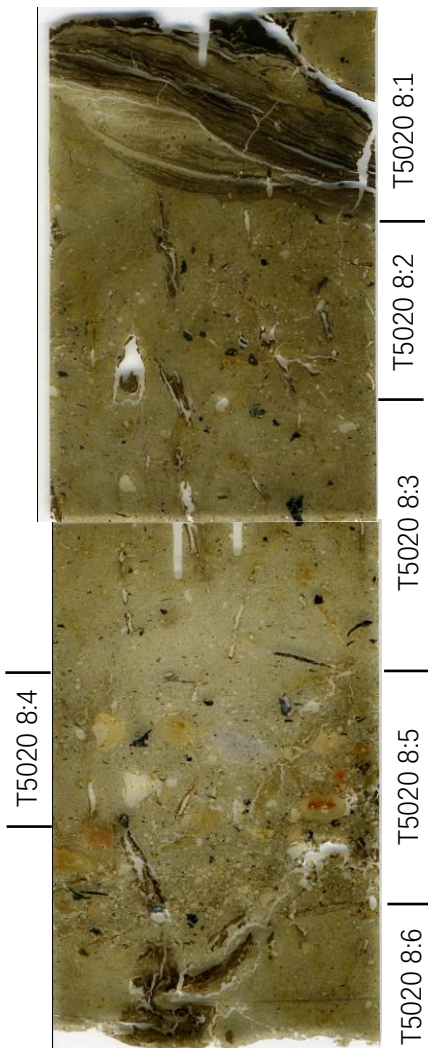


Slide thickness: 40µm, even, no loss

Micro-fabric	Micromorphological Description	Interpretation
T5020 9: 1 Lower part of Layer 5A	<p><i>Thickness:</i> 6cm. <i>Lower boundary:</i> faint, diffuse.</p> <p><i>Structure and porosity:</i> moderately well-developed sub-angular blocky; 7% channels, <6cm long, <1mm thick, accommodated, weakly serrated; 3% vesicles, 0.5-1mm.</p> <p><i>Mineral components:</i> CF limit: 50µm; CF ratio: 5/95; Texture: 20% clay, 75% silt, 5% sand; <i>Related distribution:</i> open porphyric; <i>Coarse fraction:</i> 5% sub-angular to sub-rounded fine to medium sand-size rock fragment, 50-500µm, random; <i>Fine fraction:</i> mixture of 60% light yellow (PPL) dotted fine silty clay and 35% reddish brown (PPL) humic silty clay as infillings; 20% of the micromass stained by reddish yellow (PPL) amorphous sesquioxides as hypo-coatings and mottles; stipple-speckled b-fabric.</p> <p><i>Organics:</i> 2% black/dark brown humified/charred tissue residues, 0.2-0.5mm, random.</p> <p><i>Artefacts:</i> none.</p> <p><i>Pedofeatures: Textural:</i> 1) dusty clay frequently impregnated by the iron oxides as hypo-coating of channels and root voids and complete dense infillings, 3% of the fabric, reddish yellow (PPL and XPL), medium to high birefringence, 0.2-0.5mm thick; 2) 35% dense complete infills of crescent, laminated, reddish brown (PPL) humic silty clay in root voids, 2-3cm large; <i>Crystalline:</i> 1) 3% vivianite crystals, 0.5-2mm, incomplete infillings in the voids; <i>Amorphous and cryptocrystalline:</i> 1) reddish-yellow amorphous sesquioxides as hypo- and quasi-coatings of voids with diffuse boundaries, 0.5-2mm thick, and as mottles randomly distributed in the groundmass, 10% of total groundmass.</p>	Silty clay alluvial sediments in a more oxidized, wet-dry alternated environment.
T5020 9:2 Upper part of Layer 5B	<p><i>Thickness:</i> 7cm. <i>Lower boundary:</i> none.</p> <p><i>Structure and porosity:</i> massive with vertical channels; 3% vertical root voids and channels, unaccommodated, 0.5-2cm; 2% vesicles/passages, 0.5-1mm.</p> <p><i>Mineral components:</i> CF limit: 50µm; CF ratio: 5/95; Texture: 15% clay, 80% silt, 5% sand; <i>Related distribution:</i> open porphyric; <i>Coarse fraction:</i> 5% sub-angular to sub-rounded fine to medium sand-size rock fragment, 50-500µm, random; <i>Fine fraction:</i></p>	Humic accumulation suggestive of period of surface stability and

	<p>mixture of 70% subangular to sub-rounded, moderate-sorted, medium to coarse silt-size quartz and 25% light grayish yellow (PPL) dotted fine silty clay; 15% of the micromass stained by reddish yellow (PPL) amorphous sesquioxides; stipple-speckled b-fabric.</p> <p><i>Organics:</i> 3% black/dark brown humified/charred tissue residues; 0.2-0.5mm, random.</p> <p><i>Artefacts:</i> none.</p> <p><i>Pedofeatures: Textural:</i> 1) Very thin (0.2mm) hypo-coating of dusty clay of root voids frequently impregnated by the iron oxides, 3% of the fabric; 2) 10% large infills of crescent, laminated, dusty clay in root voids; <i>Crystalline:</i> 1) 5% vivianite crystals, 0.5-2mm, incomplete infillings in the voids; <i>Amorphous and cryptocrystalline:</i> 1) 10% reddish-yellow mottles of amorphous iron oxides, randomly seen in the groundmass.</p>	<p>incipient soil formation.</p>
--	--	----------------------------------

T5020 8



Micro-fabric	Micromorphological Description	Interpretation
<p>T5020 8: 1 Middle part of Layer 5B</p>	<p><i>Thickness:</i> 1-3cm. <i>Lower boundary:</i> distinct, clear, sloping.</p> <p><i>Structure and porosity:</i> platy microstructure; 10% platy fissures, 1-3cm long; 2% small vesicles/root voids, 0.5-2mm.</p> <p>This fabric is the rhythmic alternation of two facies: Facies 1, 50% of the fabric, is 0.2-0.5mm thick fine laminations. The bottom 20% of the Facies 1 is reddish-brown to brownish slightly fluctuated, weakly fining upward, dusty, humic silty clay crusts. The upper 80% is more than fifty layers of reddish-brown laminations mixed of both dusty silty clay crusts and iron oxide impregnated or replaced laminations of organic matter.</p> <p>Facies 2, 50% of the fabric. <i>Mineral components:</i> CF limit: 50µm; CF ratio: 10/90; CF related distribution: open porphyric; <i>Texture:</i> 10% sand, 85% silt, 5% clay; <i>coarse fraction:</i> 10% sub-angular, fine to medium sand-size rock fragments, 500-500µm, random; <i>fine fraction:</i> 80% well-sorted, weakly banded, sub-angular to sub-rounded, medium to coarse silt-size quartz grains; 10% light yellow (PPL) dotted silty clay with a stipple-speckled b-fabric.</p> <p><i>Organics:</i> 3% black/dark brown humified/charred tissue residues and amorphous organic fine material.</p> <p><i>Artefacts:</i> none.</p> <p><i>Pedofeatures: Amorphous and cryptocrystalline:</i> 1) reddish brown (XPL) amorphous iron oxides complexed with organic fine material coated the root voids, commonly found in the fine material laminations (Facies 1), 2% of the fabric; <i>Fabric:</i> 1)1% dark brown aggregates of amorphous iron impregnated silty clay, randomly mixed in Facies 2, 2% of the fabric.</p>	<p>Near bank quiet and shallow environment with the introduce of organic matter that were later replaced by iron oxides.</p>

<p>T5020 8:2 Lower part of Layer 5B</p>	<p><i>Thickness:</i> 3-4.5cm. <i>Lower boundary:</i> faint, diffuse.</p> <p><i>Structure and porosity:</i> weakly developed sub-angular blocky microstructure, the ped is around 2cm in size, accommodated; 5% vertical root voids and passages, 0.5-10mm; 3% unaccommodated fissures, 0.5-2cm long.</p> <p><i>Mineral components:</i> <i>CF limit:</i> 50µm; <i>CF ratio:</i> 10/90; <i>CF related distribution:</i> close porphyric; <i>Texture:</i> 10% sand, 75% silt, 15% clay; <i>coarse fraction:</i> 10% poorly sorted, sub-angular to sub-rounded, medium to coarse sand-size rock fragments, 200-1500µm, random; <i>fine fraction:</i> 60% moderately sorted, medium to coarse silt, 30% light grayish yellow (PPL) dotted silty clay with a stipple-speckled b-fabric; 10% of the micromass stained by yellow (PPL) amorphous sesquioxides.</p> <p><i>Organics:</i> 5% randomly mixed, disoriented fine charcoal, 0.5-3mm; 2% dark brown, humified tissue residues around voids.</p> <p><i>Artefacts:</i> <1% fine bone fragments, 0.2-0.5mm; a possible phytolith slag.</p> <p><i>Pedofeatures: Textural:</i> 1) reddish brown hypo- and quasis-coatings around the voids, composed of amorphous sesquioxides and complexed with organic matter and fine silty clay, some shows crescentic features, and are alternated by limpid and dusty silty clay with moderate birefringence, varied thickness from 0.2-3mm, 5% of the fabric; 2) 3% dense infillings of dusty clay, orange (XPL), dark brown (PPL), moderate birefringence, 0.2-0.5mm; <i>Amorphous and cryptocrystalline:</i> 1) 10% mottles and impregnations of yellow to reddish yellow (PPL) amorphous sesquioxides; 2) 3% vivianite crystals with yellowish weathered rim, 1-2mm; <i>Fabric:</i> 1) 5% dark brown (PPL) dusty silty clay aggregates around voids, 0.5-1mm.</p>	<p>Decreased depositional energy with incipient soil formation process.</p>
<p>T5020 8:3 Lower part of Layer 5B</p>	<p><i>Thickness:</i> 6cm. <i>Lower boundary:</i> faint, diffuse.</p> <p><i>Structure and porosity:</i> massive with a few channels; 2% vertical, elongate, discontinuous root channels, 1mm wide; 2% 0.2-1mm large root voids/passages.</p> <p><i>Mineral components:</i> <i>CF limit:</i> 50µm. <i>CF ratio:</i> 10/90; <i>CF related distribution:</i> close porphyric; <i>Texture:</i> 10% sand, 75% silt, 15% clay; <i>coarse fraction:</i> 10% sub-angular to sub-rounded, medium to coarse sand-size rock fragments, 100-1000µm; <i>fine fraction:</i> 65% moderate-sorted, very weakly laminated, sub-angular to sub-rounded, coarse silt-size quartz 20-50µm; 20% light yellow (PPL) dotted silty clay, 3-5% parallel laminated muscovite flakes; stipple-speckled</p>	<p>Fluvial deposit with the highest depositional energy of the profile.</p>

	<p>b-fabric.</p> <p><i>Organics:</i> fine charcoal occupy around 5% of the groundmass and are parallel laminated, 1-10mm; 1% brown, humified remnant organic matter around voids.</p> <p><i>Artefacts:</i> none.</p> <p><i>Pedofeatures: Textural:</i> 1) Very thin hypo-coating of dusty clay frequently impregnated by the iron oxides, 1% of all slide. 2) <1% crescent laminated dusty silty clay crusts, found in the upper part of this fabric; <i>Amorphous and cryptocrystalline:</i> 1) 2% reddish yellow mottles of iron oxides, increase with height; 2) 1% amorphous iron compound (reddish) thin hypo-coating of voids with diffuse boundaries; 3) a single case of pyrite framboids around root voids; <i>Fabric:</i> 1) <1% 1-2mm large dusty silty clay aggregates.</p>	
T5020 8:4 Lower part of Layer 5B	<p><i>Thickness:</i> 0-3cm. <i>Lower boundary:</i> distinct, clear, sloping.</p> <p>The same as T5020 8:3 except that pebble-size and sand-size rock fragments are mixed in and occupy around 40% of the fabric.</p>	Alluvium deposit with coarse material rolled over the slope.
T5020 8: 5 Upper part of Layer 7	<p><i>Thickness:</i> 1-3.5cm. <i>Lower boundary:</i> distinct, clear, slightly fluctuating.</p> <p><i>Structure and porosity:</i> massive; 2% root voids, 0.5-1cm; 2% chambers, 1cm in width; 1% fissures near silty clay crusts.</p> <p><i>Mineral components: CF limit:</i> 50µm. <i>CF ratio:</i> 60:40; <i>Related distribution:</i> Close Porphyric; <i>Texture:</i> 5% clay, 35% silt, 60% sand; <i>coarse fraction:</i> 50-70% very poorly-sorted, sand-size to fine pebble-size rock fragments, 0.05-7mm, weakly coarser upward grading, the long axis of the flatten pebbles are horizontal laminated; <i>fine fraction:</i> 20-40% fine to medium silt-size, poorly-sorted quartz and 10% light gray (PPL) silty clay with a speckled to undifferentiated b-fabric.</p> <p><i>Organics:</i> 3% clusters of fine charcoal in-between the coarse materials, 0.5-2mm.</p> <p><i>Artefacts:</i> <1% burnt soil aggregates; three highly degraded, rounded pottery sherds, 2-5mm.</p> <p><i>Pedofeatures: Textural:</i> 1) laminated silty clay crusts covered this fabric, 1mm thick, 5% of the fabric; 2) iron impregnated dusty clay hypo-coating around the root void, 0.3-0.5mm thick, moderate birefringence, 2% of all slide; <i>Crystalline:</i> 1) <1% crystallized vivianites with weathered rims in root voids, 2-3mm; <i>Fabric:</i> 1) clay rich soil aggregates, 1-3mm, 1% of the fabric.</p>	Debris flow

<p>T5020 8: 6 Upper part of Layer 7</p>	<p><i>Thickness:</i> 2cm. <i>Lower boundary:</i> none. <i>Structure and porosity:</i> Massive with channels; 2% unaccommodated planar voids with serrated walls; 1% root voids 1-5mm in size. <i>Mineral components:</i> the same as T5020 7:1. <i>Organics:</i> Weakly laminated charcoal fragments and dark humified organic matter 0.1-2mm in size, 8% of the fabric, random. <i>Artefacts:</i> none. <i>Pedofeatures:</i> <i>Textural:</i> 1) 5% illuviated clay coatings around the void, reddish brown in XPL with moderate birefringence; <i>Crystalline:</i> 1) <1% crystallized vivianites with weathered rims, 1-2mm; <i>Amorphous and cryptocrystalline:</i> 1) 15% amorphous iron compound (reddish brown to dark brown) hypo-coating and quasi-coating of voids with diffuse boundaries, replaced of organic matter; 2) 2% iron-oxide mottles around root voids; <i>Fabric:</i> 1) 1% rounded topsoil aggregates, 0.3-0.5mm.</p>	<p>Alluvial deposits with higher depositional energy.</p>
---	--	---

T5020 7



T5020 7:1

T5020 7:2

Slide thickness: 40µm, even, minor loss.

Micro-fabric	Micromorphological Description	Interpretation
<p>T5020 7:1 Mid-lower part of Layer 7</p>	<p><i>Thickness:</i> 10cm. <i>Lower boundary:</i> distinct, clear.</p> <p><i>Structure and porosity:</i> massive with a few channels and chambers; 5% 0.2-2cm, root voids and passages.</p> <p><i>Mineral components:</i> <i>CF limit:</i> 50µm; <i>CF ratio:</i> 10/90; <i>CF related distribution:</i> open porphyric; <i>Texture:</i> 10% sand, 75% silt, 15% clay; <i>coarse fraction:</i> 5% moderate-sorted, sub-angular to sub-rounded, very fine sand size quartz, 50-80µm; 5% sub-angular medium to coarse sand size rock fragments, 100-1000µm, more concentrated in the upper part; <i>fine fraction:</i> light grayish yellow (PPL) dotted silty clay; stipple-speckled b-fabric.</p> <p><i>Organics:</i> weakly laminated charcoal fragments and dark humified organic matter 0.1-2mm in size, 5% of the fabric; 1% larger charcoal pieces around 5mm in size, concentrate in the upper part.</p> <p><i>Artefacts:</i> two obliquely laid, 3cm and 0.7cm long pottery sherds in the bottom of this layer, <1% burnt bones, 1mm.</p> <p><i>Pedofeatures:</i> <i>Crystalline:</i> 1) <1% crystallized vivianite with weathered rims, 1-2mm; <i>Amorphous and cryptocrystalline:</i> 1) 3% amorphous iron compound (reddish brown to dark brown) hypo-coating and quasi-coating of voids with diffuse boundaries, replaced of organic matter; 2) 2% amorphous iron oxide mottles around root voids; <i>Depletion:</i> 1) two lesser depleted zone of light brown (PPL) silty clay with a higher content of organic matter, 20% of the fabric; <i>Fabric:</i> 1) 1% rounded topsoil aggregates, 0.3-0.5mm, concentrate in the upper part.</p>	<p>Alluvial deposit with plant growth and pedogenesis, slightly higher depositional energy in the upper part.</p>
<p>T5020 7:2 Upper part of Layer 8</p>	<p><i>Thickness:</i> 2.5cm. <i>Lower boundary:</i> none.</p> <p><i>Structure and porosity:</i> massive microstructure with a few fissures; 60% lost in slide making; 5% 0.2-1mm round to oval root voids with remnant organic material; 3%</p>	<p>Accumulating alluvial deposit.</p>

	<p>fissures, 0.5-1mm wide, serrated walls.</p> <p><i>Mineral components: CF limit: 50µm; CF ratio: 5/95; CF related distribution: open porphyric; Texture: 5% sand, 75% silt, 20% clay; coarse fraction: 5% moderate-sorted, sub-angular to sub-rounded, very fine sand size quartz, 50-80µm; 1% sub-angular medium sand size rock fragments, 100-300µm; fine fraction: light brown (PPL) dotted humic silty clay; stipple-speckled b-fabric.</i></p> <p><i>Organics: 3% black humified tissue residues and fine charcoal 0.5-5mm in size, mostly randomly distributed, a few fine organic materials were parallel oriented.</i></p> <p><i>Artefacts: None.</i></p> <p><i>Pedofeatures: Amorphous and cryptocrystalline: 1) 1% amorphous iron compound (reddish) hypo-coating of voids with diffuse boundaries.</i></p>	
--	---	--

T5020 6



Slide thickness: 40µm, even, no loss

T5020 6:1
T5020 6:2
T5020 6:3

Micro-fabric	Micromorphological Description	Interpretation
T5020 6: 1 Middle part of Layer 8	<p><i>Thickness:</i> 5cm. <i>Lower boundary:</i> faint, diffuse.</p> <p><i>Structure and porosity:</i> moderately developed angular blocky structure, the peds are around 0.3-0.5cm in size, accommodated; 7% fissures, 0.1-0.5mm, accommodated, smooth walls; 3% vesicles, 1-4mm.</p> <p><i>Mineral components:</i> <i>CF limit:</i> 50µm; <i>CF ratio:</i> 8/92; <i>CF related distribution:</i> open porphyric; <i>Texture:</i> 8% sand, 72% silt, 20% clay; <i>coarse fraction:</i> 5% moderate-sorted, sub-angular to sub-rounded, very fine sand size quartz, 50-80µm; 3% poorly sorted, sub-angular medium to coarse sand size rock fragments, 200-1000µm, random; <i>fine fraction:</i> light yellow (PPL) dotted silty clay, 10% of the micromass moderately impregnated by reddish yellow (PPL) amorphous iron oxides; stipple-speckled to poro-striated (95:5) b-fabric.</p> <p><i>Organics:</i> 5% black humified tissue residues and fine charcoal 0.5-5mm in size, randomly distributed.</p> <p><i>Artefacts:</i> <1% 2mm bone fragments.</p> <p><i>Pedofeatures: Textural:</i> 1) micro-laminated, dusty clay hypo-coatings around voids in various thickness (0.1-0.5mm), some of which were impregnated by iron-oxide, yellow to orange in XPL, 3% of all slide; <i>Amorphous and cryptocrystalline:</i> 1) 10% crystallized vivianites with weathered rims, mostly found in voids, 1-3mm; 2) 2% clusters (1-2mm) of iron-oxide mottles were seen around crystallized vivianites and voids; <i>Fabric:</i> 1) <1% rounded dark brown topsoil fragments, 0.3-0.5mm.</p>	Accumulating alluvial plain underwent pedogenic processes and may be partly dried out.
T5020 6:2 Lower part of Layer 8	<p><i>Thickness:</i> 4cm. <i>Lower boundary:</i> faint, diffuse.</p> <p><i>Structure and porosity:</i> weakly developed angular blocky structure, the peds are around 0.5-1cm in size, accommodated; 3% planar voids, 0.1-0.5mm, smooth to slightly serrated walls; 3% vesicles and root voids, 2-10mm.</p> <p><i>Mineral components:</i> same as T5020 6:1.</p>	Accumulating alluvial plain

	<p><i>Organics:</i> 5% black humified tissue residues and fine charcoal 0.5-2mm in size, random to weakly laminated.</p> <p><i>Artefacts:</i> a 2mm large, reddened burnt soil fragment; <1% fine burnt bone, 0.3-0.5mm.</p> <p><i>Pedofeatures: Textural:</i> 1) micro-laminated hypo-coating of dusty, high birefringence clay, some of which were impregnated and further quasi-coated by iron oxides, orange in XPL, 0.1-0.3mm thick, 2% of the fabric; <i>Amorphous and cryptocrystalline:</i> 1) 7% crystallized vivianites with weathered rims, 1-3mm.</p>	
T5020 6:3 Upper part of Layer 9B	<p><i>Thickness:</i> 4cm. <i>Lower boundary:</i> none.</p> <p><i>Structure and porosity:</i> moderately developed angular blocky microstructure, accommodated peds 0.5-1cm in size; 3% channels, 1-2mm wide, partially accommodated, slightly serrated walls; 2% 1-2mm wide vesicles, smooth walls.</p> <p><i>Mineral components: CF limit:</i> 50µm; <i>CF ratio:</i> 7/93; <i>CF related distribution:</i> open porphyric; <i>Texture:</i> 7% sand, 73% silt, 20% clay; <i>coarse fraction:</i> 5% moderate-sorted, sub-angular to sub-rounded, very fine sand size quartz, 50-80µm; 2% poorly sorted, sub-angular medium to coarse sand size rock fragments, 200-2000µm, random; <i>fine fraction:</i> mixture of light brown (PPL) dotted humic silty clay, 10% dark brown (PPL) fragmented dusty silty clay crusts and 5% amorphous organic fine material; stipple-speckled to parallel striated to poro-striated (85:10:5) b-fabric.</p> <p><i>Organics:</i> 5% random to weakly laminated, black humified/charred organic matter, 0.1-1mm long; 5% 5mm large charcoal, random to weakly laminated.</p> <p><i>Artefacts:</i> burnt topsoil fragment (2cm in size); a 3cm long pottery sherd obliquely inserting into the top of the fabric.</p> <p><i>Pedofeatures: Textural:</i> 1) thick (0.5-1mm), partially fragmented, brown, dusty silty clay crusts, moderate birefringence, 10% of the fabric; <i>Amorphous and cryptocrystalline:</i> 1) 5% crystallized vivianite in the voids and incorporated in the groundmass, 1-2mm; 2) 1% amorphous iron compound (reddish) hypo-coating of voids with diffuse boundaries.</p>	Alluvium formed under slow-moving water that was later dried out.

	<i>Fabric:</i> 1) <1% silty clay topsoil aggregates.	
--	--	--

T5020 5



Slide thickness: 40µm, even,
no loss

Micro-fabric	Micromorphological Description	Interpretation
<p>T5020 5:1 Lower part of Layer 9B</p>	<p><i>Thickness:</i> 9cm. <i>Lower boundary:</i> distinct, diffuse.</p> <p><i>Structure and porosity:</i> massive with a few channels, vesicles and chambers; 5% vesicles/root voids, 2-10mm; 5% chambers, 2cm wide; 2% channels, 1mm wide, slightly serrated walls.</p> <p><i>Mineral components:</i> <i>CF limit:</i> 50µm; <i>CF ratio:</i> 10/90; <i>CF related distribution:</i> open porphyric; <i>Texture:</i> 10% sand, 80% silt, 10% clay; <i>coarse fraction:</i> 5% moderate-sorted, subangular to subrounded, very fine sand size quartz, 50-80µm; 5% poorly sorted, sub-angular medium sand size to fine pebble-size rock fragments, 0.2-7mm, random; <i>fine fraction:</i> light brown (PPL) dotted humic silty clay; stipple-speckled to poro-striated (95:5) b-fabric.</p> <p><i>Organics:</i> 5% charcoal fragments 1mm to 13mm in size, 3% humified, brownish amorphous organic fine material and tissue residues, 1/5 may be fragments of bast fibres, 0.1-2mm, both are weakly laminated to disoriented in the bottom, and laminated in the middle; 1% remnant of humified, brownish plant tissues in voids.</p> <p><i>Artefacts:</i> two pottery sherds with sharp boundaries, one is coated with fine charred material, 1-1.5cm, three rounded, degraded daubs, 1-1.5cm, <1% fine burnt bones, 0.5mm, all more concentrated in the upper part of the fabric.</p> <p><i>Pedofeatures: Textural:</i> 1) thin (0.2mm), dusty clay hypo-coated of voids, orange interference colour, moderate to high birefringence, 2% of all slide; 2) thick (0.5-2mm), iron compound (reddish) impregnated, micro-laminated, dusty silty clay hypo-coatings and quasi-coatings of large chambers and channels, moderate birefringence, 2% of all slide; <i>Amorphous and cryptocrystalline:</i> 1) 1% black pellets of manganese compound around voids; <i>Fabric:</i> 1) 1% dark reddish brown, possibly burnt aggregates with >20% micro-charcoal, 0.5-2mm; 2) aggregates composed of >70% well-sorted coarse silt-size quartz, 5% micas and 10% fine tissue residues in a less humic groundmass, 3% of all</p>	<p>Constructed platform in a dryer land with input of human occupational debris and incipient pedogenesis.</p>

	slide, appear in the upper part of the slide, 5-10mm.	
T5020 5:2 Upper part of Layer 10A	<p><i>Thickness:</i> 4cm. <i>Lower boundary:</i> none.</p> <p><i>Structure and porosity:</i> massive with a few channels; 2% vertical channels, 1mm wide, slightly serrated walls; 2% root voids/vesicles, 0.5-1mm.</p> <p><i>Mineral components:</i> <i>CF limit:</i> 50µm; <i>CF ratio:</i> 7/93; <i>CF related distribution:</i> open porphyric; <i>Texture:</i> 7% sand, 78% silt, 15% clay; <i>coarse fraction:</i> 5% moderate-sorted, sub-angular to sub-rounded, very fine sand size quartz, 50-80µm; 2% sub-angular medium sand size rock fragments, 200-400µm, random; <i>fine fraction:</i> light yellow (PPL) dotted silty clay; stipple-speckled to parallel striated b-fabric.</p> <p><i>Organics:</i> 5% weakly laminated, 1-5mm humified tissue residues; 2% 1-5mm charcoal, random.</p> <p><i>Artefacts:</i> none.</p> <p><i>Pedofeatures:</i> <i>Textural:</i> 1) incomplete dense infillings of brown fine silty clay from upper micro-fabric T5020 5:1 in vertical channels, 4/5 of the channel being filled, 1mm thick, 5% of all slide; <i>Amorphous and cryptocrystalline:</i> 1) amorphous iron compound (yellow) hypo-coating of voids with diffuse boundaries, 1% of all slide; <i>Fabric:</i> 1) 1% aggregates composed of >70% well-sorted coarse silt-size quartz, 5% micas and 15% fine organic material with a less humic groundmass, random, 1-2mm.</p>	Alluvium, slightly stronger depositional energy.

T5020 4



T5020 4:1
|
T5020 4:2

Slide thickness: 60-100µm, uneven, no loss

Micro-fabric	Micromorphological Description	Interpretation
T5020 4: 1 Lower part of Layer 10A	<p><i>Thickness:</i> 5cm. <i>Lower boundary:</i> faint, diffuse.</p> <p><i>Structure and porosity:</i> moderately separated platy microstructure; 10% planar voids, 0.5-3mm wide, slightly serrated walls. 2% vesicles and root voids, 0.2-0.5mm.</p> <p><i>Mineral components:</i> <i>CF limit:</i> 50µm; <i>CF ratio:</i> 7/93; <i>CF related distribution:</i> open porphyric; <i>Texture:</i> 7% sand, 78% silt, 15% clay; <i>coarse fraction:</i> 5% moderate-sorted, sub-angular to sub-rounded, very fine sand size quartz, 50-80µm; 2% sub-angular medium sand size rock fragments, 200-400µm, random; <i>fine fraction:</i> mixture of brown (PPL) dotted humic silty clay, 15% dark brown (PPL) fragmented dusty silty clay crusts and 3% amorphous organic fine material; stipple-speckled b-fabric.</p> <p><i>Organics:</i> 5% inclined laminated, humified tissue residues, 1-5mm, including 1% of them are a possible bast fibres, 1% fresh root fragments incorporating in the groundmass or as residues near voids; 2% randomly distributed charcoal, 0.1-2mm large.</p> <p><i>Artefacts:</i> none.</p> <p><i>Pedofeatures:</i> <i>Textural:</i> 1) thin (0.1-0.2mm), partially fragmented, dark brown, laminated, very dusty silty clay crusts, weak birefringence, 15% of the fabric; 2) 3% dense incomplete infillings of dark brown, organic-rich silty clay in cracks, commonly half-filled the cracks; <i>Crystalline:</i> 1) 2% crystallized vivianite, random, 0.2-0.5mm; <i>Amorphous and cryptocrystalline:</i> 1) amorphous iron compound (reddish) hypo-coating of voids with diffuse boundaries, 3% of all slide; <i>Fabric:</i> 1) aggregates of topsoil, 1%, 0.2mm.</p>	Alluvium, slightly stronger depositional energy.
T5020 4:2 Upper part of Layer 10B	<p><i>Thickness:</i> 8cm. <i>Lower boundary:</i> none.</p> <p><i>Structure and porosity:</i> moderately developed angular blocky microstructure, accommodated peds 0.5-2mm in size; 12% interconnected planar voids, smooth to slightly serrated walls.; 1% root voids, 0.5mm wide.</p> <p><i>Mineral components:</i> <i>CF limit:</i> 50µm; <i>CF ratio:</i> 7/93; <i>CF related distribution:</i> open</p>	Quiet, shallow water environment with mixed in of anthropogenic

	<p>porphyric; <i>Texture</i>: 7% sand, 58% silt, 35% clay; <i>coarse fraction</i>: 5% moderate-sorted, sub-angular to sub-rounded, very fine sand size quartz, 50-80µm; 2% sub-rounded medium sand size rock fragments, 200-400µm, random; <i>fine fraction</i>: mixture of brown (PPL) dotted humic silty clay, 40% dark brown (PPL) fragmented dusty silty clay crusts with weak to moderate birefringence and 3% amorphous organic fine material; parallel striated to stipple-speckled b-fabric (40:60).</p> <p><i>Organics</i>: 3% dark brownish to black, weakly laminated, humified fine organic matter; 2% 2-5mm large tissue residue, including both brown woody material, black humified grass and stem fragments and fresh root fragments incorporating in the groundmass or as residues near voids; 2% randomly distributed charcoal, 0.1-5mm large.</p> <p><i>Artefacts</i>: A small sherd was found inserting into the vertical crack on top of the fabric.</p> <p><i>Pedofeatures</i>: <i>Textural</i>: 1) thick (0.2-0.5mm), partially fragmented, dark brown, laminated, dusty silty clay crusts, weak to moderate birefringence, 40% of the fabric; 2) 2% dense incomplete infillings of dark brown, organic-rich silty clay in cracks, commonly half-filled the cracks; <i>Crystalline</i>: 1) 1% crystallized vivianite, random, 0.1-0.5mm; <i>Amorphous and cryptocrystalline</i>: 1) amorphous iron compound (reddish) hypo-coating of voids with diffuse boundaries, 3% of all slide; <i>Fabric</i>: 1) 5% aggregates composed of >70% well-sorted coarse silt-size quartz, 5% micas and 5% fine organic material with a less humic groundmass, random, 1-2mm.</p>	<p>materials.</p>
--	--	-------------------

T5020 3



T5020 3:1

T5020 3:2

Slide thickness: 60µm, even,
no loss

Micro-fabric	Micromorphological Description	Interpretation
T5020 3: 1 Lower part of Layer 10B	<p><i>Thickness:</i> 6cm. <i>Lower boundary:</i> faint, diffuse.</p> <p><i>Structure and porosity:</i> same as T5020 3:2.</p> <p><i>Mineral components:</i> same as T5020 2:1.</p> <p><i>Organics:</i> same as T5020 3:2.</p> <p><i>Artefacts:</i> none.</p> <p><i>Pedofeatures:</i> same as T5020 3:2 with 1% thin hypo-coating of dusty clay with high birefringence and orange interference colour around voids and <1% crystallized vivianites with yellowish weathered rims, random, 1-2mm.</p>	Alluvium deposited under slow-moving water.
T5020 3:2 Upper part of Layer 10C	<p><i>Thickness:</i> 6cm. <i>Lower boundary:</i> none.</p> <p><i>Structure and porosity:</i> channels and vesicles microstructure; 12% interconnected 2mm wide channels, accommodated, smooth walls; 3% vesicles and root voids 1-5mm in size, smooth to slightly serrated void walls.</p> <p><i>Mineral components:</i> same as T5020 2:1.</p> <p><i>Organics:</i> 3% dark brownish to black humified amorphous organic fine matter; 2% humified tissue residue, mostly found around root voids; 1% randomly distributed micro-charcoal, 0.1-0.2mm.</p> <p><i>Artefacts:</i> none.</p> <p><i>Pedofeatures: Textural:</i> 1) 5% fragmented, laminated dusty silty clay crusts, parallel striated, dark orange (XPL), 0.1-0.5mm thick; 2) 5% dense incomplete infillings of dark brown, organic-rich silty clay in cracks, commonly half-filled the cracks; <i>Amorphous and cryptocrystalline:</i> 1) amorphous iron compound (reddish) hypo-coating of voids with diffuse boundaries, 3% of all slide; <i>Fabric:</i> 1) 3% aggregates composed of >70% well-sorted coarse silt-size quartz, 5% micas and 5% fine organic material with a less humic groundmass, random, 1-2mm.</p>	Alluvium deposited under slow-moving water.

T5020 2



T5020 2:1

T5020 2:2

Slide thickness: 60µm, even,
minor loss

Micro-fabric	Micromorphological Description	Interpretation
T5020 2: 1 Layer 10C	<p><i>Thickness:</i> 6cm. <i>Lower boundary:</i> faint, diffuse.</p> <p><i>Structure and porosity:</i> channels and vesicles microstructure; 15% interconnected channels, 0.5-2mm, slightly serrated walls; 5% vesicles and root voids 1-12mm in size, smooth to slightly serrated void walls.</p> <p><i>Mineral components:</i> <i>CF limit:</i> 50µm; <i>CF ratio:</i> 2/98; <i>CF related distribution:</i> open-porphyric; <i>Texture:</i> 5% sand, 65% silt, 30% clay; <i>coarse fraction:</i> 5% quartz, moderate-sorted, subangular to subrounded, very fine sand size, 50-80µm; <i>fine fraction:</i> light brown (PPL) dotted mixture of silty clay with high birefringence and light yellow interference colour, pale gray micritic calcite (5%), and organic pigments (3%); stipple-speckled to porostriated to calcitic crystallitic (85:10:5) b-fabric.</p> <p><i>Organics:</i> 5% dark brown to black humified amorphous organic fine material, random, 0.1-0.5mm; 1% randomly distributed micro-charcoal, 0.1-0.2mm; 1% root fragment incorporated in the groundmass or near voids, 0.5-1cm.</p> <p><i>Artefacts:</i> none.</p> <p><i>Pedofeatures: Textural:</i> 1) 10% fragmented dusty silty clay crusts, parallel striated, light orange (XPL), 1mm thick; 2) 5% dense incomplete infillings of dark brown, organic-rich silty clay in cracks, commonly half-filled the cracks; <i>Crystalline:</i> 1) 2% micritic calcium carbonate clusters with diffuse boundaries, 0.5mm; <i>Amorphous and cryptocrystalline:</i> 1) amorphous iron compound (reddish) hypo-coating of voids with diffuse boundaries, 3% of all slide; 2) 1% pyrite framboids near humified organic matter or voids, as clusters, 0.1-0.5mm; 3) a single case of crystalized vivianite near humified organic tissues, 1-2mm; <i>Fabric:</i> 1) 3% aggregates composed of >70% well-sorted coarse silt-size quartz, 5% micas and 5% fine organic material with a less humic groundmass, random, 1-2mm.</p>	Alluvium deposited under slow-moving water and were later dried and exposed.
T5020 2:2	<i>Thickness:</i> 6.5cm. <i>Lower boundary:</i> none.	Alluvium

<p>Upper part of Platform III-2</p>	<p><i>Structure and porosity:</i> same as T5020 2:1 with a lower porosity of 15%.</p> <p><i>Mineral components:</i> <i>CF limit:</i> 50µm; <i>CF ratio:</i> 5/98; <i>CF related distribution:</i> open porphyric; <i>Texture:</i> 5% sand, 70% silt, 25% clay; <i>coarse fraction:</i> 4% moderate-sorted, sub-angular to sub-rounded, very fine sand size quartz, 50-60µm; 1% sub-angular medium sand size rock fragments, 200-400µm, random; <i>fine fraction:</i> light yellow (PPL) dotted mixture of silty clay with high birefringence and light yellow interference colour, micritic calcium carbonate (5%), and organic pigments (3%); stipple speckled to grano-striated to calcitic crystallitic (90:5:5) b-fabric.</p> <p><i>Organics:</i> 3% disoriented, humified organic residue, random, 1-5mm in size; 3% charcoal 0.5-3mm in size, random to clustered; 2% amorphous organic fine material, random to clustered, 0.1-0.2mm.</p> <p><i>Artefacts:</i> none.</p> <p><i>Pedofeatures: Textural:</i> 1) 5% dense incomplete infillings of dark brown, organic-rich silty clay in cracks, commonly half-filled the cracks; 2) 3% perpendicular laminated fine silty clay crusts, 1mm thick, concentrated in the lower part of the fabric; 3) thin hypo-coating of dusty clay with moderate to high birefringence and orange interference colour around voids, 1%; <i>Amorphous and cryptocrystalline:</i> 1) amorphous iron compound (reddish) hypo-coating of voids with diffuse boundaries, 3% of all slide; 2) 1% pyrite framboids near humified organic matter or voids; 3) a single case of crystalized vivianite near humified organic tissues, 0.5mm; <i>Fabric:</i> 1) 5% dark brown, rounded soil aggregates that contain >20% highly broken fine humified or charred organic material, randomly mixed in the fabric, 0.2-1mm.</p>	<p>disrupted by pedogenic processes and possible human activity. May be an exposed surface with vegetation growth.</p>
-------------------------------------	--	--

T5020 1



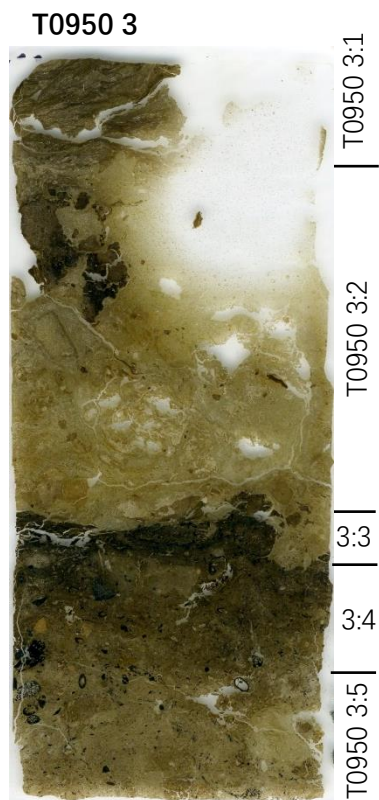
T5020 1:1

T5020 1:2

Slide thickness: 100µm,
uneven, no loss

Micro-fabric	Micromorphological Description	Interpretation
<p>T5020 1: 1 Lower part of Platform III-2</p>	<p><i>Thickness:</i> 5cm. <i>Lower boundary:</i> faint, diffuse.</p> <p><i>Structure and porosity:</i> Channel and sub-angular blocky, channels separate the fabric into four accommodated clods, each clod is 2-3cm large and shows a sub-angular blocky to platy structure; 12% cracks and planar voids, 2-4cm wide, 0.5-5cm long with serrate walls; 2% root voids with remnant organic matter, 2-3mm.</p> <p><i>Mineral components:</i> <i>CF limit:</i> 50µm; <i>CF ratio:</i> 2/98; <i>CF related distribution:</i> fine monic; <i>Texture:</i> 2% sand, 73% silt, 25% clay; <i>coarse fraction:</i> 2% quartz, well-sorted, sub-angular, very fine sand size, 50-60µm; <i>fine fraction:</i> light brown (PPL) dotted mixture of silty clay with high birefringence and light yellow interference colour, and organic pigments (3%); random striated b-fabric.</p> <p><i>Organics:</i> 5% dark brown, humified, highly fragmented organic residues (0.1-1mm), varied orientations, clustered to randomly distributed.</p> <p><i>Artefacts:</i> none.</p> <p><i>Pedofeatures:</i> <i>Textural:</i> 1) 1% iron impregnated clay hypo-coating of voids with diffused boundaries; <i>Amorphous and cryptocrystalline:</i> 1) 4% black manganese compound, as clustered pellets with diffuse boundary, nodules and hypo-coating of voids, 0.1-2mm; 2) 1% pyrite framboids near humified organic matter; <i>Fabric:</i> 1) 2-3% aggregates of organic topsoil, randomly mixed in the groundmass, 3-5mm.</p>	<p>Constructed layers by 'soil wrapped with grass'</p>
<p>T5020 1:2 Pre-occupation sediment</p>	<p><i>Thickness:</i> 7cm. <i>Lower boundary:</i> none.</p> <p><i>Structure and porosity:</i> channel and sub-angular blocky microstructure, channels separate the fabric into four accommodated clods, each clod is 2-3cm large and shows a sub-angular blocky structure; 15% cracks and planar voids, accommodated, 2-4cm wide, 0.5-3cm long with smooth to slightly serrated walls; 2% root voids with remnant organic matter, 2-5mm.</p>	<p>Slowly built-up alluvial plain with aggregating A horizon under repeat alternations of wet and periodic</p>

	<p><i>Mineral components: CF limit: 50µm; CF ratio: 0/100; CF related distribution: fine monic; Texture: 70% silt, 30% clay; fine fraction: brown (PPL), dotted mixture of silty clay with moderate birefringence, micritic pale gray calcite (10%) and black organic punctuations (3%); reticulate- to parallel-striated and calcitic crystallitic (90:10) b-fabric.</i></p> <p><i>Organics: 3% dark brown, humified, mostly horizontally oriented amorphous organic fine material, 0.1-2mm, random; 2% humified root in channels, 0.2-2cm long.</i></p> <p><i>Artefacts: none.</i></p> <p><i>Pedofeatures: Amorphous and cryptocrystalline: 1) 3% black manganese compound, as clustered pellets with diffuse boundary or nodules, 0.2-2mm; 2) 2% amorphous iron oxide (reddish yellow) replaced organic matter and hypo-coatings of root voids and passages; 3) 1% pyrite framboids near humified organic matter; Fabric: 1) 3% rounded topsoil aggregates with higher content of organic matter, randomly mixed. 2) 3% fragments of dusty silty clay crusts, randomly mixed.</i></p>	<p>dry, exposed stages.</p>
--	--	-----------------------------



Slide thickness: 50µm, even, minor loss

Micro-fabric	Micromorphological Description	Interpretation
T0950 3: 1 Lower part of Layer 9	<p><i>Thickness:</i> 2cm. <i>Lower boundary:</i> prominent, sharp, curving.</p> <p><i>Structure and porosity:</i> channel microstructure with alternations of dusty silty clay and silt-size material; 50% zone of groundmass lost during thin section making; 15% planar channels, accommodated, 0.2-3mm, serrated walls.</p> <p><i>Mineral components:</i> <i>CF limit:</i> 10µm; <i>CF ratio:</i> 60/40; <i>CF related distribution:</i> close porphyric; <i>Texture:</i> 10% sand, 75% silt, 15% clay; <i>coarse fraction:</i> 60% moderate-sorted, rounded, medium silt to very fine sand-size quartz, 20-60µm, banded; <i>fine fraction:</i> laminae of brown (PPL), humic silty clay with weak birefringence; striated to undifferentiated b-fabric.</p> <p><i>Organics:</i> 3% black/dark brown humified/charred, amorphous organic matter, laminated, 0.5-2mm.</p> <p><i>Artefacts:</i> none.</p> <p><i>Pedofeatures:</i> <i>Textural:</i> 1) Wavy micro-laminations of dusty silty clay crusts, 40% of the fabric, 0.2-0.5mm thick of each micro-bedding, alternates with the sandy silt lenses.</p>	Slow-moving channel deposition.
T0950 3: 2 Layer 10	<p><i>Thickness:</i> 6cm. <i>Lower boundary:</i> prominent, clear.</p> <p><i>Structure and porosity:</i> massive microstructure; 15% zone of groundmass lost during thin section making, 5% of the loss form 3-5mm vughs; 2% channels, serrated walls, accommodated, 1-2mm wide.</p> <p><i>Mineral components:</i> <i>CF limit:</i> 10µm; <i>CF ratio:</i> 80/20; <i>CF related distribution:</i> close porphyric. <i>Texture:</i> 25% sand, 70% silt, 5% clay; <i>coarse fraction:</i> 70% well-sorted, sub-rounded coarse silt-size and very fine sand-size quartz, 30-60µm, random to weakly laminar; 10% moderate silt-size mica flakes, 20-50µm, random; <i>fine fraction:</i> light to dark brown(PPL) silty clay aggregates (1-15mm) and striae (3-8mm); undifferentiated b-fabric.</p> <p><i>Organics:</i> <1% humified, brown, amorphous organic matter, 1-2mm long.</p>	Aeolian soil material with occasional overland flow.

	<p><i>Artefacts:</i> none.</p> <p><i>Pedofeatures:</i> <i>Fabric:</i> 1) rounded, dark brown, humic silty clay aggregates with undifferentiated b-fabric, 2-15mm, random, 17% of the fabric; 2) fragments of dusty silty clay crusts with weak birefringence, 100-200µm thick, 3-5mm long, intermittently found, 3% of the groundmass.</p>	
T0950 3: 3 Layer 11	<p><i>Thickness:</i> 0.7cm. <i>Lower boundary:</i> prominent, diffuse.</p> <p><i>Structure and porosity:</i> platy microstructure. 10% planar fissures, accommodated, serrated walls, 0.5-2mm wide, 4-15mm long.</p> <p><i>Mineral components:</i> <i>CF limit:</i> 50µm; <i>CF ratio:</i> 10:90; <i>CF related distribution:</i> close porphyric. <i>Texture:</i> 10% sand, 80% silt, 10% clay; <i>coarse fraction:</i> 5% moderate-sorted, very fine sand, 40-60µm, random; 5% medium to coarse sand-size rock fragments, 300-500µm, random. <i>fine fraction:</i> dark reddish brown (PPL) humic silty clay, undifferentiated b-fabric.</p> <p><i>Organics:</i> 30% dark brown to black, humified/charred, laminar organic material, 0.2-4mm.</p> <p><i>Artefacts:</i> none.</p> <p><i>Pedofeatures:</i> <i>Crystalline:</i> 1) 10% blueish vivianite crystals in the groundmass, 0.5-1mm, random.</p>	Edge of the burning event, a possible occupational surface with remnant matting materials.
T0950 3: 4 Layer 12	<p><i>Thickness:</i> 2cm. <i>Lower boundary:</i> faint, diffuse.</p> <p><i>Structure and porosity:</i> massive microstructure; 2% vughs, 1-3mm, irregular; 1% fissures, 0.5-1mm, accommodated, serrated walls.</p> <p><i>Mineral components:</i> <i>CF limit:</i> 50µm; <i>CF ratio:</i> 5:95; <i>CF related distribution:</i> close porphyric. <i>Texture:</i> 10% sand, 70% silt, 20% clay; <i>coarse fraction:</i> 5% sub-angular, medium to coarse sand-size rock fragments, 0.2-2mm, random; 5% sub-angular very fine sand, 40-50µm, random; <i>fine fraction:</i> brown (PPL) humic silty clay, 30% stained by amorphous iron oxides and shows reddish brown colour (PPL); undifferentiated b-</p>	Occupational layer with occupational debris.

	<p><i>fabric.</i></p> <p><i>Organics:</i> 10% black/dark brown humified/charred organic material, random to weakly laminated, 200-800 µm; 5% charred plant material including grass stems and wood, 1-5mm, random.</p> <p><i>Artefacts:</i> shell fragment, <1%, 200-400µm.</p> <p><i>Pedofeatures:</i> <i>Crystalline:</i> 1) 1% blueish vivianite in the groundmass, 0.5-1mm, random. <i>Fabric:</i> 1) a 1cm large silty clay soil fragment, high birefringent, striated b-fabric, 10% of the fabric; 2) burnt soil fragment, 2-3mm, 1% of the fabric.</p>	
T0950 3: 5 Upper part of Layer 13	<p><i>Thickness:</i> 1.5cm. <i>Lower boundary:</i> none.</p> <p><i>Structure and porosity:</i> massive microstructure; 2% channels, mostly planar, accommodated, serrated walls, 0.5-1mm wide.</p> <p><i>Mineral components:</i> <i>CF limit:</i> 10µm. <i>CF ratio:</i> 70/30. <i>Related distribution:</i> close porphyric; <i>Texture:</i> 20% sand, 60% silt, 20% clay; <i>coarse fraction:</i> 68% moderate-sorted, sub-rounded coarse silt-size and fine sand-size quartz, 30-60µm, random; 2% sub-angular, medium to coarse sand-size rock fragments, 0.5-1mm, random; <i>fine fraction:</i> light brown (PPL) humic silty clay aggregates; undifferentiated b-fabric.</p> <p><i>Organics:</i> 10% humified, brown to black, amorphous organic matter, 0.2-2mm long, random. 5% fine charred materials, 0.2-1mm, random and clustered.</p> <p><i>Artefacts:</i> none.</p> <p><i>Pedofeatures:</i> <i>Textural:</i> 1) dark greyish calcium carbonate in the voids or hypo-coating voids in the upper part of the fabric, 2% of the fabric; <i>Crystalline:</i> 1) 3% blueish vivianite in the groundmass, 0.5-1mm, random; <i>Fabric:</i> 1) rounded, dark brown, humic silty clay soil aggregates, 2-10mm, random, 30% of the fabric; 2) a 1cm large, light yellowish soil aggregates composed of well-sorted coarse-silt size quartz and micas, similar to the aeolian material in T0950 3: 2, 10% of the fabric. 3) clusters of fragmented fine (20-200µm) charred material, 0.5cm, 1% of the fabric.</p>	Physically mixture of various soil materials.

T0950 2



Slide thickness: 40µm, even, minor loss

Micro-fabric	Micromorphological Description	Interpretation
T0950 2: 1 Lower part of Layer 10	<p><i>Thickness:</i> 1cm. <i>Lower boundary:</i> distinct, sharp, wavy.</p> <p><i>Structure and porosity:</i> massive with 30% slide loss.</p> <p><i>Mineral components:</i> <i>CF limit:</i> 10µm; <i>CF ratio:</i> 90/10; <i>CF related distribution:</i> close porphyric; <i>Texture:</i> 25% sand, 70% silt, 5% clay; <i>coarse fraction:</i> 80% well-sorted, sub-rounded coarse silt-size and very fine sand-size quartz, 30-60µm, random; 10% moderate silt-size mica flakes, 20-50µm, random; <i>fine fraction:</i> yellowish brown (PPL) clay aggregates and streaks, 100-200µm in size, with reddish yellow to yellow interference colour; striated b-fabric.</p> <p><i>Organics:</i> clusters (1-2mm) of fine charred material, 2% of the fabric.</p> <p><i>Artefacts:</i> none.</p> <p><i>Pedofeatures:</i> none.</p>	Aeolian sediment.
T0950 2:2 Layer 11	<p><i>Thickness:</i> 3cm. <i>Lower boundary:</i> distinct, clear.</p> <p><i>Structure and porosity:</i> channel microstructure. 5% planar channels, partially accommodated, 6cm long, 1-3mm wide. 5% vughs between charred aggregates, 1-2mm, irregular.</p> <p><i>Mineral components:</i> <i>CF limit:</i> 50µm; <i>CF ratio:</i> 50/50; <i>CF related distribution:</i> close enaulic; <i>Texture:</i> 50% sand, 40% silt, 10% clay; <i>coarse fraction:</i> 50% sub-angular to angular, sand-size, potential burnt rock fragments, 100-400µm, random; <i>fine fraction:</i> mixture of dark brown (PPL) silty clay and micritic calcium carbonates, calcitic crystallitic b-fabric.</p> <p><i>Organics:</i> carbonized material including charred wood, stem, and seed, random, size ranging from 0.1 to 2cm, some of the highly broken charred materials are weakly laminated, 80% of the fabric.</p> <p><i>Artefacts:</i> 1% small (2-3mm) rounded, pottery fragments, random.</p>	<i>In situ</i> burning event with abundant charred materials.

	<p><i>Pedofeatures: Crystalline:</i> 1) concentration of crystallitic groundmass between the charred material, 10% of the fabric, more concentrated in the lower part of this fabric, potential ashes; <i>Fabric:</i> 1) burnt soil lumps with reddish yellow groundmass and iron oxides nodules, 0.4-5mm, 8% of the fabric.</p>	
T0950 2:3 Top of Layer 12	<p><i>Thickness:</i> 0.5cm. <i>Lower boundary:</i> prominent, diffuse.</p> <p><i>Structure and porosity:</i> platy microstructure; 2-3% planar voids, 2-5cm long, 0.2mm wide.</p> <p><i>Mineral components: CF limit:</i> 50µm; <i>CF ratio:</i> 5/95; <i>CF related distribution:</i> close porphyric; <i>Texture:</i> 5% sand, 75% silt, 25% clay; <i>coarse fraction:</i> 5% sand-size, potential burnt rock fragments, 100-200µm, random; <i>fine fraction:</i> mixture of brownish to reddish brown (PPL) micritic calcium carbonate and silty clay; calcitic crystallitic b-fabric.</p> <p><i>Organics:</i> 15% black/dark brown laminar, humified/charred organic material, half of them are probably bast fibres, 0.2-3mm long.</p> <p><i>Artefacts:</i> none.</p> <p><i>Pedofeatures: Crystalline:</i> 1) concentration of calcitic crystallitic groundmass between the lenses of charred material, 80%; 2) 3% blueish vivianite in the groundmass, 0.5-1mm, random.</p>	Substrate of the burning event, possibly occupation surface with matting material.
T0950 2:4 Layer 12	<p><i>Thickness:</i> 3.5cm. <i>Lower boundary:</i> faint, diffuse.</p> <p><i>Structure and Porosity:</i> massive microstructure; 3% vughy voids, irregular, 2-3mm.</p> <p><i>Mineral components: CF limit:</i> 50µm; <i>CF ratio:</i> 10:90; <i>CF related distribution:</i> close porphyric; <i>Texture:</i> 10% sand, 65% silt, 25% clay; <i>coarse fraction:</i> 10% sub-angular, poorly-sorted, sand-size rock fragments, 60-600µm, 1/3 of them are potentially burnt, random; <i>fine fraction:</i> 65% light brownish (PPL) humic silty clay; 20% light yellowish (PPL), silty clay aggregates 0.5-1cm in size, planar; 5% reddish brown (PPL) clay aggregates (200µm); undifferentiated to striated b-fabric (70:30).</p>	Occupational layer with heavy trampling.

	<p><i>Organics:</i> 10% black/dark brown humified/charred, organic material, mostly laminar, 0.2-2mm; 5% charred plant material, 1-5mm, random.</p> <p><i>Artefacts:</i> <1% shell fragments, 0.8mm.</p> <p><i>Pedofeatures: Crystalline:</i> 1) 3% blueish vivianite crystals in the groundmass, 0.5-1mm, random.</p>	
T0950 2:5 Layer 13	<p><i>Thickness:</i> 2cm. <i>Lower boundary:</i> none.</p> <p><i>Structure and Porosity:</i> mixture of two sediment material and as a whole shows a massive microstructure; 3% lost during thin section making; 2% vugus, 2-3mm, irregular.</p> <p><i>Sediment-1,</i> 70% of the fabric. <i>Mineral components: CF limit:</i> 50µm; <i>CF ratio:</i> 5/95; <i>CF Related distribution:</i> close porphyric; <i>Texture:</i> 5% sand, 75% silt, 20% clay; <i>coarse fraction:</i> 5% sub-angular, very fine sand-size, rock fragments, 40-80µm, random; <i>fine fraction:</i> light yellowish (PPL) silty clay with yellowish interference and striated b-fabric.</p> <p><i>Organics:</i> 1% black/dark brown humified, amorphous organic matter, 400-800µm, random.</p> <p><i>Artefacts:</i> none.</p> <p><i>Pedofeatures: Crystalline:</i> 1) 2% greenish blue vivianite crystals, 0.2-0.5mm, random; <i>Amorphous and cryptocrystalline:</i> 1) iron mottles (50µm) and nodules (0.2-5mm) widely distributed in the groundmass, 40% of the sediment-1; <i>Fabric:</i> 1) fine charcoal (0.2-0.8mm) rich soil aggregate composed of >70% reddish brown (XPL), potential calcium carbonate pseudomorphs of prismatic crystals, 5cm in size, 10% of sediment-1.</p> <p><i>Sediment-2,</i> 30% of the fabric. <i>Mineral components: CF limit:</i> 50µm; <i>CF ratio:</i> 30/70; <i>CF Related distribution:</i> close porphyric; <i>Texture:</i> 15% sand, 65% silt, 20% clay; <i>coarse fraction:</i> 20% poorly sorted, sub-angular, medium to coarse sand-size, rock fragments, 200-500µm, random; 10% sub-rounded fine sand-size quartz, 50-100µm, random; <i>fine</i></p>	Physically mix of two different soil material, could be a constructed layer.

	<p><i>fraction:</i> light brownish (PPL) silty clay, striated b-fabric.</p> <p><i>Organics:</i> 1% black/dark brown humified, amorphous organic matter, 400-800µm, random.</p> <p><i>Artefacts:</i> none.</p> <p><i>Pedofeatures:</i> Textural: 1) yellow (PPL), limpid, clay aggregates (0.1-0.4mm) with high birefringent, 2% of sediment-2; <i>Fabric:</i> 1) reddish brown (PPL) micritic calcium carbonates as lens (1cm long, 0.2cm thick) and aggregates (0.2-0.4mm), 10% of the sediment-2.</p>	
--	---	--

T0950 1



Slide thickness: 100µm, uneven, medium loss

Micro-fabric	Micromorphological Description	Interpretation
T0950 1: 1 Layer 14	<p><i>Thickness:</i> 6.5cm. <i>Lower boundary:</i> prominent, sharp.</p> <p><i>Structure and porosity:</i> massive microstructure; 3% chambers, 1cm, irregular, formed to the loss of slide. 2% fissures, 0.2-1mm wide, 2-5cm long, accommodated, slightly serrated walls. 1% 1-3mm vughs, irregular.</p> <p><i>Mineral components:</i> <i>CF limit:</i> 50µm; <i>CF ratio:</i> 5:95; <i>CF Related distribution:</i> close enaulic to close porphyric; <i>Texture:</i> 5% sand, 70% silt, 25% clay; <i>coarse fraction:</i> 5% sub-angular, fine sand-size rock fragments, 80-100µm, random; <i>fine fraction:</i> reddish brown (PPL) humic silty clay aggregates with very weak birefringence, 100-400µm in size; undifferentiated b-fabric.</p> <p><i>Organics:</i> 2-3% black/dark brown, humified, amorphous organic matter, 0.2-2mm, mostly found in voids.</p> <p><i>Artefacts:</i> none.</p> <p><i>Pedofeatures:</i> none.</p>	‘Soil wrapped with grasses’ material
T0950 1:2 Top of Layer 15	<p><i>Thickness:</i> 1cm. <i>Lower boundary:</i> diffuse, faint.</p> <p><i>Structure and porosity:</i> massive; 30% chambers, 3-15mm, irregular, formed due to the loss of slide.</p> <p><i>Mineral components:</i> <i>CF limit:</i> 50µm; <i>CF ratio:</i> 0/100; <i>coarse fraction:</i> <i>fine fraction:</i> 70% gray (PPL) micritic calcium carbonate, partially laminated; micritic calcitic crystallitic b-fabric; 30% silty clay stained by humic organic matter or iron compounds, weakly laminar.</p> <p><i>Organics:</i> 2% humified, brown, amorphous organic matter, 0.2-0.5mm, random.</p> <p><i>Artefacts:</i> none.</p> <p><i>Pedofeatures:</i> none.</p>	Top of horizon, suggestive of sharply reduced hydraulic conductivity of the soil by cementation
T0950 1:3 Layer 15	<p><i>Thickness:</i> 5cm. <i>Lower boundary:</i> None.</p> <p><i>Structure and porosity:</i> massive; 25% lost during thin section making; 2% planar</p>	Alluvium deposited under a

	<p>fissures, 0.5-2mm wide, 1-3cm long, accommodated, slightly serrated wall; 1% 1-3mm vughs, irregular; 3% chambers, 3-15mm, irregular, formed due to the loss of slide.</p> <p><i>Mineral components: CF limit: 50µm; CF ratio: 2/98; CF related distribution: close porphyric; Texture: 2% sand, 73% silt, 25% clay; coarse fraction: 2% sub-angular, very fine sand-size quartz, 50-100µm, random; fine fraction: 85% brownish (PPL) humic silty clay with lower first-order yellow interference colour, 10% micritic calcium carbonate; weakly reticulate-striated to calcitic crystallitic b-fabric.</i></p> <p><i>Organics: 3% humified, brown, amorphous organic matter, 0.2-2mm, mostly laminar; 1% charcoal fragments, 2-3mm, random.</i></p> <p><i>Artefacts: none.</i></p> <p><i>Pedofeatures: Crystalline: 1) 10% clusters (0.5-4mm) of yellow to reddish brown (XPL) micritic calcium carbonate with diffuse boundary around voids and nearby groundmass; 2) 3% vivianite crystal, 0.5-1mm, random; Fabric: 1) 5% laminated, partially fragmented dusty silty clay crusts on the top of the fabric, 1mm thick.</i></p>	<p>gentle water flow, with periodic dry episode.</p>
--	---	--

T3131 7



T3131 7:1

T3131 7:2

Micro-fabric	Micromorphological Description	Interpretation
T3131 7: 1 Unit 2	<p><i>Thickness:</i> 7cm. <i>Lower boundary:</i> diffuse, faint.</p> <p><i>Structure and porosity:</i> moderately developed prismatic microstructure; 5% planar voids, 10-20mm long, partially accommodated, serrated wall; 3% small vughs, 0.2-3mm, irregular shape, random.</p> <p><i>Mineral components:</i> <i>CF limit:</i> 50µm; <i>CF ratio:</i> 50/50; <i>Texture:</i> 10% clay, 40% silt, 50% sand. <i>CF related distribution:</i> close porphyric; <i>coarse fraction:</i> 15% sub-rounded, very fine sand-size quartz, 40-80µm, random; 35% sub-angular, fine sand to fine pebble-size rock fragments, 0.08-60mm, clustered; <i>fine fraction:</i> 50% silty clay, 80% of the fine fraction is heavily stained by amorphous iron and manganese oxides and shows reddish brown to black colour (PPL), unstained part is light yellow (PPL); striated b-fabric.</p> <p><i>Organics:</i> charcoal, 0.5-5mm, 2% of the fabric, random to clustered.</p> <p><i>Artefacts:</i> burnt bone fragments, 0.5mm, <1%, random; three rounded burnt clayey soil material (daub), 10-15mm, random; two slightly degraded pottery sherds, 18-20mm, random.</p> <p><i>Pedofeatures: Amorphous and Cryptocrystalline:</i> 1) amorphous iron and manganese oxides staining reddish yellow showing reddish brown to black colour (PPL), 80% of the fabric, around voids and channels; <i>Fabric:</i> 1) burnt, rounded clayey soil aggregates, 2-10mm, 15% of the fabric.</p>	Constructed layer, mixed with abundant burnt archaeological materials.
T3131 7:2 Unit 5-1	<p><i>Thickness:</i> 13cm. <i>Lower boundary:</i> none.</p> <p><i>Structure and porosity:</i> weakly developed sub-angular-blocky microstructure in the lower part to prismatic microstructure in the upper part; 5% short planar voids, 1-10mm long, accommodated, in the lower part; 5% vertically aliened planar voids, 1-6cm long, partially accommodated, in the upper part; 3% small vughs, 0.2-3mm, irregular shape, random; a 3cm long crack form around fresh woody material.</p> <p><i>Mineral components:</i> <i>CF limit:</i> 50µm; <i>CF ratio:</i> 40/60; <i>Texture:</i> 10% clay, 50% silt,</p>	Constructed layer mixed of fine silty clay and coarse sand-size rock fragments with a few fine

Slide thickness: 40µm, even, no loss.

	<p>40% sand. <i>CF related distribution</i>: close porphyric; <i>coarse fraction</i>: 20% sub-rounded, very fine sand-size quartz, 40-80µm, random; 20% sub-angular, fine sand to fine pebble-size rock fragments, 0.08-10mm, clustered; <i>fine fraction</i>: 60% light yellow (PPL) limpid silty clay with high birefringence, 25% of the fabric is moderately stained by amorphous iron oxides and shows reddish brown colour (PPL); random striated to grano-striated b-fabric (90:10).</p> <p><i>Organics</i>: charcoal, 1-6mm, 5% of the fabric, random to clustered; dark humified/amorphous organic fine material, 0.2-2mm, 1%, random; two pieces of platy wood materials, 1-2cm.</p> <p><i>Artefacts</i>: burnt bone fragments, 1-3mm, 3%, random.</p> <p><i>Pedofeatures: Textural</i>: 1) crescentic coating and hypo-coating composed of juxtaposed limpid and dusty clay, high birefringence, light yellow to reddish yellow interference colour, 200-400µm thick, concentrated in the mid-lower part of the fabric, 3%; 2) welding of rounded soil aggregates coated with very dusty reddish brown (PPL) silty clay, 50-100µm, concentrated in the mid-lower part of the fabric, 3% of the fabric; 3) micro-laminated intercalation of dusty silty clay, reddish yellow interference colour, 100-200µm, more concentrated in the mid-lower part of the fabric, <1%; <i>Amorphous and Cryptocrystalline</i>: 1) stains and nodules of reddish yellow iron oxides with diffuse boundaries, 5% of the fabric, mostly found in the lower part of the fabric; 2) hypo-coating and depletion quasi-coating of iron oxides of voids and channels, 1-3mm thick, 20% of the fabric, mostly found in the upper part of the fabric; <i>Fabric</i>: 1) rounded clayey soil aggregates, 2-12mm, 1/3 of them are possibly burnt, 20% of the fabric; 2) clusters (5-10mm) of fine charcoal, 2%, random.</p>	<p>occupational debris.</p>
--	--	-----------------------------

T3131 6



T3131 6:1

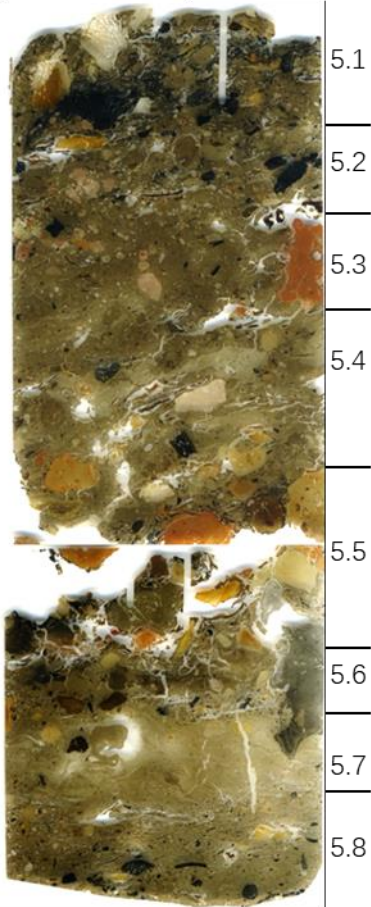
T3131 6:2

Slide thickness: 40µm, even, no loss.

Micro-fabric	Micromorphological Description	Interpretation
T3131 6: 1 Unit 5-1	<p><i>Thickness:</i> 4.5-7cm. <i>Lower boundary:</i> prominent, sharp, inclined.</p> <p><i>Structure and porosity:</i> vesicular microstructure; 10% vesicles, 0.2-20mm long, 0.2-3mm thick, irregular shape, random, smooth voids; 3% fissures, 2-10mm long, 0.2-0.5mm thick, random.</p> <p><i>Mineral components:</i> <i>CF limit:</i> 50µm; <i>CF ratio:</i> 25/75; <i>Texture:</i> 10% clay, 65% silt, 25% sand. <i>CF related distribution:</i> close porphyric; <i>coarse fraction:</i> 15% sub-rounded, very fine sand-size quartz, 40-80µm, random; 10% sub-angular to sub-rounded, fine to medium sand-size rock fragments, 80-400µm, random; <i>fine fraction:</i> 75% light yellow (PPL) limpid silty clay with high birefringence; random to grano-striated b-fabric (90:10).</p> <p><i>Organics:</i> charcoal, 1-6mm, 5% of the fabric, random or clustered; dark humified/amorphous organic fine material, 0.2-2mm, 1%, random.</p> <p><i>Artefacts:</i> burnt bone fragments, 3-15mm, 3%, random;</p> <p><i>Pedofeatures: Textural:</i> 1) crescentic coating and hypo-coating of juxtaposed limpid and dusty clay of voids, high birefringence, light yellow interference colour, 200-400µm thick, 1%; 2) microlaminated intercalation of dusty silty clay, reddish yellow interference colour, 100-200µm, <1%; 3) a possible rotational feature showing the rotated fine sand material in the lower part of this fabric, 1cm in size; <i>Amorphous and Cryptocrystalline:</i> 1) stain, nodules with diffuse boundaries and hypo-coating of reddish yellow amorphous iron oxides, 5% of the fabric; <i>Fabric:</i> 1) rounded soil aggregates with various groundmass, 2-5mm, 10% of the fabric, soil aggregates in the bottom part are similar to the fine fraction of this fabric but are cleaner and clay-rich; 2) fine charcoal rich soil aggregates, 5-10mm. 3%, random.</p>	Constructed layer mixed of fine silty clay and coarse sand-size rock fragments with a few fine occupational debris.
T3131 6:2 Unit 5-2-1	<p><i>Thickness:</i> 7.5-5cm. <i>Lower boundary:</i> none.</p> <p><i>Structure and porosity:</i> massive; 5% planar vegetal voids form after the decay of organic</p>	Heavily trampled, open-

	<p>material, 2-10mm long, 0.5-3mm thick, smooth wall; 3% slide loss.</p> <p><i>Components:</i></p> <p><i>35% Organics:</i> lenses of humified/charred blackish brown grass material, 1-5mm thick, 27%, some grass materials show <i>in situ</i> breakages; charcoal with cell structures, 1-8mm, 5% of the fabric, random, laminar; fresh woody plant material, 1-13mm, 3%; a phytolith slugs, 200µm.</p> <p><i>25% Sediment-1:</i> <i>CF limit:</i> 50µm; <i>CF ratio:</i> 30/70; <i>Texture:</i> 30%, 45% silt, 15% clay; <i>coarse fraction:</i> 30% sub angular, very fine to fine sand-size (40-150µm) quartz grains, random; <i>fine fraction:</i> light yellow (PPL), homogenous, random striated b-fabric; few (3%) organic inclusions; 15% as rounded to elongated aggregates (0.4-13mm) and groundmass between the lenses of organic material, 1/3 of which are possibly burnt; 10% coated the Soil Fabric 2.</p> <p><i>20% Sediment-2:</i> <i>Texture:</i> similar to Sediment 1; light reddish brown (PPL), possibly stained by amorphous iron oxides; as rounded soil aggregates in the bottom of the fabric, 5-25mm, mostly coated with fine charred materials.</p> <p><i>10% Rock fragments:</i> 30% poorly-sorted, sub-angular, fine to medium sand-size rock fragments, 80-350µm, random; sub-rounded, coarse sand to fine pebble-size rock fragments, 0.35-5mm, randomly distributed in-between organic materials.</p> <p><i>5% Artefacts:</i> two pottery sherds, 7-10mm, laminar.</p> <p><i>5% Pedofeatures:</i> <i>Textural:</i> 1) thick, micro-laminated, partially fragmented, reddish yellow (XPL) dusty silty clay with high birefringence filled in the gaps between the humified plant material in the lower part of the fabric, 50-400µm, 3% of the fabric; 2) thin, dusty, light yellowish clay coatings with high birefringence, inbetween laminated plant material, mostly found in the upper part of the fabric, 50µm thick, 2% of the fabric.</p>	<p>air living surface with repeat matting of grass materials.</p>
--	---	---

T3131 5



Micro-fabric	Micromorphological Description	Interpretation
<p>T3131 5:1 Unit 5-2-2</p>	<p><i>Thickness:</i> 2cm. <i>Lower boundary:</i> distinct, sharp.</p> <p><i>Structure and porosity:</i> weakly separated platy microstructure; 10% planar voids, 2-25mm long, 0.5-2mm thick, slightly serrated wall.</p> <p><i>Mineral components:</i> <i>CF limit:</i> 50µm; <i>CF ratio:</i> 60/40; <i>Texture:</i> 8% clay, 52% silt, 40% sand. <i>CF related distribution:</i> close porphyric; <i>coarse fraction:</i> 20% poorly-sorted, sub-angular, fine to medium sand-size rock fragments, 80-350µm, random; 20% sub-rounded, coarse to very coarse sand-size rock fragments, 0.35-2mm, half of them are burnt and reddened, random; <i>fine fraction:</i> 60% brownish (PPL) very humic silt clay; undifferentiated b-fabric.</p> <p><i>Organics:</i> lenses of humified/charred blackish brown grass material, 10mm thick, 30%; charcoal, 1-14mm, 10% of the fabric, laminar; humified/amorphous organic fine material, 0.2-2mm, 5%, laminar; fresh woody plant material, 1-15mm, 5%.</p> <p><i>Artefacts:</i> burnt bone fragments with <i>in situ</i> fractures, 3-10mm, 10%, overlaid the lenses of grass material.</p> <p><i>Pedofeatures:</i> Textural: 1) compound coatings of limpid clay with orange interference colour and high birefringence and dusty clay coating incorporating very fine charcoals, in the upper 1cm of the fabric around the bones and voids, 50-500µm thick, 3% of the fabric. Fabric: 1) rounded soil aggregates with various groundmass, 2-5mm, 15% of the fabric, 1/2 of which are burnt.</p>	<p>Dumped and trampled occupational debris and grass matting material</p>

Slide thickness: 40µm, even, no loss.

<p>T3131 5:2 Unit 5-2-3</p>	<p><i>Thickness:</i> 1.8cm. <i>Lower boundary:</i> distinct, sharp.</p> <p><i>Structure and porosity:</i> weakly separated platy microstructure; 10% planar voids, 2-15mm long, 0.5-1mm thick, smooth wall.</p> <p><i>Mineral components:</i> <i>CF limit:</i> 50µm; <i>CF ratio:</i> 60/40; <i>Texture:</i> 8% clay, 32% silt, 60% sand. <i>CF related distribution:</i> close porphyric; <i>coarse fraction:</i> 20% poorly-sorted, sub-angular, fine to medium sand-size rock fragments, 80-350µm, random; 40% sub-angular to sub-rounded, coarse sand to pebble size rock fragments, 0.35-5mm, mostly burnt and reddened, crudely bedded; <i>fine fraction:</i> 40% light brownish (PPL) humic silt clay; undifferentiated to speckled b-fabric.</p> <p><i>Organics:</i> humified plant tissues and bast fibres, 0.5-3mm, 10%, laminar; charcoal, 1-10mm, 5% of the fabric, random to weakly laminar; lenses of humified/charred blackish brown grass material, 1mm thick, 5%; fresh woody plant material, 1-7mm, 5%.</p> <p><i>Artefacts:</i> none.</p> <p><i>Pedofeatures:</i> <i>Fabric:</i> 1) rounded soil aggregates with various groundmass, 2-5mm, 10% of the fabric, 1/3 of which are burnt.</p>	<p>The same groundmass as 5:3, constructed layer mixed with deliberately added or accidentally brought-in burnt rocks.</p>
<p>T3131 5:3 Unit 5-2-4</p>	<p><i>Thickness:</i> 2cm. <i>Lower boundary:</i> distinct, clear.</p> <p><i>Structure and porosity:</i> moderate separated granular microstructure; 10% star-shape vughs inbetween two soil aggregates (sediment 1 and 2), 0.5-15mm.</p> <p>Sediment-1, 80% of the fabric: <i>Mineral components:</i> <i>CF limit:</i> 50µm; <i>CF ratio:</i> 40/60; <i>Texture:</i> 8% clay, 52% silt, 40% sand. <i>CF related distribution:</i> close porphyric; <i>coarse fraction:</i> 20% poorly-sorted, sub-rounded, fine to medium sand-size rock fragments, 50-350µm, random; 20% sub-angular to sub-rounded, coarse sand to fine pebble-size rock fragments, 0.35-5mm, random; <i>fine fraction:</i> 60% brown (PPL) humic silt clay; undifferentiated to speckled b-fabric.</p> <p><i>Organics:</i> humified plant tissues and amorphous fine organic material, 0.5-3mm, 15%, mostly parallel laminated, vertically laminated in the conjunction between two soil aggregates; fine charcoal, 0.2-3mm in size, 3% of the fabric, weakly laminar or as clusters; fresh woody plant material, 1-3mm, 1%, laminated.</p> <p>Sediment 2, 20% of the fabric: a reddish, 15mm, highly degraded pottery sherd surrounded by similar soil material of sediment 1.</p> <p><i>Pedofeatures:</i> <i>Textural:</i> 1) infilling and coating of thin (200µm) very dusty clay in the voids between sediment 1 and 2,</p>	<p>Kneading of two different soil materials, constructed layer.</p>

	some of the coatings show alternations between dusty and limpid clay, 5% of the fabric.	
T3131 5:4 Unit 6A-1	<p><i>Thickness:</i> 3cm. <i>Lower boundary:</i> distinct, sharp.</p> <p><i>Structure and porosity:</i> weakly separated platy microstructure; 10% planar voids, 2-15mm long, 0.5-1mm thick, slightly serrated wall.</p> <p><i>Components:</i></p> <p><i>40% Sediment 1:</i> <i>CF limit:</i> 50µm; <i>CF ratio:</i> 40/60; <i>Texture:</i> 8% clay, 52% silt, 40% sand. <i>CF related distribution:</i> close porphyric; <i>coarse fraction:</i> 40% poorly-sorted, sub-angular, fine to coarse sand-size rock fragments, 80-2000µm, random; <i>fine fraction:</i> 60% light brown (PPL) humic silt clay; speckled to undifferentiated b-fabric; as groundmass inbetween the coarse materials.</p> <p><i>25% Sediment 2:</i> <i>CF limit:</i> 50µm; <i>CF ratio:</i> 50/50; <i>CF related distribution:</i> close porphyric; <i>Texture:</i> 10% clay, 40% silt, 50% sand; <i>coarse fraction:</i> 50% well-sorted, sub-rounded, very fine to fine sand-size rock fragments, 40-150µm, weakly laminated; light yellow (PPL) silty clay with striated b-fabric; as laminar, elongate soil aggregates, 3-40mm long, 2-6mm thick.</p> <p><i>20% Organics:</i> humified plant tissues and bast fibres, 0.5-3mm, 10%, laminated, mostly found in the Sediment-1, a lamina of bast fibre overlies this fabric; fresh woody plant material, 1-4mm, 5%, laminated; fine charcoal, 0.2-5mm in size, 5% of the fabric, weakly laminar or as clusters, mostly found in the Sediment 1.</p> <p><i>10% Rock fragments:</i> sub-rounded, fine pebble size rock fragments, 2-10mm, laminated.</p> <p><i>5% Artefacts:</i> two pottery sherds with sharp boundaries, 5-10mm, laminar; 1% bright orange burnt clay materials, 2mm, random.</p> <p><i>1% Pedofeatures:</i> <i>Textural:</i> 1) a thin lamina of very dusty silty clay, 40mm long, 0.2-0.4mm thick, in the upper part of this fabric, inbetween coarse clasts.</p>	Open-air, heavily trampled, occupation zone
T3131 5:5 Unit 6A-2	<p><i>Thickness:</i> 3cm. <i>Lower boundary:</i> none.</p> <p><i>Structure and porosity:</i> highly separated granular microstructure; 40% voids caused by both loss during thin section making and the open structure of the aggregates.</p> <p><i>Components:</i></p> <p><i>40% Soil aggregates:</i> rounded soil aggregates in various types and sizes, commonly coated with fine charred materials or</p>	Loosely-packed, dumped burnt soil aggregates

	<p>clay coatings, at least 1/2 are burnt, 1-15mm.</p> <p><i>20% Organics:</i> fine charcoal, 0.2-2mm in size, 8% of the fabric, random or hypo-coated soil aggregates; fresh woody plant material, 8-10mm, 7%, random, in-between the soil aggregates; bast fibres and humified plant tissues, 1-8mm, laminated in the Sediment-1, 5%; phytoliths, <1%, 0.2mm, in the bottom of this fabric.</p> <p><i>10% Artefacts:</i> rounded, highly degraded pottery sherds, 5-12mm, random.</p> <p><i>10% Rock fragments:</i> fine pebble size rock fragments, 2-4mm, random.</p> <p><i>10% Sediment-1: CF limit:</i> 50µm; <i>CF ratio:</i> 40/60; <i>Texture:</i> 8% clay, 52% silt, 40% sand. <i>CF related distribution:</i> close porphyric; <i>coarse fraction:</i> 40% poorly-sorted, sub-angular, fine to coarse sand-size rock fragments, 80-2000µm, random; <i>fine fraction:</i> light brown (PPL) humic silt clay; speckled to undifferentiated b-fabric; concentrate in the lower part of this fabric.</p> <p><i>10% Pedofeatures: Textural:</i> thick (200-400µm), compound clay coatings consist of alternating dark brown (XPL) dusty and light yellow (XPL) limpid clay materials with high birefringence coating the soil aggregates and pottery sherds.</p>	
T3131 5:6 Unit 6A-3	<p><i>Thickness:</i> 1cm. <i>Lower boundary:</i> distinct, sharp.</p> <p><i>Structure and porosity:</i> platy structure; 10% planar voids, 2-15mm long, 0.5-1mm thick, slightly serrated wall.</p> <p><i>Mineral components:</i> the same as T3131 5:8.</p> <p><i>Organics:</i> humified plant tissues and amorphous fine organic material (10%), at least 1/3 are bast fibres, 1-20mm, parallel laminated; charcoal, 0.5-3mm in size, 10% of the fabric, random to weakly laminated.</p> <p><i>Artefacts:</i> fine pottery sherds, 2-5mm, random, 2%; burnt bone fragments, 0.5-2mm, 1%.</p> <p><i>Pedofeatures: Fabric:</i> 1) rounded, dark brown, burnt soil aggregates, 1-5mm, 10% of the fabric.</p>	Brought-in of occupational debris by trampling.
T3131 5:7 Unit 6A-4	<p><i>Thickness:</i> 2cm. <i>Lower boundary:</i> distinct, sharp.</p> <p><i>Structure and porosity:</i> massive structure; 5% planar voids, accommodated, serrated wall.</p> <p><i>Mineral components: CF limit:</i> 10µm; <i>CF ratio:</i> 70/30; <i>Texture:</i> 10% clay, 70% silt, 20% sand. <i>CF related distribution:</i> close porphyric; <i>coarse fraction:</i> 70% moderate-sorted, sub-angular to sub-rounded, coarse silt to fine sand-size rock fragments, 30-100µm; <i>fine fraction:</i> 30% light yellow (PPL) humic silty clay; random striated b-fabric.</p> <p><i>Organics:</i> amorphous fine organic material, 4mm, 3%, random.</p> <p><i>Artefacts:</i> none.</p>	Dumped constructional material or natural aeolian sediment

	<p><i>Pedofeatures: Textural:</i> 1) intercalations of dusty silty clay, 5% of the fabric; 2) thin (40-100µm) coating of dusty clay with high birefringence in voids; <i>Fabric:</i> 1) rounded, soil aggregates with various groundmass, 0.2-0.4mm, 3% of the fabric.</p>	
T3131 5:8 Unit 6A-5	<p><i>Thickness:</i> 1.5cm. <i>Lower boundary:</i> none.</p> <p><i>Structure and porosity:</i> weakly developed platy structure; 8% planar vegetal voids, 2-25mm long, 0.5-2mm thick, smooth wall, formed after the shrinkage and decay of organic matter.</p> <p><i>Mineral components: CF limit:</i> 50µm; <i>CF ratio:</i> 30/70; <i>Texture:</i> 8% clay, 62% silt, 30% sand. <i>CF related distribution:</i> close porphyric; <i>coarse fraction:</i> 30% poorly-sorted, sub-angular to sub-rounded, fine to coarse sand-size rock fragments, 80-2000µm; <i>fine fraction:</i> 65% light brown (PPL) humic silt clay; 5% light yellow (PPL) limpid clay aggregates (200-400µm) and fine striae (10-20µm) with bright yellowish interference colour; undifferentiated to parallel striated.</p> <p><i>Organics:</i> humified plant tissues and amorphous fine organic material (20%), at least 1/3 are bast fibres, 1-20mm, parallel laminated; charcoal with cell structures, 1-10mm in size, 10% of the fabric, parallel laminated; fresh woody plant material, 5-7mm, 3%, parallel laminated.</p> <p><i>Artefacts:</i> none.</p> <p><i>Pedofeatures: Fabric:</i> 1) rounded, dark brown, humic soil aggregates, 0.2-0.4mm, 3% of the fabric.</p>	<p>Trampled surface containing fine aggregates of bast fibres and occupational debris.</p>

T3131 4



Slide thickness: 40µm, even, minor loss.

Micro-fabric	Micromorphological Description	Interpretation
T3131 4:1 Unit 6A-4	<p><i>Thickness:</i> 6-7cm. <i>Lower boundary:</i> faint, diffuse.</p> <p><i>Structure and porosity:</i> weakly developed platy structure; 10% planar vegetal voids, 2-40mm long, 0.5-2mm thick, smooth wall, formed after the shrinkage and decay of organic matter.</p> <p><i>Mineral components:</i> <i>CF limit:</i> 50µm; <i>CF ratio:</i> 30/70; <i>Texture:</i> 8% clay, 62% silt, 30% sand. <i>CF related distribution:</i> close porphyric; <i>coarse fraction:</i> 25% poorly-sorted, sub-angular to sub-rounded, fine to coarse sand-size rock fragments, 80-2000µm; 5% rounded, fine pebble size rock fragments, 2-5mm, random; <i>fine fraction:</i> 62% light yellowish (PPL) humic silt; 8% light yellow (PPL) limpid clay aggregates (200-400µm), coatings and fine striae (10-20µm) with bright yellowish interference colour; granostriated to parallel striated.</p> <p><i>Organics:</i> charcoal with cell structures, 1-25mm in size, 40% of the fabric, random to obliquely laminated, concentrated in the bottom part; bast fibres, 2-40mm, obliquely (angle of 30°) laminated, 10% of the fabric; humified plant tissues and amorphous fine organic material (8%), 1-25mm long, mostly parallel laminated; fresh woody plant material, 1cm, 1%.</p> <p><i>Artefacts:</i> bone fragments, 0.5-1, 1%.</p> <p><i>Pedofeatures: Textural:</i> 1) the charcoals concentrate in the bottom part of the fabric and are covered by laminated bast fibres, the soil material and fine charred material in-between or underly the bast fibres are compacted and parallel to the slope direction;</p> <p><i>Fabric:</i> 1) rounded burnt soil aggregates, 5-15mm, 5% of the fabric.</p>	Trampled occupational layer with matting and occupational debris such as charcoals and bones.
T3131 4:2 Unit 6B	<p><i>Thickness:</i> 7cm. <i>Lower boundary:</i> none.</p> <p><i>Structure and porosity:</i> massive; 5% fissures and vughs near organic materials, 2-10mm long, 0.5-5mm thick, slightly serrated wall, formed after the shrinkage and decay of organic matter; 3% slide loss.</p>	Dumped archaeological material in

	<p><i>Mineral components: CF limit: 50µm; CF ratio: 30/70; Texture: 5% clay, 62% silt, 33% sand. CF related distribution: close porphyric; coarse fraction: 30% poorly-sorted, sub-angular to sub-rounded, fine to coarse sand-size rock fragments, 80-2000µm; 3% rounded, fine pebble size rock fragments, 2-5mm, random; fine fraction: 62% light brownish (PPL) humic silt; 5% light yellow (PPL) limpid clay aggregates (200-400µm) and coatings with bright yellowish interference colour; grano-striated to random striated.</i></p> <p><i>Organics: humified plant tissues and amorphous organic material (10%) and fragmented bast fibres (5%), 1-7mm long, mostly random, laminae of horizontal oriented organic matter appear at intervals; charcoal with cell structures, 2-10mm in size, 5% of the fabric, random; fresh woody plant tissues, 3-10m, 3% of the fabric.</i></p> <p><i>Artefacts: a single piece of highly degraded, rounded, pottery sherd, 5mm.</i></p> <p><i>Pedofeatures: Textural: 1) laminae (2-3mm) of horizontal oriented organic matter appear at intervals, the soil material trapped in-between the laminar organic beddings shows a darker colour with finer particle sizes and are weakly laminated, 10% of the fabric; Fabric: 1) aggregates (3-7mm) mixed by reddened calcium carbonate rich groundmass and fine charred material, possibly burnt, 10% of the fabric; 2) various rounded possibly burnt soil aggregates, including a 10mm large, rounded soil aggregates composed of light brownish (PPL) limpid silty clay with high birefringence and striated b-fabric, the outer rim was burnt; a 5mm large, light black (PPL) sandy silt aggregates containing abundant very fine charred materials; a 4cm long, reddish brown (PPL) burnt daub; 3) a bimodal paste mixed by very fine silty clay and angular sand size rock fragments, 1cm large.</i></p>	alluvial deposits
--	--	-------------------

T3131 3



Slide thickness: 40µm, even, no loss.

Micro-fabric	Micromorphological Description	Interpretation
T3131 3: 1 Unit 6B	<p><i>Thickness:</i> 5cm. <i>Lower boundary:</i> distinct, clear, sloping.</p> <p><i>Structure and porosity:</i> weakly developed platy microstructure; 10% planar vegetal voids, 2-30mm long, 0.5-4mm thick, slightly serrated wall, formed after the shrinkage and decay of organic matter.</p> <p><i>Mineral components:</i> <i>CF limit:</i> 50µm; <i>CF ratio:</i> 45/55; <i>Texture:</i> 5% clay, 50% silt, 45% sand. <i>CF related distribution:</i> close porphyric; <i>coarse fraction:</i> 25% poorly-sorted, sub-angular to sub-rounded, fine to coarse sand-size rock fragments, 80-2000µm, random; 20% rounded, pebble size rock fragments, 5-15mm, concentrate in the upper 3cm; <i>fine fraction:</i> 50% light brown (PPL) humic silt; 5% light yellowish (PPL) limpid clay aggregates and coatings with bright yellowish interference colour, 200-400µm; <i>b-fabric:</i> striated.</p> <p><i>Organics:</i> 15% parallel bedded humified plant tissues and amorphous organic material, 5% of which are potential bast fibres, 1-20mm long; charcoal with cell structures, 2-20mm in size, 10% of the fabric, random to weakly laminar; bedded fresh woody plant tissues, 3-15mm, 2% of the fabric.</p> <p><i>Artefacts:</i> 2% burnt bone fragments, 0.5-1mm, random; a 2cm large pottery sherds, obliquely inserted into Microfabric 3:2.</p> <p><i>Pedofeatures: Textural:</i> 1) the sediment in the bottom 2cm is more compacted, organic material and pottery sherd are mostly laminated. 2) limpid clay coating around pebble size rock fragments, strong birefringence, bright yellowish interference colour, 2% of the fabric. <i>Fabric:</i> 1) rounded soil aggregates with diverse groundmass, 1-25mm in size, 20% of the fabric. 2) laminar of fine charcoal rich, humic silty clay similar to the fine matrix in Microfabric 3:2, intercalated between the coarse materials, 5% of the fabric.</p>	Trampled layer mixed with dumped rock fragments and occupational debris.
T3131 3:2 Unit 6C-1	<p><i>Thickness:</i> 7cm. <i>Lower boundary:</i> none.</p> <p><i>Structure and porosity:</i> weakly developed platy microstructure; 15% planar vegetal</p>	Trampled and intensively

	<p>voids, 2-50mm long, 2-5mm thick, slightly serrated wall, formed after the shrinkage and decay of organic matter.</p> <p><i>Mineral components: CF limit: 50µm; CF ratio: 30/70; Texture: 5% clay, 65% silt, 30% sand. CF related distribution: close porphyric; coarse fraction: 27% poorly-sorted, sub-angular to angular, fine to coarse sand-size rock fragments, 80-800µm; 3% rounded, fine pebble size rock fragments, 5-10mm; fine fraction: 70% dark brown (PPL) humic silty clay with low interference colour; b-fabric: stipple to striated.</i></p> <p><i>Organics: parallel bedded humified plant tissues and amorphous organic material (10%) and bast fibres (10%), 1-20mm long; charred material in-between the bast fibres, with cell structures, 2-10mm in size, 8% of the fabric, random to weakly laminar, more concentrate in the upper part; bedded fresh woody plant tissues, 0.3-1cm, 3% of the fabric, some are broken <i>in situ</i>; <1% phytolith slugs, 0.2-0.4mm.</i></p> <p><i>Artefacts: 5% burnt bone fragments, 0.5-10mm, laminar.</i></p> <p><i>Pedofeatures: Textural: 1) bast fibres are more concentrated in the lower part, charred material and burnt bones are more concentrated in the upper part. Fabric: 1) rounded soil aggregates with diverse groundmass and sizes and are commonly coated with fine charred materials, 1-25mm in size, found in-between bast fibres in the lower part, random in the upper part, at least 1/5 of which are potentially burnt, 40% of the fabric. 2) an amorphous, yellowish brown (PPL), optically isotropic, phosphate rich aggregate with imprints of various organic matter or phytoliths, 7mm large, potential coprolite.</i></p>	<p>occupied floor sequence with intact woven bast fibres and abundant occupational debris.</p>
--	---	--

T3131 2



Slide thickness: 40µm, even, no loss.

Micro-fabric	Micromorphological Description	Interpretation
<p>T3131 2: 1 Unit 6C-1</p> <p>2:1</p> <p>T3131 2:2</p>	<p><i>Thickness:</i> 0.5cm. <i>Lower boundary:</i> faint, diffuse.</p> <p><i>Structure and porosity:</i> moderately developed platy microstructure; 15% planar vegetal voids, 0.5-1mm wide, 0.5-4cm long, smooth wall.</p> <p><i>Mineral components:</i> <i>CF limit:</i> 50µm; <i>CF ratio:</i> 15/85; <i>CF related distribution:</i> close porphyric; <i>Texture:</i> 20% clay, 70% silt, 15% sand; <i>coarse fraction:</i> 15% sub-rounded, very fine to fine sand-size single quartz grains, 40-150µm, random; <i>fine fraction:</i> light yellow (PPL) humic silty clay; <i>b-fabric:</i> parallel striated.</p> <p><i>Organics:</i> Parallely bedded bast fibres, 3cm long, 40% of the fabric; fine charred material in-between the bast fibres, 0.2-0.5 mm in size, 5% of the fabric; 3% amorphous organic fine material, 0.2-0.5mm, mostly laminar.</p> <p><i>Artefacts:</i> none.</p> <p><i>Pedofeatures:</i> none.</p>	<p>Matting with trampling.</p>
<p>T3131 2:2 Unit 6C-2</p> <p>T3131 2:3</p> <p>T3131 2</p>	<p><i>Thickness:</i> 5cm. <i>Lower boundary:</i> faint, diffuse.</p> <p><i>Structure and porosity:</i> massive; 3% porosity formed by soil lost during slide making; 3% fissures and cracks, 1-2mm wide, serrated wall; 2% root voids, 0.5-1cm long, smooth wall.</p> <p><i>Mineral components:</i> <i>CF limit:</i> 50µm; <i>CF ratio:</i> 15/85; <i>CF related distribution:</i> close porphyric; <i>Texture:</i> 20% clay, 65% silt, 15% sand; <i>coarse fraction:</i> 10% sub-rounded, very fine to fine sand-size single quartz grains, 40-150µm, random; 5% sub-rounded, medium to coarse sand-size rock fragments, 400-800µm, random; <i>fine fraction:</i> yellowish brown (PPL) humic calcareous silty clay. <i>b-fabric:</i> striated.</p> <p><i>Organics:</i> 10% charcoal fragments with various size from 1mm to 2.5cm, random; 8% mostly laminar humified plant tissues and amorphous organic fine material, half of which are potential bast fibres, 0.2-2mm; fresh woody plant tissues, 0.2-1cm, 3% of the fabric;</p>	<p>Alluvium deposited under shallow and slow water with input of occupational debris from nearby occupation areas</p>

	<p><i>Artefacts:</i> <1% fine burnt bone fragments, 0.2mm, random; <1% shell fragments, 0.5mm, random.</p> <p><i>Pedofeatures: Textural:</i> 1) iron oxides impregnated clay material and pyrite framboids coated root voids that have remnant organic matter, <1% of the fabric; <i>Crystalline:</i> 1) 8% reddened clusters of micritic calcium carbonates with diffuse boundaries, 0.2-2mm, and a 2cm long, elongate cluster of iron impregnated micritic calcium carbonate incorporating fine charred materials; 2) <1% blueish vivianite crystals near decayed organic matter; <i>Fabric:</i> 1) burnt soil aggregates, 3mm, random, 2% of the fabric.</p>	
<p>T3131 2:3 Unit 7-1</p>	<p><i>Thickness:</i> 7cm. <i>Lower boundary:</i> none.</p> <p><i>Structure and porosity:</i> weakly developed platy microstructure; 10% planar vegetal voids, 2-20mm long, 0.2-2mm thick, slightly serrated wall, formed after the shrinkage and decay of organic matter.</p> <p><i>Mineral components: CF limit:</i> 50µm; <i>CF ratio:</i> 10/90; <i>Texture:</i> 10% clay, 80% silt, 10% sand. <i>CF related distribution:</i> close porphyric; <i>coarse fraction:</i> 9% sub-angular, fine to coarse sand-size rock fragments, 80-800µm; 1% rounded, pebble size rock fragments, 7mm, potentially burnt; <i>fine fraction:</i> 75% light brownish (PPL) humic silty clay with low interference colour; 15% light yellow (PPL) to reddish brown (PPL) sparite calcium carbonates, unevenly distributed in the groundmass; <i>b-fabric:</i> undifferentiated to calcitic crystallitic.</p> <p><i>Organics:</i> parallelly bedded humified amorphous organic material (10%) and bast fibres (10%), 160-2000µm long; charred material in-between the bast fibres, with cell structures, 2-7mm in size, 10% of the fabric, random to laminar; bedded fresh woody plant tissues, 0.3-1cm, 3% of the fabric; a 4cm long, 1mm thick wood plank laid on top of this fabric.</p> <p><i>Artefacts:</i> 3% pottery sherds, 3-10mm, random; 1% fine burnt bones, 300-400µm; <1% shell fragments, 400-600µm.</p> <p><i>Pedofeatures: Textural:</i> 1) lower 1cm of this fabric are more compacted with higher content of bast fibres and more fragmented charred materials; <i>Crystalline:</i> 1) lumps (2cm) and small aggregates (40-800µm) of reddened micritic/sparite calcium carbonates unevenly scattered in-between the laminated bast fibres, mostly with diffuse boundaries, more concentrated in the lower 1cm, a few fine charred materials are incorporated in the large lumps, 15% of the fabric; 2) 1% blueish vivianite crystals near decayed organic matter, 0.2-0.5mm; 3) an intact calcium carbonate pseudomorphs after plant structure, 3mm long, in the lower part of the fabric; <i>Fabric:</i> 1) a single piece of 1cm large, burnt soil aggregate coated with fine charcoals, found on top of one of the bedded bast fibres.</p>	<p>Heavily trampled occupation layer with well-preserved matting in the bottom 2cm.</p>

T3131 1



Slide thickness: 40µm, even, minor loss.

Micro-fabric	Micromorphological Description	Interpretation
T3131 1: 1 Unit 7-1	<p><i>Thickness:</i> 0.5-1cm. <i>Lower boundary:</i> distinct, faint.</p> <p><i>Structure and porosity:</i> massive. 5% planar vegetal voids around plant materials, 0.5-1mm wide, smooth wall.</p> <p><i>Mineral components:</i> <i>CF limit:</i> 50µm; <i>CF ratio:</i> 10/90; <i>Related distribution:</i> close porphyric; <i>Texture:</i> 15% clay, 75% silt, 10% sand; <i>coarse fraction:</i> 10% moderate-sorted very fine sand-size single quartz grains, random; <i>fine fraction:</i> light yellow (PPL) humic silty clay. <i>b-fabric:</i> striated.</p> <p><i>Organics:</i> Parallely bedded bast fibres, 5-6cm long, 20% of the fabric; charred material in-between the bast fibres, 1-2mm in size, 5% of the fabric.</p> <p><i>Artefacts:</i> <1% reddened clusters of micritic calcium carbonates, potential ash lumps, 0.5-1mm; a single piece of fine pottery sherds, 2mm.</p> <p><i>Pedofeatures:</i> none.</p>	Trampled, 'clean' matting surface.
T3131 1:2 Unit 7-2	<p><i>Thickness:</i> 4cm. <i>Lower boundary:</i> distinct, clear, sloping.</p> <p><i>Structure and porosity:</i> massive; 3% fissures and cracks, 1-2mm, serrated wall.</p> <p><i>Mineral components:</i> <i>CF limit:</i> 50µm; <i>CF ratio:</i> 15/85; <i>CF related distribution:</i> close porphyric; <i>Texture:</i> 20% clay, 65% silt, 15% sand; <i>coarse fraction:</i> 10% poorly-sorted sub-angular fine sand-size single quartz grains, 40-150µm, random; 5% randomly distributed coarse sand-size or fine pebble-size rock fragments, 400-800µm, random; <i>fine fraction:</i> light brown (PPL) humic calcareous silty clay. <i>b-fabric:</i> striated.</p> <p><i>Organics:</i> 15% charred material and fresh woody material 1-2cm in size, long-axis parallel to the surface; 5% weakly laminated amorphous organic fine materials, half of which are potential bast fibres, 0.2-2mm.</p> <p><i>Artefacts:</i> 1% reddened clusters of micritic calcium carbonates, potential ash lumps;</p>	Alluvium deposited under shallow and slow water with input of occupational debris from nearby occupation areas

	<p>0.5-1mm, random.</p> <p><i>Pedofeatures: Crystalline:</i> 1) <1% blueish vivianite crystals near decayed organic matter, 0.2-0.5mm.</p>	
T3131 1:3 Unit 8-1	<p><i>Thickness:</i> 3.5-4cm. <i>Lower boundary:</i> distinct, sharp, wavy.</p> <p><i>Structure and porosity:</i> massive; 3% lost during thin section making; 2% vughs formed after the decay organic matter.</p> <p><i>Components:</i></p> <p>30% Rock fragments: sub-angular, coarse sand-size to fine pebble-size rock fragments, 1-7mm, mostly random, weakly laminated and parallel to the slope direction in the upper part of this fabric.</p> <p>30% <i>Sediment-1: Mineral components: CF limit:</i> 50µm. <i>CF ratio:</i> 40/60. <i>CF related distribution:</i> close porphyric; <i>Texture:</i> 10% clay, 50% silt, 40% sand; <i>coarse fraction:</i> 40% poor-sorted sub-rounded, fine to coarse sand-size single quartz grains, 100-1000µm, random; <i>fine fraction:</i> dark brown (PPL) humic silty clay; <i>b-fabric:</i> speckled to undifferentiated; found in-between the coarse materials.</p> <p>25% <i>Organics:</i> 15% amorphous organic fine material, 0.2-1mm; 5% uncharred organic residues, 2-10mm, random; 3% charcoal with cell structure, 2-5mm, random; 2% bast fibres, 2cm long, weakly laminated.</p> <p>15% <i>Artefacts:</i> 5% burnt bones (including fish bones and a reptile bone), 1-7mm, random; 5% dark brown micritic calcium carbonate aggregates, possibly reworked ash lumps or plaster materials, 3-5mm, random; a single piece of pottery sherds with sharp edges, 5mm; a single piece of stone artefact, 1.5cm; 1% burnt soil aggregates, 4mm, random.</p> <p>2% <i>Pedofeatures: Crystalline:</i> 1) 1% blueish vivianite crystals near burnt bone materials, 0.2-0.5mm.</p>	Inclined dumped layer containing large amount of burnt anthropogenic materials.
T3131 1:4 Unit 8-2	<p><i>Thickness:</i> 2cm. <i>Lower boundary:</i> distinct, sharp.</p> <p><i>Structure and porosity:</i> massive; 1% planar fissures, 0.5mm, serrated wall.</p> <p><i>Mineral components: CF limit:</i> 50µm; <i>CF ratio:</i> 8/92; <i>CF related distribution:</i> close porphyric; <i>Related distribution:</i> close porphyric; <i>Texture:</i> 10% clay, 82% silt, 8% sand; <i>coarse fraction:</i> 8% of sub-angular, coarse sand-size and fine pebble-size rock fragments, 0.5-3mm, random; <i>fine fraction:</i> brown (PPL) humic silty clay; <i>b-fabric:</i> undifferentiated.</p> <p><i>Organics:</i> 20% charred or humified amorphous organic fine material, 0.2-0.5mm, parallelly laminated in the bottom, no orientation in the middle and upper part.</p> <p><i>Artefacts:</i> a single piece of possible lime plaster fragment with four layers of lime plasters interlaced with layers of micro-charcoal, 4mm.</p>	Alluvial deposits, possibly dumped

	<i>Pedofeatures:</i> none.	
T3131 1:5 Unit 8-3	<p><i>Thickness:</i> 2cm. <i>Lower boundary:</i> none.</p> <p><i>Structure and porosity:</i> massive with a few channels; 5% zone of groundmass loss during thin section making; 3% voids formed after the shrinkage or decay of organic matter.</p> <p><i>Components:</i></p> <p><i>30% Rock fragments:</i> sub-angular to sub-rounded, fine pebble-size rock fragments, 2-6mm, random, >50% light yellow (PPL) calcite-rich metamorphic rock fragments.</p> <p><i>30% Sediment-1: Mineral components:</i> CF limit: 50µm. CF ratio: 40/60. CF related distribution: close porphyric; <i>Texture:</i> 10% clay, 50% silt, 40% sand; <i>coarse fraction:</i> 40% poorly-sorted, sub-angular, fine to coarse sand, 100-1000µm, random; <i>fine fraction:</i> 50% brownish (PPL) humic silty clay mixed with 10% micritic calcium carbonate; <i>b-fabric:</i> undifferentiated to micritic calcitic crystallitic; found inbetween the coarse materials.</p> <p><i>28% Organics:</i> 10% humified organic fine material, 0.2-1mm, commonly found incorporating in Sediment-1; 10% charcoal with cell structure, 2-10mm; 6% uncharred organic residues, 0.5-1mm; 2% bast fibres, 3-5mm long; all organic materials are randomly distributed.</p> <p><i>5% Artefacts:</i> a single piece of pottery sherd with sharp boundaries, 1.2cm long.</p> <p><i>7% Pedofeatures: Crystalline:</i> 1) 5% micritic calcium carbonate clusters with diffuse boundary, 0.5-3mm. <i>Fabric:</i> 1) 2% rounded soil aggregates, 2mm, random.</p>	Dumped anthropogenic materials.

T1812 7



T1812 7:1

T1812 7:2

Slide thickness: 20-40µm,
uneven, major loss

Micro-fabric	Micromorphological Description	Interpretation
T1812 7: 1	<p><i>Thickness:</i> 4cm. <i>Lower boundary:</i> faint, diffuse.</p> <p><i>Structure and porosity:</i> the same as T1812 7:2.</p> <p>Mixture of different soil materials with 2% coarse sand-size rock fragments, which is similar to the Micro-fabric T1813 7:2. Around 50% of the groundmass is heavily stained by orange (PPL) amorphous iron oxides.</p> <p><i>Organics:</i> 2% dark brown humified and amorphous organic fine material, random, 0.1-1mm.</p> <p><i>Artefacts:</i> none.</p> <p><i>Pedofeatures: Textural:</i> 1) a thin (50µm) lamina of dusty (orange in XPL) silty clay crusts with high birefringence, demarcates the Micro-fabrics T1812 7:1 and 7:2; 2) thin (20-50µm) hypo- and quasi-coating of dusty (orange in XPL) clay with high birefringence around voids, 1% of the fabric; <i>Amorphous Crypocrystalline:</i> 1) reddish yellow (PPL) stain of amorphous iron oxides as depleted quasi-coating of voids and mottles, 50%.</p>	Constructed layer using various soil materials.
T1812 7: 2	<p><i>Thickness:</i> 7cm. <i>Lower boundary:</i> none.</p> <p><i>Structure and porosity:</i> mixture of moderately developed sub-angular blocky and vesicular structure, the peds are accommodated, 1-2cm in size; 15% interconnected planar voids, unaccommodated, 0.2-1mm thick, slightly serrated walls; 5% vesicles, 0.2-1mm large, smooth walls, irregular shape; 50% zone of groundmass lost during thin section making.</p> <p><i>Mixture of different soil materials</i> with 2% coarse sand-size rock fragments, which is similar to the Micro-fabric T1813 6:1. Around 50% of the groundmass is heavily stained by orange (PPL) amorphous iron oxides.</p> <p><i>Organics:</i> 2% dark brown humified and amorphous organic fine material, random, 0.1-1mm.</p>	Constructed layer using various soil materials.

	<p><i>Artefacts:</i> none.</p> <p><i>Pedofeatures: Textural:</i> 1) thin (20-50μm) hypo-coating of dusty (yellow to orange in XPL) clay with high birefringence around voids, 1% of the fabric; <i>Amorphous Crypocrystalline:</i> 1) reddish yellow (PPL) stain of amorphous iron oxides as depleted quasi-coating of voids and mottles, 50%.</p>	
--	---	--

T1813 6

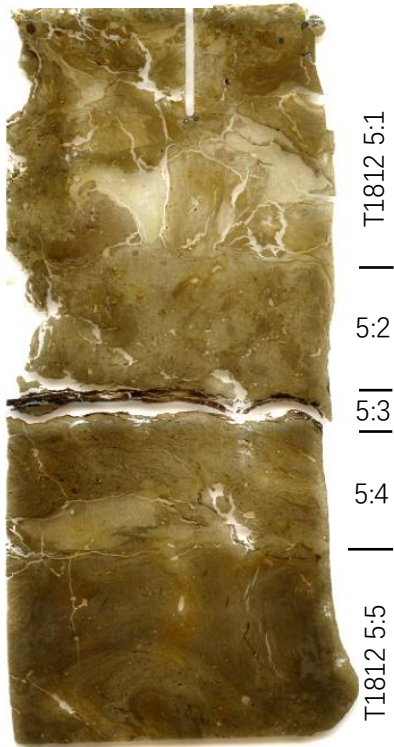


Slide thickness: 40µm, even,
no loss

Micro-fabric	Micromorphological Description	Interpretation
T1813 6:1 Bottom of Platform I-2	<p><i>Thickness:</i> 2cm. <i>Lower boundary:</i> faint, diffuse.</p> <p><i>Structure and porosity:</i> mixture of weakly developed sub-angular blocky and vesicular structure, the peds are accommodated, 0.5-1cm in size; 10% vesicles, 0.2-5mm large, smooth walls, irregular shape; 5% interconnected planar voids, unaccommodated, 0.2-1mm thick, slightly serrated walls.</p> <p>The groundmass is the unevenly but well-incorporated mixture of four sediment materials similar to the Micro-fabric T1813 6:3 with 2% randomly distributed coarse to very coarse sand-size rock fragments and 1% clusters of charred material, 1-2mm, random.</p> <p><i>Artefacts:</i> none.</p> <p><i>Pedofeatures: Textural:</i> 1) hypo-coating and quasi-coating of micro-laminated thin (20-100µm) limpid and dusty (orange in XPL) clay with high birefringence around voids and organic materials, 1% of the fabric. <i>Crystalline:</i> 1) vivianite crystals, 1-3mm, 1% of the fabric.</p>	Constructed layer using various soil materials.
T1813 6:2 Between Platform II-2 and I-2	<p><i>Thickness:</i> 2cm. <i>Lower boundary:</i> faint, diffuse.</p> <p><i>Structure and porosity:</i> mixture of moderately developed sub-angular blocky and vesicular structure, the peds are partially accommodated, around 0.5-1cm in size; 10% interconnected planar voids, unaccommodated, 0.2-1mm thick, slightly serrated walls. 5% vesicles, 0.2-2mm large, smooth walls, irregular shape; 5% slide loss.</p> <p><i>Mineral components:</i> the same as the Sediment-2 of Micro-fabric T1813 6:3.</p> <p><i>Organics:</i> A inclined (30°) layer of black, humified grass materials, 5-20mm, 30% of the fabric.</p> <p><i>Artefacts:</i> A thin lamina of fragmented bone material, 3% of the fabric.</p> <p><i>Pedofeatures: Textural:</i> 1) crescent hypo-coatings and intercalations of alternating dusty</p>	Open-air matting of grass materials

	and limpid clay with high birefringent, yellow (XPL), 0.3-0.5mm thick, around voids and laminar organic materials, 5% of the fabric; 2) hypo-coating of thin (20-100µm) limpid (yellow in XPL) and slightly dusty (orange in XPL) clay with high birefringence around voids and organic materials, 1% of the fabric.	
T1813 6:3 Top of Platform II-2	<p><i>Thickness:</i> 5cm. <i>Lower boundary:</i> none.</p> <p><i>Structure and porosity:</i> mixture of moderately developed sub-angular blocky and vesicular structure, the peds are partially accommodated, around 0.5-1cm in size; 10% interconnected planar voids, unaccommodated, 0.2-1mm thick, slightly serrated walls; 10% vesicles, 0.2-2mm large, smooth walls, irregular shape.</p> <p>The groundmass is the unevenly but well-incorporated mixture of four sediment materials and 2% randomly distributed coarse to very coarse sand-size rock fragments and 2% fragments of charred material, 1-2mm, random.</p> <p>Sediment 1, 40% of the fabric: the same as the Sediment-1 in Micro-fabric T1812 4:1.</p> <p>Sediment 2, 40% of the fabric: the same as the Sediment-2 in Micro-fabric T1812 4:1.</p> <p>Sediment 3, 10% of the fabric, as soil aggregates, 5-7mm, random: the same as the groundmass in Micro-fabric T1812 4:2.</p> <p>Sediment 4, 5% of the fabric, as soil aggregates, 5-7mm, random: the same as the Sediment 3 in Micro-fabric T1812 4:1.</p> <p><i>Pedofeatures: Textural:</i> 1) intercalations of limpid and dusty micro-layers of clay with high birefringence, light yellow to orange (XPL), 0.5mm thick, random, 1% of the fabric. 2) thin (20-100µm) hypo-coating of limpid (yellow in XPL) and slightly dusty (orange in XPL) clay with high birefringence around voids, 1% of the fabric.</p>	Constructed layer using various soil materials.

T1812 5



Slide thickness: 40µm, even, no loss

Micro-fabric	Micromorphological Description	Interpretation
T1812 5: 1 Platform I-3	<p><i>Thickness:</i> 4cm. <i>Lower boundary:</i> prominent, clear.</p> <p><i>Structure and porosity:</i> fissures microstructure; 10% fissures between soil aggregates, unaccommodated, 0.5-1mm thick, slightly serrated walls.</p> <p>This fabric is the closely compacted of at least four different types of soil materials:</p> <p><i>Soil aggregates-1</i>, 25% of the fabric: light brown (PPL) fine silty clay (c/f 30/70, limit:10µm) with lamination of silty clay crusts (30% of the soil aggregate), some of aggregates have vertical laminated silty clay crusts.</p> <p><i>Soil aggregates-2</i>, 25% of the fabric: yellow (PPL) very fine silty clay with reticulated-striated b-fabric and high birefringence (c/f 5/95, limit:10µm), similar to the T1813 4:2 micro-fabric, 2-12cm, random.</p> <p><i>Soil aggregates-3</i>, 25% of the fabric: light yellow (PPL) limpid silty clay soil aggregates (c/f 70/30, limit:10µm), similar to the groundmass of Micro-fabric T3131 6:1 of profile T3131, 5-15mm, random.</p> <p><i>Soil aggregates-4</i>, 25% of the fabric: brown (PPL) humic silty clay with a high content of humified amorphous fine material (c/f 50/50, limit:10µm), 3-14mm, random.</p> <p><i>Pedofeatures: Crystalline:</i> 1) vivianite crystals, 1-1.5mm, 1% of the fabric, in the upper part of the fabric.</p>	Constructed layer using various soil materials.
T1812 5:2 Top of Platform I-4	<p><i>Thickness:</i> 2cm. <i>Lower boundary:</i> prominent, clear.</p> <p><i>Structure and porosity:</i> vesicular microstructure; 5% vesicles, 0.5-6mm large, smooth walls, irregular shape.</p> <p><i>Mineral components: CF limit:</i> 50µm; <i>CF ratio:</i> 20/80; <i>CF related distribution:</i> close porphyric; <i>Texture:</i> 20% sand, 60% silt, 20% clay; <i>coarse fraction:</i> 20% moderate-sorted, sub-rounded to sub-angular, very fine to fine sand-size quartz, 40-200µm,</p>	Constructed layer made with water and stirring with the soil sourced in nearby stratum.

	<p>random; <i>fine fraction</i>: light grayish yellow (PPL) humic silty clay with moderate birefringence, commonly as small aggregates 0.1-1mm in size, 3% of the fine fraction is stained by light reddish yellow (PPL) amorphous iron oxides; <i>b-fabric</i>: random striated.</p> <p><i>Organics</i>: 3% dark brown humified and amorphous organic fine material, random, 0.1-1mm.</p> <p><i>Pedofeatures: Amorphous Crypocrystalline</i>: 1) light reddish yellow (PPL) stain of amorphous iron oxides as hypo-coating of voids and mottles, 3%; <i>Fabric</i>: 1) fragmented fine silty clay soil aggregates with irregular boundaries, 20%, 1-5mm, random.</p>	
T1812 5:3 Middle of Platform I-4	<p><i>Thickness</i>: 0.5cm. <i>Lower boundary</i>: prominent, sharp.</p> <p><i>Structure and porosity</i>: platy microstructure; 60% porosity formed due to the shrinkage of organic material.</p> <p>60% laminar, humified organic residue, 50-100µm thick, more than 30 layers.</p> <p>40% light brown (PPL) dusty, very fine silty clay with moderate birefringence, filled in the interspace of the laminar organic materials.</p>	Organic laminae placed by human in a ponding condition.
T1812 5:4 Bottom of Platform I-4	<p><i>Thickness</i>: 2cm. <i>Lower boundary</i>: prominent, clear.</p> <p><i>Structure and porosity</i>: massive microstructure; 5% horizontal planar voids, accommodated, 0.1-0.5mm thick, slightly serrated walls; 3% vughs, 2-5mm, irregular shape.</p> <p><i>Mineral components: CF limit</i>: 50µm; <i>CF ratio</i>: 15/85; <i>CF related distribution</i>: open porphyric; <i>Texture</i>: 15% sand, 60% silt, 25% clay; <i>coarse fraction</i>: 15% moderate-sorted, sub-rounded to sub-angular, very fine to fine sand-size quartz, 40-200µm, random; <i>fine fraction</i>: light grayish yellow (PPL) humic silty clay with moderate birefringence; <i>b-fabric</i>: parallel striated.</p> <p><i>Organics</i>: 10% dark brown humified and amorphous organic fine material, laminar, 0.1-5mm.</p> <p><i>Pedofeatures: Textural</i>: 1) fragmented fine dusty silty clay crusts near the laminar organic materials, 20%; <i>Fabric</i>: 1) soil aggregates composed of coarse silt-size and very fine sand-size quartz and light yellow (PPL) silty clay (c/f 40/60, limit: 10µm) with fewer fragmented humified organic material, 5-20mm, 20% of the fabric, horizontal laminar in the bottom of this fabric.</p>	Alluvium with flushed in of soil aggregates by rainfall events.
T1812 5:5 Top of Layer 5	<p><i>Thickness</i>: 3cm. <i>Lower boundary</i>: none.</p> <p><i>Structure and porosity</i>: massive microstructure with secondary sedimentary structures of convoluted laminations of dusty silty clay crusts; 2% vertical planar voids, accommodated, 0.1-0.5mm thick, serrated walls; 2% small root voids coated with remnant humified organic material, 0.5-2mm.</p> <p><i>Mineral components: CF limit</i>: 50µm; <i>CF ratio</i>: 10/90; <i>CF related distribution</i>: open porphyric; <i>Texture</i>: 10% sand, 70% silt,</p>	Alluvium deposited under repeat wetting and drying with deformed

	<p>20% clay; <i>coarse fraction</i>: 10% moderate-sorted, sub-rounded to sub-angular, very fine to fine sand-size quartz, 40-200µm, random; <i>fine fraction</i>: light grayish yellow(PPL) fine calcareous silty clay with low birefringence, 15% stained by reddish yellow (PPL) amorphous iron oxides; <i>b-fabric</i>: stipple-speckled to micritic calcitic crystallitic.</p> <p><i>Organics</i>: 5% dark brown humified and amorphous organic fine material, random, 0.1-5mm; <1% very fine charcoal, 0.1-0.3mm, random.</p> <p><i>Artefacts</i>: a single piece of burnt bone, 1mm, on top of this fabric.</p> <p><i>Pedofeatures: Textural</i>: 1) convoluted laminations of dusty silty clay crusts, each crust is 0.1-0.2mm thick, 50% of the fabric; 2) thick (1-1.5mm) laminations of very fine silty clay crusts with moderate birefringence, on top of the fabric, 3%; <i>Amorphous Crypocrystalline</i>: 1) light reddish yellow (PPL) stain of amorphous iron oxides as quasi-coating of voids and mottles in the groundmass, 15% of the fabric; 2) manganese pellets incorporated near voids and humified organic materials, <1% of the fabric.</p>	<p>features. Covered by thin silty clay crusts formed under very quiet, ponding condition.</p>
--	--	--

T1813 4



Slide thickness: 40µm, even,
no loss

Micro-fabric	Micromorphological Description	Interpretation
T1813 4: 1 Platform II-2	<p><i>Thickness:</i> 5cm. <i>Lower boundary:</i> prominent, clear.</p> <p><i>Structure and porosity:</i> moderately-developed prismatic microstructure, the pedes are accommodated, 1-2cm in size; 10% vertical planar voids and fissures, accommodated, 0.2-0.5mm thick, slightly serrated walls.</p> <p>The groundmass is the unevenly but well-incorporated mixture of four sediment materials and 2% coarse sand-size rock fragments:</p> <p>Sediment 1, 50% of the fabric: <i>Mineral components:</i> CF limit: 50µm; CF ratio: 5/95; <i>CF related distribution:</i> open porphyric; <i>Texture:</i> 5% sand, 75% silt, 20% clay; <i>coarse fraction:</i> 5% moderate-sorted, sub-rounded, very fine to fine sand-size quartz, 40-100µm, random; <i>fine fraction:</i> light brown (PPL) calcareous humic silty clay with low birefringence; <i>b-fabric:</i> stipple-speckled to striated. <i>Organics:</i> 5% black to dark brown charred and humified, amorphous organic fine material, random, 0.1-1mm.</p> <p>Sediment 2, 30% of the fabric: <i>Mineral components:</i> CF limit: 50µm; CF ratio: 10/90; <i>CF related distribution:</i> close porphyric; <i>Texture:</i> 10% sand, 65% silt, 25% clay; <i>coarse fraction:</i> 10% well-sorted, sub-rounded, very fine sand-size quartz, 40-50µm, random; <i>fine fraction:</i> light grayish yellow (PPL) calcareous silty clay with high birefringence; <i>b-fabric:</i> random to parallel striated. <i>Organics:</i> 5% black to dark brown charred and humified, amorphous organic fine material, random, 0.1-1mm.</p> <p>Sediment 3, 10% of the fabric, as soil aggregates, 0.1-5mm, random: <i>Mineral components:</i> CF limit: 50µm; CF ratio: 5/95; <i>CF related distribution:</i> open porphyric; <i>Texture:</i> 5% sand, 75% silt, 20% clay; <i>coarse fraction:</i> 5% moderate-sorted, sub-rounded, very fine to fine sand-size quartz, 40-100µm, random; <i>fine fraction:</i> dark brown (PPL) very humic silty clay, undifferentiated b-fabric. <i>Organics:</i> 50% finely fragmented humified and charred organic materials, 50-500µm, random.</p>	Construction material, possibly 'soil wrapped with grass' material.

	<p>Sediment 4, 10% of the fabric: the same the groundmass of micro-fabric 1813 4:2.</p> <p><i>Artefacts:</i> none.</p> <p><i>Pedofeatures: Textural:</i> 1) Thin (20-50µm) dusty clay hypo-coating around voids, high birefringent, orange (XPL), 1%.</p>	
<p>T1813 4:2 Top of Layer 5</p>	<p><i>Thickness:</i> 6cm. <i>Lower boundary:</i> none.</p> <p><i>Structure and porosity:</i> strongly developed angular-blocky structure, the peds are accommodated, size ranging from 1 to 10mm; 20% interconnected planar voids and fissures, accommodated, 0.2-5mm thick, slightly serrated walls.</p> <p><i>Mineral components: CF limit:</i> 50µm; <i>CF ratio:</i> 2/98; <i>CF related distribution:</i> open porphyric; <i>Texture:</i> 2% sand, 73% silt, 25% clay; <i>coarse fraction:</i> 2% moderate-sorted, sub-rounded, very fine sand-size quartz, 40-100µm, random; <i>fine fraction:</i> light brownish (PPL) humic silty clay with moderate birefringence; <i>b-fabric:</i> reticulated-striated.</p> <p><i>Organics:</i> 2% dark brown humified and amorphous organic fine material, random, 0.1-1mm; 1% very fine charcoal, 0.1-0.2mm, random.</p> <p><i>Artefacts:</i> none.</p> <p><i>Pedofeatures: Amorphous Crypocrystalline:</i> 1) light reddish yellow (PPL) stain of amorphous iron oxides in the groundmass, 3% of the fabric; 2) 2% blueish vivianite crystals, 100-400µm, random; <i>Fabric:</i> 1) soil aggregates composed of fragmented humified organic material and silt-size quartz, 0.5mm, 1% of the fabric, random.</p>	<p>Quiet, ponding environment with high clay content, repeat shrink-swell process.</p>

T1812 3



Slide thickness: 40µm, even, no loss

Micro-fabric	Micromorphological Description	Interpretation
T1812 3:1 Layer 5 Unit 5-1	<p><i>Thickness:</i> 5cm. <i>Lower boundary:</i> distinct, clear.</p> <p><i>Structure and porosity:</i> massive microstructure with secondary sedimentary structures of convoluted laminations of dusty silty clay crusts; 2% channels, partially accommodated, 2.5 cm long, serrated walls; 3% slide lost.</p> <p><i>Mineral components:</i> <i>CF limit:</i> 50µm; <i>CF ratio:</i> 5/95; <i>CF related distribution:</i> open porphyric; <i>Texture:</i> 5% sand, 75% silt, 20% clay; <i>coarse fraction:</i> 5% moderate-sorted, sub-rounded, very fine to fine sand-size quartz, 40-100µm, random; <i>fine fraction:</i> light grayish yellow(PPL) fine calcareous silty clay with low birefringence; <i>b-fabric:</i> stipple-speckled to micritic calcitic crystallitic.</p> <p><i>Organics:</i> 2% dark brown humified and amorphous organic fine material, random, 0.1-2mm; <1% very fine charcoal, 0.1-0.3mm, random.</p> <p><i>Artefacts:</i> none.</p> <p><i>Pedofeatures:</i> <i>Textural:</i> 1) convoluted laminations of dusty silty clay crusts, each crust is 0.1-0.2mm thick, 50% of the fabric; <i>Amorphous Crypocrystalline:</i> 1) a cluster of micritic calcium carbonate with diffuse boundaries near the channel, 5mm; 2) light reddish yellow stain of amorphous iron oxides, 1% of the fabric; 3) <1% blueish vivianite crystals, 50-100µm, random; 4) manganese pellets incorporated near voids and humified organic materials, <1% of the fabric.</p>	Accumulation of alluvial material under repeat wetting and drying conditions.
T1812 3:2 Bottom of Layer 5 Unit 5-2	<p><i>Thickness:</i> 2cm. <i>Lower boundary:</i> distinct, clear.</p> <p><i>Structure and porosity:</i> massive microstructure; 3% slide loss; 1% channels, partially accommodated, 2.5 cm long, serrated walls.</p> <p><i>Mineral components:</i> <i>CF limit:</i> 50µm; <i>CF ratio:</i> 20/80; <i>CF related distribution:</i> close porphyric; <i>Texture:</i> 20% sand, 65% silt, 15% clay; <i>coarse fraction:</i> 20% poorly-sorted, angular to sub-angular, very fine to medium sand-size quartz, 40-200µm, random; <i>fine</i></p>	Alluvial deposit with higher depositional energy.

	<p><i>fraction</i>: light grayish yellow(PPL) humic silty clay with low birefringence; <i>b-fabric</i>: stipple-speckled to striated.</p> <p><i>Organics</i>: 5% dark brown humified and amorphous organic fine material, random, 0.1-5mm; 1% very fine charcoal, 0.1-0.3mm, random.</p> <p><i>Artefacts</i>: none.</p> <p><i>Pedofeatures</i>: none.</p>	
T1812 3:3 Pre- occupation sediment-1	<p><i>Thickness</i>: 6cm. <i>Lower boundary</i>: none.</p> <p><i>Structure and porosity</i>: massive microstructure; 3% slide loss; 1% channels, partially accommodated, 2.5 cm long, serrated walls.</p> <p><i>Mineral components</i>: <i>CF limit</i>: 50µm; <i>CF ratio</i>: 5/95; <i>CF related distribution</i>: open porphyric; <i>Texture</i>: 5% sand, 75% silt, 20% clay; <i>coarse fraction</i>: 5% moderate-sorted, sub-rounded, very fine to fine sand-size quartz, 40-100µm, random; <i>fine fraction</i>: light grayish yellow(PPL) humic, calcareous silty clay with low birefringence; <i>b-fabric</i>: stipple-speckled to striated.</p> <p><i>Organics</i>: 2% dark brown humified and amorphous organic fine material, laminated, 0.1-1mm; 1% very fine charcoal, 0.1-0.3mm, random.</p> <p><i>Artefacts</i>: none.</p> <p><i>Pedofeatures</i>: <i>Textural</i>: 1) dusty silty clay crusts (50-400µm) alternates with coarse silt size material in the lower part of the fabric, 10% of the fabric; 2) fragmented dusty silty clay crusts, 100-200µm thick, mid-upper part of the fabric, 40% of the fabric; <i>Fabric</i>: 1) rounded fine silty clay soil aggregates, 2% of the fabric, random.</p>	Alluvial deposit

T1812 2



Slide thickness: 40-50µm,
even, no loss

Micro-fabric	Micromorphological Description	Interpretation
T1812 2: 1	<p><i>Thickness:</i> 6cm. <i>Lower boundary:</i> none.</p> <p><i>Structure and porosity:</i> massive microstructure; 1% channels, unaccommodated, 1.5 cm long, serrated walls.</p> <p><i>Mineral components:</i> <i>CF limit:</i> 50µm; <i>CF ratio:</i> 2/98; <i>CF related distribution:</i> open porphyric; <i>Texture:</i> 2% sand, 75% silt, 23% clay; <i>coarse fraction:</i> 2% well-sorted, sub-rounded, very fine to fine sand-size quartz, 40-100µm, random; <i>fine fraction:</i> light yellowish (PPL) dusty silty clay with low birefringence; <i>b-fabric:</i> reticulate-striated.</p> <p><i>Organics:</i> 3% dark brown humified and amorphous organic fine material, random, 0.1-5mm.</p> <p><i>Artefacts:</i> none.</p> <p><i>Pedofeatures:</i> <i>Crystalline:</i> 1) clusters of micritic calcium carbonate with diffuse boundary, 10-15mm, 10% of the fabric; <i>Amorphous and Cryocrystalline:</i> 1) A trace amount of blackish manganese compound is incorporated in the groundmass, <1%; 2) a few pyrite framboids around humified organic matter, <1%.</p>	<p>Gradually deposited alluvium or intertidal flat sediment under very weak depositional energy.</p>

T1812 1



Slide thickness: 40µm, even,
no loss

Micro-fabric	Micromorphological Description	Interpretation
T1812 1: 1	<p><i>Thickness:</i> 7.5cm. <i>Lower boundary:</i> none.</p> <p><i>Structure and porosity:</i> massive microstructure; 3% channels, unaccommodated, 0.2-1mm, 1.5-4 cm long, serrated walls; two 5mm root voids with remnant organic material.</p> <p><i>Mineral components:</i> <i>CF limit:</i> 50µm; <i>CF ratio:</i> 2/98; <i>CF related distribution:</i> open porphyric; <i>Texture:</i> 2% sand, 78% silt, 20% clay; <i>coarse fraction:</i> 2% well-sorted, sub-rounded, very fine sand-size quartz, 40-60µm, random; <i>fine fraction:</i> light yellowish (PPL) silty clay with moderate birefringence, 8% evenly distributed micritic to sparitic calcium carbonate (8%), 10-30µm; <i>b-fabric:</i> reticulate-striated to micritic calcitic crystalline (90:10).</p> <p><i>Organics:</i> 3% dark brown humified and amorphous organic fine material, random, 0.1-5mm.</p> <p><i>Artefacts:</i> none.</p> <p><i>Pedofeatures: Textural:</i> 1) channels are partially (1/4) infilled by finer silty clay with serrated void walls; 2) alternated micro-laminations of fine silty clay and calcium carbonate rich fine silt material, in the upper part of the fabric, 5% of the fabric; <i>Crystalline:</i> 1) clusters of micritic calcium carbonate with diffuse boundary, 10mm, 1/3 stained by amorphous iron oxides, 3% of the fabric; <i>Amorphous and Crypocrystalline:</i> 1) A trace amount of blackish manganese compound is incorporated in the groundmass, <1%; 2) a few pyrite framboids around humified organic matter, <1%; 3) red amorphous iron oxides coated humified organic material with diffuse boundary, <1%.</p>	<p>Gradually deposited alluvium or intertidal flat sediment under very weak depositional energy.</p>

JCN 4



Slide thickness: 40µm, even, no loss

JCN 4:1

Micro-fabric	Micromorphological Description	Interpretation
<p>JCN 4:1 Top of Unit 2</p>	<p><i>Thickness:</i> 6cm. <i>Lower boundary:</i> none.</p> <p><i>Structure and porosity:</i> moderately developed sub-angular blocky microstructure, the peds are partially accommodated, 5-20mm; 8% planar voids, accommodated, 0.5-3cm long, 0.5-1mm thick, smooth to slightly serrated walls, more concentrated in the upper right of the slide.</p> <p><i>Mineral components:</i> <i>CF limit:</i> 50µm; <i>CF ratio:</i> 25/75; <i>CF related distribution:</i> close porphyric; <i>Texture:</i> 25% sand, 50% silt, 25% clay; <i>coarse fraction:</i> 15% poorly-sorted, sub-rounded, very fine to fine sand-size quartz, 40-200µm, random; 10% sub-angular coarse sand-size to fine pebble-size rock fragments, random, 0.3-3mm; <i>fine fraction:</i> light yellow (PPL) silty clay with moderate birefringence, 40% of the groundmass stained by red (PPL) amorphous sesquioxides, mostly concentrated in the lower left part; 10% grayish yellow to yellow (PPL) dusty to limpid clay intercalations and hypo-coating of voids, moderate to high birefringent; <i>b-fabric:</i> random striated.</p> <p><i>Organics:</i> 5% fine charred material, 0.1-1mm, randomly distributed.</p> <p><i>Artefacts:</i> none.</p> <p><i>Pedofeatures:</i> <i>Textural:</i> 1) grayish yellow (PPL) dusty clay with moderate birefringence and yellow (PPL) limpid clay with high birefringent and high order interference colour as intercalations (100-200µm, random orientation) and hypo-coating (100-500µm) of voids, some show alternations of micro-laminated dusty and limpid clay, 10% of the fabric; 2) depletion hypo-coating of dusty silty clay around planar voids, 5%; <i>Amorphous Cryptocrystalline:</i> 1) red staining of amorphous iron oxides as nodules (0.5-5mm) and mottles, 50% of the fabric;</p>	<p>Constructed layer.</p>

JCN 3



JCN 3:1

Slide thickness: 40µm, even, no loss

Micro-fabric	Micromorphological Description	Interpretation
JCN 3:1 Bottom of Unit 2	<p><i>Thickness:</i> 6cm. <i>Lower boundary:</i> none.</p> <p><i>Structure and porosity:</i> moderately developed sub-angular blocky microstructure, the peds are partially accommodated, 2-5mm; 5% channels and associated vughs, unaccommodated, 0.3-1 cm long, 0.5-2mm thick, smooth to slightly serrated walls.</p> <p><i>Mineral components:</i> <i>CF limit:</i> 50µm; <i>CF ratio:</i> 30/70; <i>CF related distribution:</i> close porphyric; <i>Texture:</i> 30% sand, 50% silt, 20% clay; <i>coarse fraction:</i> 15% moderate-sorted, sub-rounded, very fine to fine sand-size quartz, 40-200µm, random; 15% sub-angular coarse sand-size to fine pebble-size rock fragments, random, 0.3-3mm; <i>fine fraction:</i> light brown(PPL) humic silty clay with moderate birefringence, 50% of the groundmass stained by red (PPL) amorphous sesquioxides; <i>b-fabric:</i> random striated.</p> <p><i>Organics:</i> 5% fine charred material, 0.1-1mm, clustered to randomly distributed.</p> <p><i>Artefacts:</i> none.</p> <p><i>Pedofeatures:</i> <i>Textural:</i> 1) dusty clay hypo-coatings of voids and grano-coating of soil aggregates and rock fragments, moderate birefringence, reddish brown (XPL), 100µm thick, 1% of the fabric; <i>Amorphous Crypocrystalline:</i> 1) red staining of amorphous iron oxides as nodules (0.5-5mm) and mottles, 50% of the fabric; <i>Fabric:</i> 1) rounded, 'clean', soil aggregates mainly composed of sub-angular silt size minerals, 10% of the fabric, 3-15mm, random.</p>	Constructed layer.

JCN 2



Slide thickness: 40µm, even, no loss

Micro-fabric	Micromorphological Description	Interpretation
JCN 2:1 Unit 3-1	<p><i>Thickness:</i> 4.5-6cm. <i>Lower boundary:</i> distinct, clear.</p> <p><i>Structure and porosity:</i> Platy microstructure; 5% horizontal planar voids, partially accommodated, 0.5-1mm thick, slightly serrated walls, 2% voids formed after the decay/shrinkage of organic material.</p> <p><i>Mineral components:</i> <i>CF limit:</i> 50µm; <i>CF ratio:</i> 20/80; <i>CF related distribution:</i> close porphyric; <i>Texture:</i> 20% sand, 65% silt, 15% clay; <i>coarse fraction:</i> 15% moderate-sorted, sub-angular to sub-rounded, very fine to fine sand-size quartz, 40-200µm, random; 5% sub-angular coarse sand-size rock fragments, random, 200-500µm; <i>fine fraction:</i> light yellow(PPL) silty clay with moderate birefringence; <i>b-fabric:</i> parallel to random striated (80:20).</p> <p><i>Organics:</i> 15% charcoal fragments, 1-10mm, mostly horizontally laminated, laminae of very fine charred materials are found in the upper part of the fabric; 10% light brown to black, humified organic residues and amorphous organic fine material, parallel laminar, 0.1-5mm, 1/4 of which are fragmented bast fibres; phytolith, random, 1%.</p> <p><i>Artefacts:</i> burnt bone fragments, 0.5-6mm, 3%, horizontal laminated; phytolith slags, <1%, random; fat-derived char, 0.5-1mm, random, <1%.</p> <p><i>Pedofeatures: Textural: Fabric:</i> 1) small rounded, 'clean', fine silty clay soil aggregates mainly composed of sub-angular silt size mineral, 1-5mm, 10% of the fabric, more concentrated in the upper of the fabric.</p>	<p>Intense human activity of cooking, dumping, trampling and bring in of material by foot traffic in a groundmass of alluvial sediment.</p>
JCN 2:2 Unit 3-2	<p><i>Thickness:</i> 1cm. <i>Lower boundary:</i> distinct, clear.</p> <p><i>Structure and porosity:</i> massive; 2% horizontal planar voids, accommodated, 0.3mm thick; 2% planar voids around organic material.</p> <p>The unit is formed by two intact layers of bast fibre, soil material between the bast fibres, and 0.5cm compacted lamina rich in horizontally laminated fine charcoals and</p>	<p>Matting and possible trampling on the activity surface.</p>

	<p>fragmented bast fibres on top of the bast fibres.</p> <p><i>Bast fibres:</i> inclined (30°) laminated, 0.1-0.2mm thick.</p> <p><i>Soil material in between the bast fibres:</i> similar to the groundmass of JCN 2:1.</p> <p><i>Compacted lamina:</i> groundmass similar to JCN 2:3, mixed with 20% charcoal, 0.5-5mm, horizontally laminated; 5% fragmented, laminated bast fibres, 0.5mm; 5% humified, laminar amorphous organic fine material, 0.2-1mm; 2% burnt bone fragments, 0.5-1mm; 1% fat-derived char; 1% phytolith.</p>	
JCN 2:3 Unit 3-3	<p><i>Thickness:</i> 3.5-5cm. <i>Lower boundary:</i> none.</p> <p><i>Structure and porosity:</i> massive microstructure; 2% fissures, partially accommodated, 0.2-0.5mm thick, slightly serrated walls, 2% voids formed after the decay/shrinkage of organic material.</p> <p><i>Mineral components:</i> <i>CF limit:</i> 50µm; <i>CF ratio:</i> 20/80; <i>CF related distribution:</i> close porphyric; <i>Texture:</i> 20% sand, 65% silt, 15% clay; <i>coarse fraction:</i> 15% moderate-sorted, sub-angular to sub-rounded, very fine to fine sand-size quartz, 40-200µm, random; 5% sub-angular coarse sand-size to fine pebble-size rock fragments, random, 0.3-5mm; <i>fine fraction:</i> light brown (PPL) humic silty clay with moderate birefringence; <i>b-fabric:</i> random striated.</p> <p><i>Organics:</i> 10% light brown to black, humified organic residues and amorphous organic fine material, random to parallel laminar, 0.1-10mm, 1/4 of which are possible bast fibres; 3% charcoal fragments, 0.1-1mm, random.</p> <p><i>Artefacts:</i> fine burnt bone fragments, 0.2-1mm, 2%; fine pottery debris, 0.2mm, <1%.</p> <p><i>Pedofeatures:</i> <i>Amorphous Crypocrystalline:</i> 1) pyrite framboids near and humified organic materials, <1% of the fabric. <i>Fabric:</i> 1) small rounded soil aggregates, 1mm, 1% of the fabric.</p>	Fine alluvium sediments with a few fine anthropogenic remains.

JCN 1



Slide thickness: 40µm, even, no loss

Micro-fabric	Micromorphological Description	Interpretation
<p>JCN 1:1 Unit 4</p>	<p><i>Thickness:</i> 8.5cm. <i>Lower boundary:</i> none.</p> <p><i>Structure and porosity:</i> platy microstructure; 5% horizontal planar voids, partially accommodated, 0.2-1mm thick, slightly serrated walls; the upper part of this fabric may be distorted during the hand augering.</p> <p>This fabric shows a rhythmic bedding with alternating coarse Facies 1 and fine laminae Facies 2 that do not grade into each other.</p> <p>Facies 1, 60% of the fabric: <i>Mineral components:</i> CF limit: 10µm; CF ratio: 95/5; CF related distribution: chitonic to enaulic; <i>Texture:</i> 30% sand, 65% silt, 5% clay; <i>coarse fraction:</i> well-sorted, sub-rounded, coarse silt-size to very fine-sand size minerals, including 50% quartz, 20% micas, 20% dark brown heavy mineral and 10% calcium carbonate, 20-50µm, weakly laminar; <i>fine fraction:</i> light yellow (PPL) silty clay, undifferentiated b-fabric.</p> <p>Facies 2, 30% of the fabric, silty clay crusts with varied thickness from 0.2-2mm: <i>Mineral components:</i> CF limit: 10µm; CF ratio: 30/70; CF related distribution: close porphyric; <i>Texture:</i> 30% sand, 65% silt, 5% clay; <i>coarse fraction:</i> the same as Unit 1, weakly laminar; <i>fine fraction:</i> brown (PPL) humic silty clay, undifferentiated b-fabric; <i>Organics:</i> 2% dark brown humified and amorphous fine organic matter, laminar, 0.1-1mm.</p> <p><i>Artefacts:</i> none.</p> <p><i>Pedofeatures:</i> <i>Textural:</i> 1) thin (100µm) laminae of medium silt-size, black heavy mineral, 5% of the fabric; 2) occasional cross-stratification of fine laminae, 5%.</p>	<p>Well-preserved intertidal flat sediment.</p>

HXT 3



HXT 3:1

Micro-fabric	Micromorphological Description	Interpretation
<p>HXT 3:1 Unit 2</p>	<p><i>Thickness:</i> 12.5cm. <i>Lower boundary:</i> none.</p> <p><i>Structure and porosity:</i> massive; 3% vughs, irregular shape, 0.5-5mm, random; 2% fissures, unaccommodated, mostly vertical, 1-3mm long, 0.5mm thick, slightly serrated walls.</p> <p><i>Mineral components:</i> <i>CF limit:</i> 50µm; <i>CF ratio:</i> 20/80; <i>CF related distribution:</i> close porphyric; <i>Texture:</i> 20% sand, 60% silt, 20% clay; <i>coarse fraction:</i> 18% moderately-sorted, sub-angular, very fine to fine sand-size quartz, 40-200µm, random; 2% sub-rounded coarse sand-size rock fragments, random, 0.3-0.5mm; <i>fine fraction:</i> light yellow (PPL) silty clay with moderate birefringence; 15% of the micromass stained by reddish yellow (PPL) amorphous sesquioxides <i>b-fabric:</i> stipple-speckled to random striated.</p> <p><i>Organics:</i> 2% very fine charred material, 0.1-0.3mm, random; 2% iron-impregnated organic residues, mostly around voids.</p> <p><i>Artefacts:</i> none.</p> <p><i>Pedofeatures: Textural:</i> 1) limpid to dotted clay hypo-coating of voids, high birefringence, orange (XPL), 100-200µm thick, 2% of the fabric; 2) dusty clay hypo-coatings of voids, low to moderate birefringence, dull red (XPL), 100µm thick, 1% of the fabric; <i>Amorphous Crypocrystalline:</i> 1) reddish yellow (PPL) staining of amorphous sesquioxides as mottles, vertical fine striations (2-5mm) and hypo-coatings of voids, 15% of the fabric.</p>	<p>Alluvial deposits formed under a higher depositional energy. Under long-term saturation.</p>

Slide thickness: 40µm, even,
no loss

HXT 2



Slide thickness: 40µm, even,
no loss

Micro-fabric	Micromorphological Description	Interpretation
HXT 2:1 Unit 3	<p><i>Thickness:</i> 6cm. <i>Lower boundary:</i> distinct, clear, distorted due to the mechanical transformation in hand augering.</p> <p><i>Structure and porosity:</i> massive; 2% fissures and cracks, partially accommodated, mostly horizontal, 0.5-1mm long, 0.5-2mm thick, slightly serrated walls; 1% slide loss forming irregular vughs, 3-5mm.</p> <p><i>Mineral components and Organics:</i> The same as Micro-fabric HXT 3:1.</p> <p><i>Pedofeatures: Textural:</i> 1) intercalation and hypo-coating of dusty clay, low to moderate birefringence, dull red to reddish yellow (XPL), 100-300µm thick, 2% of the fabric; <i>Amorphous Crypocrystalline:</i> 1) reddish yellow (PPL) staining of amorphous sesquioxides as mottles, vertical fine striations (2-5mm) and hypo-coatings of voids, 15% of the fabric.</p>	Alluvial deposits formed under a higher depositional energy.
HXT 2:2 Top of Unit 4	<p><i>Thickness:</i> 5.5cm. <i>Lower boundary:</i> none.</p> <p><i>Structure and porosity:</i> massive; 8% vughs, irregular shape, diffuse boundary, some may form due to slide loss, 0.3-5mm; 1% fissures and cracks, unaccommodated, 0.5-1mm long, 0.5-1mm thick, slightly serrated walls.</p> <p><i>Mineral components: CF limit:</i> 50µm; <i>CF ratio:</i> 30/70; <i>CF related distribution:</i> close porphyric; <i>Texture:</i> 30% sand, 50% silt, 20% clay; <i>coarse fraction:</i> 15% moderate-sorted, sub-rounded, very fine to fine sand-size quartz, 40-200µm, random; 15% sub-angular coarse sand-size to fine pebble-size rock fragments, random, 0.3-13mm; <i>fine fraction:</i> light grayish brown(PPL) humic silty clay with moderate birefringence; <i>b-fabric:</i> parallel to random striated (80:20).</p> <p><i>Organics:</i> 3% humified organic residues, 0.1-2mm, random; 3% charred material, 0.5-2mm, randomly distributed.</p> <p><i>Artefacts:</i> three horizontally laminated pottery sherds, 5-15mm.</p>	Shallow water area with input of archaeological remains from nearby activity zones.

	<p><i>Pedofeatures: Textural:</i> 1) micro-laminated, thin dusty clay crusts, low birefringence, reddish brown (XPL), 100µm thick, 3% of the fabric; <i>Amorphous Crypocrystalline:</i> 1) yellow (PPL) staining of amorphous iron oxides around the pottery sherds, 2% of the fabric; 2) vivianite crystals, 0.5mm, 1% of the fabric; <i>Fabric:</i> 1) brown to reddish brown (PPL), rounded, organic-rich, silty clay soil aggregates, 2% of the fabric, 0.5-1mm, random. 2) dark brown (PPL) organic topsoil fragments rich in fine charred materials, 0.5-1mm, 1%; 3) burnt soil aggregates, 1mm, <1%.</p>	
--	--	--

HXT 1



HXT 1:1

Micro-fabric	Micromorphological Description	Interpretation
HXT 1:1 Unit 4	<p><i>Thickness:</i> 6cm. <i>Lower boundary:</i> none.</p> <p><i>Structure and porosity:</i> massive; 1% small vughs, irregular shape, 0.5-2mm; <1% small fissures, accommodated, 5mm long, 0.5mm thick, slightly serrated walls.</p> <p><i>Mineral components:</i> <i>CF limit:</i> 50µm; <i>CF ratio:</i> 10/90; <i>CF related distribution:</i> close porphyric; <i>Texture:</i> 10% sand, 70% silt, 20% clay; <i>coarse fraction:</i> 10% poorly-sorted, sub-angular, very fine to fine sand-size quartz, 40-200µm, random; <i>fine fraction:</i> brown(PPL) humic silty clay with low birefringence; <i>b-fabric:</i> stipple-speckled to undifferentiated.</p> <p><i>Organics:</i> 5% very fine dark brown to black humified organic residues and amorphous organic fine material, 0.05-1mm, random; 1% very fine charred material, 0.1-0.5, random.</p> <p><i>Artefacts:</i> none.</p> <p><i>Pedofeatures:</i> <i>Crystalline:</i> 1) vivianite crystals, as 0.1-0.5mm aggregates incorporating in the groundmass, 3% of the fabric.</p>	<p>Very fine alluvium accumulated under a very weak depositional energy and waterlogged condition.</p>

Slide thickness: 40µm, even,
no loss

DZ 1



DZ 1:1

DZ 1:2

Micro-fabric	Micromorphological Description	Interpretation
DZ 1:1	<p><i>Thickness:</i> 6cm. <i>Lower boundary:</i> none.</p> <p><i>Structure and porosity:</i> moderately separated granular microstructure, peds are 1-3mm in size; 15% compound packing voids, 0.5-2mm, smooth to slightly serrated walls.</p> <p><i>Mineral components:</i> <i>CF limit:</i> 50µm; <i>CF ratio:</i> 70/30; <i>CF related distribution:</i> chitogeferic; <i>Texture:</i> 70% sand, 15% silt, 15% clay; <i>coarse fraction:</i> 30% poorly-sorted, sub-rounded to sub-angular, very fine to fine sand-size minerals, 50-200µm, random; 40% sub-angular to sub-rounded coarse sand-size to fine pebble-size rock fragments, random, 0.2-3mm; <i>fine fraction:</i> 15% light yellow (PPL) silty clay with high birefringence; 15% reddish yellow (PPL) amorphous sesquioxides; <i>b-fabric:</i> grano-striated to stipple-speckled.</p> <p><i>Organics:</i> 1% dark brown humified or charred very fine amorphous organic fine material, 0.1mm, randomly distributed.</p> <p><i>Artefacts:</i> none.</p> <p><i>Pedofeatures:</i> <i>Textural:</i> 1) <i>Amorphous Crypocrystalline:</i> 1) red staining of amorphous iron oxides as nodules (0.5-5mm) and grano-coatings inbetween the coarse rock fragments, one concentric nodule (2mm), 15% of the fabric; <i>Fabric:</i> 1) clayey aggregates, bright yellow in PPL and XPL, unclear extinction band, 0.2-1mm, 5% of the fabric, inbetween coarse rock fragments.</p>	River sand.
DZ 1:2	<p><i>Thickness:</i> 2.5-6cm. <i>Lower boundary:</i> none.</p> <p>The same as DZ 1:1</p>	River sand.

Slide thickness: 40µm, even,
no loss

Appendix 3 Results of bulk analysis

Sample No.	pH	Mag sus ($10^{-9} \text{ m}^3\text{kg}^{-1}$)	P (mg/L)	Carbon (%)	CaCO ₃ (%)	Total Organic (%)	Elevation (m)	Clay (%)	Silt (%)	Sand (%)
T0950 1-1	6.62	135.10	0.10	2.29	5.20	6.40	3.10	26.36	73.26	0.39
T0950 1-2	6.51	85.40	1.40	1.36	4.12	6.04	3.20	25.85	70.98	3.17
T0950 2-1	6.84	129.00	0.60	1.51	4.37	3.70	4.28	25.85	70.98	3.17
T0950 2-2	6.69	185.00	0.70	3.14	4.17	17.54	4.35	10.79	65.32	23.89
T0950 2-3	6.80	79.80	0.70	0.64	2.60	1.40	4.50	5.50	72.64	21.86
T0950 3-1	6.85	105.10	0.20	1.48	4.30	3.64	4.55	14.36	79.34	6.31
T2621 1-1	7.68	116.90	0.10	1.53	5.21	2.16	1.12	17.83	73.50	8.67
T2621 2-1	7.01	119.60	0.20	0.92	6.31	2.31	1.42	19.49	78.40	2.11
T2621 2-2	7.01	104.50	0.00	0.62	5.67	1.56	1.62	16.25	80.17	3.58
T2621 3-1	6.38	90.60	0.40	0.84	3.56	1.93	1.78	10.51	81.96	7.53
T2621 3-2	7.13	147.20	0.30	0.90	3.59	2.37	1.88	5.39	76.72	17.89
T2621 3-3	6.92	106.70	0.00	0.25	4.34	1.91	1.99	8.17	78.27	13.56
T2621 4-1	7.13	115.00	0.00	0.37	4.23	1.99	1.92	7.53	76.31	16.16
T2621 4-2	7.27	77.70	0.10	0.44	3.02	1.22	2.07	6.26	77.85	15.88
T2621 5-1	7.43	89.80	0.60	0.36	2.98	1.43	2.16	6.38	73.97	19.65
T2621 5-2	7.51	87.30	0.30	0.34	3.37	1.37	2.22	5.91	75.03	19.06
T2621 5-3	7.46	78.00	0.40	0.55	4.70	1.79	2.30	8.03	86.79	5.18
T2621 6-1	7.44	43.20	0.20	0.71	6.19	1.41	3.10	13.31	51.22	35.46
T2621 6-2	7.31	99.70	0.50	1.19	4.49	2.77	3.20	12.48	80.48	7.03

T2621 7-1	7.32	111.10	0.10	1.05	5.05	2.46	3.33	12.68	81.64	5.68
T2621 7-2	7.34	135.10	0.10	1.72	5.74	3.44	3.40	21.83	64.24	13.93
T2621 8-1	7.30	114.80	0.10	1.35	5.12	2.93	3.50	14.39	78.69	6.92
T2621 8-2	7.30	175.30	0.20	1.21	4.51	2.75	3.60	17.20	77.23	5.58
T3131 1-1	6.66	171.40	0.40	0.60	5.45	5.70	1.15	14.60	59.41	25.99
T3131 1-2	6.78	128.80	0.40	0.99	6.09	5.21	1.35	21.66	66.68	11.66
T3131 2-1	7.14	191.10	0.40	1.79	4.52	7.16	1.35	20.25	69.41	10.34
T3131 2-2	7.37	126.50	1.00	1.36	6.86	8.30	1.50	17.69	67.96	14.35
T3131 3-1	5.84	132.20	0.40	1.31	3.87	10.64	1.62	6.85	67.03	26.12
T3131 3-2	6.16	128.00	0.80	1.22	3.89	7.31	1.79	7.06	66.56	26.39
T3131 4-1	7.28	240.00	0.60	1.12	4.15	6.05	1.59	6.33	65.14	28.53
T3131 4-2	7.22	158.70	0.80	1.50	3.88	5.89	1.79	9.12	67.59	23.29
T3131 5-1	6.76	325.80	0.20	1.52	3.54	5.62	1.70	8.29	76.37	15.34
T3131 5-2	7.25	110.60	1.00	1.07	3.19	7.46	1.90	7.31	61.34	31.35
T3131 6-1	6.99	100.50	0.60	1.62	4.38	15.84	1.95	7.67	64.16	28.18
T3131 6-2	7.58	121.90	0.40	1.22	3.70	3.01	2.13	7.98	70.19	21.83
T3131 7-1	7.64	139.40	0.60	1.34	3.65	3.45	2.25	8.65	72.75	18.60
T3131 7-2	7.45	1783.80	1.00	0.79	2.77	2.44	2.36	8.38	67.60	24.02
T5020 10-2	7.20	71.70	2.50	1.47	3.91	3.69	2.66	19.19	75.59	5.22
T5020 10-1	7.07	108.50	0.20	1.14	4.02	2.78	2.51	20.34	75.99	3.67
T5020 9-2	6.63	84.20	0.20	1.12	4.24	2.98	2.40	15.30	80.57	4.13
T5020 9-1	6.87	111.90	0.80	0.88	3.42	2.38	2.23	11.54	81.57	6.89
T5020 8-2	6.87	110.00	0.40	1.05	3.18	2.80	2.00	13.69	78.69	7.62
T5020 8-1	6.90	85.60	0.20	0.91	2.37	2.47	1.82	11.23	80.82	7.95
T5020 7-2	6.59	66.40	0.20	1.03	2.63	2.83	1.76	14.18	79.70	6.12

T5020 7-1	6.52	74.70	0.40	1.26	3.51	3.51	1.62	19.42	77.21	3.37
T5020 6-2	6.64	157.80	0.40	1.28	3.79	4.11	1.74	19.90	72.63	7.47
T5020 6-1	6.76	85.80	0.10	1.36	3.39	4.74	1.59	20.06	74.49	5.45
T5020 5-2	6.45	77.00	0.10	1.35	2.72	5.53	1.60	7.67	82.31	10.02
T5020 5-1	6.78	119.30	0.30	1.34	4.05	5.05	1.38	15.11	80.18	4.71
T5020 4-2	5.83	97.60	0.40	1.40	3.83	5.75	1.05	15.64	79.77	4.59
T5020 4-1	5.92	101.60	0.70	1.45	4.03	6.44	0.90	35.65	60.25	4.10
T5020 3-2	6.41	122.50	0.90	1.78	5.07	6.09	0.68	20.99	76.24	2.77
T5020 3-1	6.63	121.80	0.90	1.91	5.44	6.22	0.54	25.81	72.38	1.82
T5020 2-3	6.70	118.90	0.90	2.04	5.35	6.11	0.82	22.51	75.02	2.47
T5020 2-2	6.63	109.80	0.10	1.60	4.64	6.27	0.75	29.29	69.31	1.39
T5020 2-1	5.83	114.30	0.10	1.70	5.80	6.23	0.69	30.60	68.09	1.31
T5020 1-2	6.55	116.10	0.40	2.25	5.11	6.44	0.52	25.88	72.82	1.30
T5020 1-1	6.75	231.30	0.10	1.18	10.75	3.55	0.37	30.70	69.30	0.00
HXT 1	6.81	128.40	0.80	0.79	4.20	3.78	0.40	15.19	78.96	5.84
HXT 2	6.51	116.30	0.10	0.89	3.79	3.87	1.00	15.31	80.55	4.14
HXT 3	7.07	71.10	0.20	0.77	3.03	2.10	1.50	10.75	74.62	14.63
HXT 4	7.08	95.10	0.70	0.98	3.70	2.52	1.70	18.32	73.76	7.91
JCN 1-1	7.71	183.00	1.10	0.24	6.06	1.46	1.50	6.13	61.71	32.16
JCN 1-2	6.91	149.60	1.40	0.81	4.86	3.83	1.80	17.97	73.98	8.06
JCN 1-3	6.97	181.30	0.30	0.91	5.16	3.63	2.00	21.16	71.69	7.15
JCN 2-2	6.76	204.40	0.40	1.00	5.73	2.39	2.10	15.97	77.39	6.65
JCN 1-4	6.96	118.70	1.00	0.64	4.98	2.58	2.60	22.43	73.15	4.41
JCN 2-4	7.35	109.30	1.10	0.40	3.63	0.96	3.20	5.96	74.61	19.43
JCN 2-5	7.53	115.90	0.80	0.77	4.57	2.39	3.40	14.81	82.99	2.20

T1812 1	7.78	156.50	0.20	1.14	8.16	3.26	-0.30	20.58	78.63	0.79
T1812 2	7.84	160.40	0.10	1.33	7.79	3.54	0.25	23.65	75.50	0.85
T1812 3	7.57	110.60	0.60	0.81	5.18	3.42	0.30	18.29	79.39	2.33
T1812 4	7.73	122.30	1.40	0.91	6.37	3.48	0.40	17.67	80.69	1.64
T1812 5	7.56	139.70	0.10	1.08	6.96	2.48	0.90	24.23	74.48	1.29
T1812 6	7.33	74.60	0.10	1.30	5.89	4.54	1.00	20.53	78.13	1.34
T1812 7	7.07	106.40	0.70	0.84	6.48	3.94	1.10	19.95	77.22	2.83
T1812 8	7.25	137.00	0.40	1.18	5.70	3.14	1.20	22.57	75.46	1.96
T1812 9	7.51	74.80	0.20	1.51	5.06	3.90	1.90	22.65	75.31	2.04
T1812 10	7.56	100.30	2.80	1.38	5.45	3.59	2.00	21.31	75.92	2.78
T1812 11	6.82	128.20	0.20	1.16	5.43	3.11	2.20	23.32	74.80	1.88
T1812 12	7.45	104.10	0.40	1.29	3.56	3.04	2.30	15.58	78.41	6.02
TSB 1-1	7.25	274.70	0.10	0.75	2.83	1.66	5.30	17.12	78.06	4.82
TSB 1-2	7.25	98.90	0.20	1.17	2.49	2.11	5.80	21.38	75.93	2.69
TSB 1-3	7.32	507.00	0.50	1.20	3.04	2.61	5.90	23.69	57.45	18.86
TSB 1-4	7.41	115.60	0.30	1.67	3.79	3.04	6.30	19.36	75.85	4.78
TSB 2-2	5.26	1.13	0.40	0.83	2.53	2.59	/	14.67	35.50	47.96
TSB 2-1	5.90	1.14	0.30	0.90	2.71	1.79	/	16.54	42.00	43.33
Average	6.98	144.41	0.50	1.15	4.52	4.01	2.07	16.28	73.13	10.60
Maximum	7.84	1783.80	2.80	3.14	10.75	17.54	6.30	35.65	86.79	47.96
Minimum	5.26	1.13	0.00	0.24	2.37	0.96	-0.30	5.39	35.50	0.00
Standard deviation	0.50	187.74	0.47	0.47	1.40	2.69	1.30	6.87	8.25	10.34